Freeforms in architecture

Shaping of discrete, doubly-curved grid-shells in planar quadrilateral topology using the bottom-up approach

by

Michał Święciak

M.Sc. Eng. in Architecture

Thesis submitted for the degree of

Doctor of Philosophy in Architecture

Thesis Supervisor

Romuald Tarczewski

PhD Eng., Hab., Associate Professor

Faculty of Architecture
Wrocław University of Science and Technology

February 2019

Table of contents

1. Introduction to issues addressed in the dissertation

1.1. Subject of the research

This dissertation develops a new methodology for shaping and implementing discrete freeform structures, commonly called *freeforms*, in architecture using existing and newly developed methods of their generation and transformation.

Although their definition is not yet explicit and well-established, as will be discussed further, *freeforms* are becoming increasingly popular in architectural designing practice (Soeren, Sánchez-Alvarez, and Knebel 2004), (Huzefa 2013), (Pottmann, Schiftner, and Wallner 2008), (Liu et al. 2006), (Hambleton et al. 2009).

1.1.1. What are freeforms

Freeforms should not be confused with design freedom, which is an indispensable attribute of both architecture and structural design. This term refers primarily to the geometrical features of objects and their visual perception.

As already mentioned above, *freeform* geometry does not have a well-established definition, see e.g. (Hambleton et al. 2009). It is characterized by smooth flowing lines, unique and varying shapes and lack of inherent symmetries. In (Adriaenssens et al. 2014), *freeforms* are associated with free-curved or sculptural shells whose geometry does not consider any structural performance – unlike *mathematical* and *form-found* surfaces. In (Soeren, Sánchez-Alvarez, and Knebel 2004) and (Sánchez-Alvarez 2002), *freeforms* are associated with *NURBS* surfaces allowing to specify any imaginable form. In a general case, the *freeform* surface has a permanently changing curvature and parts of that surface are non-symmetric (irregular). Irregularity and variable curvature are indicated as main features of *freeforms* also in (Gidófalvy, Katula, and Ma 2016). However, *freeforms* can be shaped as discrete models (i.e. grid shells or meshes) without a corresponding, continuously curved surface, as mentioned in (Yang et al. 2011). According to (Pottmann, Eigensatz, et al. 2015), *freeforms* that are shaped under a certain regime – i.e. including fabrication requirements – are not fully free formed due to the fact that *fabrication-aware design* restricts the freedom of design.

1.1.2. *Freeforms* in architecture

Although known for a long time in other areas of technical activity, *freeforms* found application in architecture only when some computer based design tools have become available that did not exist before, or for various reasons were only available in specific applications, e.g. in automotive, aviation and naval industries (Bagneris et al. 2007), (Gonzales-Pulido, Vaggione, and Ackley 2002). In contrast to these areas, in architecture *freeforms* are strongly connected with the uniqueness of structural parts of a building or a structure.

The first large scale use of such design tools in architecture was during design and construction of the Guggenheim Museum in Bilbao (from 1993 to 1997) (Gonzales-Pulido, Vaggione, and Ackley 2002). In contrast to the majority of architects, the designer of Guggenheim Museum, Frank O. Gehry, was supported by structural engineers (from Skidmore, Owings & Merrill) as well as technicians formerly associated with the aviation design industry. They made designing decisions together since

the very beginning. As emphasized in (Schober 2015a): *"designing completely freeforms requires special skills which very few designers possess".*

The incredible international success of the building accelerated the adoption of *NURBS* surfaces and parametric design in architectural practice. Since then the number of designers who followed the style of its designer, and started to design similar forms has been constantly growing.

In a simplified, but very popular approach, *freeforms* are associated with all forms for which the geometric basis are surfaces with a two-way curvature, usually changing according to an adopted formula.

Such objects, popular at one time in architecture, were shells, made mainly of reinforced concrete, but also of small-size elements like bricks and stones, which were designed and constructed even before the advent of the aforesaid methods. Single-layer, thin shells achieved a high degree of structural efficiency and enabled the construction of many objects that are outstanding in terms of architectural form. Notable examples of such forms are objects designed by Felix Candela, Eduardo Torroja, Heinz Isler, Anton Tedesko and others. In (Schober 2015a) an elegant justification for doubly curved shells is provided:

"Shells are naturally beautiful and efficient structures. The reason for this is that their flowing double-curved form is able to transfer loads without bending, by transmitting tension and compression forces solely within the surface. They therefore require significantly less material than flat structures under bending stress, as for instance beam or slab structures. There is however a discrepancy between favourable load-bearing behaviour and difficult double-curved construction. Solving this discrepancy is an important step towards successful shell design."

Another type of structures in which two-way curvature is a prerequisite for implementation are structures made of textile membranes. The distinguishing designers of membrane structures were Frei Otto and Jörg Schlaich.

Although traditional shell and membrane structures are usually classified as *freeforms*, they clearly break out of the trend initiated by the emergence of the Guggenheim Museum. It's because their form is shaped on the basis of structural logic, often by means of physical modeling. "Contemporary" *freeforms* are distinguished by the fact that – thanks to the above-mentioned computer tools – their complex double-curved geometric form has been created apart from any material and structural constraints and limitations.

Such freedom, however, has its price. Iconic architectural forms often break technological boundaries, e.g. Sydney Opera House[1] and Guggenheim Museum in Bilbao, but in the first case, however, overwhelmingly exceeding the budget. Some ambitious architectural forms fail to successfully overcome the barrier between the design and the construction. A good example is Milano Convention Centre which form was inspired by *pappardelle* pasta and the resultant structure supporting the architectural form was a challenge for both its designers: Mario Bellini – architect and Massimo Majowiecki – structural engineer (Tarczewski 2011).

In (Majowiecki 2013) and (Majowiecki 2007), professor Massimo Majowiecki, on the base of his personal experience as being a structural engineer of many important freeform objects, notes that new morphologies adopted in the present conceptual design methodology cause significant uncertainties in the assessment of reliability. Majowiecki highlights that nowadays more and more

[1] The architect of the Sydney Opera House was Jørn Oberg Utzon, later awarded the Pritzker Prize

architects and engineers, absorbed by this new challenge which is the pursuit of ever new *freeforms* in design, put aesthetics over static rationality.

Apart from the introduction of CAD tools, which allow shaping *freeforms*, a new trend has emerged – the parametric designing. It allows one to grasp complicated structural systems which, in the context of *freeform design,* are composed of numerous and unique structural elements. These elements are designed as a result of a parametric model, predefined by the designer (Oosterhuis 2016):

"Parametric design means modelling associations between the components which a ship or a building is made of. Associations are a form of dynamic entanglement. When one part changes its values, the associated parts change with it".

These facts may cause a false impression that any architectural form is possible and the purpose of structural engineering is merely supporting an architectural vision. Nowadays, it is possible to design complicated forms not getting away from the computer screen, whereas in the past designers had been limited to relying on physical tools and models.

Before the invention of digital tools intended for designing *freeforms*, empirical (physical) and analytical (mathematical and geometrical) methods had been used, (Lienhard 2014), p. 51. Shaping forms in empirical way allows for almost immediate evaluation of their structural properties. The physical modelling methods, give precise shapes in which a structure performs optimally. Gaudí's experiments with the structure of Sagrada Familia with the use of strings, and Frei Otto experiments with shapes of tensile membrane structures with the use of soap film are widely known.

While new design tools give architects opportunities to design new forms, they often go far beyond the available and feasible technologies of their construction (Veltkamp 2015) and even force solutions that are detached and inadequate from the logic of structural systems (Hambleton et al. 2009):

"Although there is no doubt that this newly found freedom has given rise to some incredible and beautiful forms, it has also widened the gap between the original design intent of a project and what can reasonably be constructed."

Separating the form from its physical sense in the shaping process makes it ineffective and sometimes even dangerous. For this reason, many authors recommend a return to the use of form finding procedures, which were developed for the purpose of shaping shell and membrane structures. It is defined by Patrik Schumacher as follows (Hassel 2016):

"Form finding is a physical setup where form self-organizes and it is not drawn by hand or invented or preconceived. It emerges in a physical process".

On the other hand, ignoring purely aesthetical and compositional reasons for using *freeforms* in architecture, when reasonably well-designed, they allow for obtaining optimal forms from the structural point of view, making it possible to increase the span and height of a structure and reduce material consumption and total costs. Parametric designing tools allow to look at *freeforms* in terms of their non-physical – i.e. geometrical and topological properties and form-find them in these fields. This is very important because, while the application of physical modelling or its numerical equivalent allows to obtain an optimal form in terms of flow of forces and mechanical properties, in the case when there are additional limitations of topological or geometric nature, such modelling becomes inadequate.

One of the sources of such constrains is the very strong tendency now to introduce large glazed surfaces in both façades of buildings and roofs over various surfaces. The consequence of this is that

most *freeforms* are not realized as continuous structures with a homogeneous surface but as reticulated structures also called lattice or grid structures. Such solutions are very spectacular, however, they impose restrictions, the fulfilment of which is often very difficult in practice.

1.1.3. Glossary of basic terms

Below are explained some of the most basic terms related to *freeforms*, which are used in further considerations.

1.1.3.1. Curvature

The curvature associated with *freeforms* is a function showing how much each part of the curve or curved surface is deformed. The curvature $\boldsymbol{\kappa}$ of a curve is reciprocal to the radius $\boldsymbol{R}$ of a circle tangent to that curve at measured point, see formula (1.1).

$$\boldsymbol{\kappa = \frac{1}{R}} \tag{1.1}$$

The curvature of the curve on Fig. 1.1 is measured at two points – P_1 and P_2. The lesser the curvature, the greater the tangent circle and its radius. Location of the centre of curvature on different sides of the curve is expressed by a curvature sign: positive or negative.

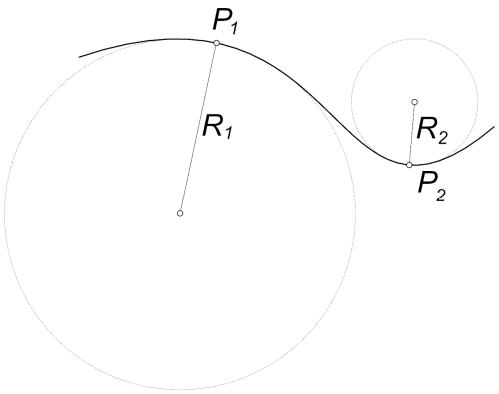

Fig. 1.1 Circles tangent to a curve at its specified points and their radii.

Surfaces have two distinct directions along which they can be curved. The *freeformed* surfaces are curved along both directions, and are called *doubly curved* surfaces. Depending on the relation between curvatures in both directions, doubly curved surfaces are distinguished by two types:

- synclastic (positive Gaussian curvature) – when curvatures are compatible, e.g. sphere;
- anticlastic (negative Gaussian curvature) – when curvatures are opposite, e.g. saddle (*hypar*) surface.

Spheres are synclastic surfaces of constant curvature in both directions. Despite the identical curvature on the whole surface, spheres can be classified as a *freeform* due to the fact that there is only a finite number of ways a sphere can be divided into identical fragments. All other forms of surfaces whose curvatures are varying are classified as *freeforms* due to their lack of regularity.

The curvature is also defined as a derivative of the direction of a curve. The faster the tangent direction changes along a curve, the greater is the curvature of that curve, see Fig. 1.1. On doubly curved

surfaces the curvature may be examined in any chosen direction, therefore Gaussian and mean curvatures are defined, see section 1.1.3.3.

1.1.3.2. Curvature continuity

The continuity of curves and surfaces is represented as level of the *curvature continuity* (Golay, Hambly, and Fugier 2014), p. 39. The curvature continuity levels are as follows:

- Positional continuity – ***G0***
- Tangency continuity – ***G1***
- Curvature continuity – ***G2***

*G*0 continuity at a point means that the tangent vectors at the infinitesimal distances around the measured point are not equal. There is a kink on a curve or between two line segments, see Fig. 1.2. Consequently there can be a positional continuity between two surfaces. The necessary condition is that the segments must have common point.

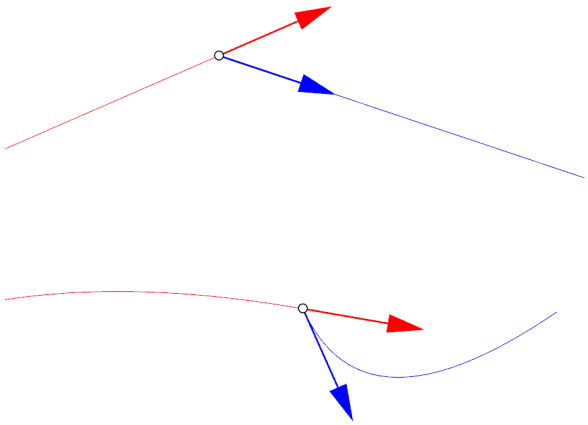

Fig. 1.2 Two line segments and two curve segments with G0 *continuity.*

*G*1 continuity have the necessary condition of *G*0, with additional condition, that the tangent vectors must be equally directed, see Fig. 1.3.

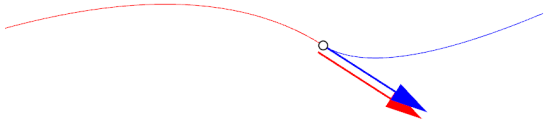

Fig. 1.3 Two curve segments with G1 *continuity – the tangent vectors are shown separately for clearance.*

*G*2 continuity have the necessary conditions of *G*1, with the additional condition, that the centres of tangent circles of both curve segments have to be at the same point. The distances *R* of the tangent circles of both curve segments are therefore equal so as the curvatures – $\boldsymbol{\kappa}$. Thus, the graphs of the curvatures in Fig. 1.4, right, are continuous, i.e. have the same value on both sides of the measured point, contrary to the graphs of the curvatures in Fig. 1.4, left.

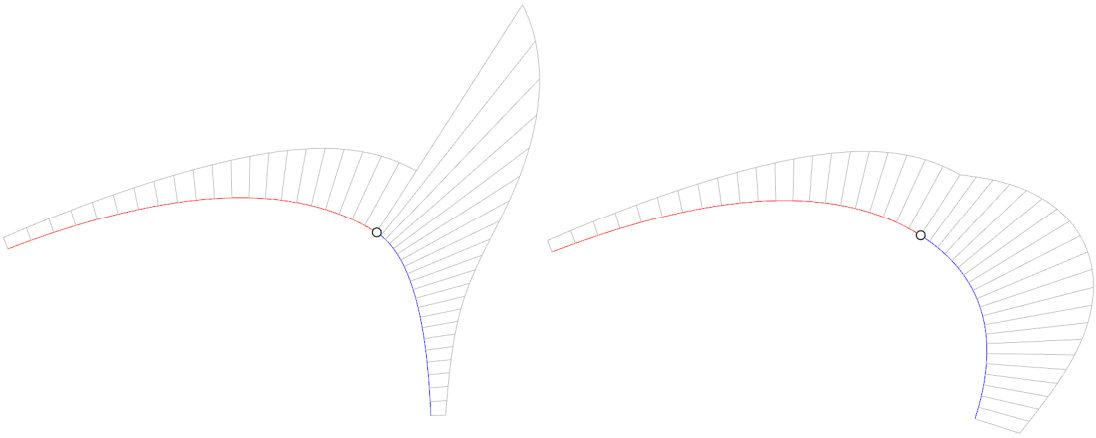

Fig. 1.4 Curvature graphs of G1 *(left) and* G2 *(right) continuities.*

There are also ***G3***, ***G4*** levels of continuity and the next ones. The *G3* continuity have the necessary conditions of *G*2, with the additional condition that the curvature graph has to be smooth, i.e. without the kink as in Fig. 1.4, right. However above the ***G3*** there is no visible significance to the shape of the curve of surface. An example is shown in Fig. 1.5.

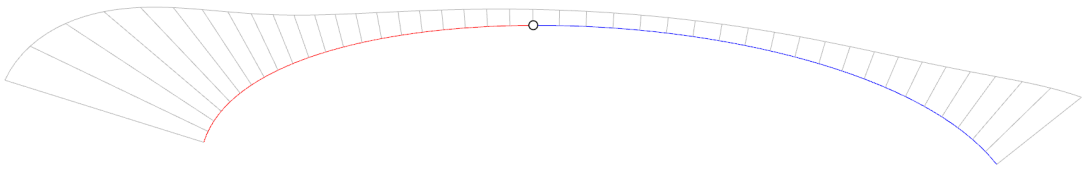

Fig. 1.5 Curvature graph of G3 *continuity.*

1.1.3.3. Gaussian and mean curvature[2]

The Gaussian curvature ***K*** at a point ***P*** of a surface is the product of two principal curvatures $\boldsymbol{\kappa_1}$and $\boldsymbol{\kappa_2}$, see equation (1.2). At each point of surface a normal vector exists. A plane containing that normal vector intersects with the surface and the intersection is a curve. Such curve has a curvature at the point on a surface. There are infinitely many planes containing one normal vector and infinitely many curves. The principal curvatures are the maximum and minimum values among all the curves obtained by intersection between the surface and plane.

Mean curvature ***H*** is a half of the sum of curvatures $\boldsymbol{\kappa_1}$ and $\boldsymbol{\kappa_2}$, see equation (1.3).

$$\boldsymbol{K = \kappa_1 \kappa_2} \tag{1.2}$$

$$\boldsymbol{H = \frac{1}{2}(\kappa_1 + \kappa_2)} \tag{1.3}$$

The values of $\boldsymbol{\kappa_1}$ and $\boldsymbol{\kappa_2}$ may have opposite signs if the curvatures are opposite, i.e. when the centres of tangent circles are on the opposite sides of the surface. Anticlastic surfaces have opposite principal curvatures, therefore the Gaussian curvature is negative. Synclastic surfaces have the principal curvatures compatible, therefore their Gaussian curvature is positive. When the surface is single curved one of the principal curvatures is equal to zero, therefore the Gaussian curvature of such surface is also equal to zero.

[2] Exact definitions and formulas for *principal curvatures* can be found in (Weisstein 2018k).

1.1.3.4. Continuous and discrete forms

Curves and doubly-curved surfaces may have continuous or discrete representations. The term continuous refer to the curvature function, i.e. the graph of that function is continuous. Discrete representations are composed of elements in straight or planar configurations, see Fig. 1.6. The curvature continuity of the discrete forms is ***G0***.

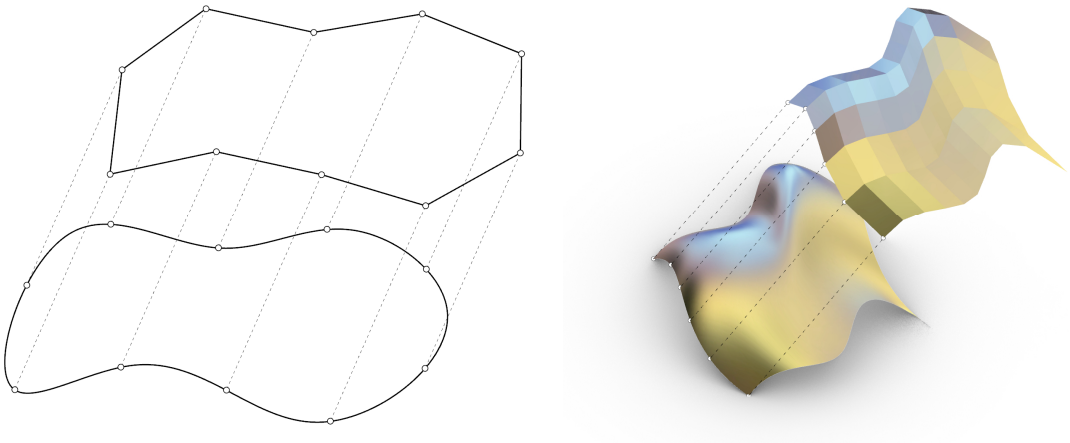

Fig. 1.6 Left: curve in the discrete (top) and the continuous (bottom) form. Right: surface in the discrete (top) and the continuous (bottom) form.

Discrete forms of surfaces, i.e. polyhedral surfaces, are also have Gaussian curvature ***G*** (A. I. Bobenko et al. 2008), p. 180, expressed by formula (1.4).

$$\boldsymbol{G} = (\boldsymbol{2\pi} - \sum_{\boldsymbol{j}} \boldsymbol{\phi_j})/\boldsymbol{A} \tag{1.4}$$

Where $\boldsymbol{\phi_j}$ are the angles in radians between edges of facets that are adjacent to a point ***P***, around which the curvature is measured. The ***A*** is the area around the measured point.

Figure 1.7 shows that the sum of angles around a vertex can be less than 360°[3]. Areas around vertex are marked by rectangular borders.

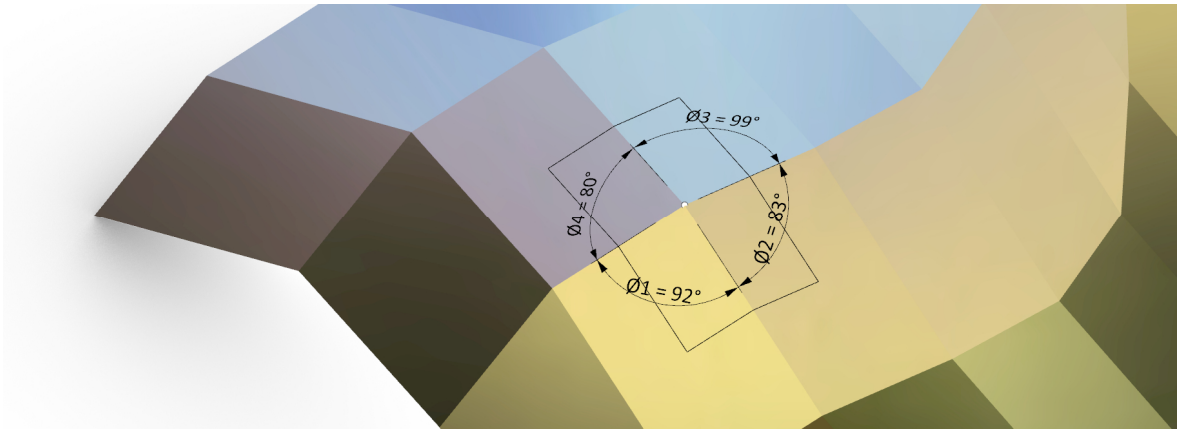

Fig. 1.7 Angles around a vertex.

[3] The difference between full angle (2π) and the sum of angles around a vertex in polyhedron is called angular defect, see (Weisstein 2018b).

1.2. Scope of the research

Based on previous considerations, the term freeforms has been specified for the purpose of this work, in order to achieve unambiguity and certain ordering of content. In this dissertation *freeforms* are always associated with the forms that are not regular. Unlike in (Adriaenssens et al. 2014) and (Pottmann, Eigensatz, et al. 2015), the term *freeforms* here also covers the structurally optimized forms. Although *freeforms* can be represented by *NURBS* surfaces or discrete models (grid shells) this work focuses on the methods of shaping discrete models only. Discrete representations of doubly curved surfaces with constant curvature (spheres) are also included in the group of *freeformed* if their topology (panelization) is irregular, therefore meeting the requirement of irregularity.

Freeforms that are created purely for the sculptural reasons are excluded from the scope of this thesis. The example of such form is the Milwaukee Art Museum designed by Santiago Calatrava. In this building ribs based on ruled surface create the "wings" which spread over the building. However, they carry no structural improvement or significance to the building, and only function as a moving sculpture. The imperative of the aesthetical aspects over the structural and economical logic makes the necessity of optimization and reasoning less significant.

Additionally, in this work the methods of implementation of *freeforms* as grid shells are narrowed down to planar-quadrilateral (PQ) topologies. The meaning of this term is explained in the following. The decision is supported by analyses provided in Chapter 3 which prove superiority of PQ topology in terms of functional, economical and fabrication aspects.

The methods of formation and implementation of *freeforms* in this work are investigated together in accordance with the *fabrication-aware design* principle. Consequently, the newly proposed methods of formation of *freeforms* should always:

- act in accordance with the implementation rules, and
- offer sufficient freedom of design.

The change of the design paradigm is imposed due to the requirements of *fabrication-aware design*. The approach assumes the awareness of specific fabrication methods that will be used during the construction from the very first design phases. Hence, the scope of this work is narrowed down to the bottom-up paradigm, see section 3.4.

Since the author of this work is an architect, not a structural engineer, the geometrical aspects of creating *freeforms* are mainly emphasised. The issues related to the geometric stability, selection of the member cross-sections and other structural aspects are out of the scope of this work.

1.3. Theses of the dissertation

The emergence of the unique Guggenheim Museum in Bilbao in 1997 coincided with the dissemination and wide availability of computer tools allowing relatively easy creation and manipulation of objects with complex geometry, in particular with NURBS surfaces. This caused an avalanche effect of using such forms in architectural design, soon named the *Bilbao effect*.

Henceforth the designers, felt free from many previous limitations, were able to realize all their ideas, at least on the geometric level of forms. Therefore, this design trend is now referred to as *freeform* design and the architectural forms designed and realized in this manner are called *freeforms*.

After the initial, quite enthusiastic period, when numerous objects formed on the basis of *freeforms* were created, numerous problems were identified, which are the result of the detachment of geometric shaping from the material conditions related to the implementation. These are problems related to, for example, issues of stability and dynamics, which are solved as part of structural design, as well as problems concerning the form itself, which require certain solutions at the topological and geometric level.

An especially important and interesting example of such *freeforms* are discrete grid shells covered with glass or other types of panels, which are coverings of buildings, their parts or their structural skins i.e. façades.

- **Thesis 1**

  Grid shells are one of the main means of expression within the free-form design trend in architecture and belong to the most characteristic and most frequently implemented objects in this group.

- **Thesis 2**

  Free-form grid shells based on planar quadrilateral topology (PQ) have many advantages over grid shells based on a triangular topology.

- **Thesis 3**

  It is possible to develop design tools that allow for the effective design of PQ meshes based on a bottom-up methodology.

- **Thesis 4**

  Guided by the principles of bottom-up design, desirable grid shells can be obtained with a small and acceptable restriction of freedom in shaping their form.

1.4. Scientific objectives and research methods

Research carried out in connection with the preparation of this doctoral dissertation was aimed at gathering and systematizing knowledge on the methods of designing doubly curved grid shells, in particular of PQ topology and preparing a monographic study based on it, that would depict these issues in a comprehensive way.

The specific aim of the dissertation was to develop proprietary methods of generating and transforming meshes for doubly curved grid shells and formulating the procedure for their design according to the bottom-up methodology taking into account non-geometric structural and implementation aspects.

During the implementation of the main objective, the following intermediate goals were also set:

- Capturing the common features and the way of shaping *freeforms* in architecture;
- Analysis and evaluation of topological and geometric features of discrete *freeforms*;
- Gathering and systematizing information on the methods of shaping meshes of grid shells;
- Proposing new, proprietary methods for shaping grid shells;
- Gathering and systematizing information on the methods of transformation of meshes of grid shells;

- Proposing new, proprietary methods for transforming grid shells;
- Proposing a systematic and comprehensive methodology for the design of grid shells shaped on freeform surfaces;
- Verification of the proposed methods through their application in practical examples.

These objectives were accomplished through the analysis of existing facilities, observation of applied solutions, analysis of the current state of knowledge and own conceptual work. The conclusions drawn from the research and new design tools developed can be used for implementation a more effective methodology for the design of grid shells shaped on freeform surfaces.

The problems of shaping the PQ mesh on *freeforms* presented in the dissertation are divided into chapters which present the history of application of *freeforms* in technology; issues and problems related to their application in architecture; methods of forming PQ meshes; methods of transforming PQ meshes; a comprehensive concept of the design process for PQ meshes; case studies and mechanical assessment of the presented solutions. In the course of work on the dissertation, classical research methods used in architecture (Niezabitowska 2014) were applied, such as the logical analysis, observational - descriptive method, comparative case studies, numerical experiments, modelling and simulation research as well as combinations of these methods.

1.5. Current state of research

The glazed PQ grid shell at the courtyard of the Museum of Hamburg History is considered as the pioneer structure of its type. Designed by the architect Volkwin Marg, engineered by Jörg Schlaich, built in 1989. The geometrical solutions, beside the structural properties, were described by Jörg Schlaich in *Conceptual Design of Long-Span Roofs* (Schlaich and Bergermann 1994) with Rudolf Bergermann and in *Glass-covered lightweight spatial structures* (Schlaich and Schober 1994) with Hans Schober, both in 1994. Prior, German-speaking sources are form 1992 - (Schlaich and Schober 1992b) and (Schlaich and Schober 1992a). Technical description of the structure occurred in 1991 in DETAIL magazine (*DETAIL* 1991). *Conceptual Design of Long-Span Roofs* also contain the argumentation for application of doubly curved grid shells.

Hans Schober, a structural engineer cooperating on numerous PQ grid shell designs with Jörg Schlaich, summarizes achievements and realizations in the field of doubly curved PQ grid shells in the article *A parametric strategy for free-form glass structures using quadrilateral planar facets*[4] (Glymph et al. 2004) and in his comprehensive and important in the field book titled *Transparent Shells: Form Topology Structure* (Schober 2015a). The last position describes in details the various aspects of designing PG grid shells, among which there are geometrical aspects of designing doubly curved PQ grids. Selected case studies of doubly curved PQ grid shells, designed with Schober complicity, are chronologically:

- Aquatoll in Neckarsulm, Germany, built in 1989, (Schlaich and Bergermann 1994) and (Schlaich and Schober 1994);
- Rostocker Hof in Rostock roof, Germany, built in 1994, (Schober 2003a);
- House for Hippopotamus in Berlin Zoo, Berlin, Germany, built in 1997, (Schlaich and Schober 1998);
- Bosch Areal roof over the pedestrian zone built in 2001, (Schober 2003a) and (Schober 2003b);

[4] Hans Schober was a representant of Schlaich Bergermann & Partners structural engineering office, while other authors represented Gehry Partners architectural office.

- Schubert Club Band Shell, St. Paul, Minnesota, USA, built in 2001, (Schober 2003a);
- German Historical Museum inner courtyard roof, Berlin, Germany, built in 2002, (Schober 2003a);
- Uniqa Tower atrium roof, Vienna, Austria, built in 2004, (Woltron and Zugmann 2004);
- Cabot Circus Bristol roof built in 2007, (Schober and Justiz 2012).

Geometric solutions adopted by Schober and Schlaich may be described as bottom-up, whereas majority of publications in the field of generating *freeform* PQ tessellations represent the other approach, which is top-down. Among them, most are the theoretical works of a mathematician Helmut Pottmann, a Professor of Geometry at Vienna University of Technology. His most important work is the *Architectural Geometry*, published in 2007 (Pottmann, Asperl, et al. 2007). The content of the book expands the methods invented by Schober by introducing to the field of architectural geometry conepts like *parallel meshes* and *conjugate curve networks*. Both are derived from the fields of *discrete geometry* and *discrete differential geometry* and are bases to further researches of Helmut Pottmann. Prior to the *Architectural geometry*, a *Geometric Modeling with Conical Meshes and Developable Surfaces*, (Liu et al. 2006) and *Discrete Surfaces for Architectural Design* (Pottmann, Brell-Cokcan, and Wallner 2007) were published by Helmut Pottmann et al.. Also in 2007 the article titled *Geometry of multi-layer freeform structures for architecture* (Pottmann, Liu, et al. 2007) was published, which was focused on the properties of parallel PQ meshes, as well of those of other topologies.

Helmut Pottmann also introduced solutions derived from computer graphics in the subdivision method of obtaining the PQ meshes. Originally, this method was created for the needs of 3D modelling in PIXAR studio movies by Edwin Catmull and Jim Clark: *Recursively generated B-spline surfaces on arbitrary topological meshes* (Catmull and Clark 1978).

Selected works of Helmut Pottmann et al., or those which he contributed in the field of obtaining and optimizing PQ meshes are listed chronologically:

- *Geometric modeling with conical meshes and developable surfaces*, (Liu et al. 2006);
- *Discrete surfaces for architectural design*, (Pottmann, Brell-Cokcan, and Wallner 2007);
- *Geometry of multi-layer freeform structures for architecture,* (Pottmann, Liu, et al. 2007);
- *Architectural geometry,* (Pottmann, Asperl, et al. 2007);
- *Geometry of architectural freeform structures,* (Pottmann, Schiftner, and Wallner 2008);
- *The focal geometry of circular and conical meshes,* (Pottmann and Wallner 2008);
- *Architectural freeform structures from single curved panels,* (Schiftner et al. 2008);
- *New strategies and developments in transparent free-form design: from facetted to nearly smooth envelopes,* (Baldassini et al. 2010);
- *A curvature theory for discrete surfaces based on mesh parallelity,* (A. I. Bobenko, Pottmann, and Wallner 2010);
- *Case studies in cost-optimized paneling of architectural freeform surfaces,* (Eigensatz et al. 2010);
- *Edge offset meshes in Laguerre geometry,* (Pottmann, Grohs, and Blaschitz 2010);
- *Tiling freeform shapes with straight panels: algorithmic methods,* (Wallner et al. 2010);
- *Shape space exploration of constrained meshes*, (Yang et al. 2011);
- *Freeform honeycomb structures*, (Caigui Jiang, Wang, et al. 2014);
- *Form-finding with polyhedral meshes made simple*, (Tang et al. 2014);
- *Interactive modelling of architectural freeform structures: combining geometry with fabrication and statics*, (Caigui Jiang, Tang, et al. 2014);

- *Architectural geometry*, (Pottmann, Eigensatz, et al. 2015);
- *Cell packing structures*, (Pottmann, Jiang, et al. 2015);
- *Geometry and freeform architecture*, (Pottmann and Wallner 2016);
- *Vertex normal and face curvatures of triangle meshes*, (Sun et al. 2016);
- *Measuring and Controlling Fairness of Triangulations*, (Cagui Jiang et al. 2016).

In 2015 paper *Architectural Geometry*, (Pottmann, Eigensatz, et al. 2015) the authors summarize the state of knowledge, that has been developed since 2006 – mainly focusing on the aspects of the discretization problems of arbitrary *freeform* shapes. It is mentioned, that the other approach for *freeform* designing – i.e. *fabrication aware design*, or as called in this work *bottom-up* approach – poses more unsolved problems. The article also highlights different problematic aspects related with the panelization and topology such as: the existence of parallel meshes (offsetting meshes), geometrical torsion-free support structures, developable (single curved) panelling, optimization of the doubly curve panelling, repetitiveness of elements and obtaining patterns in the panelization of *freeform* surfaces.

A significant part of the mathematical theory used in the research on PQ meshes derives from *discrete geometry* and *discrete differential geometry*, especially that represented by the top-down approach. Robert Sauer is referred by Pottmann as the author describing the existence and geometry of planar quadrilateral meshes since 1930's, see (Pottmann, Brell-Cokcan, and Wallner 2007). *Differenzengeometrie* (Sauer 1970) summarizes the knowledge of the time about PQ meshes. Recently this area of knowledge is widely described in *Discrete differential geometry. Integrable structure* (A. I. Bobenko and Suris 2008) by Alexander I. Bobenko and Yuri B. Suris, in *Discrete Differential Geometry: An Applied Introduction* (Desbrun et al. 2006) by Mathieu Desbrun and Konrad Polthier and in the *Discrete differential geometry* (A. I. Bobenko et al. 2008) by Alexander I. Bobenko et al.. Alexander I. Bobenko cooperated with Helmut Pottmann et al. in the following articles dedicated to the geometry of PQ meshes:

- *Geometry of multi-layer freeform structures for architecture*, (Pottmann, Liu, et al. 2007);
- *A curvature theory for discrete surfaces based on mesh parallelity*, (A. I. Bobenko, Pottmann, and Wallner 2010);
- *Vertex Normals and Face Curvatures of Triangle Meshes*, (Sun et al. 2016).

The subject of PQ meshes and their intrinsic properties is discussed and studied by Bobenko et al. independently in the following articles and works:

- *Discrete isothermic surfaces*, (A. Bobenko and Pinkall 1996);
- *Discrete conformal maps and surfaces*, (A. Bobenko 1999);
- *Variational principles for circle patterns and Koebe's theorem*, (A. Bobenko and Springborn 2004);
- *Minimal surfaces from circle patterns: Geometry from combinatorics*, (A. I. Bobenko, Hoffmann, and Springborn 2006);
- *On organizing principles of discrete differential geometry*, (A. I. Bobenko and Suris 2007);
- *Quasiisothermic Mesh Layout,* (Sechelmann, Rörig, and Bobenko 2012).

Important contribution of the *differential geometry* and *discrete differential geometry* into the field of *architectural geometry* and the geometry of PQ meshes is the correspondence of the principal curvature lines of the discretized surface with the alignment of the quads.

Johannes Wallner, professor of Geometry affiliated with TU Graz and TU Wien, contributed to the field with following works:

- *An angle criterion for conical mesh vertices*, (Wang, Wallner, and Liu 2007);
- *Designing quad-dominant meshes with planar faces*, (Zadravec, Schiftner, and Wallner 2010).

However, most of articles and works published by Johannes Wallner were developed in cooperation with Helmut Pottmann et al.:

- *Geometric Modelling with Conical Meshes and Developable Surfaces*, (Liu et al. 2006);
- *Discrete Surfaces for Architectural Design*, (Pottmann, Brell-Cokcan, and Wallner 2007);
- *Geometry of Architectural Freeform Structures*, (Pottmann, Schiftner, and Wallner 2008);
- *The focal geometry of circular and conical meshes*, (Pottmann and Wallner 2008);
- *Tiling Freeform Shapes With Straight Panels: Algorithmic Methods*, (Wallner et al. 2010);
- *Interactive Modelling of Architectural Freeform Structures: Combining Geometry with Fabrication and Statics*, (Caigui Jiang, Tang, et al. 2014);
- *Freeform Honeycomb Structures*, (Caigui Jiang, Wang, et al. 2014);
- *Form-finding with polyhedral meshes made simple*, (Tang et al. 2014);
- *Architectural Geometry*, (Pottmann, Eigensatz, et al. 2015);
- *Cell packing structures*, (Pottmann, Jiang, et al. 2015);
- *Measuring and Controlling Fairness of Triangulations*, (Cagui Jiang et al. 2016);
- *Geometry and freeform architecture*, (Pottmann and Wallner 2016).

Helmut Pottmann, Alexander Bobenko and Johannes Wallner et al. published together following works:

- *Geometry of multi-layer freeform structures for architecture*, (Pottmann, Liu, et al. 2007);
- *A curvature theory for discrete surfaces based on mesh parallelity*, (A. I. Bobenko, Pottmann, and Wallner 2010);
- *Vertex Normals and Face Curvatures of Triangle Meshes*, (Sun et al. 2016).

Quoted works of Helmut Pottmann, Alexander Bobenko and Johannes Wallner concern the intrinsic properties of PQ meshes as well as case studies of structures the authors contributed to. Other topologies of grid shells such as triangular and 3-valent are also discussed, together with the form finding and optimization strategies. Recent practice of these authors is focused on the discretization of freeforms into single curved and developable panels and unification of the single and doubly curved panels.

Different to the top-down approach represented by Hans Schober (who has, nevertheless, occasionally cooperated with Helmut Pottmann) is the one represented by Romain Mesnil. His approach, named by him the *bottom-up* approach, promises new morphologies of *freeform* PQ grid shells and the change of the way these are designed. Works of Romain Mesnil et al. are chronologically:

- *Isogonal moulding surfaces: A family of shapes for high node congruence in free-form structures*, (Mesnil, Douthe, Baverel, Léger, et al. 2015);
- *Möbius Geometry and Cyclidic Nets: A Framework for Complex Shape Generation*, (Mesnil, Douthe, Baverel, and Léger 2015);
- *Generating high node congruence in freeform structures with Monge's Surfaces,* (Mesnil, Santerre, et al. 2015);
- *New shapes for elastic grid shells covered by planar facets*, (Douthe et al. 2016);
- *Marionette mesh: from descriptive geometry to fabrication-aware design*, (Mesnil et al. 2016);

- *Structural explorations of fabrication-aware design spaces for non-standard architecture*, (Mesnil 2017).

The position is the Doctoral Dissertation of Romain Mesnil summarizing the knowledge according to the *bottom-up* approach (accurately called *fabrication-aware design*). Among others his contribution to the field is the introduction of the Tchebycheff[5] networks for generating isoradial meshes, Monge surfaces, Möbius geometry and his original method, i.e. *Marionette* projections. This approach coincides in many respects with the one presented in this work.

Argumentation for the advantages of *freeform* shells and grid shells over conventional forms from the point of view of statics is presented in the following works:

- *Conceptual Design of Long-Span Roofs*, (Schlaich and Bergermann 1994);
- *Ethics and Structural Reliability in Free-Form Design (FFD)*, (Majowiecki 2007);
- *New Strategies and Developments in Transparent Free-Form Design: From Facetted to Nearly Smooth Envelopes*, (Baldassini et al. 2010);
- *Parapluie - Ultra Thin Concrete Shell Made of UHPC By Activating Membrane Effects*, (Eisenbach et al. 2014);
- *Non-parametric Free-form Optimization for Grid-shell Structures*, (Shimoda et al. 2013);
- *Computational Techniques For Designing Shell Structures*, (Tish 2015);
- *The end of Free-Form Design, long live Free-Form Design!*, (Veltkamp 2015).

Argumentation for the advantages of PQ meshes over other topologies in case of glazed grid shells is presented in:

- *Conceptual Design of Long-Span Roofs*, (Schlaich and Bergermann 1994);
- *A parametric strategy for free-form glass structures using quadrilateral planar facets*, (Glymph et al. 2004);
- *Study of Panelization Techniques to Inform Freeform Architecture*, (Hambleton et al. 2009);
- *Architectural Geometry*, (Pottmann, Eigensatz, et al. 2015);
- *The end of Free-Form Design, long live Free-Form Design!*, (Veltkamp 2015).

The following works in this field also deserve attention:

- *Reticulated Structures on Free-Form Surfaces*, (Soeren, Sánchez-Alvarez, and Knebel 2004);
- *Constrained planar remeshing for architecture*, (Cutler and Whiting 2007);
- *Thrust Network Analysis: a new methodology for three-dimensional equilibrium*, (Block and Ochsendorf 2007);
- *Glazing Technology: the Hidden Side of Freeform Design*, (Baldassini 2008);
- *On Vertex Offsets of Polyhedral Surfaces*, (Liu and Wang 2008);
- *Planar hexagonal meshes by tangent plane intersection*, (Troche 2008);
- *Study of Panelization Techniques to Inform Freeform Architecture*, (Hambleton et al. 2009);
- *A new method of generating grids on free-form surfaces*, (Ding and Luo 2013);
- *Form-finding and planarisation of glass domes with quad elements*, (Estrada and Baldassini 2013);
- *Design and Construction of a Free-Form Reticulated Glazed Canopy*, (Sánchez-Alvarez, Schwarnowski, and Wolkowicz 2013);

[5] Pafnouti Lvovitch **Tchebychev** or **Tchebycheff** are transliterations of Пафнутий Львович **Чебышёв** used by French authors, whereas later in this work English transliteration will be used: Pafnuty Lvovich **Chebyshev**.

- *Approximating a Funicular Shape with a Translational Surface, Example of a Glass Canopy*, (Menard, Fayette, and Azzopardi 2013);
- *Shell Structures for Architecture: Form Finding and Optimization*, (Adriaenssens et al. 2014);
- *Biomimetic Lightweight Timber Plate Shells: Computational Integration of Robotic Fabrication, Architectural Geometry and Structural Design*, (Krieg et al. 2014);
- *Surface Panelization Using Periodic Conformal Maps*, (Rörig et al. 2014);
- *Exact face-offsetting for polygonal meshes*, (Hambleton and Ross 2015);
- *Pattern and Form - Their Influence on Segmental Plate Shells*, (J.-M. Li and Knippers 2015);
- *Planar Hexagonal Meshing for Architecture*, (Y. Li, Liu, and Wang 2015);
- *Computational Techniques For Designing Shell Structures*, (Tish 2015);
- *Face-offsetting polygon meshes with variable offset rates*, (Ross, Hambleton, and Aish 2016).

Apart from the scientific works listed above there are also many others like those written by architects and structural engineers who had been working on the design of completed structures. Number of such structures and people cooperating during their design and construction processes is large and still growing. However, in authors conviction, listed works represent the most important ones in the field and those which contribute most to the scientific aspects of the PQ designing methods. It is also worth noting, that there are situations, when the industry is ahead of the science as it was during the construction of Museum Guggenheim Bilbao, see (Veltkamp 2015).

2. A brief history of *freeforms* and their application in architecture

Freeforms were present throughout the history in various fields of science, technology and art, among them also in architecture. Among the areas which are very important areas of their application should be mentioned boatbuilding and naval industry. In this chapter selected examples are described chronologically allowing to look at the modern *freeform design* paradigms in architecture from a more general perspective. Since nowadays the empirical methods have started to be replaced by analytical methods, ongoing evolution of *freeforms* shaping tools is subsequently described. Finally, selected modern examples, relevant for further considerations are described.

2.1. Mudhif – an ancient example of the use of *elasticas*

Vernacular architecture have had more in common with curved, irregular forms than the modern architecture. Limiting the materials used only to the most easily available, naturally occurring ones, requires great ingenuity from the builders. Adjusting the form of the building to the specific features of the material allows to obtain the most effective structural system, with the desired span and load capacity.

The so-called bending-active structures attract nowadays more and more attention due to the effectiveness of material usage in such forms and some specific aspects of the shaping process, see (Lienhard 2014), (La Magna, Schleicher, and Knippers 2016). However the idea itself is not new. Mad'an people, inhabitants of marshy areas in the south of Iraq build their homes in the same way their Sumerian ancestors did five thousand years ago, see Fig. 2.1, (Ochsenschlager 1998). Buildings called *Mudhif* are made of flexibly bent reed bundles, see Fig. 2.2 and 2.3. Reed is the only material abundantly available in the area, however, Mad'an (also called Marsh Arabs) did not use it in a banal way, building simple huts, but were able to develop an unusual structural system that has survived on this areas to this day. A straight reed bundle is easily deformable. But the initial deformation of such bundle is done through applying force prior to any external loads are applied, thus introducing pre-stress to the system. As with all prestressed systems, initially introduced stresses superimpose with stresses resulting from the external loads, so that their final value is much smaller than in non-prestressed components. Significant deformation of an initially straight, highly deformable and elastic structural element results, paradoxically, in a more rigid and structurally effective element[6].

The geometrical shape of those deformed reed bundles is close to the *elastica*, i.e. a curve representing axis of an elastic rod deformed by bending. The mathematical concept of the *elastica* developed by James Bernoulli at the end of XVIIth century and published in the article *Curvatura laminae elasticae* (Bernoulli 1694) was later improved by Christiaan Huygens and Leonhard Euler (Goss 2003). Although the mathematical concept for the shape of a bent elastic rod is well elaborated, in practice it's not used in computer aided design (CAD). The evolution of digital tools for creating curved forms brought more comprehensive and reliable geometrical concepts. These forms, however, are purely mathematical creations and do not directly relate to the mechanical properties of the materials from which they would have been realized in reality and do not correspond to forms occurring in nature.

[6] Julian Lienhard's definition of *bending-active* structures (Lienhard 2014):
"Bending-active structures are structural systems that include curved beam or shell elements which base their geometry on the elastic deformation from an initially straight or planar configuration"

Seemingly simple *Mudhif* buildings are a great example of an intuitive connection of three important architectural and structural concepts. First, their architectural form is based on double-curved surfaces. Secondly, the use of these surfaces is not a purely formal procedure, but it is based on the rational use of available resources. Thirdly, their construction is carried out by means of the bending-active method, which allows to convert relatively slender plant material into a fully-fledged structural element. This last aspect is at the same time a clasp linking these buildings with one of the most creative structural ideas of recent years.

Fig. 2.1 Dated ca. 3000 BC relief presenting architectural form similar to the mudhifs built today.[7]

Fig. 2.2 Bending the bundles bufixed at the ends to the ground and tying them together at the top.[8]

[7] Source: http://www.unc.edu/depts/classics/courses/clar241/UrukTrgh.jpg
[8] Source: http://www.arch.mcgill.ca/prof/sijpkes/abc-structures-2005/Lectures-2005/term-work/50-questions/marsh-arabs-construction.jpeg

Fig. 2.3 Interior of a finished Mudhif.[9]

2.2. Catenary forms in vernacular and contemporary architecture

Catenary forms are known to man for ages. They can be seen in the shape of hanging ropes, or in some natural rock formations. Richard L. Handy also described the form of Rainbow Natural Bridge in Utah, U.S.A, see Fig. 2.4, (Handy 1973). The shape of the bridge has been previously recognized as elliptical in 1961 by Clifton W. Livingston (Livingston 1961). However, Handy states that just as accurately that shape is described by the catenary curve, which is less general since it has only one constant instead of two as in ellipse[10]. He puts forward an interesting thesis about how nature prefers catenary forms:

"Perhaps nature dislikes tension almost as much as it abhors a vacuum, and microfractures held open by tensile stress become localized sites for weathering with attendant expansion and spalling parallel to the direction of tension […]. Furthermore where tension does not exist as a boundary condition, tensile crack propagation still occurs within a brittle material normal to the direction of compression […]; thus the shape of a weathered natural arch in uniform nonlayered material should describe a trajectory of maximum compressive stress near the surface, i.e., a catenary."

[9] Source: http://www.arch.mcgill.ca/prof/sijpkes/abc-structures-2005/Lectures-2005/term-work/50-questions/mars-arabs-mudhif-1.jpeg

[10] Ellipses belong to the same class of curves – conical sections or second degree curves. Before Huygens argumentation, Galileo's opinion was widely accepted, that catenaries are equal to the parabola (which is also a conical section curve).

Fig. 2.4 Rainbow Natural Bridge, Utah, USA.[11]

No wonder then, that this form appeared at the earliest in the vernacular architecture created by the Inuit. Although the Inuit tribes (native inhabitants of arctic regions of Greenland, Canada and Alaska) never devised any mathematical methods to design optimal shape of an igloo, their trial and error practice resulted in the structural perfection confirmed recently analytically by scientist Richard L. Handy (Handy 1973). It reveals, that the shape of an igloo is nearly perfect approximation of catenary curve[12] that is revolved. While most ideas of domes picture spherical shape, they cannot be constructed of snow and ice, as these materials are not able to carry tensile forces. Ancient engineers building domes in the Mediterranean area introduced tensile rings and heavy supports at the bases of their domes to prevent them from collapse, as the bases were loaded by forces transmitted from the top of the structure that tried to push them outside. Due to insufficiency of various construction materials, Inuit people had to use the only material available without limitations – snow. Similarly to some other construction materials like stone and bricks snow has much higher strength for compression than for tension or shear and bending. Thus they had to find a form in which the whole structure is only in compression and there are no horizontal tensile forces at the base. The catenary form is a perfect candidate for this purpose. Through subsequent attempts they analysed if the built form performed well in its shape or not, having the possibility of evaluating it almost immediately. Gathering experience and possibly by the way of evolution of form, the final, perfect solution was achieved. In the catenary form the forces are in pure compression and the performance is not related to the thickness of the walls since buckling is in practice eliminated and mass increases proportionally to the thickness. The widespread occurrence of snow enabled easy change of the place of residence, which corresponded to the nomadic lifestyle of the Inuit.

[11] Source:
https://upload.wikimedia.org/wikipedia/commons/0/06/Rainbow_Bridge_Natural_Arch_Utah_USA.jpg

[12] Mathematical equation for catenary curve was derived by Gottfried Leibniz, Christiaan Huygens and Johann Bernoulli in 1691, although earlier in 1646, seventeen year old Christiaan Huygens proves analytically that catenary is not parabola.

Catenary forms are often used in modern architecture as well. Probably the most well-known example of their very wide use are the buildings designed by Antoni Gaudí. Their most notable application was shaping the form of the structure of Sagrada Familia church by means of a physical model, see Fig. 2.5. Antoni Gaudí, as an astute nature observer, noticed that the best performing forms are those created by nature. Therefore, he let the nature to find the form for Sagrada Familia, limiting himself to setting the external conditions for the *form-finding*[13] (see Patrik Schumacher's definition in section 3.6).

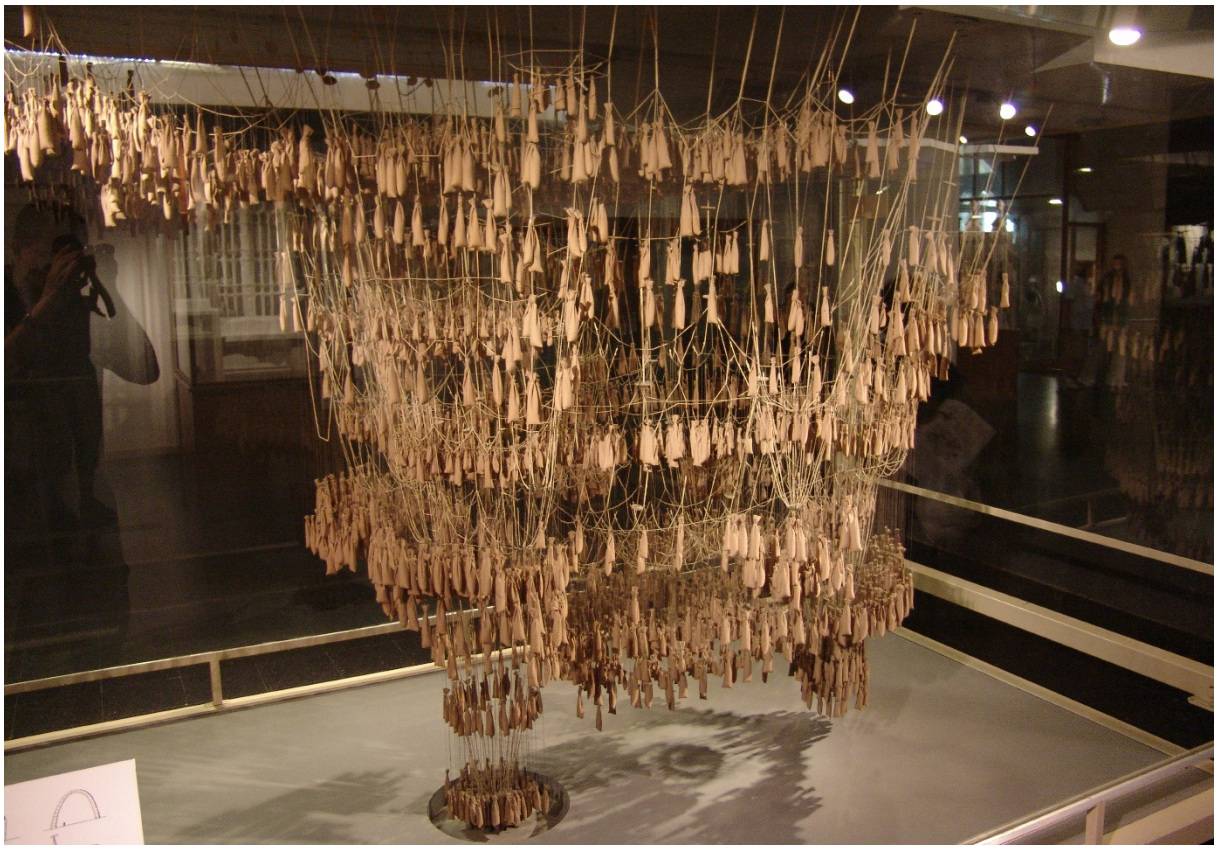

Fig. 2.5 Catenary model of the structural system of the Sagrada Familia.[14]

Before the age of computer aided design, the empirical, i.e. physical methods were frequently used for form-finding. Such approach allowed one for almost immediate judgement of structural properties of obtained shape. Nowadays, so fashionable and popular designing of arbitrary "free" shapes often deprives the form of structural and fabrication logic. What those quoted above examples have in common, is firstly that the specific form is the main source of outstanding efficiency of the structure. Secondly, these forms are derived from nature, i.e. they are not abstract concepts. Lastly, they fulfil the criteria of *freeform* in terms of irregularity of curvature.

[13] The term *form-finding* (ger. *Formfindung*) was first used by Klaus Linkwitz in 1974, see (Linkwitz, Schek, and Gründig 1974), who developed the method of calculating membrane structures. In times Antoni Gaudí the term was not yet used.

[14] Source: https://commons.wikimedia.org/wiki/File:SagradaFamiliaStatikmodell.jpg

2.3. Discovery of perspective and its impact on the architecture of Renaissance and Baroque

The usage of *freeform* shape was not necessarily narrowed to the structural efficiency. In the XVIth century the development of sciences brought the shift from the empirical to the analytical way of thinking due to the aforesaid scientists - Leibnitz, Galileo, Bernoulli etc.

The Renaissance brought Europe a refreshing return to the classic desire to learn about and describe the surrounding world by the language of science. Classical thinking and the knowledge accumulated on its basis in antiquity, has survived partly to modern times in Byzantine Empire, as well as in the Arab world, which gradually took over this heritage. It has reached Western Europe thanks to the contacts of Italian trade republics such as Venice and Genoa. The fall of Constantinople in 1453 brought the final wave of this "transfer of knowledge".

2.3.1. Perspective

The beginnings of the aforementioned revolution took place in the art of painting, then artists' talent merged with their mathematical and geometric knowledge. Artists such as Paolo Uccello, Piero Della Francesca and Filippo Brunelleschi searched for the rules that govern the perspective. Symbolism began to be replaced by realism, and its achievement required an analytical approach.

Paolo Uccello (1397 - 1475) was a painter and perspective pioneer in painting. Changes in the approach to the representation of the world are visible in differences between his early and late works. The symbolic perspective in the sense of the Gothic art was replaced with a natural perspective, this trend has remained in art for several hundred years. In addition to these discoveries, his studies on the form itself in the perspective and manner of its recording are also important. His analytical approach is surprisingly consistent with the approach currently common in computer graphics.

Paolo Uccello's study of a vase, see Fig. 2.6, is a sketch showing the revolving body in perspective as a collection of points connected by section lines. What he did over five centuries ago is today the basis for the recording of spatial form and its presentation on the computer screen. Instead of attempting to present the vase in a complete perspective, he made the discretization of its form, i.e. dividing it into a finite set of points and edges, through which it is sufficiently and unambiguously represented. Such approach allows for calculations or activities leading to the creation of a perspective sketch, that could be done on a finite number of elements.

Later another artist - Piero della Francesca (ca. 1412[15] - 1492) was also a painter and a mathematician. He was the author of the works: *De prospectiva pingendi* (On the perspective in painting, (Della Francesca 1474)) and *Libellus de Quinque Corporibus Regularibus* (Short Book on the Five Regular Solids). In addition to art, he was deeply interested in arithmetic, geometry of spatial solids and perspective.

[15] The year of birth of Piero della Francesca is not exactly known and vary depending on the source between 1410 and even 1420. Here the year of birth of the artist is taken from the introduction to the polish edition of *De prospective pingendi* (Della Francesca 1474).

In 1465, Piero della Francesca finished the *Resurrection*, a painting on which he placed his self-portrait. The figure in the painting depicts the author and has an unnaturally deviated – by the standards of that time – head, however, it is a realistically accurate image obtained by the artist through strictly analytical approach, see Fig. 2.7, bottom, right.

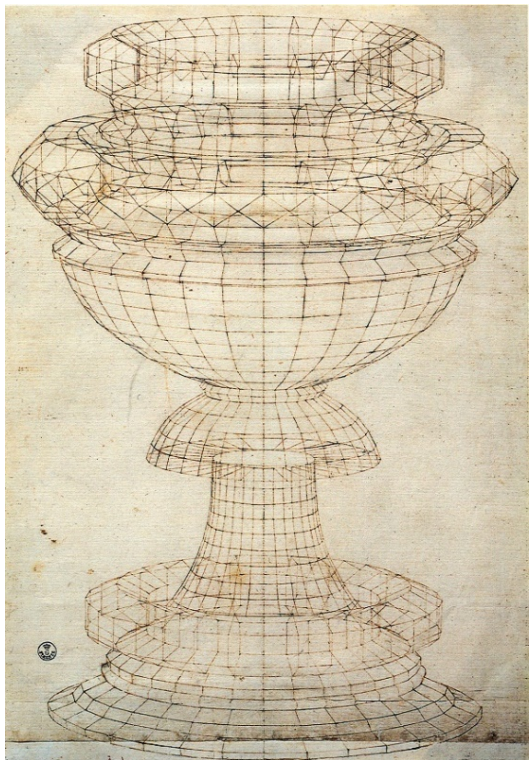

Fig. 2.6 Paolo Uccello, Studio di vaso in prospettiva.[16]

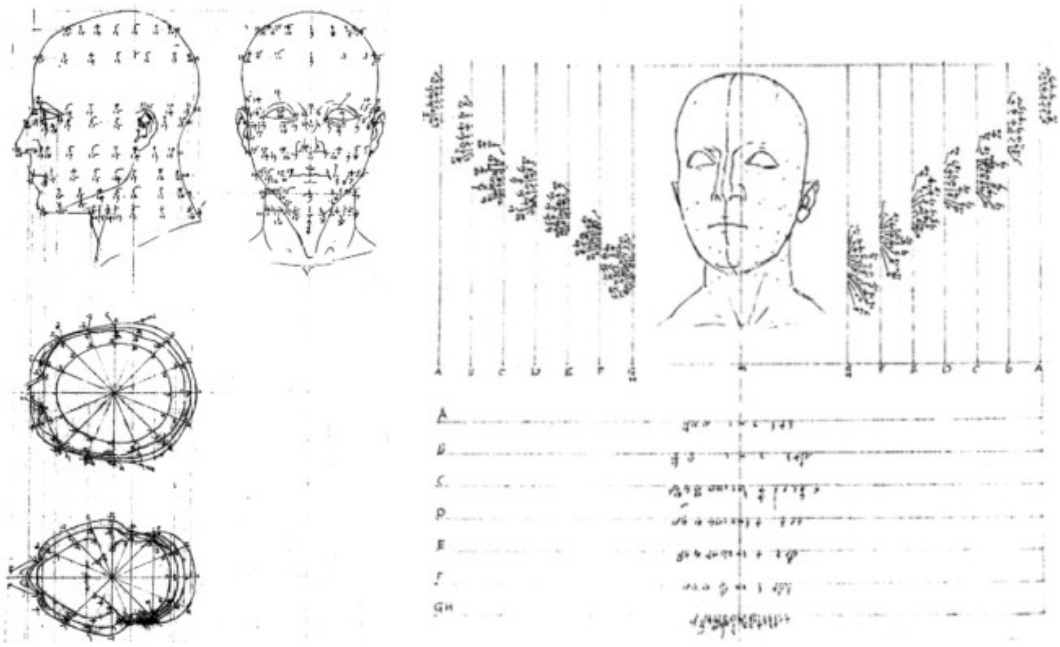

Fig. 2.7 Drawings from "De prospectiva pingendi" (Della Francesca 1474) including a fragment of the "Ressurection" with autoportrait of Piero della Francesca.

[16] Source: https://commons.wikimedia.org/wiki/File:Paolo_uccello,_studio_di_vaso_in_prospettiva_02.jpg

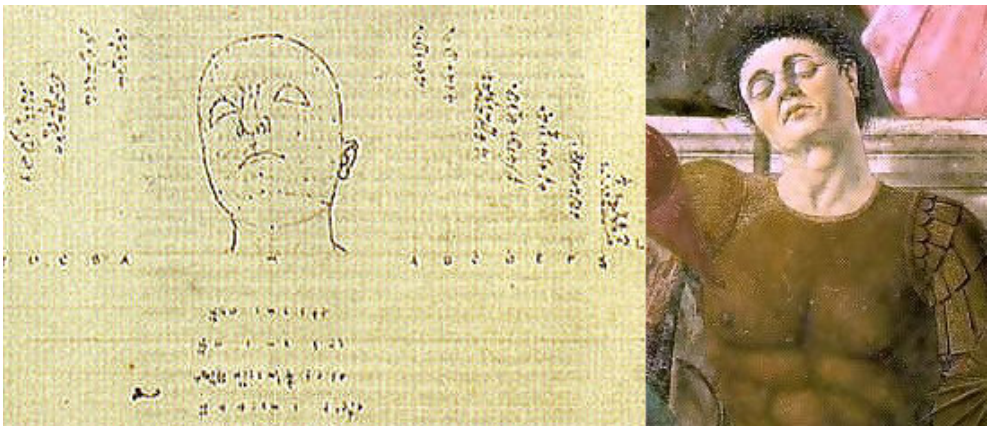

Fig. 2.7 – continued.

Piero della Francesca made a discretized record (like Paolo Uccello) for the set of points of his head, written in the form of four orthographic projections[17], see Fig. 2.7, top, left. By projecting any three-dimensional image on the plane, information about the position of elements of this object in the direction perpendicular to the projection plane is lost. Francesca recovered this information and recorded it by introducing orthogonal projection. Having unambiguous information about the position in the space of points on the head, he could subject them to any manipulation (rotation around the selected axis and perspective projection) thus achieving the position of the head captured in the image.

Thus, Piero della Francesca confirmed the discovery of Paolo Uccello of the possibility of writing a continuously curved object as a discrete set of points in space, interpolating the described shape. However, a shift between the record of a regular rotary body and a shape as subtle as a human face is worth emphasizing. At the same time, he proposed a form of representing spatial solids in a two-dimensional form, very convenient and used until today in various areas when a three-dimensional object is displayed in perspective on a flat screen, whether in CAD programs, computer games, computer animation films and even in neuroimaging (Schott 2008). Also, Piero della Francesca's orthogonal projection is the oldest known example of this type of projection.

However, correctness of discoveries of the two discussed artists had still to be confirmed. Although works of Paolo Uccello and Piero della Francesca looked to be correct, only an experiment carried out by Filippo Brunelleschi (1377 - 1446) proved their utility.

Filippo Brunelleschi was an architect known primarily for the work of his life - *Il Duomo* in Florence. Like Paolo Uccello and Piero della Francesca he was deeply interested in mathematics, geometry and perspective. He proposed a method of comparing the perspective image recorded on the panel with the view of the image in nature, see Fig. 2.8. This comparison was to take place not by looking at the object and its image separately, but by looking at both simultaneously. As objects for comparison he chose the Baptistery and Palazzo Vecchio in Florence (unfortunately, paintings used for the comparison has not survived until today). For the experiment he used a painting of the Baptistery (in a mirror image) with a hole at the vanishing point and a mirror with a similar hole. Filippo Brunelleschi held the mirror in front of him in an upright hand. The mirror was facing toward him. The painting was held in his other hand, in front of his face, however it was facing the opposite

[17] It is worth mentioning here that both the Cartesian concept of axis and coordinate system as well as the Gaspard Monge's orthographic projection (first-angle projection) were not known at that time. Piero della Francesca was a precursor in this area.

direction, i.e. toward the mirror. The architect was looking through both holes – in the painting and in the mirror – at the Baptistery, while he was able to see the reflection of the painting at the mirror simultaneously. Looking at the object and the reflection of his image, he could immediately assess the similarity of both. This experiment confirmed the practical usefulness of the perspective and correctness of geometrical principles developed by mathematicians and artists.

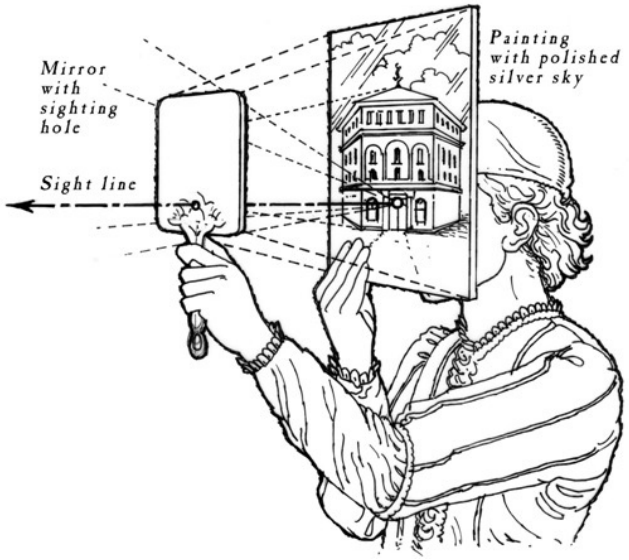

Fig. 2.8 Brunelleschi linear perspective experiment.[18]

2.3.2. Renaissance and Baroque eras

Paolo Uccello and Piero della Francesca proved analytically that circles are transformed into ellipses in the perspective projections[19] and elliptical forms were willingly adopted in the architecture of the Renaissance and Baroque eras. Rediscovery of works of Vitruvius changed the paradigm of creation into a new one, which was focused on the search for beauty in the perfection of forms and their proportions. Therefore, the newly constructed buildings were oriented on the human-scale and their plan composition was centralized. They were intended for human perception in contrast to the Gothic architecture, which was concentrated on the divine scale characterized by high rise buildings with a structure brought to the limit. Altering the attention from the scale of the building to its form allowed to design and built within fraction of an architect's lifetime. That eventually led to creation of individuality of architects henceforth conceived as artists. The new challenge among architects was to search for unknown forms of expression – new proportions, details and compositions. Initially, the antique architecture was a sufficient source of inspirations. The evolution of forms lasted until breaking the strict geometrical rules of Renaissance, what have led to the development of Baroque architecture.

Elliptical plans of churches allowed to combine the centralized plan with the traditional, linear division of the temple. It also created an optical illusion that the objects at the opposite sites of an ellipse quadrants are closer to each other, e.g. an entrance of the church to the altar. The most famous

[18] Source: https://maitaly.files.wordpress.com/2011/04/0328p_duomo6_b.jpg
[19] In fact, through a general perspective projection a circle can be transformed into any second degree curve – i.e. a circle, ellipse, parabola and hyperbola, as well as into a line segment.

example of deliberate use of perspective shortening the space is the elliptical part of St. Peter's Square designed by Giovanni Lorenzo Bernini.

The Mascarino Staircase in Palazzo del Quirinale designed by Ottaviano Mascarino, San Giacomo in Augusta designed by Carlo Maderno, San Andrea al Quirinale designed by Giovanni Lorenzo Bernini and Santa Maria in Montesanto designed by Carlo Rainaldi and revised by Giovanni Lorenzo Bernini all share elliptical plans. The ellipse can also be easily plotted both on the plan and on the construction site.

2.3.3. Francesco Borromini

Francesco Borromini (1599 -1667) went a step further in creating of the *freeform* architecture. He was a pioneer in the application of *freeform* lines, waviness, concavity and convexity and was able to transfer his visions into full-size buildings. In the paper "*Elasticas* in shaping architectural form – a hypothesis about Borromini's approach" (Święciak and Tarczewski 2018) author of this work argues the hypothesis, that Borromini was familiar with *elasticas* and their usefulness in shaping architectural forms. The most notable examples of his works, that match that hypothesis are the staircase in Palazzo Barberini and the dome in San Carlo alle Quattro Fontane. The forms of both do not fit exactly any analytical forms of ellipses, nor ovals as suggested in (Mazzotti 2014), while the *elastica* curve could have been easily obtained in both: plan and full scale.

Flexible slat (i.e. *spline*) could have been used by Borromini due to an important fact: *elastica* curve can be easily scaled between drawing and full-scaled object. Given the scale, the length of the slat, positions and directions at its ends builders could have used wooden slat of length according to the scale. Such method was widely used by shipbuilders tracing ship hulls and structures also in Francesco Borromini's time.

Digital tools currently available for architects allow them to design *freeform* curves and surfaces. These tools had been evolving, starting from simple splines through Bezier curves ending at complex NURBS surfaces. Nevertheless, the problem of scaling the *freeforms*, which Borromini could have encountered, is still actual. Moreover, many designs fail due to the underestimated technological threshold between what is possible to design and what is possible to be built.

Borromini might have used the *splines* to trace the shapes of his architectural works. Such tools were already known and commonly used in the naval architecture, however, these might have also be the subject of closely protected technologies, also due to their military applications. The path of evolution of *freeform* design tools in naval architecture is described in the following sections.

2.4. Naval architecture - *spline curves*

Free forms were present in the naval architecture ever since people started to taming the element of water. The earliest archaeological findings are reed-bundled (compare with section 2.1 – *Mudhif*) boats from sixth and fifth millennia BC (Carter 2006), located around the Persian Gulf. Another ancient form of boat is Inuit *umiak*, i.e. boats intended for whale hunting, used by the inhabitants of the far north (Greenland, Siberia). Due to the lack of resources like wood, these boats were made of whalebones with seal skins stretched over the skeleton. These structures could have been classified as hybrid – bending-active and membrane structures – naturally taking on a *freeform* defined by the equilibrium of both counteracting forces caused by expanding skeleton and compressive membrane.

The slenderness and flexibility guaranteed the reed-bundle and *umiak* boats better performance, i.e. stability, capacity and speed, than in case of rigid constructions. Early Viking ships were built on similar principles. The hull was built independently from overlapping, cleaved along fibres planks, with strut braces added later. Individual planks, divided with the use of an axe, were joined together in the clinker-built style, creating self-supporting hull (Garrison 1998). The process of shipbuilding in the reversed fashion, where the hull was built before the internal skeleton was dominant in Europe in the first millennium. Usually ships were built without plans and hulls were assembled on moulds (Rieth 2003), (Olaberria 2014).

Technological progress in the shipbuilding made by the Portuguese and Castilians in the XVth century brought to reaching America. A technique called carvel-built allowed for creating vessels that were characterized by smoother hulls, lighter structures and faster speeds than common at the time clinker-built vessels. The caravel type of ship (por. *caravela*) was able to navigate the ocean thanks to the features carvel-built hull, which resulted from the arrangement of planks on the ship's frame. Instead of overlapping the planks like in the clinker planking, the carvel planking assumed tight arrangement of planks one next to each other so that individual planks were touching each other only along the narrow edges. Such hulls were thinner and smoother. Additionally, the planks swelling when in contact with water expanded and clamped each other, enabling resignation from sealants. Building ships in such a manner required more detailed planning, also the frame had to be prepared before the hull was built. Each individual plank should have been prepared for its exact destination.

Rapid development of science since the XVth century was present not only in mathematics, art and architecture. In the shipbuilding industry new technologies were subjects of economic secrets. *Arsenale di Venezia*, the Venetian shipyard and armoury complex, since its establishment in 1104 until the industrial revolution was the greatest industrial complex in Europe. Technological secrets were protected according to strict rules, e.g. a worker of a shipyard leaving Venice was obliged to leave members of his family as hostages. Individual workshops in the complex were specialized in prefabricating specific parts for ships, what on one hand allowed for faster production and storage of components. The ship built of stockpiled parts took Venetians around eight months to finish, comparing to four years per similar ship in the similar period for Maltans, see (Atauz 2005), p. 179. The same source claims that Venetians managed to assemble a galley within 24 hours. On the other hand such approach required specialized planners and draftsmen. Once prepared plan was the subject of highest protection, yet it could have been divided into incomplete parts that were sent separately to the corresponding workshops. Also, many ships could have been built according to the same plans.

One of many tools and methods used for drafting the plans for ships was the *spline*, see Fig. 2.9. It was a long, flexible, wooden or metal strip fixed in position at several points. Passing through that points the strip relaxes forming a smooth curve. The *spline* was very convenient for transferring curves between drawings and scales, any curve drawn with the use of *spline* could be defined by the position of control points and the length of the strip. The same technique could have been used by Francesco Borromini at the San Carlo alle Quattro Fontane, according to the author's hypothesis (Święciak and Tarczewski 2018). Draftsmen of boat and ship plans used *splines* to trace the courses of wooden planks on the hulls. In the full scale the control points were placed at the frame sections, and the planks running along the hull took the shape of elastically deformed *splines*. Drawings were redrawn on greater scales in the only dry and spacious places in the shipbuilding workshops, i.e. at lofts, hence the today's name of a loft function commonly used in the computer aided design software. However, the modern *spline* understood as a 3D CAD tool is not equivalent with the shapes obtained by elastically deformed strips.

In the 18th century boatbuilding draughtsmanship began to become naval architecture (Nowacki 2006). The growing influence of the natural sciences (e.g. hydromechanics) left its impact also in the ship design industry. Empirical methods usually supported by experience for designing hulls were since then also supported by analytical methods. Gradually physical hull models were completely replaced by drawings generated with use of other tools.

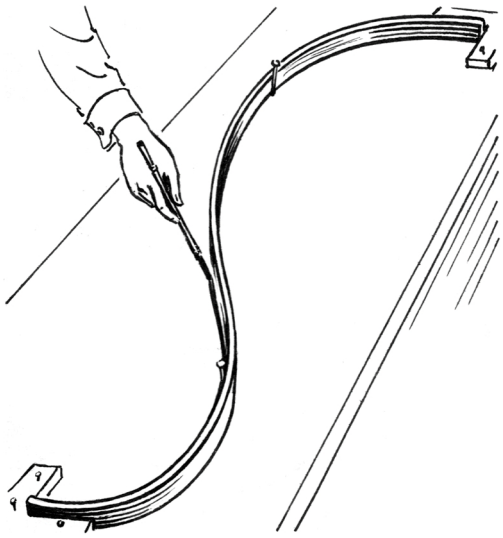

Fig. 2.9 A spline slat attached to a drawing board with pins[20],[21]

Naval architecture and draft methods were successfully adapted by the newly established aviation industry in the first decades of 20th century. Boeing's first production facility, *Boeing Plant 1*, was located in wooden boat shipyard, whose previous owner became the master woodsman of Boeing (Spitzer 1998). The draftsman *spline* curves were utilized at Boeing until the introduction of computer aided design methods of interpolating curves (Grandine 2005). Although the same name for computational curves is used -*splines*, these are not representations of elastically deformed draftsman *splines*[22]. Due to detachment from physical properties of the tool it's possible to manipulate their shape in a much larger range. This is also the cause of many problems related to the constructional aspects of the realization of *freeform* objects.

2.5. Influence of naval and aerospace design on architecture

"For me as an architect it has been ideal to have been attached to a large shipyard, where all trades were represented, and large-scale work was carried out. When I was about to draw the Opera House in Sydney, I was not really worried that I had to convert sketches into curved surfaces towering 60 meters, define them geometrically and have them constructed. As a child I had seen huge ship-hulls. My father helped me construct the large-scale models required. Without any specific agreement he made the wooden models. After a couple of days the delicate forms were in the drawing room"

Jørn Utzon[23]

[20] Instead of pins so-called *ducks* are preferred. The name *duck* refers to the shape of a weight, which holds a pin in position.

[21] Source: https://en.wikipedia.org/wiki/File:Spline_(PSF).png

[22] The broadly described history of splines is described in the article of Alastair Townsend *On the spline* (Townsend 2014).

[23] Jørn Utzon about his father, Aage Utzon in the conversation with Bent Aarre, source:

The history of construction of the Sydney Opera House[24] clearly emphasizes the threads and opportunities accompanying the architecture of *freeforms*. Jørn Utzon (1918-2008) was a son of a naval architect. Naval design was also a subject of interest for young Jørn Utzon who spent many hours with his father designing ships and building models. Naval architecture, being merely one of many sources of inspiration for Jørn Utzon, took the primary role for the competition project for Sydney Opera House in 1957. The competition drawings resembled the more of a free-flowing and organic shapes than the actually built structure. Shell structures implemented at that time by Pier Luigi Nervi, Felix Candela and Eero Saarinen convinced the legitimacy of the solution proposed by Jørn Utzon. However, Ove Arup, whose company was assigned as the structural and civil engineers for the project, told Jørn Utzon at their first interview that proposed shells are not structurally suitable. Also, being unexperienced with projects of such scale Jørn Utzon might have underestimated the rationalization of the shape in terms of repetitiveness of structural elements. The shape of the shells went through 12 iterations – including parabolic sections, circular ribs and ellipsoids. It became clear to engineers that some form of unification of structural elements is essential in order to rationalize the prefabrication costs and preform structural calculations correctly. Eventually each shell took a form of the sphere section, each one was assembled of repetitive, convenient for prefabrication ribs. For the structural analysis Arup used computer systems, which was one of the earliest attempts of such use of computers. Nevertheless, physical models were also used for verification of these calculations.

The completion of the construction and opening of the Sydney Opera House took place in 1973, six years behind the planned schedule. Most of the technologies involved in the design and construction of the shell were innovative at the time. The originally assumed cost estimate was exceeded over tenfold. The building that had become one of the most iconic architectural works of the modern times required unexpectable effort to complete. However, it also highlighted the problems of implementation of *freeform* in architecture. Its construction revealed, that forms that were previously available for the naval architecture occurred to be problematic in architectural applications. The problems encountered were related to unification of used structural elements, thickness of the shells and uniqueness of the design, all of which is characteristic for architecture. Importance of these properties in context of mechanical industry and architectural design in further explained in section 3.1.

Implementation of architectural *freeforms*, especially when talking about continuously curved, solid, smooth surfaces require solutions so much sophisticated, that nowadays the most iconic implementations are prefabricated by specialized shipyards, because only they have technical capability to produce them. Manufacturer like *Central Industry Group*[25] (Veltkamp 2015) is a shipyards specialized in architecture, which was the brain behind the construction of some iconic architectural works like components for the Porsche Pavilion in Wolfsburg (Fig. 2.10, left), curved walls in Central Station in Arnhem (Fig. 2.10, right) and link bridge at Yas Island in Abu Dhabi (Fig. 2.11).

http://www.utzonphotos.com/about-utzon/curriculum-vitae-and-biography/biography/aage-utzon-father/

[24] The history of Sydney Opera House is broadly described in the book titled *The saga of Sydney Opera House* by Peter Murray (Murray 2003).

[25] CIG is also a manufacturer who produced *freeformed* claddings on topologically optimized supporting structure in Qatar National Convention Centre, see more in introduction to chapter 3.

Fig. 2.10 Left: Porsche Pavilion[26], right: Central Station in Arnhem[27].

Fig. 2.11 Link bridge in Yas Marina Hotel. Left: in CIG shipyard[28], right: completed structure[29].

2.6. Digital *freeform* design tools

Aircraft design before the second world war was actually based on the similar drafting techniques as the ones used in the naval industry. However, the requirements for the smoothness and streamlines in the aircrafts was much more demanding, especially during the armaments race. North American Aviation airplane manufacturer met the new challenges by introducing the conical sections into the design and manufacturing process, (Wagner 1990), p. 57. The first plane designed in such a fashion was the P-51 Mustang fighter. Its shape was based to a large extent on conical sections. Conical sections are the curves obtained from the intersection of the surface of a cone with a plane. Generally they include circles, ellipses, parabolas and hyperbolas. It is possible to represent these curves as second degree equations, hence their other name *second degree curves*. Engineers working at NAA had to find new solutions enabling a fast and reliable way of transferring and scaling shapes of these curves, because in the contract with the British Government NAA was obliged to build and test a prototype within 100 days, see (Wagner 1990), p. 55. Adapting a new technology gave such opportunity due to several advantages. In order to solve this problem they developed a new technology, which, as it turned out, had many advantages over previously used ones.

[26] Source: http://www.centralindustrygroup.com/mediadepot/779ccdaddf6/1024/EP02690-277.jpg
[27] Source: http://www.centralindustrygroup.com/mediadepot/2160c3ff1ca7/1024/OVTArnhem2.jpg
[28] Source: http://www.centralindustrygroup.com/mediadepot/740a512f6c5/1024/IGP1876SP.jpg
[29] Source: http://www.centralindustrygroup.com/mediadepot/462323de003/678/480/LinkBridgeFinished.jpg

The design recorded in the form of blueprints and formulations describing every curve on it was scale–free. Typically the plans for the plane required redrawing into the 1:1 scale, what usually caused some inaccuracies and errors. Scaling the formulations describing the shape was based on multiplication in which the possible error was minimized. Therefore, it was possible to record the design in form of encrypted numerical tables and send it by radio. Thanks to the reduction of scaling inaccuracies, the plane segments like wings, tail, fuselage etc. could have been manufactured separately and simultaneously, while ensuring that these parts will match each other perfectly. Hence, the applied solution not only ensured greater accuracy but it also allowed to save production time.

National Advisory Committee for Aeronautics (an organization that was the predecessor of today's NASA) was involved in the project cooperating at designing laminar flow airfoils for the wing sections and performing tests in aerodynamic tunnel, see (Wagner 1990), p. 18. Apart from delivering the first prototype after 102 days after the contract was signed, the engineers managed to construct one of the best performing fighters of the second world war. Roy A. Liming, the Head of Engineering Loft Mathematics in North American Aviation published a book summarizing the theoretical concepts behind the design of Mustang in *Practical Analytic Geometry with Applications to Aircraft* in 1944 (Liming 1944). Until the nineteen eighties different algorithms and CAD systems for spline evaluation had emerged, with De Casteljau's algorithm and Bézier curves in early 1960s as the most notable examples, see (Mortenson 1999), pp. 264-276. Paul de Casteljau was a physicist and mathematician working at Citroën and Pierre Bézier was an engineer working at Renault. Both individually developed CAD and CAM systems for their companies capable of plotting curves and doubly curved surfaces[30]. In 1979 Boeing, which at the time used several separate CAD systems for different design tasks, appointed *TIGER Geometry Development Group* whose goal was to unify several used systems for curve and curved surfaces interpolation into one stable and compatible system. As the authors of the cited source admit (Blomgren and Kasik 2002):

"Early commercial airplane design was derived from ship design. Both the terminology (airplanes have waterlines; they roll, pitch, and yaw; directions include fore, aft, port and starboard) and the fundamental design of surfaces (lofting to make airplanes fly smoothly in the fluid material called air) are still in use today."

Aerodynamic forms with the curvature degrees higher than G1 were required especially for the airplane design industry, therefore the boundaries were pushed forward. The result of their development were NURBS (short for *Non-Uniformal, Rational B-Splines*) which spread further and became a standard for representing *freeform* curves and surfaces in CAD and CAM (Blomgren and Kasik 2002). The NURBS documentation was published and further projects of Boeing were carried on CATIA CAD CAM software originating from Dassault Systems – a French airplane designer and manufacturer. CATIA was also the first CAD CAM platform used for the architectural purposes, for details see section 2.8.

Nowadays NURBS have also spread into the architectural design world. Their applicability is constantly growing. Their applications are not limited only to geometric problems, but they also entered the field of mechanical calculations, through the emergence and rapid development of isogeometric analysis[31]. The ease of use of NURBS surfaces results in appearing new building morphologies which, however, are also the subject of "old" problems of which the Sydney Opera House is a great example. They concern designing *freeform* shapes prior to the decisions how those shapes would be divided

[30] After revealing the details of these systems the Bézier curves became standard geometrical objects available in almost every CAD and graphical systems.
[31] Abbreviation for Isogeometric analysis is *IGA*, in contrast to *FEA* for the finite element analysis.

into parts, what materials should be used and generally, how could the *freeform* be built. Such approach, called top-down (see section 3.4), dominates the architectural *freeform* design. Unfortunately, some contemporary designs containing *freeforms*, which repeat the history of Sydney Opera House, frequently win competitions, eventually creating unprecedented problems in the realization phase. Nevertheless, as these designs may be very good from the other points of view, they are the source of opinions about *freeforms* as risky, bringing them merely to the level of temporary fashion. Whereas the source of the problem are not the *freeforms* themselves, but the top-down approach to their design. The problems related with designing *freeform* architecture according to the top-down approach is shown in the following section. Although it is a successful realization, it highlights problems related to this approach.

2.7. POLIN - Museum of the History of Polish Jews

A *freeform* object representing the top-down approach to design is the Museum of History of Polish Jews located in Warsaw. It is the embodiment of the competition winning design by Finnish design studio Lahdelma & Mahlamäki. The details of the construction process are described more profound in (Ferenc 2013).

The volume of the building is split by the 20 m high lobby. In contrast to the cubic volume of the building, the lobby has the form inspired by a canyon formed by the flowing water as a reference to the passage of the Israelites through the Red Sea. These walls of the lobby are designed as NURBS surfaces. Additionally designers assumed, that these *freeform* walls will act as construction supporting the roof. Designers began to look for the methods to implement them as reinforced concrete, but quickly realized that there are not feasible and economically justified methods to design and construct formwork for this type of surface.

The decision was taken to perform the walls as a steel, structural frame (shown during the construction in Fig. 2.12), with fiber concrete doubly curved panels attached to it. Each corner of NURBS surface replicating panel was given spatial coordinates. The starting material for the implementation of cladding a digital model of the wall was made in Rhino 3D and was submitted to contractor. Shortly after the start of construction, the contractor returned to the discussion on possible ways to construct the wall, finally the sprayed concrete method was adopted. In the first phase the steel structure that reproduces the pre-wall geometry was completed. The structure consists of vertical and diagonal tubes with a diameter of 273 mm and horizontal transoms that were fire secured to provide 120 minutes fire resistance.

Flat MDF panels and reinforcing mesh was mounted to the construction as a basis for 35 mm thick layer of sprayed concrete. Finally, to obtain the desired geometry of wall, the dividing network of horizontal, vertical and diagonal curves was designed on a freeform surface in the 3D model. Such grid was implemented with flexible PVC strips trailed on the implemented wall. Specific coordinates of the grid points taken from the model were used by the surveyors to verify the geometry of the resulting wall. These moldings formed an expansion joints and act as guides during the final modeling of the wall.

Although the final realisation was a success and the implementation of *freeform* walls does not diverge from the assumed design, the insufficient recognition of the implementation methods led to some uncertainties. The structural system had to be redesigned into heavy steel frame, which hidden behind continuously curved cladding still impose problems of freeform grids. Final thickness of the wall is higher than the assumed one, therefore some spatial and functional changes were also required.

Fig. 2.12 Steel structure behind the freeform walls.[32]

2.8. The Bilbao Effect

The construction of the Guggenheim Museum has paved the way to modern methods of designing and implementing *freeforms* in architecture (Gonzales-Pulido, Vaggione, and Ackley 2002). In addition to the architect of the project - Frank O. Gehry, the executive architect and investment supervisor was the IDOM office (Gonzales-Pulido, Vaggione, and Ackley 2002), (Skylakakis 2005) pp. 11 - 15. The office was responsible for the execution of the project, including preparation of detailed solutions and maintaining the flow of information between contractors. Without modern digital recording and data processing methods, the implementation would probably take much longer.

All major design and implementation units involved in the project were equipped with the CATIA software used as the platform for digital recording and processing of the geometry of the building, see (Gonzales-Pulido, Vaggione, and Ackley 2002) pp. 16-18. Aerospace designers who had earlier experience with CATIA were assigned to the key units in Frank O. Gehry's office in Santa Monica in California and at the construction site in Bilbao, i.e. SENER, the largest Bilbao-based engineering firm concerned with aerospace, naval and industrial projects (Skylakakis 2005) pp. 11-12.

The general physical model of the Museum was created in California by Frank O. Gehry's team. It was then 3D scanned and transformed into a computer model. Recorded on several magnetic tapes it was sent to Spain, where it was further processed. Based on the general 3D model engineers prepared documentation for the structure of the building, substructures for cladding and detailed CAM files for doubly curved cladding elements.

There are three types of pioneering implementations of *freeforms* in the Museum Guggenheim Bilbao – developable metal sheet cladding attached to curvilinear latticework; CNC carved, doubly curved stone cladding and triangular, glazed grid shell. In each of the implementation type specific problems appear, which were recognized early in the design process. All types of implementations of *freeforms* are discussed in (Gonzales-Pulido, Vaggione, and Ackley 2002) pp. 9-16.

[32] Source: https://architektura.nimoz.pl/wp-content/uploads/2013/03/Budynek-7.jpg

Cladding made of titanium sheets cover the area of over 25,000 m^2. It was implemented in number of steps beginning with the execution of regular, maximally modularized main structure. It consists of steel, diagonally stiffened modules connected with reinforced strength bolts. Consecutive layer, substructure for the cladding, was adapted for the final, *freeform* shape of the cladding. It consist of horizontal steel profiles every 3 meters. The profiles are connected to the main structure via consoles of variable lengths. These horizontal profiles are continuously curved according to the data obtained from the main 3D model. Each profile was deformed by CNC bending machine and marked with an individual barcode, which was used for the proper localization of the element at the construction site. Horizontal profiles served as a support for the next layer, i.e. another set of continuously curved profiles in oriented vertically, which were additionally in geometrical torsion. The geometrical torsion was applied in order to ensure the tangency of profiles to the final *freeform* surface. Available technology allowed for the maximal 4° of torsion. Subsequent layers of steel plates, watertight insulation and laminated titan sheets were mounted on that *freeformed* construction grate. Due to the fact that each titanium sheet is fixed to the structure at four points, that are not coplanar, the sheets are slightly folded.

Second type of implemented *freeforms* was realized in the form of steel-reinforced concrete structure covered with stone cladding. Similarly to the titanium cladded structure, the concrete structure was rationalized and simplified in order to be casted in advance, before the documentation for the stone cladding substructure was started being prepared. Each piece of the stone cladding was individually prepared in the 3D model. Numerical data obtained from the models was used to control CNC milling machine. The CNC machine used for that purpose was previously used in the machine industry for milling metals. Its modifications, preparation and assemble at the construction site lasted around six months. It worked continuously, 24 hours a day, 7 days a week for two years (Gonzales-Pulido, Vaggione, and Ackley 2002) p. 18.

The scale of the project allowed for non-standard solution in the form of individual technological solution at the construction site. The stone cladding is, however, the only realized as continuously curved *freeform*.

Third type of the *freeform* implementation is the doubly curved, glazed, triangular grid shell. The adopted form of implementation is by so far the most popularized in the field of architectural *freeform* structures. The triangular shape of each panel gave the certainty, that each one is planar and simultaneously reasonable freedom of design was assured – especially, when the initial form was obtained from the physical, sculpture-like, arbitral model. Doubly curved, quadrilateral glass panels would have been economically unreasonable in that case. Among the total number of 2200 glass plates, 2000 have unique shapes. Individually pre-prepared technical drawings of each panel were sent to the construction site, where slight modifications were made according to the actual surveys of the grid shell and executive tolerances. Finally each panel was cut by a CNC machine and assembled at the right spot on the grid shell.

The construction of the Museum according to the investor's assumption was associated with many technical problems not observed previously in the construction industry. Javier Aja, being a representative of a company dealing with the realization of interiors and building installations, stated that:

"80% of the construction systems and materials used in the Guggenheim Bilbao project were totally innovative in the building industry."[33]

The investor's awareness led him to an attitude in which he insisted that the budget for the construction should be used to the maximum extent in order to improve the quality of implementation by seeking innovative solutions instead of seeking savings. Cooperation and communication between engineers and managers from various industries resulted in the development of new solutions forming the base for further architectural implementations of *freeforms*.

The term *Bilbao Effect* appeared in the literature as a common name for bundle of various aspects: social, economic and technological and has rather unfavorable connotation, see (Rybczynski 2002). From the technological point of view, it was a conscious operation and cooperation on the interface between investor, architect, executive architect and structural engineers[34], which resulted in solutions that are still used today. It should be emphasized that it was a planned activity was and included in costs of the investment.

2.9. Latest generation of *freeform* design tools

An alternative to the described above method for shaping doubly curved surfaces was invented for the purposes of entertainment industry. PIXAR studio working on the short motion pictures before their first full-length featured movie - Toy Story, used NURBS models, see chapter 5 in (Chopine 2011), which were controlled by a finite number of control points that revealed to be insufficient for the animation purposes. Characters were made of several patches of NURBS surfaces which, during animation, had the tendency to create creases and gaps between each other. The consistency of curvature continuity between patches was also an issue. NURBS surfaces are also constrained topologically into patches consisting of four edges (possibly an edge can be shrined into a singularity, i.e. a point). The solution for that problem was the application of subdivided meshes. This method was invented by Edwin Catmull, the founder of PIXAR studio together with Jim Clark and published in 1978 (Catmull and Clark 1978). In the Catmull-Clark mesh subdivision method, a coarse mesh with small amount of vertices is treated as a control frame. The control frame consist only of vertices that are necessary to represent the object topology and characteristic geometrical feature. In each frame of the movie the control frame vertices are animated (translated) and then the control frame is subdivided into larger amount of vertices and facets. Each subdivision iteration is followed by reaction of the vertices, so that new mesh is smooth and almost continuously curved. Such approach eliminated the problem of mismatching the patches and allowed the usage of facets with more complex topologies.

[33] According to (Skylakakis 2005), p. 14.
[34] Skidmore, Owings & Merrill (Petroski 1998).

The subdivision method with slightly modified vertex relocation algorithm is also used for obtaining PQ meshes of complex topologies, see (Liu et al. 2006), (Pottmann, Brell-Cokcan, and Wallner 2007), (Pottmann and Wallner 2008), (Baldassini et al. 2010) and (Tang et al. 2014). A technology equivalent to subdivision meshes that utilize NURBS patches is T-splines (Sederberg et al. 2003), in which the problems of curvature consistency and complex topology were solved.

An invaluable contribution to the development of design techniques and the implementation of *freeforms* can be attributed to Zaha Hadid. However, one must be aware that behind those successes there was her former mathematical education, and the desire to create her designs with the use of advanced CAD technologies.

3. Problems associated with the use of *freeforms* in architecture

The importance of problematic aspects of *freeforms* may be emphasized by the case of Qatar National Convention Centre, where part of the structure, the tree-like columns, was designed as *freeformed* reinforced concrete structure. Particularly, the purpose of designing it as such was an effect of ESO and topology optimization (see (Veltkamp 2015), (Cui, Ohmori, and Sasaki 2003) and (Donofrio 2016)) which objective was to find the optimal shape for the tree-like, branched columns. In fact, what had to increase the structural capability and reduce expenses turned out to cause unacceptable technological issues. Eventually, the structure was built in more conventional way with straight steel tubes and was covered by *freeformed* cladding to leave the visual impression of what was originally intended, see Fig. 3.1.

Fig. 3.1 Tree-like structure at Qatar National Convention Centre. Internal, octagonal structure made of planar steel plates partially covered by freeform cladding.[35]

In cases like the described one the technical difficulties of constructing *freeforms* prevail over potential benefits resulting from adopting them. Without prior consideration of problems that may occur during the construction of *freeformed* structures it may never be construct as desired. Especially, when designing methods and tools, which originate from mechanical industry but used for architectural design may cause problems unknown before. These and other problems related with *freeforms* in architecture will be discussed in this section.

[35] Source: https://dohanews.co/wp-content/uploads/2014/05/Dohaqnccnov08.jpg

3.1. Differences between *freeforms* in mechanical industry and architecture

Bearing in mind that the majority of tools and design methods available today originate from the mechanical industry, there are several differences between the design methodologies in mechanical and architectural design.

3.1.1. Thickness and layers of the walls

The bodyworks and hulls of vehicles are most often made of thin composite or metal sheets. In the original form the metal, carbon fibre or fibreglass sheets are initially flat and they are subjected to moulding. The thickness of the sheets of these materials is usually negligible, therefore their final forms may be represented as parametrical surfaces, with no thickness at all (i.e. equivalent to *NURBS* surfaces)[36]. In architecture surfaces are usually associated with substantial thickness, which in turn cannot be sufficiently represented by single surface – with the exception of membrane structures. The external surface of continuously curved architectural surfaces made of metal (moulded claddings), stone (CNC milled claddings), casted claddings (Enrique Monzó and Schwartz 2017), curved glass, and laminates may be defined by *NURBS* surface. However, cladding and glazing require substructure that has to be hidden beside the external surface. The curvatures of corresponding surfaces (sub and external) diverge. The external surface's shape affects the substructure's shape directly. While the substructure's shape is responsible for the structural performance it is largely defined by aesthetical aspects of external surface.

Additionally, discrete, doubly curved surfaces constructed as glazed grid shells are related to the offsetability problem, see chapter 19 in (Pottmann, Asperl, et al. 2007). Grid shells are constructed with longitudinal[37] members whose cross sections have defined orientation (rotation around the longest direction of a member) – usually normal to the doubly curved surface they discreetly represent. Normal vectors of the ruled surface along a straight line drawn on that surface have various directions. Thus, structural member drawn on that surface would be in geometrical torsion, what is undesirable from the structural point of view. Most doubly curved surfaces (not only ruled ones) have that geometrical torsion involved in their geometry and such fact may be overlooked in the structural detail design process. Even when the constraint of member normal to surface alignment is abandoned, the topology of second mesh may be inadequate to the original one, i.e. corresponding edges adjacent to a point on the external side of the structure may not cross in one point on the internal side. Those issues are more precisely described in section 3.5 and in selected works: (Liu et al. 2006) (Pottmann and Wallner 2008), (Wang, Wallner, and Liu 2007), (Pottmann, Grohs, and Blaschitz 2010) and (Hambleton and Ross 2015).

Apart from the necessity of maintaining the geometrical structure of discrete meshes on several layers of the free formed grid – architectural shells, walls, roofs and facades are divided into layers, each of which has a separate function. From external, decorative function, trough thermal and hydro insulation to structural support – each one has to be placed at some distance, preferably constant, from the doubly curved surface describing the global geometry of the wall. Such problem was clearly visible at the POLIN Museum (section 2.7), where the structural truss described by smooth and light

[36] However, ever for sheets of materials with negligible thicknesses, applying curvature to them also require folding or tearing.

[37] Construction parts, in which one direction is dominant, i.e. significantly larger than two other.

surface had to be construct of members whose diameters ranged up to 273 mm, eventually reducing the usable area inside the building.

3.1.2. The scale of the building components

Unlike most of automobiles, planes and ships, buildings, due to their scale cannot be manufactured in a factory out of their desired location. Each of building's components has to be manufactured, transported to the construction site and assembled on its destined place in the construction separately. Every step of that process limits the size of the components: the production line, transportation and construction cranes capabilities determine the reasonable size of the components. The scale of these components is much smaller than the scale of the entire building – unlike in the case of vehicles.

Also, in case of most vehicles, each component of its body is unique. In an automobile, plane and ship the component destined for a specific place is shaped in such a manner, that it fits only there. Minimalization of number of components is a result of production and mechanical aspects of vehicles. Each component is designed individually, accordingly to its place of destination. Front and back doors of a car are designed and manufactured as separate parts, although functionally and structurally they are similar. In turn, the construction industry uses universal structural components which can be used repeatedly even in different buildings although the final product of their assembly is very individual. Therefore, designing *freeforms* in architecture require additional rationalization of component variety in order to reduce the complexity and costs of the construction.

Concluding *–freeformed* structure of a building should be divided into a set of components that are possible to manufacture, transport and place built in a desired place on the building. Since the absolute regularity of the components is unobtainable, each component of the same type (glazing, cladding, rods, nodes) should be as similar to other components of the same set as possible. I.e. the facets (glazing, cladding) should be planar with varied outlines (possibly with similar external dimensions[38]); bar elements should have the same cross sections and vary between lengths and cut angles at their ends.

3.1.3. Aerodynamics and hydrodynamics

The level of complexity of the design tools for shaping the forms of air, water and land vehicles results from the necessity to minimize frictions generated by movement. Shapes of these vehicles have to be aero- or hydrodynamic. Although skyscrapers and large spanned structures are also objects for aerodynamic optimizations, this characteristic is not always the most important one. Unlike in vehicles, the structural load capacity, thermal performance and technological versality are the priorities.

The technological leaps which led to the contemporary *freeform* design tools were dictated by the necessity of more aerodynamic vehicles.

[38] External dimensions of quadrangular glass panes of PQ grid shells described in (Schober 2015b), pp. 190-207, range from 1000 mm to 2400 mm – depending on the construction.

3.1.4. Production scale

Majority of vehicles are manufactured in large series. Thanks to this fact the cost of development and implementation of the technology of production is distributed on numerous manufactured copies. Whereas buildings are designed and built in their unique forms only once. In the second case the cost of development of technology has much higher share in the total cost of constructing the building.

In order to avoid the necessity of developing new technology each time a free form is constructed, system solutions are adopted. Such approach reducs freedom of shaping *freeforms*, in turn reducing the technological difficulties. Moreover, the same system can be adopted in multiple buildings.

In conclusion, in order to reduce implementation costs of *freeforms* it is required to seek for technological simplifications allowing their construction to be based on the common principles and components.

3.1.5. Importance of *freeforms* in architectural challenge

Throughout the history architects had been searching for new ways to express their artistic visions of buildings they were designing while competing between each other. A significant example of such competition resulted in most extraordinary forms created by Francesco Borromini, i.e. the dome of San Carlo alle Quattro Fontane and the Mascarino Staircase in Palazzo Barberini, see (Święciak and Tarczewski 2018). Apart from the structural and functional purposes architectural designing allows for greater freedom of shaping the forms. In contrast to the vehicles, for which the most important aim is to be safe, efficient, reliable – the imperative for representative buildings such as palaces, churches, opera houses, stadiums, etc. is to be unique, however also safe and functionally correct. The form is only one of the features of the building, however it may be more important for the building than for the automobile, plane or ship.

The available unique morphologies for the buildings and the sources of inspiration are in the growing deficit (Tarczewski 2011). Therefore, the architectural designers are demanding for even greater freedom of design and new sources of inspiration. *Freeforms* open great opportunities in this area, allowing to go far beyond routine design.

3.1.6. Conclusion

While designing *freeformed* architectural structures in modern CAD environments originating from mechanical industry, previously mentioned differences have to be taken into consideration. Depending on type, thickness and details of designed *freeform* structure, the designer have to know what intrinsic properties the geometry he is creating possesses. With different set of issues requiring consideration during designing of mechanical industry object, CAD environments can lead an architectural designer on a wrong path at the end of which the designed structure is hard and expensive to construct and may be a subject to failures. A different approach in which those intrinsic geometrical properties related with details of *freeformed* structures in architecture are taken into consideration right from the beginning of design process is called bottom-up approach and is more precisely described in sections 3.4 and 3.7.

3.2. The types of *freeform* implementations in architecture

Examples of *freeforms* shown in appendix A-3 allow to emphasize diversity of their applications in architecture and richness of forms in terms of morphology. The following summarizes the most important features, on the basis of which the initial general classification of *freeforms* was made.

Among forms several are distinguished:

- orthogonal – composed of elements in flat configuration;
- developable – composed of elements in single-curved configuration;
- doubly-curved - i.e. *freeformed*.

Among the doubly curved forms in architecture several types of implementation are distinguished. Among the most important there are (see section 1.1.2):

- membrane,
- pneumatic,
- shells,
- grid shells.

The curvature of the form may be (see section 1.1.3.4):

- continuous,
- discrete.

Membranes and pneumatic structures are continuously curved, whereas shells and grid shells can be discrete and continuous.

Types of grid shells are distinguished due to their topological structure (see section 3.2.5), i.e.:

- triangular,
- quadrilateral,
- polygonal.

Triangular grid shells always have planar facets, whereas quadrilateral and polygonal grid shell can have all types of facets.

Among the grid shell type another typology is distinguished depending on the curvature of individual facets, which can be:

- planar,
- single-curved,
- doubly-curved.

Triangular grid shells always have planar facets, whereas quadrilateral and polygonal grid shell can have all types of facets.

Regardless of the above classification, the grid shells can be designed using two different methodologies (see section 3.4):

- top-down,
- bottom-up.

Arguing for particular types the scope of this research has been narrowed to: discrete, doubly-curved grid shells in planar quadrilateral topology obtained using the bottom-up method, see Table 3.1.

Table 3.1 General classification of freeforms applied in architecture

Form	Curvature	Type	Facets	Topology	Design method
Discrete	Doubly-curved	Grid shells	Planar	Quadrilateral	Bottom-up
Continuous	Developable	Shells	Developable	Triangular	Top-down
	Orthogonal	Membranes	Doubly curved	Polygonal	
		Pneumatic			

A brief overview of differentiation of *freeforms* on the basis of these features is presented further in this section.

3.2.1. Geometry

Implementations of *Freeforms* in architecture are firstly distinguished between continuously curved and discrete, see Fig. 3.2. In the discrete form, the structures representing doubly curved surfaces are composed of planar or straight components, which approximate those surfaces. Continuous forms usually do not have visible divisions into segments. Examples of the continuous forms are membrane and pneumatic structures. There are also examples of continuously curved concrete shells, composite claddings (e.g. Heydar Aliyev Centre designed by Zaha Hadid) and glass façades (e.g. Emporia Shopping Centre in Malmö).

Geometrically, *freeforms* may be synclastic, anticlastic or any composition of the previous two types.

Additionally, one more geometrical type may be specified. Discrete, reticulated shells can be constructed as continuously curved networks of curves, i.e. curvilinear networks. Examples of such networks are elastic grid shells designed by Frei Otto and rigid curvilinear grids designed by Shigeu Ban, for example Centre Pompidou-Metz.

Fig. 3.2 Left: continuously curved shell (Crematorium in Kakamigahara)[39], right: discrete lattice shell (Złote Tarasy, Warszawa)[40].

[39] Source: http://www.toyo-ito.co.jp/WWW/Project_Descript/2005-/2005-p_07/2-800.jpg
[40] See appendix A-3, p. 268, source: https://upload.wikimedia.org/wikipedia/commons/d/de/Zlote_tarasy_zima2011.jpg

3.2.2. Structure

Freeforms are constructed either as building elements which have structural importance, or such which carry only aesthetical value. In some cases a structure designed as *freeformed* is constructed in the conventional manner and covered with *freeform* cladding resembling structural element (see the introduction to section 3, i.e. the case of Qatar National Convention Centre). Economic and technological factors may determine whether the structure is performed as *freeformed* or the structure is conventional and is covered by *freeformed* cladding. Whereas other types of structures like tensile, membrane, pneumatic, concrete shells and lattice shells have intrinsically double curved shape.

3.2.3. Function

Functionally, *freeforms* may have various purposes – they can be constructed as walls, vaults, roofs, shells etc. These are the examples of opaque building skins. From the other hand *freeforms* are preferably constructed as transparent skins – façades, glazed canopies and roofs, reticulated shells and space trusses. Transparent forms are necessarily discrete, i.e. flat glass panels are preferred and they fill the holes in grid shell made of straight bar members (again preferably straight). However, also in case of reticulated shells facets can be made of opaque cladding, which can be as well curved.

3.2.4. Material

There are various materials *freeformed* structures can be made of. Depending on the structural role membrane structures are made of fabrics such as industrial textiles: PVC coated polyester, PTFE coated fibreglass or silicon coated fibreglass. Pneumatic cushions are made of PVC, fibreglass and ETFE. Shells are made of concrete (reinforced by steel or microfibres), brick or stone. Grid shells and space trusses are made of structural steel, although timber structures are also common. Claddings are made of metal sheets, GFRC panels, laminates, membrane, ETFE cushions and glass panes (as fillings), etc.

3.2.5. Topology

Topology is an important characteristic of discrete grid shells based on doubly curved surfaces. In this respect, topologies of all layers within lattice structure and geometrical relations are also a subject of interest (see section 3.5). Grid shells are represented by a polyhedral mesh, which consist of facets, edges and vertices. Facets correspond to glass panes or ETFE cushions, edges correspond to structural rods and vertices correspond to structural nodes. The topology describes the properties of a mesh regardless of its shape. Such property can be for example the number of edges each vertex is adjacent to or the number of vertices each facets is surrounded by. The topologies of the most often implemented grid shells are as follows:

- Triangular meshes – each facet is triangular, the vertices are adjacent to 6 edges;
- Quadrilateral meshes – each facet is quadrilateral, the vertices are adjacent to 4 edges;
- Hexagonal meshes – each facet is hexagonal, the vertices are adjacent to 3 edges;
- Hybrid – combination of the above topologies[41].

[41] Irregular topologies are least common. From over 50 representative cases listed in the appendix A-3, only six belong to the group of irregular topologies.

It is possible that a vertex in a specific topology is adjacent to more or less edges than described above. Hexagonal meshes are also called 3-valent – according to the number of edges each vertex is adjacent to. Such topologies are adequate to the external layers of space trusses or to the plate stable shells. For more information about plate stable shells refer to *Structural order in space: the plate-lattice dualism* (Wester 1981), also (Święciak and Tarczewski 2015) and (Święciak and Tarczewski 2016).

3.3. Evaluation of lattice shell topologies

When designing a *freeform* grid shell one has to consider all aspects listed in the previous section. Certain aspect of the design is topology of grid shell. Each of the available topologies has its pros and cons. Every form of a shell requires tessellation for creation of a grid shell. From the point of view of economy and feasibility the tessellation is equally important as the initial global form. Appropriately shaped and discretized grid shell allows to avoid many technological problems, improve structural properties and reduce the costs of construction and operation of the structure. Some tessellations require specific methods for designing the global shape. Generally the more profits from the proper tessellation, the more freedom of the design of the global shape has to be given up.

The most important available topologies are:

- triangular,
- quadrilateral with planar facets – PQ.

The first one is most frequently implemented. It gives designer great freedom of shaping since any *freeform* surface can be discretized into a triangular mesh with significant freedom. Sufficient conditions of a triangular mesh is planarity of facets and collinearity between edges of facets. Firstly, the triangular facet is always planar, since any random set of three points in space always constitute a common plane. Secondly, pairs of points forming edges are common between adjacent facets, therefore the edges are colinear. The possibility of placing the vertices anywhere on the discretized surface allows for many optimization criteria, like the best possible unification of rod lengths and the best possible approximation of triangles into equilateral form, although these criteria can never be fully met. Nevertheless, all are important both from the aesthetic (legible grid layout) and static (flow of forces on supports on a regular grid of bars) point of view.

The second type of topology – the planar quadrilateral meshes (PQ) are more constrained. The quadrilateral facet contains four vertices. Any selection of three vertices from the four constitutes a plane - the fourth one is constrained to that plane, i.e. the freedom of its positioning is narrowed. In case of discretizing the *freeform* surface the vertices of quadrilateral facets must lie on an intersection of plane and the surface, or the positioning the vertices on that surface has to be given up. In the following sections it will be explained, that while it is possible to discretize arbitrarily shaped *freeform* surface into a PQ mesh, it is also possible to shape that surface in the particular manner or shape the PQ mesh instantly.

The requirement of coplanarity of facet vertices can be met by detaching the vertices from the discretized surface. The vertices are then projected onto a plane, e.g. tangent to that surface. The requirement of collinearity of adjacent edges may still be not met. An example of such compromise is the glazed roof over the Kogod Courtyard, see Fig. 3.3. It needs to be highlighted that despite the design disadvantages, the PQ topology has several advantages improving feasibility. Table 3.2 presents the most important differences between two major topologies of grid shells.

Fig. 3.3 Planar, quadrilateral glass panels with non-colinear adjacent edges. Kogod Courtyard glazed roof, Smithsonian Institution, Foster + Partners.[42]

Table 3.2. Comparison between triangular and PQ meshes

Triangular	**PQ**
+ Great freedom of shaping	- Limited freedom of shaping
- 6 rods in the node, greater complexity of each element	+ 4 rods in the node, less complexity of each element
- Lower surface ratio of glazing to bar elements	+ Better surface ratio of glazing to bar elements
- Triangular glass panes increase the amount of waste in production	+ Quadrilateral glass panes reduce the amount of waste in production
- Higher risk of leakage through additional rods, as well as through more complicated nodes	+ Lower risk of leaks through reduced amount of rods, as well as through smaller nodes
- Increased amount of thermal bridges	+ Reduced amount of thermal bridges
- Heavier structure	+ Lighter structure
+ No necessity to stiffen geometrically stable triangular facets	- Necessity to stiffen geometrically variable four-sided facets
+ Numerous possibilities of geometry optimization	- Limited optimization possibilities
- Less possibility of shaping parallel meshes	+ More possibility of shaping parallel meshes

Results of comparison from Table 3.2 allow each designer to choose which topology is more suitable for a given project. Growing awareness of their benefits, PQ topologies are recently gaining increasing popularity. The superiority of PQ topology is further reasoned in (Pottmann, Asperl, et al. 2007), p. 676. Apart from the mentioned properties, additional properties of PQ meshes are claimed in the cited source, i.e. the lesser costs per area of construction of PQ based glazed grid shells. Additionally, the properties like torsion-free nodes and parallel meshes (see in sections 3.5) are only available for simple forms of triangular meshes, while they can be obtained in PQ meshes. In (Mesnil, Douthe, Baverel, Léger, et al. 2015) triangular meshes are qualitatively compared with three types of PQ meshes. The results are presented on Table 3.3.

[42] See appendix A-3, p. 317, source: https://www.fosterandpartners.com/media/2635088/1276_fp342827.jpg

Table 3.3. Assessment of different methods of geometrical optimisation, table from (Mesnil, Douthe, Baverel, Léger, et al. 2015), p. 39.

Optimisation	Angles reception	Length uniformity	Panels planarity	Node complexity	Design freedom
Triangular mesh	-	++	++	--	++
Scale-trans surface[43]	--	++	++	-	--
PQ conical mesh[44]	+	+	++	+	+
Edge offset mesh	+	-	++	++	-

As seen from the table, triangular meshes have the worst node complexity in turn for the greatest freedom of design. Other properties depend on the intrinsic properties, which might be obtained by certain design methods or optimizations.

In (Hambleton et al. 2009) several discretization methods were compared, among others: triangulated surfaces, primitively approximated PQ meshes, fitted rotational PQ meshes and PQ meshes obtained by conjugate curvature networks (see section 3.7.1). Aassessment of the comparison is presented on Table 3.4, where lower rating values mean inferior properties.

Table 3.4. Assessment of different methods of geometrical optimisation, table from (Hambleton et al. 2009), p. 242.

Design solution comparison	Node simplicity	Structural transparency	Design intent	Material efficiency
Triangulated meshes	1	1	3.5	2.5
Primitive approximated PQ	1.5	3	2	3.5
Fitted rotational PQ	4	3.5	2	3.5
Principal curvature PQ	4	4	4	3.5

Triangulated meshes in the comparison above have the worst properties in the field of node simplicity, structural transparency and material efficiency. Again they have the advantage in freedom of design.

While the first cited comparison (Table 3.3) consists of PQ meshes exanimated through different geometrical, intrinsic properties, the second one (Table 3.4) consists of few methods of obtaining PQ's, which do not include most of the methods presented and proposed in this work.

3.4. Top-down and bottom-up paradigms

In the context of designing *freeform* grid shells, the design paradigms apply to the order in which three main aspect are considered, see Fig. 3.4. Generally, grid shells are characterized by:

- Global shape (**form**) – a continuously curved surface (usually NURBS) characterizing global shape of the façade or glazed canopy. Usually it is very convenient to design the shape of the shell using NURBS surfaces in the initial stage of the design process. However, as it will be explained further in the text, specifying the **form** by means of continuously curved surface

[43] Scale-trans surfaces are continuously curved equivalents of scalar-translational meshes described in the section 4.1.3.
[44] Conical and edge offset meshes are described in the section 3.5.3.

is not necessary for the design. The form may be a derivative of topologically specified mesh. The **form** can also be a result of a form finding process.

- Discretization (**tessellation** or **panelization**) – the way the form is divided into finite elements such as vertices, edges and faces. It also describes topologies of such division e.g. how many edges are connected at each vertex, or how many edges each face consists of. The group includes also properties such as: planarity or no-planarity of faces, possibility of concave outlines of faces and coplanarity or no-coplanarity of corresponding node axes. These properties will be described further in the section.

- Structural properties (**mechanics**) – contrary to the previous two groups describing geometrical properties, this group deals with the mechanical properties of elements representing edges, faces and vertices. Each vertex corresponds to the node, the edge to the bar and the facet to the panel. Mechanical properties describe material, sections, thickness, weight and other properties that affect the performance of a structure and are not included in any of the previous two groups.

Structural performance of *freeformed* grid shell depends on those three groups of properties which are interrelated one to each other in all possible ways.

With the use of these three groups, a grid shell can be designed and characterized. A design process is a methodical series of steps that designer follow to find, optimize and make a decision over properties in each group. Depending on the order between the groups, two different approaches are possible: **bottom–up** and **top–down**, see Fig. 3.5.

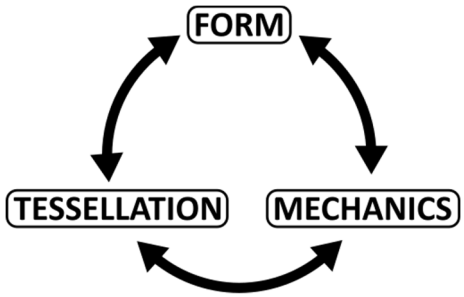

Fig. 3.4 Three interdependent properties of freeformed grid shells.

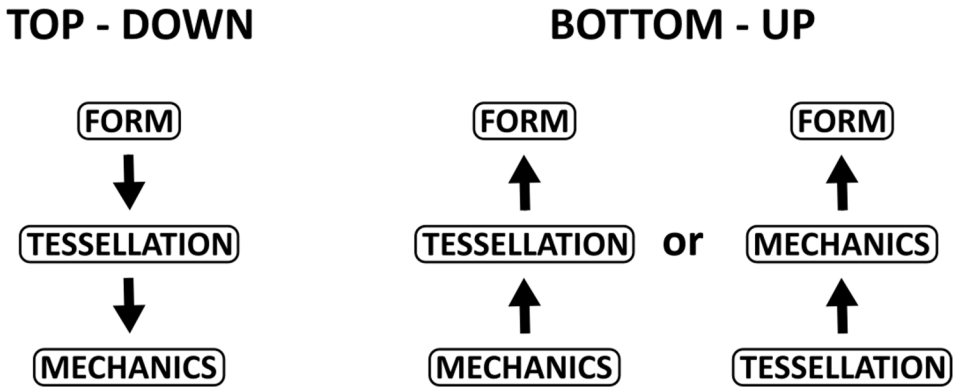

Fig. 3.5 The sequences of specifying the properties of the design, according to top-down and bottom-up paradigms. The resultant design vary depending on the adopted paradigm.

First approach to the form finding process refers to a procedure with its aim to find an optimal (or close to the optimum) **form** of the structure. Such a form is a subject for further tessellation and mechanical decisions and optimisations. This is the **top-down** procedure.

Second approach to the form finding process refers to a process which goal is to find a form that will be best suited depending on mechanical and tessellation decisions taken before. Thus, the freedom of shaping form will be limited to some extent. This is the **bottom-up** procedure.

In the top-down approach form is assumed before tessellation and mechanical decisions are made, whereas in the bottom-up approach mechanical and tessellation decisions are made preliminarily and form is derived from them.

Some specific cases[45] require a specific approach. However, the common practice is the facilitation of the top-down approach. We argue with this statement, what will be explained further in this section. Top-down approach is not necessarily the best option for some cases of grid shells, therefore, some new strategies based on bottom-up approach will be presented.

As fitting planar, quadrilateral facets to a *freeform* surface is significantly difficult, a bottom-up procedure for shaping a mesh is more rational approach. However it is also possible to shape PQ nets using top-down approach.

The state of the art method for generating PQ meshes according to the top–down paradigm utilizes the *conjugate principal curvature lines network* – see section 3.7.1 and (Pottmann, Asperl, et al. 2007), p. 684. The methods proposed in (Mesnil, Douthe, Baverel, Léger, et al. 2015), (Mesnil, Douthe, Baverel, and Léger 2015), (Mesnil, Santerre, et al. 2015), (Douthe et al. 2016), (Mesnil et al. 2016) and (Mesnil 2017) work according to the bottom-up paradigm. A particular one – *Marionette method* is described in sections 3.7.2 and 4.1.6. Between the top-down and bottom-up paradigms stands the subdivision method described in section 3.7.3, following papers (Pottmann, Schiftner, and Wallner 2008), (Pottmann, Brell-Cokcan, and Wallner 2007), (Pottmann and Wallner 2008), (Tang et al. 2014) and (Pottmann, Asperl, et al. 2007), pp. 684-686.

Romain Mesnil, author of the Marionette method based on the bottom-up paradigm, uses the phrases *fabrication-aware design* and *construction-aware design*. These phrases accurately reflect the nature of bottom-up paradigms. According to *fabrication* and *construction-aware design* the designer should concern the fabrication and construction aspects since the very beginning. The global form of the structure should be result of those concerns. He also claims that: *no new shapes for fabrication-aware design have been introduced since the 1990's* (Mesnil 2017), p. 29. Romain Mesnil also distinguish two modelling methods: *surface-based* and *mesh-based* (Mesnil 2017), pp. 30-31. The first one is more convenient for the designer since available tools (i.e. NURBS surfaces) allow him for great control over the global shape through the limited amount of control points. On the other hand *mesh-based modelling* tools are limited and require more effort from the designer – in turn *mesh-based models* contain information important for the fabrication and structural behaviour of the grid shell.

The tools incorporating *surface-based modelling* are suitable for the top-down paradigm, while *mesh-based modelling* tools are more suitable for the bottom-up paradigm. As claimed, the second group of design tools is in deficit for modern requirements of *freeform* design.

[45] Such as bending-active grid shells, see section 2.1.

The three stages division is also proposed in the chapter *Multi-criteria grid shell optimization* in *Shell structures for architecture* (Adriaenssens et al. 2014), p. 265. The stages are defined as follows:

1. *Surface form – conceptual shape by the designer.*
2. *Grid layout – defining member layout (also referred to as 'rods') on a given surface.*
3. *Member size – section sizes are chosen once geometry is defined.*

The optimization criteria are however narrowed to the grid layout in the cited source and the surface form is arbitrarily given by a sculptor. In that case, the approach is top-down.

In his book, *Transparent Shells: Form, Topology, Structure*, Hans Schober defines the two approaches in the following words:

"There are now computer tools available that generate grids with the desired properties on unmeshed, completely freeform surfaces, thus producing homogeneous structures. Whilst this would be impossible without this software, I do believe that simple, understandable principles, whose basic mathematical and geometric concepts can be reconstructed and which therefore do not constitute a black box, still have their place." – from (Schober 2015b), p. 7.

The methodology of Hans Schober and methods described in his book can be classified as bottom-up.

Sections 5 and 6 present methods of obtaining (forming) and transforming PQ meshes in accordance with the bottom–up approach. They cover only *Form* and *Tessellation* parts of the approach, see Fig. 3.5. The *Mechanics* is not taken into consideration in this work. The recognition of the rules of how to create PQ meshes according to the presented rules, allow to recognise what morphologies are possible. From those geometrically appropriate possible morphologies mechanical optimums can be searched and reached. Parametrization of the presented methods and rules of obtaining and transforming PQ meshes is the base for creation of an interface, through which optimization methods can be applied. The bottom-up methods give the designer narrowed freedom of design in which the planarity of facets and geometrical consistency is guaranteed.

Descriptions of the methods of obtaining PQ meshes are contained in section 4, whereas section 5 contains descriptions of the methods of transformation of PQ meshes.

3.5. Parallel meshes

Two meshes are parallel, when corresponding edges and facets between them are mutually parallel. The existence of parallel meshes[46] allows for designing multi layered structures, where each layer is defined by one of the meshes.

3.5.1. Types of parallel meshes

Two parallel meshes can be defined by the distance between each other. That distance can be measured in three possible ways: between vertices, edges and facets. A parallel mesh is called a vertex, edge or face offset, when the distances between the respective elements is constant for the whole mesh.

[46] Parallel PQ meshes and offsets are discussed precisely in (Pottmann, Asperl, et al. 2007) in section *Offset Meshes*.

In order to generate a specific type of an offset, the base mesh has to meet specific geometrical requirements. On the Fig. 3.6 a simple PQ mesh is shown for which a set of four equally distanced facets was generated. The corresponding facets and edges are parallel, however the topology of the upper mesh is not PQ. The requirement for the vertex valence is not met, i.e. a 4-valent vertex was split into two 3-valent vertices connected with an additional edge. The additional edge can be reduced into a single vertex, then however, its adjacent edges will not be parallel to the base mesh anymore, see Fig. 3.7.

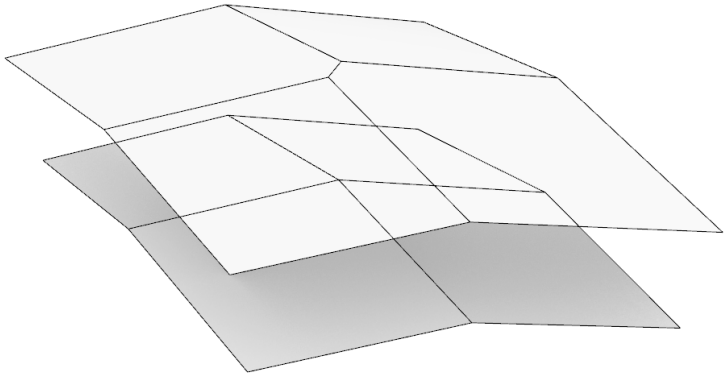

Fig. 3.6 Two PQ meshes with parallel edges and facets and equal distance between facets. However the topologies are different, since the upper mesh has an additional edge

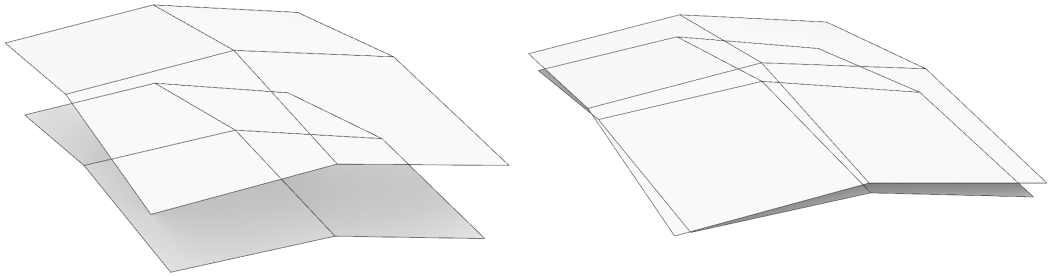

Fig. 3.7 Additional edge collapsed into a single vertex. Right: the meshes situated closer to each other to highlight the non-parallel edges.

3.5.2. Geometrical torsion in meshes

In real structures a single layered grid shell constructed of rods with rectangular[47] cross-sections also requires consideration of meshes parallel to its base mesh. Edges of base PQ mesh indicate the directions of rods, whereas orientation (rotation around edges) of rods' also require consideration. A second mesh, with respect to the base mesh, can be obtained by selecting two points over a cross section of rods, see Fig. 3.8, right. The first point (e.g. at the bottom) will always lie along an edge of the base mesh and the cross section will be aligned normal (perpendicular) to edges of that mesh. Then, the second mesh can be obtained by drawing edges traced by the upper point on cross sections. Depending on orientations of rods along edges of the base mesh two scenarios are possible:

- The second mesh has distorted topology, as in Fig. 3.6,
- Both meshes are parallel and have proper topologies.

[47] Rods with circular cross sections are not subject to geometric torsion, however, rectangular cross sections are preferred by architects in grid shells.

The second case is highly unlikely without proper alignment of the rods' orientations.

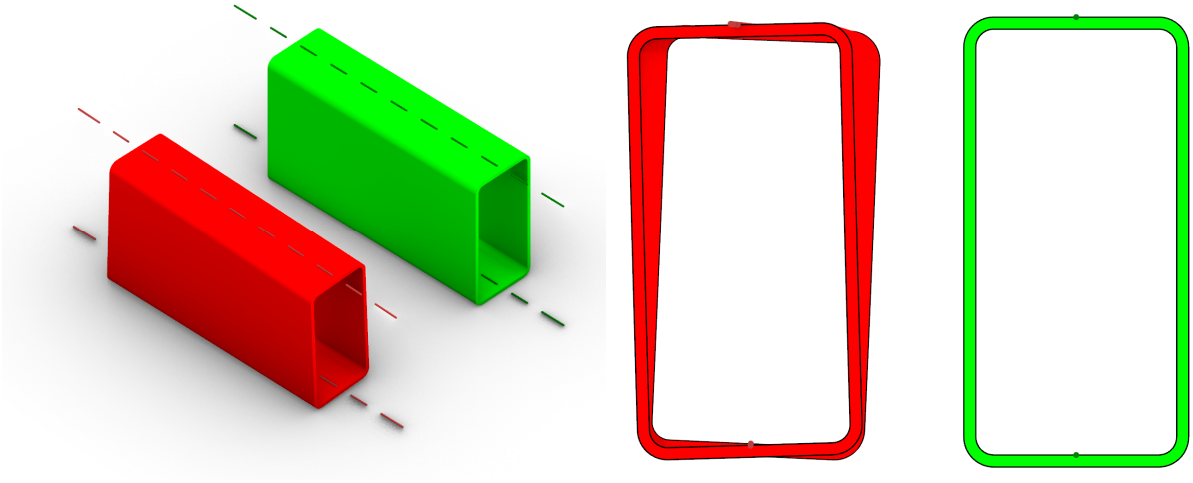

Fig. 3.8 Two RHS members along parallel (green) and non-parallel edges. The red member is in torsion.

A different approach is possible, which may also lead to two scenarios. When normal axes of the base mesh are assigned before orienting rods' cross sections, see blue dashed lines in Fig. 3.9 to 3.11, rods may be oriented alone edges by alignment with those normal axes. In such case the orientation of normal axes has to be adjusted in such a way, that adjacent normal axes[48] are co-planar. Otherwise rods spanned between non co-planar normal axes would be in geometrical torsion[49], as in Fig. 3.7, red rods in Fig. 3.8 and Fig. 3.10.

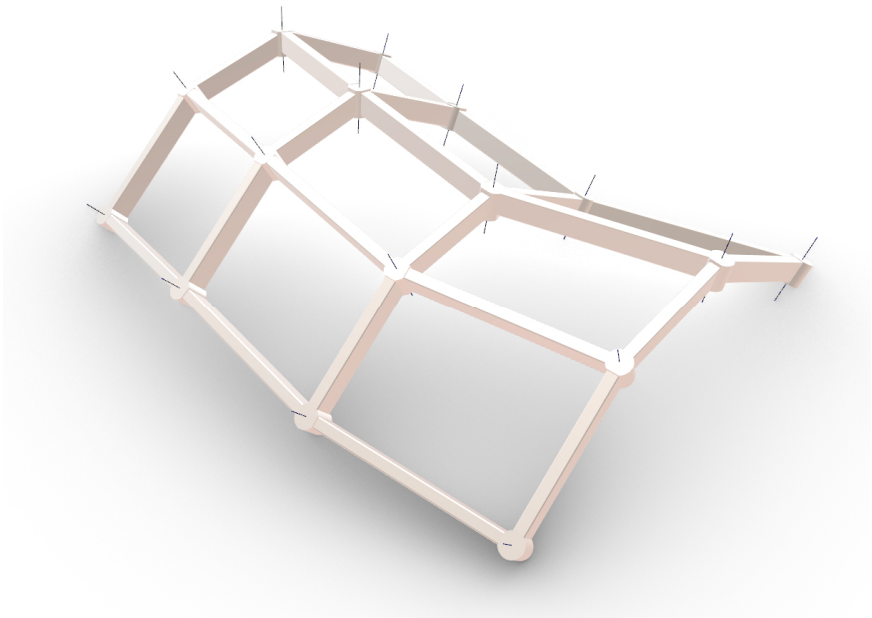

Fig. 3.9 9-cell PQ grid shell (nom-circular and non-conical) with node axes.

[48] Pairs of normal axes that lie at both ends of each edge of a mesh.
[49] Attempt to construct incorrectly designed grid shell with geometrical torsion in rods would lead to real, structural torsion in members.

It is desirable to design meshes and adjust cross sections and normal axes in such a manner, that rods are not in geometrical torsion. Such solutions are possible only for simple forms of triangular meshes, while in PQ meshes an optimal alignment can always be found. Eventually, when properly designed, nodes in PQ meshes can have reduced complexity with respect to equivalent nodes in triangular topologies, i.e. the geometry of these nodes may not take into account the yaw angles (rotation along mesh edges) of rods. Figures 3.10 and 3.11 shows two cases of grid shells and nodes, where rods are not in physical torsion, but the first one is in geometrical torsion. Both cases are based on the same meshes and cross sections of rods. However, in the second case normal axes of vertices are optimized.

It may also happen, that two meshes describing the upper and down sides of the rods are not parallel to each other, since their topologies were forced into PQ (pairs of 3-valent varices were collapsed into single 4-valent ones). Then the rods are in geometrical torsion. When this fact is not considered while determining the nodes it may cause implementation and operation problems. The solution to solve that geometrical problem is to consider the rake angle of the rod with respect to the node axis. The other solution considers the usage of circular cross section rods, which in turn complicate the application of glass plates. Figure 3.12 show both pairs of normal axes for comparison.

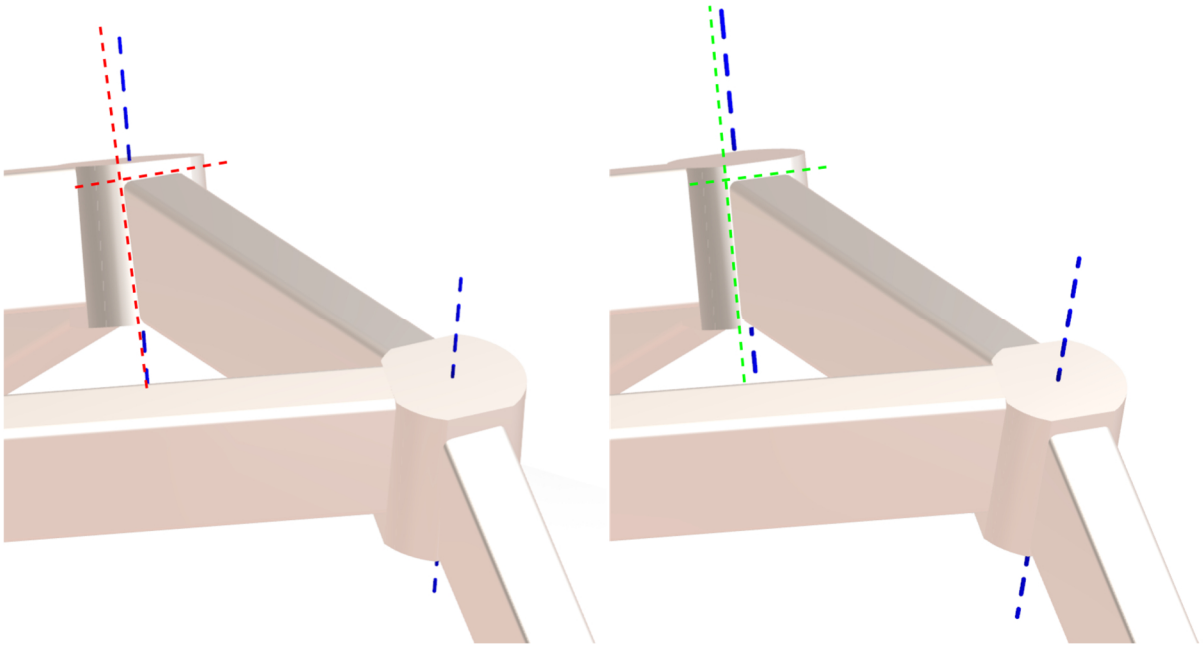

Fig. 3.10 Node-rod-node connections in geometrical torsion grid shell (left) and torsion free grid shell (right). On the left side the rod's axis in not aligned with the axes of adjacent nodes. On the right side the node axes were oprimized and corresponding ones lie on a common plane, therefore the axes of rods may be aligned with them.

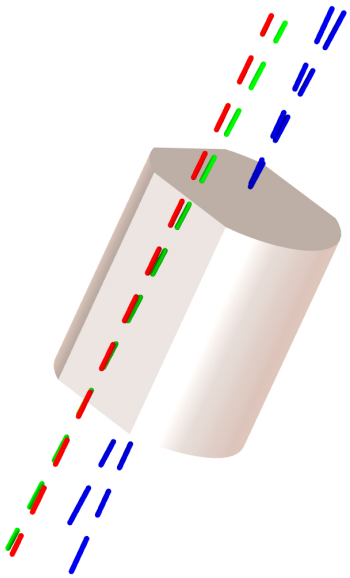

Fig. 3.11 Node from the grid's from previous figure without and with optimized axes (blue) and axes of adjacent rods. Red dashed line marks axis of rod without optimization, whereas green dashed line marks axis or rod with optimization. Green axis lies on a common plane with corresponding blue axis of the node.

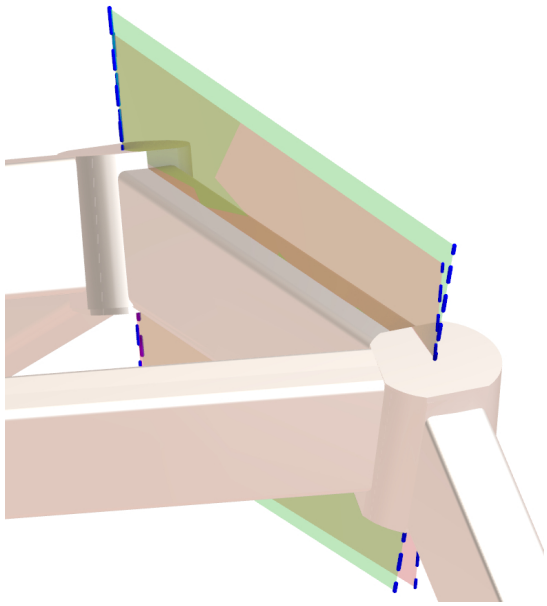

Fig. 3.12 Planes between corresponding node axes of torsion and torsion-free adjustment. Red plane is in torsion, whereas green one is planar.

When the mentioned intrinsic properties of meshes are not considered during the detailing of the grid shell, a series of unexpected problems may occur during the fabrication, assembly and operating the structure. The consciousness of those properties may result with better design and construction. Generally, geometrical constructs favoured from the point of view of fabrication and assembly processes are more available for the free formed PQ meshes than in the triangular ones. For example torsion-free meshes in triangular topologies have very limited number of available morphologies.

Torsion-free meshes can be obtained by adoption of the constrained meshes described further in this section, i.e. conical and circular meshes. However, it is also possible to optimize normal axes alignment of PQ meshes to eliminate torsion.

3.5.3. Conical meshes

In order to design a PQ mesh with torsion-free offset, a certain construction may be used. Generally, face offsets (with constant distances between all pairs of corresponding facets) are torsion-free. Mesh having a face offset has such property, that each quadruple of facets adjacent to the common vertex is tangent to a cone. The angles between edges surrounding a vertex have to meet the condition of the equation (3.1), see (Liu et al. 2006).

$$\boldsymbol{\omega_1 + \omega_3 = \omega_2 + \omega_4} \tag{3.1}$$

Where ω_n are the angles and the *n* marks the consequent one. That is the sum of diagonally opposing angles is equal. When the above condition is met a cone can be created, which apex is located at the vertex of a mesh, and the surrounding facets are tangent to that cone. Such cone has an axis, which is equivalent to the normal axis of a vertex. An offset of the quadruple of conical facets can be then performed by translating them along the normal axis (axis of the cone). Doing so, each facet will be translated by the same distance. Additionally, in the conical meshes the pairs of cone axes located on the both sides of an edge are coplanar – therefore the mesh is also torsion-free.

Node axes are also equivalents of surface normal vectors in case of meshes devised according to the top-down paradigm. In such case however, the corresponding normal axes (pairs adjacent to common edge) are usually not coplanar. In case of triangular topologies each normal axis has to be aligned with 6 more vectors (instead of 4 in case of PQ topology) and that limits the available morphologies of torsion-free triangular meshes into the discrete equivalents of spheres and certain types of anticlastic surfaces.

3.5.4. Circular meshes

Circular PQ meshes are such meshes, whose facets are cyclic quadrilaterals[50], see Fig. 3.13, left. Such meshes have families of parallel meshes with constant vertex distances (Liu and Wang 2008). Additionally, circular meshes are allowed for some transformations that preserve the planarity of facets – see sections 5.1.2 and 5.1.3. Examples in Fig. 3.13 and 3.14 show examples of circular meshes obtained through diverse methods. On the right side of figures a constant vertex distance offsets of those meshes are presented.

[50] A cyclic quadrilateral is a quadrilateral for which a circle can be circumscribed so that it touches each polygon vertex (Weisstein 2018f). The opposite angles of a cyclic quadrilateral sum to π radians (see Euclid, Book III, Proposition 22).

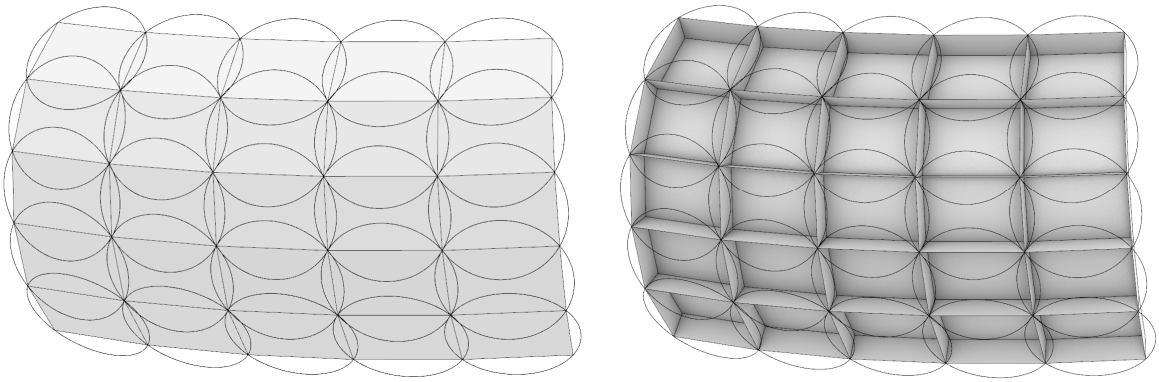

Fig. 3.13 Left: circular PQ mesh obtained as spherical inversion of a sweep PQ mesh. Right: the same mesh with vertex offset.

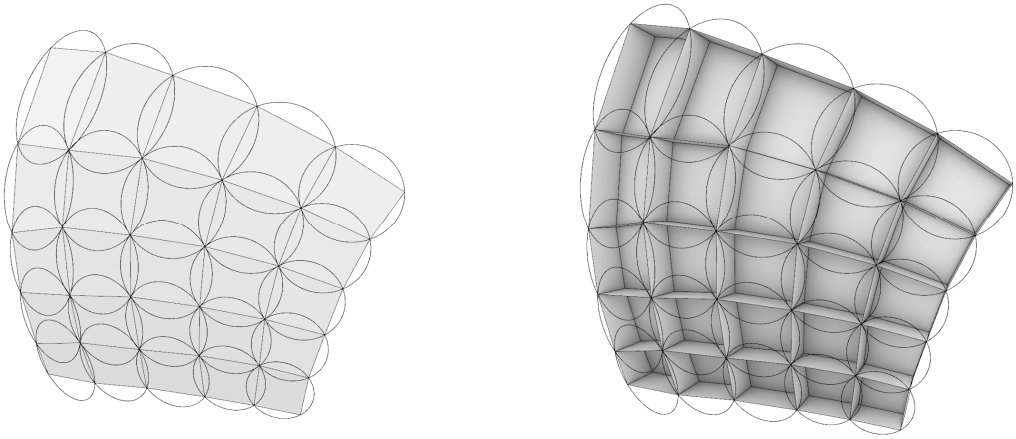

Fig. 3.14 Left: circular PQ mesh obtained as stereographic projection of planar isoradial mesh. Right: the same mesh with vertex offset.

In Fig. 3.15 particular geometrical properties of vertex offset meshes are shown. All normal axes edges marked by dark blue colour have equal lengths. There are infinitely many solutions for the directions of the vertex normals[51] which met the vertex offset requirements in circular meshes. These directions can be chosen arbitrarily, however, vertex normal directions are conjugated, i.e. only one axis can be chosen arbitrarily and the rest is derived from it. Examples of different alignment of normal axes of equal lengths creating parallel meshes are shown in Fig. 3.16.

[51] Vertex normal – normal axis of a vertex

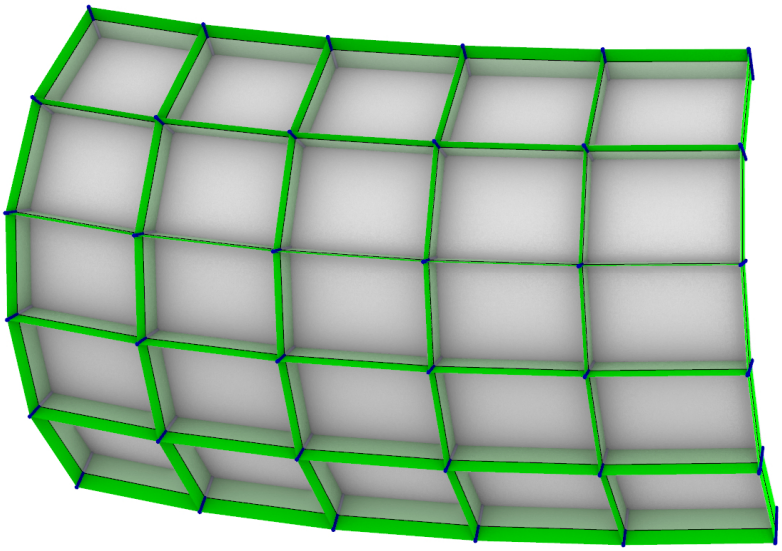

Fig. 3.15 Vertex offset of a circular PQ mesh. All edges marked by blue colour have equal lengths. Green facets are planar.

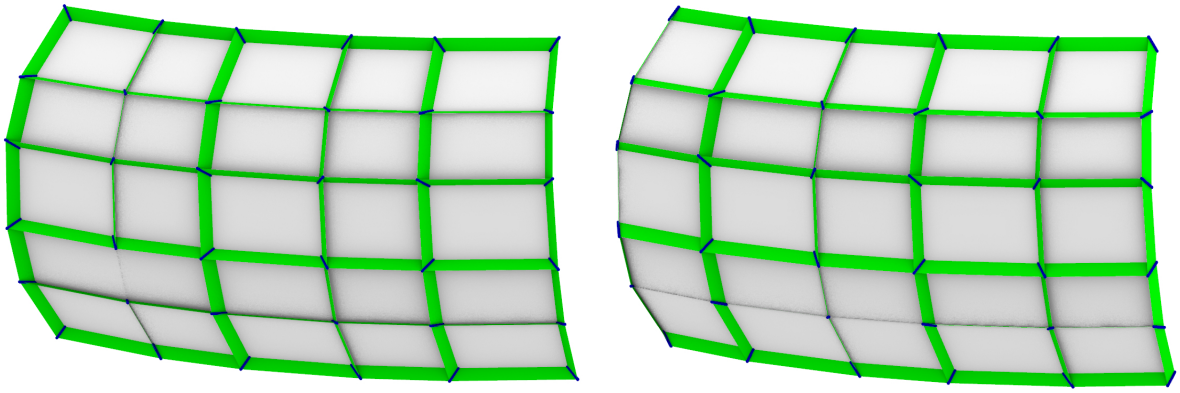

Fig. 3.16 Examples of allowed directions of the vertex normals.

Semi-transparent facets in Fig. 3.15 are planar and all their vertices are equally distanced to the original mesh. Finally, faces marked in green colour are planar, i.e. adjacent vertex normals always line on a common plane. Mechanically, RHS pipes from which the grid shell is built can be aligned with those green, planar faces eliminating geometrical torsion. Therefore, the class of PQ meshes, to which circular meshes belong, is called torsion-free.

Nevertheless, it is possible to generate torsion-free offsets for non-circular meshes. An example is shown in Fig. 3.17. In the presented example all green facets are planar, therefore they can constitute guiding planes for RHS[52] rods without geometrical torsion. However, in such non-circular networks, the distances between vertices, facets nor edges are not constrained to constant lengths. Finally, vertex normals are less conjugated, i.e. in case of circular networks only one normal axis was arbitrarily chosen and the rest was derived from it, whereas in case of non-circular meshes a whole row or column of normal vector direction can be arbitrarily chosen.

[52] RHS – Rectangular Hollow Section

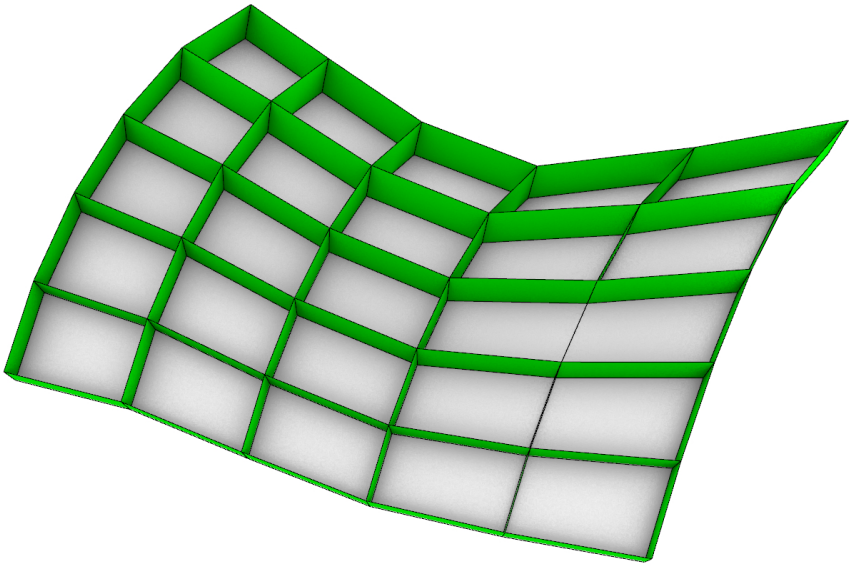

Fig. 3.17 An example of non-circular PQ mesh with torsion-free edges.

In general, torsion-free meshes exist only for very limited forms of triangular meshes, what is an additional argument for the PQ meshes as bases for the glazed grid shell design.

3.6. Form and form-finding

General form of a shell is one of the factors determining static performance of a structure. Such forms are preferred, for which normal forces in rods are dominant, i.e. compression and tensile forces. Vectors of such forces should be tangent to the surface of a shell. In grid shells forces are transferred by rods, which are optimal elements in transferring tensile and compressive forces. The presence of bending moments and shear forces in rods require increase of the cross sections of the rods, which is undesirable.

A form of a grid shell devoid of non-axial forces can be obtained using form-finding methods. In (Hassel 2016), Patrik Schumacher explains:

"Form finding is a physical setup where form self-organizes and it is not drawn by hand or invented or preconceived. It emerges in a physical process".

Examples of form-finding methods are the funicular model, force polygon, funicular polygon, force density method or thrust network analysis. Form-finding methods for shells are extensively discussed in *Shell Structures in Architecture: Form Finding and Optimization* (Adriaenssens et al. 2014). Diverse form-finding strategies are used for different grid shell requirements.

Arbitrarily shaped shells are also a subject of optimizations. A notable example of such optimization is the shell roof of Crematorium in Kakamigahara (Pugnale and Mario 2007), see Fig. 3.2, left. The shape of the shell was described with the use of NURBS surface with finite amount of control points, whose positions were parametrized. The factor to optimize was a minimum deformation of a shell under dead and live load. The genetic algorithm was used to find the optimal configuration of control point positions. The form was optimized by finding the best positions for each of the parametrized control points. The criterium of the optimization was minimalization of deflection of the shell under load. Genetic algorithms are abstract models which have no physical equivalent allowing for form-finding process in physical manner, whereas funicular forms and minimal surfaces are possible to obtain through both computer and physical simulations.

Apart from the form of grid shell, its tessellation also has influence on the static performance of a structure. However, PQ shells are geometrically constrained and available form-finding processes not considering those constraints are insufficient. The change of paradigm into the bottom-up one is therefore proposed for this reason. The space of possible morphologies should be narrowed by geometrical constraints in the first place, before the structural optimization of form-finding process is performed. Optimizing methods should be then able to find the best solution within the geometrically correct morphologies.

Tessellation of a form-found shape can result with less favourable result than optimizing a geometrically consistent PQ mesh.

3.7. Designing PQ *freeforms* in context of bottom-up and top-down approaches

In this section, three exemplary and selected methods are discussed for forming PQ meshes representing top-down, bottom-up and intermediate approach.

3.7.1. Top-down method example – conjugate curvature network

As fitting planar quadrilateral facets to a *freeform* surface is significantly difficult, a bottom-up approach for shaping a PQ grid shell is usually taken. However it is also possible to shape PQ grid shells using top-down approach.

Among top–down approaches the state-of-the-art method utilizes curvature line networks of predefined *freeform* surfaces (Liu et al. 2006), (Pottmann, Liu, et al. 2007). The method assumes determining on the free surface such a curved grid, which consists of two families of curves marked in red and blue colours in Fig. 3.18. Curves from the same family cannot cross each other, but can intersect with the curves from the other family. The way the curves intersect is strictly defined. A series of points along one curve (blue) is created by intersections with curves from the opposite family (red). From these points a series of lines (green) are designated in such a manner, that these are tangent to corresponding red curves (also, these green lines are tangent to the base surface). If the neighbouring tangent lines (green) lie on a common plane, they create opposite edges of planar quad. A series of these quads along one curve is called PQ strip, see Fig. 3.19. The network of curvature lines is proper, if the tangents create PQ strips. This condition is fulfilled, when the curves are the principal curvature lines, i.e. lines that follow greatest (red) and the smallest or opposite (blue) curvatures. The whole surface is panelized by assigning PQ strips along all curves from one family and intersecting neighbouring strips. The distances between the curves of the same family can be varied, therefore the dimension of the panels can be controlled.

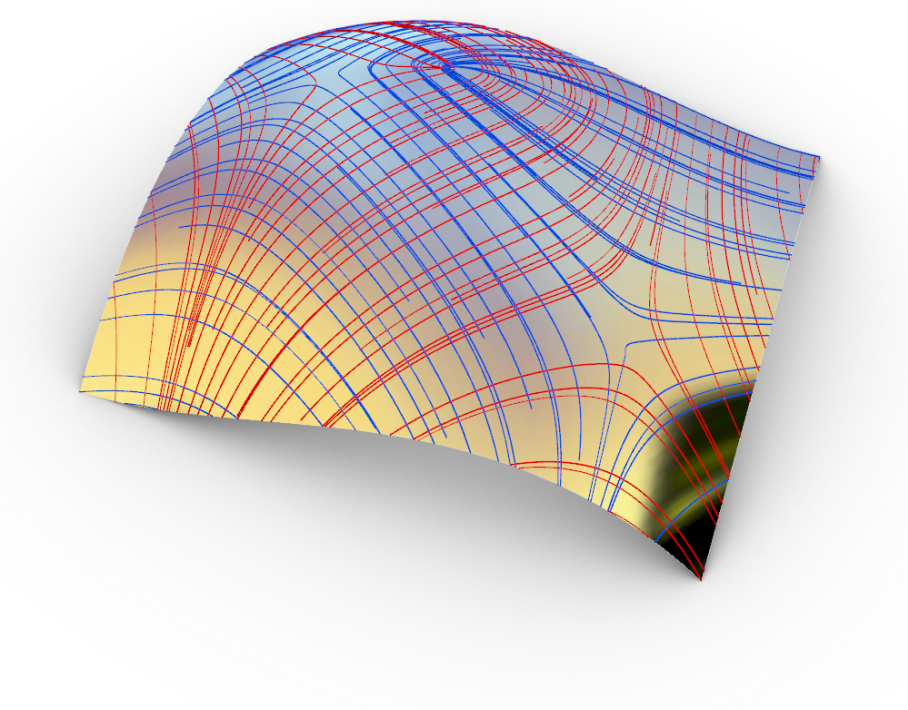

Fig. 3.18 Freeform surface covered by conjugated network of principal curvature lines

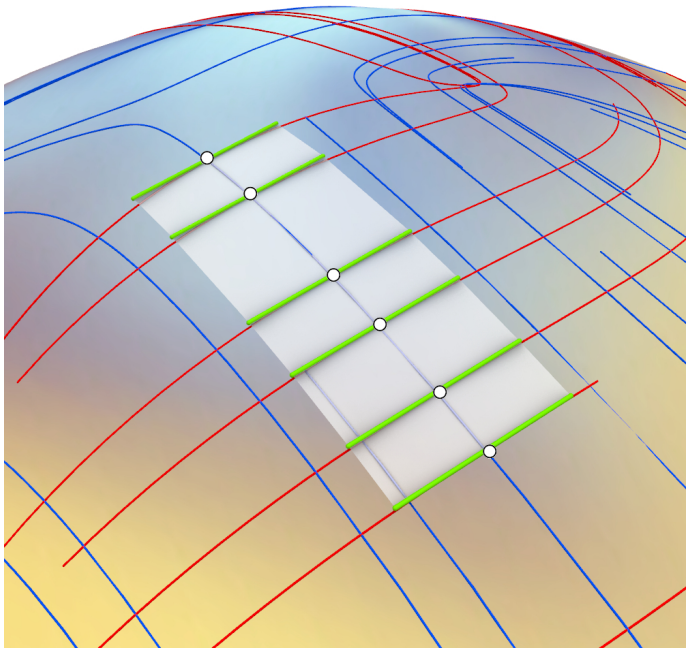

Fig. 3.19 PQ strip between lines (green) tangent to the consequent principal curvature lines

The weakness of this method is the inability to change direction of PQ strips, what may sometimes be necessary. Secondly, when the previously designed free formed surface has transitions between synclastic and anticlastic parts, the singularities occur. Finally, there are surfaces (and parts of surfaces) in which the curvatures in all directions are equal (e.g. a sphere). Therefore, the network of curves has to be assigned arbitrarily.

3.7.2. Bottom-up method example - Marionette

In the Marionette method[53] the global form of the PQ mesh is obtained algorithmically, from the user controlled parameters consisting of directrix and generatrix curves. In Fig. 3.20 each curve is represented in a form of two projections – vertical and horizontal. Designer also have to define quadrilateral mesh on plane. Each vertex of that mesh in planar configuration is iteratively projected on a plane already containing three other vertices of the final mesh. The first set of three vertices of final mesh is at the corner, where directrix and generatrix intersect. As new vertices are projected, new planes for further projections are created until all vertices from the planar mesh are projected and construct PQ mesh.

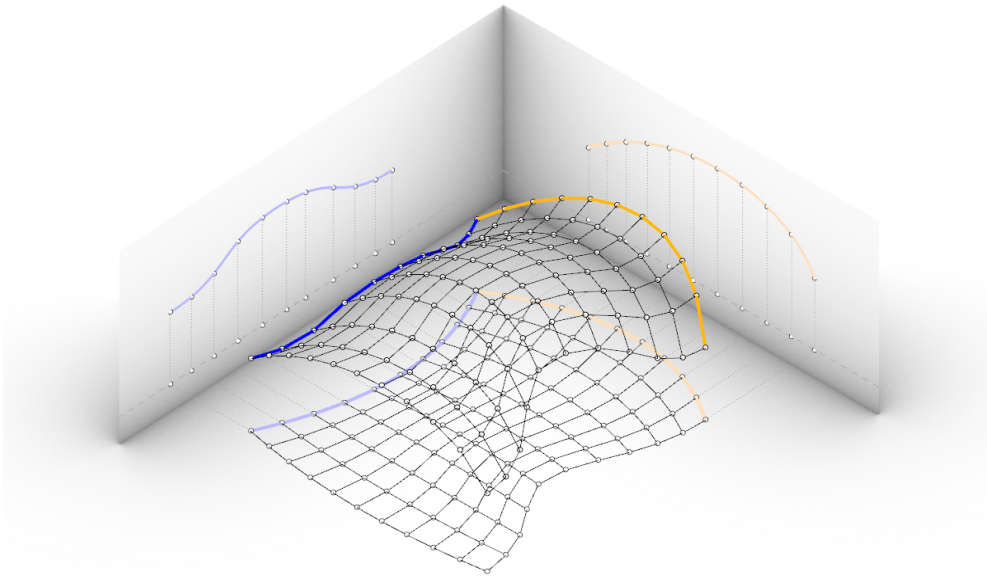

Fig. 3.20 PQ mesh designed with the use of Marionette method. Two profiles (blue and orange, directrix and generatrix) are user defined.

In this method there is no necessity of defining the shape of a continuously curved surface. The tessellation (topology) and user defined parameters control the final shape, therefore the method works according to the bottom-up paradigm.

3.7.3. Mesh subdivision method

Other method, which stands between top–down and bottom–up method, uses mesh subdivision and planarity optimization iterative algorithm. According to this method, a global shape of the roof or façade is roughly defined by few facets (significantly bigger comparing to final ones), which are iteratively subdivided and planarized (Pottmann, Asperl, et al. 2007), p. 684. This method uses algorithm which was originally devised for the purpose of 3D animation by Edwin Catmull[54] and Jim Clark in Pixar studio (Catmull and Clark 1978). Its greatest advantage is the ability to consider various topological properties of the global form like holes, funnels or wormholes (see Fig. 3.22) between two meshes, what brings the consequences of topology change, i.e. more or less than four bars connected in one node. In Fig. 3.21 some vertices in the last stage are 3- or 5-valent, analogically to corresponding vertices from the first stage of subdivision.

---

[53] Marionette method is described in [74] and [75], also in the section 4.1.6.
[54] The founder of Pixar Studio.

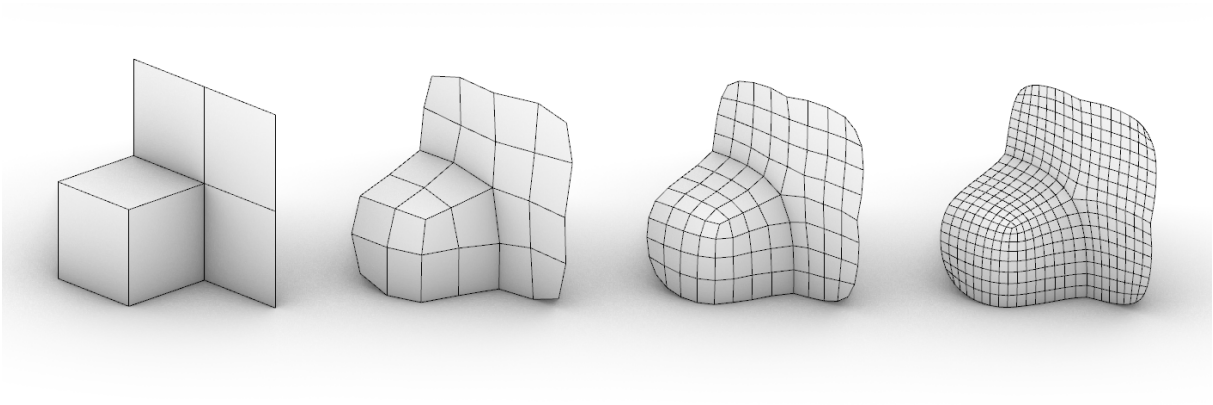

Fig. 3.21 Consecutive stages of subdivision and planarization steps.

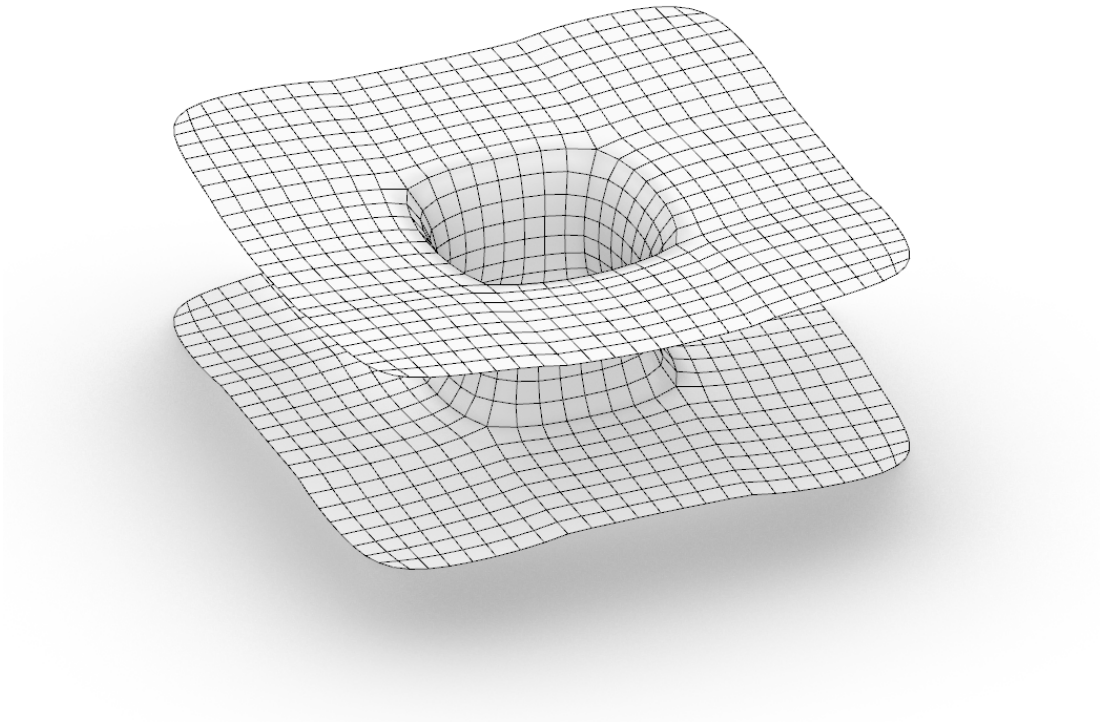

Fig. 3.22 PQ mesh containing a wormhole.

Although the method is suitable for meshes, where the required morphology is complex, i.e. containing holes, funnels or wormholes it also imposes the planarization step, what in case of doubly curved grid shells based on planar perimeters would lead to solutions, in which the resultant mesh would be completely flat.

4. Methods of formation of PQ meshes

This section describe selected methods of shaping the PQ mashes representing the bottom–up approach. They cover only *Form* and *Tessellation* parts of this approach. The *Mechanics* is not taken into consideration. The recognition of the rules of how to create PQ grid shells according to the bottom-up approach, offers the opportunity to recognise the possibilities and the range of freedom of their design. Parametrization of the formation methods allows the optimization algorithms (e.g. genetic algorithms) to be further applied.

The following section 5 describes the methods of transformation of PQ meshes, which preserve the planarity and topology of meshes.

4.1. The existing methods of formation

The methods described in this section have been adopted previously for the design and construction of glazed grid shells or have been proposed as methods for designing grid shells.

A PQ mesh is a system of vertices, edges and facets that are characterized by the following features:

- all facets are quads, i.e. they contain exactly 4 edges and 4 points;
- all points incident with a facet lie on the common plane, i.e. corresponding points are co-planar;
- all edges incident with a facet create a convex, simple quadrilateral, i.e. non self-intersecting, closed polygon.

One of the most simple objects that fulfil the above requirements is a cube, Fig. 4.1. It has 6 facets, all of which contain exactly 4 edges and 4 points. All points that surround each facet are co-planar. Finally, all edges that surround a facet create convex and simple quadrilateral polygon, i.e. a square.

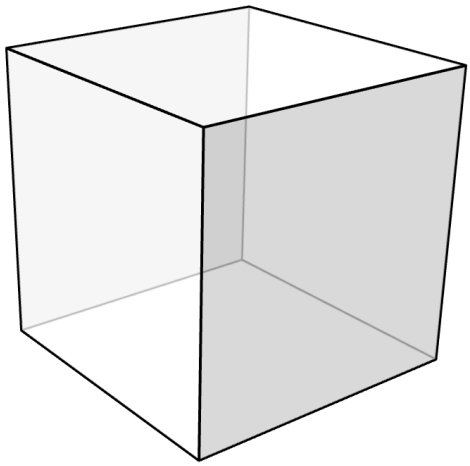

Fig. 4.1 Cube

What is more, in this case all edges are incident with exactly two facets. That is because the cube is a solid object and all facets tightly close the space within the cube. It is not required for the PQ form, in which open edges which are incident with one facet are allowed.

Figure 4.2 shows an example of the PQ form whose all facets are congruent and lie on the same plane. Those two simple examples are important for the future considerations as a determinants of validity. Any strategy that is valid for a complex case is inadequate if fails for a simple case.

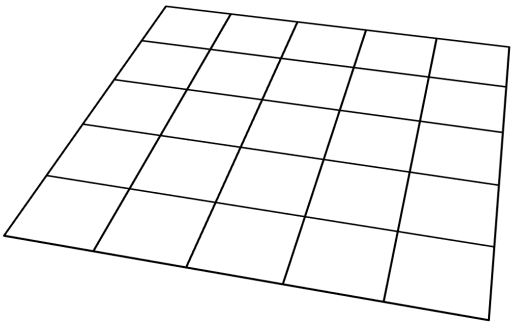

Fig. 4.2 Planar PQ mesh

4.1.1. Translational method

A single quadrilateral created from two pairs of points, where the second pair is image of translation of the first pair, fulfils all the requirements for PQ grids. Simplest case of such transformation is shown in Fig. 4.3. Translation of the line segment AB by vector *v* produces another segment A'B' which is parallel to the previous one. Together with two additional segments (AA' and BB'), a facet surrounded by exactly 4 points and 4 edges is obtained. This fulfils the first requirement.

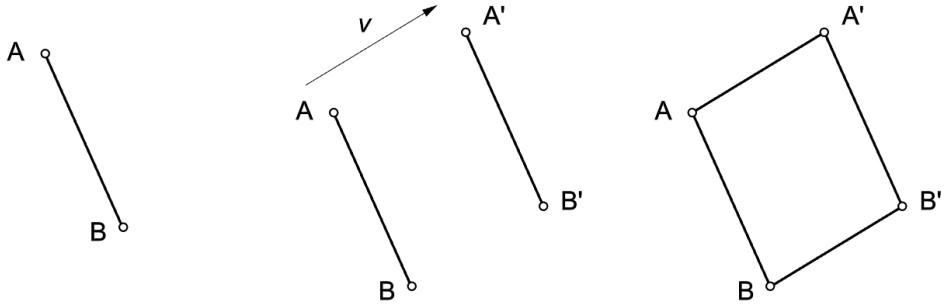

Fig. 4.3 Parallelogram - a simple planar quadrilateral

The sufficient condition for coplanarity of lines is their parallelism. Segments AA' and BB' are parallel, because they are directed along the same vector *v*. Also AB and A'B' are mutually parallel, because translation does not change the direction. Consequently, all segments and all points lie on the same plane, what fulfils the second requirement.

Finally, the obtained quad is a parallelogram which is contained in a set of simple-quads. That fulfils the third requirement.

This simple construction allows to be performed on more complex sets of line segments producing strips of planar quads, see Fig. 4.4. Any pair from a set of line segments: AA', BB', CC', DD' and EE' is mutually parallel.

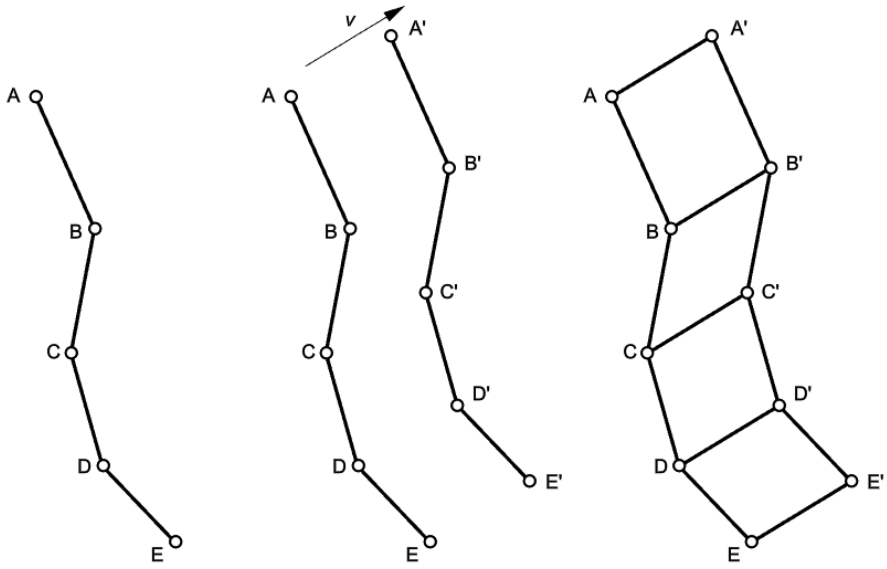

Fig. 4.4 PQ strip of parallelograms

Repeating the steps of applying new vector of translation to the lately created set of points, allows to produce a whole mesh of planar quads, see Fig. 4.5.

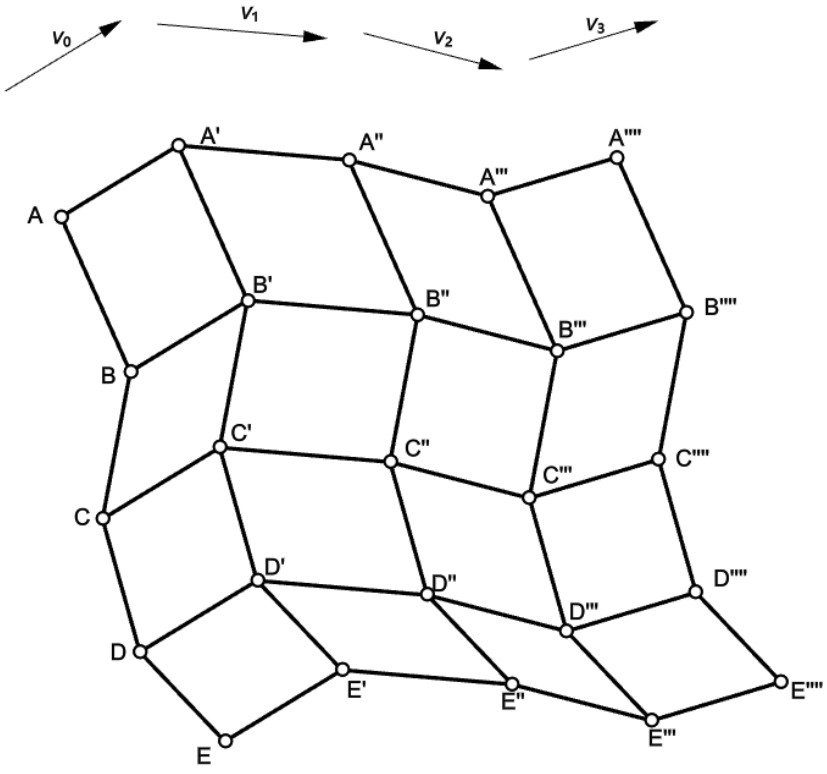

Fig. 4.5 Translational PQ mesh

The same mesh would be obtained if the polygonal chain is created with the use of points: A, A', A'', etc. and would be translated with the use of the vectors $\overrightarrow{AB}$, $\overrightarrow{AC}$, $\overrightarrow{AD}$, etc., see Fig. 4.6.

Each vector can also be denoted as a pair of points on a curve. By shifting the positions of the points on curves, the sizes of the facets can be manipulated, while preserving all of the required properties for the PQ meshes.

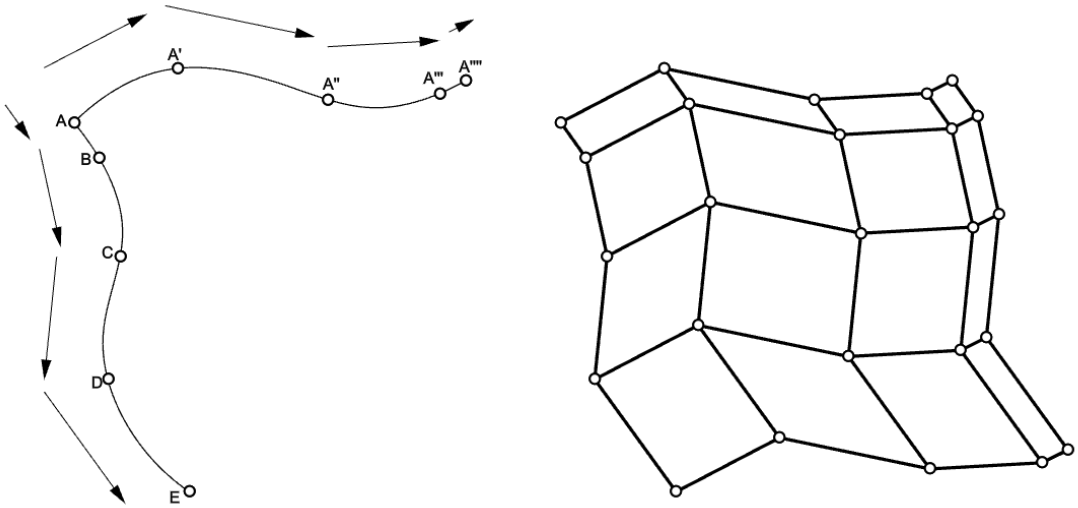

Fig. 4.6 PQ mesh generated from continuously curved directrix and generatrix.

The PQ meshes described so far, lie on a plane but the objective is to construct a doubly curved grid shell. As a matter of fact, if curves containing points do not lie on a common plane or are not even planar, the method will still be valid for PQ meshes. In such case, the created grid is three dimensional, see Fig. 4.7.

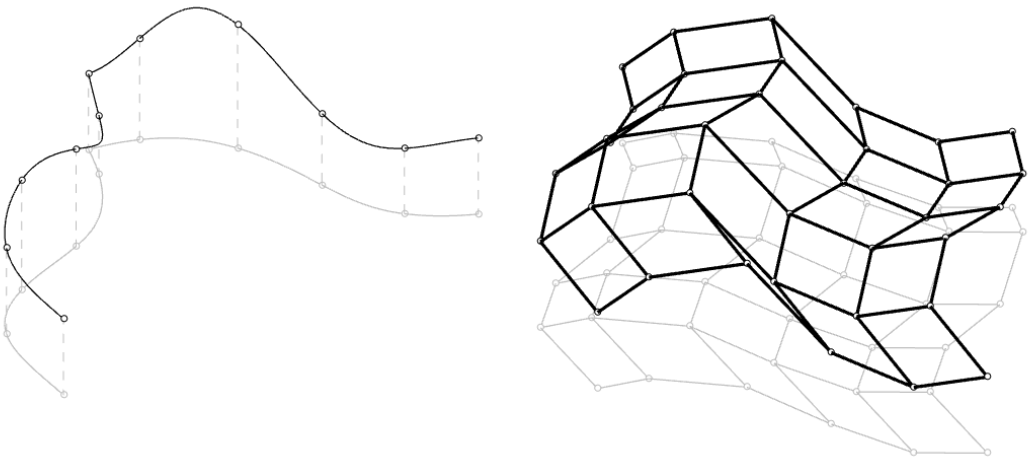

Fig. 4.7 PQ mesh from spatial curved directrix and generatrix

Such a mesh is also a discrete equivalent for a translational surface (Fig. 4.8), i.e. the surface which is generated by sliding a generatrix curve along directrix curve. Both directrix and generatrix can be treated interchangeably.

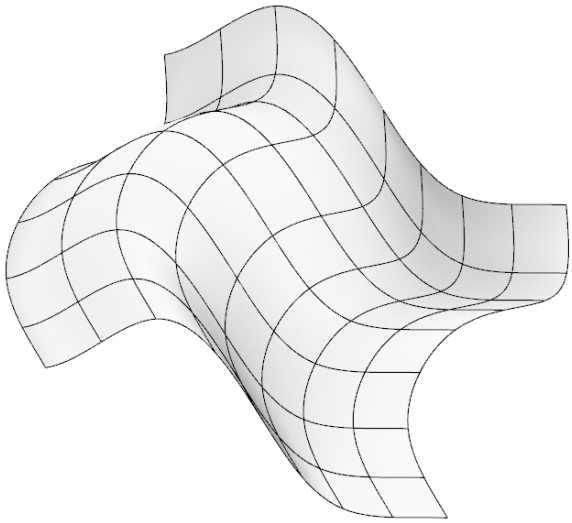

Fig. 4.8 Translational surface

In architecture, translational PQ grid shells are used frequently. Important examples are the Museum of Hamburg History glass roof shown in Fig. 4.9 and glass roof of the House for Hippopotamus in Berlin Zoo, shown in Fig. 4.10.

Fig. 4.9 The glazed canopy over the courtyard of Museum of Hamburg History - an example of translational PQ grid shell.[55]

[55] The geometry was additionally optimized changing some parts of translational mesh, see appendix A-3, p. 293.
Sources:
http://www.gmp-architekten.com/typo3temp/_processed_/csm_06_L_2549-01_a79814d9a4.jpg,
http://www.gmp-architekten.com/typo3temp/_processed_/csm_05_L_2513-01_0f9457573f.jpg.

It is worth mentioning, that most of the glass panels in the first example are planar quads obtained through translational method, however some panels near the corners of the dome were divided diagonally into two triangles for the sake of structural optimisations, see (Schober 2015b), p. 46.

Fig. 4.10 House for Hippopotamus, Zoo Berlin - an example of translational PQ grid shell.[56]

Translational meshes are discussed in (Schober 2015b), pp. 51–52.

4.1.2. Translational with planar base method

A successful application of translational method was introduced in the design of glazed roof over Rennes University Library courtyard, see Fig. 4.11. The glazed lattice shell was based on PQ, translational grid, which was constrained by a planar, rectangular outline of the courtyard. The method of its creation is described in (Menard, Fayette, and Azzopardi 2013) and was recreated by the author for further analysis.

To ensure the planarity of panels for the grid, previously described translational method was applied. The planarity of the grid base was ensured by a proper construction of the directrix and generatrix curves used to create translational curvilinear network. According to (Menard, Fayette, and Azzopardi 2013), both directrix and generatrix curves are the same curves. Each one consist of 4 symmetrical segments: C_1, C_2, C_3, C_4, see Fig. 4.12.

Segment C_1 is a point symmetry of C_2, the other two segments C_3, C_4 are a mirror symmetry of C_1 and C_2. Each segment is a second degree spline curve interpolated between two points and extrapolated by one point P_e which position is parametrized, see Fig. 4.12, left and formula (4.1).

[56] See appendix A-3, p. 294, source: https://www.sbp.de/fileadmin/sbp.de/projects/0559DF968B4E8CE1C1257E750035BD85_0_1_1642_97_a_MAX.jpg

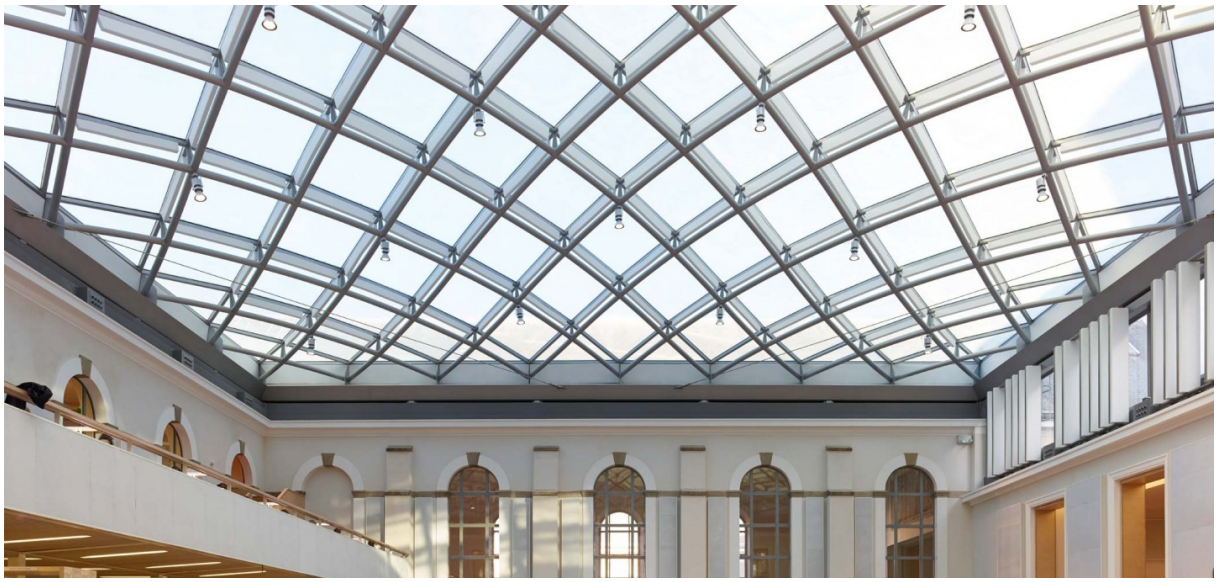

Fig. 4.11 Bibliothèque Universitaire Rennes – an example of PQ translational glazed canopy with planar base.[57]

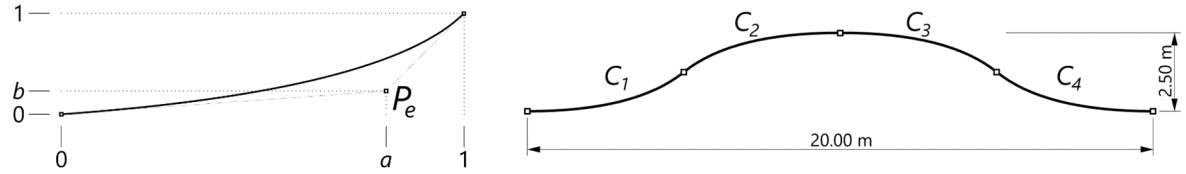

Fig. 4.12 Left: construction of the C_1 segment curve, parametrized by the $P_e(a,b)$ extrapolated point. Right: construction of the profile curve composed of C_1, C_2, C_3 and C_4 segments.

$$\boldsymbol{P_e} = [\boldsymbol{a}, \boldsymbol{b}]: \boldsymbol{a} \in \langle \mathbf{0}, \mathbf{1} \rangle, \boldsymbol{b} \in \langle \mathbf{0}, \mathbf{1} \rangle \tag{4.1}$$

By changing the P_e parameters different shapes of the profile curves are obtained, see Fig. 4.13. For values of *b* greater than 0 the profile curve breaks curvature continuity at the middle, see Fig. 4.13, right, whereas if *a* = *b* the profile is composed of two straight sections.

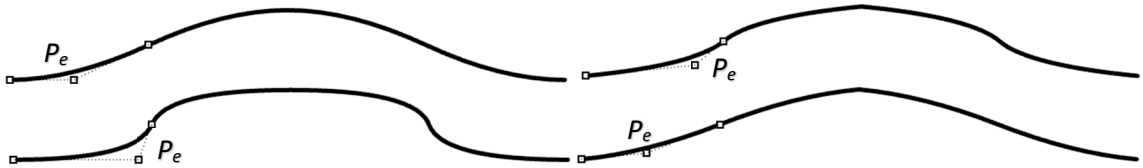

Fig. 4.13 Examples of possible shapes of the profile curve according to the position of P_e extrapolating point. Left: for b = 0 the profile curve has G1 continuity at whole span; right: for b > 0 the profile curve has G0 curvature continuity (in the middle).

A curvilinear network created from the profile curves is trimmed by a horizontal plane, see Fig. 4.14. That intersection is a perfect, planar square marked in blue color in Fig. 4.14, right. In order to fit the base plane into a rectangular shape, the network can be scaled anisotropically[58] along the selected base edge.

[57] Source: http://www.bruno-gaudin.fr/images/projets/352/357.jpg
[58] See anisotropic scale transformation in section 5.1.1.5.

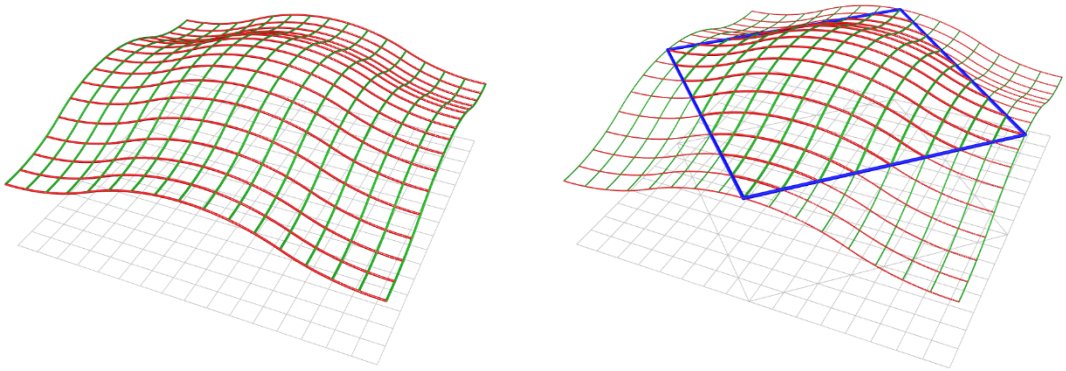

Fig. 4.14 Perspective views of a curvilinear networks obtained as a translational network with the profile curves as directrix and generatrix (red and green). Blue rectangle (right) marks the intersection of a translational surface with a horizontal plane.

Intersections of curves in created curvilinear network are points that create panels' outlines. A projection of this network on the horizontal plane is a regular square grid.

Possible shapes depending on the values of the *a* and *b* parameters are shown in Fig. 4.15. The space of *a* and *b* parameters contain parts, where the shapes of curvilinear networks lack curvature continuity along the diagonals. Also, pyramidal form is possible to obtain for particular combination of *a* and *b* values.

PQ mesh is obtained from curvilinear network by circumscribing quads on the points of intersection between directrix and generatrix curves of the network, theses quads are planar.

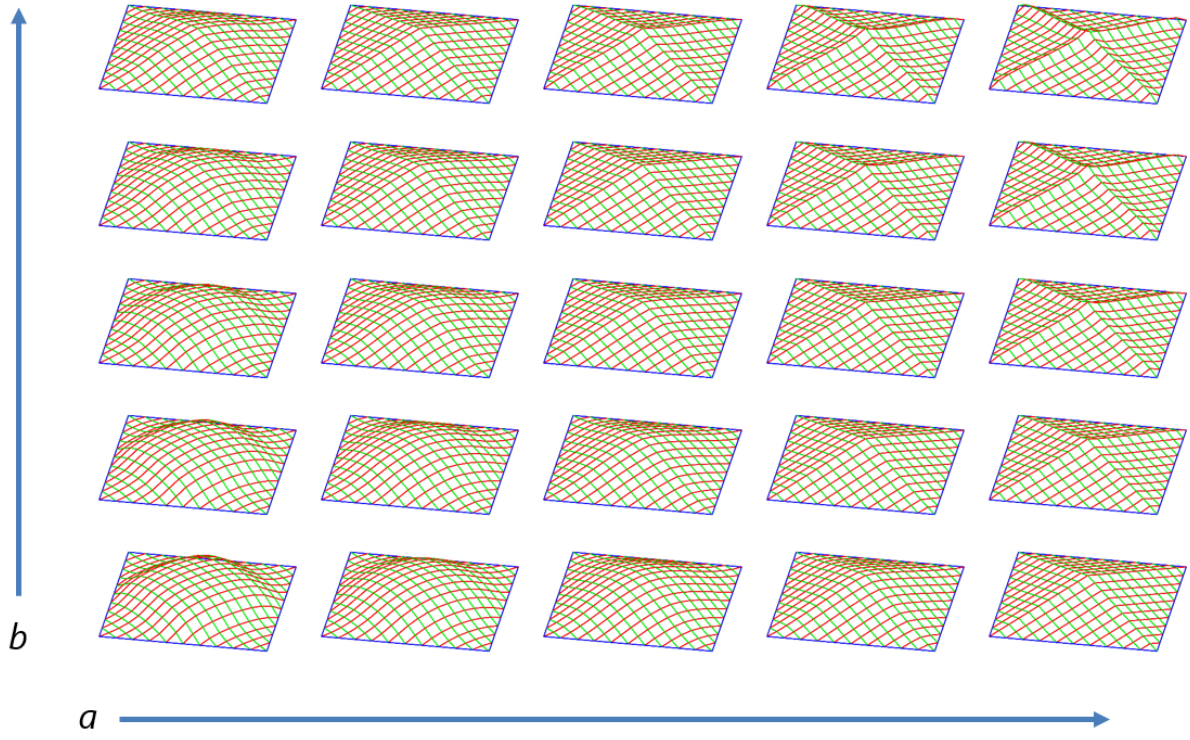

Fig. 4.15 The diagram of possible curvilinear networks depending on the values of a *and* b *parameters.*

4.1.3. Scalar-translational method

Beside translation, there is another transformation that preserves parallelism of line segments, which is a sufficient condition to construct PQ meshes. It is uniform or isotropic scaling. This transformation is characterised by a centre point and a factor. In the following example a planar quadrilateral trapezoid is created by scaling the line segment *AB*, see Fig. 4.16. Image of transformation, the *A'B'* segment, is parallel to *AB* and therefore quad *ABB'A'* is also planar. The opposing edges *AA'* and *BB'* are no longer parallel as it was in the previous method. Nonetheless, the parallelism of the opposing edges is only a sufficient but not necessary condition for PQ meshes.

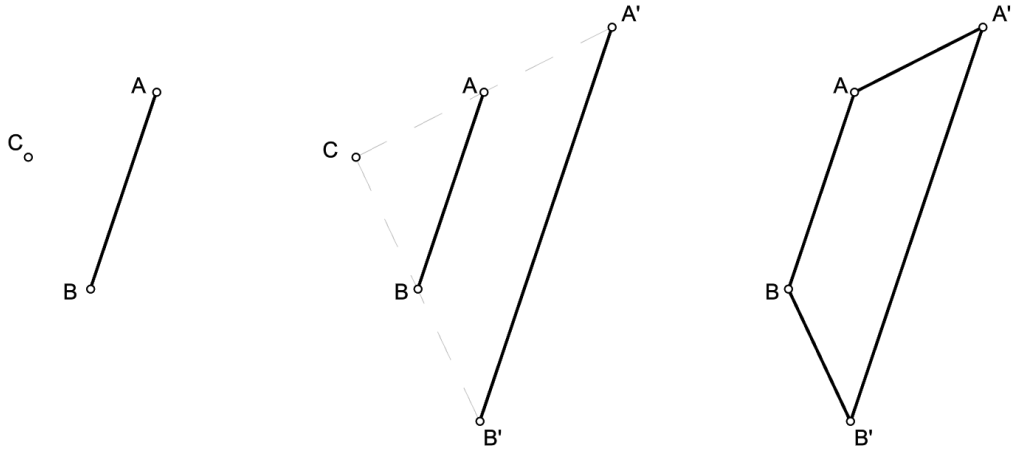

Fig. 4.16 Construction of a planar trapezoid obtained by scaling of a line segment.

Scaling can be combined with transformation of translation as both transformations preserve parallelism. *A''B''* segment is an image of translation of *A'B'* segment along vector *v*. The resulting *ABB''A''* quad is still planar, see Fig. 4.17.

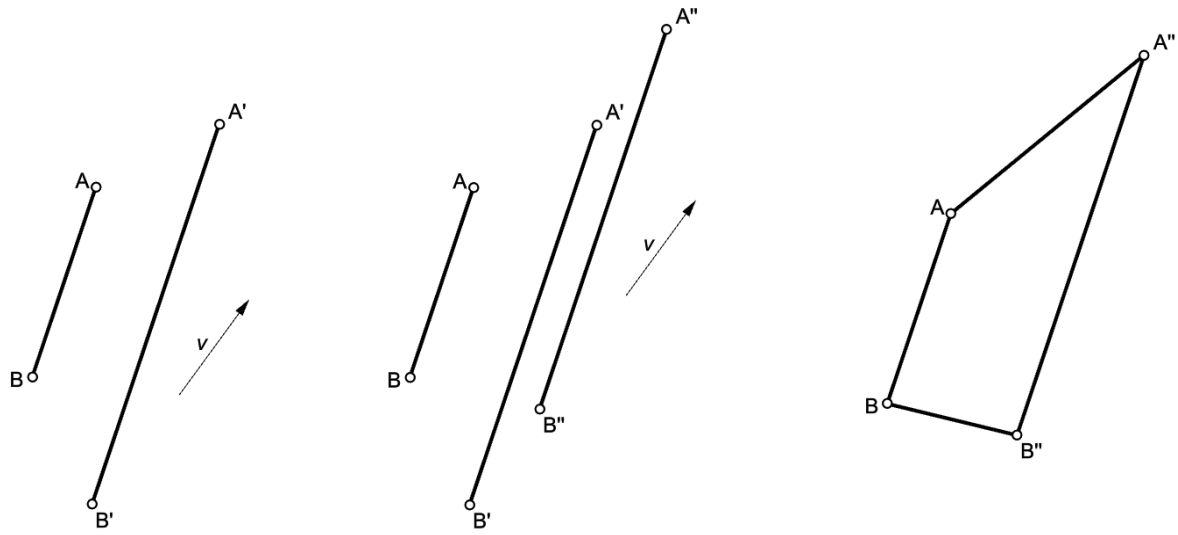

Fig. 4.17 Construction of a planar trapezoid obtained by scaling and translation of a line segment

Order of performing the transformations is important. Scaling before the translation will not result with the same image as translation of a scaled object. In order to obtain the same result the centre of scaling transformation has to be translated together with the object, if the desired order is the translation and then scaling.

In the reversed procedure, where the line segment, translation vector, scaling factor and centre points are known, the centre of scaling has to be translated along the vector in order to obtain the same results as in Fig. 4.18. Points A', B' and C' are the images of translation the *v* vector. In the next step line segment *A''B''* is obtained by the scale transformation of *A'* and *B'* points from the *C'* centre point. The scale factor is preserved.

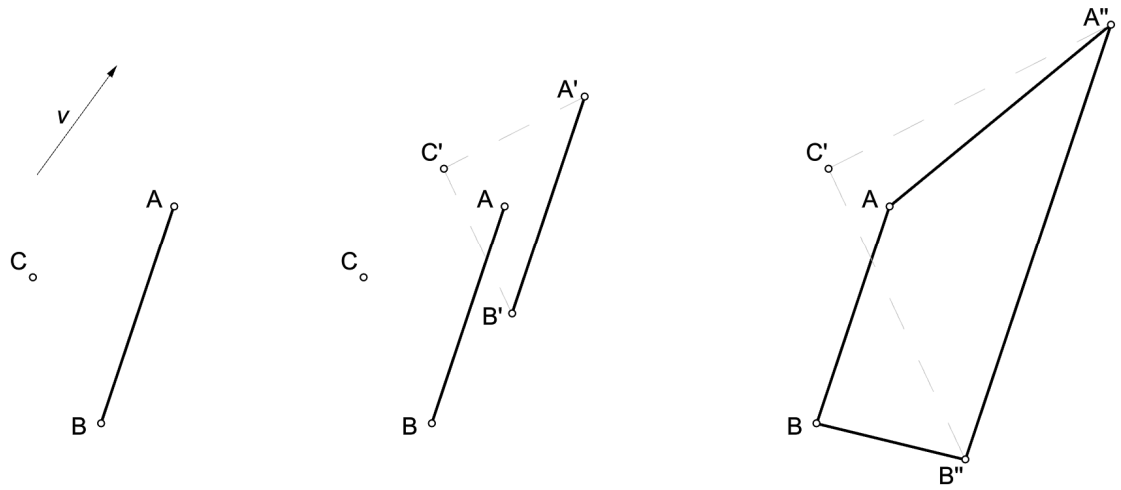

Fig. 4.18 Construction of a planar trapezoid obtained by translation and scaling of a line segment

Performing scale-trans transformations on a chain of segments results in a strip of planar quads, see Fig. 4.19. There should be only one centre point for scaling for all segments in a chain, however, at each step different centre point and scale factor can be used.

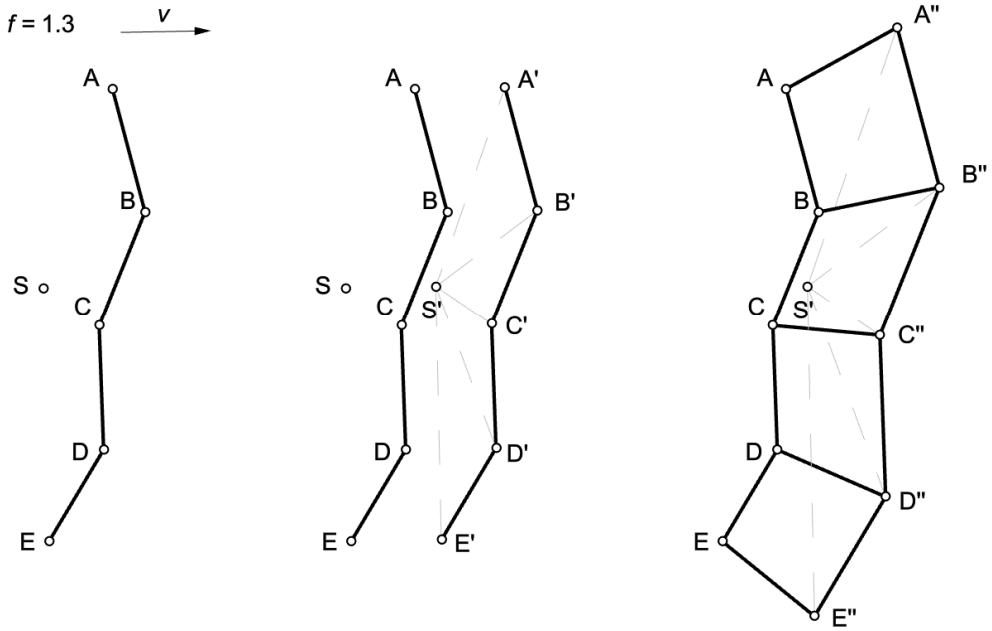

Fig. 4.19 A chain o planar trapezoids obtained by translation and scaling

Instead of defining a centre point for scaling each PQ strip a different approach can be taken. Scale factors, translation vectors and centre points can be derived from a continuously curved directrices and a generatrix curves as in Fig. 4.20. Generatrix curve ***g*** can be a spatial curve.

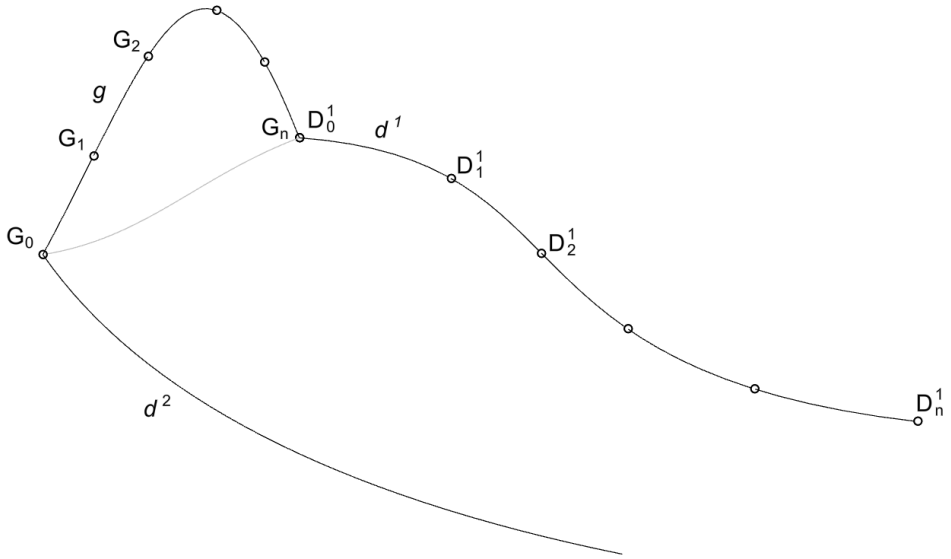

Fig. 4.20 Continuously curved directrices d^1, d^2 *and a generatrix* g.

In Fig. 4.21 the generatrix curve ***g*** contains a set of points G_0 to G_n, whereas from two directrix curves d^1 and d^2 only the first one contains points: from $D_0{}^1$ to $D_n{}^1$. Subsequent translation vectors are created by the pairs of points $D_i{}^1$ and $D_{i+1}{}^1$. The ***g*** curve, together with the points it contains, is translated along these vectors. The scaling centres for the following $g_n - g_{n+1}$ curves are corresponding to $D_i{}^1$ points.

In order to get scaling factors, another set of points has to be created on the second directrix curve d^2. These points are projections of $D_i{}^1$ points on the d^2 curve along the G_nG_0 vector. The scaling factors are equal to the quotient between $|G_0G_n|$ and $|D_i{}^2D_i{}^1|$. The resultant PQ mesh is shown in Fig. 4.22.

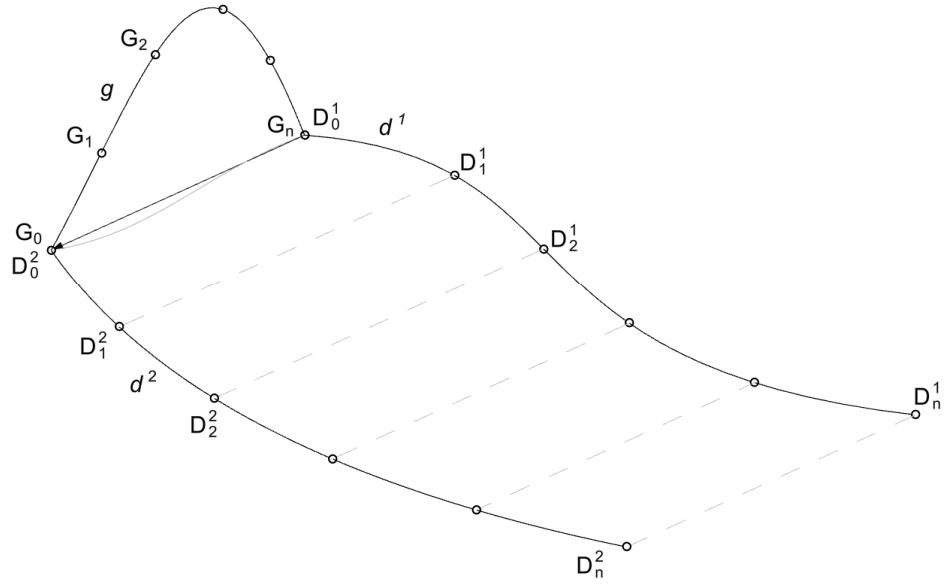

Fig. 4.21 Consequent $D_n{}^2$ *points derived from projections of* $D_n{}^1$ *points along the* d^1 *directrix curve.*

The corresponding edges $G_i{}^jG_{i+1}{}^j$ and $G_i{}^{j+1}G_{i+1}{}^{j+1}$ are parallel. As a result of this fact the sufficient condition for PQ mesh is fulfilled. The curve ***g*** not necessarily has to be planar.

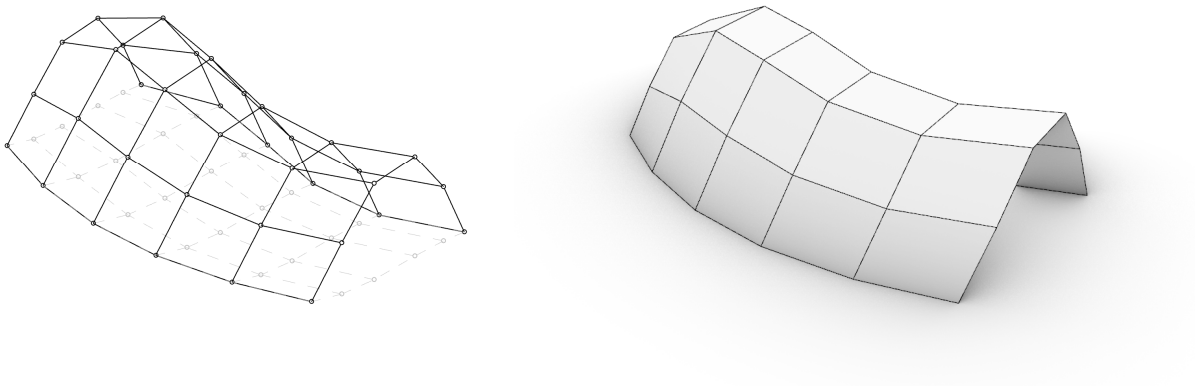

Fig. 4.22 A scalar - translational PQ mesh. Right: the same mesh with shading.

This approach allows to obtain a PQ mesh with user specified shape of the boundary. The global form is the result of these user controlled parameters and the scaling–translation rules. Most notable example of this approach is Sage Gateshead building, see Fig. 4.23.

Fig. 4.23 Sage Gateshead - architecture: Foster + Partners. An example of scalar - translational PQ mesh.[59]

Presented scalar translational PQ meshes are also partially described in (Glymph et al. 2004) as scale-trans surfaces, and more widely in (Schober 2015b), pp. 124–131.

[59] See appendix A-3, p. 301, source:
https://upload.wikimedia.org/wikipedia/commons/4/49/The_Sage_Gateshead.jpg

4.1.4. Rotational method

The last presented basic transformation that allows to create PQ meshes is the rotation. A planar rotation is characterized by a centre point and an angle. In 3D space a centre point is insufficient, therefore an axis or a centre point and a plane of rotation have to be additionally defined.

The image of rotation of the line segment *AB* around the centre point *O* by the angle *α* (or *β*) is the line segment *A'B'*, see Fig. 4.24. Neither *AB* and *A'B'*, nor *AA'* and *BB'* are parallel, therefore resulting quads are neither parallelograms, nor trapezoids. The ABB'A' quad is planar due to the fact that both: line segment *AB* and the centre of rotation *O* lie on a common plane.

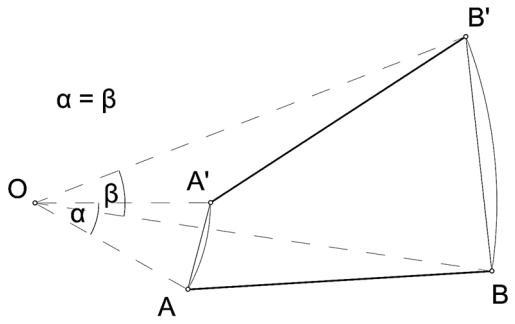

Fig. 4.24 Planar quadrilateral obtained by a rotation of a line segment.

For a rotation in space, the resultant quads are not parallelograms or trapezoids without additional constraints. In order to produce quad with at least one pair of parallel edges the required condition is that the centre of rotation and the primary line segment lie on a common axis, see Fig. 4.25. Newly created quad is a isosceles trapezoid since *AB* and *A'B'* have the same lengths, and *AA'* and *BB'* are parallel one to another.

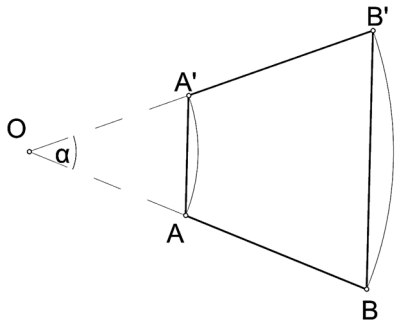

Fig. 4.25 An isosceles trapezoid obtained by a rotation of a line segment. The rotation point O is colinear with the rotated line segment.

In 3D space, a rotation is performed around an axis. In order to produce two line segments that are parallel one to another, the original points have to be placed on plane which contains the axis of rotation, see Fig. 4.26, right.

The rotation in Fig. 4.26 is performed around the vertical axis ***r***, which is perpendicular to the horizontal plane of projection. The intersection of the ***r*** axis with the horizontal plane is marked with the point ***O***. The projection of line segment ***AB*** on the horizontal plane is a line segment that is not colinear with the ***O*** point. The ***AB*** segment is not co-planar with the ***r*** axis. The resultant ***ABB'A'*** quad in the Fig. 4.26, left, is not planar.

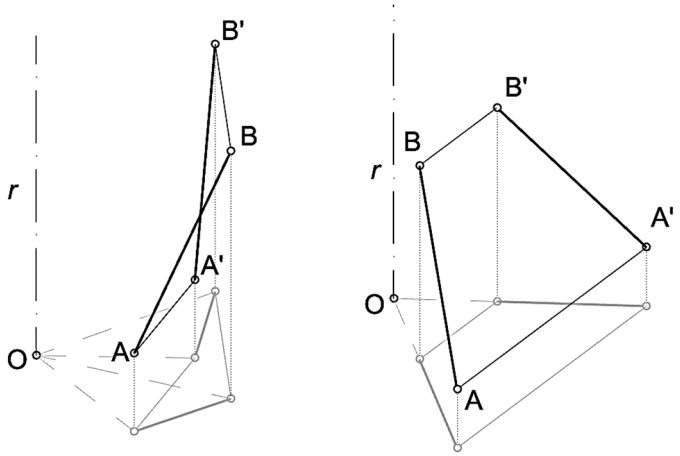

Fig. 4.26 Rotation around an axis. Left: non-planar quad. Right: planar quad - the AB *line segment and* r *axis lie on a common plane.*

In the second case (Fig. 4.26, right), ***A***, ***B*** and ***r*** lie on the common plane and projections of ***A*** and ***B*** are co-linear with ***O***. The image of rotation creates ***A'B'*** segment, whose projection on the horizontal plane containing ***O*** is a line segment, also co-linear with ***O***.

The projected quadrangle $A_pA_p'B_p'B_p$ in Fig. 4.27 is an isosceles trapezoid with pair of points A_p-A_p' and B_p-B_p' equally distanced to the point ***O***. Line segments A_pA_p' and B_pB_p' are parallel. Points ***A*** and ***A'*** lie on the same level over the horizontal plane, i.e. $|A_pA| = |A_p'A'|$. Also $|B_pB| = |B_p'B'|$. Therefore, pairs ***BB'*** and ***AA'*** are also parallel. Finally the quad ***AA'B'B*** is planar and has circumcircle.

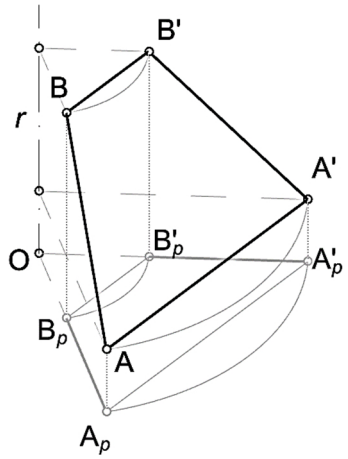

Fig. 4.27 Isosceles trapezoid obtained by a rotation

Rotating chains of segments around the axis by sequences of angles, create rotational PQ meshes which are discrete representations of rotational surfaces, see Fig. 4.28.

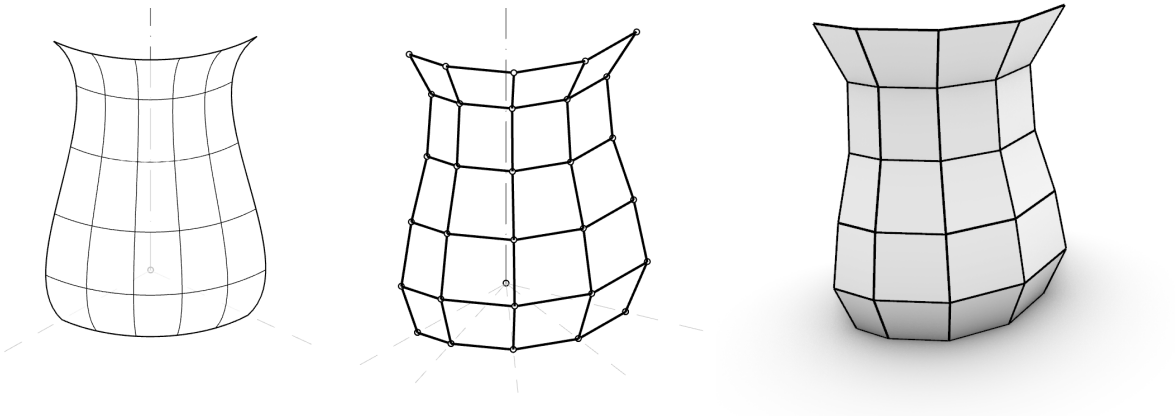

Fig. 4.28 Left: rotational surface, centre: the same surface discretized, i.e. the PQ mesh obtained by rotation. Right: rotational PQ mesh with shading.

In Galeria Katowicka shown in Fig. 4.29 the vertical axis of rotation lies within the glazed façade.

Fig. 4.29 Galeria Katowicka, Katowice.[60]

In Pearl River Tower shown in Fig. 4.30 the vertical axis of rotation is situated in front of the building. The form of the building's elevation is simple and balanced, i.e. the glazed façades are doubly curved and maintain significant repeatability of glazed panels and nodes.

[60] See appendix A-3, p. 322, source: http://pl.apsysgroup.com/wp-content/uploads/2015/12/GaleriaKatowicka_12.jpg

Fig. 4.30 The Pearl River Tower, Guangzhou.[61]

In Jaca Ice Pavilion (Fig. 4.31) the axis of rotation is horizontal and lies underground. The rotated chain of segments is inscribed in circle and the whole figure of rotation is a torus.

Fig. 4.31 Jaca Ice Pavilion, Spain. Right: scheme of the mesh.[62].

[61] See appendix A-3, p. 308, source:
http://legacy.skyscrapercenter.com/class-image.php/userpics/10005/?width=1000&height=800&image=/images/albums/userpics/10005/PearlRiverTower_ext-LookingUp6(c)TM.jpg

[62] Sources: https://www.arup.com/-/media/arup/images/projects/j/jaca-ice-pavilion/2000x1125-jacaicerink.jpg

Additional advantage of the rotational mesh is the fact, that all facets are isosceles trapezoids and therefore are also cyclic quadrilaterals[63]. This geometrical property has mechanical meaning, which is explained in the section 3.5.4 Circular meshes.

The method of creating PQ meshes with rotations is described in (Schober 2015b), pp. 64–66.

4.1.5. Sweep method

Following presented method is further discussed in (Pottmann, Asperl, et al. 2007) pp. 431–433 and (Mesnil, Douthe, Baverel, Léger, et al. 2015). In (Schober 2015b), pp. 67–69 part of the method using rotations is named *arrays of surfaces of revolution*. In the following method a freeform guiding (or directrix) curve not necessarily have to be planar. A directrix curve contains a point which is also a common point between that curve and a vertical plane. The projection of that plane on a horizontal plane intersects with the projection of the curve perpendicularly, see Fig. 4.32.

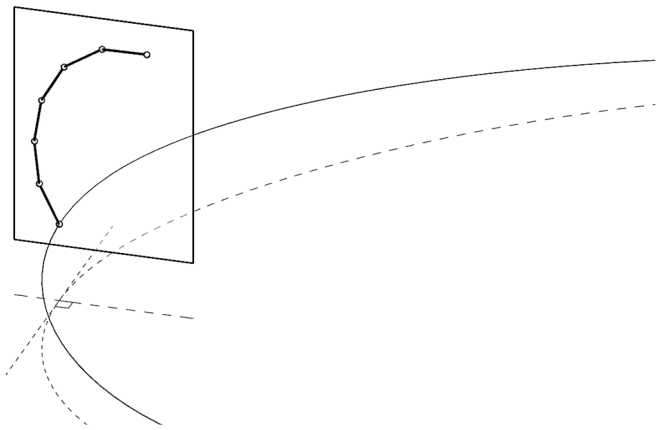

Fig. 4.32 The chain of segments lies on a vertical plane, which is perpendicular to the projection of the directrix curve.

The vertical plane also contains a profile chain of segments, i.e. a generatrix. These segments need to be transformed along the spatial directrix curve in such a manner, that the corresponding vertices of consequent generatrix chains produce planar quads. In order to specify the following generatrix chains it is required to generate the vertical planes that will contain them. Those planes should contain selected points lying on the spatial directrix curve and their projections on the horizontal plane should intersect perpendicularly with the projection of the directrix curve, see Fig. 4.33.

The intersections of consequent pairs of planes are vertical lines, which can be used as axes of rotations, see Fig. 4.34, left. Since the directrix curve is spatial and the planes are vertical, the image of a rotation of the generatrix chain of line segments is not incident with the point contained on the directrix curve. The resultant generatrix profile requires translation on its plane in order to touch the directrix curve, see Fig. 4.34, right. However, the resultant composition of rotation and translation transformations results with non-coplanar pairs of line segments generated by original points and their projections.

---

https://www.arup.com/~/media/Images/Projects/J/Jaca_Pavilion/Jaca5218x275CreditsArup.ashx?bc=ffffff&as=1&mw=218&thn=0&w=218

[63] The opposite angles in isosceles quadrilateral sum to π radians, therefore meet the condition for cyclic quadrilateral.

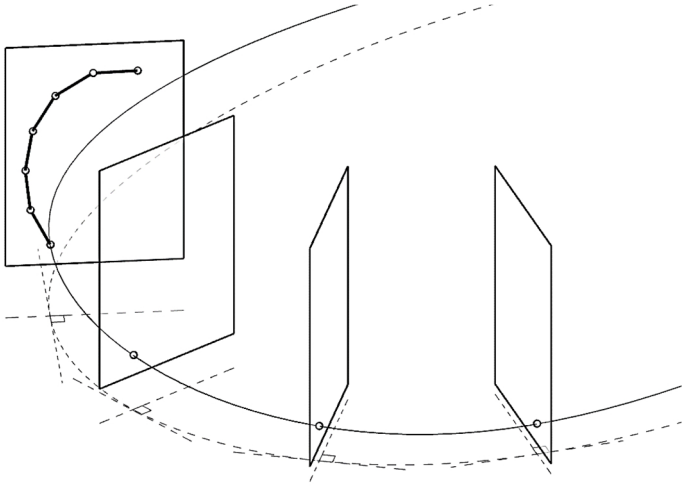

Fig. 4.33 Consequent vertical planes perpendicular to the projection of a directrix curve.

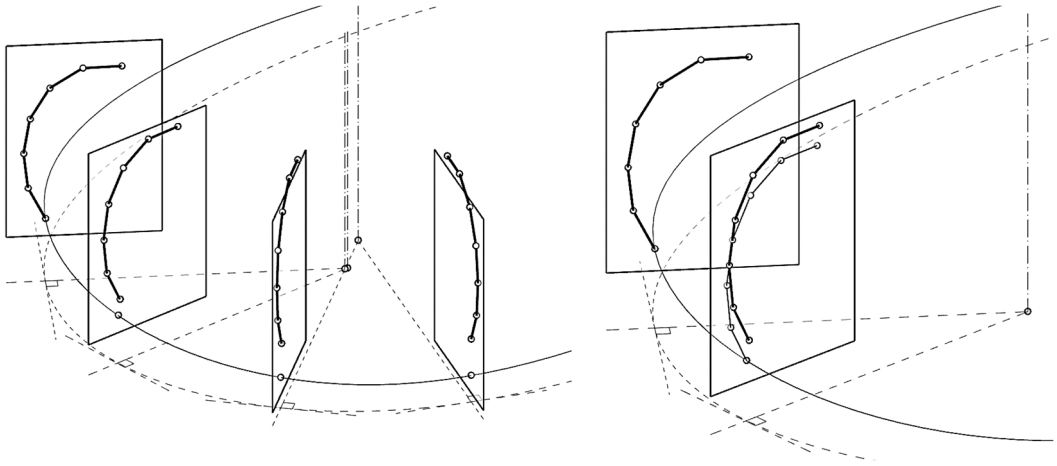

Fig. 4.34 Left: vertical axes of intersection of consequent pairs of planes. Right: a chain of segments rotated around the intersection axis and translated along the vector lying on the plane.

In this case neither the rotation, scaling and translation give the proper solution, nor any of their combinations. The proper solution assume facilitation of parallel projections, where each point of the profile chain is projected on the adjacent plane along the same direction creating pairs of parallel edges. That way, each pair of original and image points will create a line segment. All line segments between corresponding planes will be parallel to each other. The parallelism guarantees the planarity of created quads.

The direction of projection is determined by the consequent points contained on the directrix curve, see Fig. 4.35. All points along the generatrix chain are projected on the neighbouring plane along the same direction. The procedure is performed for all plane pairs, see Fig. 4.36, left.

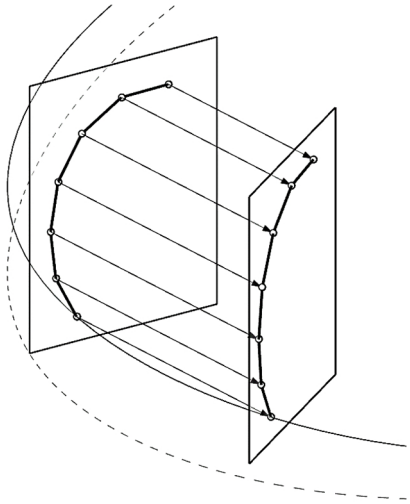

Fig. 4.35 A chain of segments obtained by projections. All points are projected along the same direction.

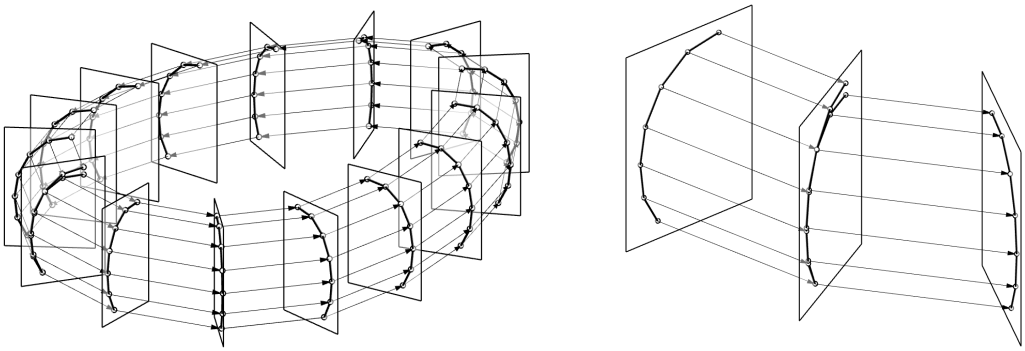

Fig. 4.36 Left: consequent projections of line segments. Right: the last projection results with a chain of segments which is not similar to the first one.

What has to be noted is the loop closure. The first and the last profile chains are not equivalent, i.e. points creating those profile chains lie on a common plane, however, these are not congruent. In Fig. 4.37 two profile chains at the left side of the mesh are co-planar, but no congruent.

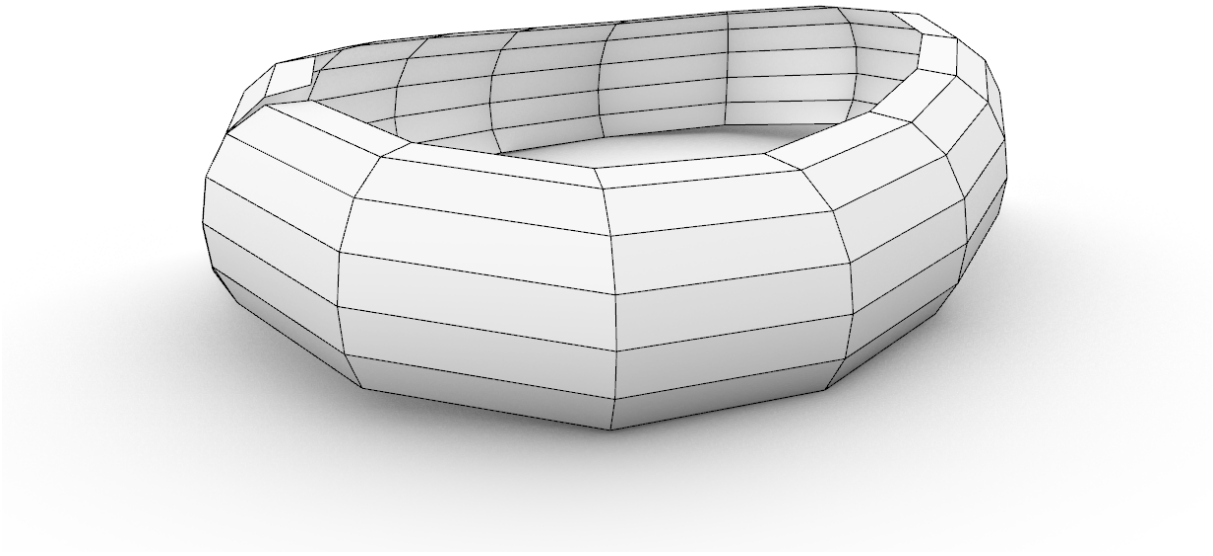

Fig. 4.37 A PQ mesh obtained by projections, with shading of facets.

By so far the presented method assumed, that all profile chains lied on vertical planes, what is a reasonable solution from a constructional viewpoint. Structural elements of the façade can be fastened to a corresponding, vertical structural elements of the building, e.g. column or truss. On the other hand, PQ meshes obtained according to the presented solution lack a certain geometrical property, i.e. the mesh is not circular (see section 3.5.4 Circular meshes). Almost similar PQ mesh which are also circular are possible to obtain by adoption of the method described in the further part of this section.

The rotations of the profile chains produce strips of isosceles trapezoids, see section 4.1.4. Such figures are always cyclic quadrilaterals. Additionally, the following generatrix profiles should be rotated in such a manner, that the image of rotation is coincident with the directrix curve at the adequate point. Since the points on the guiding curve are on various levels, the rotations cannot be performed around vertical axes. Therefore, the axes of rotations are defined by the intersections between corresponding neighbouring planes. The question remains how to select the positions and orientations of the planes. Such planes should be incident with points contained on the directrix curve and the rotations between the consequent planes should generate proper images of the generatrix line of segment chains.

The first plane containing the generatrix chain of line segments is perpendicular (normal) to the spatial, directrix curve, see Fig. 4.38. Since the directrix is a spatial curve, the plane is not necessarily vertical. Rotational PQ meshes are created around axes, that lie on a common plane with the generatrixes, see section 4.1.4. Therefore the path of rotation of a point on generatrix chain is an arch, which is perpendicular to the plane containing generatrix chain of line segments. One pair of original and image of rotation points is known, i.e. the neighbouring points contained on the directrix curve. Those points and the tangent direction at the start determine the arch, from which the centre point is derived, see Fig. 4.39. The centre of rotation and a point on the directrix define the bundle of planes[64]. In order to finally determine the second plane one more constraint is required.

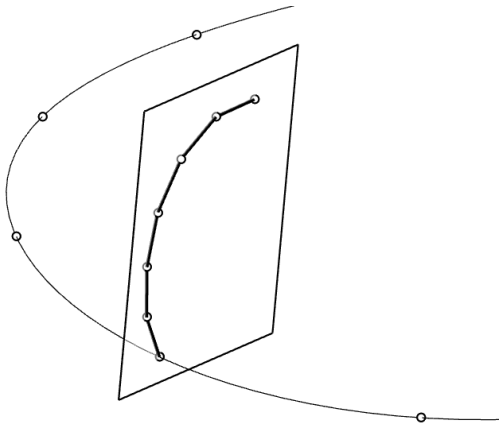

Fig. 4.38 A non-vertical plane containing the generatrix profile (chain of line segments). The plane is incident with a point contained on the directrix curve and is perpendicular to the directrix curve at that point.

[64] A set of planes which intersect at a common line.

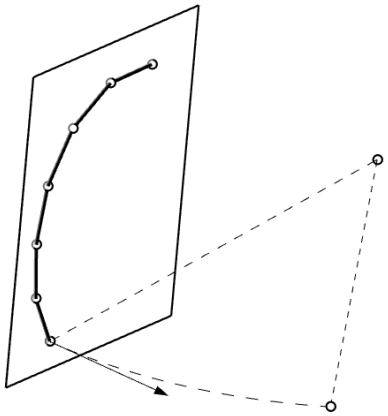

Fig. 4.39 The path of rotation determined by the tangent vector at start and two points. The point at the apex is the centre point of the arch.

The centre point of the arc, together with its endpoints constitute a plane. A line that is normal to that plane, and starts at the centre point of arc is the rotation axis - Fig. 4.40. That rotation axis explicitly determines the position and orientation of the second plane. The axis of rotation is also the intersection line between two neighbouring planes.

The next plane contains the next point on the guide curve and the axis of rotation. All the other points on the original generatrix chain of segments land after rotation on that newly created plane. Trough rotation a series of cyclic isosceles trapezoids is created, Fig. 4.41.

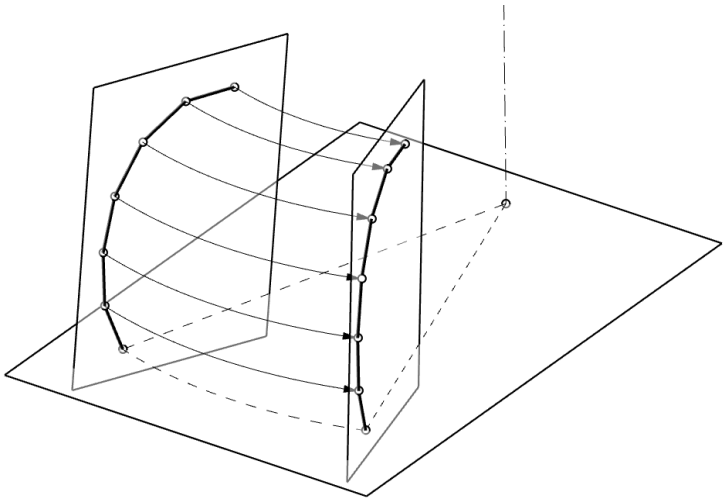

Fig. 4.40 The arch which is the path of the rotation lies on a plane. The axis of rotation is perpendicular (normal) to that plane.

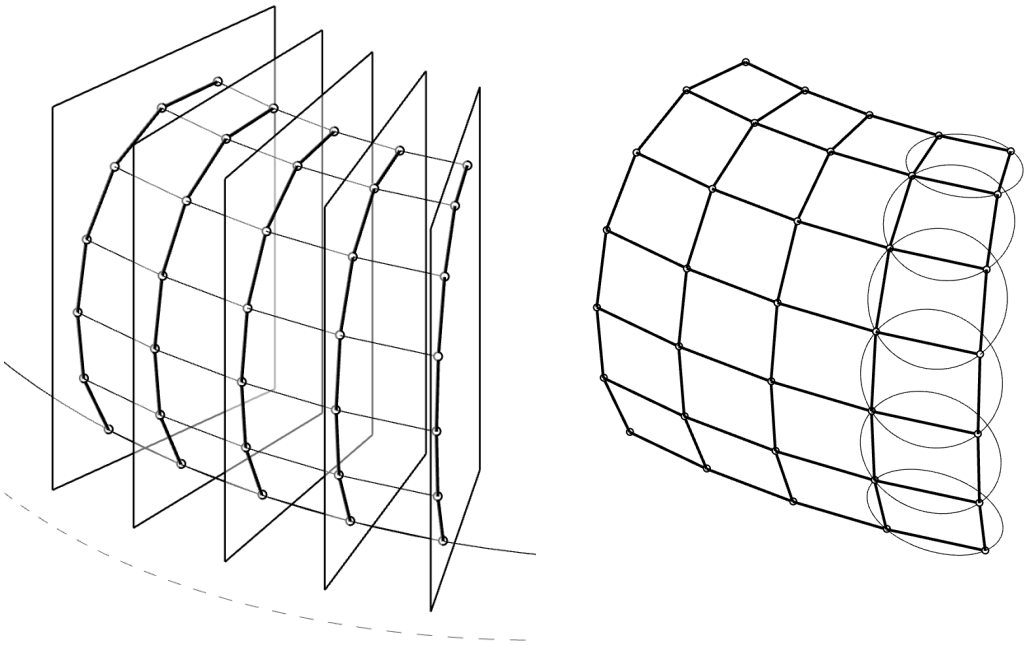

Fig. 4.41 Left: a series of rotations of a chain of line segments. Right: cyclic quadrilaterals are obtained by rotations.

Figure 4.42 shows a series of planes containing generatrix chains of segments. Between each pair of adjacent planes auxiliary extension lines and a rotation axis is shown. In Fig. 4.43 a PQ mesh created according to sweep method is shown. The result is visually similar to the one in Fig. 4.37. However, here an advantage is that facets are cyclic in exchange for the fact, that generatrix sections are not vertical. In this case, as in the previous one, the loop of generatrix profiles in not congruent, i.e. the first and the last profile is co-planar but no congruent.

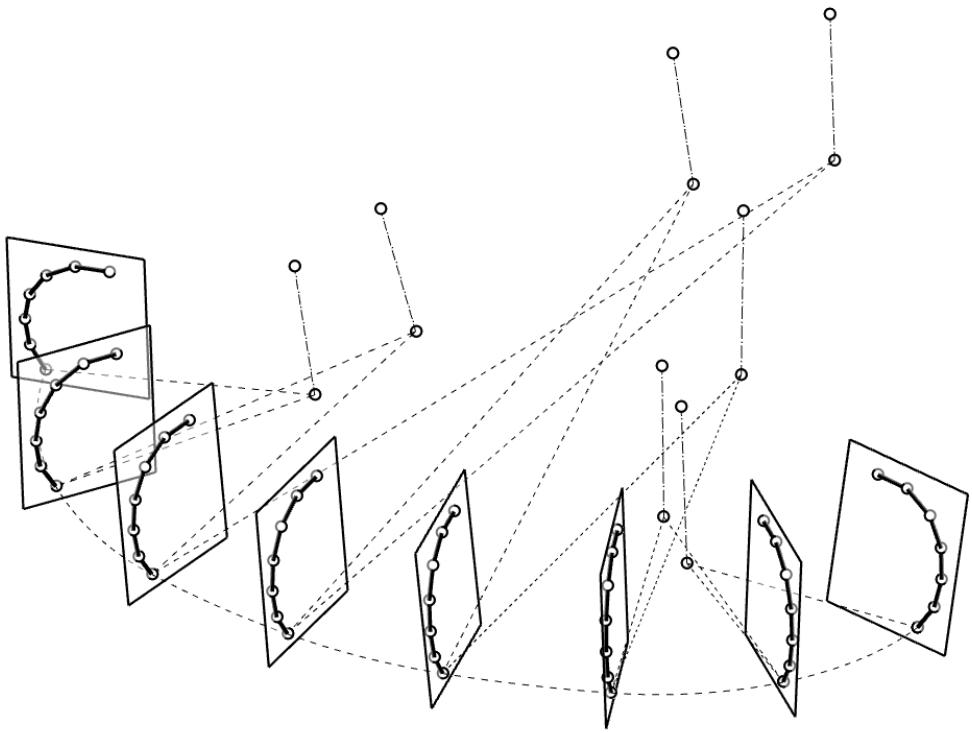

Fig. 4.42 A series of planes containing generatrixes. Between all the corresponding pairs of planes the paths of rotations and the rotation axes are shown.

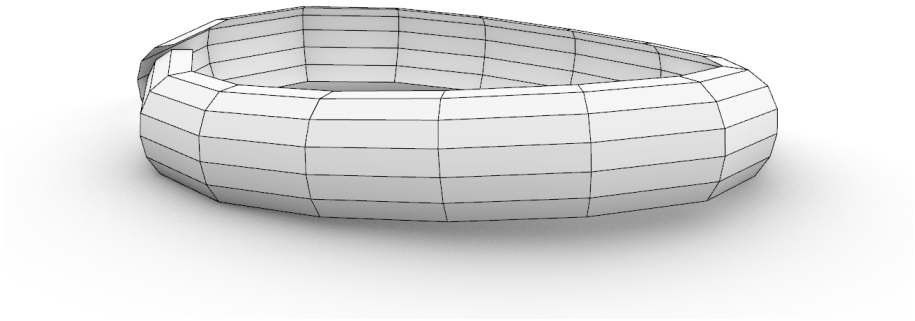

Fig. 4.43 Circular PQ mesh obtained by rotations shown with shading of facets.

Although the planes containing the profile chains are no longer vertical, the shape of the profiles achieved through this alternative of sweep method give significant geometrical and technological advantages, see 3.5.4 Circular meshes.

4.1.6. Marionette method

Marionette meshes are the proposition for constructing PQ meshes according to the bottom-up paradigm (*fabrication-aware design*) presented in (Mesnil et al. 2016) and broadly in (Mesnil 2017).

For each facet of a PQ mesh there is a constraint that refers to the co-planarity of 4 adjacent points. For 3 points any configuration of their positions fulfils the co-planarity constraint, since any 3 points constitute a plane. If there is 4^{th} point added, its position is limited to the plane of previous 3 points – the 3D space of solutions is limited to a 2D plane. However, within that plane there are infinite solutions for the 4^{th} point location.

In the previously presented methods, the final plane was a result of rotation or translation. The co- planarity of all four points was guaranteed by the parallelism of any of two pairs of opposing edges. Since the parallelism is only the sufficient condition, there is another possibility to obtain planar quad. It assumes that the plane on which the quad will eventually lie is known before all the points are transformed. The necessary condition of the planarity of quad is the situation of all four points lying on a common plane. Therefore, the sufficient condition has not to be met, i.e. the resultant quad is not restricted to be trapezoid or parallelogram. Although the method does not exclude the possibility that the resultant quads are cyclic, usually they lack that property contrary to isosceles trapezoids. The Marionette method enables different approach to the PQ mesh design according to the external guiding parameters. Methods presented before were defined by directrix and generatrix curves with the additional information defining the allowed transformations. In this method the resultant mesh is parametrized by two directrix curves (or chain of line segments) and a quad mesh in the flat configuration on the horizontal plane.

The procedure of generating PQ mesh according to Marionette method requires a quadrilateral mesh defined in horizontal projection. For better understanding the method, let that initial mesh consist of one, horizontal quad *ABCD*, see Fig. 4.44. The positions of A^s, B^s and C^s are selected arbitrarily along the vertical axes passing through the corresponding points *A*, *B* and *C*. Line segments A^sB^s and B^sC^s are in this simplified example equivalents of arbitrarily defined directrix and generatrix profiles, where the parameters are the vertical distances of points over the quad in horizontal configuration. Points A^s, B^s and C^s constitute a plane. Finally, the position of D^s is defined by an intersection of a vertical axis passing through the corresponding point *D* and a plane defined by A^s, B^s and C^s. From that definition the A^s, B^s, C^s and D^s point create a planar quad, which points are situated directly above the points *A*, *B*, *C* and *D*, see Fig. 4.45.

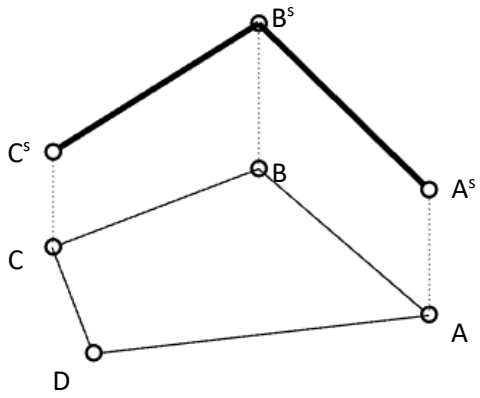

Fig. 4.44 ABCD *quad lying on the horizontal plane.*
Correspongind points Aˢ, Bˢ *and* Cˢ *are situated directly above* A, B *and* C *points creating two edges.*

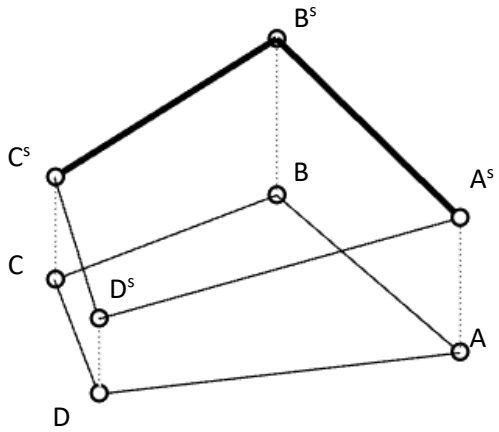

Fig. 4.45 Point Dˢ *is situated directly above the point* D *and lies on the plane determined by points* Aˢ, Bˢ *and* Cˢ.
Newly created spatial quad AˢBˢCˢDˢ *is planar.*

The name of the method *Marionette* refers to the procedure of raising the fourth point to the plane of destination - like a marionette on a string. The procedure for a single cell is expanded by adding more quads in planar configuration and two directrix chains of line segments, Fig. 4.46. Each quad requires three defining points and results with one additional point, which will define the construction of following quads in following iterations. That inequality makes it necessary to add more defining points externally. Those external points are defined by the directrix chains situated on two vertical, mutually perpendicular planes.

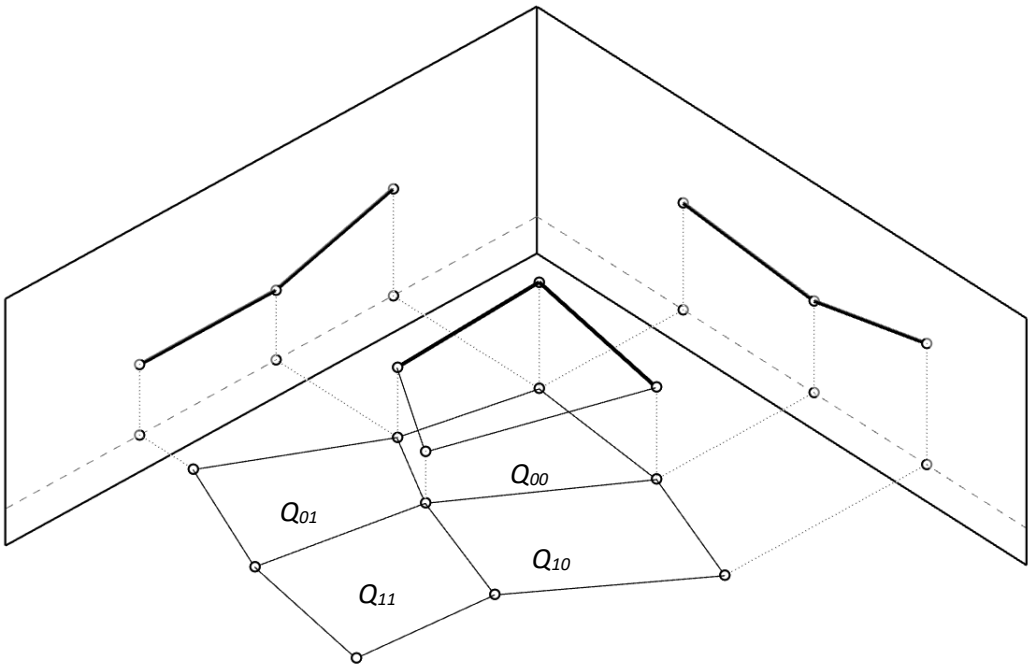

Fig. 4.46 Expansion of the basic definition described before.
A PQ mesh in flat configuration is expanded and two directrix profiles are added.

Quad projections Q_{01} and Q_{10} already have two adjacent points in space, so there is one missing for each. In order to determine the position of those missing points, two vertical planes are introduced, perpendicular to each other (Monge projections). Each of those planes contains a directrix chain of segments. The third point is constructed by the intersection of a vertical axis passing through the corresponding point on the vertical plane and another, horizontal axis passing through the corresponding point on the directrix chain. The second axis has to be perpendicular to a vertical plane with which it intersects, see Fig. 4.47. As the missing point altitude is defined, the fourth point of Q_{01} and Q_{10} is projected on the plane constituted by the previous three points. Eventually the quad Q_{11} will have 3 adjacent points in space that are required to define the quad position in space. The whole procedure is repeated until the whole projection of a PQ mesh is raised into space, such as a marionette.

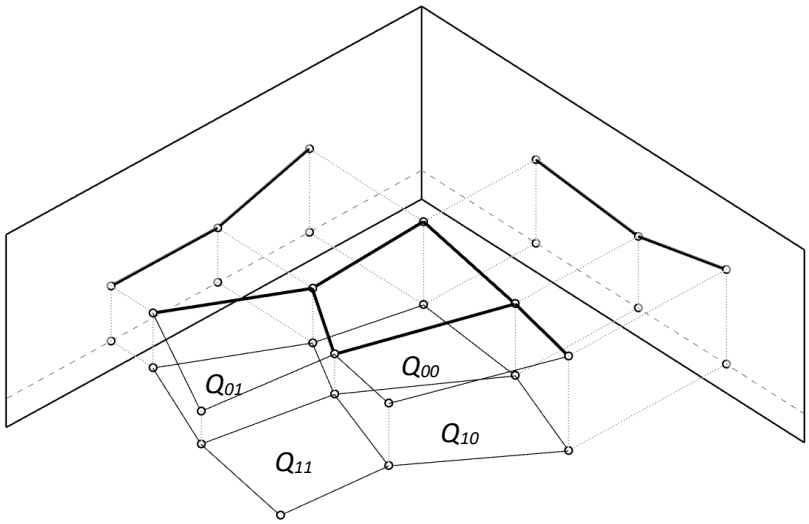

Fig. 4.47 Missing third points of two quads are defined by the intersections of vertical axes with the axes that are perpendicular to the vertical planes and pass through the corresponding points on the directrix chains of segments.

In Fig. 4.48 more complex PQ, Marionette mesh is shown together with projection on horizontal plane and projections of directrix and generatrix curves.

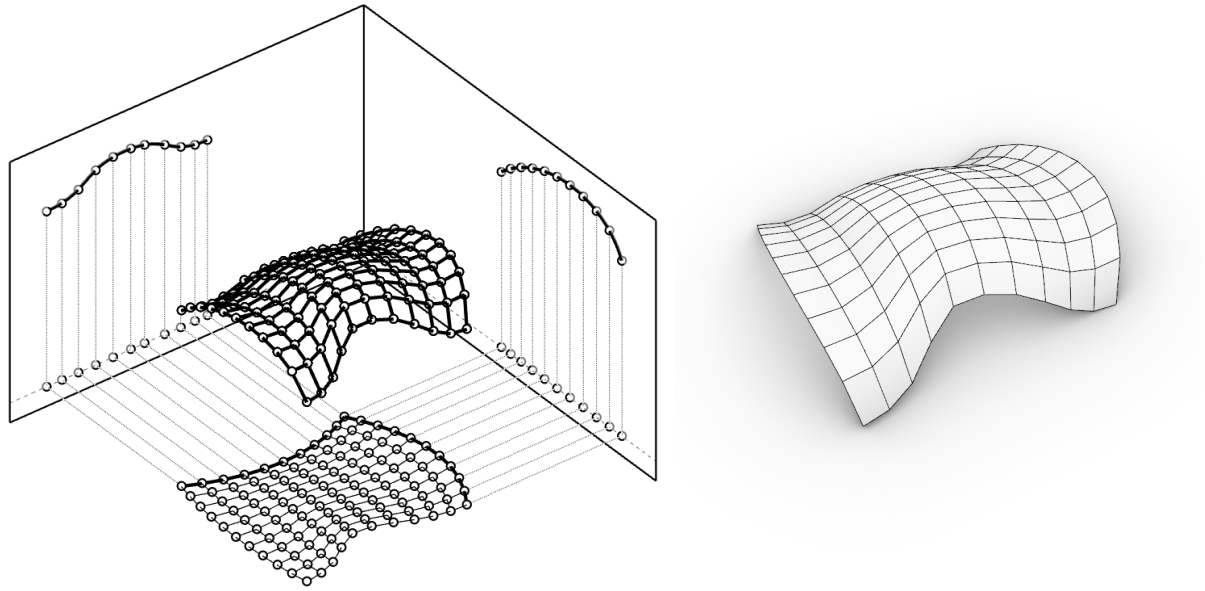

Fig. 4.48 An example of Marionette mesh. Left: the construction with parameters as directrices and planar mesh, right: the same mesh with shading.

The designer has the control over the shape of mesh in planar configuration and the directrix chains (or curves). However, the network in planar configuration has so many parameters (the position of each of its points), that it would be difficult for a manual control. Additionally, the designer is given control only over the shape of the two edges (not directly), whereas the shape of two another edges of resultant PQ mesh are hard to predict.

4.1.7. Isoradial meshes from Chebyshev nets

A mesh composed of planar isosceles trapezoids is called circular mesh, since any isosceles trapezoid is cyclic. Circular PQ meshes can be obtained by rotations according to the methods described in sections 4.1.4 and 4.1.5. Circularity of a mesh is required for certain types of transformations described in sections 5.1.2 and 5.1.3, in order to keep planarity of individual facets after the transformation. Those transformations allow to obtain spatial PQ meshes from planar, circular meshes. Therefore, a method for formation of planar, circular meshes is also useful. Potentially useful concept is the Chebyshev net (Bazylev 2002), i.e. a mesh composed of edges of constant length.

Chebyshev nets covering three dimensional, doubly curved surfaces also exist and are used for the estimation of shapes of elastic grid shells, see (Masson and Monasse 2017). However, in context of obtaining circular meshes only planar Chebyshev nets are concerned.

Both meshes in Fig. 4.49 are constrained to a plane and consist of segments of lengths. Each cell is a rhombus or a square – having all edges equal in lengths. This construction can be obtained according to the translational method (section 4.1.1), where the directrix and generatrix chains are divided into sections of equal length. As translation transformation preserves the distances between points, the resultant edges maintain the original length. Therefore, the whole mesh is composed of edges with equal lengths.

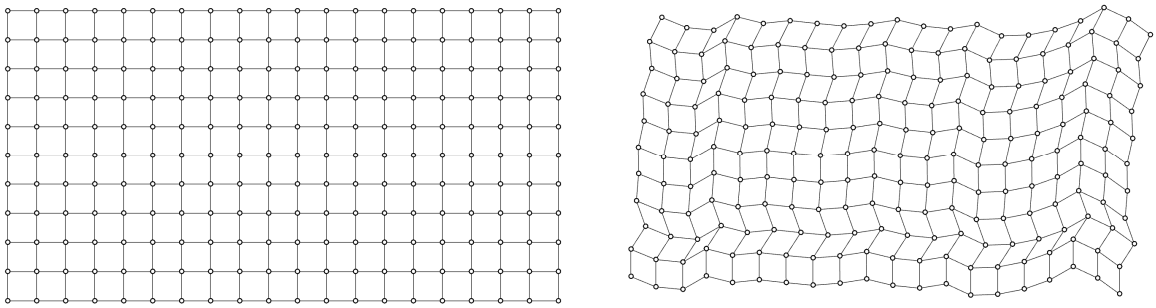

Fig. 4.49 Chebyshev nets - two examples of quadrilateral meshes in planar configuration composed of edges of equal enghts.

Each vertex of a Chebyshev net can be used as a centre point of a circle, whose radius is equal to the lengths of surrounding edges, see Fig. 4.50, left. Four points adjacent to the centre point of the circle lie on that circle. Connecting these points with line segments will result in cyclic quad. The pairs of opposing edges of the resultant quads are not necessarily parallel, however the quad is planar, since the whole construct was performed on a plane. Also, since all edges have equal lengths, all circles have the same radii. Therefore, the resultant mesh is also called *isoradial mesh*.

Planar, isoradial mesh obtained from Chebyshev net is shown in Fig. 4.51.

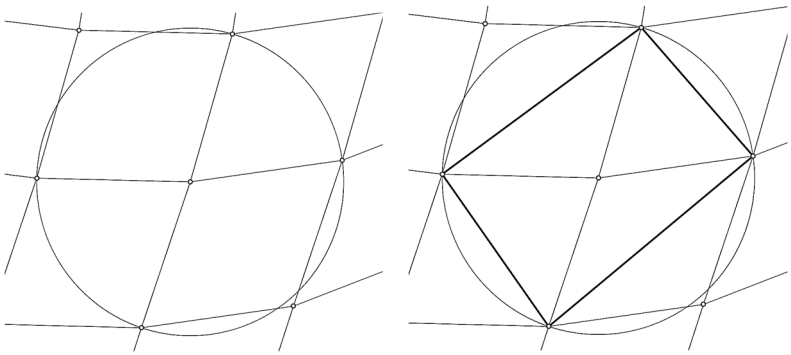

Fig. 4.50 A circle drawn around a vertex of Chebyshev net with radius equal to the length of its edge is incident with all four points adjacent with the centre point. Right: quad created from the four points adjacent to the centre one is cyclic.

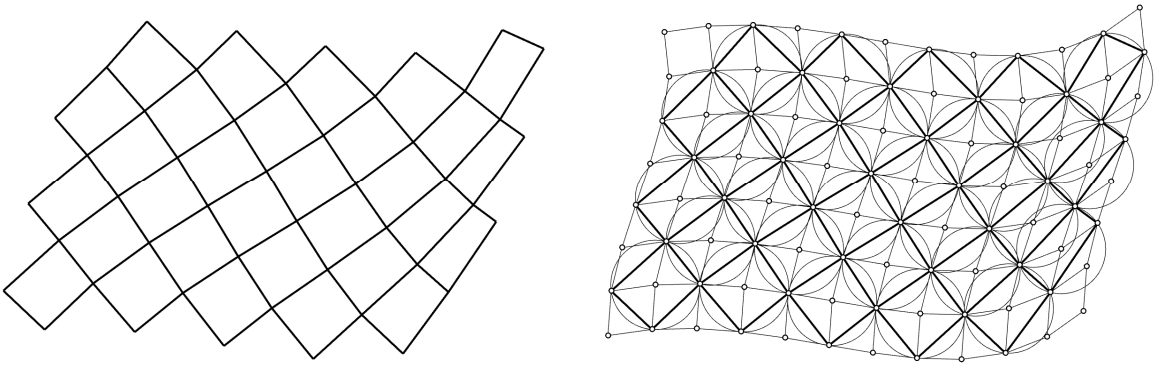

Fig. 4.51 Planar, isoradial mesh obtained from Chebyshev net shown separately, left and with corresponding Chebyshev net and circumcircles, right .

The construction described above uses only half of the mesh vertices as the centre points of circles, whereas a denser isoradial mesh can be obtained. Two neighbouring cyclic quads intersect creating new quad, which is also cyclic, see Fig. 4.52. The newly created quad is inscribed into a circle, whose diameter is an edge of the Chebyshev net.

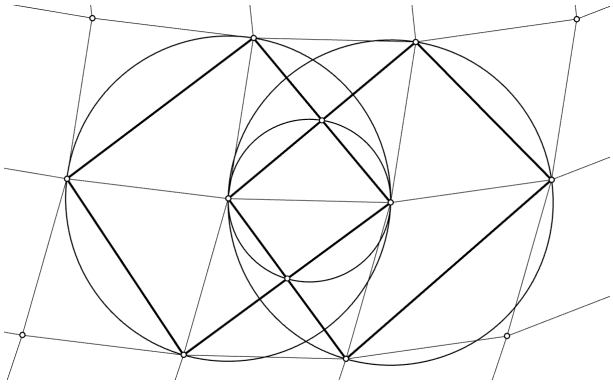

Fig. 4.52 A quad obtained by intersection of two other neighbouring quads. The small quad is also cyclic.

Filling all the points on the initial mesh with circles and cyclic quads will result in an isoradial mesh with 4 times more cells, see Fig. 4.53.

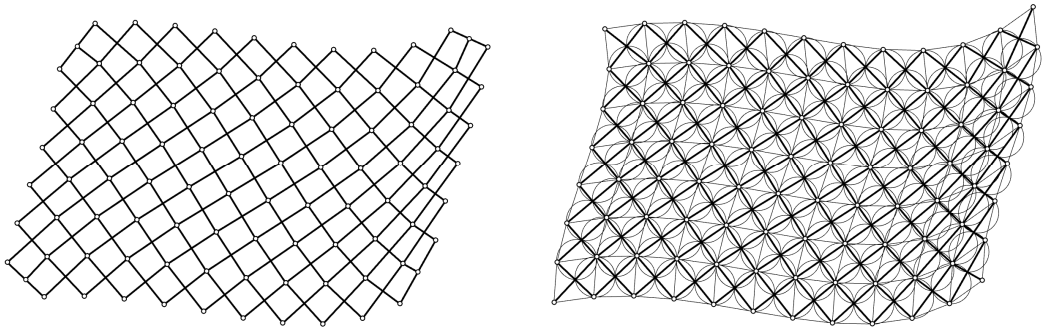

Fig. 4.53 Left: a mesh of quads obtained by intersections of neighbouring quads. Right: the same mesh with translational mesh and circles. The meshes obtained by this method are circular meshes.

Edges of isoradial mesh are also diagonals of facets of Chebyshev net. This example was based on planar isoradial meshes and spatial isoradial meshes will not be further explored in this section.

Although potential of Chebyshev nets for generating PQ meshes has already been reported in mathematics, e.g. in (Douthe et al. 2016), they have not been used in design and construction of PQ grid shells yet.

4.2. New methods of formation of PQ meshes proposed by the author

The methods of shaping PQ meshes described in this section are propositions and modifications proposed by the author of this work.

4.2.1. Circular Marionette method

To some extent, the Marionette method proposed by Romain Mesnil in (Mesnil et al. 2016), briefly described in section 4.1.6, may be modified in order to obtain circular PQ meshes, i.e. the meshes, which facets are planar quadrilaterals, that are also cyclic. This modification is an author's proposition. Having the initial constraints, i.e. the projected mesh and the vertical projections of the profile chains - the procedure is carried out in a standard manner. The first triple of points are raised and the fourth is projected on a plane set by those. However, as it is shown in Fig. 4.54, the last point is not coincident with the circle that contains three previous points.

In order to construct cyclic quad the fourth point has to remain on the plane defined by the three initial points and additionally has to be placed on the circle containing those three points.

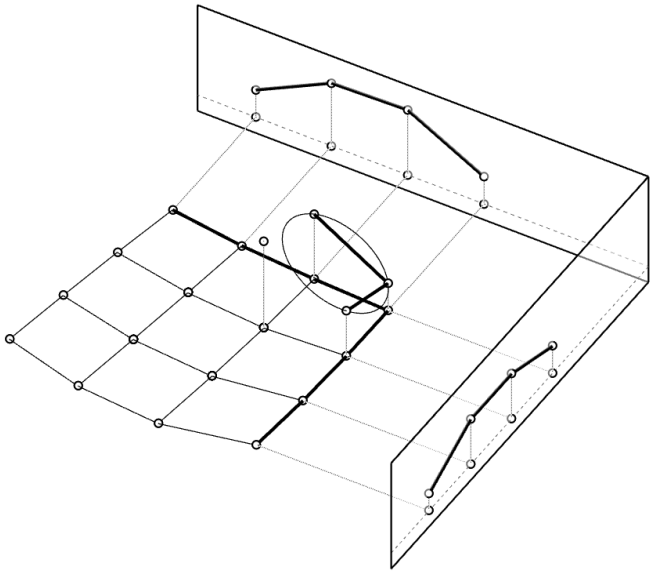

Fig. 4.54 First three points define a circle, which is not coincident with the fourth point.

As a circle is a planar shape which is already on a plane defined by first three points, the fourth point is projected onto a closest point on the circle to meet all the defined constraints, see Fig. 4.55.

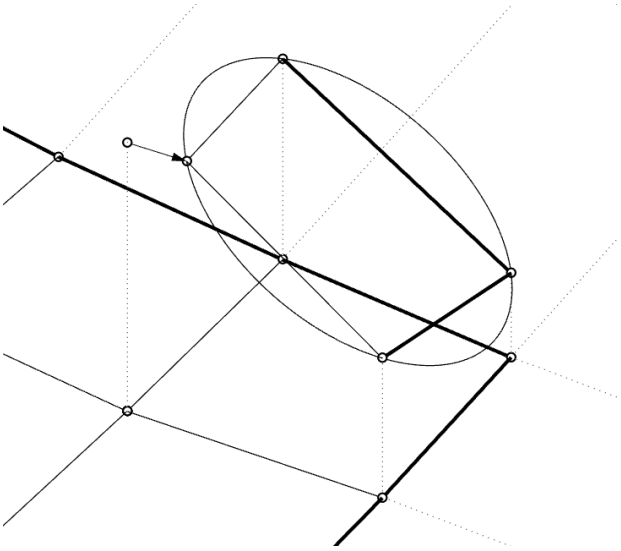

Fig. 4.55 Closest projection of the fourth point on a circle.

Iterative process of creating PQ mesh according to the Marionette method is carried with the additional step of projecting each fourth point onto a circle until all points are projected. In Fig. 4.56 a simple circular PQ mesh obtained with the described method is shown together with projection on horizontal plane in two versions: thicker line segments indicate the user defined mesh, whereas thin lines indicate the projection of actually obtained mesh. The difference between both can be observed. That difference in general shape can also be observed between PQ meshes shown in Fig. 4.57 and 4.58.

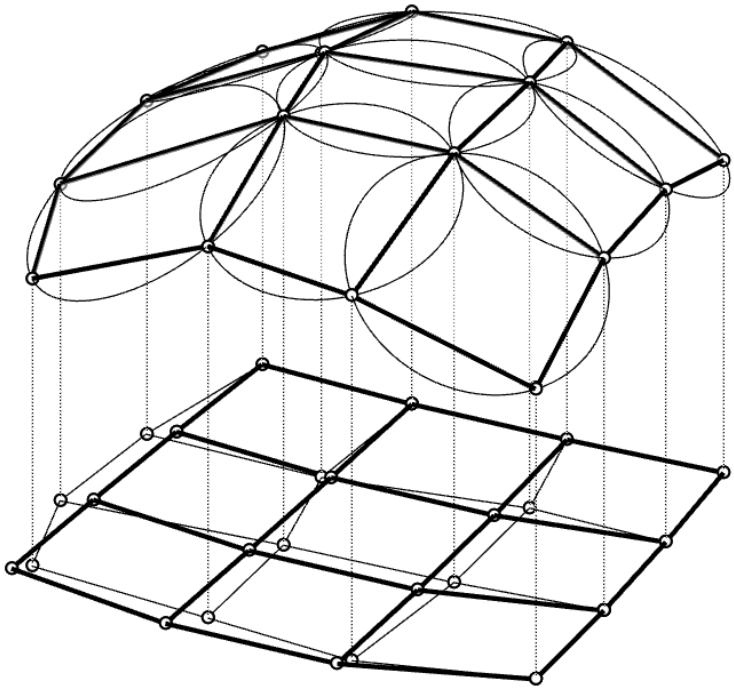

Fig. 4.56 Projection of the obtained mesh compared with the initial mesh in the flat configuration.

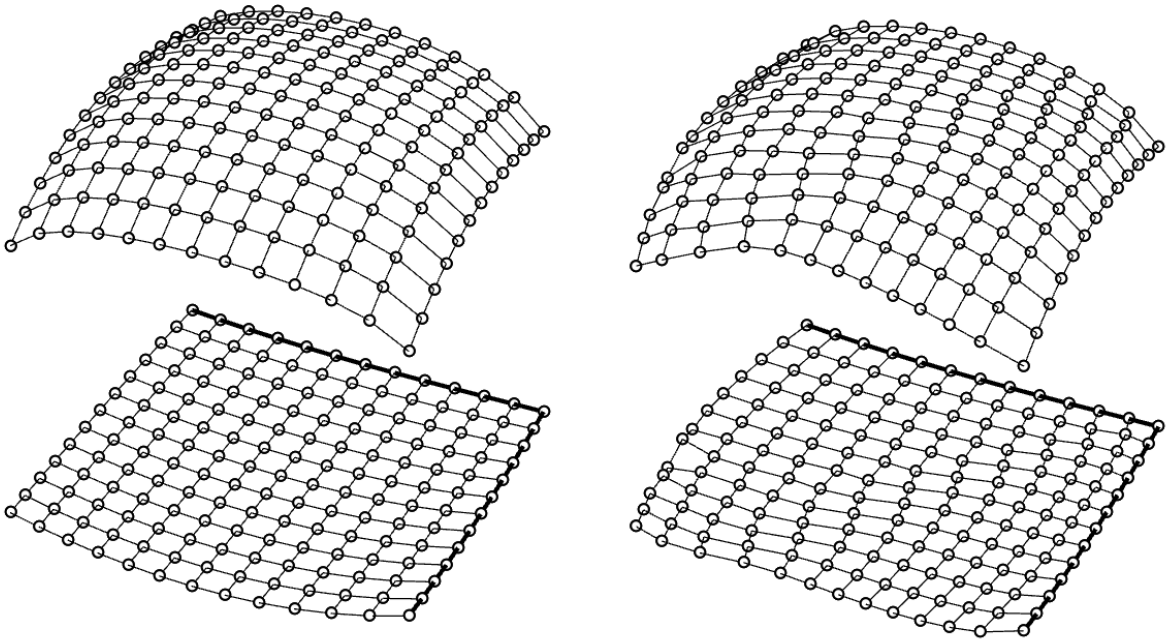

Fig. 4.57 Comparison of two meshes derived from the same parameters. Left: conventional Marionette, right: circular modification. A difference in regularity is visible.

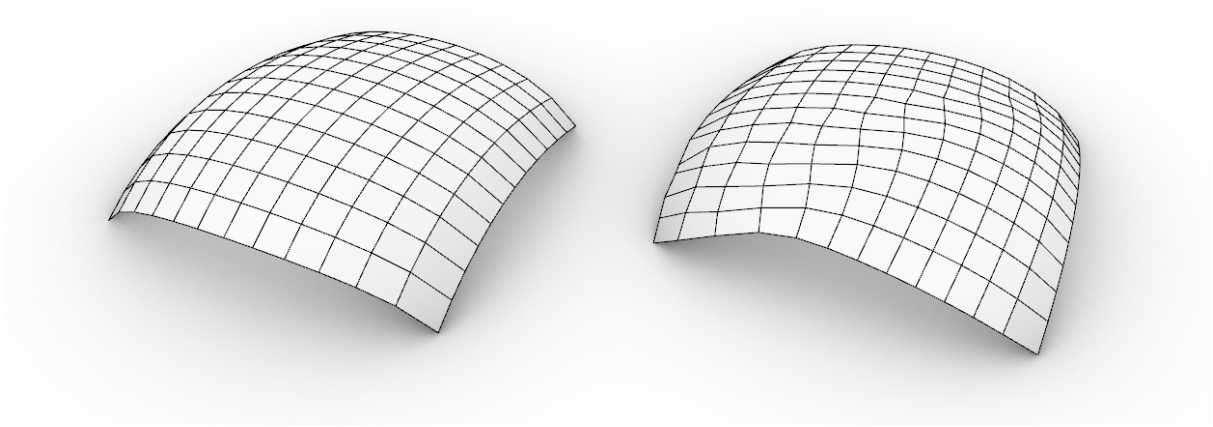

Fig. 4.58 Two marionette PQ meshes with shading applied. Left: conventional, right: circular.

The presented modification have certain limitations. After several iterations a vertex projected vertically onto a desired plane may have be closer to the wrong side of the circle, resulting with concave or self-intersecting quad. Due to that disadvantage, further work on this modification is not carried. Instead, different ways of obtaining the circular PQ meshes and the ways of their deformation will be discussed in the following sections. However, it is possible that the mentioned limitations will be eliminated in future and the presented method will turn out to be useful tool for creating PQ meshes, therefore its description is included in this work.

4.2.2. Super-ellipsoids

'Man is the animal that draws lines which he himself then stumbles over. In the whole pattern of civilization there have been two tendencies, one toward straight lines and rectangular patterns and one toward circular lines. There are reasons, mechanical and psychological, for both tendencies. Things made with straight lines fit well together and save space. And we can move easily, physically or mentally, around things made with round lines. But we are in a straitjacket, having to accept one or the other, when often some intermediate form would be better. To draw something freehand, such as the patchwork traffic circle they tried in Stockholm, will not do. It isn't fixed, isn't definite like a circle or square. You don't know what it is. It isn't aesthetically satisfying. The super-ellipse solved the problem. It is neither round nor rectangular, but in between. Yet it is fixed, it is definite — it has a unity.'

Piet Hein[65]

Discrete representations of spheres (as in Fig. 4.59), i.e. networks of points at the intersections of their longitude and latitude lines, are also a proper PQ meshes. Discrete PQ sphere is in fact a rotational mesh, where the rotation axis is an axis or of the sphere and the profile chain is interpolated between a family of consequent points lying on a single longitude line of that sphere. Such PQ mesh is also circular – since obtained by rotations.

[65] Quote from (Hicks 1966).

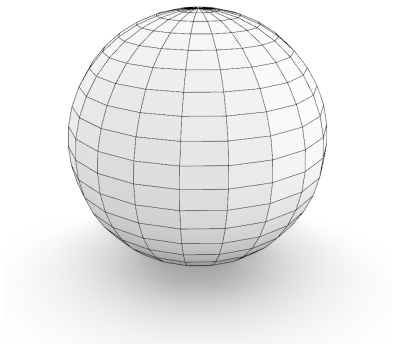

Fig. 4.59 PQ mesh obtained by a discretization of a sphere.

A sphere is defined as the set of all points in three-dimensional Euclidean space R^3 that are located at a distance (the "radius") from a given point (the "centre") (Weisstein 2018o). If the centre point is at the beginning of the 3-dimensional cartesian coordinate system and the radius of the sphere is equal to 1, then all the points whose *x*, *y* and *z* coordinates satisfy the equation (4.2).

$$\boldsymbol{x^2 + y^2 + z^2 = 1} \tag{4.2}$$

The equation above is the 3 dimensional generalization of Pythagorean theorem. If the exponents of *x*, *y* and *z* are replaced by parameters *r, s* and *t* the possible solutions of the equation become a family of super-ellipsoids (Weisstein 2018p). It is a 3–dimensional version of super–ellipse, a mathematical concept popularized by Piet Hein[66].

General implicit equation of a super-ellipsoid has a following form of formula (4.3).

$$\boldsymbol{|x|^r + |y|^s + |z|^t = 1} \tag{4.3}$$

Exponents *r*, *s* and *t* replace square exponents from the sphere equation. Since the values of exponents can be fractions and irrational positive numbers, the values of *x*, *y* and *z* parameters are absolute. The value of each exponent is responsible for bulging or denting the form in each corresponding *x*, *y* or *z* direction. For values larger than 2 the shape is bulging outwards. When the exponent is approaching infinity, the shape becomes two perpendicularly intersecting surfaces. For values smaller than 2, the form dents inward becoming two perpendicularly intersecting surfaces, when the exponent approaches 0.

The symmetry of super-ellipse is increased by reducing the exponents to two as in formula (4.4). In such form, the form has 4-fold rotational symmetry around vertical axis.

$$\boldsymbol{(|x|^r + |y|^r)^{r/t} + |z|^t = 1} \tag{4.4}$$

The super-ellipsoid in Fig. 4.60, middle, is a discrete representation of the above equation with the exponents *r* = 2 (thus the same as for sphere, therefore latitudes are circular) and *t* = 3. As the *r* exponent is responsible for the *x* and *y* coordinates, the horizontal, latitude chains remain circumscribed in circle. Different values of parameter *t* are responsible for the shape of meridian chains of segments. Changing the value of *t* below 2 makes the form pinched at the equator (Fig. 4.60, left) and as *t* strives to infinity, the form becomes tubular, see Fig. 4.60, right. The *t* exponent is therefore responsible for the shape of meridian chains of segments in super-ellipsoids.

[66] Piet Hein was a Danish mathematician, inventor, designer, author and poet, who, for the first time in history used the concept of Lamé curves in a design and popularised them as super-ellipses.

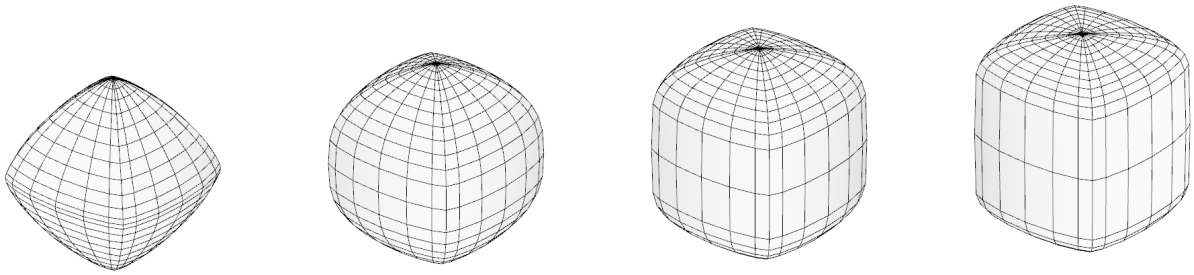

Fig. 4.60 Available forms of super-ellipsoid depending on value of the t *exponent with the same values of the* r *exponent.*

Shapes of latitudes are controlled by the value of the exponent *r*, see Fig. 4.61.

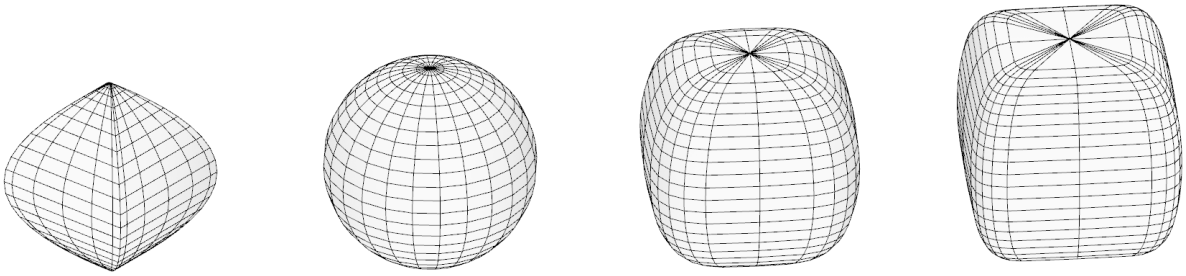

Fig. 4.61 Available forms of super-ellipsoid depending on value of the r *exponent with the same values of the* t *exponent.*

Various combinations of *r* and *t* exponents result in extensive family of various shapes. The example in Fig. 4.62 represents the shape for $r = 2.5$ and $t = 3$. Overview of possible super-ellipsoid forms depending on *r* and *t* exponents is in Fig. 4.63.

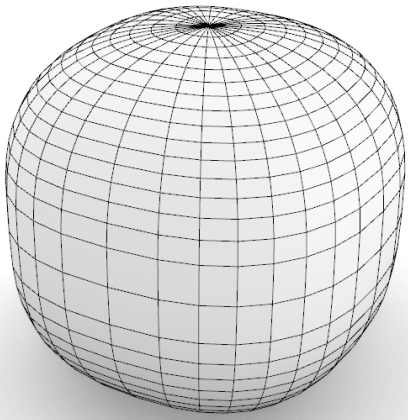

Fig. 4.62 A variant of super-ellipsoid with exponents r *and* t *larger than 2. This discrete version is an example of PQ mesh.*

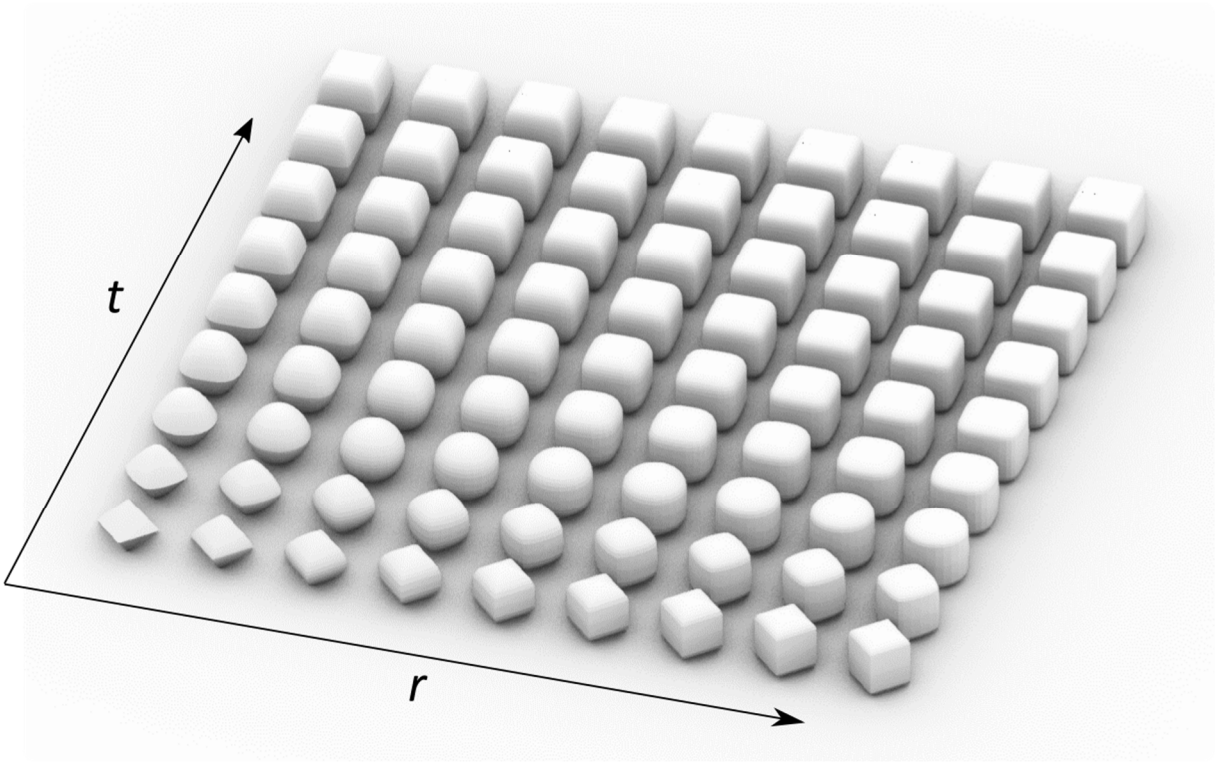

Fig. 4.63 Space of possible super-ellipsoid shapes depending on r *and* t *exponent values.*

All discrete forms of super-ellipsoids are PQ meshes due to the fact, that between each pair of latitude chains of segments there are pairs of parallel line segments. In fact, each latitude in a super-ellipsoid is the same super-ellipse which is scaled and as it was already mentioned in section 4.1.3, scaling transformation preserves parallelism. Also, each chain of segments is a projection of previous, neighbouring longitude profile, therefore can be constructed according to sweep method described in section 4.1.5.

5. Methods of transformation of PQ meshes

This section describes methods of transformation of PQ meshes, which **preserve the exact planarity** of all facets. PQ meshes obtained according to the methods described in the previous section can be transformed increasing the spectrum of available forms. In some cases of transformations, the base PQ mesh is required to meet some geometrical conditions in order to keep planarity of facets after the transformation. These requirements are described for each type of transformation. However, most of the basic transformations have no restrictions.

The *mechanical* aspects are not concerned in this chapter.

5.1. The existing methods of transformation

The methods described in this section have been adopted previously for the design and construction of glazed grid shells or have been proposed as methods for designing grid shells. Nevertheless, these transformation methods require definition and systematization as complementary for other, more complex transformations proposed in this work.

The presented description of existing methods includes only the basic principles of described methods, omitting the detailed mathematical formulations that can be found in (Gallier 2011).

5.1.1. Affine transformations

The planarity deflection of a single quad can be measured as the proportion between the distance between two diagonals and the sum of their lengths, see formula (5.1) and Fig. 5.1.

$$\boldsymbol{P = \frac{d}{D_1 + D_2}} \tag{5.1}$$

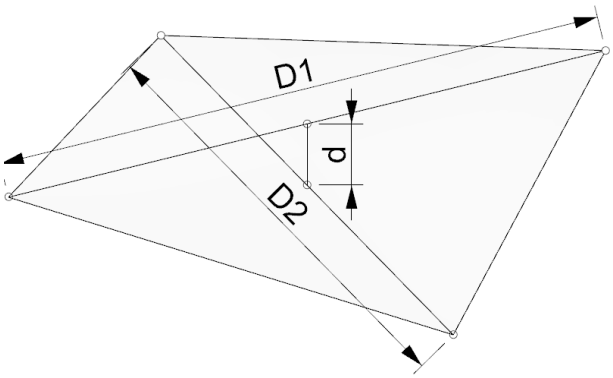

Fig. 5.1 Diagonals D1, D2 *and the distance between them* – d.

If a quad is exactly planar, then *d* is equal to 0, so is the *P*.

Figure 5.2 shows three cases of quads – one is planar and two are non-planar. In planar quadrilateral two conditions must be met: diagonals must intersect at a single point and diagonals must be a straight line segments. Therefore a transformation preserving planarity must transform lines into lines (preserves linearity) and be a one-to-one correspondence function (a bijection). Preserving linearity excludes situations like in Fig. 5.2, centre.

Bijection is a function transforming elements from one set into another one, where each element of one set is paired with exactly one element of the other set, and each element of the other set is paired with exactly one element of the first set. i.e. a single point is transformed into exactly one point (it cannot be transformed into a line like in Fig. 5.2, right) and two points cannot be transformed into one point.

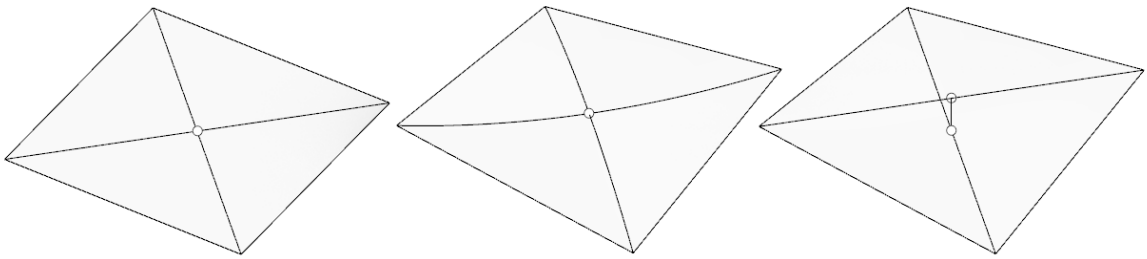

Fig. 5.2 Left: planar quad, diagonals are straight and intersect at single point. Centre: distorted, non-planar quad, diagonals intersect in one point, but were deformed into curves. Right: non-planar quad diagonals do not intersect at one point. The shortest distance between them is marked by two points and a line section.

Both requirements are features of all the affine transformations, see (Weisstein 2018a) and (Sung, Shirley, and Baer 2008), p. 209. That is the transformations transform line segments into line segments and they are bijections. Therefore, all affine transformations and their combinations preserve planarity of facets.

Additional properties of the affine transformations are: preserving parallelism and preserving proportions. Images of affine transformation of two parallel lines are always parallel and have the same proportion of their lengths as their original forms. The proportion is preserved between any pair of chosen segments.

Among the affine transformations in 3D space, the following are distinguished:

- Translation (Weisstein 2018q), (Sung, Shirley, and Baer 2008), pp. 194-198
- Rotation (Weisstein 2018m), (Sung, Shirley, and Baer 2008), pp. 204-208
- Reflection (Weisstein 2018l)
- Scaling (Sung, Shirley, and Baer 2008), pp. 198-204:
    - Isotropic
    - Anisotropic
- Shear (Weisstein 2018n)

5.1.1.1. Translation

Translation is the most obvious method of transforming a PQ grid in such a manner, that the planarity of the facets is preserved.

Figure 5.3 shows an object an its translated image, the following convention is used:

- $\boldsymbol{v}$ - the vector of translation
- $\boldsymbol{T_v}$ - the translation
- $\boldsymbol{T_v^{-1}}$ - the inverse operation when the transformed object needs to be displaced back to its original position

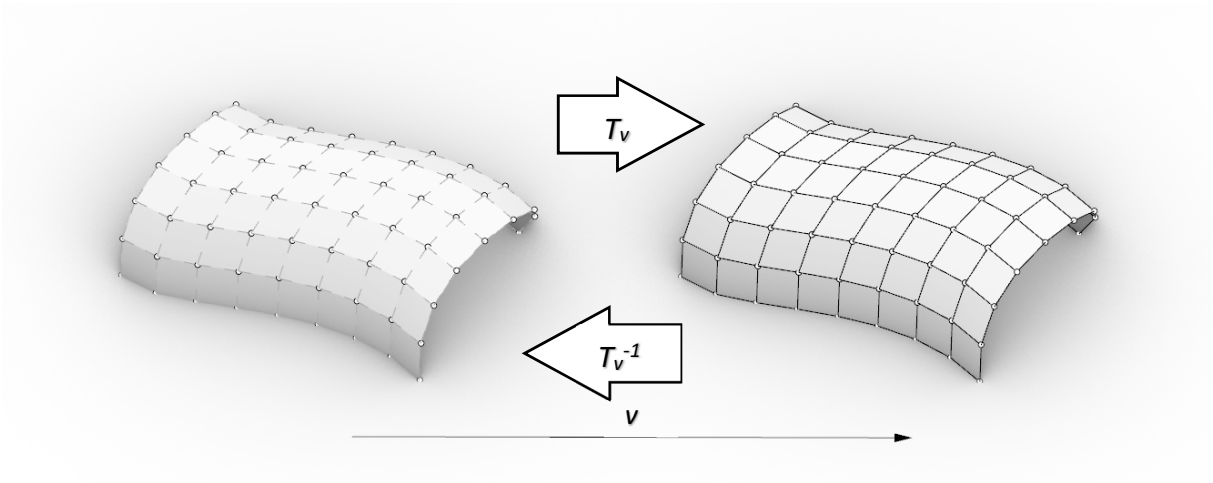

Fig. 5.3 Translation of a PQ mesh along the vector. All vertices are translated along the same vector.

5.1.1.2. Rotation

The rotation is a transformation that preserves the similarity of figures and preserves planarity of facets. It is characterized by an axis of revolution (rotation) and an angle.

Figure 5.4 shows an object an its rotated image, the following convention is used:

- ***a*** - the axis of rotation
- ***Θ*** - the angle of rotation
- $R_{a,\Theta}$ - the rotation
- $R_{a,\Theta}^{-1}$ the inverse operation

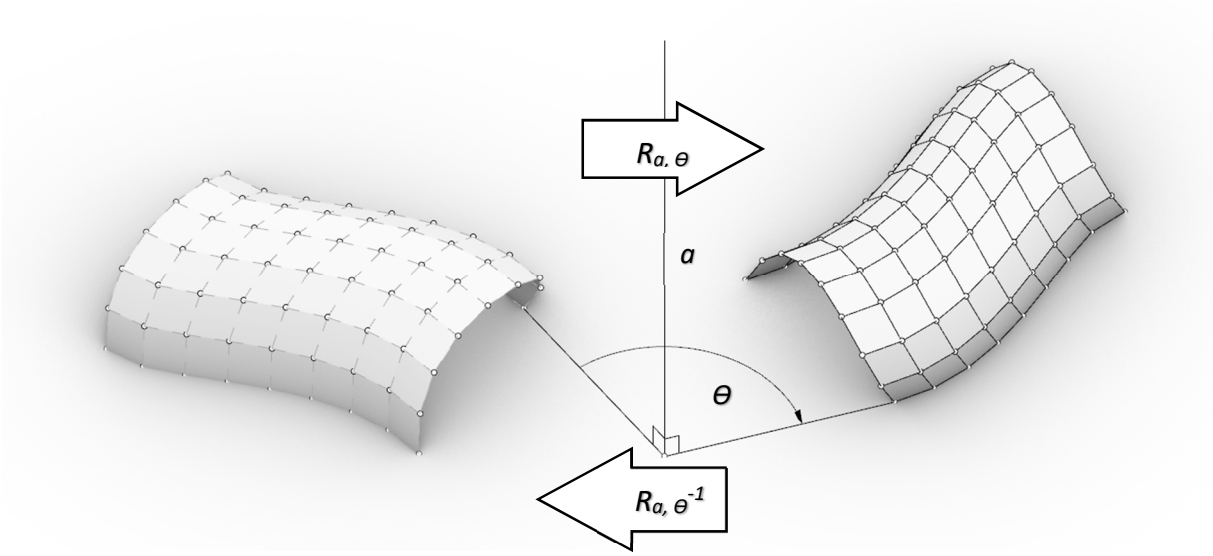

Fig. 5.4 Rotation of a PQ mesh around the axis of rotation.

5.1.1.3. Reflection

The reflection is a transformation, in which objects are reflected on the other side of a reflection axis (in two dimensional space) or plane (in three dimensional space). Each pair of original and image points is equally distanced to the axis or plane of the transformation. Reflections will be denoted as M_p, where ***p*** will denote the plane of reflection, see Fig. 5.5.

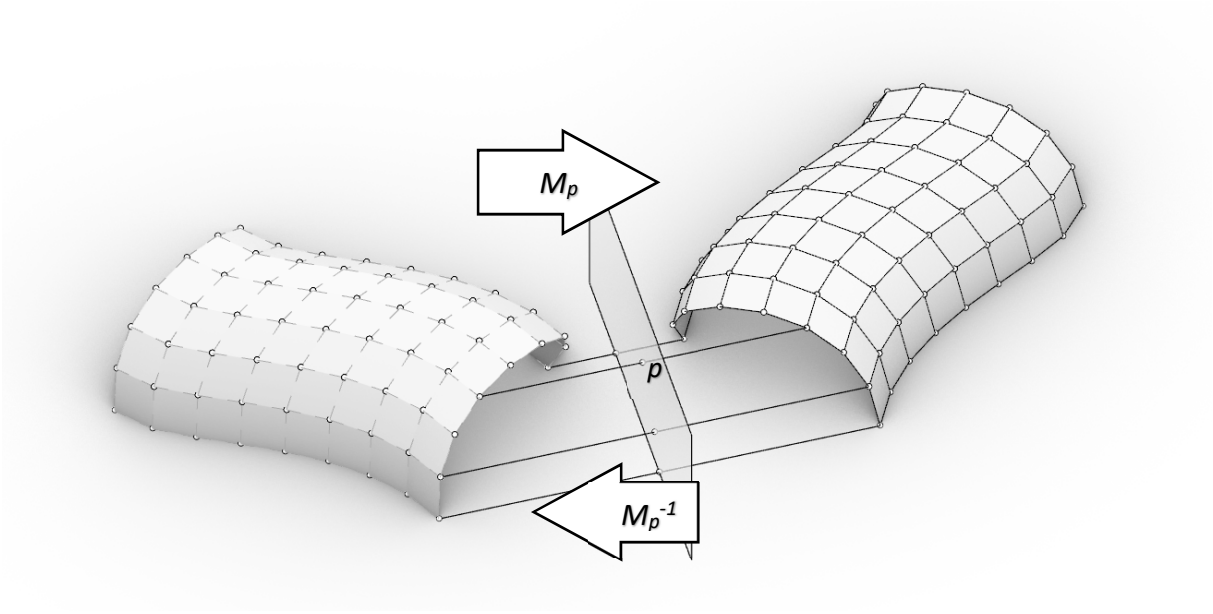

*Fig. 5.5 Reflection of a PQ through the plane **p**.*

5.1.1.4. Isotropic scaling

Isotropic scaling is a transformation characterized by a centre point and a factor. All points of the object are moved along individual axes passing through the centre point. The proportion of the distances between centre - original point and centre – image point is equal to the factor of scaling. This transformation will be denoted as $S_{C,f}$, where C is the centre point of the transformation and f is the factor, see Fig. 5.6. Isotropic means that the transformation is 'the same' regardless of the direction in space, contrary to the next described transformation, i.e. anisotropic scaling.

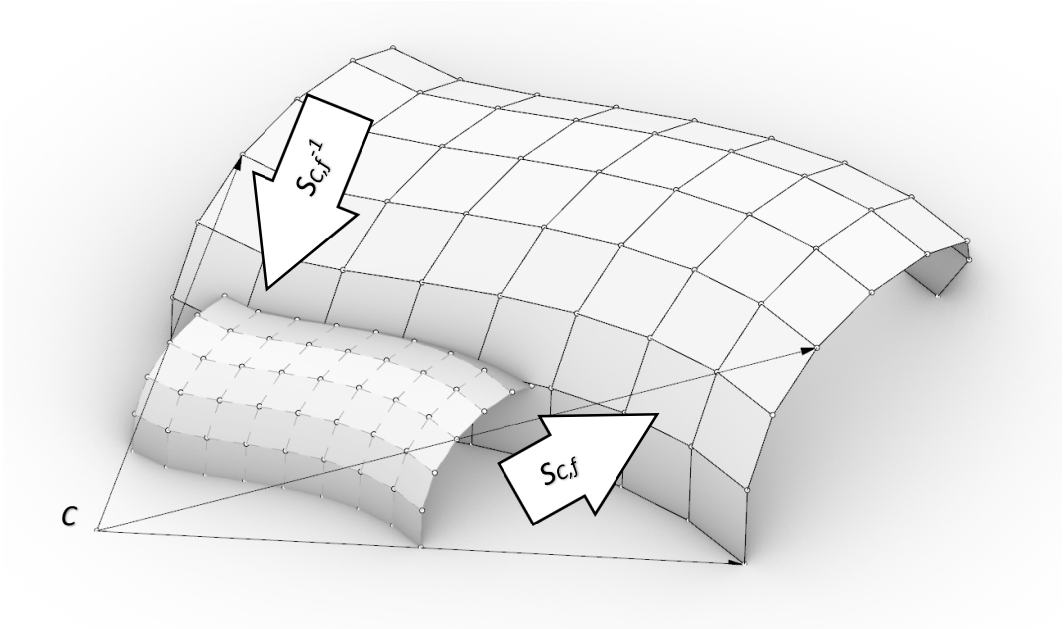

Fig. 5.6 Isotropic scale of a PQ mesh.

5.1.1.5. Anisotropic scaling

Anisotropic scaling is characterized by a factor and a plane. A plane can be deconstruct into a point (like in previous isotropic scaling) and a direction, i.e. a point and direction define a plane. Objects are stretched or shrank along the direction. The further from the transformation plane the transformed objects are, the more they are translated outward or inward (depending on factor). When a transformed point is on the transformation plane, it is incident with its image of transformation. Therefore a slice of a PQ mesh intersection with a plane of scaling remains unchanged. The factor of scale denotes the proportion between point-to-plane and image-to-plane. This transformation will be denoted as $\boldsymbol{C}_{P,\ f}$ further in the text, where $\boldsymbol{P}$ denotes the plane and $\boldsymbol{f}$ is the factor, see Fig. 5.7.

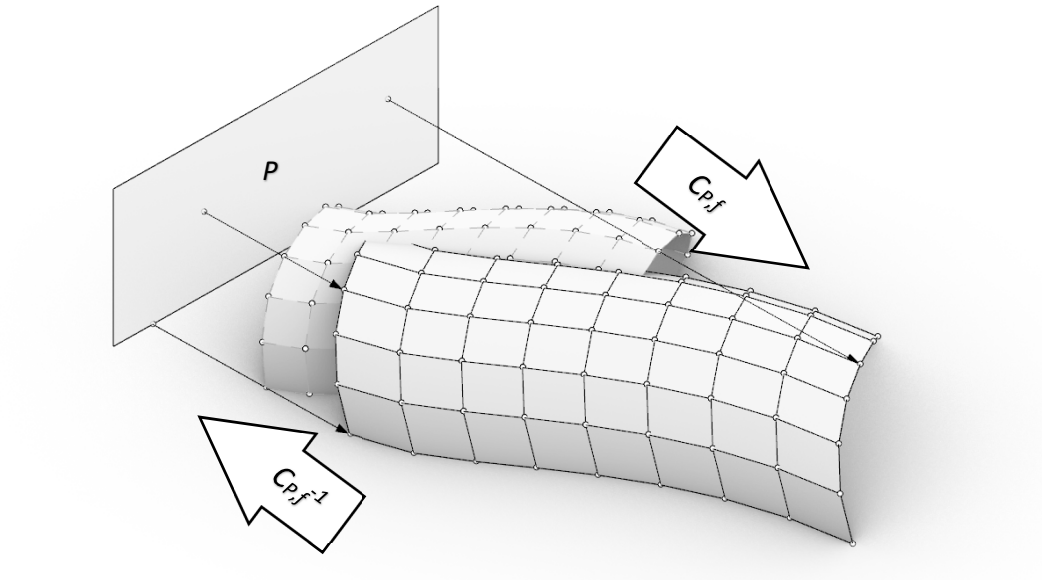

Fig. 5.7 Anisotropic scale of a PQ mesh.

Scaling transformation, both isotropic and anisotropic is described in (Schober 2015b), pp. 137–139.

5.1.1.6. Shear

Shear is a transformation which translates each point of an object along a specified direction $\boldsymbol{d}$ by a factor that is proportional to a distance of that point to a specified plane $\boldsymbol{P}$. The direction $\boldsymbol{d}$ of the translation is always parallel to the plane $\boldsymbol{P}$. Given 3 parameters the shear transformation is denoted as $\boldsymbol{H}_{P,\ f,\ d}$, where $\boldsymbol{P}$ is the plane, $\boldsymbol{f}$ is the factor and $\boldsymbol{d}$ is the direction, see Fig. 5.8. All points contained on the plane $\boldsymbol{P}$ are preserved.

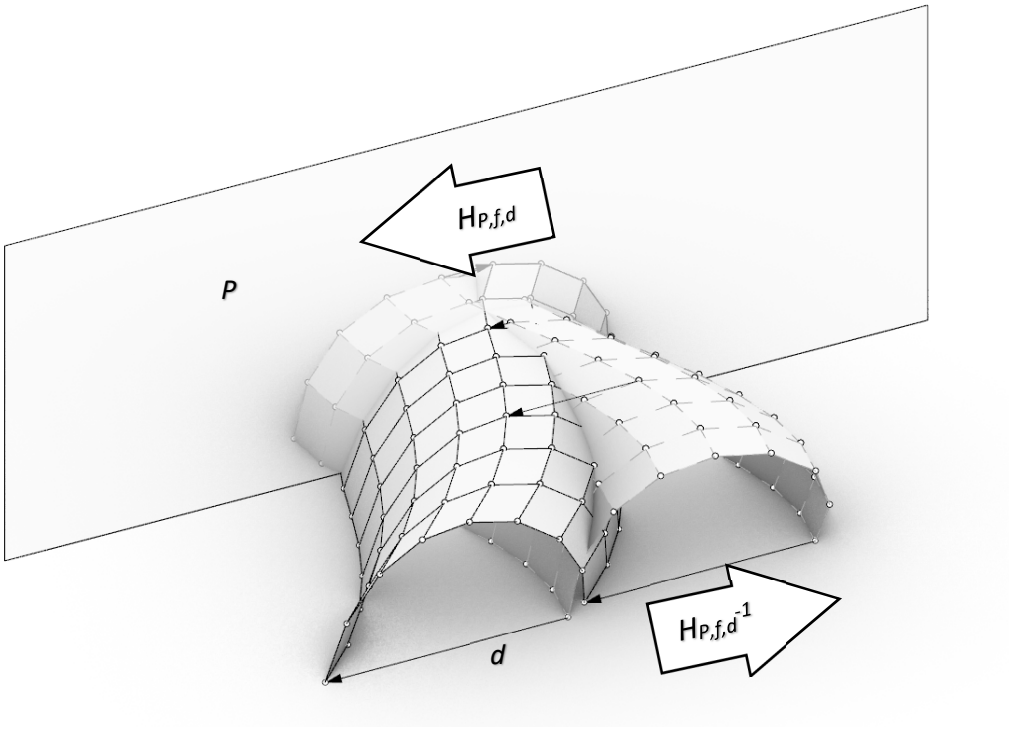

Fig. 5.8 Shear transformation of a PQ mesh

Shear transformation is described in details in (Schober 2015b), pp. 113–121.

5.1.2. Stereographic projection

The illustration form the *Opticorum Libri Sex philosophis juxta ac mathematicis utiles* (Aguilón 1613), Fig. 5.9, drawn by Rubens figuratively presents the principles of stereographic projections, which were already known by Hippoarchos (c. 190 – c. 120 BC) (Howarth 1996). The book, among other terms widely accepted in the optic's nomenclature, introduced the term *stereographic projections*, although these projections were known before. Stereographic projection is a projection of points on a sphere onto a plane, which is tangent to that sphere at its 'south' pole. Each point from a sphere is projected along a line that passes through the 'north' pole. The terms 'south' and 'north' are used to emphasize, that these points are on the opposite sides of the sphere.

Fig. 5.9 Peter Paul Rubens, an illustration for Six Books of Optics*, by François d'Aguilon. Source: (Aguilón 1613).*

Stereographic projections are mapping functions, in which surface of the sphere is projected onto a plane. These projections were historically known by the cartographers, as on maps portions of the Earth's surface are represented on planar map sheets. Construction of such function is based on two, basic assumptions:

- The plane and the sphere are tangential, i.e. share one and only one common point;
- Projected points lie on the plane and the axis passing through original point on the sphere and the point at the top of the sphere.

Although stereographic projections are neither isometric nor area preserving (distances and areas are distorted), they have one particularly useful property which is preserving the circles unchanged, see Fig. 5.10. Such property means, that if a closed curve is circular on the sphere, it will remain circular after projection, although points on that circle are shifted along the curve. It is also important to accent, that a circle on a surface of a sphere constitutes a plane. It is the only shape possible to obtain from the intersection between a plane and sphere apart from a point, when the plane is tangent to a sphere.

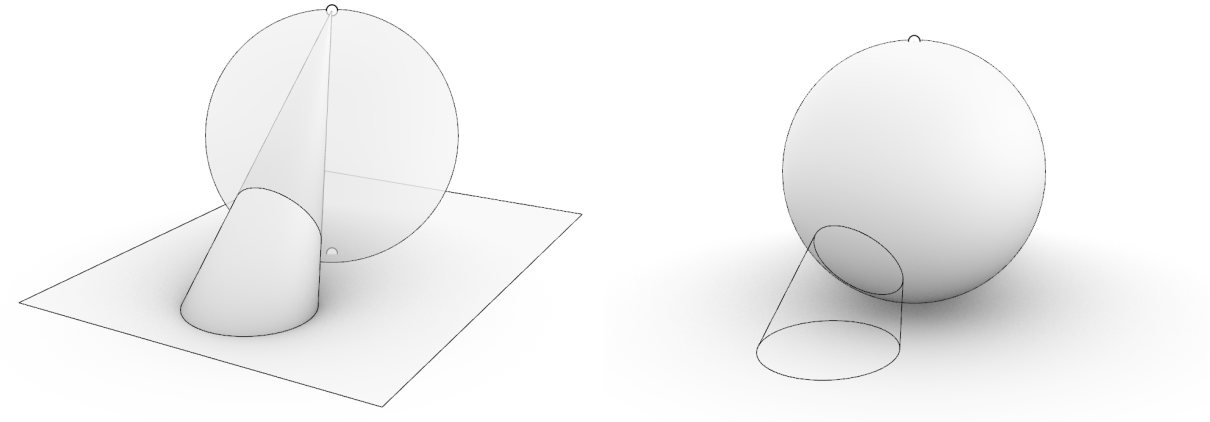

Fig. 5.10 Stereographic projection of a circle onto a plane results with a circle. A circle on a sphere is planar. Apart from a point (singularity) it is only possible shape that can be obtained by an intersection between sphere and plane.

An intersection between a sphere and a plane, if exist, is either a point or a circle. Consequently, as a circle is a planar construct, circle lying on a surface of a sphere can always be a result of intersection of sphere and plane. By mapping a circle with a stereographic projection from a surface of a sphere onto a plane, geometries from the intersection surface are simultaneously mapped onto a projection surface. The following Fig. 5.11 show the procedure of mapping from a plane intersecting with the sphere onto a stereographic projection plane. Except for the circle the image of Poland's boarder is visibly distorted.

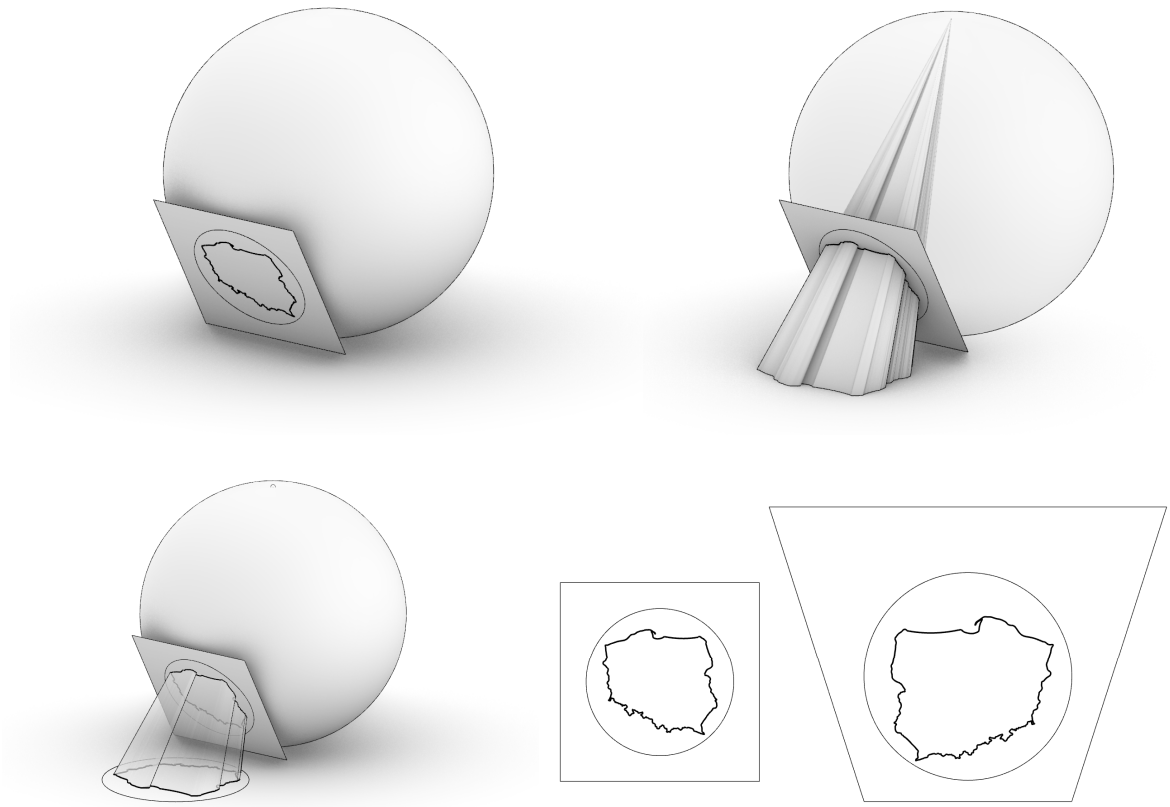

Fig. 5.11 Boundaries of Poland stereographically projected on a plane.
Distortion are visible, however the circular shape was preserved.

Another important feature of the stereographic projections is that these are bijective functions, i.e. all mapping are unambiguously reversible. That means that the shape on a plane can be projected back onto the surface of the sphere to create the exact image as the original one from the first, stereographic projection. For the purposes of the transformation of PQ meshes, only the points lying on a common circle, that constitute a quad are concerned. Since circles are preserved, so are their planarity and the co-planarity of points lying on those circles. Therefore, stereographic projections of circular PQ meshes in flat configurations preserve planarity, see Fig. 5.12.

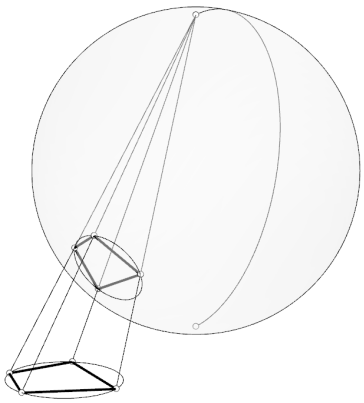

Fig. 5.12 Cyclic quad projected onto a surface of a sphere preserves planarity.
Vertices of the quad lie on the surface of a sphere, whereas in order to maintain the straight edges of projected quad, the edges were reconected after the projection.

Any planar, circular PQ mesh can be raised up onto a surface of a sphere with facets planarity preserved (see Fig. 5.13), not only isoradial ones like in the example above. Only one method of obtaining circular PQ meshes was presented in this work in section 4.1.7[67]. Those are isoradial meshes, whereas the radii of circumcircles do not have to be the same. A circular PQ mesh can be obtained from isoradial mesh by adoption of the method described in the following section. However, the applications of that transformation are much wider.

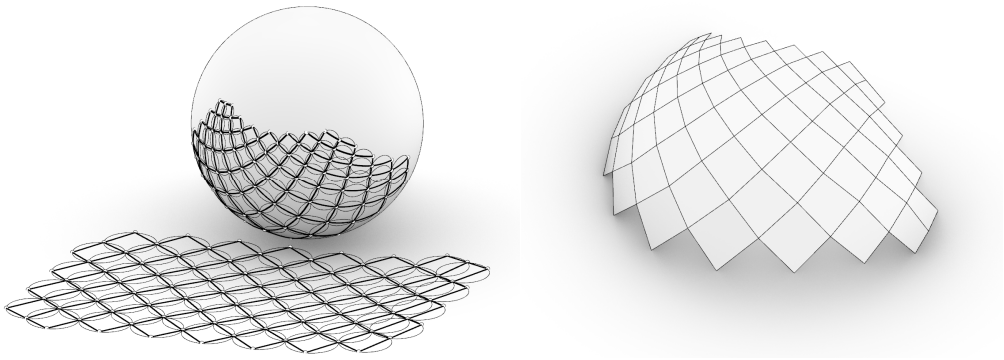

Fig. 5.13 Left: stereographic projection of isoradial mesh in flat confuguration obtained from Chebyshev net. Right: the resultant PQ mesh with shading.

Stereographic projection method have not been used for design and construction of PQ grid shell yet.

5.1.3. Inversions

Inversions (Weisstein 2018g), (Lachlan 1893) are conformal, i.e. angle preserving (Weisstein 2018d), geometric transformations, which are defined by a circle of inversion on a plane or a sphere of inversion in space (Weisstein 2018h). Points that are situated inside the circle of inversion are reflected outside and vice versa – from outside to inside of the circle. One particular point inside the circle, its centre point, is reflected into infinity and vice versa – points at infinity are mapped onto the centre of inversion circle. When a point in the centre of a circle of inversion is inverted, the direction is not specified – it is all around at infinity. Whereas image points (except of the point at infinity, and points placed at the circle of inversion) lie at the straight axes passing through the original points and the centre point of the inversion circle. Points that lie on the circle of inversion remain at the same place.

Each inversed point is reflected along the direction perpendicular to the circle of inversion, i.e. along the direction defined by the centre point of inversion and the inversed point. The distances between original point *X*, its image of inversion *X'* and the centre point of inversion circle *O* must meet the equation (5.2).

$$|\boldsymbol{OX}||\boldsymbol{OX'}| = \boldsymbol{r^2} \tag{5.2}$$

Where *r* is the radius of the circle of inversion. In other words – the distance from the centre point of inversion to the original point times the distance from the centre point of inversion to the image point is equal to the radius of inversion circle squared. From this equation the distance of the image from the centre point is derived. The exact position of the image point is defined by that distance and the line along which the centre and original points lie.

[67]Among others, a lot of methods for obtaining non-isoradial, planar, circular meshes belong to the wide scope of circle covering theorem, see (Rocha et al. 2013).

Figure 5.14 presents inversion of two points with defined distances.

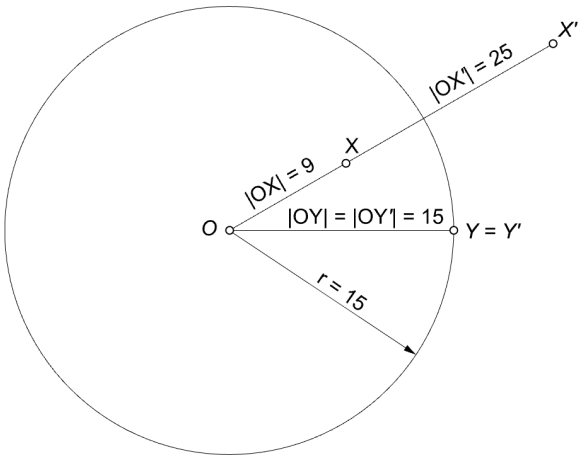

Fig. 5.14 Inversion of points X, Y *and* Z *by a circle with the centre point* O *and radius* r = 15.

The product of absolute distances from the centre of inversion to original and image points are equal the radius of the inversion circle squared, see equation (5.2). Knowing, that points: *O*, *X* and *X'* lie at a common line, all parameters are given to clearly specify the location of the image point. While if the point *Y* lies on the inversion circle, the equality (5.3) takes place.

$$|\boldsymbol{OY}| = \boldsymbol{r} \tag{5.3}$$

Therefore, additional equality (5.4) must also be satisfied in order to satisfy equation (5.2).

$$|\boldsymbol{OY'}| = |\boldsymbol{OY}| \tag{5.4}$$

It proves the statement, that if a point lies at the circle of inversion, it is coincident with its own image. Whereas, when the original point lies at the centre point of the inversion circle, then the equality (5.5) takes place.

$$|\boldsymbol{OO}| = \boldsymbol{0} \tag{5.5}$$

Therefore, the image point must be placed at infinity, see equation (5.9).

$$|\boldsymbol{OO'}| = \infty \tag{5.6}$$

The above reasoning is intuitive. However, the assumption that inversion of a point placed at the centre of inversion circle is a point at infinity gives very reasonable solutions in terms of geometry. The argumentation and intuitive explanation is given on the example of an inversion of a straight, infinite line, which is tangent to the inversion circle, see Fig. 5.15. Thirteen points were assigned on along the line ***a***. An inversion of each of these points was calculated and placed inside the inversion circle. As it happens, image points lie on a common circle, which is tangent to the inversion circle at the same point as the line ***a***. The extension of arc created by image points also passes through the centre point of inversion circle ***O***. It is also noticed, that points more distant from the tangent point on the line ***a***, have images closer to the point ***O***, which are also closer and closer to each other. By continuing adding points on the inverted circle ***a'*** closer to the point ***O*** the axes passing through ***O*** and image points would become almost parallel to the line ***a***. Eventually, at the infinitesimal distance to the point ***O***, the axis would be parallel to line ***a*** and by definition, two parallel lines intersect at infinity.

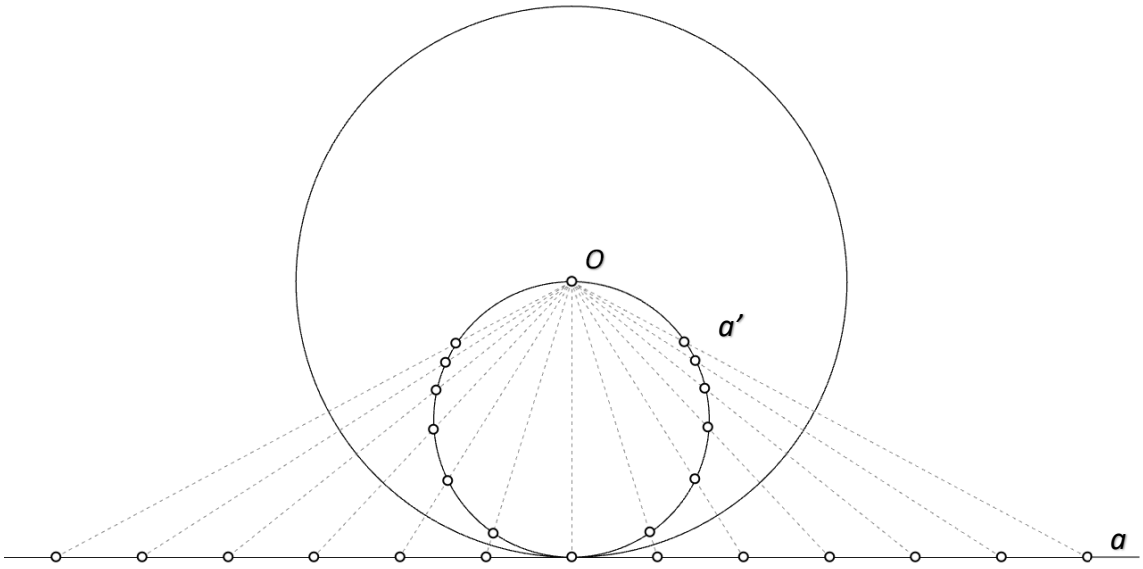

Fig. 5.15 Inversion of circle a', *tangent to circle of inversion* c *and passing through its centre point* O *is line* a, *which is also tangent to the circle of inversion at the same point and spans into infinity.*

Figure 5.16 shows a simple case, when the object of inversion is a circle *b*, which is concentric with the circle of inversion *c*. Since all points on that original circle are equally distant from the centre point of inversion, all the image points will also be equally distant from the centre point *O*. Hence, the image will be a circle *c'* with the same centre point as the original one.

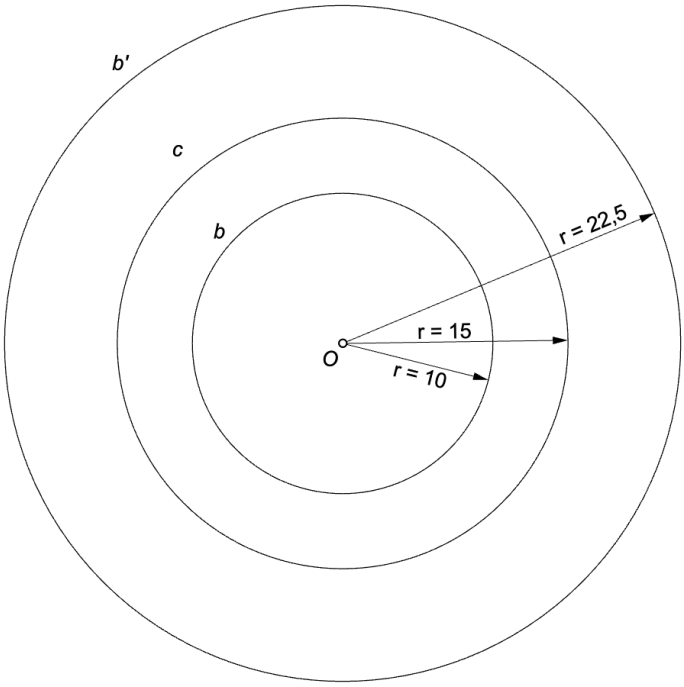

Fig. 5.16 Circle b *is inverted by circle* c. *All circles are concentric.*

Circle *b* in Fig. 5.17, which is randomly placed inside the inversion circle *c*, was divided into eight points. The inversions of those points were calculated, resulting in image points that lie on a common circle, i.e. *b'*. The *b'* circle is an image of inversion of *b*. However, the inversion of the centre point *B* of original circle *b* is not the centre point *B'* of image circle *b'*. Consequence of that is the fact, that although circles are preserved, their internal structures are not, i.e. the position of the centre point image is not in the centre of circle image and distance ratios between original and image points are not preserved.

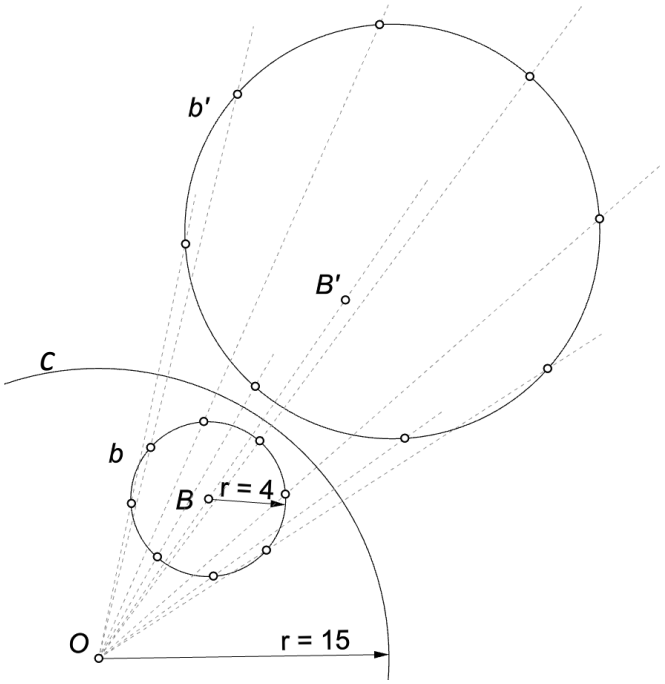

Fig. 5.17 Inversion of circle b*, randomly placed inside the inversion circle.*

Concluding, if the subject of inversion is a circle, the image is also a circle (Lachlan 1893), p. 221, except for the case, when the original circle intersects with the centre of inversion circle[68]. In such a case the image figure is a line which has points at infinity[69], see (Lachlan 1893), p. 235. Any other shapes are distorted as shown in Fig. 5.18.

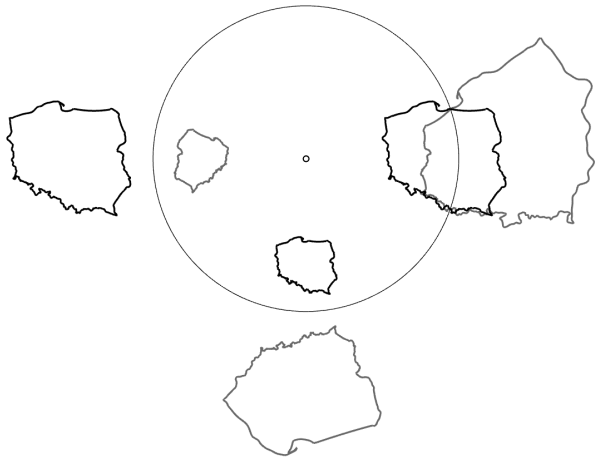

Fig. 5.18 Distortions in images of inverted non circular shapes.

For the purpose of planarity preserving inversions, only circular PQ meshes[70] are useful. Inversion of a straight line segment between two vertices of a quad generates an arch, therefore discrete transformation is performed, i.e. such that inverses only the vertices and connects their images with a straight line segment. The resultant quads are also cyclic.

[68] It not necessarily have to be tangent with the inversion circle as in Fig. 5.15.
[69] Such line by some interpretations is also considered as a circle, which has an infinite radius.
[70] Circular PQ meshes are PQ meshes in which all facets are cyclic quadrilaterals, i.e. all four vertices of each single facet lie on a common circle.

In Fig. 5.19 an isoradial[71] PQ mesh in planar configuration, obtained from Chebyshev net[72] (left) is inversed (right). Inversed mesh remains circular but individual line segments are deformed, i.e. straight edges have been inversed into arches. Those sections of arches can be replaced by straight line segments by connecting end points of the arches, which lie on the circles, see Fig. 5.20. The result of that replacement is a proper circular PQ mesh.

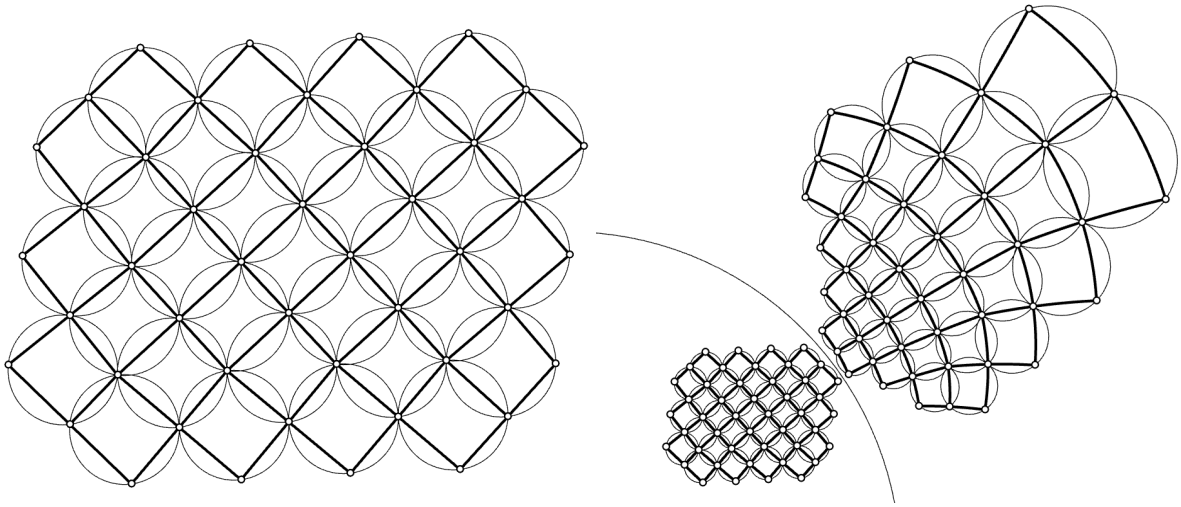

Fig. 5.19 Left: isoradial PQ mesh in flat configuration obtained from Chebyshev net. Right: inversion of that mesh. An image is also isoradial, with circles of various radii.

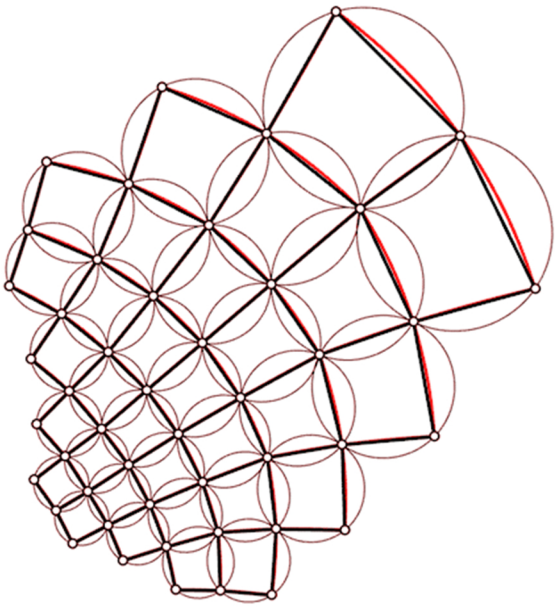

Fig. 5.20 Replacement of arched (red) edges into straight line segments (black).

By using inversions, an isoradial mesh in planar configuration[73] can be deformed into a planar, circular mesh with circles of various radii. Inversed, planar circular PQ meshes can be successfully projected stereographically according to the method described in section 5.1.2. Combination of both of these transformations increase the freedom of design of PQ meshes.

[71] Isoradial – all circles have equal radii.
[72] See section 4.1.7
[73] For example obtained by the method described in section 4.1.7.

Circular PQ meshes in planar configuration are also easily obtained in a manual manner. In such a case, the designer draws consequent circles, specifying their radii. Such approach would however require to specify many parameters manually, whereas combination of inversions and stereographic projections limits the necessary parameters, i.e. the initial parameters of isoradial mesh described in section 4.1.7, the parameters of inversion and the parameters of stereographic projection.

Combination of the two transformations: inversion and stereographic projection, and their potential for shaping meshes of reticulated shells is shown in the following figures. A simple, orthographic, planar, isoradial mesh in Fig. 5.21, left, is transformed by means of inversion, Fig. 5.21, right. Then, both original and inversed meshes are transformed by stereographic projection, Fig. 5.22. Comparison of both meshes after the last transformation is shown in Fig. 5.23.

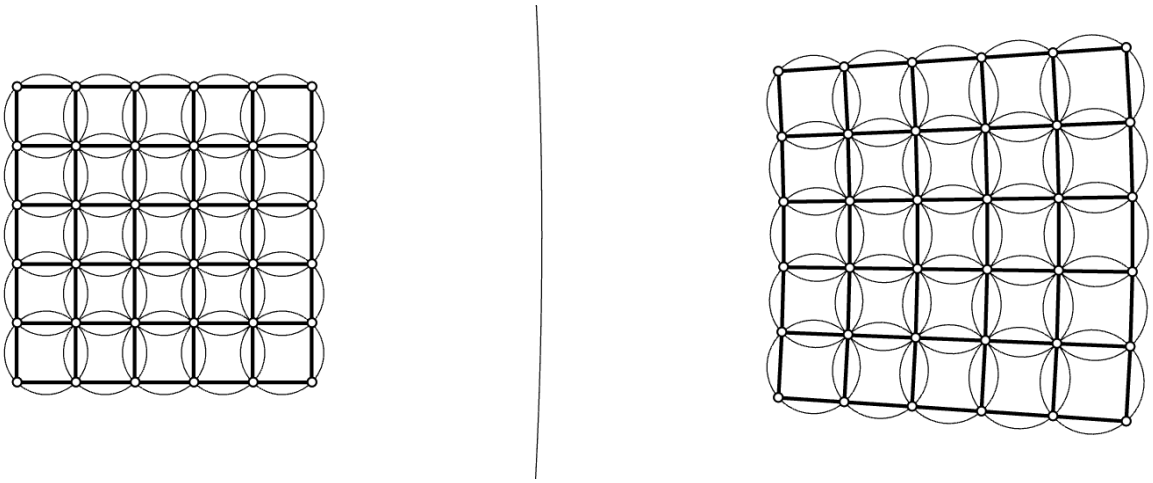

Fig. 5.21 An inversion of a simple, orthographic, planar, isoradial mesh. Left: original mesh, right: inversed mesh.

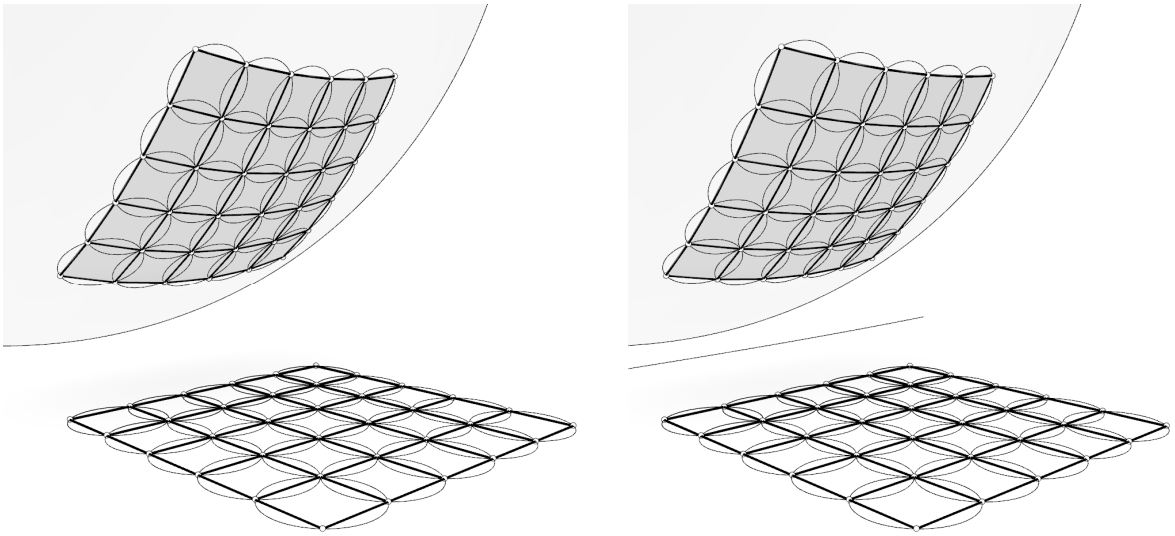

Fig. 5.22 Left: stereographic projection of simple, orthographic PQ mesh. Right: stereographic projection of that planar mesh after inversion.

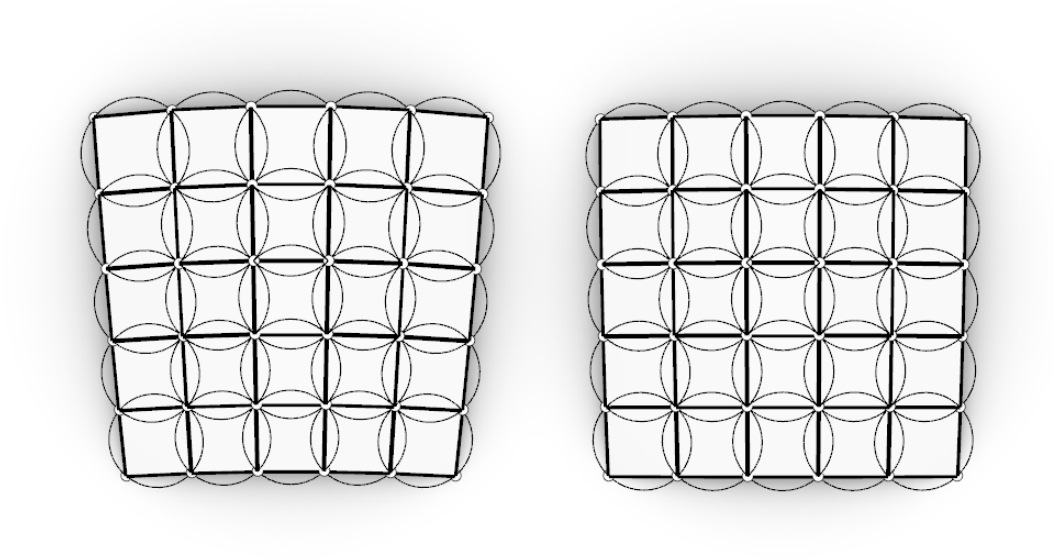

Fig. 5.23 Top view at stereographically projected meshes: the original one (left) and previously inversed (right). Previously inversed mesh (right) has more homogeneous radii of circles.

Inverse geometry on a plane allow to differentiate the radii of PQ circular meshes in planar configuration. However, the method can be expanded into third dimension. Then, inversion is made through the surface of a sphere, which is defined by a centre point and a radius – therefore the same parameters as in planar inversions. In this case, all points are reflected on the other side of the surface of a sphere. Similarly as in planar inversions, the points coincident with the centre of the inversion sphere are inversed into infinity, whereas point that lie on the surface of the sphere remain in place. Spherical inversion also preserves circles, if they do not intersect with the centre point. Moreover, spheres are also preserved under the same condition. Spheres intersecting with the centre of the sphere inversion are inverted into planes. A circular PQ mesh in planar configuration can be inversed by a sphere, resulting in discrete spherical PQ mesh – similarly to the meshes obtained through stereographic projections. Those transformation in the context of PQ meshes are studied and described in (Mesnil, Douthe, Baverel, and Léger 2015).

Two dimensional, circular inversions also have three dimensional equivalent in which an object is inversed by an inversion sphere. In spherical inversions all the rules from circular inversion are preserved, i.e.:

- centre point of the inversion sphere, original and image point are always colinear;
- equation (5.2) is still valid, i.e. quotients of distances between pairs of original and image points to the centre point of the inversion sphere is equal to the radius of the inversion sphere squared.

Spherical inversions also preserve circles and therefore preserve planarity of circular PQ meshes as well. These circular PQ meshes not necessarily have to be planar. Any spatial, single or doubly curved circular PQ meshes can be inversed by a sphere while preserving planarity of its facets. Figures 5.24 to 5.27 show a circular PQ mesh obtained according to the sweep method[74]. On the left side of each figure an original mesh is shown, whereas on the right side the mesh after inversion is shown. Additional transformations of reflection and scaling were performed on the inversed mesh in order to unify its size with the original mesh, so that both can be compared visually.

[74] Method described in section 4.1.5.

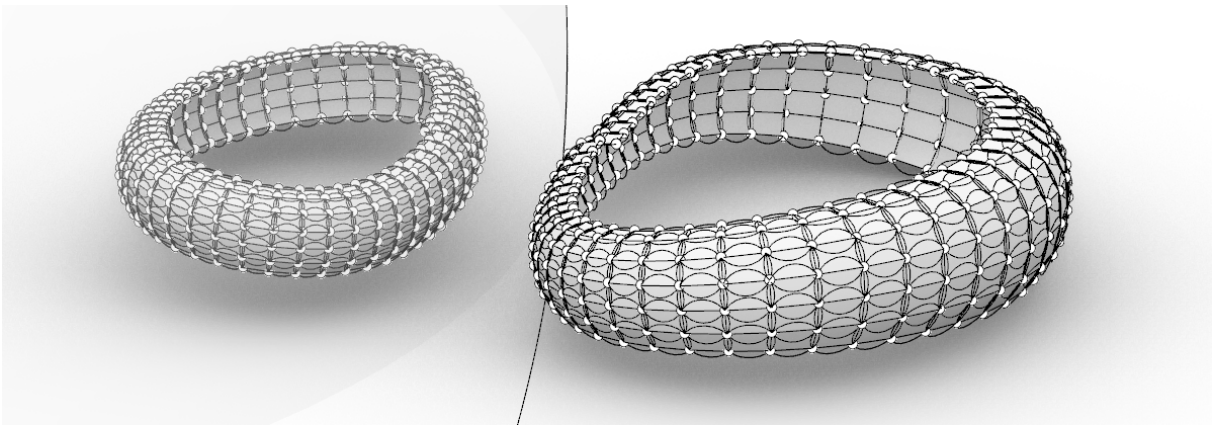

Fig. 5.24 Inversion of a circular PQ mesh obtained with the use of sweep method discussed in section 4.1.5. Original mesh located on the left side, within the inversion sphere.

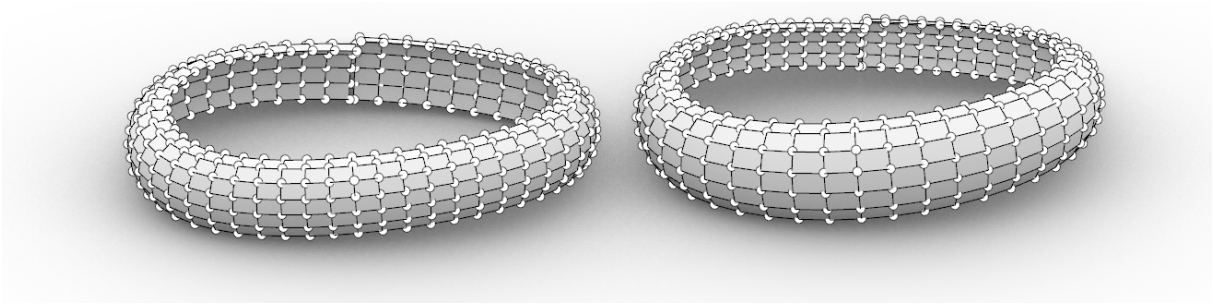

Fig. 5.25 Comparison of circular, sweep PQ mesh from Fig. 5.24 - before (left) and after inversion (right). Axonometric view.

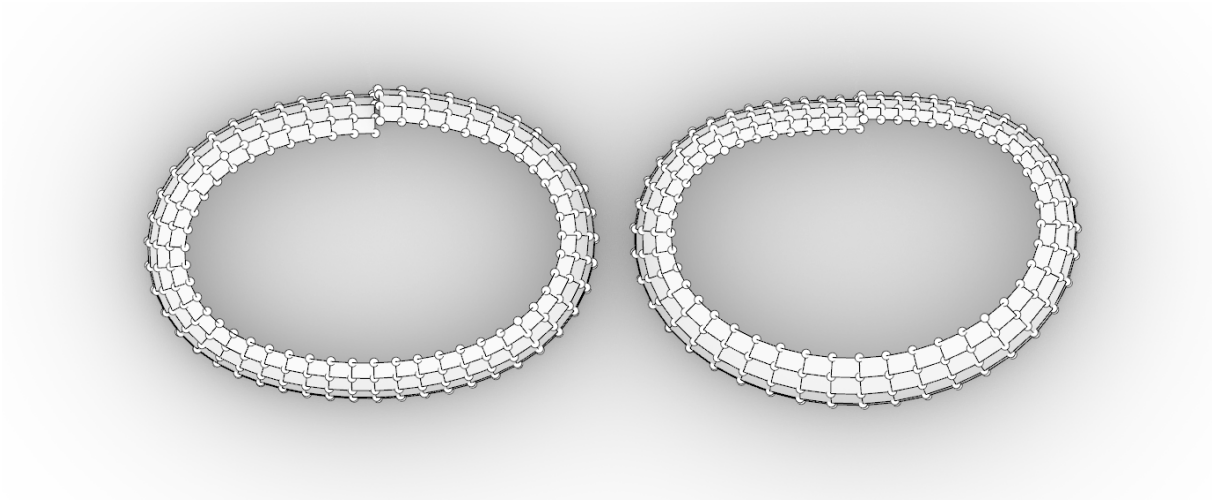

Fig. 5.26 Comparison of circular, sweep PQ mesh from Fig. 5.24 - before (left) and after inversion (right). Top view.

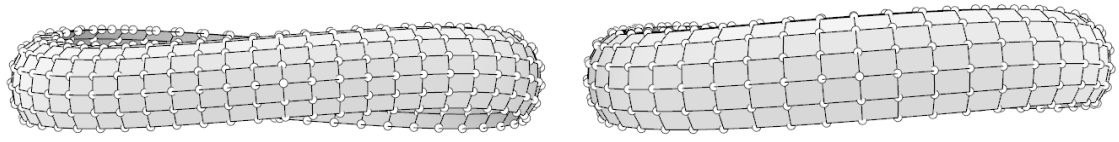

Fig. 5.27 Comparison of circular, sweep PQ mesh from Fig. 5.24 - before (left) and after inversion (right). Front view.

Inversions as a method for transforming circular PQ meshes are described in details in context of designing PQ meshes in (Mesnil et al. 2017). However, the described method have not been used for design and construction of PQ grid shell yet.

5.2. New methods of transformation proposed by the author

In this section new methods of transformation of PQ meshes preserving their planarity, developed by the author of this work, are presented and explained. All this methods significantly increase possibilities of transforming and adjusting PQ meshes.

5.2.1. Spherical-cylindrical (SC) mapping

Spherical–cylindrical mapping is a function developed by the author of this work. It belongs to the groups of projection maps and outputs exactly one value for each element in the input set (Weisstein 2018i). In this case, an input and an output sets contain points in 3D space that form the mesh. Projection maps are well known from cartography. Their purpose is to assign individual point on a plane to a point on a sphere, i.e. the globe. There are many types of projection maps. Each one has its specific advantages and disadvantages. There are types of map projections that preserve angles (conformal maps), distances (equidistant) or areas. Mapping is always associated with distortions and it is impossible to map a sphere onto a plane without distortions, i.e. preserving all three properties (angles, distance and areas) with one particular mapping.

Whereas projection maps in cartography concern transformations between surfaces (two dimensional domains), mapping of a doubly curved PQ mesh requires a function that will map every point in the three dimensional domain into another one, also three dimensional. Such 3D mapping transformation assigns exactly one point in the three dimensional image space to each point from the original three dimensional space. The assignment has to be done is such a manner, that point lying on a common plane will remain co-planar after the mapping. Hence the SC mapping transformation can also be called iso-planar.

5.2.1.1. Systems of coordinates

As mentioned above the essence of spherical-cylindrical mapping is transformation of points from Cartesian system of coordinates to spherical-cylindrical system of coordinates. These systems of coordinates and relations between them are discussed below.

Cartesian system of coordinates

Location of points in three dimensional space can be specified by means of three coordinates of the Cartesian system of coordinates, i.e. *x*, *y* and *z*), see Fig. 5.28.

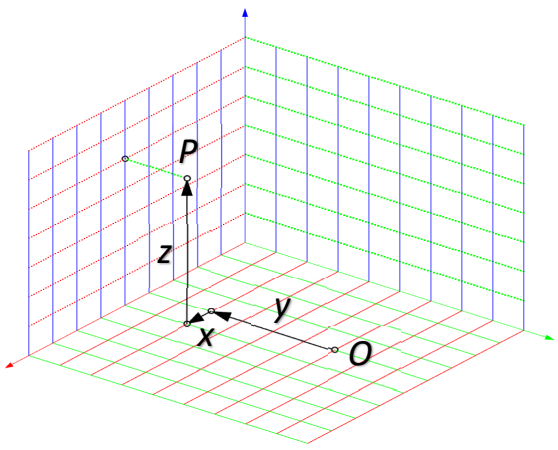

Fig. 5.28 Location of the point P *relative to the point* O *in Cartesian coordinate system.*

Cylindrical system of coordinates

In a cylindrical system of coordinates (see Fig. 5.29) the position of a point, measured relative to the beginning of the coordinate system in point *O*, is defined by three coordinates - *ρ*, *φ*, *z*. Coordinate *ρ* describes the distance of *P* from the central, vertical axis passing through the point *O*. Coordinate *φ* is the angle between the red axis and the vertical plane containing point *O*, on which lies the point *P*. The last coordinate – *z*, is the distance of the point *P* from the horizontal plane containing *O*. The real distances increase proportionally to the increment of coordinate values, i.e. when coordinate *ρ* is doubled, the distance of *P* to the central axis is also doubled.

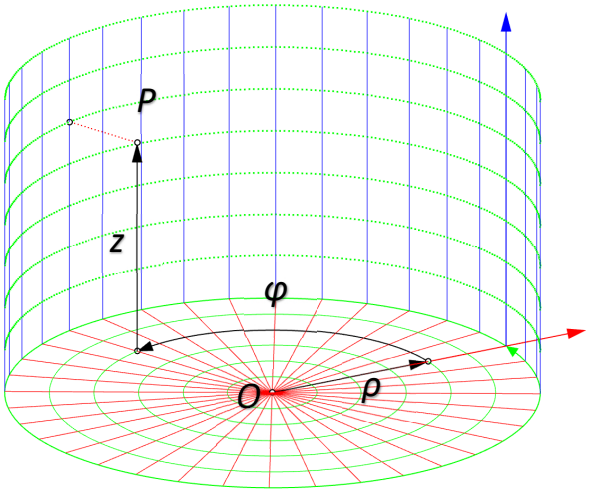

Fig. 5.29 Location of the point P *relative to the beginning of the coordinate system in cylindrical coordinate system.*

Spherical system of coordinates

In the spherical coordinate system (see Fig. 5.30) the position of point *P* measured relative to the beginning of the coordinate system in point *O*, is defined by three coordinates - *ρ*, *φ* and *ϑ*. Coordinate *ρ* describes the distance of *P* from the central point *O*. Coordinate *φ* is the angle between the red axis and the vertical plane containing point *O*, on which lies the point *P*. The last coordinate *ϑ* is the angle between the horizontal plane containing point *O* and the axis passing through points *O* and *P*. Again, as in cylindrical coordinate system, the real distances increase proportionally to the increment of coordinate values.

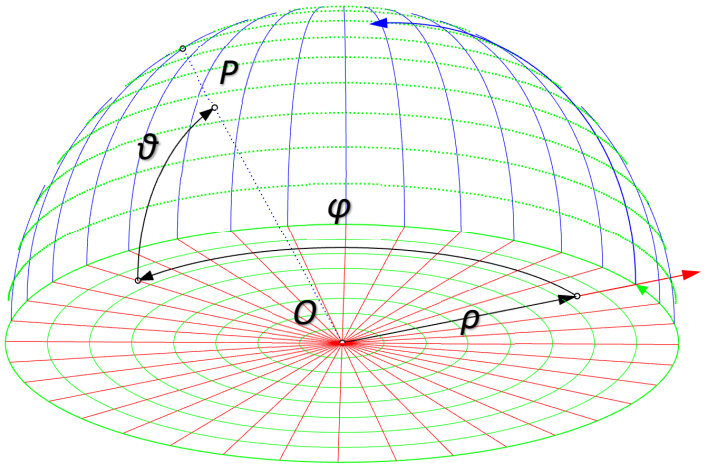

Fig. 5.30 Location of the point P *relative to the beginning of the coordinate system* O *in spherical coordinate system.*

Spherical-cylindrical (SC) system of coordinates

In the spherical-cylindrical system of coordinates (see Fig. 5.31) coordinate φ is similar to the both: cylindrical and spherical coordinate systems, i.e. it is an angle of rotation around the point *O*. Coordinate *z* is similar to that in the cylindrical coordinate system – it is the distance above the horizontal plane containing point *O*. Coordinate λ resembles coordinate ρ from both previously described coordinate systems, which measure the distance from the centre point *O*. However, contrary to the coordinate ρ, the measure of coordinate λ is heterogenic, i.e. the real distances increase disproportionately to the increment of coordinate value. It can be seen comparing distances between successive green circles in Fig. 5.31 – the further from the centre point, the closer to each other are the circles.

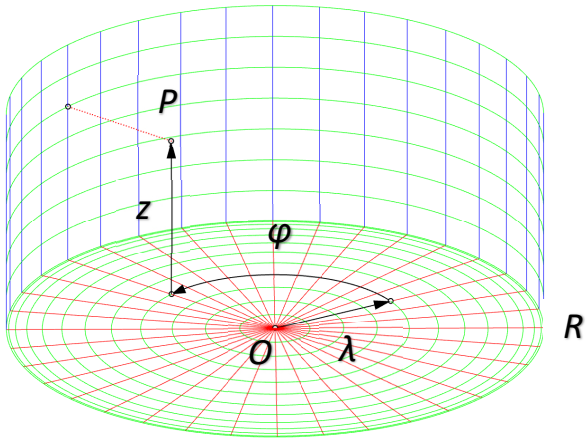

Fig. 5.31 Location of the point P *relative to the beginning of the coordinate system* O *in spherical-cylindrical coordinate system. The coordinate system has additional property –* R*, which stands for the radius of the edge of the coordinate system.*

The real distances between consequent green circles are derived from the spherical coordinate system, see Fig. 5.32. However, it is required to determine one particular parameter *R*, which is the radius of the sphere in the spherical coordinate system. To measure the distance between point *P* to the beginning of the coordinate system *O*, point *P* is firstly vertically projected on a sphere with radius *R*, resulting with the *P'* image point. Then an angle is measured between the horizontal axis containing point *O* and the axis passing through points *O* and *P'*. In the particular case shown in Fig. 5.32 the angle is equal 30^o and the same is the value of the coordinate λ. The domain of coordinate λ is limited to the range $[0^o, 90^o]$. At the edge of the coordinate system, coordinate λ is equal 90^o and cannot exceed that value.

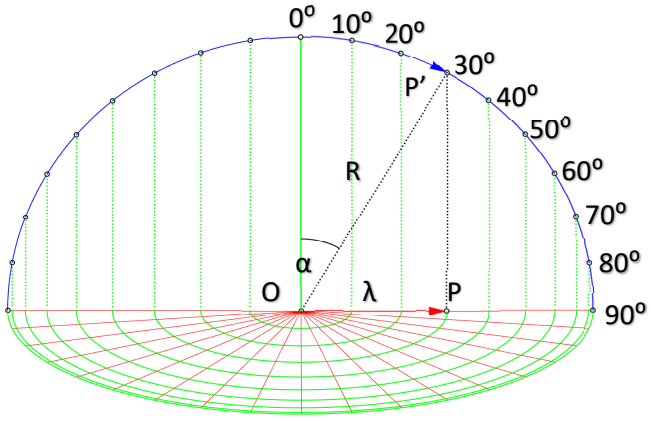

Fig. 5.32 Hemisphere of spherical coordinate system projected onto a plane containing O*. The values of angle α determine the value of coordinate* λ*.*

5.2.1.2. Transformation of coordinates between SC and Cartesian systems

Spherical–cylindrical mapping transforms objects by mapping between Cartesian and SC coordinate systems (see Fig. 5.33). Position of original point is defined by three Cartesian coordinates: *x*, *y* and *z*, whereas in the SC system of coordinates, the position of a point is defined by the coordinates *λ*, *φ* and *z*. SC mapping is a linear function, which outputs the values of SC coordinates from the values of Cartesian coordinates. New points created by SC mapping require conversion back to the Cartesian coordinate system, i.e. new coordinates *x'*, *y'* and *z'* are calculated for each SC mapped point. Both steps: mapping and conversion are represented in (5.7), where first symbol → denotes mapping and the second one denotes conversion.

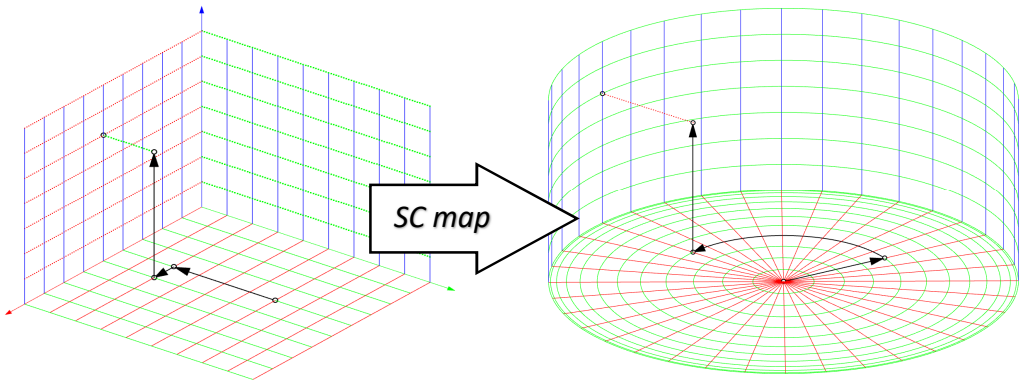

Fig. 5.33 SC mapping is a transformation between orthogonal and spherical-cylindrical spaces.

$$(\boldsymbol{x}, \boldsymbol{y}, \boldsymbol{z}) \rightarrow (\boldsymbol{\lambda}, \boldsymbol{\varphi}, \boldsymbol{z}) \rightarrow (\boldsymbol{x'}, \boldsymbol{y'}, \boldsymbol{z'}) \tag{5.7}$$

Mapping of the first coordinate: *x* → *λ* requires setting some additional constraints. It is crucial to emphasize the fact, that the values of *λ* are within the range of angles: [0°, 90°] (see Fig. 5.32), where *λ* is directly related to *α*), whereas a point in orthogonal space can be placed in unbounded domain of *x* values (-∞, +∞). Therefore, in order to assign proper mapping, the bounds of *x* domain have to be set. Precisely, if the domain of *x* is within closed interval [X_1, X_2], then any value of *x* between X_1 and X_2 can be linearly mapped to a value of *λ* within closed interval [0°, 90°], see formula (5.8). Values of X_1 and X_2 are derived from the shape of the original object, see Fig. 5.34 top.

$$[\boldsymbol{X_1}, \boldsymbol{X_2}] \rightarrow [\boldsymbol{0}°, \boldsymbol{90}°] \tag{5.8}$$

If the boundaries given by right side of equation (5.8) are exceeded, the mapped object would wrap and turn back to the origin of the coordinate system after mapping – see Fig. 5.32 and Fig. 5.34. However, it is not necessary to use the whole domain of *λ* given by (5.8). By changing the domain of *λ* values different final forms of transformed object can be obtained. Narrowed domain of *λ* coordinate is expressed by interval (5.9).

$$\boldsymbol{\lambda} \in [\boldsymbol{\lambda_1}, \boldsymbol{\lambda_2}] \tag{5.9}$$

Where λ_1 is the distance from the origin point, and λ_2 is the distance from the external boundary of SC space. Eventually, mapping of coordinate *x* has a form of expressed by (5.10) and is calculated by the formula (5.11).

$$[\boldsymbol{X_1}, \boldsymbol{X_2}] \rightarrow [\boldsymbol{\lambda_1}, \boldsymbol{\lambda_2}] \tag{5.10}$$

$$\boldsymbol{\lambda} = \boldsymbol{aX} + \boldsymbol{b} \tag{5.11}$$

Parameters a and b are computed by solving the system of two equations with values of X_1, X_2, λ_1 and λ_2. Then, the cylindrical distance of any point represented by coordinate λ to the vertical axis passing through central point O is calculated from the formula (5.12), where R is the real radius of SC space which can be defined arbitrarily.

$$\boldsymbol{\rho = R \sin \lambda} \tag{5.12}$$

Additionally, mapping of y coordinate: $y \rightarrow \varphi$ also requires determination of narrowed domain of φ. Absolute boundaries of the domain of φ are within the closed interval [0^o, 360^o]. Thus, narrowed domain of φ is expressed by formula (5.13), where φ_1 is the value of angle between lower boundary and main axis of the coordinate system ($\varphi = 0^o$) and φ_2 is the value of angle between upper boundary and main axis of the coordinate system ($\varphi = 0^o$), see Fig. 5.34 bottom.

$$\boldsymbol{\varphi \in [\varphi_1, \varphi_2]} \tag{5.13}$$

Values Y_1 and Y_2 are analogically to the x coordinates derived from original object, see Fig. 5.34 top.

The boundaries of coordinate y are set as before in the form of closed interval: [Y_1, Y_2]. Coordinate y of each transformed point is mapped to a value from range [φ_1, φ_1], see mapping (5.15). The formulation of this mapping is given by formula (5.15).

$$\boldsymbol{[Y_1, Y_2] \rightarrow [\varphi_1, \varphi_2]} \tag{5.14}$$

$$\boldsymbol{\varphi = cY + d} \tag{5.15}$$

Finally, the z coordinate remains unchanged as an isotropic distance above horizontal plane containing point O.

Cylindrical coordinates (ρ, φ, z) are calculated with the formula (5.12) or taken directly from SC coordinates (λ, φ, z). Finally, cylindrical coordinates of mapped points are converted into Cartesian system of coordinate (x', y', z'). Conversion between systems is calculated according to the formulations (5.16), (5.17) and (5.18).

$$\boldsymbol{x = \rho \cos \varphi} \tag{5.16}$$

$$\boldsymbol{y = \rho \sin \varphi} \tag{5.17}$$

$$\boldsymbol{z = z} \tag{5.18}$$

Example of two dimensional SC mapping

Example shown in Fig. 5.34 shows mapping of the shape of Poland's boundaries between two-dimensional Cartesian space and two-dimensional SC space. The third coordinate stays unchanged, therefore it is omitted in this example. The bounds on the SC space along the λ direction are chosen arbitrarily as:

- $\lambda_1 = 20^o$,
- $\lambda_2 = 70^o$,

and bounds around the coordinate φ are:

- $\varphi_1 = -30^o$,
- $\varphi_2 = 30^o$.

The domains of x and y coordinates are set by the external parts of the original shape and are represented by closed intervals $[X_1, X_2]$ and $[Y_1, Y_2]$.

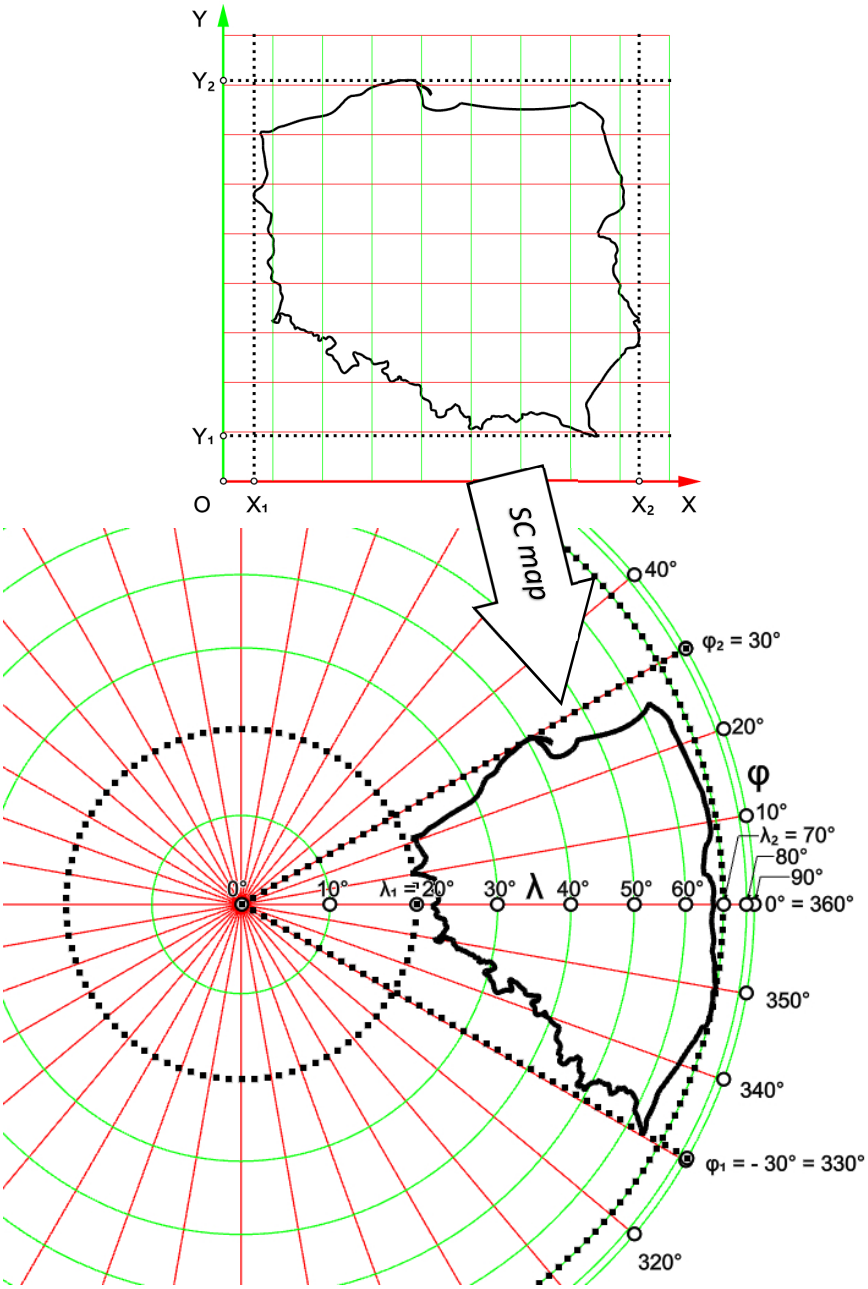

Fig. 5.34 SC mapping of a planar shape.

5.2.1.3. Extension of the methodology to 3D PQ meshes

Previous paragraph of this section described the details of SC mapping on plane. The following part of this section will explain how, why and when such mapping may be applied to a three dimensional PQ mesh in such a way that it preserves planarity of its facets.

The SC mapping transformation preserve facets planarity in two particular cases. The first case is a SC mapping of a translational PQ mesh with straight directrix, see Fig. 5.35, left. The image of mapping is a rotational mesh with slightly deformed generatrix, see Fig. 5.35, right. Planarity is preserved since individual pairs of opposing edges remain parallel after the transformation.

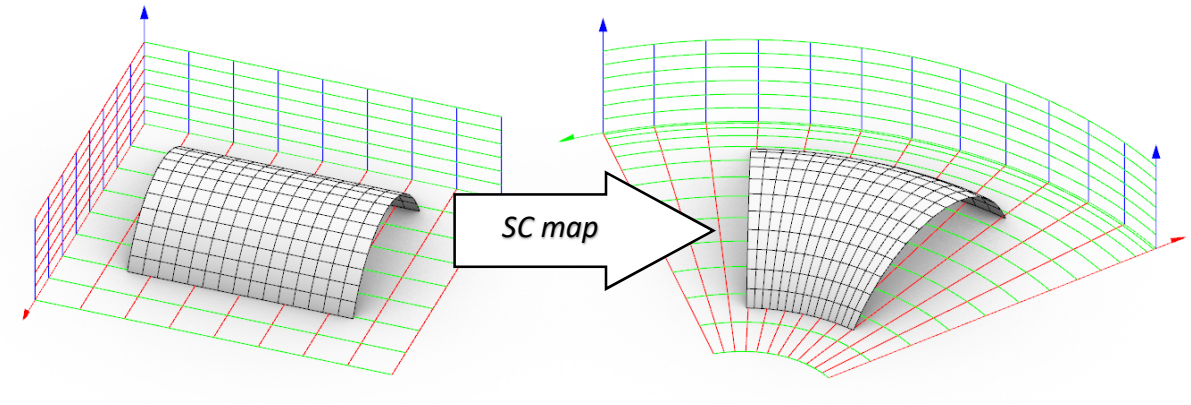

Fig. 5.35 Planarity preserving case of SC mapping: a simple, translational mesh.

The SC mapping maintains planarity of facets of PQ meshes if parallelism of opposite edges of each facet is maintained. There are two conditions that have to be fulfilled together in order to preserve this parallelism:

1. Within one of the two families[75] of edges in the mesh for each facet two opposite edges has to be of equal length.
2. Alternatively:
   2.1. If the edges from the concerned family are horizontal, they must be:
      2.1.1. Parallel to the *y* axis, or
      2.1.2. Diagonal to *x* and *y* axes (the angle between the edge and the axes is equal 45° or -45°).
   2.2. If the edges from the concerned family are not horizontal, their projection on the horizontal plane (normal to *z* axis) must be diagonal to *x* and *y* axes (the angle between the edge and the axes is equal 45° or -45°).

In continuous form of cylindrical–spherical space, for chosen value of φ all tangents to the green circles are parallel, see Fig. 5.36. Therefore, if edges of a PQ mesh are parallel to each other and to the *y*-axis, then they remain (discretely) parallel after the SC mapping. In other words, the green, parallel lines in Fig. 5.35 and every line segment which is parallel to them is transformed into green circles and circular segments concentric with them in plain projection, see Fig. 5.35 right. Knowing, that some edges remain parallel in the plan view, it is only required to keep their heights above the horizontal plane, i.e. coordinate *z*. In cylindrical–spherical space, the parallelism is considered discreetly. Tangent directions of the green circles in Fig. 5.36 along particular λ direction are parallel to each other.

[75] A family of edges is composed of edges lying on the same type of profile chains of segments or profile curves. For example one family of edges is composed of those edges that lie along directrix profiles, whereas second family is composed of those edges that lie along generatrix profiles. Within individual facets two edges of the same family are not adjacent and are situated on opposite sides the facet. Edges from two families are in alternate array around each vertex in mesh.

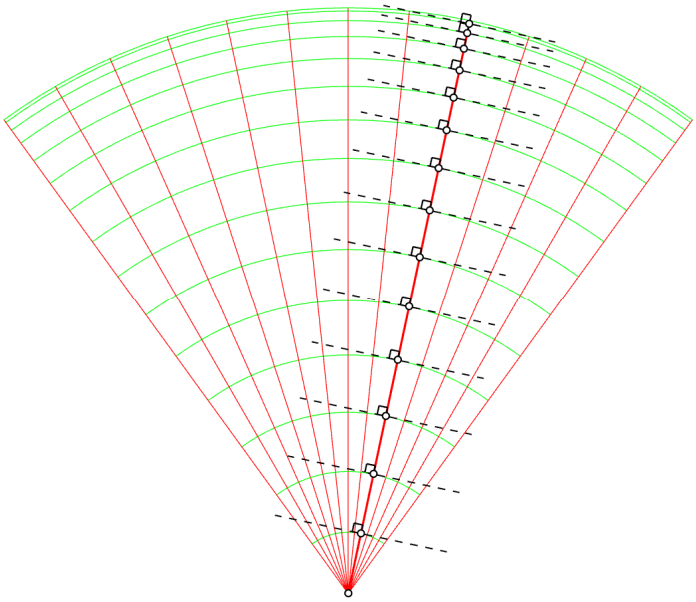

Fig. 5.36 The red, λ axis intersects with green φ circles.
All dashed, that are tangents to the green φ circles at the points of intersection with the red λ axis are mutually parallel.

Second case when SC mapping preserves planarity of facets is when conditions described before: (1 and 2.1.2) or (1 and 2.2) are met. In Fig. 5.37, top, line *D* is diagonal with respect to the orthogonal coordinate system, so is the set of lines *d*. Line *D* intersects with lines *d* perpendicularly. Lines *T* indicate the tangent direction of consequent *d* lines at the points of intersection with *D*. This system is SC mapped, see Fig. 5.37. In the result of that mapping, the *D* line becomes circle *D'* and lines d_i become circles d_i'. All the circles *D'* and d'_i pass through the centre point of the SC space and are tangent to the external boundary of that space. Consequent tangent directions T_i' in the mapped system, which are the tangents of d_i' at the points of intersections with *D'*, are also mutually parallel. Consequently, these intersection directions remain discretely perpendicular after mapping.

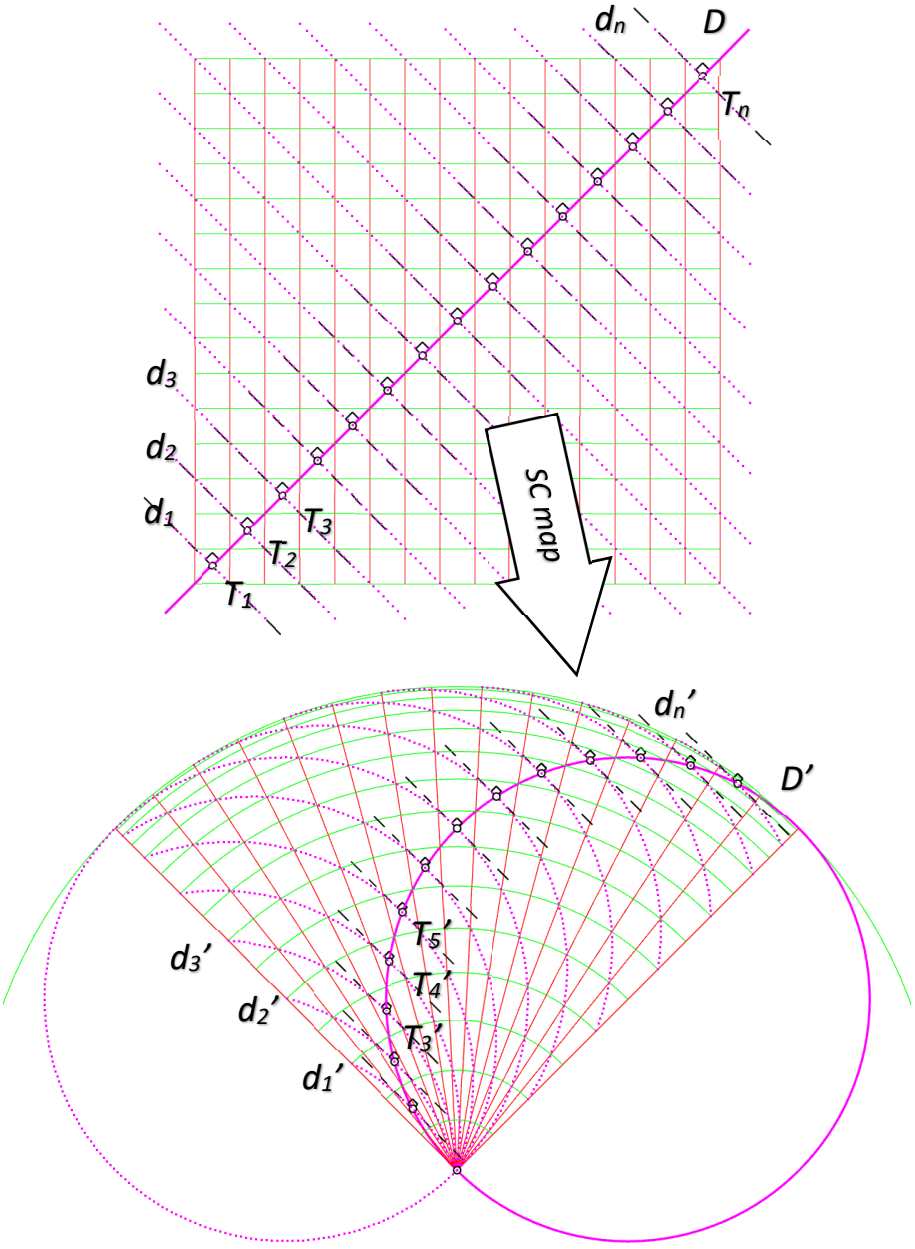

Fig. 5.37 Top: a set of diagonal lined d and one line D, which is diagonal in opposite direction. Bottom: images of D and d becomes circles, which pass through the centre point of the SC space, and which are tangent with its external boundary.

An example of application of previously presented method is SC mapping of a translational PQ mesh diagonally aligned with the orthogonal coordinate system, see Fig. 5.38. All edges of that mesh which are parallel to each other and diagonal to the system of coordinates preserve parallelism after mapping and therefore also the planarity of faces they define.

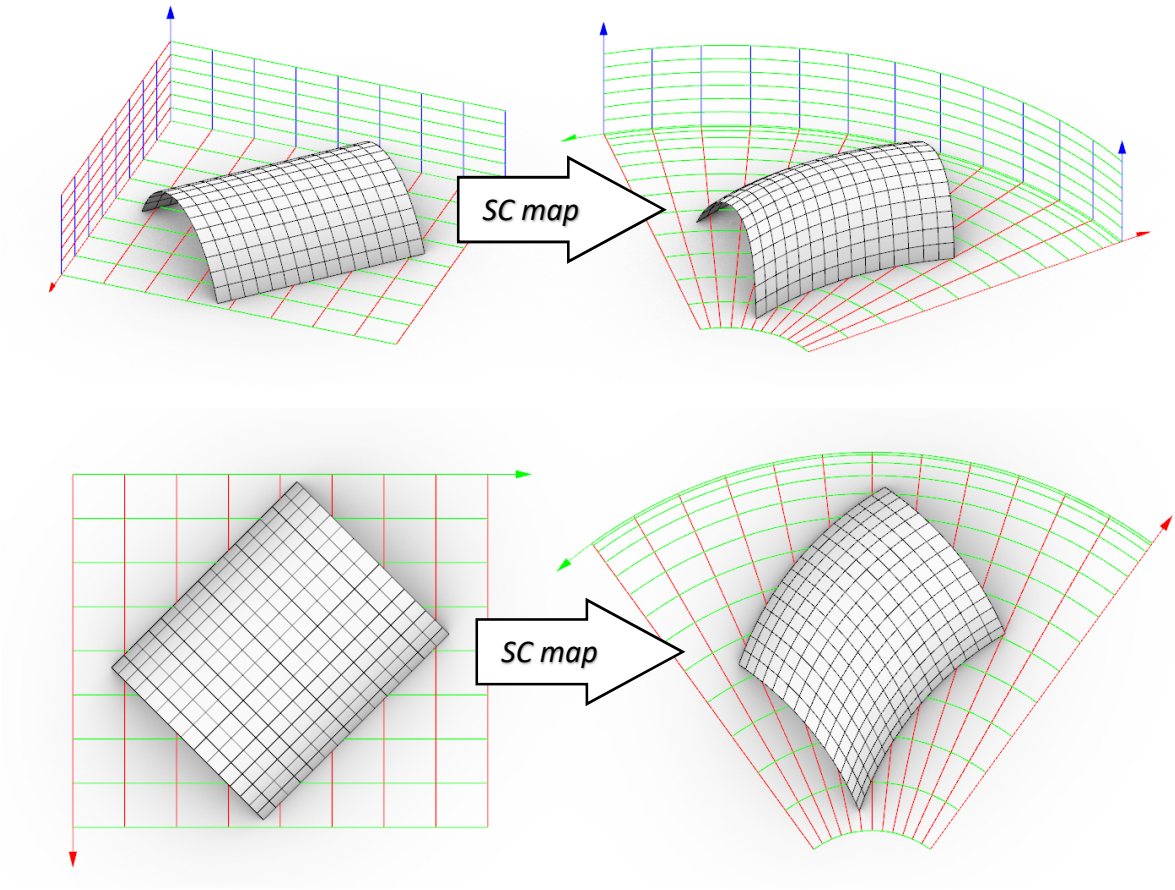

Fig. 5.38 Planarity preserving SC mapping of a translational PQ mesh with straight directrix. The PQ mesh is aligned diagonally to the orthogonal system directions.

When parallel to the *y* axis of the Cartesian coordination system, the edges change their lengths after mapping. It can be noted in Fig. 5.35 to 5.40 that the lengths of green segments vary. The *z* coordinate of vertices (edges' endpoints) is preserved, thus initially parallel edges of the same length are not parallel after mapping, unless the *z* coordinate is the same for vertices at both sides of each edge, i.e. edges remain horizontal. However, the parallelism is preserved also for non-horizontal pairs of edges, when they are aligned diagonally (condition 2.2 on page 122), see examples in Fig. 5.40 and 5.40. It is determined by the fact, that all diagonal of SC coordinate system are of equal length, see Fig. 5.41.

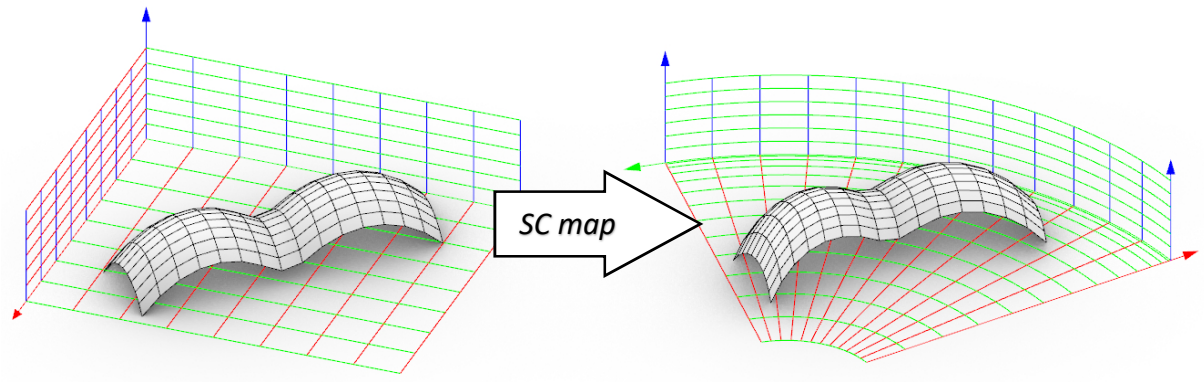

Fig. 5.39 Planarity preserving SC mapping of a translational PQ mesh with spatial directrix. The PQ mesh is aligned diagonally to the orthogonal system directions. Axonometric view.

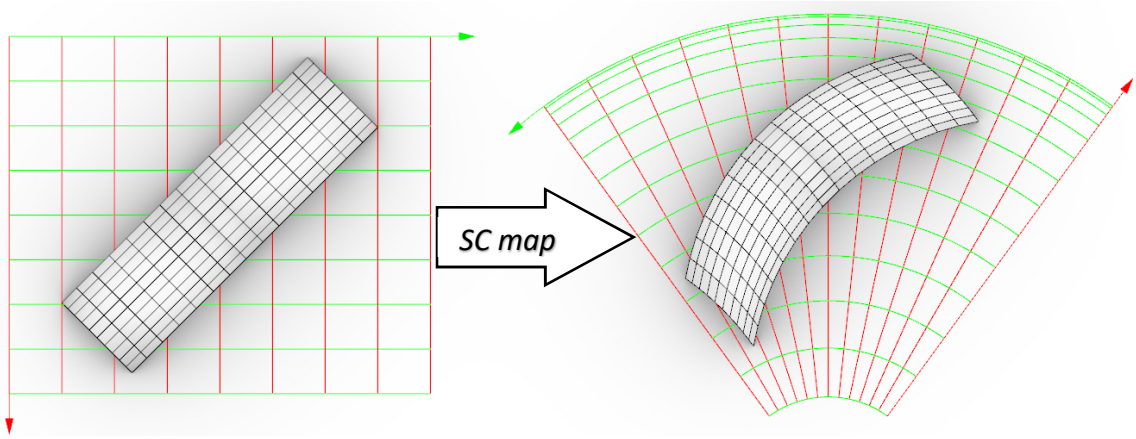

Fig. 5.40 Planarity preserving SC mapping of a translational PQ mesh with spatial directrix. The PQ mesh is aligned diagonally to the orthogonal system directions. Top view.

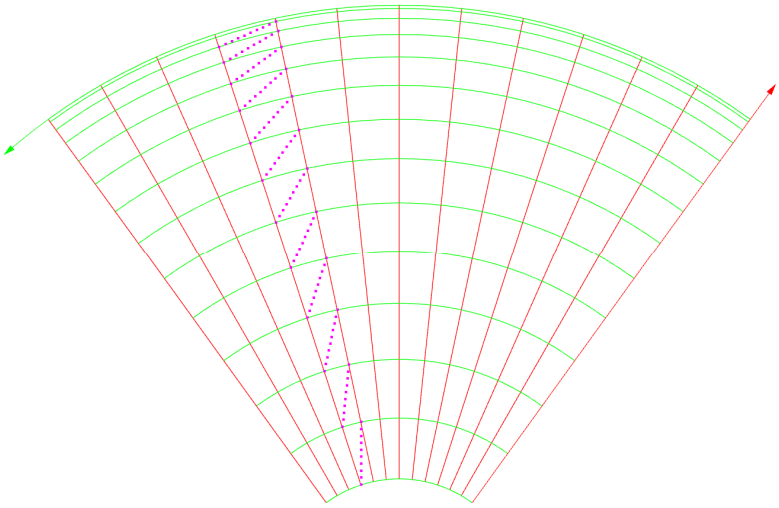

Fig. 5.41 Lengths of green segments vary along the coordinate λ, so do lengths of red segments around coordinate φ. Whereas purple, dotted diagonals have constant lengths all over the SC space.

5.2.1.4. SC mapped quasi-PQ meshes

In section 5.2.1.3 conditions for proper SC mapping of PQ meshes are given. This conditions are source of limitations in the use of presented method. However, if constraints are released within some reasonable limits, SC mapping results in meshes with non-planar facets which distortion of planarity is also within reasonable range. These meshes will be called quasi-planar quadrilateral (quasi-PQ) meshes. Despite the fact that their facets are not planar, these meshes are still useful for design purposes. This is due to the fact that they can be further optimized by means of an algorithm and finally become a proper PQ meshes. This procedure will be called *planarization* and is discussed further in this section. Usage of the quasi-PQ meshes is justified because it extends the catalogue of available PQ forms.

Measure of the planarity distortion

The planarity measure *P* is a proportion between the distance between facet's diagonals and half of their summed length given in percent, see formula (5.19) and Fig. 5.42. It represents credible planarity, regardless of the shape of the facet and its size. Green colour means exact planarity, colours between yellow and red represent distortions values between 0,0% – 2,0% and above. In further examples facets are colorized according to the planarity measure.

$$P = \frac{d}{(D_1 + D_2)/2} * 100\% \tag{5.19}$$

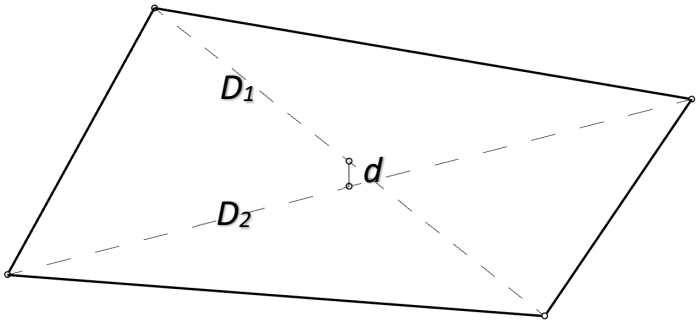

Fig. 5.42 Distance - d - between two diagonals - D_1 and D_2.

Table 5.1 shows examples of PQ meshes in their orthogonal form and SC mapped in aligned and diagonal versions. All images of diagonal mapped PQ meshes show negligible distortions in planarity of facets. The same meshes occur slightly higher distortions, when aligned for the SC mapping. In both cases, quasi-PQ meshes are eligible for optimization.

Table 5.1. Results of SC mapping of different types of original PQ meshes.

Type of initial PQ mesh	Shape of initial PQ mesh	Image of aligned SC mapping	Image of diagonal SC mapping
Translational mesh, with straight directrix			
Translational mesh with horizontal, planar directrix			
Translational mesh with vertical, planar directrix			
Translational mesh with non – planar directrix			
Scalar – translational mesh			
Sweep mesh			

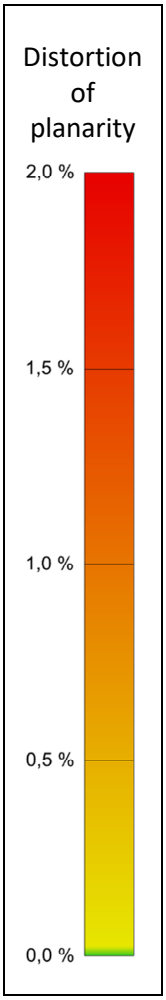

Super-elliptical-cylindrical mapping

As it was shown previously in this work (section 4.2.2 Super-ellipsoids) the concept of sphere can be extended into super-ellipses. An example of that proposition is shown in Fig. 5.43.

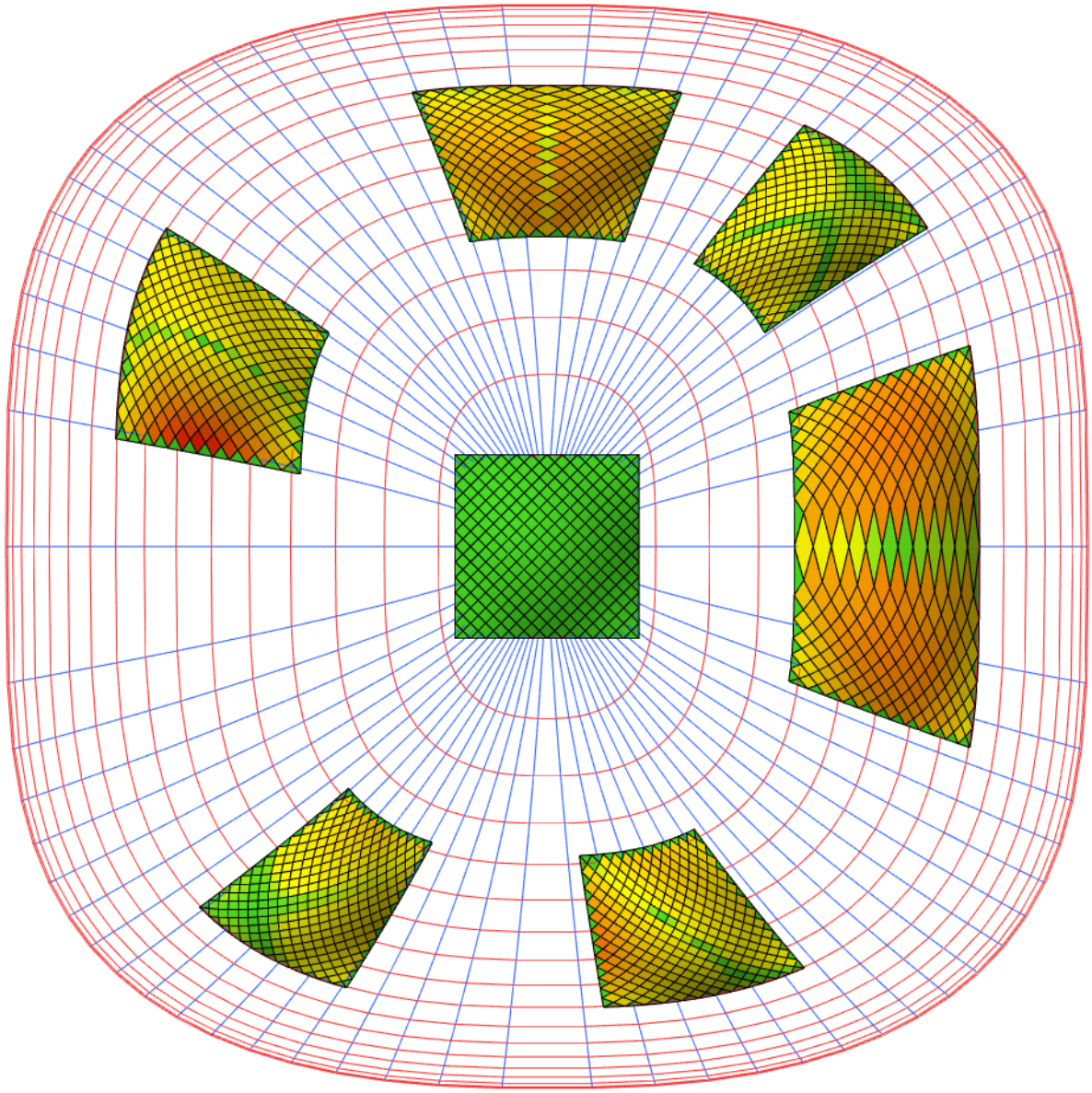

Fig. 5.43 Proposition of the extension of SC mapping: Super-elliptical-cylindrical mapping. The resultant meshes are quasi-planar, however capable of planarity optimization. The mesh (scalar with planar base) in the middle is in orthogonal configuration.

The SEC mapping (Super-elliptical-cylindrical) is a specific subgroup of quasi-PQ mappings extending further the catalogue of available PQ forms. More deep exploration of possibilities offered by SEC mapping are out of scope of this work.

Planarization of SC mapped quasi-PQ meshes

In this work quasi-PQ meshes are planarized by the Kangaroo Live Physics engine in Grasshopper/Rhino. In such optimization process each vertex has a goal to land on a plane defined three other vertices, with whom it creates a common facet. The goal is defined by a vector indicating the desired position of the vertex. As each vertex of a quadrilateral mesh (not including those on edges)

is adjacent to four facets, the goal is an average of four vectors. For each vertex the goal vector is computed and scaled down by a certain factor. The optimization is an iterative process. When each vertex is translated along reduced goal vector, the calculation of new goals is repeated. The iteration steps are repeated until, the system converges, and all facets are planar.

Figure 5.44 shows some iteration steps of planarization. The initial mesh was highly distorted, i.e. most facets revealed over 2% of distortion. The result of the planarization is a PQ mesh with all facets exactly planar. Moreover, the global shape of the mesh was preserved with slight shifts of the vertices, whereas positions of all vertices on the edge of the mesh were preserved.

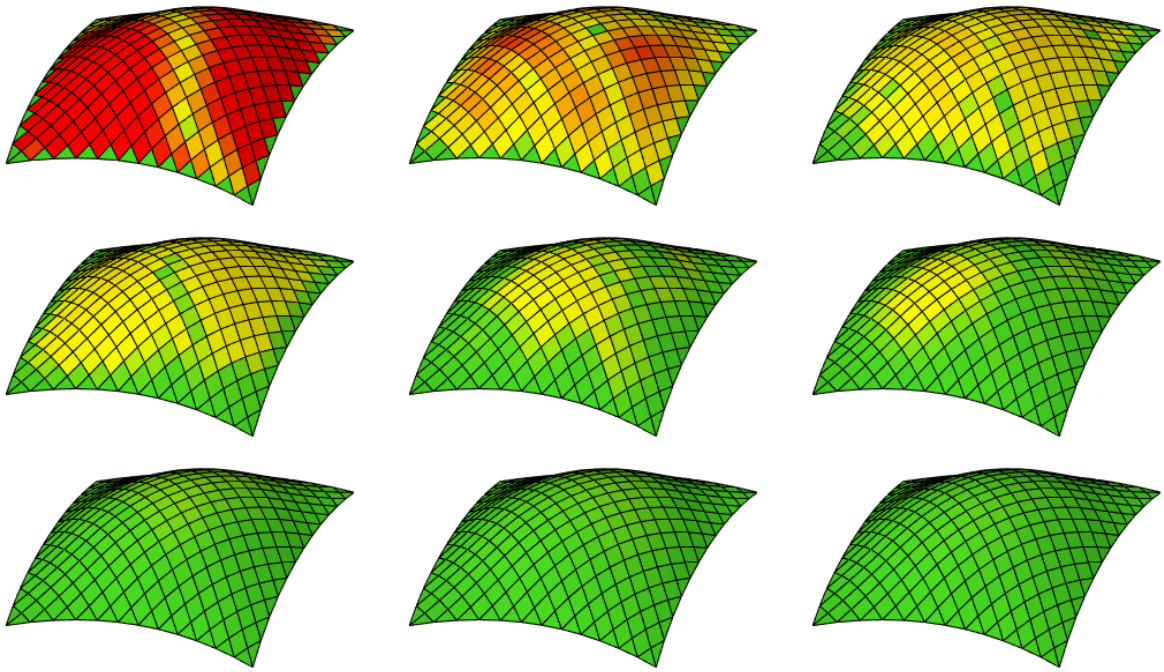

Fig. 5.44 Steps of the optimization of quasi-PQ mesh. The initial mesh (translational with planar base) was diagonally SC mapped. The resultant mesh is exactly planar and preserved the global form.

In the above example all supporting points (vertices) of the mesh are fixed. It is not a necessary condition. In the example below this condition was released for two of the four edges (arched edges in Fig. 5.45 to 5.48).

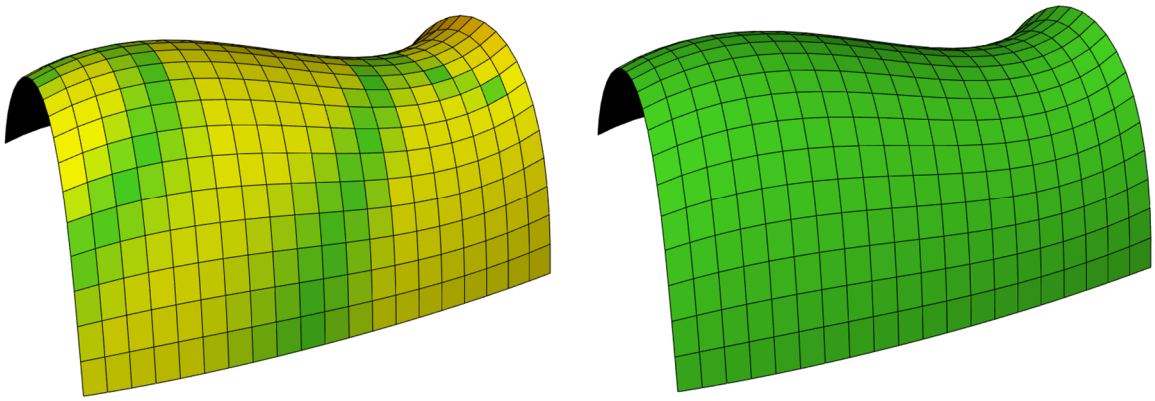

Fig. 5.45 Quasi-PQ, diagonally SC mapped scalar-translational mesh and the result of its planarization.

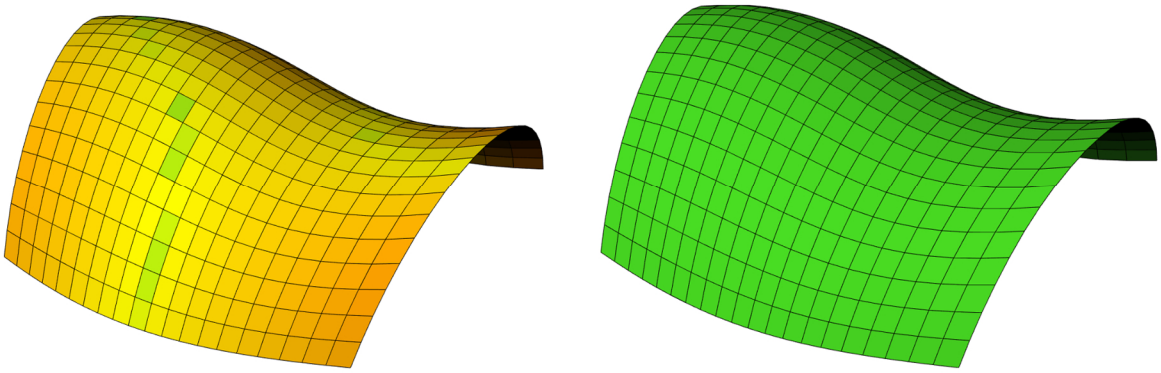

Fig. 5.46 Quasi-PQ, aligned SC mapped sweep mesh and the result of its planarization.

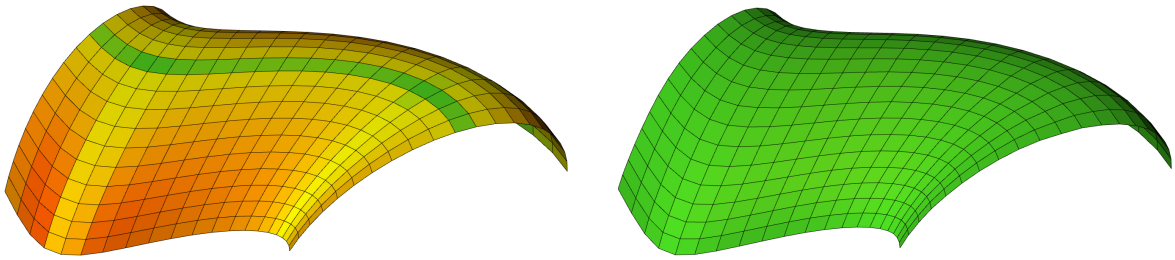

Fig. 5.47 Quasi-PQ, aligned SC mapped scalar-translational mesh and the result of its planarization.

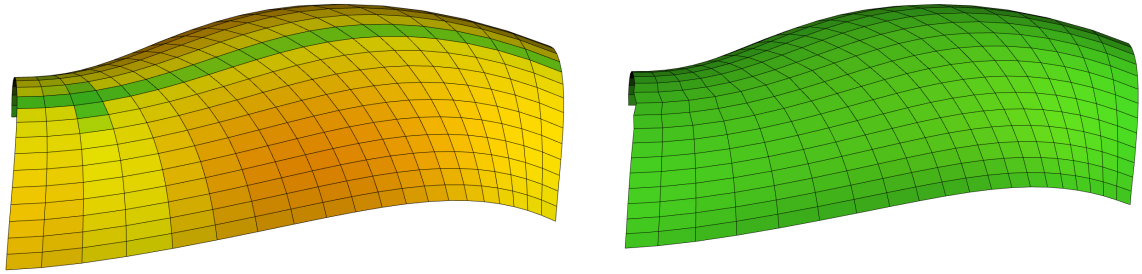

Fig. 5.48 Quasi-PQ, diagonally SC mapped sweep mesh and the result of its planarization.

Depending on a design constraints any combination of fixed points can be selected for the optimization process. However, the more points are fixed, the greater displacements occur in other points (vertices).

As shown in the Fig. 5.49 the attempt to planarize an arbitrarily shaped quadrilateral mesh results with highly distorted shape. That fact emphasizes usability of SC maps, even when it results in quasi-PQ meshes. That particular planarization attempt shows the complexity of the quadrilateral panelization of arbitrarily shaped forms as it is in the top-down approach and the strong relationship between the form and the tessellation – proving one of the claims of this research.

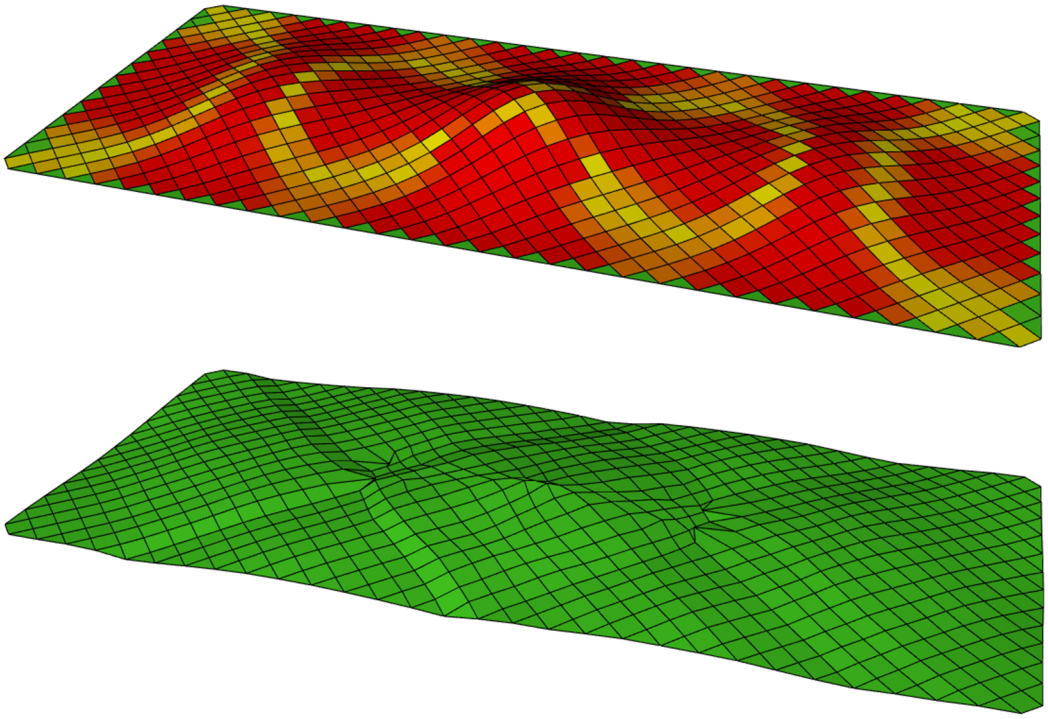

Fig. 5.49 Attempt of planarization of non-planar, quadrilateral mesh, resembling the glass roof over the Kogod Courtyard, see Fig. 3.3. The result is PQ mesh, which has highly distorted form.

5.2.2. Perspective transformation

The following method of *perspective transformation* facilitates rules of perspective in the sense of mathematics, computer graphics and modern digital tools, which allow displaying three dimensional objects on a computer screens. Although this transformation has been known for a long time, it has not been used for shaping PQ meshes yet. Perspective transformations used by Paolo Uccello and Piero della Francesca (see section 2.3.1) were based on discretization of continuous objects (surfaces) into sets of points comprehensively defined by three Cartesian coordinates – *x*, *y* and *z*. The way in which three-dimensional objects are displayed in perspective on computer screens today are based on the same principles. Every single point, which builds a mesh of three-dimensional object is transformed according to certain linear algebra formulations in order to create a perspective image.

A projection of an object from three-dimensional space onto a two-dimensional plane, whether orthogonal (see Fig. 5.52) or perspective (see Fig. 5.52), changes the values of two of its points coordinates: *x* and *y*, while the information about the third coordinate *z* is discarded. It is impossible to reverse such projection without maintaining the information about the third coordinate, i.e. it is impossible to ambiguously project a two-dimensional image of three-dimensional object back to its original, three-dimensional form without some additional information, basin only on the final, planar image. However, Piero della Francesca was able to record the information about the third coordinate on two-dimensional, planar paper. Apart from introducing orthogonal, side-views, he assigned numerical values to each of the points in order to store additional information for further computations. Thanks to these 'hidden' data (or meta-data in modern terms), he was able to mathematically raise the two-dimensional image into the virtual three-dimensional space, manipulate with it (rotate) and project it back on the two-dimensional paper (see Fig. 2.7 on page 28).

The same happens when the three dimensional image is displayed on the two dimensional computer screen. The computer stores in its memory additional information about the position of each point (vertex) of 3D object, even though that finally it is displayed as 2D image, in order to allow for numerous transformations of that object without the necessity for excessively complex calculations. However, in order to generate perspective projections of PQ meshes in the presented method, a fourth coordinate was introduced. In practice it means storing the information about 3D objects as four dimensional. Adding an extra dimension for the computations allows for obtaining 3D objects from transformation, as eventually 3D PQ mesh is required to design grid shell upon it. An explanation of the importance of this solution is given later in this section.

5.2.2.1. Justification of the method's usefulness

Two features of perspective projections are important from the point of view of planarity preserving transformations of PQ meshes. Firstly, perspective transformation preserves lines, i.e. straight line is transformed into a straight line (or a point in specific cases), thus a straight line segment always be straight after perspective transformation.

Secondly, perspective projection is a function, which means, that for each argument (original point) there is exactly one value (image point). This fact excludes the possibility of generating more than one image points by perspective projection of a single point, in another words: **perspective projection of a point cannot produce a line.**

These two aspects of perspective projections: **linearity preservation** and **point preservation** lead to the following conclusion: if a spatial quadrangle is planar, its diagonals intersect each other at a singular point. After perspective projection both diagonals remain straight and a point of intersection remains a singular point. Therefore projected quadrangle meets the necessary conditions of planarity.

Figure 5.50 shows comparison between two types of transformations that externally result with the same shapes (red and blue grids), however, the internal structure decides whether the transformed object will preserve linearity.

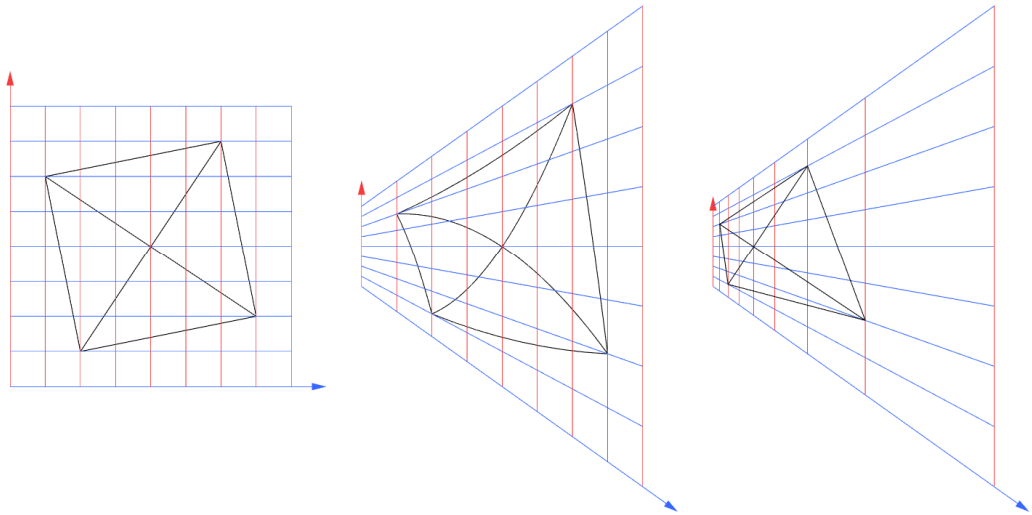

Fig. 5.50 Left: a square with diagonals in original form described on auxiliary orthogonal grid.
Centre: deformation of the square and grid by means of tapering transformation[76], the result is a quadrilateral with curved edges and diagonals.
Right: perspective transformation (planar) of the square and auxiliary grid, edges of the square remain straight, whereas the distances between red lines of auxiliary grid vary unlike in case of tapering transformation.

Perspective image of an object can be obtained by means of two possible approaches. Firstly, as a central projection onto a plane of original object as in Fig. 5.51. In this approach each point of the object is projected along the line, which also passes through the projection centre point.

In the second approach exactly the same image as in Fig. 5.51 is obtained by parallel projection of previously deformed original object, see Fig. 5.52. In this case, all projection lines (blues) are parallel. In order to obtain exactly the same image as before, the original object is deformed by the perspective transformation.

[76] Tapering is a transformation similar to scaling (i.e. anisotropic scaling, see section 5.1.1.5) where the factor of scale differentially changes along axis. For more details see (Barr 1987) p. 23.

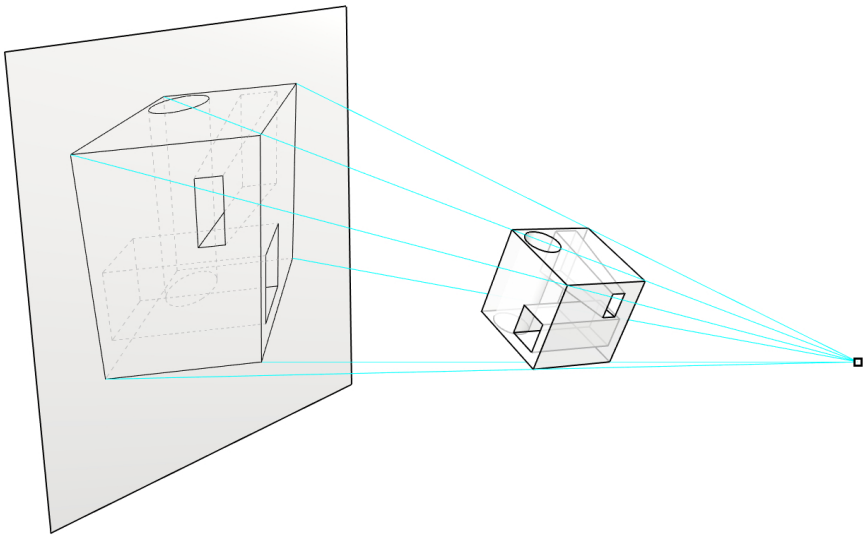

Fig. 5.51 Central projection of three dimensional object.

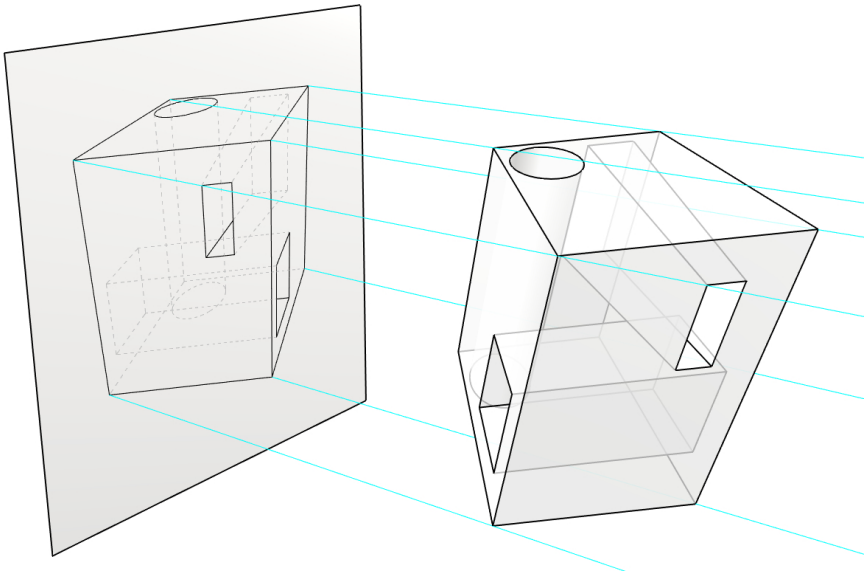

Fig. 5.52 Parallel projection of previously deformed object.

5.2.2.2. Transformation of the *viewing frustum*

Both images in Fig. 5.51 and Fig. 5.52, although obtained through different approaches are exactly the same, regardless of the used method. However, the second one is more convenient for computations in computer graphics due to the application of linear algebra methods and performing all the computations for each vertex simultaneously.

In order to obtain perspective image with respect to the second approach, the 3D object has to be initially deformed. Such transformation is a perspective transformation and utilizes the idea of a *viewing frustum*[77], which is a volume that defines how 3D models are projected. For mathematical details of perspective transformations utilizing viewing frustums see (Sung, Shirley, and Baer 2008) pp. 379–408.

[77] Another name appearing in the literature is the *pyramid of vision*, see (Parekh 2006), p. 413.

Essentially the viewing frustum is a cut-off pyramid with a camera (observer) positioned on its cut-off apex, see Fig. 5.53. The side facets of viewing frustum define field of view of the camera, beyond which projected objects will be not visible (beyond the edges of perspective projection image). In order to obtain perspective image through parallel projection a viewing frustum has to be transformed into a canonical viewing volume together with all 3D objects within viewing frustum, see Fig. 5.53, right. Such transformation is computed according to following properties:

- position of the camera in 3D space,
- direction of the camera,
- field of view of the camera (opening angle of viewing frustum),
- distances of far and near facets of viewing frustum to the camera.

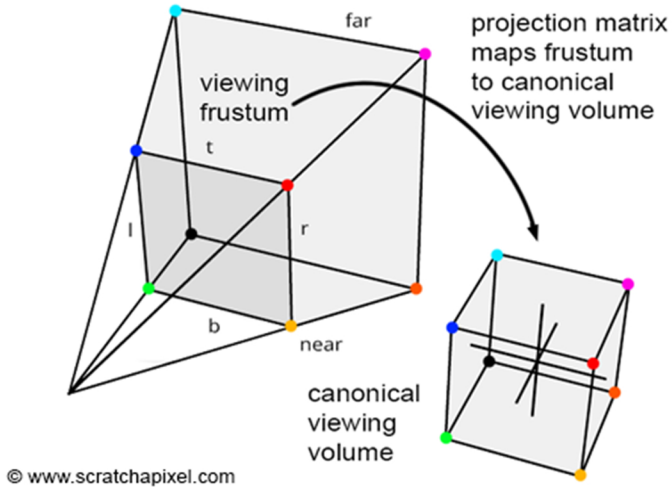

Fig. 5.53 Viewing frustum (left) and canocnical viewing volume (right).[78]

Depending on those properties the projection matrix transforming viewing frustum into a canonical viewing volume (a cube) is calculated. A 3D object contained within viewing frustum is transformed by that projection transformation defined by matrix and then it is parallelly projected onto a plane resulting with perspective image as in Fig. 5.52.

Perspective transformations used for the purpose of transforming PQ meshes work according to the same principles as in 3D graphics, however in reversed order, i.e. a 3D object (e.g. PQ mesh) is contained within canonical viewing volume (a cube) and then it is transformed into a different shape defined by the viewing frustum, see Fig. 5.54. It is assumed, that the initial and final shapes (canonical viewing volume and viewing frustum) are positioned at the beginning of the coordinate system, hence the properties such as the position of the camera, its direction and its field of view are not considered, what in turn simplifies all the calculations.

[78] Source: http://www.scratchapixel.com/lessons/3d-basic-rendering/perspective-and-orthographic-projection-matrix/projection-matrices-what-you-need-to-know-first

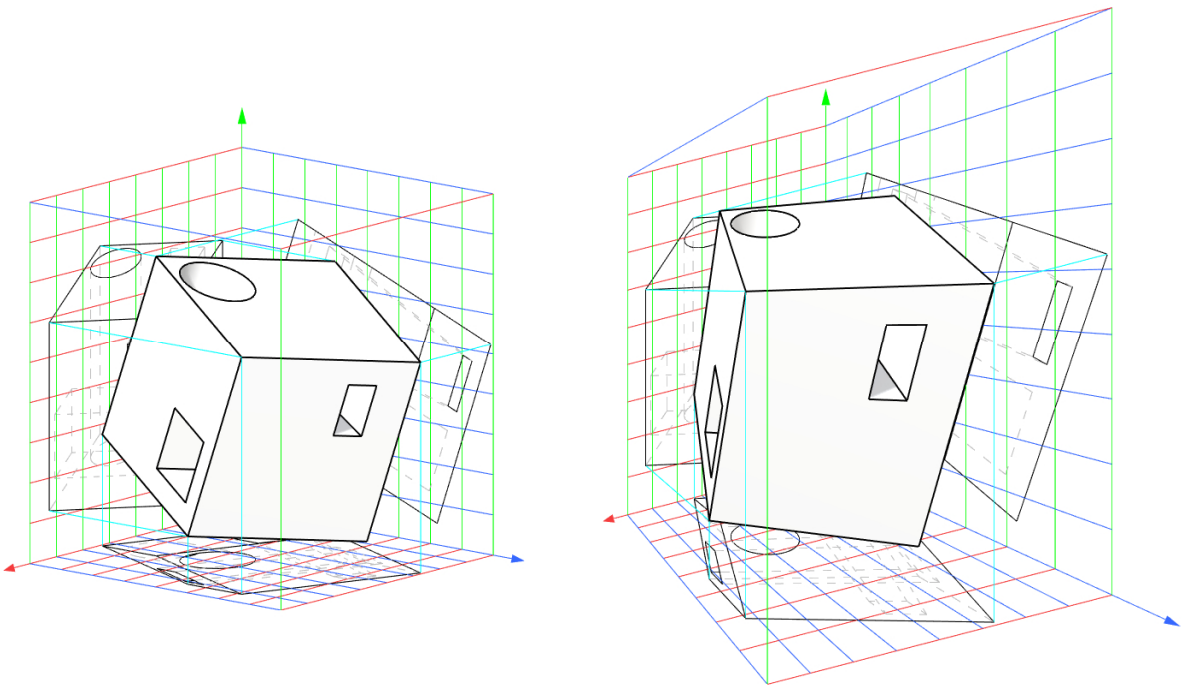

Fig. 5.54 Three dimensional object deformed within viewing frustum. All straight lines and planes are preserved.

In Fig. 5.54 viewing frustum and an object inside are shown in two configurations. On the left side, the object in original configuration is embedded in viewing frustum in orthogonal configuration. All lines in particular colour are parallel (only those on the edges and back wall of frustum are shown, however they fill all the space inside of it). The space in such configuration is isomorphic, meaning that all distances, areas and surfaces are proportional between corresponding steps (lines).

On the right side viewing frustum is deformed. The near, right face is enlarged. The faces adjacent to the enlarged one are now trapezoids, which are filled with deformed grid (such as on the Fig. 5.50, right). The distances, areas and volumes are no longer isomorphic in that configuration. Object embedded within that frustum was deformed simultaneously. All points of the object, which were incident to the particular intersections of lines (red, green, blue) before the transformation, remain incident with the intersections of the same lines, which are now deformed by the frustum.

5.2.2.3. Example of two dimensional perspective transformation

In order to intuitively understand the structure of homogenous matrix its two dimensional equivalent is used as the example below. This 2D example will help to extend the problem to 3D objects.

If a two dimensional object (shape) is raised above the plane by adding a third coordinate, it can be point projected back onto a plane resulting with image, which is a scaled version of the original object, see Fig. 5.55, right. When the object is additionally manipulated above the plane (e.g. rotated in 3D space), the central projection results with perspective image of that object, see Fig. 5.56, 5.57 and 5.58. In order to mathematically perform such manipulations in the extended dimension, the transformation matrix is expanded by additional (homogenous) row and column, see equation (5.20) on page 138.

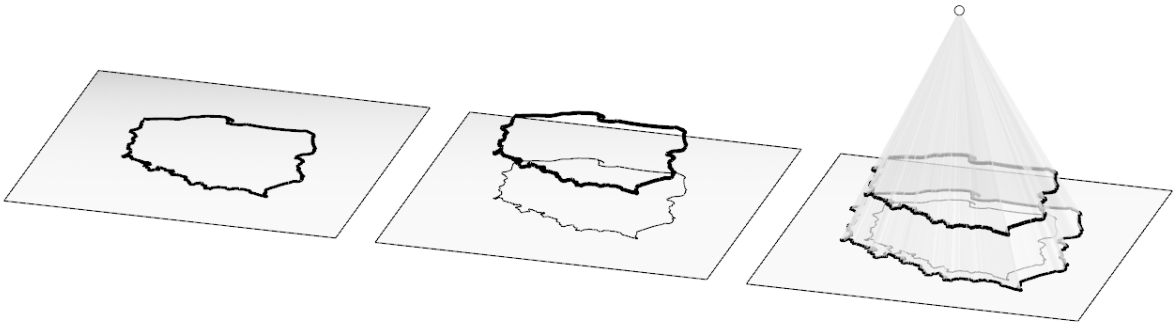

Fig. 5.55 Central projection of two-dimensional shape transformed in third dimension.

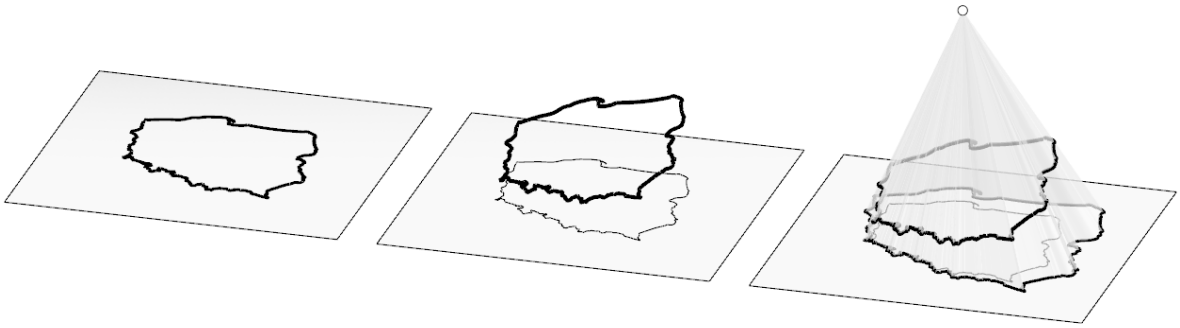

Fig. 5.56 Central projection of two dimensional shape rotated in third dimension.

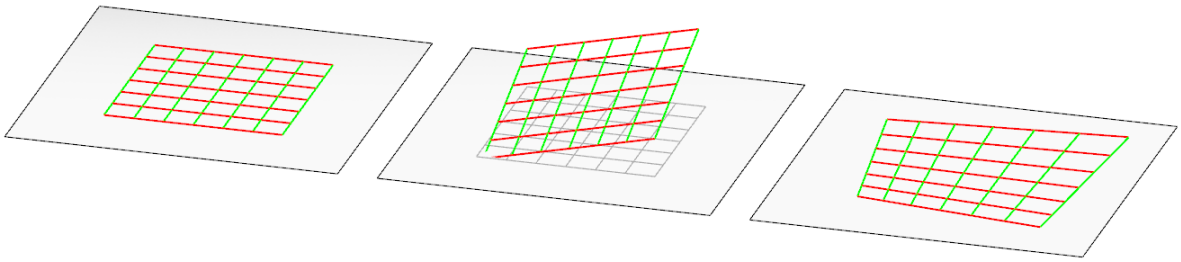

Fig. 5.57 Central projection of two dimensional grid rotated in third dimension.

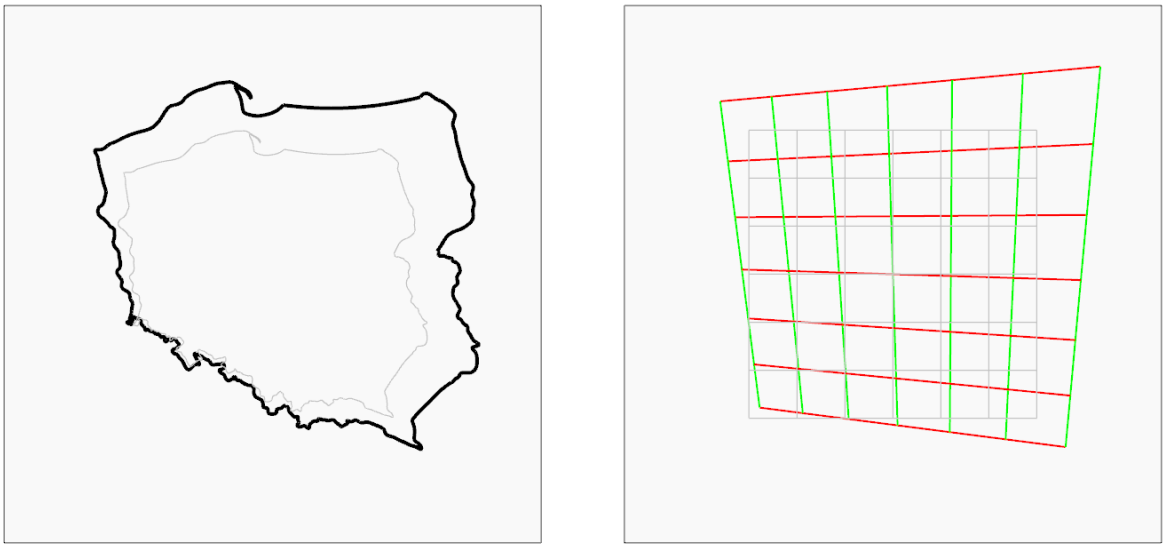

Fig. 5.58 Comparison of original shapes (light grey) and images of their homogenous transformations.

This analytical way of applying a perspective transformation is a composition of several transformations: raising an object above the plane, rotating the object around an axis (or several axes) in 3D space and point projection back onto a plane. Equivalent of this procedure for three dimensional object is raising it to the fourth dimension, rotating it in that fourth dimension, and projecting it back onto the three dimensional space.

5.2.2.4. Perspective transformation matrix

The perspective projection matrix used for the purpose of 3D computer graphic has diverse forms depending on applied technology. It may be a composition of several matrices which are additionally responsible for transformations such as rotations (considering the rotation of the camera) and translation (considering the position of the camera). For the purpose of transforming PQ meshes in this work only the essential form of the perspective transformation matrix, derived by the author, is used[79], i.e. the positions of transformed points are calculated by the multiplication of two matrices by the formulation as in equation (5.20).

$$\begin{bmatrix} \boldsymbol{x_c} \\ \boldsymbol{y_c} \\ \boldsymbol{z_c} \\ \boldsymbol{w_c} \end{bmatrix} = \begin{bmatrix} \boldsymbol{1/f} & \boldsymbol{0} & \boldsymbol{0} & \boldsymbol{0} \\ \boldsymbol{0} & \boldsymbol{1/g} & \boldsymbol{0} & \boldsymbol{0} \\ \boldsymbol{0} & \boldsymbol{0} & \boldsymbol{1/h} & \boldsymbol{0} \\ \boldsymbol{\frac{1-f}{f}} & \boldsymbol{\frac{1-g}{g}} & \boldsymbol{\frac{1-h}{h}} & \boldsymbol{1} \end{bmatrix} \begin{bmatrix} \boldsymbol{x} \\ \boldsymbol{y} \\ \boldsymbol{z} \\ \boldsymbol{1} \end{bmatrix} \tag{5.20}$$

The left side of the equation is the matrix record of the coordinates after the transformation. The 4x4 matrix is the homogenous matrix of perspective transformation. The 1x4 matrix on the right side is the matrix record of the coordinates of an original object. The fourth, ***w***, is called *homogenous* coordinate, see (Sung, Shirley, and Baer 2008), p. 214 and (Foley et al. 1995), pp. 253–258, was added to a conventional record containing three coordinates (*x*, *y*, *z*). Therefore the transformation matrix is called *homogenous* and consists of additional row and column. The deformation of viewing frustum is parametrized by *f*, *g* and *h* parameters. Each parameter corresponds to the scaling of one of three (from six in total) faces of frustum.

From the equation (5.17) results a 1x4 matrix containing the vectors of coordinates. These coordinates are the real ones if for their given values the fourth coordinate w_c is equal to 1. This form is calculated by the equation (5.21), where the real coordinates are *x'*, *y'* and *z'*.

$$\begin{bmatrix} \boldsymbol{x'} \\ \boldsymbol{y'} \\ \boldsymbol{z'} \\ \boldsymbol{1} \end{bmatrix} = \frac{\boldsymbol{1}}{\boldsymbol{w_c}} \begin{bmatrix} \boldsymbol{x_c} \\ \boldsymbol{y_c} \\ \boldsymbol{z_c} \\ \boldsymbol{w_c} \end{bmatrix} \tag{5.21}$$

The final form of the homogeneous matrix used for perspective transformation is the composition of transformation matrices of all used basic transformations (rotation, translation, orthographic projection). The matrix in (5.17) is simplified by the author of this work into such form, that the deformations driven by change of factors *f*, *g* and *h* can be intuitively understood.

---

[79] Perspective and orthographic projection matrices used for the purpose of computer graphic are more broadly explained in several publications under the link:
https://www.scratchapixel.com/lessons/3d-basic-rendering/perspective-and-orthographic-projection-matrix/orthographic-projection-matrix

Each one of these three factors is responsible for rotation around particular axis in the fourth dimension. The fourth axis of rotation has no impact for the shape in three dimensional projection.

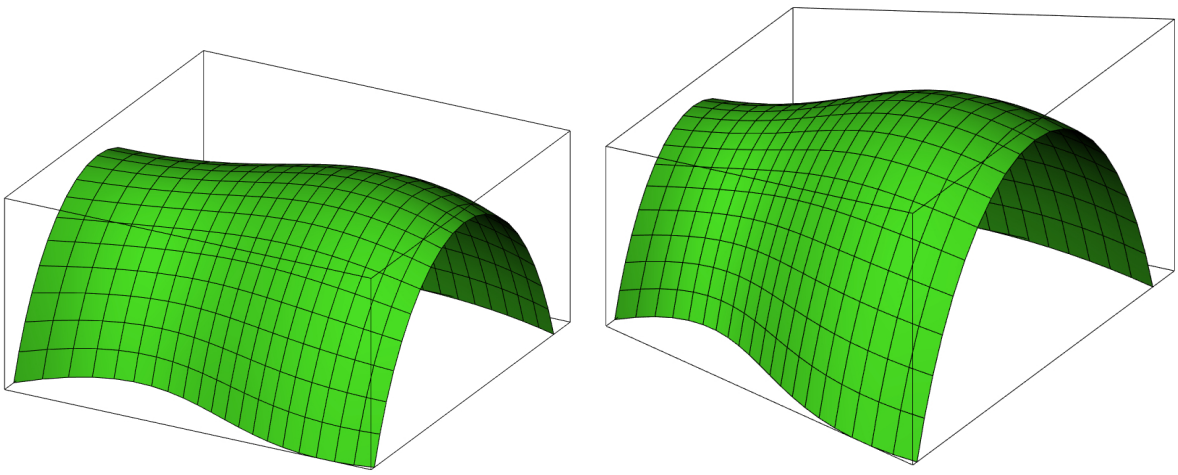

Fig. 5.59 Left: original PQ mesh in cuboid frustum. Right: homogenous rotation around f-axis.

Left image in Fig. 5.59 is the original object embed in orthogonal frustum. All factors are equal to 1, hence resulting in unit homogenous matrix, see equation (5.22).

$$\begin{bmatrix} \mathbf{1/f} & \mathbf{0} & \mathbf{0} & \mathbf{0} \\ \mathbf{0} & \mathbf{1/g} & \mathbf{0} & \mathbf{0} \\ \mathbf{0} & \mathbf{0} & \mathbf{1/h} & \mathbf{0} \\ \mathbf{\frac{1-f}{f}} & \mathbf{\frac{1-g}{g}} & \mathbf{\frac{1-h}{h}} & \mathbf{1} \end{bmatrix} = \begin{bmatrix} \mathbf{1} & \mathbf{0} & \mathbf{0} & \mathbf{0} \\ \mathbf{0} & \mathbf{1} & \mathbf{0} & \mathbf{0} \\ \mathbf{0} & \mathbf{0} & \mathbf{1} & \mathbf{0} \\ \mathbf{0} & \mathbf{0} & \mathbf{0} & \mathbf{1} \end{bmatrix} \tag{5.22}$$

In the same figure, right (Fig. 5.59) the value of factor *f* is different from 1 resulting with changed form of PQ mesh. Then the matrix multiplication has a following form of equation (5.23).

$$\begin{bmatrix} \mathbf{x_c} \\ \mathbf{y_c} \\ \mathbf{z_c} \\ \mathbf{w_c} \end{bmatrix} = \begin{bmatrix} \mathbf{1/f} & \mathbf{0} & \mathbf{0} & \mathbf{0} \\ \mathbf{0} & \mathbf{1} & \mathbf{0} & \mathbf{0} \\ \mathbf{0} & \mathbf{0} & \mathbf{1} & \mathbf{0} \\ \mathbf{\frac{1-f}{f}} & \mathbf{0} & \mathbf{0} & \mathbf{1} \end{bmatrix} \begin{bmatrix} \mathbf{x} \\ \mathbf{y} \\ \mathbf{z} \\ \mathbf{1} \end{bmatrix} = \begin{bmatrix} \mathbf{x/f} \\ \mathbf{y} \\ \mathbf{z} \\ \mathbf{x\left(\frac{1-f}{f}\right)+1} \end{bmatrix} \tag{5.23}$$

The result of equation (5.23) is then normalized by dividing the right side by the value of w_c, the right side of the equation gets the form of equation (5.24).

$$\mathbf{\frac{1}{x\left(\frac{1-f}{f}\right)+1}} \begin{bmatrix} \mathbf{x/f} \\ \mathbf{y} \\ \mathbf{z} \\ \mathbf{z\left(\frac{1-f}{f}\right)+1} \end{bmatrix} = \begin{bmatrix} \mathbf{\frac{x/f}{x\left(\frac{1-f}{f}\right)+1}} \\ \mathbf{\frac{y}{x\left(\frac{1-f}{f}\right)+1}} \\ \mathbf{\frac{z}{x\left(\frac{1-f}{f}\right)+1}} \\ \mathbf{1} \end{bmatrix} \tag{5.24}$$

The last row in the matrix has to be equal 1, in order to get the real values of *x*, *y* and *z* coordinates. In that form the positions of points along *y* and *z* coordinates are also influenced by their position along the *x* coordinate, and the factor *f*. The same principle applies to two other parameters: *g* and *h*; each one responsible is for perspective deformation along axes *y* and *z*, see Fig. 5.60 left and right.

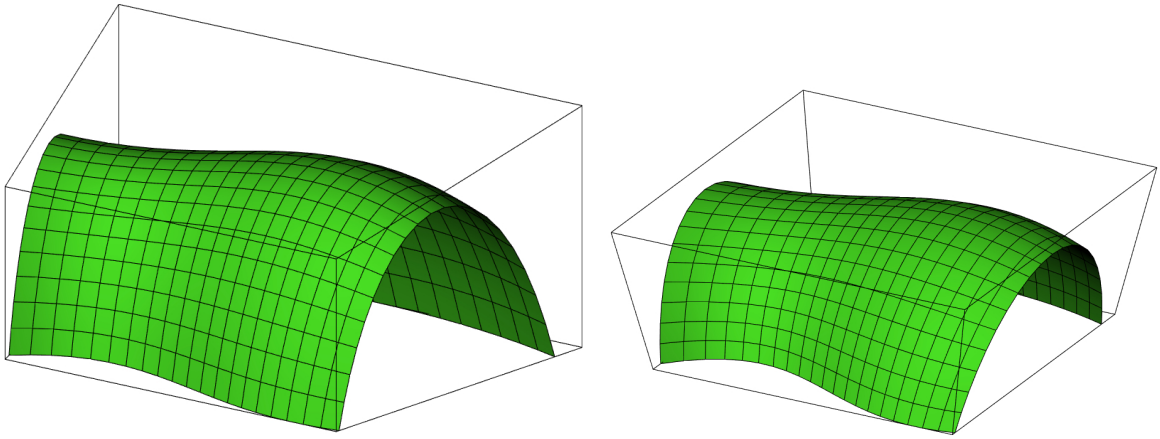

Fig. 5.60 Left: homogenous rotation of PQ mesh around g-axis*. Right: homogenous rotation of PQ mesh around* h-axis*.*

Analogously to equations (5.23) and (5.24), changed values of parameters *g* and *h* result with equations (5.25) and (5.26). Normalized values of resultant vectors have the forms of equations (5.27) and (5.28).

$$\begin{bmatrix} x_c \\ y_c \\ z_c \\ w_c \end{bmatrix} = \begin{bmatrix} 1 & 0 & 0 & 0 \\ 0 & 1/g & 0 & 0 \\ 0 & 0 & 1 & 0 \\ 0 & \frac{1-g}{g} & 0 & 1 \end{bmatrix} \begin{bmatrix} x \\ y \\ z \\ 1 \end{bmatrix} = \begin{bmatrix} x \\ y/g \\ z \\ y\left(\frac{1-g}{g}\right)+1 \end{bmatrix} \tag{5.25}$$

$$\begin{bmatrix} x_c \\ y_c \\ z_c \\ w_c \end{bmatrix} = \begin{bmatrix} 1 & 0 & 0 & 0 \\ 0 & 1 & 0 & 0 \\ 0 & 0 & 1/h & 0 \\ 0 & 0 & \frac{1-h}{h} & 1 \end{bmatrix} \begin{bmatrix} x \\ y \\ z \\ 1 \end{bmatrix} = \begin{bmatrix} x \\ y \\ z/h \\ z\left(\frac{1-h}{h}\right)+1 \end{bmatrix} \tag{5.26}$$

$$\frac{1}{y\left(\frac{1-g}{g}\right)+1} \begin{bmatrix} x \\ y/g \\ z \\ y\left(\frac{1-g}{g}\right)+1 \end{bmatrix} = \begin{bmatrix} \frac{x}{y\left(\frac{1-g}{g}\right)+1} \\ \frac{y/g}{y\left(\frac{1-g}{g}\right)+1} \\ \frac{z}{y\left(\frac{1-g}{g}\right)+1} \\ 1 \end{bmatrix} \tag{5.27}$$

$$\frac{1}{z\left(\frac{1-h}{h}\right)+1}\begin{bmatrix} x \\ y \\ z/h \\ z\left(\frac{1-h}{h}\right)+1 \end{bmatrix} = \begin{bmatrix} \frac{x}{z\left(\frac{1-h}{h}\right)+1} \\ \frac{y}{z\left(\frac{1-h}{h}\right)+1} \\ \frac{z/h}{z\left(\frac{1-h}{h}\right)+1} \\ 1 \end{bmatrix} \tag{5.28}$$

As changes of the *f*, *g* and *h* parameters influence the shape of a 3D object in particular manner it can be assumed, for the ease of use of the method, that the object is *rotated* around some *f*, *g* or *h* axes in fourth dimension. Rotation around *f* axis in 4D space deforms an object along *x* axis, whereas analogously rotation around *g* axis influences deformation along *y* and *h* along *z* axes.

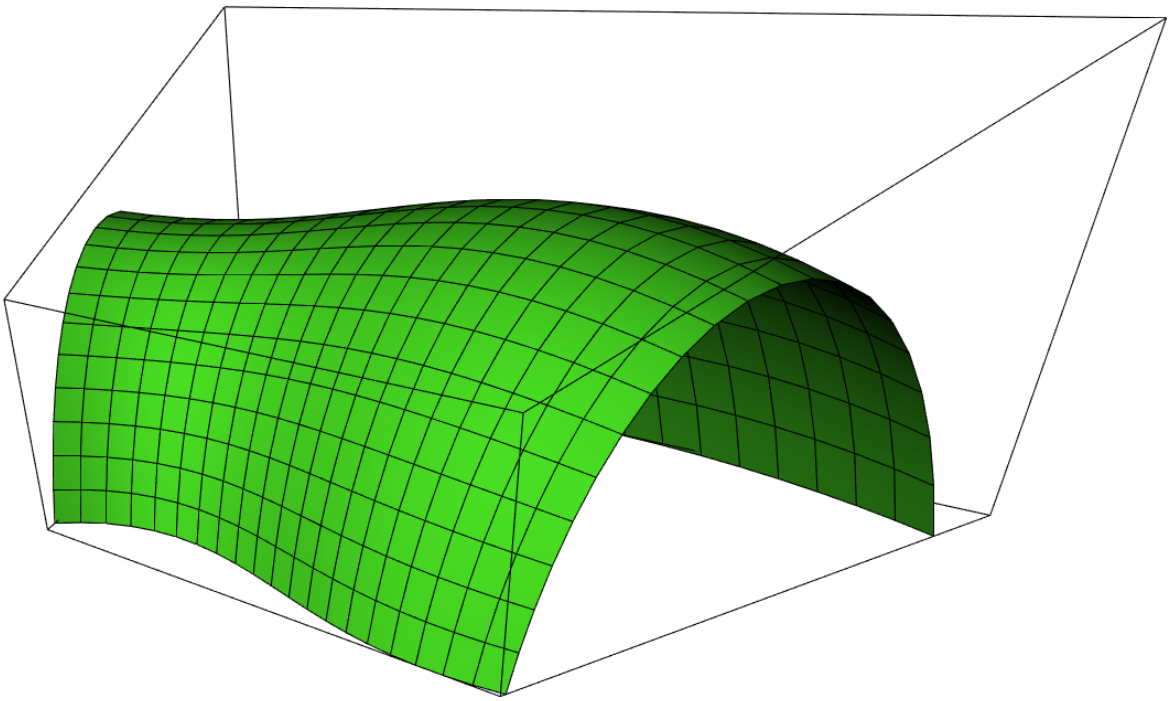

Fig. 5.61 Composition of homogenous rotations around all f, g *and* h *axes. The resultant mesh have all facets preserved planar.*

When all parameters have values other than 1, the rotations are combined and the frustum is deformed along each direction, see Fig. 5.61. The resultant form is always a valid PQ mesh, regardless of the intrinsic properties of the initial PQ mesh. It is not required for the initial mesh to be circular, isoradial or conic. Although SC method proposed in the previous chapter is much more constrained, it allows for other deformations, which are not available for the perspective transformation. Therefore it is possible to combine both transformation. Due to the fact, that the SC mapping is geometrically constraint to particular types of PQ meshes it is performed as the first one. Then the perspective transformation can be applied. A particular geometrical application for that combination of transformations is proposed in the section 5.2.2.9, where PQ meshes with circular base shapes, that are possible to obtain by SC mapping, are perspective transformed to align their base shapes into forms of conical sections.

5.2.2.5. Perspective transformation matching

In the computer graphics the perspective transformation matrix parameters relate to the parameters of the camera, i.e. the focal lenght. Generally, for obtaining natural, human eye views, only one parameter is changed. The scene is transformed, so that one with its main axes aligns with the axis of view. Although, perspective transformation meant for PQ mesh transformations is based on the same principles, it is controlled by different constraints. It is not important for the designer what values does the *f*, *g*, *h* or any other parameters have. From the designer point of view, it is important to set the positions of few, key vertices of transformed PQ mesh and automatically perform the transformation for all the other vertices.

For a praticular case study described in the section 7.1, a translational PQ mesh with planatr,square base (from section 4.1.2) is selected for the perspective transformation matching , see Fig. 5.62, left. The assumption is that the designer specifies the four vertices of the desired quadrilateral base, and the transformation is calculated automatically according to the rules described below. These user defined vertices are allowed in any planar configuration in wich they construct non self-intersecting, convex quadrilateral.

Further discussion concerns the case study mentioned above (from the section 7.1). The perspective transformation matrix is convenient to work with, when the transformed object is unitized, i.e. the centre of the mesh lies at the beginning of the coordinate system *O*(0,0) and its corners are at points *A*(1,1), *C*(1,-1), *E*(-1,-1) and *G*(1,-1), see Fig. 5.62, right. Auxilary points: *B*(0,1), *D*(-1,0), *F*(0,-1) and *H*(1,0) are also introduced at the middle points of the edges of mesh. The height of the mesh is temporarly negligible, therefore point locations are specified without *z* coordinates, assuming it is equal zero.

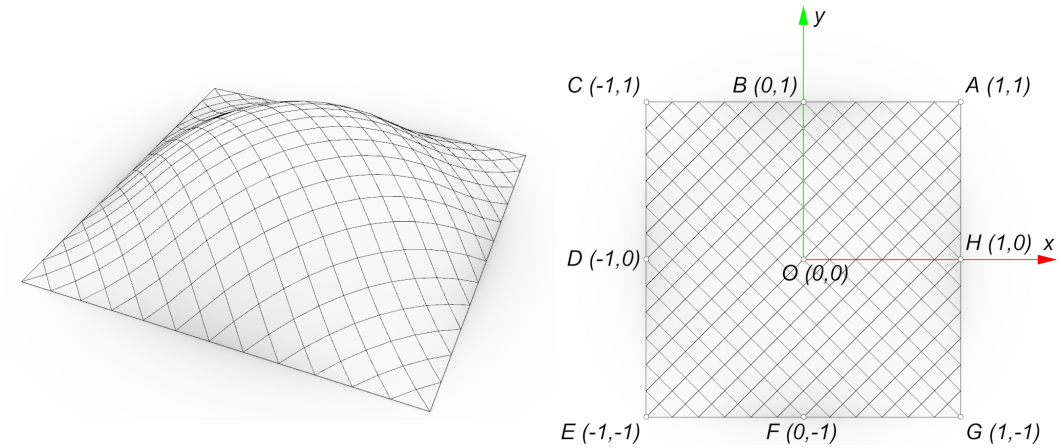

Fig. 5.62 Translational PQ mesh with planar, square base. Right: unit dimensions and orientation of the mesh.

When performing a perspective transformation on any mesh in space, it can be unitized before by the adoption of all the planarity preserving transformations. The most convenient are affine transformations, described is the section 5.1.1, which include translations, rotations, shear, isotropic and anisotropic scaling. Once object is unitized, the perspective transformation is performed on it and the result is transformed by the inversion of unitizing transformations used before. By means of linear algebra all the transformations are represented by matrices. All performed transformations can be combined into one by multiplying their matrices. The inversion of that combined matrix correspond to the inversion of all combined transformations. The combinations of matrices is convenient for reducing the computation time – instead of computing all the transformations for all the vertices step by step, one combined transformation is calculated for all the vertices at once.

When changing the parameter *f* in the perspective transformation on the unit mesh, some points stay invariant, i.e. the centre point *O* and edge midpoints *B*, *F* and *H*, see Fig. 5.63. Points *A* and *G* at the right corners change only their *y* coordinates, which are equal to the *f* and *-f* values. Midpoint *D* changes its *x* coordinate and points *C* and *E* change both of their coordinates, which values are shown in Fig. 5.63. For any values of *f* parameter, the opposing edges |AG| and |CE| are always parallel. It is assumed, that their intersection is at infinity (at the vanishing point).

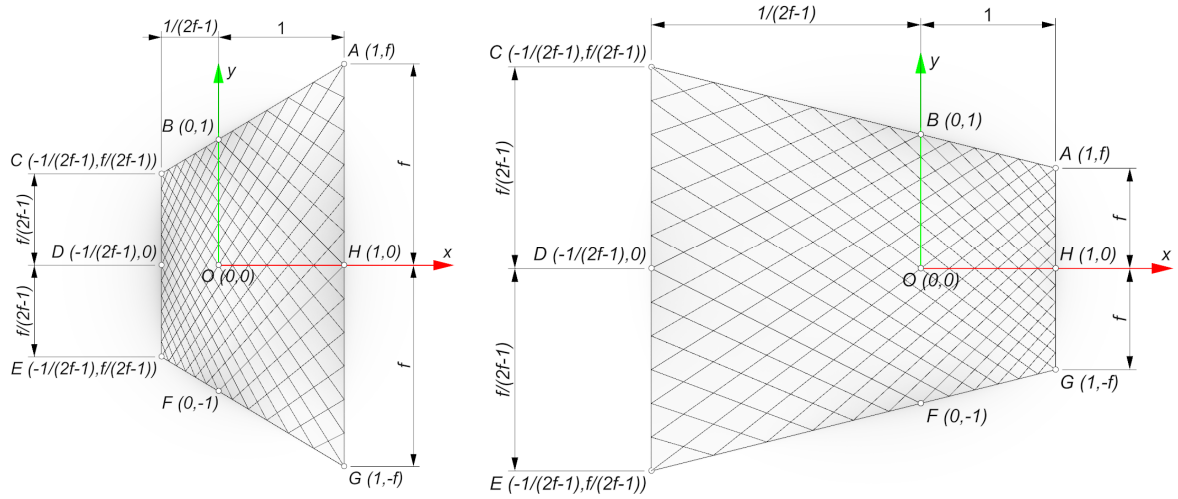

Fig. 5.63 The effects of changing the value of f *parameter. Left: for* f > 1*. Right: for* f < 1*.*

Changing the parameter *g* gives similar results as it is in the case of the parameter *f*, however the deformation happens along the *y* axis, see Fig. 5.64. The other pair of edges stay parallel and intersect at infinity. Appropriate coordinates of points are derived with respect to the vale of *g* parameter. In perspective transformation by changing the *g* parameter three points stay invariant, i.e. *B*, *D* and *H*. Two of these points are also invariant in the perspective transformation in which only the *f* parameter is changed, i.e. *B* and *H*. Both of these points lie along the poistive sides of *x* and *y* axes of the coordinate system, at their invariant markers.

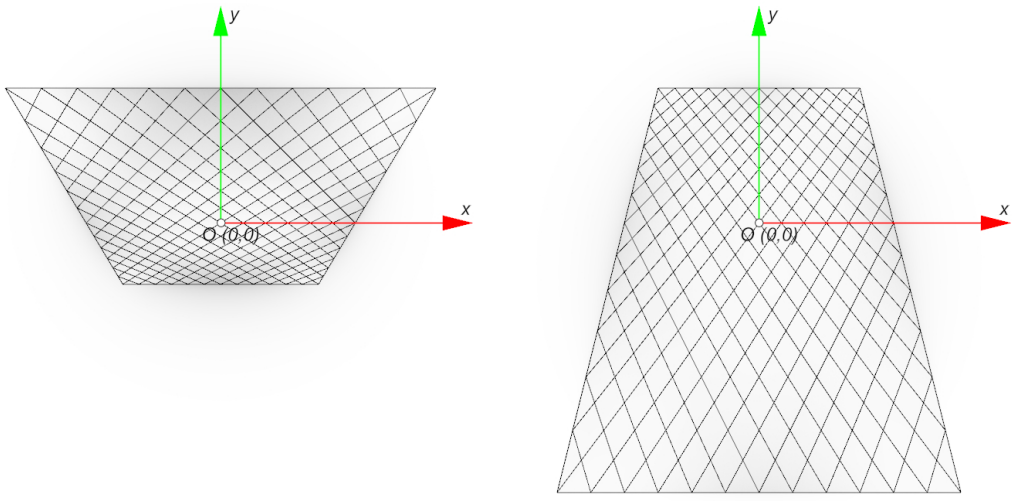

Fig. 5.64 The effects of changing the value of parameter g*. Left: for* g > 1*. Right: for* g < 1*.*

The impact of the *h* parameter is omitted in further considerations, since it has no impact on the shape of the base of mesh. The base of the mesh, when located on the *z*=0 plane is invariant for such perspective transformations.

Table 5.2. Shapes of unit PQ mesh as in Fig. 5.62 after perspective transformations with various values of parameters *f* and *g*.

	f < 1	f = 1	f > 1
g < 1	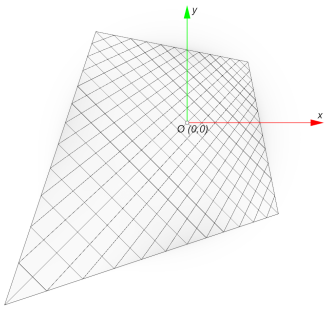	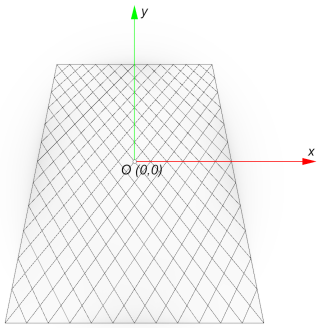	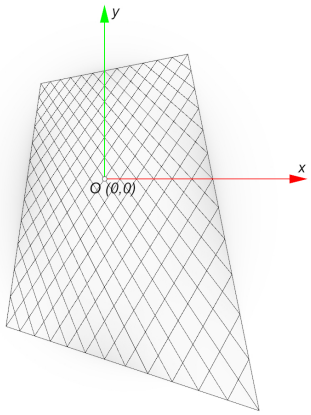
g = 1	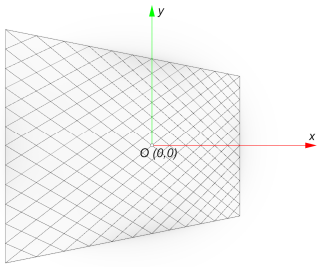	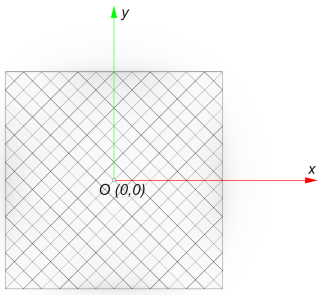	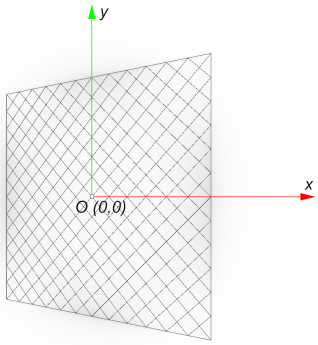
g > 1	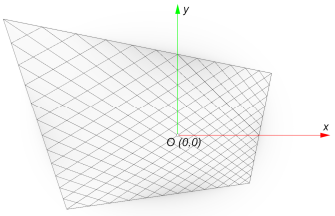	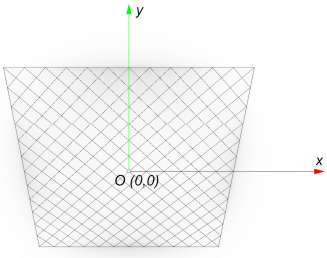	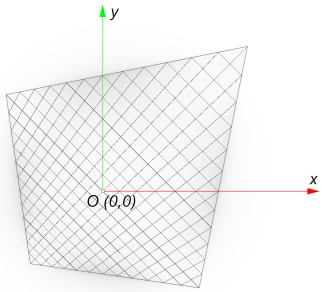

The coordinates of corner points of transformed unit mesh, with respect to the parameter *f*, are derived by the author and shown in Fig. 5.63. Analogous relations of the corner point positions with respect to the parameter *g* can be derived[80]. Knowing these formulations the exact positions of corner points with respect to the parameters *f* and *g* can be calculated and vice versa, the parameters *f* and *g* can be derived from the positions of the corner points.

[80] The exact formulations for each point are not necessary for the final calculations, only the positions of the midpoints of two edges expressed by equations (5.40) and (5.41).

However, by the sole adoption of perspective transformation it is impossible to obtain any quadrilateral shape, hence in order to allow the designer to choose any configuration of four corner points for the final mesh, additional adoption of affine transformations is required. The following part of this section concerns on the utilization of affine transformations for obtaining any quadrilateral shape for the base of PQ mesh. The composition of perspective transformation with affine transformations discussed in section 5.1.1, all of which preserve planarity, allows for creating a comprehensive system for transforming a PQ mesh with planar square base into a PQ mesh with a base perimeter in shape of any irregular quadrilateral shape.

By so far it is known, that for any combinations of *f* and *g* parameters, the *B* and *H* points are invariant. There is another invariant point which always stay at the same coordinates, i.e. point *O*, which is always located on the intersection of diagonals of quadrilateral base. There is also known that the intersection of extensions of opposing edges of perspective transformed quadrangle is always located along the *x* or *y* axes of the coordinate system, see Fig. 5.65, apart from the situation, when the edges are parallel (for *f* or *g* equal one). In such a case, the edges are also parallel to the *x* or *y* axis and intersect at their vanishing points located at adequate *x* and *y* axes.

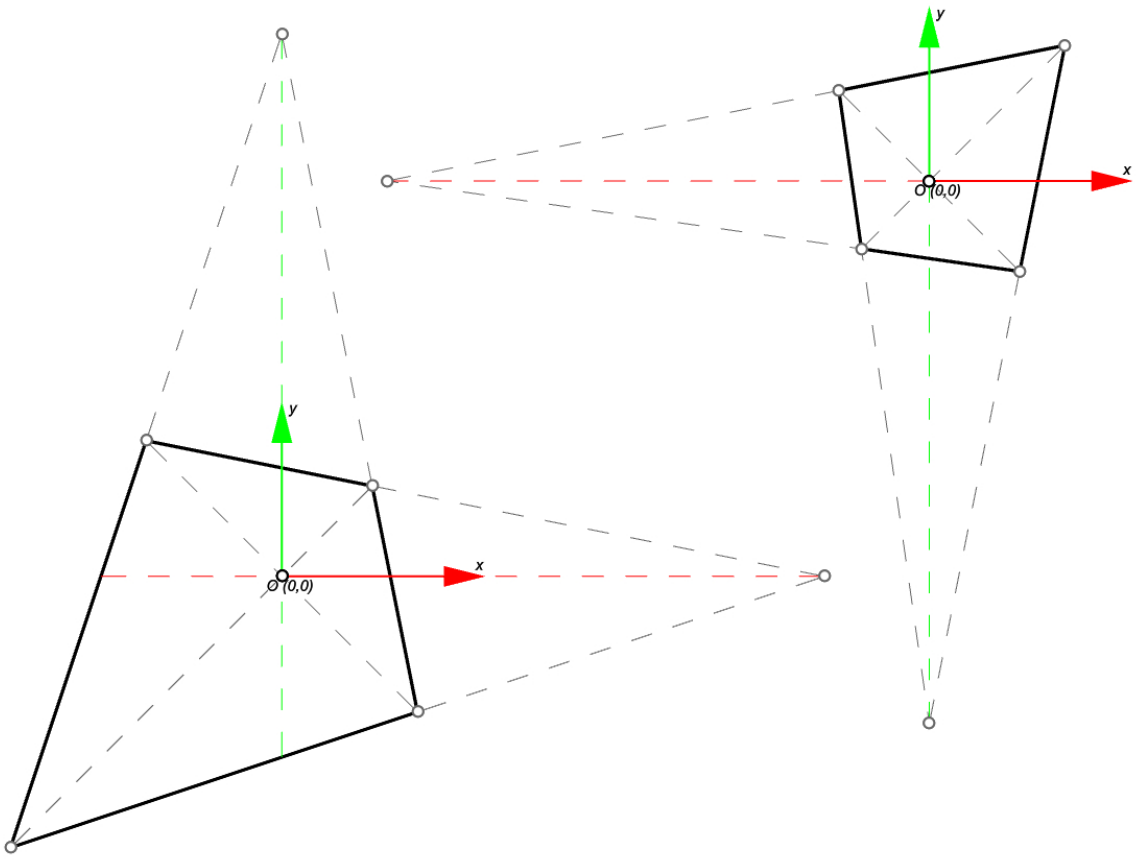

Fig. 5.65 Two example cases of perspective transformations for various combinations of parameters f *and* g*. In any case, the intersection of extensions of opposing edges is incident with the adequate,* x *or* y *axis.*

The properties mentioned above, i.e. invariant points and incidence of intersection points of opposing edges with coordinate system axes, are always true for perspective transformations of unit shapes. However, these properties also limit possible configurations of quadrangles obtained through perspective transformations. For example there are quadrilaterals whose axes (passing through the intersection of diagonals of the quad and intersections of extensions of its opposing edges, as in Fig. 5.67) are not mutually perpendicular. Therefore, in order to devise a transformation for any quadrilateral shape, a combinations of affine and perspective transformations is required.

5.2.2.6. Affine transformations

Affine transformations are chosen in such a manner, that they transform any quadrangle into a form that is possible to obtain through perspective transformations. Any quadrangle can be transformed by affine transformations into a form in which:

- the intersection of its diagonals is located at the beginning of the coordinate system $O(0,0)$;
- the intersections of extensions of opposing edges are incident with x and y axis;
- the points at two edges intersecting with positive parts of x and y axes lie at points $B(0,1)$ and $H(1,0)$.

The way all those properties are met is obtained according to the procedure described further in this section. Notations for each transformation are adopted so that their final composition could be expressed in single formulation, i.e. the equation (5.32).

The planar, *ACEG* quadrangle in Fig. 5.66 is an example of geometrically unconstrained quadrangle which will be transformed into a unit square by the adoption of affine and perspective transformations.

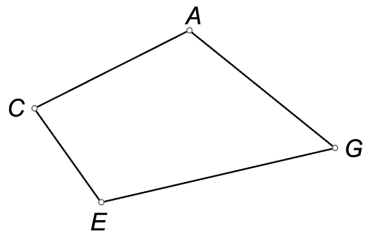

Fig. 5.66 Exemplary, geometrically unconstrained, planar quadrangle ACEG.

First step assumes the assignation of *ACEG* quadrangle characteristic points, see Fig. 5.67. Point *O* iles at the intersection of the diagonals – *CG* and *AE*. Points *V* and *W* are the vanishing points of the opposing edges: *AG* and *CE* for *V*; *AC* and *EG* for W. Points *B*, *D*, *F* and *H* not at the midpoints of corresponding edges in this configuration of the quadrangle. In order to assign their positions auxilary lines are instroduced – *WO* and *VO*. Points *D* and *H* lie at the intersections of *WO* with two edges, whereas points *B* and *F* lie at the intersections of *VO* and the second pair of edges.

First transformation is a translation along the vector $\boldsymbol{T_v} = OO'$, where *O'* lies at the beginning of the coordinate system at point (0,0). The *ACEG* quadrangle and all of its characteristic points are translated by the same vector. In this way, the first requirement of aligning point *O* with the begining of the coordinate system is met.

Translated quad *ACEG* is further transformed by rotation around the point *O*. The angle of rotation $\boldsymbol{\Theta}$ has such a value, that the rotation image of *H'* lies on the x axis, see Fig. 5.68. The rotation transformation has a $\boldsymbol{R_{O,\Theta}}$ notation, where *O* is the centre of rotation and Θ is the angle of rotation.

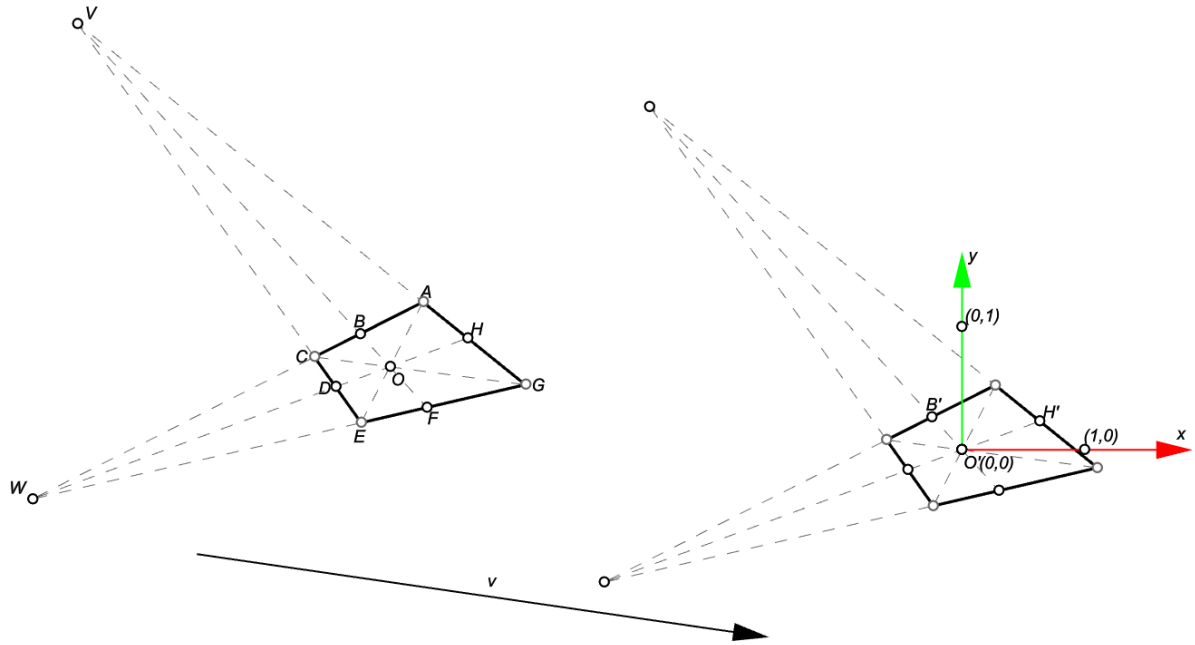

Fig. 5.67 Left: assignment of characteristic points of ACEG *quadrangle. Point* O *lies at the intersection of the diagonals. Points* W *and* V *lie at the intersections of* AC - EG *and* AG - CE *edges. Points* D, H *and* B, F *lie at the lines passing through points* W – O *and* V – O. *In this form points* B, D, F *and* H *are not located at the midpoints of the edges.*
Right: first transformation is the translation of all points along the vector OO', *where* O' *is at the beginning of the coordinate system at point* (0,0).

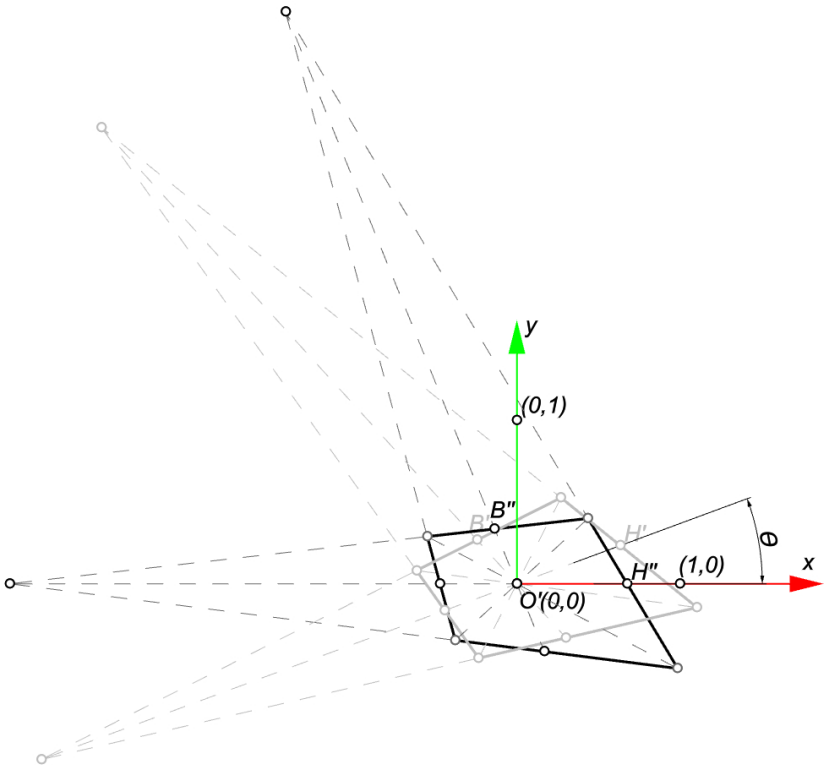

Fig. 5.68 Rotation of ACEG *quad around point* O *by the angle* Θ, *aligning point* H' *with the* x *axis.*

There are two anisotropic scale transformations used in the presented method. The first one is anisotropic scale transformation which has a notation $\boldsymbol{C_{x,\,fx}}$.

Ponit *H''* still has to be located at (1,0) coordinates. A transformation through which it can be obtained, while preserving the position of point *O'* is the anisotropic scale along the axis *x*, see Fig. 5.69. In this praticular anisotropic scale the invariant points lie along the direction perpendicular to the direction of scaling. While *O* is invariant, the invariant line runs along the *y* axis. Therefore, according to the notation assumed in section 5.1.1.5, the first parameter of anisotropic scale transformation is the *y* axis of coordinate system. The scale factor is inverse of $|O'H''|$ line segment length, see equation (5.29).

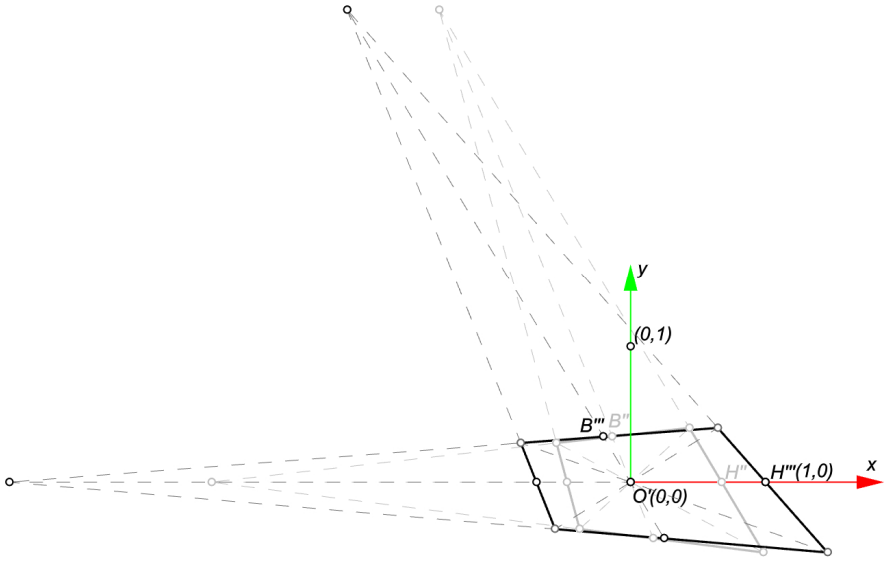

Fig. 5.69 Anisotropic scale transformation aligning point H' *with the point* (1,0) *while preserving the position of point* O.

$$\boldsymbol{f_x = \frac{1}{|O'H''|}} \tag{5.29}$$

The $\boldsymbol{C_{x,\,fx}}$ transformation changed positions of all other points (apart of *O*), together with the position of *B''*, which image (point *B'''* in Fig. 5.69) still requires the alignment with point (0,1). One transformation adopted previously, i.e. rotation is no longer suitable, since it would distort the required locations of points *O'* and *H'''*. The parameters of point *B'''* can be adjusted to the required values by two separate transformations, which will preserve the positions of points *O'* and *H'''*. First of these two transformations is again anisotropic scale. However, in this case, the invariant is the *x* axis and the factor of scaling is equal to the reciprocal of the *y* coordinate of point *B*, i.e. equation (5.30).

$$\boldsymbol{f_y = \frac{1}{B_y}} \tag{5.30}$$

The second anisotropic scale transformations has a notation $\boldsymbol{C_{y,\,fy}}$. Point *B''''* has *y* coordinate equal to 1 and *x* coordinate is the last one to be adjusted. Last transformation should preserve points lying on the *x* axis of coordinate system and the *y* coordinate of point *B''''*. Shear transformation, described in section 0, meets these requirements, see Fig. 5.70.

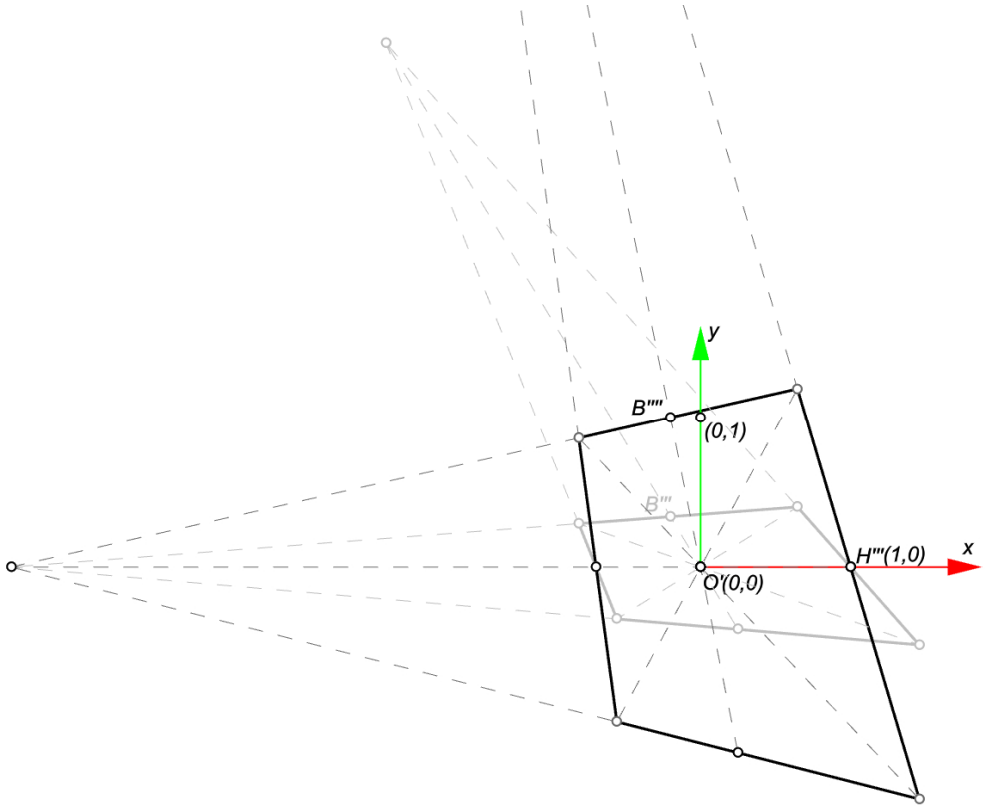

Fig. 5.70 Second anisotropic scale transformation, which aligns y coordinate of point B *with the value of 1, while preserving locations of points* O' *and* H'''.

The shear transformation (see Fig. 5.71), noted as $\boldsymbol{H_{P,h,d}}$, consists of three parameters: ***P*** – the invariant plane of transformation, which is the plane that intersects with the *x* axis of the coordinate system. The *x* axis containts points *O'* and *H'''*, which are already on the required positions. Therefore, ***P*** will be denoted as ***x***. Parameter ***d*** refers to the direction of transformation, which in this case is the vector of translation between point *B''''* and its desired position at point (0,1), see equation (5.37).

$$\boldsymbol{d} = \overrightarrow{\boldsymbol{B}''''(\mathbf{0},\mathbf{1})} \tag{5.31}$$

Parameter ***h*** is the factor of shear, i.e. the distance of transformation at along the vector ***d*** at the distane of one unit from the invariant plane ***P***. Since both points: *B''''* and (0,1) are located one unit from the invariant plane, the ***h*** factor is simply equal to the lenght of vector ***d***.

The effect of the last transformation is shown in Fig. 5.78Fig. 5.71. Although final positions of points *V* and *W* are invisible on that figure, these are already aligned with corresponding coordinate system axes *x* and *y*. After application of previously described affine transformations, the resultant quadrangle meets all the requirements of quadrangles allowed by perspective transformation of an unit square.

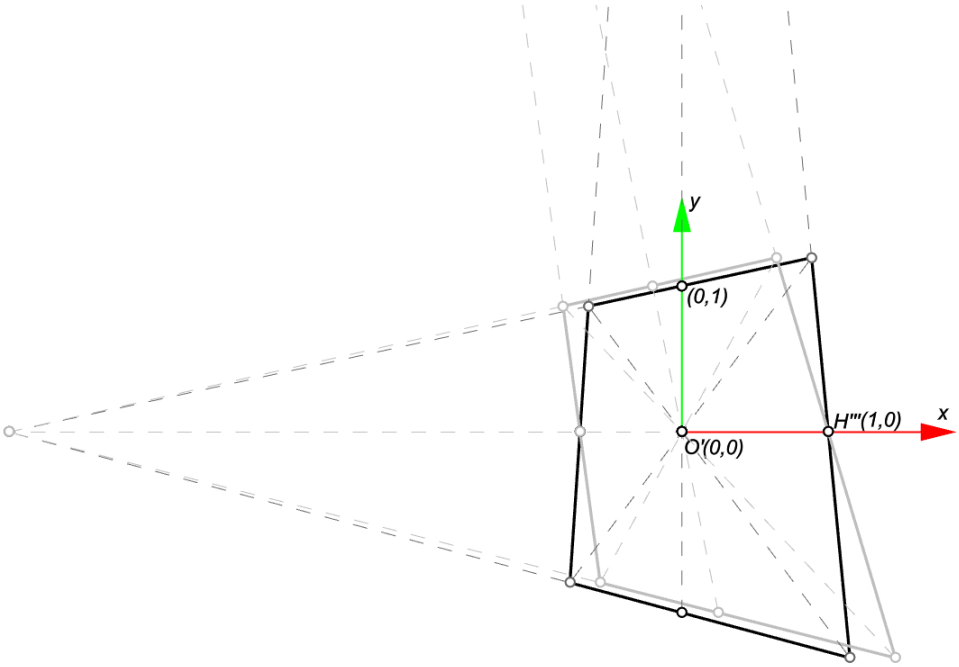

Fig. 5.71 The last of described affine transformation, shear, which aligns point B *with* (0,1) *coordinates.*

5.2.2.7. Combination of affine and perspective transformations

All the affine transformations discussed so far are allowed for the transformation of PQ meshes and preserve planarity of their facets. These transformations combined together are noted as in equation (5.38).

$$\mathcal{F} = \boldsymbol{H_{x,h,d}} \boldsymbol{C_{x,f_x}} \boldsymbol{C_{y,f_y}} \boldsymbol{R_{O,\theta}} \boldsymbol{T_v} \tag{5.32}$$

Consequent transformations are performed from right to left. The inverse transformation, which will be required later for the application of PQ mesh transformation has a form of inverse transformations combined in the inversed order as in equation (5.39).

$$\mathcal{F}^{-1} = \boldsymbol{T_v}^{-1} \boldsymbol{R_{O,\theta}}^{-1} \boldsymbol{C_{x,f_x}}^{-1} \boldsymbol{C_{y,f_y}}^{-1} \boldsymbol{H_{x,h,d}}^{-1} \tag{5.33}$$

Where:

$\mathcal{F}$ denotes the composition of affine transformations,
$\boldsymbol{T}$ denotes translation,
$\boldsymbol{v}$ denotes vector of translation,
$\boldsymbol{R}$ denotes rotation,
$\boldsymbol{O}$ denotes centre of rotation,
$\boldsymbol{\theta}$ denotes angle of rotation,
$\boldsymbol{C_x}$ denotes anisotropic scale in *x* direction,
$\boldsymbol{f_x}$ denotes the factor of scale in *x* direction,
$\boldsymbol{C_y}$ denotes anisotropic scale in *y* direction,
$\boldsymbol{f_y}$ denotes the factor of scale in *y* direction,
$\boldsymbol{H_x}$ denotes the shear transformation with eigenvector along *x* axis,
$\boldsymbol{h}$ denotes the factor of shear transformation,
$\boldsymbol{d}$ denotes the direction of shear transformation.

The *ACEG* quadrilateral in Fig. 5.72, initially transformed by affine transformations, is in configuration, which is possible to obtain by perspective transformation of a unit square. The inversed perspective transformation can be derived from that configuration, i.e. the exact parameter values of *f* and *g*, for which the *ACEG* quadrilateral can be transformed into unit square. From the coordinates of points *D* and *F* the values of parameters *f* and *g* can be calculated, from which the inversed perspective transformation matrix can be derived. These relations were initially explained in section 5.2.2.5 and in Fig. 5.63.

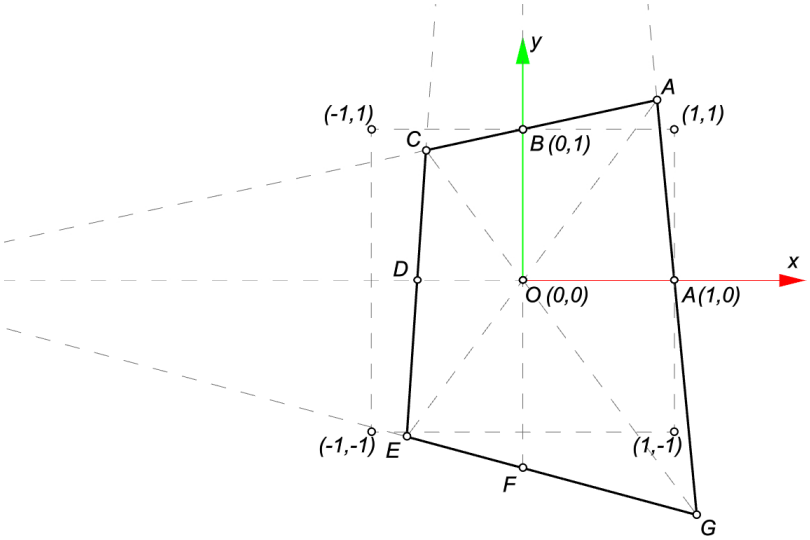

Fig. 5.72 The ACEG *quadrangle after all affine transformations and the dashed silhouette of a unit square. Points around the quadrangle were named anew for clarity.*

The *f* parameter is derived from the *x* coordinate of point *D*, which position is defined by formula (5.40).

$$\boldsymbol{D} = \left(\frac{\boldsymbol{-1}}{\boldsymbol{2f-1}}, \boldsymbol{0}\right) \tag{5.34}$$

Whereas the *g* parameter is derived from the *y* coordinate of point *F*, which position is defined by formula (5.41).

$$\boldsymbol{F} = \left(\boldsymbol{0}, \frac{\boldsymbol{-1}}{\boldsymbol{2g-1}}\right) \tag{5.35}$$

The inversed perspective transformation can be denoted as a function: $\boldsymbol{\mathcal{M}^{-1}(f,g)}$. Finally, the transformation that transforms the unit, translational PQ mesh with planar base into any, user defined quadrilateral is a set of perspective transformation and inversed combination of affine transformations and has the form expressed by (5.36).

$$\boldsymbol{\mathcal{F}^{-1}\mathcal{M}(f,g)} \tag{5.36}$$

where $\mathcal{F}^{-1}$ part is the inversed combination of affine transformations and $\mathcal{M}(f,g)$ is the perspective transformation. In Fig. 5.73 and 5.74 these two steps are visualized. Planarity of individual facets of the PQ mesh is preserved at every step.

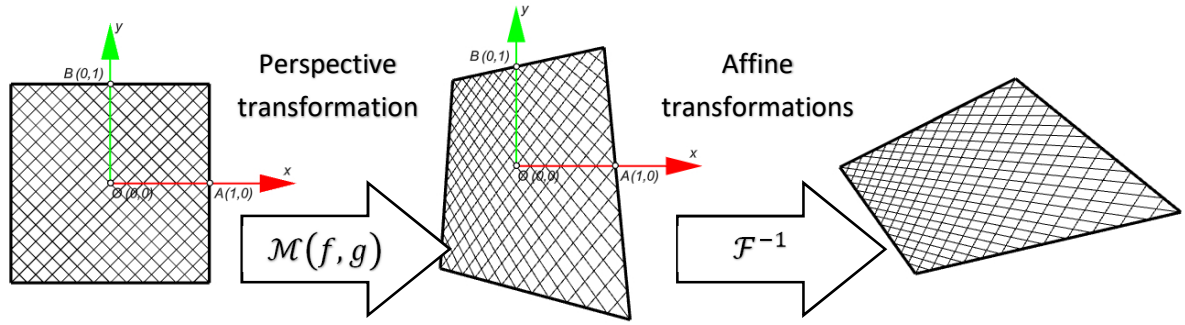

Fig. 5.73 Two steps of transforming the unit PQ mesh into any quadrilateral form.

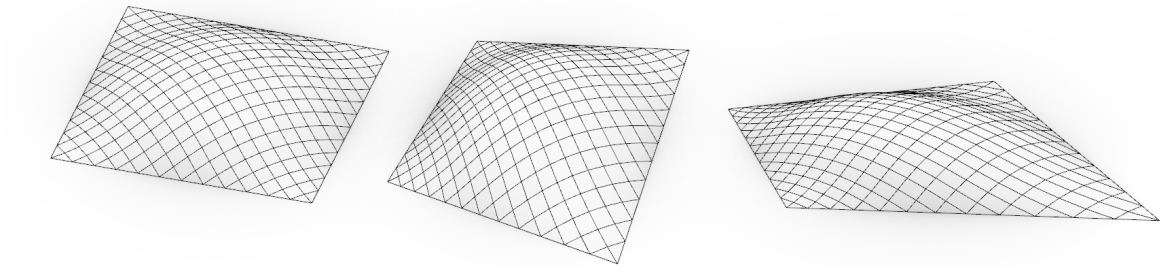

Fig. 5.74 Result of the two-step transformation in perspective view with shading.

This proposed by the author procedure of fitting PQ meshes into any quadrilateral forms assures the exact preservation of facets planarity. This method has a great potential in designing glazed grid shells especially over courtyards of historical buildings in centers of cities, where the outline of courtyard is usually distorted.

5.2.2.8. Aditional perspective transformation adjustments

The *h* factor of perspective transformation had been ignored in previous calculartions. As the horizontal plane at *z*=0 is the invariant plane of perspective transformation with *h* parameter changed, it had no influence on the shape of base quadrilateral. However, the *h* parameter has an impact on the vertical deformation of the mesh and can be utilized as an optimization factor or a parameter through which the user (e.g. an architect) can adjust the final shape of the grid shell.

Figures 5.75 and 5.76 show translational PQ meshes with planar base perimeter, which have been transformed by means of perspective transformation with varied values of the parameter *h* while both parameters *f* and *g* are equal to one. The wireframe box around the mesh is the viewing frustum, which is also deformed showing the outline of each deformation and giving a sense of how the *h* parameter influences the final shape. The top views of the mesh show how does it shrinks or expands according to the *h* parameter.

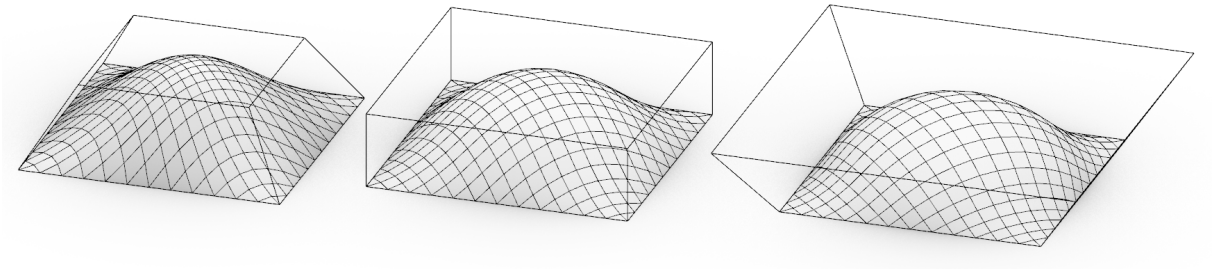

Fig. 5.75 The influence of changing the parameter h *of perspective transformation. Left:* h*<1, centre:* h*=1, right:* h*>1.*

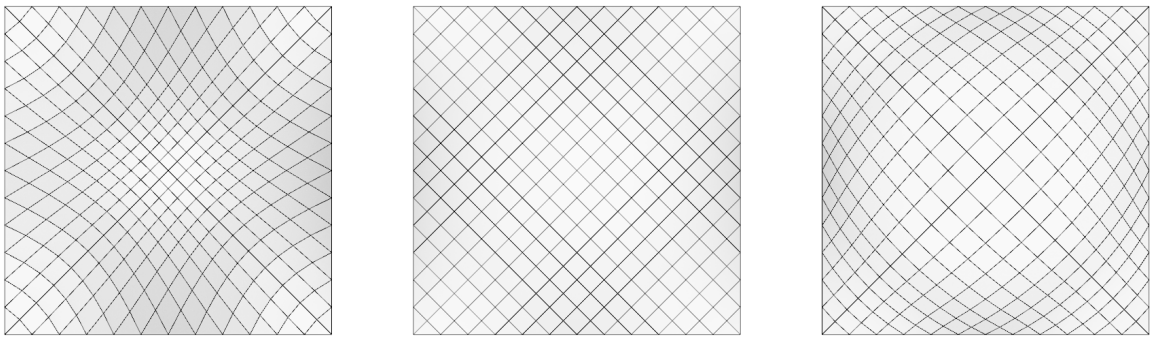

Fig. 5.76 Top view at the meshes perspective transformed with varied values of parameter h*.*
Left: h<1*, centre:* h=1*, right:* h>1*.*

Along with the possibility of changing the value of *h* parameter, the user also has the ability to control the deformation through the location of the centre point of the perspective transformation. Depending on the location, the user can control the 'leaning' direction, see Fig. 5.77.

Summarizing, the combined methods of shaping the translational, PQ mesh with planar base and the perspective transformation, the designer has the control over intuitive, from his point of view, parameters. These parameters include the control over the global shape of the initial mesh (through the parametrized location of *Pe*(*a,b*) extrapolating point, see Fig. 4.12 on page 72) and the density of the mesh. Also, he can define the outer boundary by defining control points. There is also the possibility to apply further planarity preserving transformations, e.g. anisotropic scale in vertical direction to adjust the height of the mesh and shear transformation, also in vertical direction (see transformations described in section 5.1.1). Diffeomorphism can be applied in order to adjust the distribution of edges and distances between support points. In the following chapters the concept of a designing tool and the explanation of a design process using these tools is described.

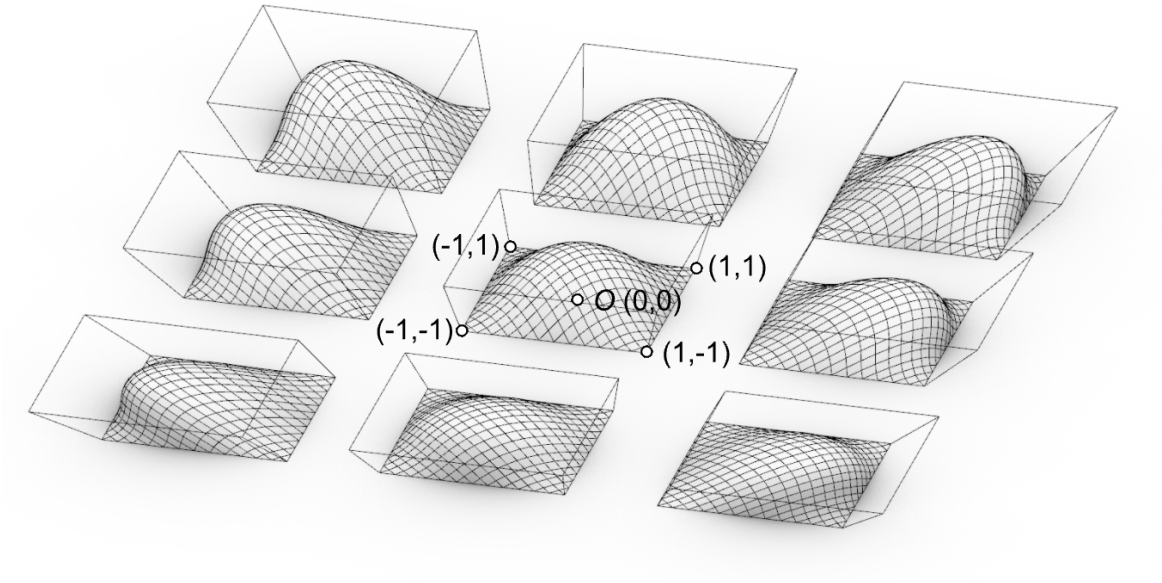

Fig. 5.77 A group of PQ meshes transformed by means of perspective transformation along vertical axis (with parameter h *different from one).*
Shapes of the resultant forms also depend on their location relative to the centre of coordinate system -point O*.*

5.2.2.9. Perspective transformation of conics and second degree surfaces – conic transformations

This section describes author's proposition of matching PQ meshes with 2nd degree base curves. The method is based on perspective transformations. In order to simplify the term 'perspective transformation matching second degree curves' the term **conic transformations** will be used further in this work.

Conic curve or conic section is a curve obtained by intersecting the conical surface with a plane, see Fig. 5.78. Conical surface is a surface formed by a set of all lines passing through a point called apex and a closed directrix curve. In the right conical surface the directrix is a circle and the apex is located directly above the centre point of that circle. A line passing through the apex and any point on the directrix is called generatrix. The axis of a cone is the line passing through the apex and the centre point of directrix.

Depending on the orientation of the plane to the conical surface, the intersection curve can have several generic forms, see (Weisstein 2018e):

- a **circle** is obtained, when the intersecting plane is perpendicular to the axis of the conical surface;
- when the angle between the axis and plane is smaller than the right angle and larger than the angle between the axis and generatrix, then the resultant intersection curve is an **ellipse**;
- when the angle between the axis and plane is equal to the angle between the axis and generatrix, then the resultant intersection curve is a **parabola**;
- when the angle between the axis and plane is smaller than the angle between the axis and generatrix, then the resultant intersection curve is a **hyperbola**.

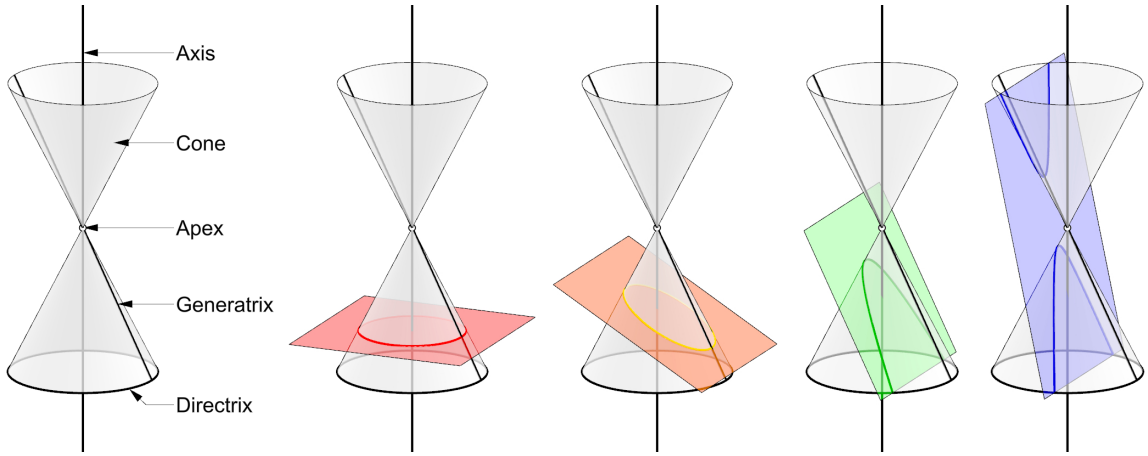

Fig. 5.78 A cone and the conic sections obtained by intersection with a plane.
Red: circular section, the plane is perpendicular to the axis.
Orange: ellipse, the plane is between the axis and generatrix.
Green: parabola, the plane is exactly planar to the generatrix.
Blue: hyperbola, the plane is between the generatrix and axis.

Apart from four types of conic curves that can be obtained by intersecting the right conical surface with a plane there is also an exceptional case, when the intersecting plane contains the apex of conical surface. In such a case the intersection is a point or two straight lines.

All these curves are also plots of second degree formulations, therefore also the term **second degree curves** is used. All points on the unit circle satisfy the equation (5.37). Ellipse is the affine image of circle, i.e. it can be obtained by affine transformation (anisotropic scale, shear) of a circle. The equation of ellipse has a form of (5.38), parabola has the equation (5.39) and hyperbola has the equation (5.40), where *a* and *b* are shape parameters.

$$\boldsymbol{x^2 + y^2 = 1} \tag{5.37}$$

$$\boldsymbol{\frac{x^2}{a^2} + \frac{y^2}{b^2} = 1} \tag{5.38}$$

$$\boldsymbol{y = ax^2 + bx + c} \tag{5.39}$$

$$\boldsymbol{\frac{x^2}{a^2} - \frac{y^2}{b^2} = 1} \tag{5.40}$$

In all the equations above, the exponents of *x* and *y* are equal to two, therefore all these curves are of second degree. This property is used for the parametrization of NURBS curves of second degree, which are composed of segments of second degree curves, i.e. circles, ellipses, parabolas and hyperbolas, see (Weisstein 2018j). Each second degree curve can be therefore decomposed into second degree segments, which can be then used as the base shapes for conic transformations of PQ meshes. The concept of this method is to allow the designer to control the shape of the PQ mesh by adjusting the control points of a second degree NURBS curve.

That concept utilizes yet another property of second degree curves: all the conical sections are perspective images of circle (see (Bradley 1834), pp. 196–206). Following consideration will explain why and how.

The fact, that circle has an elliptical shape in perspective view was well known to artists and architects since at least Renaissance era, see section 2.3.2 and (Święciak and Tarczewski 2018). In Fig. 5.79 the perspective transformation of a circle was performed. The parameter *f* was set to the value of 0,75. The resultant shape is the exact ellipse. The resultant curve is an ellipse for all the *f* values that meet the condition (5.41)[81].

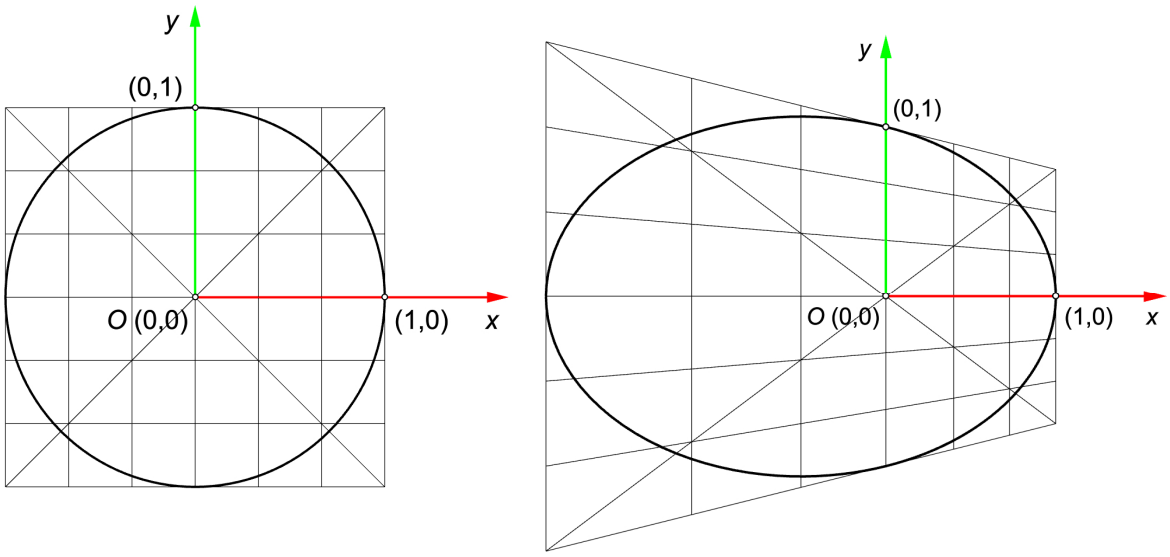

Fig. 5.79 Planar perspective transformation of a circle. In general, a circle in perspective is an ellipse.

$$\mathbf{0,5} < \boldsymbol{f} < \mathbf{1 \text{ or } 1} < \boldsymbol{f} \tag{5.41}$$

As *f* approaches the value of 0,5, the left side of the frame, goes beyond the field of view and tends toward the infinity. It cannot be displayed on paper, however it can be shown by displaying some selected lines on the frame are bolded, i.e. two pairs of edges and diagonals, see Fig. 5.80. When the condition (5.41) is met the pairs edge-and-diagonal (see bold lines in Fig. 5.80) intersect at the corners of the frame on the left side (compare Fig. 5.79, right and Fig. 5.80). However, when perspective transformation is performed with the *f* parameter value equal to 0,5 the corresponding pairs of edge-diagonal are parallel, see Fig. 5.80. Therefore it is assumed that they intersect at infinity. Concluding, the left side of the frame in Fig. 5.80, whose corners are at the edge-diagonal intersection points is also at infinity. Since the perspective transformed circle is tangent to that infinitely distanced edge, it also extends into infinity and practically never closes. In such a case, the circle is a parabola (see Fig. 5.81) and the resultant curve does not lose its second degree structure.

[81] The condition was derived by the author based on the perspective transformation principles already assumed in this work, i.e. the placement of the unit circle in the coordinate system, perspective transformation matrix (5.20) and letter notations. The cases, when parameter *f* does not met the condition in (5.41) are explained further in this section.

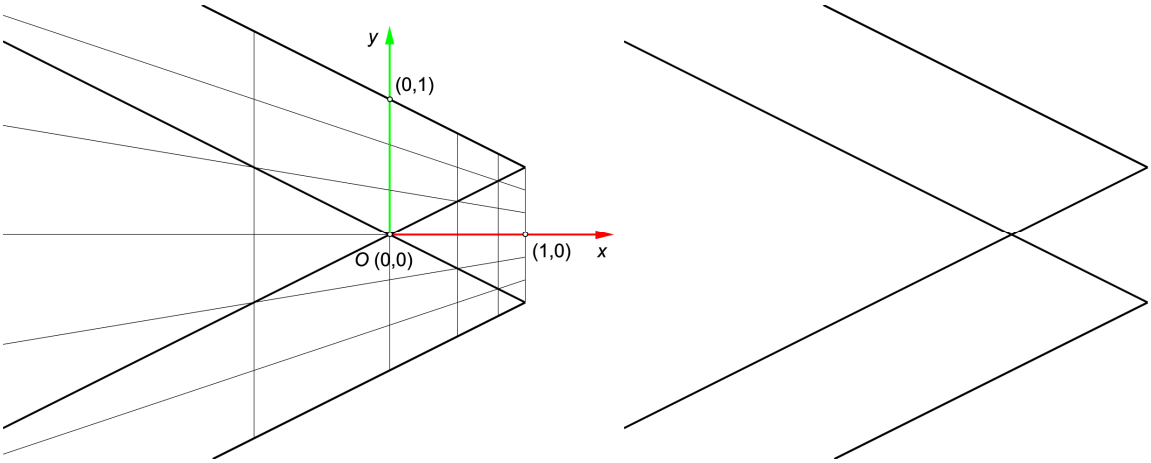

Fig. 5.80 Bold lines correspond to the diagonals and opposing edges of the frame in perspective. Right: The same bold lines without the frame, where the parallelism between corresponding pairs is visible. In perspective view pairs intersect at infinity.

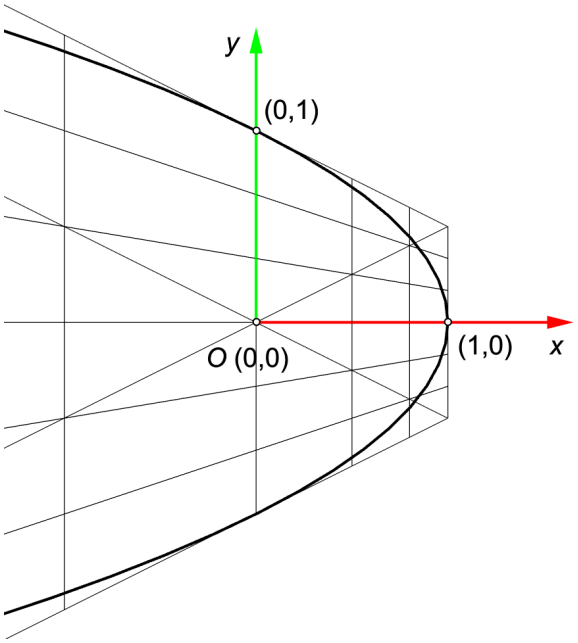

Fig. 5.81 When the left side of the image spans into infinity, the circle also closes at infinity, becoming a parabola.

When the *f* parameter value is decreased even further, beyond the value of 0,5, then the intersection points of corresponding edge-diagonal pairs come out on the right side of the image, Fig. 5.82. Part of the transformed image on the right is also inverted vertically. Proper real connection between the parts of the same line segment does not exist, therefore unexisting parts are shown with dashed lines. Since one line cannot be transformed into two lines the connection still exist, but virtually at infinity. Lines from the left side of the figure extend leftward into infinity, then flip at the right sided infinity and finish at the right side of the image.

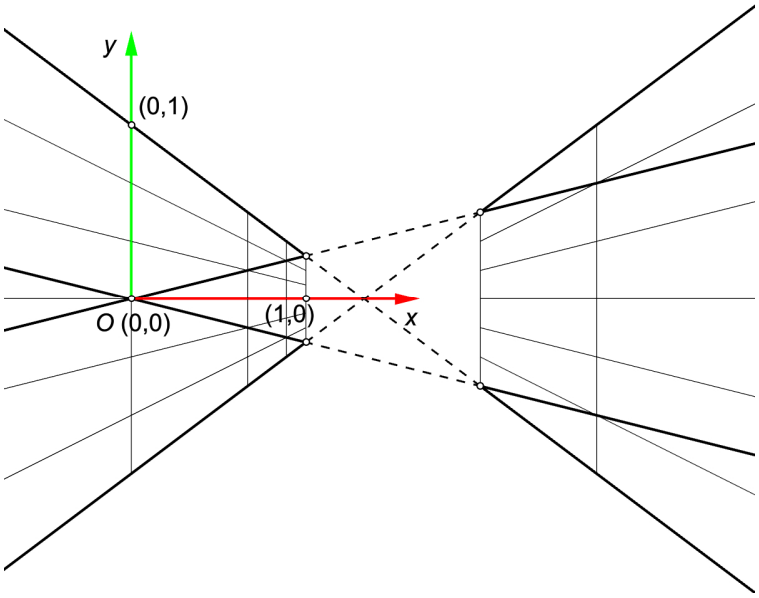

Fig. 5.82 Extensions of the opposing edges and diagonals intersect on the other side of the image. The side of the image that went into infinity to the left appears on the right side of the image.

A circle embedded into that perspective transformed frame should be tangent to all of its edges, consequently it should appear as two curves on both sides of the image. Virtually, that transformed circle is still at one piece at infinity, however, in Fig. 5.83 it is represented in two pieces. The obtained curve is a hyperbola. For further consideration only the left side of the hyperbola will be the subject of interest.

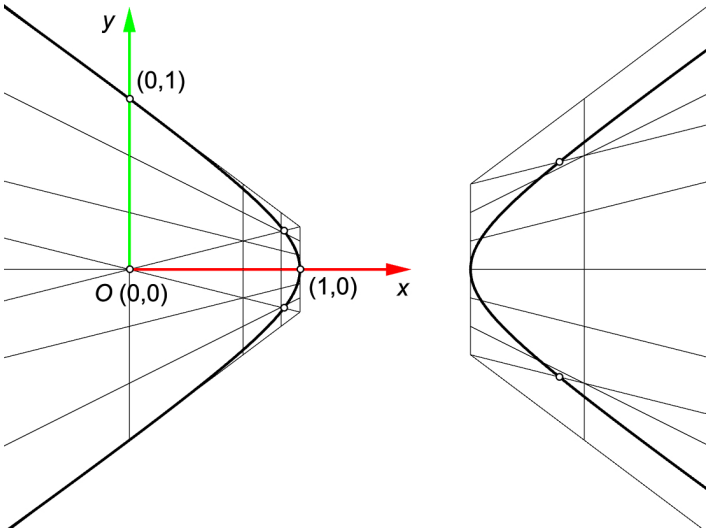

Fig. 5.83 The circle in perspective closes on the right side of the image becoming a hyperbola.

Since a circle can be transformed by perspective transformation into any second degree curve any second degree curve can be transformed into circular form by inversed perspective transformation, i.e. any ellipse, parabola and hyperbola will create circle image when point projected onto a plane from particular angle. Intuitively, an observer looking at an ellipse from particular direction will see circular image[82].

[82] Compare with Gian Lorenzo Bernini's elliptical part of St Peter's Square in Vatican.

Conic transformations can be further used for matching PQ meshes with circular base lines (e.g. obtained by stereographic projection or inverse geometry discussed in sections 5.1.2 and 5.1.3) to match them with second degree base shapes. An intersection of a sphere with a horizontal base plane results in a circle, see Fig. 5.84, left. Transforming such sphere together with the intersection curve will result in an ellipsoid, paraboloid or a hyperboloid, see Fig. 5.84. The intersection lines at the bases of obtained shapes become consequently ellipse, parabola or hyperbola. Therefore, a PQ mesh contained on a sphere can be transformed into a new family of shapes based on rotational conics by a stereographic projection or inverse geometry.

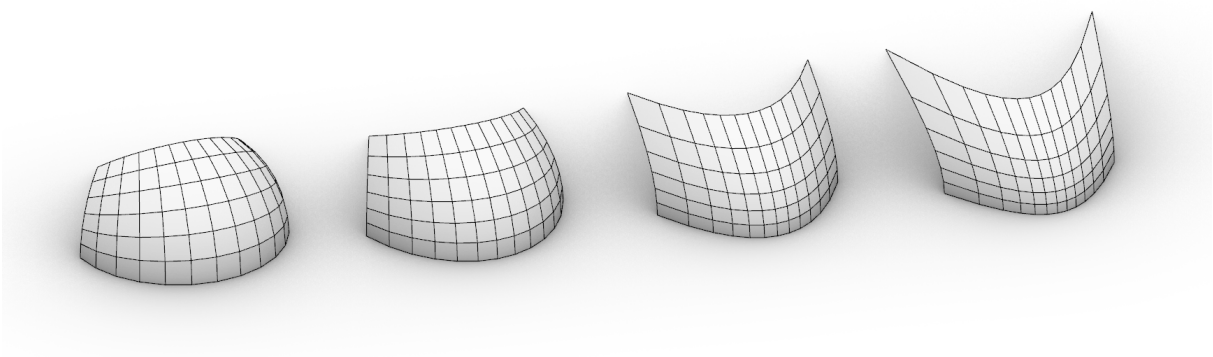

Fig. 5.84 Initial, spherical PQ mesh (left) and perspective transformations resulting with (from left to right) elliptical, parabolical and hyperbolical shapes depending on the parameter f *described in this section.*

The following study of rotational conics extends the versatility of conic transformations even further. Conic sections obtained by intersections between conical surface and plane, with respect to the relation between obtained curve and the orientation of the plane toward the cone, was already explained before at the beginning of this section, see Fig. 5.78. However, conical sections can also be obtained by intersections between plane and other family of surfaces, i.e. surface of revolution with conical generatrix, or rotational conic for simplicity. A rotational conic surface is a surface obtained by rotation of a circle, ellipse, parabola or hyperbola around its main axis, see Fig. 5.85. Consequent surfaces are: sphere, ellipsoid, paraboloid and hyperboloid. The relation between orientation of intersecting plane, the type of rotational conic and the type of resultant curve will be explained in the following part of the work. Moreover, all intersections between plane and rotational conic are second degree curves. Any rotational conics can be obtained by perspective transformations of sphere, such as any second degree curve is possible to obtain by perspective transformation of circle.

The concept of application of conic transformation is as follows: the user defines base curve as second degree NURBS curve, see Fig. 5.86. The NURBS curve is divided into segments, each of which is a conical section by the definition of second degree NURBS model, see Fig. 5.87. Selected segment, e.g. a parabola (Fig. 5.88, left) is the desired base shape, for which a reciprocal perspective transformation F^{-1} is computed. Finally, the perspective transformation F is applied onto a discrete, spherical PQ mesh with circular base resulting with a transformed PQ mesh, that fits exactly to the base line, see Fig. 5.88, right.

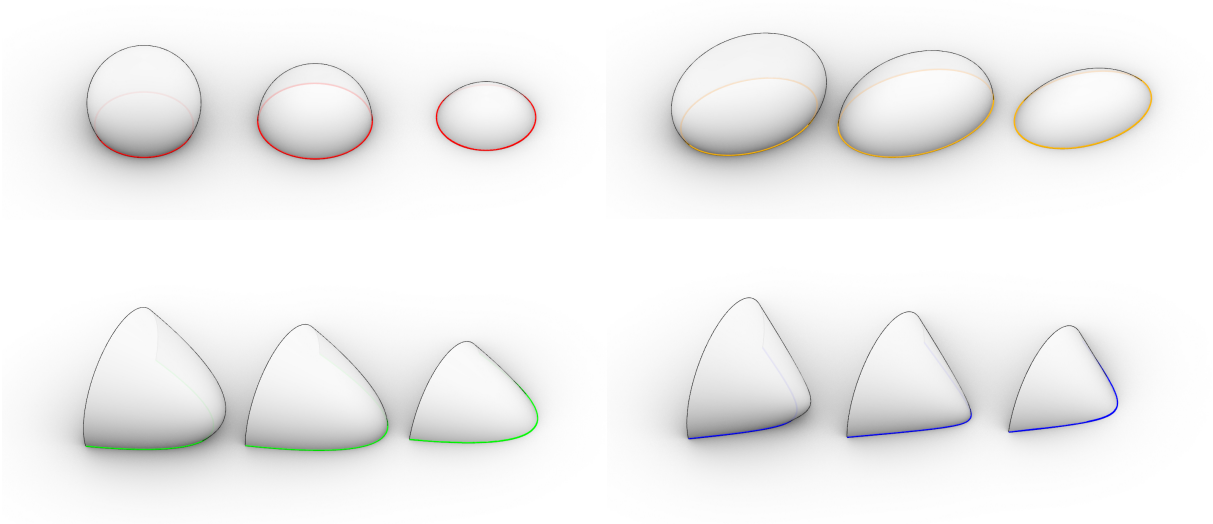

Fig. 5.85 Curves of intersection of perspective transformed spheres and plane.
Red - circle, orange - ellipse, green - parabola, blue - hyperbola.

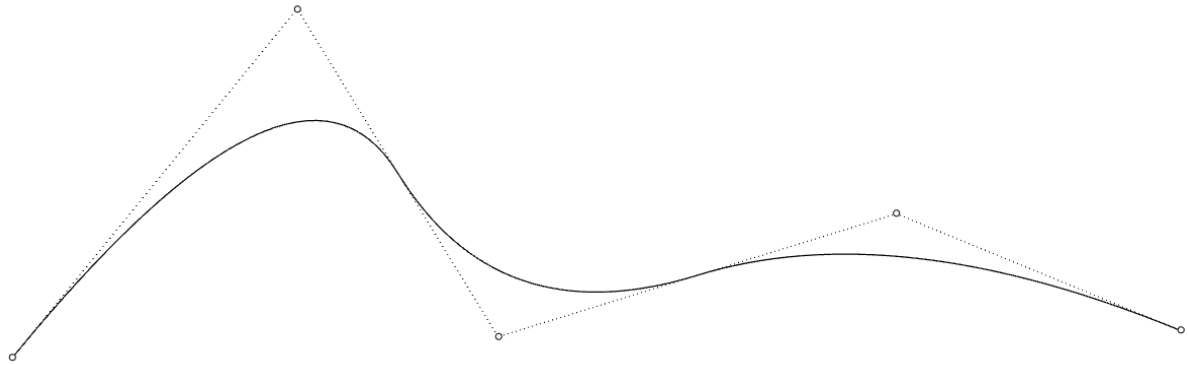

Fig. 5.86 Second degree NURBS curve with five control points.

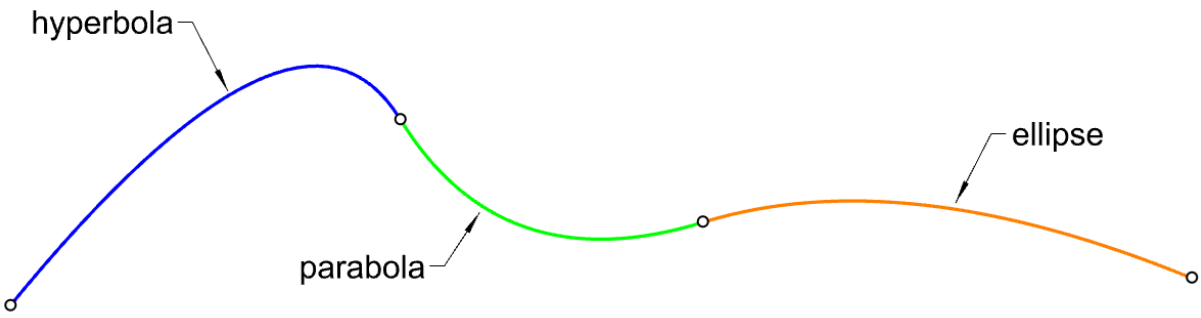

Fig. 5.87 Segmentation of the curve above into conical sections.

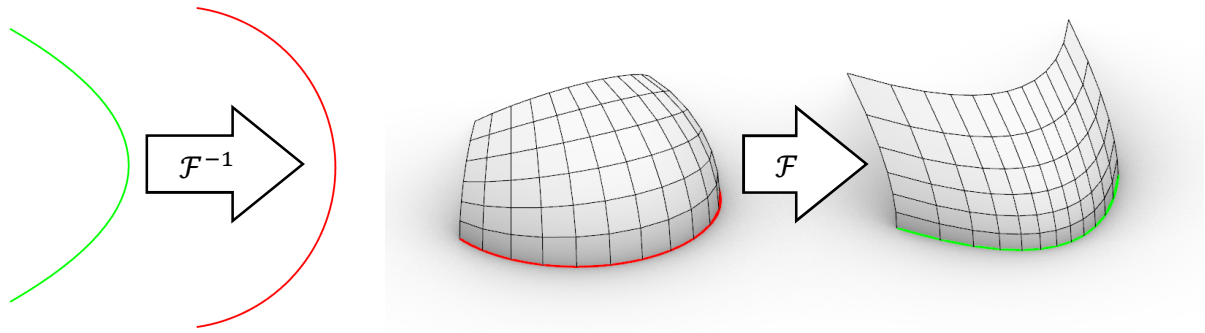

Fig. 5.88 Left: calculation of the inversed perspective transformation F^{-1} between desired base conic section and a circle segment. Right: application of the perspective transformation F onto the discrete spherical PQ mesh in order to fit the base of mesh to the desired shape.

Whole family of rotational conics can be obtained by the application of perspective transformations of spheres. The same rule applies to the discrete representations of dicussed surfaces, i.e. PQ meshes based on spheres and rotational conics.

Moreover, one particular conic curve can be obtained from a whole family of rotational conics, depending of its parameters and the orientation of intersecting plane with respect to the rotational conic main axis. Simple example is shown in Fig. 5.89, where various ellipses and a circle are obtained by intersection of a plane and ellipsoid, depending on the orientation of the ellipsoid's axis. This behaviour allows to increase the freedom of the design. The designer is allowed to change the axis inclination angle to explore possible solutions for the grid shell. The selecion of appropriate rotational conic and perspective transformation is performed by the algorithm.

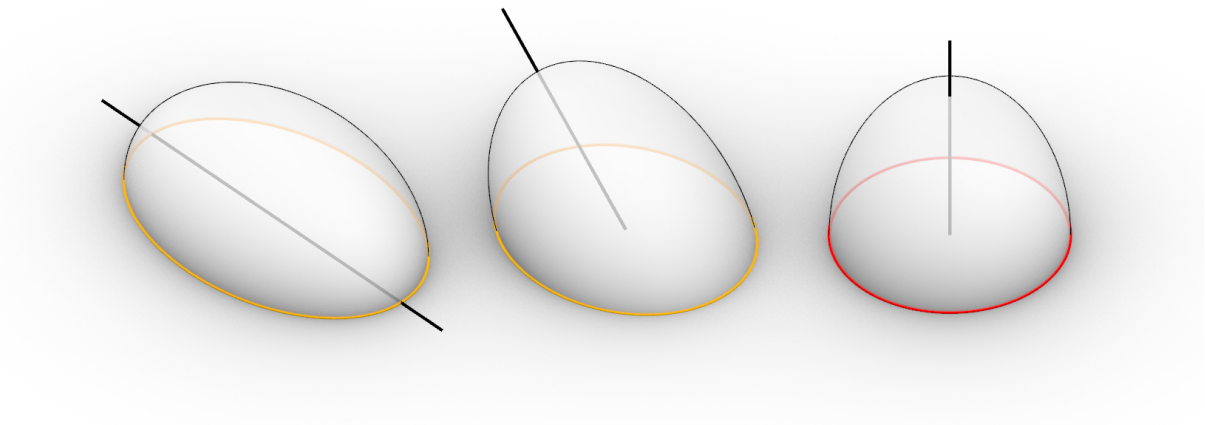

Fig. 5.89 Curves of intersection between ellipsoid and plane at various configurations. All cases result with ellipse (orange) apart when the axis of ellipsoid is perpendicular to the plane. In such case the intersection is circular.

An overview of resultant intersection curves of plane and rotational conics, whose main axes are parallel to the plane is shown in Fig. 5.85. Each type of rotational conic in the figure is shown in three different cases: with axis of rotation below, on and over the intersecting plane. The resultant curves of intersection are always affine images of the generatrix of rotational conic (except for the hyperboloid, explanation is given later in this section). It means that an ellipsoid is a surface of revolution of an ellipse and the intersection curves of that ellipsoid are also ellipses, however of a different shape than the generatrix. These different shapes are affine images of the generatrix, which means, that by application of anisotropic scaling and shear transformation one ellipse can be transformed into another ellipse or a circle.

When the main axis of rotational conic surface is not parallel to the intersecting plane, then the intersection curves are also conics. In case of ellipsoid (Fig. 5.89) the intersection curve is always an ellipse, except for the case, when the axis of rotation is perpendicular to the intersection plane. In such a case the intersection curve is a circle, which is also an affine image of any ellipse.

The intersection between paraboloid and plane is a parabola only in one case, i.e. when the axis of rotation is parallel to the intersecting plane, see Fig. 5.90, left. Second unique configuration is when the axis of rotation is perpendicular to the intersection plane. In such case, the curve of intersection is a circle, see Fig. 5.90, right. In all other cases the curves of intersection are ellipses.

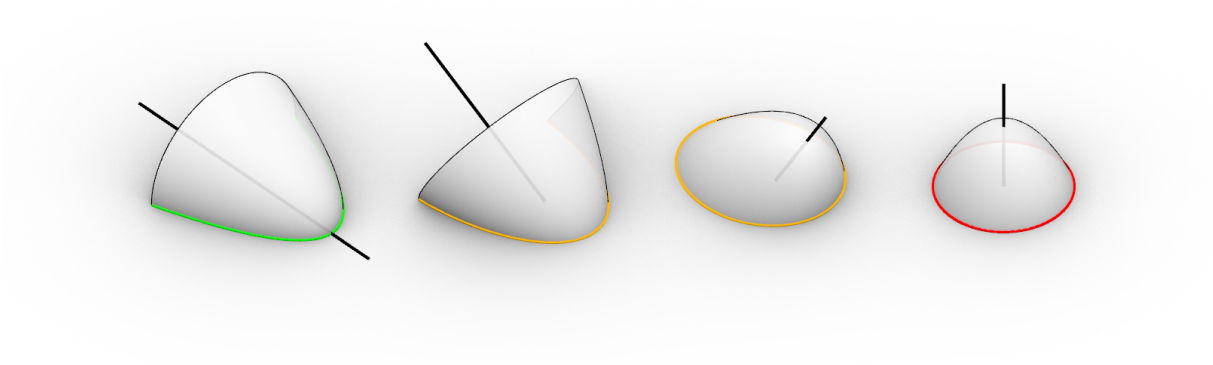

Fig. 5.90 Paraboloid obtained by perspective transformation of sphere and curves of intersection with plane. Intersection curve is a parabola (green) when the axis is parallel to the plane. Intersection curve is a circle (red) when the axis is perpendicular to the plane. Intersection curve is an ellipse (orange) in other cases.

Intersections between hyperboloids and plane allow to obtain any conical curve. Figure 5.91 shows the relation between the orientation of hyperboloid with respect to the plane and the resultant intersection, conic curve. In case of hyperboloids there is another property, which defines the type of obtained intersection, conic curve, i.e. the asymptote line (dashed in Fig. 5.91).

The specific angle that separates different types of obtained conics is the angle between asymptote of the generatrix hyperbola (dashed line) and the intersection plane. Only if that angle is equal to 0, i.e. the asymptote is parallel to the plane, obtained curve is a parabola. Rotating hyperboloid further from that angle results in elliptic curve and finally a circle, when the axis of hyperboloid is perpendicular to the plane of intersection. Rotating it backwards results in hyperbolas.

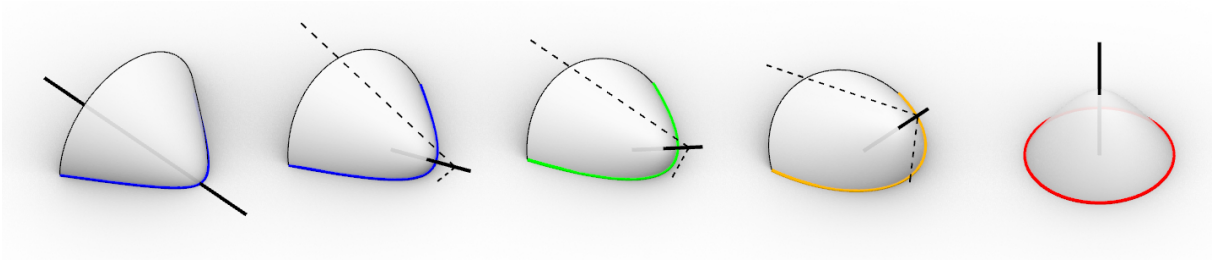

Fig. 5.91 Hyperboloid obtained by perspective transformation of sphere and curves of intersection with horizontal plane. Intersection curve is a parabola (green) when the asymptote of hyperboloid (contained in vertical plane) is parallel to the horizontal plane of intersection plane. Intersection curve is a circle (red) when the axis of hyperboloid is perpendicular to the horizontal plane. Intersection curve is an ellipse (orange) when the axis between asymptote of hyperboloid (contained in vertical plane) and plane is larger than 0. Intersection curve is a hyperbola (blue) when the axis between asymptote of hyperbola (contained in vertical plane) and the horizontal plane is smaller than 0 and when the main axis of hyperbola is parallel to the horizontal plane.

Position of rotational conic over the horizontal plane of intersection does not affect the type of obtained conic curve, while it can be used as a parameter for obtaining different shapes[83]. Therefore, position of rotational conic over the plane of intersection and the inclination of axis of rotational conic are two independent parameters. Those parameters give the designer two degrees of freedom in shaping PQ meshes through conic transformations.

Figure 5.92 shows sections of rotational conics, from left to right: cone, hyperboloid, paraboloid, ellipsoid, sphere. The cone is added illustratively, since it has no utilization in conic transformations. Colour fill refers to the type of curve obtained by intersection of particular rotational conic with a plane, which is perpendicular to the plane of section and passes through a point marked on picture. Passing the intersection plane through the blue area results with hyperbola, which is possible to obtain only in case of cone and hyperboloid. When the intersection plane passes through the green line, the resultant curve is parabola. Parabola is obtained only in particular configuration of intersection plane. The same is true for circular intersections, marked red with the exception of sphere, where any intersection is circular. Other intersections result with elliptical curves – marked in orange. All results are dependent on the position of the point, through which the intersection plane runs through. However, a change in the position of that point does not affect basic rules of resulting intersection curves – e.g. the parabolic plane is always parallel to the asymptote (in hyperboloid) or the main axis (in paraboloid).

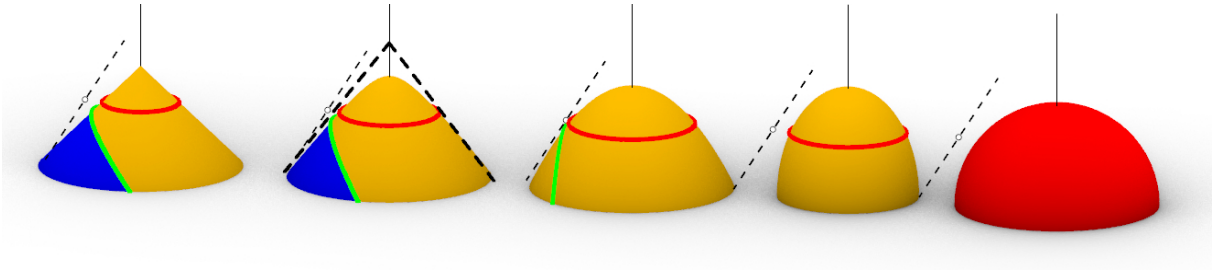

Fig. 5.92 Conic sections according to the angle of intersecting plane (containing dashed line next to each surface) with respect to the section of consequent surfaces of revolution. From left to right – cone, hyperboloid, paraboloid, ellipsoid, sphere. Colours: blue – hyperbola, green – parabola, orange – ellipse, red – circle.

Figure 5.93 presents versatility of conic transformations, i.e. for a particular base shape (a parabola) diverse forms were adjusted. The first from the left side is paraboloid, whose axis is perpendicular to the horizontal plane. Consequent pictures are rotational conics obtained by perspective transformations of unit spheres, with consequently decreasing f parameter and consequently increasing of inclination angle of the main axis. For all cases the level above the horizontal does not affect the type of obtained curve, however, except for the paraboloid, the resultant curves are affine images (i.e. parabolas in diverse scales).

Similarly, any other doubly curved surface, which is a rotational conic, can be obtained and exactly adjusted to any second degree base curve. Additionally, affine transformations can be applied to the resultant shapes, increasing the degree of freedom even further. Plane preserving affine transformations such as anisotropic scale and shear are adequate to lean the resultant shape or adjust its height.

[83] For example the designer can decide whether he wants to design a spherical dome (with circular base) which is exactly half of that sphere or which is a part of that sphere truncated above or below its great circle.

The versatility of conic transformations was presented above on continues forms, whereas their destined purpose is the transformation of PQ meshes. Figure 5.94 shows two examples of simple PQ meshes obtained through conic transformations, where the base curve was predefined by the designer. In both cases, two different methods of obtaining the initial, spherical PQ mesh were adopted, resulting with two, completely different patterns of quads. The shapes of conical curves on vertical walls are also adjustable through available parameters of conic and affine transformations. Through the adjustability of the form of vertical edge conical curves, two neighbouring PQ meshes can be tightly joined, i.e. two, neighbouring PQ meshes with different conical base curves can be adjacent to each other along one conical curve.

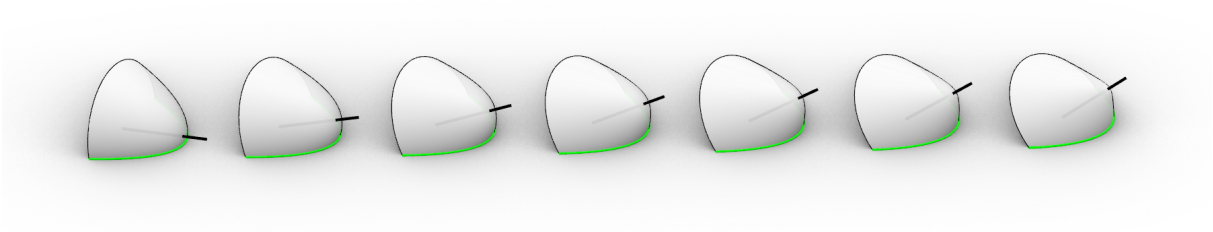

Fig. 5.93 Exactly the same parabolic curve is obtained by conic transformations with appropriately selected parameters. First parameter is the type of rotational conic obtained by perspective transformation of a unit sphere, the second parameter is the inclination of the main axis of rotational conic.

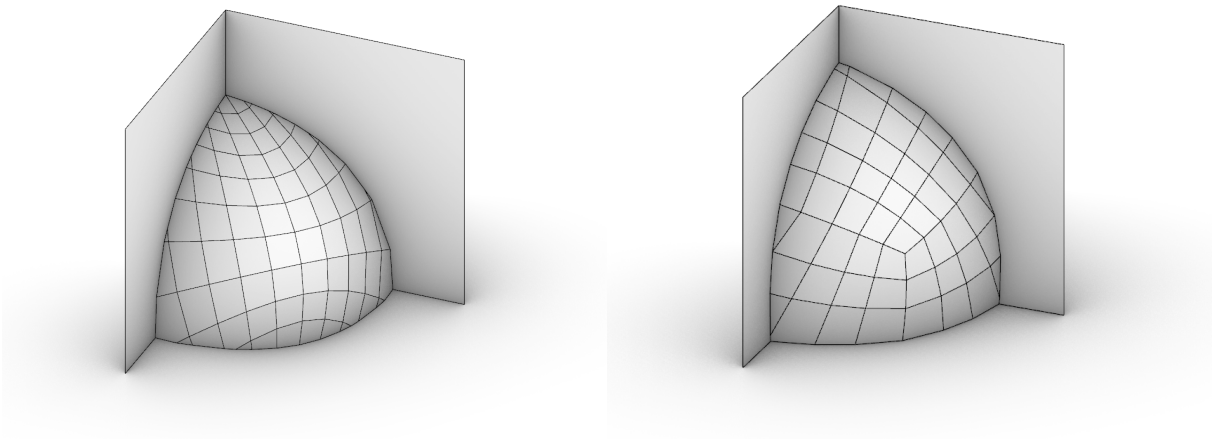

Fig. 5.94 Examples of PQ meshes aligned to the predefined, second degree boundary curves.

However, in Fig. 5.87 the neighbouring conical curves are curved on the opposite directions (inflected), meaning that the continuity of neighbouring PQ meshes requires the adoption of negatively curved mesh. For that purpose a conical transformation of the PQ mesh based on torus can be adopted, see Fig. 5.95.

Due to the fact that the real building case studies presented further in this work require only the essential version of perspective transformation and SC mapping, the conic transformations are only presented as a concept and will not be further discussed in course of this work.

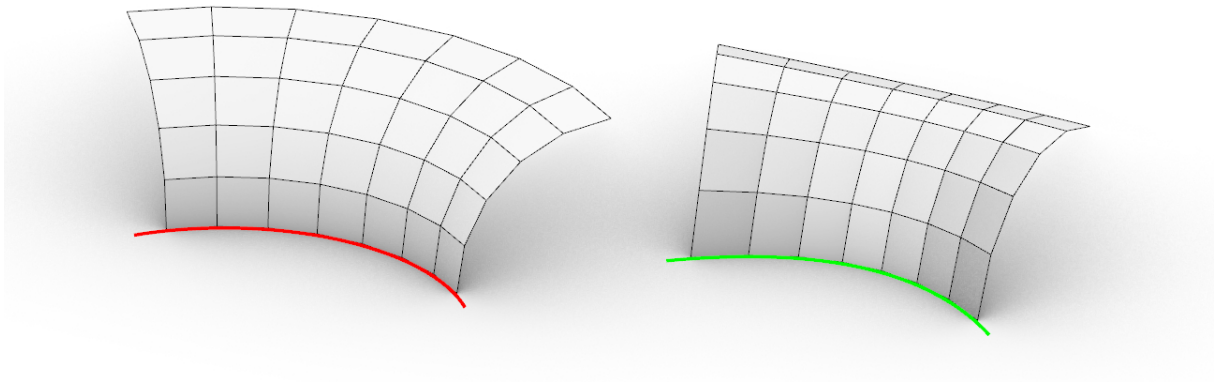

Fig. 5.95 Conic transformation of negatively curved PQ mesh based on torus.
Left: initial mesh with circular base, right: transformed mesh with parabolic base.
Auxiliary affine transformations were adopted for the mesh on the right.

5.2.3. Diffeomorphism

An intrinsic property of any surface is a coordinate system embedded into it. A coordinate system of a surface is represented by straight lines or curves that indicate positions on that surface in two directions. As long as any pair of curves from the same direction (or family) don't cross, the system can unambiguously define position of any point on that surface. There are infinitely many possible ways to embed a coordinate system on a surface. Example shown in Fig. 5.96 proves, that even flat surfaces may be parametrized by complex and irregular systems of coordinates.

Fig. 5.96 Peter Kogler optical illusion rooms. Visualization of a concept of arbitrarily parametrized flat surfaces.[84]

[84] Source: https://mymodernmet.com/wp/wp-content/uploads/2016/12/peter-kogler-room-installation-1.jpg

When designing a surface as NURBS, their coordinate systems rely on control point positions. Depending on the intervals between them and their weights, the network of coordinate system may be distorted as shown in Fig. 5.97. The first coordinate system represents unique state, when all the lines are in equilibrium, each one is divided in equal portions.

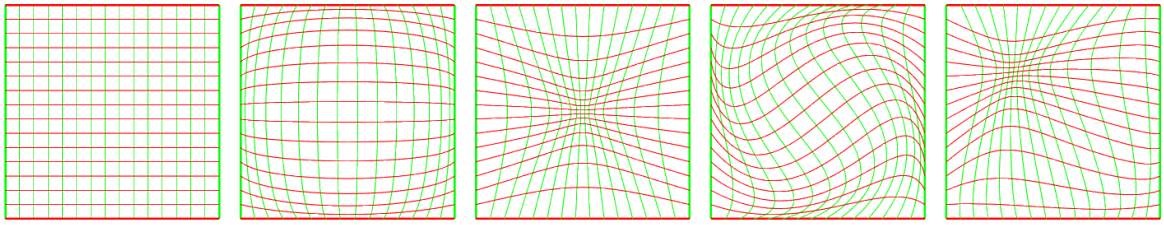

Fig. 5.97 Variations of coordinate systems over the flat NURBS surface, depending on the positions and weights of control points.

For majority of freeform surfaces it is impossible to obtain coordinate system that preserves equal distances, areas and angles for the same intervals of surface's domains. A form such simple as a sphere is itself a subject of a science. Our globe is parametrized by a system consisting of latitude and meridian curves, see Fig. 5.98. Meridians actually meet at the singularities on poles of the globe and circles of latitude are closed in loops. Circles of latitude and meridians are uniformly spread over Earth's surface. Circles of latitude intersect meridians so that they divide them into portions of equal lengths and vice versa. Although the portions of earth's surface that are trimmed by different pairs of latitudes and meridians that have equal distances to each other, they are not necessarily the same in areas. Also the portions of latitudes are different in lengths depending on distances from the equator and corners of areas closed by four portions of latitudes and meridians does not sum up to 360°.

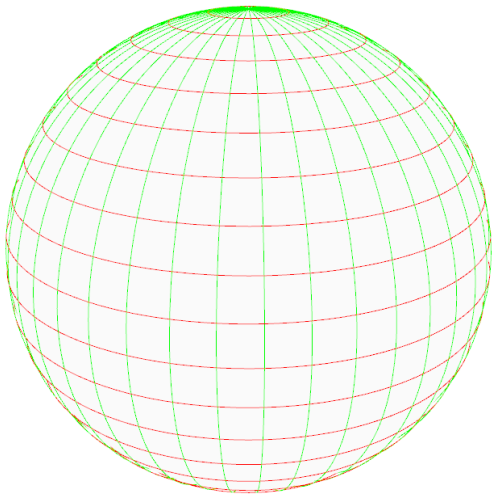

Fig. 5.98 Sphere parametrized by a system of latitude and meridian circles.

Nevertheless, the adopted system is unique one, that is in the state of equilibrium. The network of curves is uniformly distributed over the surface, at least some of the geometrical properties are preserved locally.

While designing a spatial structure, e.g. lattice shell, it is convenient to measure distances between nodes in Cartesian coordinate system. Each vertex is parametrized by 3 coordinates - x, y and z. However, while designing a grid shell over a parametrized NURBS surface according to the top-down paradigm, the position of each vertex is derived from formulation (5.42) with two argument parameters: U and V.

$$\boldsymbol{f}(\boldsymbol{U},\boldsymbol{V}) \rightarrow (\boldsymbol{x},\boldsymbol{y},\boldsymbol{z}) \tag{5.42}$$

U and V are the two dimensional coordinates of surface embedded in three dimensional space. It is desirable to optimize the distances between points (eventually uniformalise the lengths of the rods) that are separated by the same intervals of *UV* space. Distorted systems of isocurves are often obtained due to non-uniform distribution of control points and their weights. Similar issue is associated with super-ellipse and its parametric representation (5.43), which is a system of equations parametrized by *u* and *v* coordinates, where *c* and *s* are auxiliary functions.

$$\begin{cases} \boldsymbol{x}(\boldsymbol{u},\boldsymbol{v}) = \boldsymbol{c}\left(\boldsymbol{v},\frac{\boldsymbol{2}}{\boldsymbol{t}}\right)\boldsymbol{c}\left(\boldsymbol{u},\frac{\boldsymbol{2}}{\boldsymbol{r}}\right) \\ \boldsymbol{y}(\boldsymbol{u},\boldsymbol{v}) = \boldsymbol{c}\left(\boldsymbol{v},\frac{\boldsymbol{2}}{\boldsymbol{t}}\right)\boldsymbol{s}\left(\boldsymbol{u},\frac{\boldsymbol{2}}{\boldsymbol{r}}\right) \\ \boldsymbol{z}(\boldsymbol{u},\boldsymbol{v}) = \boldsymbol{s}\left(\boldsymbol{v},\frac{\boldsymbol{2}}{\boldsymbol{t}}\right) \end{cases} \tag{5.43}$$

In Fig. 5.99 a form of super-ellipsoid dome is discretely represented by two networks of lattices. Colours relate to the lengths of edges. In the first case the vertices were designated from the parametric form super-ellipsoid, with parameters *u* and *v* the same intervals – same parameter intervals result in lattices of uneven lengths. In the second case the *u* and *v* parameters have various intervals between corresponding rows and columns of vertices, whereas the real distances between vertices in column or row are equal.

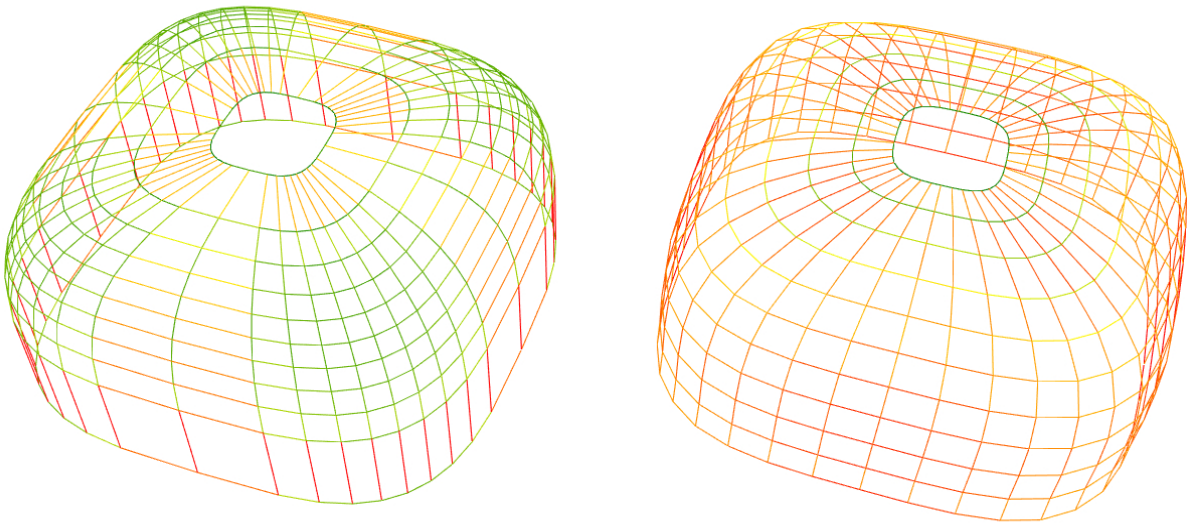

Fig. 5.99 Upper hemispheres of super-ellipses in discrete representation. Left: vertices are distributed in even parametric distances. Right: vertex distribution is optimized according to the Euclidean measure. The same colours mark edges of equal lengths. Both meshes are PQ.

The algorithm used to equalize the distances between parametrized surface is iterative. In the each step the *UV* distance between corresponding vertices is modified according to the real distance between them until the system converges.

The second case concern the disproportion of vertex distribution after some transformations that were previously presented in this chapter, e.g. perspective transformation. In that case it is possible to perform the optimization linearly.

For example a translational mesh divided into edges of equal length is transformed by means of perspective transformation, resulting in non-uniform distribution of vertices, see Fig. 5.100, right. The objective is to distribute points uniformly over the form after transformation. To do so, the points are distributed over the continuous form after the transformation along one of its edges, see Fig. 5.101, right. Pairs of those points define consequent vectors of translation for the generatrix curve of translational PQ mesh, no other points are required. The reverse transformation is then performed on these points, resulting with their non-uniform distribution over the basic surface, see Fig. 5.101, left. The last step it co construct a mesh from those points (Fig. 5.102, left) and perform the perspective transformation *T* once again on the corrected mesh. The resultant PQ mesh has equalized lengths of edges, see Fig. 5.102, right.

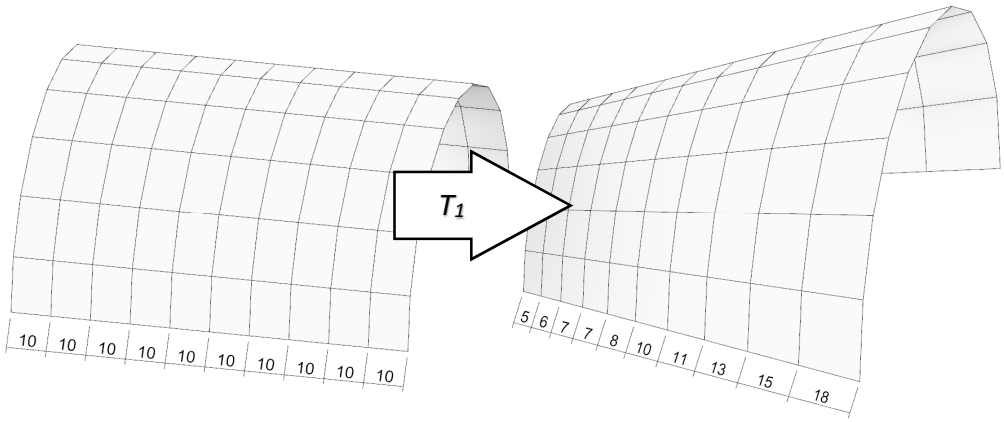

Fig. 5.100 Perspective transformation T_1 of uniformly distributed mesh.

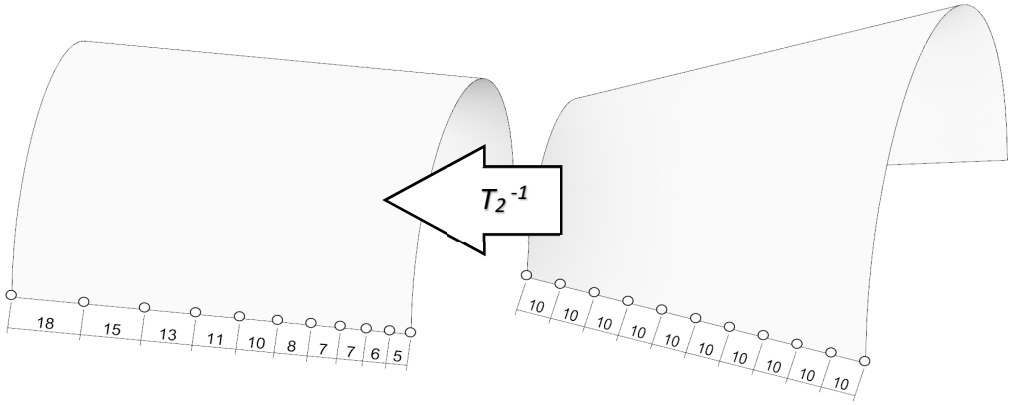

Fig. 5.101 Reverse transformation T_2^{-1} of transformed surface with uniformly distributed points along its base edge.

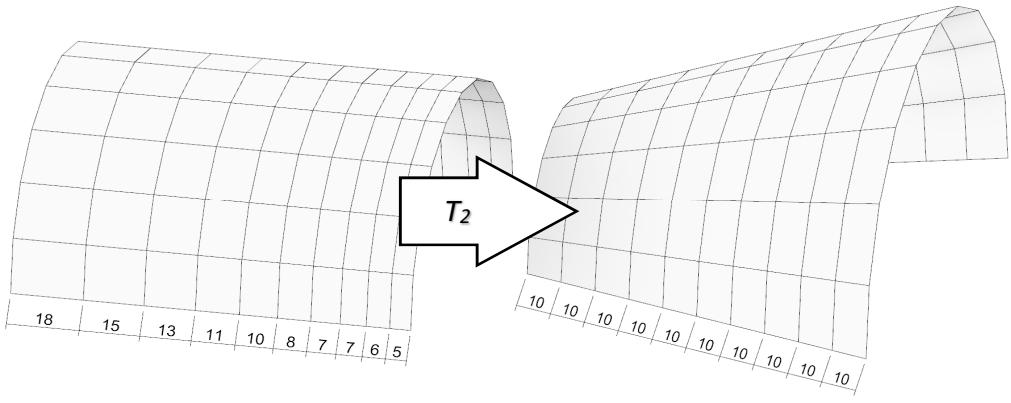

Fig. 5.102 Transformation of the basic form with modified distribution of points.

Optimisation methods vary depending on the type of PQ mesh and methods it was obtained. However, in case of translational meshes with planar base, if one wants to keep the intersections points between perpendicular chains of edges, the optimization described before will distort distribution along other edges, see Fig. 5.103 and 5.104.

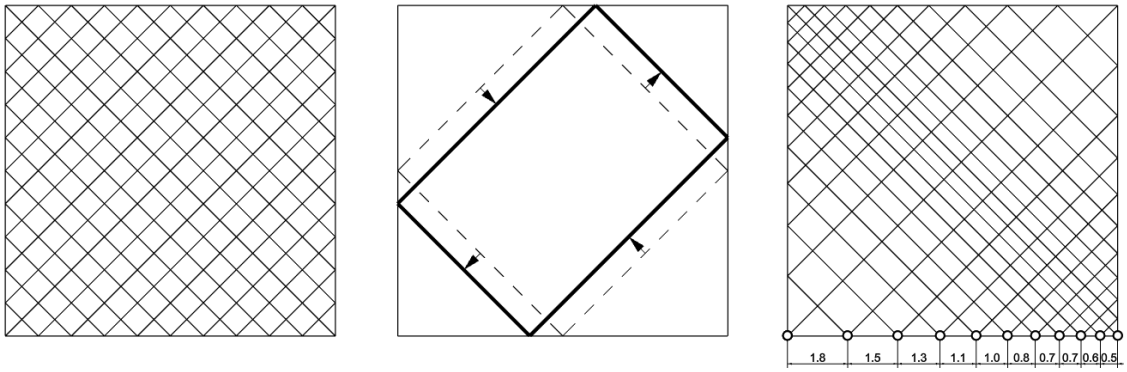

Fig. 5.103 Changing the distribution of points along one edge affects the distribution over other edges.

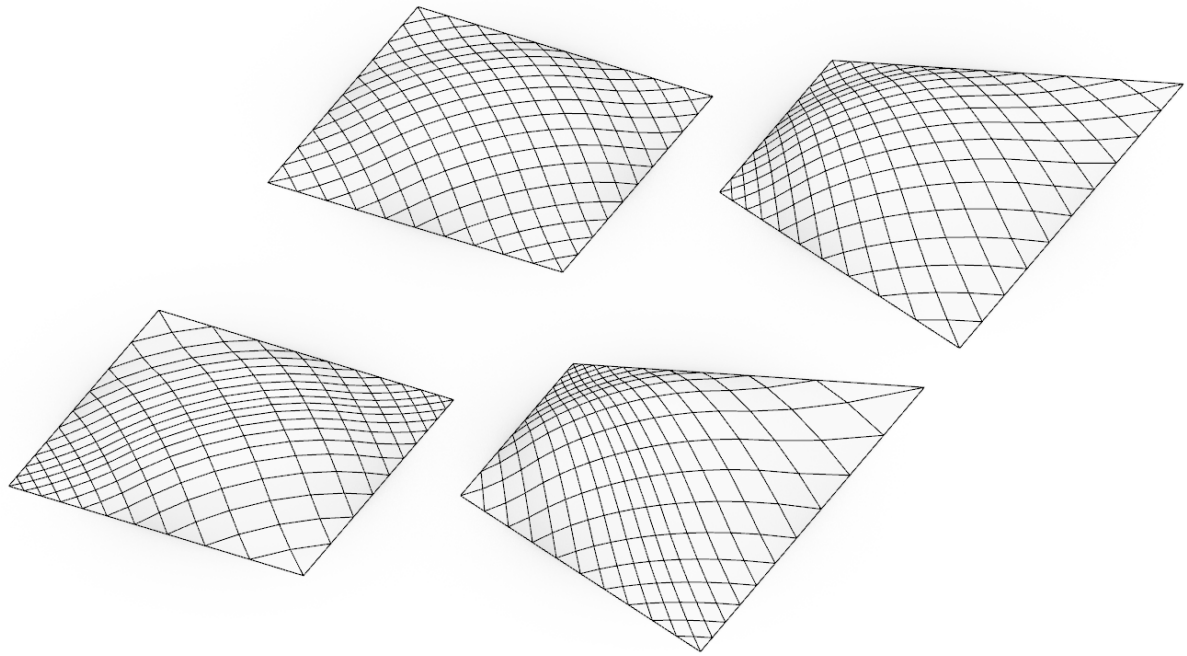

Fig. 5.104 Top: perspective transformation of evenly distributed meshes. Bottom: the distances between vertices at the along the near edge of the perspective transformed mesh are evenly distributed, however on the opposite site, the points are highly distorted.

6. Designing with the use of formation and transformation methods

The proposed designing process for PQ meshes is based on methods of formation and transformation presented in Chapters 4 and 5. Combinations of these methods allow for significant freedom of the design while ensuring the exact geometrical accuracy of PQ meshes. While formation of the PQ mesh is a single step in the design process, transformations can be performed many times according to the needs. This observation allows to build a great number of design scenarios for any combination of formation and transformation methods. However, some principles are adopted so that these combinations could be useful for designers, e.g. what was already mentioned, the formation method is performed as the first step of the design process and it is followed by further transformations.

Due to the huge amount of possibilities a particular concept of the design process is adopted in this work and is proposed as a design procedure for architects and structural engineers. According to the top-down paradigm, the designer specifies the global shape of the freeform structure by designing a doubly curved surface, which is further panelised. Whereas in the bottom-up approach presented and promoted in this work, the designer has a lot of methods, each of which is controlled by various numerical and vector parameters. Those parameters usually have indirect influence on the resultant form. Therefore, in order to combine the advantages of the top-down and bottom-up approaches (control over the final shape and exact accuracy of tessellations) the parameters controlled by the designer have to be intuitively understood. A perspective transformation of translational mesh with planar base is a particular scenario, where the designer is required to specify the boundary of the final mesh (by defining the positions of four corner points) instead of setting the values of incomprehensible f and g parameters and the details of all auxiliary, affine transformations. In this work these complex and unintuitive parameters have been converted into easily understandable interface with direct meaning for the designer.

Other design scenarios are based on the same principle, i.e. they should combine formation and transformation methods in such a manner, that the particular global shape could be easily obtained and controlled by the designer. Figure 6.1 presents the general concept of such design scenarios. At first, the designer should answer the question: “what should the final shape look like?”. The design scenario is chosen accordingly to the answer to that question. Such approach partially have the advantages of top-down approach, i.e. the designer can directly specify the base shape parameters choosing from predefined family of morphologies. The rest of the mesh based on such base is generated by algorithm using formation and transformation methods, guaranteeing the correctness of PQ mesh and its double curvature while the designer has reasonable control over the final shape through parameters.

The adoption of such approach is further reasoned by the fact, that arbitrarily shaped forms for PQ meshes are usually adopted for newly designed and constructed building envelopes, where the designer have a lot of freedom for shaping the boundary shapes. Whereas in this work, particular case studies are considered, where the base shapes are strictly defined, i.e. these are courtyards of existing buildings, which have distorted forms. Such cases are common in design practice, especially in old city centres, where irregular mesh of streets form irregular quarters with irregular courtyards.

Nevertheless, previously presented methods of formation and transformation allow for construction of much more design scenarios, even for newly designed PQ envelopes.

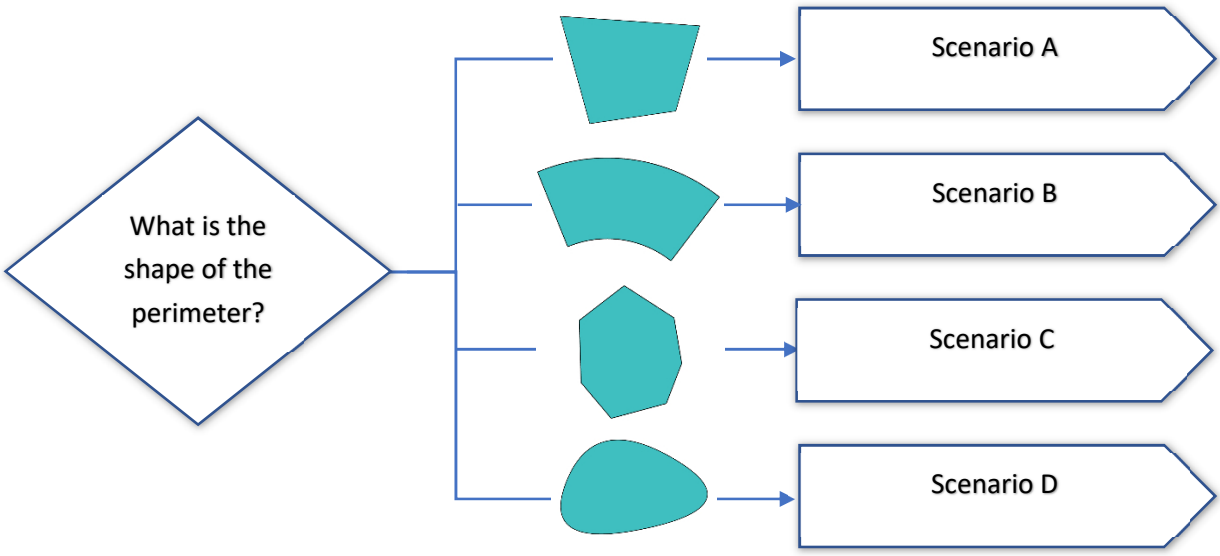

Fig. 6.1 Design scenarios are based on the global shapes of base meshes, that the designer wants to obtain

6.1. Composition of a design scenario – the sequence of activities within the designing process

Assumed design scenarios have comprehensive form, in which the final PQ mesh is a result of several steps. The scheme of design scenario is presented in Fig. 6.2. The big container with thick blue outline represents any of the design scenarios from Fig. 6.1. The scenario container contains four smaller containers, set one by one, representing consequent activities of the design process. Each step of the design process is controlled by the user through numerical and vector parameters.

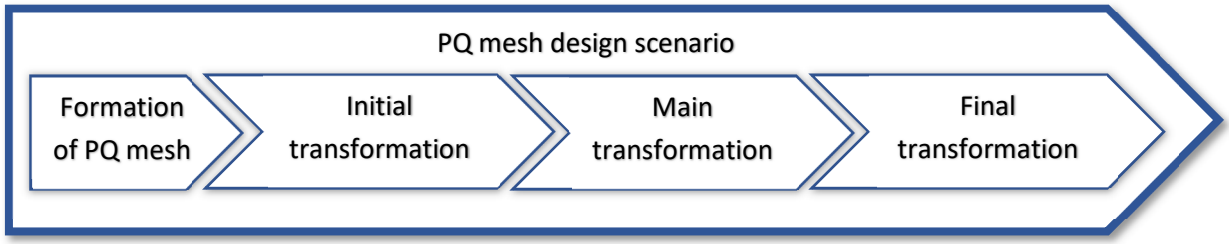

Fig. 6.2 Composition of a design scenario

First step is the formation of the basic PQ mesh which is done in such a manner, that it is eligible for further transformations. The first step is adequate for the transformation from the third step, e.g. for stereographic projection the initial PQ mesh should be formed as circular and for SC mapping, the initial mesh should have diagonally aligned edges in top projection.

Third step is the main transformation, i.e. any transformation from chapter 5. Most of these transformations have special geometrical requirements for the transformed meshes, which should be guaranteed by previous two steps.

Second step is any transformation (or composition of transformations) that can be performed on the initial mesh, which will preserve or provide the geometrical properties required by the main transformation step. For example when the designer wants to design a PQ mesh with second degree base curve, he can use planar Chebyshev net in the first step, spherical inversion in the second step and conic transformation in the third step.

The last step of the design scenario refers to any transformation (or composition of transformations) that could not be performed in the second step. If any auxiliary transformation brakes the geometrical property required by the main transformation from the third step, it should be performed at the end of the scenario, when these properties are no longer required. For example height adjusting anisotropic scaling destroys the circularity of meshes, therefore if the main transformation is any transformation requiring that property, then the anisotropic scaling should be performed in the fourth step.

It is also convenient to perform most of the transformations in the last step, when the global form is more or less visible and fits the required boundaries. For the last step following transformations are proper:

- Anisotropic scale for height adjustment. It preserves all points within one plane, which can be the base plane of the mesh. Eventually global shape is adjusted while the base shape is preserved.
- Shear transformation for inclining the mesh. Same as in previous transformation, the base plane is preserved, while the global shape can be adjusted.
- Perspective transformation along the *h* (vertical) axis. Such transformation again preserves the base plane, while the global shape can be adjusted.

In some cases planarization of the mesh can be also included into this group, when the result of previous transformation in quasi-PQ mesh (see section 5.2.1.4).

Performing these transformations for final adjustments is more convenient after the third step is performed. In the sections 5.2.1 and 0 two transformation methods were proposed in which the mesh with planar, square base outline is adjusted into user defined shape. Applying auxiliary, shape adjusting transformations before that step would result in indirect relationship between the user defined transformation parameters and the resultant mesh. Whereas in the adopted step order, the designer have direct control over the final shape adjustments.

6.2. Summary of relations between formation and transformation

Table 6.1 presents methods allowed for each step of the design process. The combination of selected methods from each column allow to construct a design scenario. Moreover, more than one method from second and fourth column can be used in single design scenario. Table 6.2 presents the proposed path of used methods for designing a special case of PQ mesh on irregular, quadrilateral base (see case study). In the first step translational mesh with planar, square base is selected, since it already have some properties of the required final mesh, i.e. it has four base vertices and four base, straight edges. In the second step all affine transformations are performed (see section 5.2.2.6) and some additional adjustments, e.g. trimming (see section 6.4.2). The main transformation is performed in the third step. Whereas in the fourth step all auxiliary transformations are performed, i.e. height adjusting anisotropic scale, shear and perspective transformation with *h* parameter.

Table 6.3 presents scenario for SC mapping, aligning PQ mesh into rounded base shape. In this case only trimming is allowed in the second step, since SC mapping requires particular alignment of edges in top projection, that could be distorted by any other initial transformations. Again, final adjusting transformations are allowed as in previous example.

The last example refers to the hypothetical conic transformation, see Table 6.4. In this case the second step allows only for one of the two methods of transformation of initial planar, circular Chebyshev net, i.e. stereographic projection or inverse geometry (spherical inversion).

Table 6.1 Allowed methods for formation and transformation according to the design scenario steps.

Formation of PQ mesh	**Initial transformation**	**Main transformation**	**Final transformation**
Translational	Affine transformations	Perspective transformation	Perspective transformation with *h* parameter
Translational with planar base	Trimming	Conic transformation	Anisotropic scale
Scalar – translational	Stereographic projections	SC mapping	Shear
Rotational	Inverse geometry	Stereographic projection	Planarization
Sweep		Inverse geometry	
Marionette			
Chebyshev net			
Circular Marionette			
Super-ellipsoid			

Table 6.2 Path of selected methods for designing a PQ mesh based on irregular quadrilateral base.

Formation of PQ mesh	**Initial transformation**	**Main transformation**	**Final transformation**
Translational	Affine transformations	Perspective transformation	Perspective transformation with *h* parameter
Translational with planar base	Trimming	Conic transformation	Anisotropic scale
Scalar – translational	Stereographic projections	SC mapping	Shear
Rotational	Inverse geometry	Stereographic projection	Planarization
Sweep		Inverse geometry	
Marionette			
Chebyshev net			
Circular Marionette			
Super-ellipsoid			

Table 6.3 Path of selected methods for designing a PQ mesh based on SC mapping.

Formation of PQ mesh	Initial transformation	Main transformation	Final transformation
Translational	Affine transformations	Perspective transformation	Perspective transformation with *h* parameter
Translational with planar base	Trimming	Conic transformation	Anisotropic scale
Scalar – translational	Stereographic projections	SC mapping	Shear
Rotational	Inverse geometry	Stereographic projection	Planarization
Sweep		Inverse geometry	
Marionette			
Chebyshev net			
Circular Marionette			
Super-ellipsoid			

Table 6.4 Path of selected methods for designing a PQ mesh based on conic transformation.

Formation of PQ mesh	Initial transformation	Main transformation	Final transformation
Translational	Affine transformations	Perspective transformation	Perspective transformation with *h* parameter
Translational with planar base	Trimming	Conic transformation	Anisotropic scale
Scalar – translational	Stereographic projections	SC mapping	Shear
Rotational	Inverse geometry	Stereographic projection	Planarization
Sweep		Inverse geometry	
Marionette			
Chebyshev net			
Circular Marionette			
Super-ellipsoid			

6.3. Design tools based on design scenario cases

Based on concept of design scenario proposed by the author, presented in Fig. 6.2, proprietary design tools are proposed. Whereas in the scenarios presented in section 6.2 the designer must follow all the steps manually, implementing these steps into the one tool allows for instant execution of all of them. Moreover, parameters for each step can be changed any time in any order and the result is calculated instantly. When the final mesh is calculated, the designer can change parameters of the first step and the algorithm will perform all consequent transformations of new base mesh according to parameters that were previously provided for all other steps. There is no necessity for the designer to concern the order of steps in this approach. The designer is only required to provide all necessary information for the algorithm. In Fig. 6.3 and 6.6 user input is marked as one block.

In the following sections 6.3.1 and 6.3.2 two examples of the design tools corresponding to the workflows shown in Table 6.2 and 6.3 are further discussed.

6.3.1. The tool for designing PQ meshes based on irregular quadrilaterals – *perspective transformation tool*

The tool for designing PQ meshes with irregular quadrilateral outlines is based on perspective transformations, i.e. third step in Fig. 6.3. Perspective transformation matching is additionally aided with auxiliary affine transformations, see sections 5.2.2.5 and 5.2.2.6.

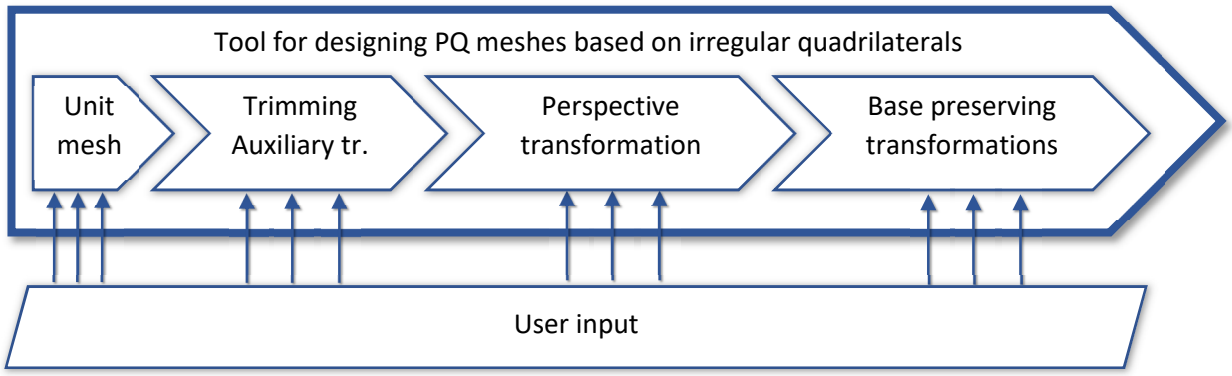

Fig. 6.3 Diagram of the workflow in the tool for designing PQ meshes based on irregular quadrilaterals.

After the PQ mesh is transformed, the tool allows for transformations that preserve the base of the mesh. These *base preserving transformations* include perspective transformation with *h* parameter, height adjusting anisotropic scale and shear transformation (see Table 6.2).

Before the main transformation and final adjustments are performed, the base mesh has to be constructed, which can be then modified. The base mesh is a parametrized translational PQ mesh with planar, square base outline – a unit mesh, which is discussed in section 6.4.1. After the base mesh is ready, additional *trimming* (see section 6.4.2) modification is done before the main transformation. Trimming changes the external dimensions of the mesh, therefore it has to be done before perspective transformation matching in order to accurately fit the desired outline.

6.3.2. The tool for designing PQ meshes with rounded outlines – *SC transformation tool*

The tool for designing PQ meshes with rounded outlines is based on SC mapping, i.e. the third step in Fig. 6.4. Similarly to the previously proposed tool, this one performs *unit mesh* formation in the first step (translational PQ mesh with planar, square base), trimming and auxiliary transformations in the second step and *base preserving transformations* in the last step. Although the purpose of these tools is different and its application will result with different morphologies of PQ meshes, most of the steps are similar.

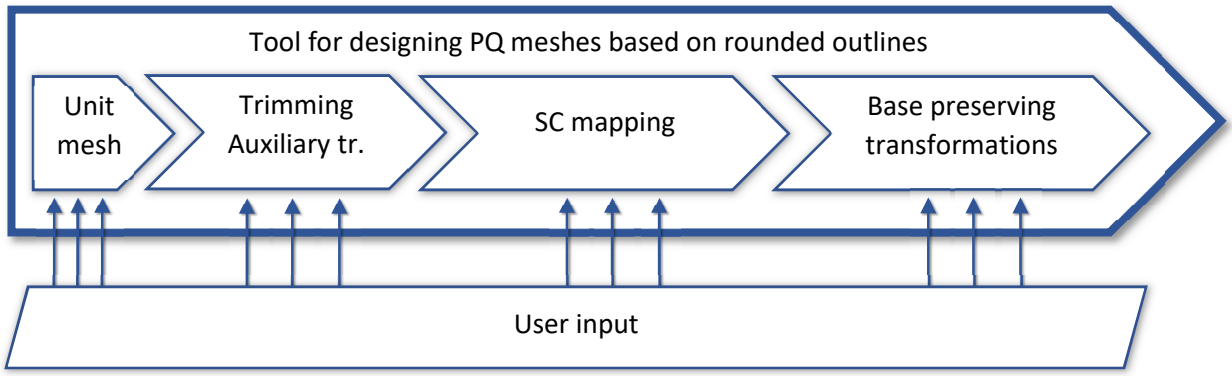

Fig. 6.4 Diagram of the workflow in the tool for designing PQ meshes based on rounded outlines.

6.4. Description of subsequent activities

In this section, the individual steps performed in *perspective* and *SC* tools are explained in details.

6.4.1. Activity 1: Formation of unit mesh

Unit mesh is an initial PQ mesh created as a translational mesh with planar, square base perimeter as described in the section 4.1.2. For the convenience of further calculations and transformations (perspective transformation and SC mapping) it has to be positioned at the origin of the coordinate system and span one unit only in each *X* and *Y* directions (see Fig. 6.5). Perimeter points must lie on the *XY* ($Z = 0$) plane. All other vertices of the mesh are positioned over the base plane. Since the final height of the mesh is adjusted in the last stage of the tool's workflow, for now the highest point *P* is positioned over the beginning of the coordinate system *O* at the level $z=1$, i.e. $P = (0,0,1)$, see Fig. 6.6.

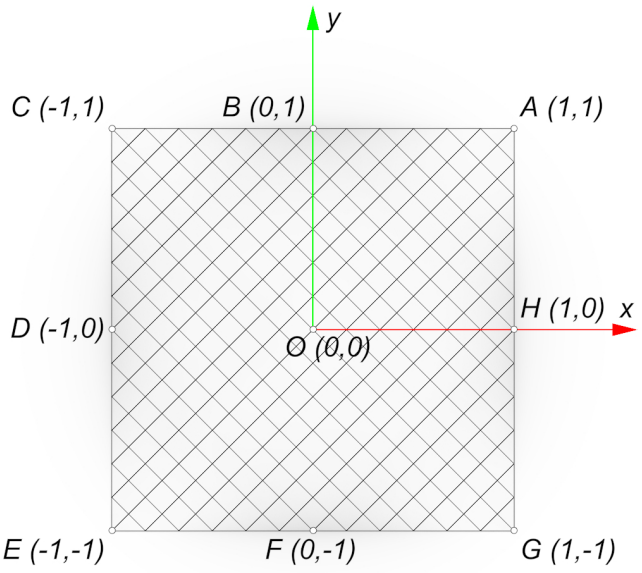

Fig. 6.5 Positioning of the unit mesh.

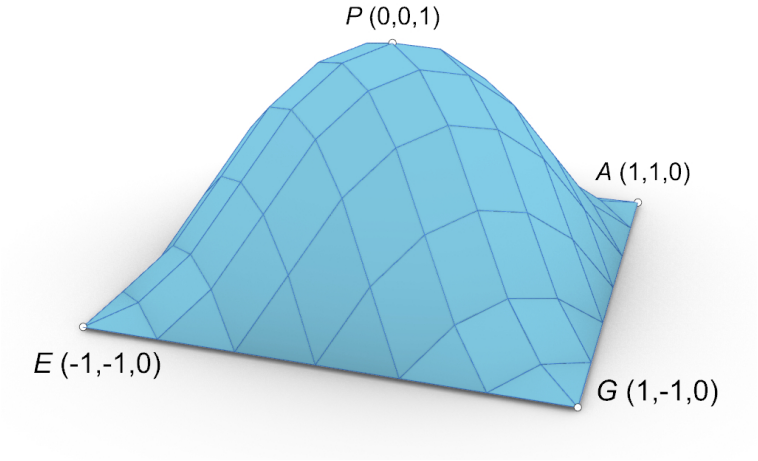

Fig. 6.6 Specification of the height of unit mesh

The scheme for *unit mesh* user controlled parameters is shown in Fig. 6.7. There are three parameters, each of them will be explained respectively further in this section, under the names of parameters their types and value ranges are specified.

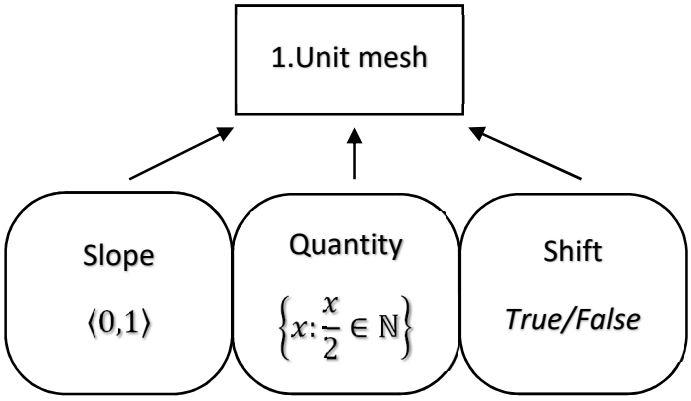

Fig. 6.7 Scheme for parameters of unit mesh.

6.4.1.1. Slope

The slope parameter *s* controls the shape of the directrix (generatrix) curve of the mesh, according to the rules described in section 4.1.2. Parameter *s* defines the position of extrapolating point P_e of the segment curve, from which the directrix is composed. The parameter *s* is within the interval $\langle 0,1 \rangle$, see Fig. 6.8. In section 4.1.2 the P_e point is defined by two coordinates, i.e. *a* and *b*. For the purpose of further parametrization only the coordinate *a* is controlled by the value of *s* – *slope*, while coordinate *b* is equal to 0, for which the resultant shape has continuous curvature all over its surface (see Fig. 8.3 on page 215).

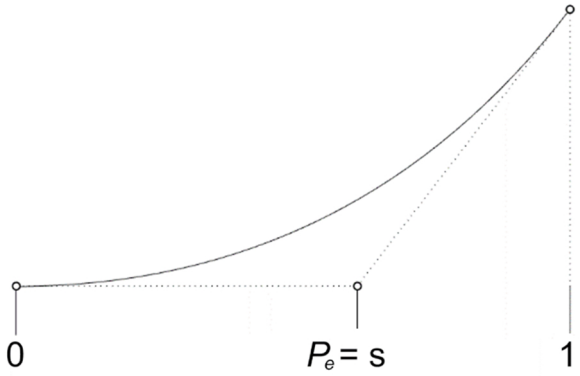

Fig. 6.8 Slope parameter s *controls the shape of the segment curve.*

Possible forms of unit mesh depending on the value of *s* parameter are shown in Fig. 6.9. When the extrapolating point is incident with the first interpolating point at (0,0), the obtained shape is a pyramid. In section 8 - *Mechanical performance of doubly curved PQ shells* the result of FEM analysis showed that the best static properties for the PQ meshes occur when the *slope* parameter has the value between 0,4 and 0,5, see tables 8.1 to 8.5. Also, for these values the mesh has the most natural form, i.e. the discrete curvature continuity is preserved, which is not the case for values near 0 (pyramidal form) and near 1 (most bulged form).

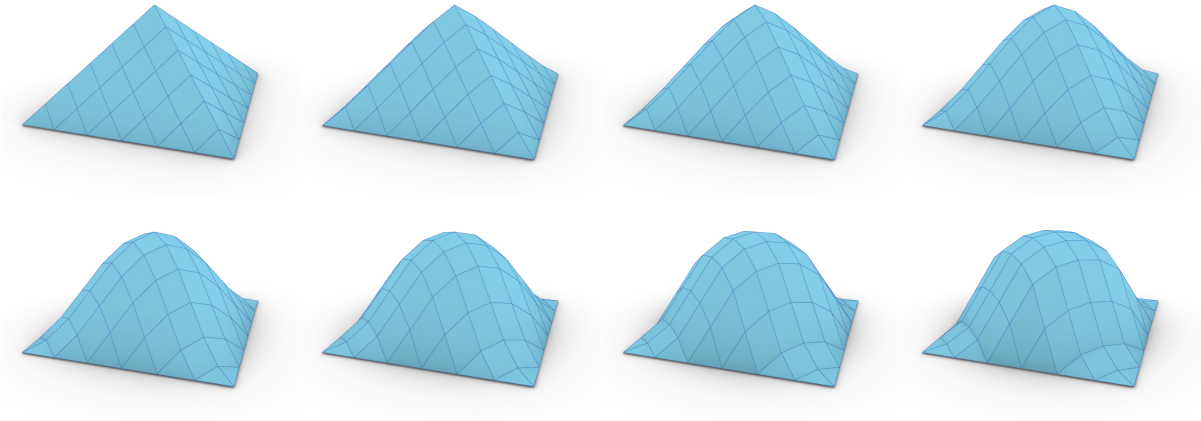

Fig. 6.9 Consecutive forms of unit mesh obtained with different values of slope*, starting from 0 with 0.1 step.*

6.4.1.2. Quantity

The *quantity* parameter is responsible for the number of PQ panels in each diagonal direction. In order to keep consistency of facets, the value of *quantity* must be even. The explanation of that assumption is shown in Fig. 6.10. The *quantity* value refers to the number of divisions along the diagonal line. If that number is odd, the diagonal line is discarded, therefore facets at the corners of the mesh are pentagonal, so is every second facets incident with the border of the mesh. Three of five vertices of each corner facets must lie on the border of the mesh, therefore they lie at the ground plane. Those three points constitute a plane on which two remaining points lie (the ground plane). Consequently every corner facet is horizontal and lies on the ground plane. Further analysis provides into a conclusion, that when the *quantity* value is odd, the only possible configuration of the mesh is flat, what is an undesirable solution in this consideration. Whereas if the *quantity* value is even, the resultant shapes of facets are only quadrilateral and triangular (at the edges) and at most only two vertices of a facet lie at the border of the mesh (at the ground plane).

Figure 6.11 presents possible configurations of the unit mesh depending on the values of *quantity*.

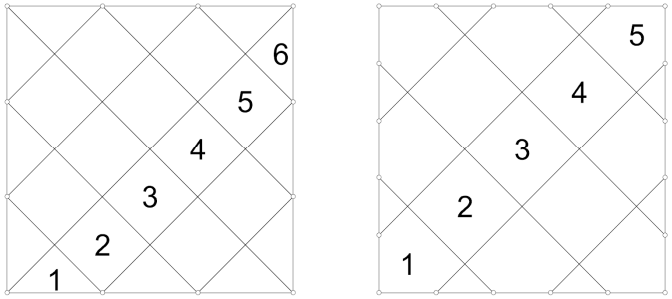

Fig. 6.10 Top projections of unit meshes with even and odd number of cells in diagonal direction.

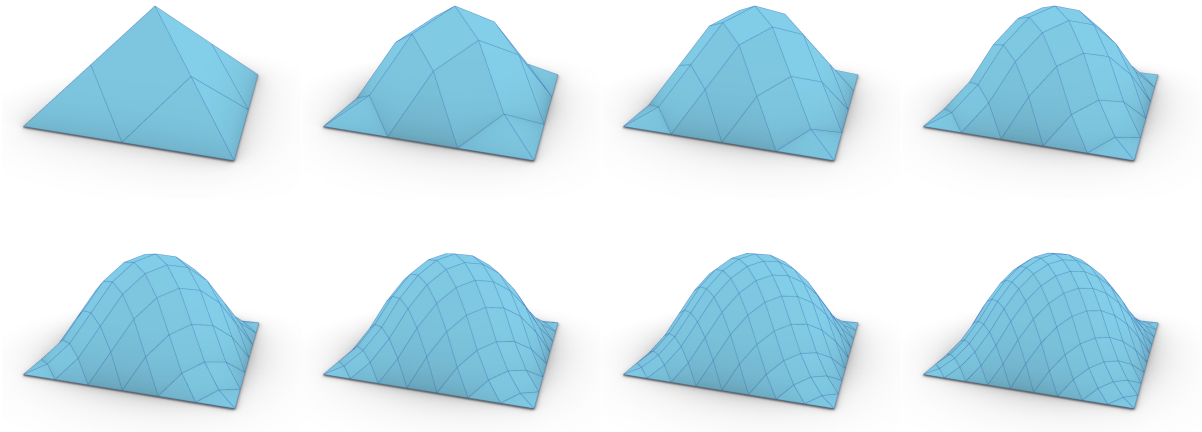

Fig. 6.11 Consecutive forms of unit mesh *obtained with different values of* quantity *parameter, starting from 4 with step equal 2.*

6.4.1.3. Shift

The last parameter of *unit mesh* is *shift*. The *shift* parameter has true/false values. It is responsible for the distribution of facets over the mesh. There are two possible ways to distribute the same amount of facets on the mesh while keeping their forms triangular and quadrilateral. In the first case shown in Fig. 6.12, left, the facets are distributed in conventional manner. On the same figure, right, the facets are shifted by half the width of the facets. The amount of facets along the diagonal direction is the same, however in the second case one facet is split into two halves.

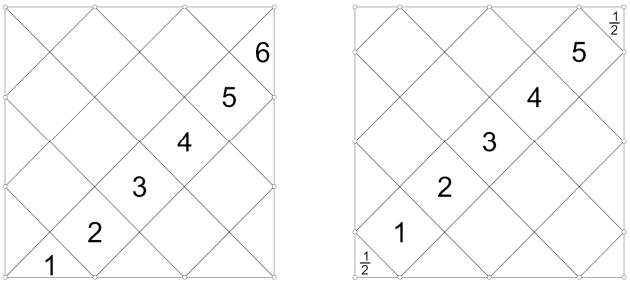

Fig. 6.12 Left: mesh with shift=false*, right: mesh with* shift=true*.*

Both types of meshes are aligned together in Fig. 6.13. In fact these two meshes are dual images. The vertices of one mesh are centres of facets of the other mesh and corresponding edges intersect at right angles.

The difference between meshes in both cases is that in the second one there is no top vertex – it is replaced by single, horizontal facet. Additionally, there is only one triangular facet at each corner (instead of two), which is however horizontal. Although horizontal facets are not desired, the practical application of this parameter is explained in the following section.

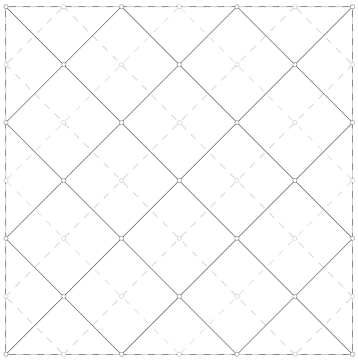

Fig. 6.13 Conventional mesh - continuous lines; shifted mesh - dashed lines.

Two meshes of the same *quantity* with *shift* false and true are shown in Fig. 6.14.

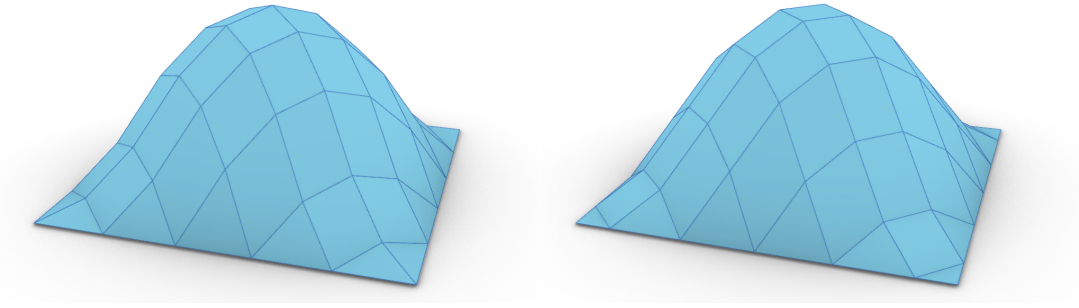

Fig. 6.14 Perspective view on the unit mesh with shift=false *(left) and* shift=true *(right).*

6.4.2. Activity 2: Trimming

In the second step, apart from the auxiliary affine transformations of the main transformation, the unit mesh can be trimmed. In some cases it is desired to transform a mesh, whose selected edges are not horizontal, e.g. trimming was used in case study in section 7.2, where only two or three sides of meshes are supported on horizontal cornices of the courtyard's walls, whereas the others are trimmed in order to form arched edges. Part of the unit mesh can be trimmed and discarded, resulting with one, two, three or four arched edges. Figure 6.15 presents a scheme of this activity, which requires four values from the range between -1 and 1. As the unit mesh spans within the values of *x* and *y* coordinates between -1 to 1, each trim parameter indicates the location of the vertical trimming plane. For example when the vertical trimming plane on the right side of the mesh has value 1 (the plane is located at point *x*=1 at the abscissa), then no trimming is performed. When that value is changed, the trimming plane is moved along the *x* axis and all vertices that are located at the right side of that vertical plane are discarded, see Fig. 6.16, left.

In order to keep the consistency of facets shapes (only triangles and quadrilateral are allowed), after discarding the points that are located on the negative side of the trimming planes the mesh is rebuilt from the remaining points. It means that the trimming plane has not necessarily to be located at the resultant edge of the mesh. Some facets are transformed from quadrilateral into triangular shapes if one of their vertices is discarded. There are also cases, when additional vertex has to be introduced into a facet, when two vertices are discarded (by two trimming planes), see Fig. 6.16, right (the triangular facet at the rightmost corner). Such additional vertex is located on the plane containing that particular facet it belongs to. Lastly, new vertex has to be introduced when triangular facet is located at the border of mesh which is trimmed, see Fig. 6.16, centre (rightmost vertex of mesh in centre located on its edge). In that case the newly added vertex is located on the base plane and at the extreme *x* or *y* parameters of all remaining points in the mesh.

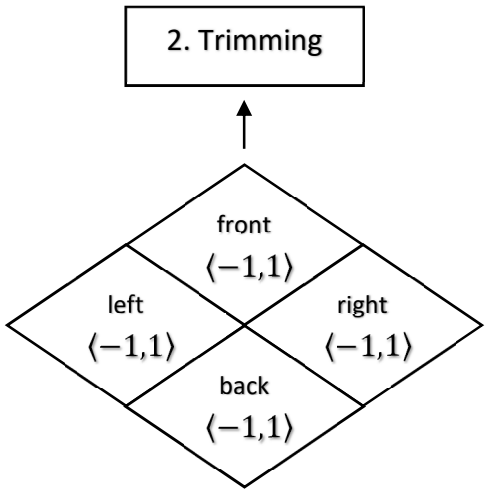

Fig. 6.15 Scheme for trimming.

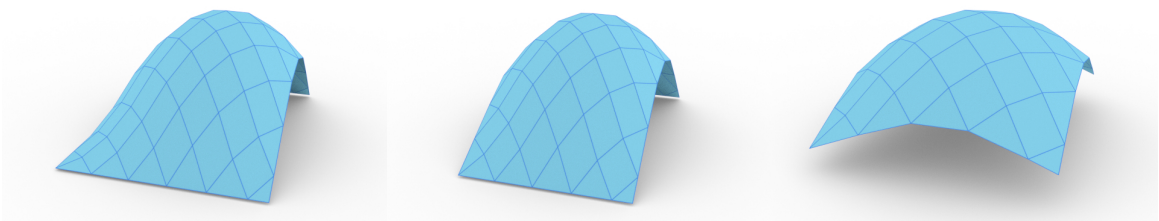

Fig. 6.16 Unit meshes trimmed from right side (right image), two -left and right side (centre image) and all four sides (right image).

In cases when trimming results with single triangular facet at the corner of the mesh, the *shift* parameter from previous activity can be switched to the opposite value. Figure 6.17 shows a case when the initial mesh has single facets at the corners (when *shift* = true), whereas after trimming the mesh has double facets at the corners. Combination of *shift* and *trimming* parameters allow to design PQ meshes by controlling the shapes of edges (horizontal or arched) and the distribution of vertices along them.

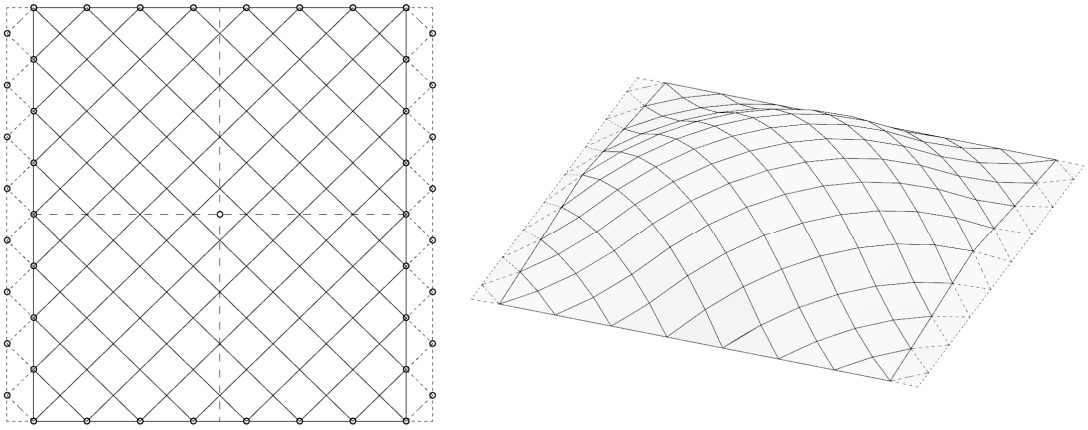

Fig. 6.17 Combination of trim *and* shift *parameters resulting with two facets adjacent with each corner of resultant mesh. Trimmed part of initial mesh whose parameter* shift=true *is marked by dashed lines.*

Once the mesh is rebuild after trimming, it has to be unitized again in order to be suitable for the main *perspective transformation* or *SC mapping*. Trimming reduced the span of the mesh along *x* and/or *y* directions. Therefore anisotropic scaling has to be introduced in order to align resultant edge with *A*, *C*, *E* and *G* points from Fig. 6.5. It is not necessary to locate those corner points on the ground plane, the *z* coordinate of all points in the mesh remain unchanged.

6.4.3. Activity 3a: Perspective transformation

The first variant of third step in the workflow shown in Fig. 6.2 is perspective transformation in which previously generated mesh is transformed into any, user defined quadrangle *A'B'C'D'*, see Fig. 6.18 and 6.19. The designer defines desired base perimeter by indicating four points at the corners. The points are provided in proper order so that the resultant irregular quadrilateral is non self-intersecting. Also, the configuration of these points have to allow the construction of convex quadrilateral, i.e. each point has to be located outside of a triangle constructed by three remaining points.

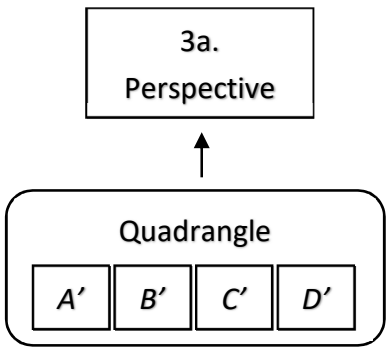

Fig. 6.18 Scheme for perspective transformation. Any irregular quadrangle is defined by positions of four points: A', B', C' and D'.

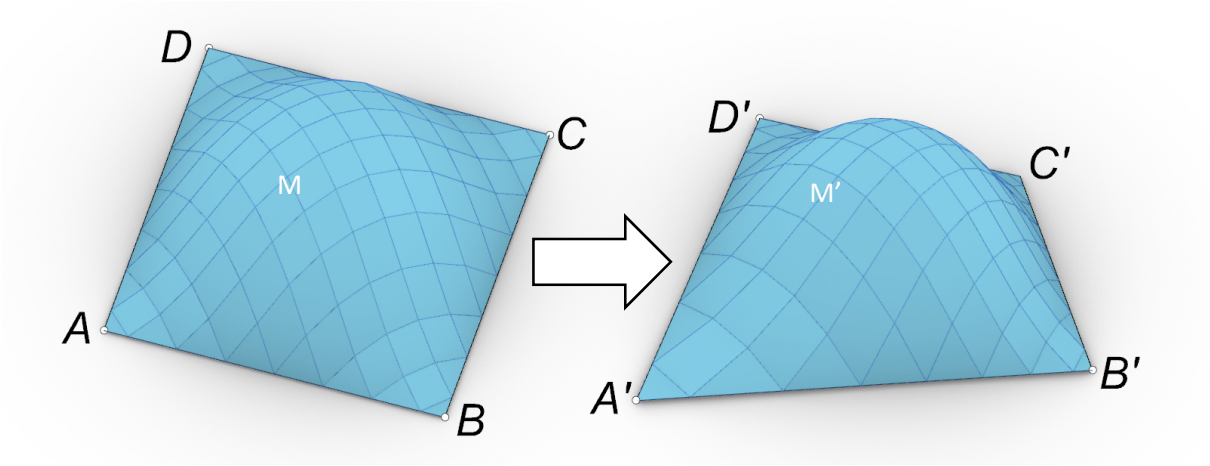

Fig. 6.19 Transformation of unit mesh M *into* M' *though perspective transformation. Mesh* M *has square base perimeter defined by points* ABCD. *Resultant mesh* M' *has base perimeter which is any irregular quadrilateral, user defined by points* A', B', C' *and* D'.

This activity of the perspective transformation design tool works according to the assumptions described in section 5.2.2.5 *Perspective transformation matching*. These mentioned assumptions are represented in Fig. 6.20: firstly, the transformation *T* (composition of perspective transformation and auxiliary affine transformations) between the desired shape and unit square is calculated. Then the inversion of *T* is applied on the unit mesh obtained by execution of previous activities. The effort of creating and unitizing the mesh in previous steps is reasoned by convenience of perspective transformation. Eventually, the mesh is aligned with desired dimensions by auxiliary affine transformations of the perspective transformation step.

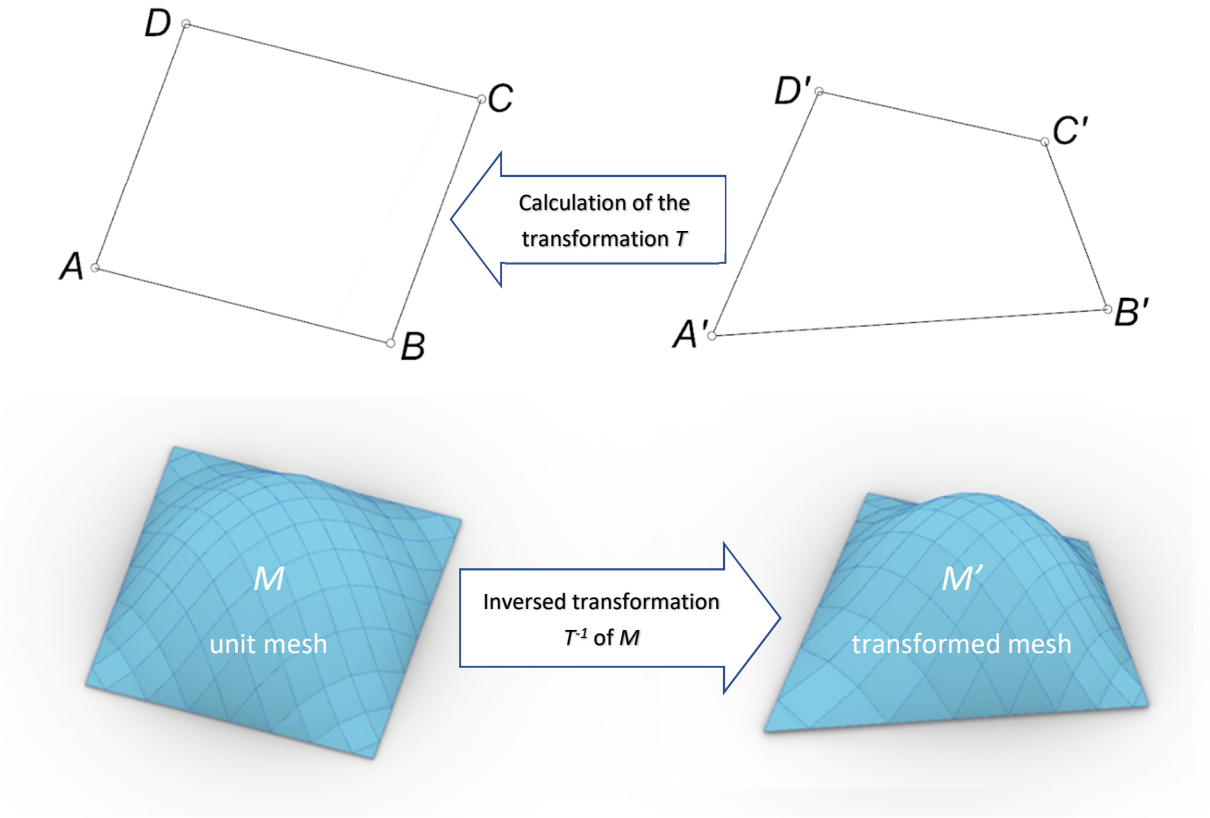

Fig. 6.20 Perspective view at transformation T *calculation procedure (top). Inversed transformation of unit mesh* M *(bottom).*

Any time the designer modifies positions of *A'*, *B'*, *C'* or *D'*, the algorithm recalculates transformations, so that the user can see the resultant *M'* mesh immediately.

Examples of perspective transformation of previously trimmed PQ meshes generated with various values of shift parameter are shown in Fig. 6.21.

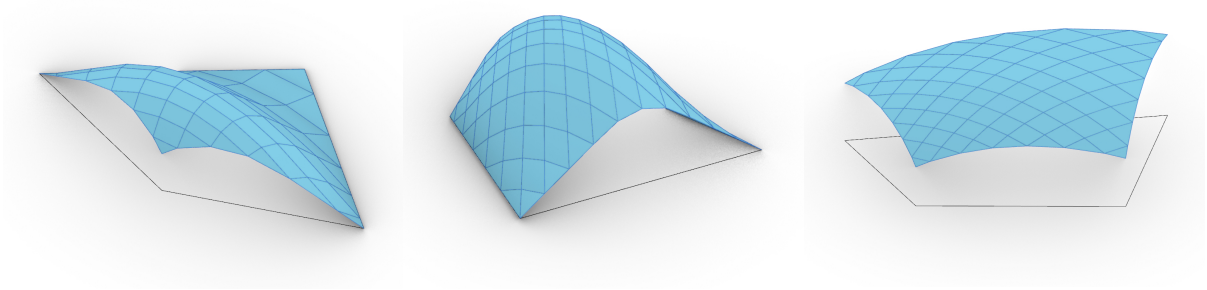

Fig. 6.21 Variety of possible PQ morphologies obtained through parametrization of first three steps.

6.4.4. Activity 3b: Spherical cylindrical mapping

The second variant of the third activity in the design tool is the SC mapping described in section 5.2.1. In this case the designer specifies only three points – *A*, *B* and *C*, see Fig. 6.22.

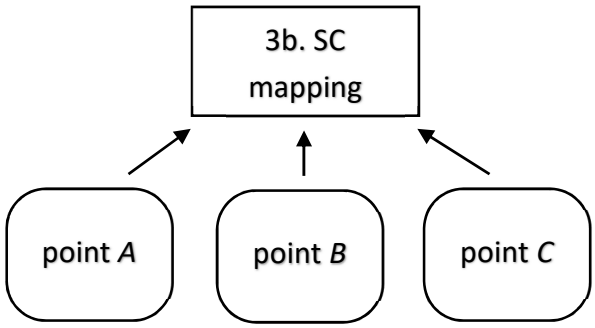

Fig. 6.22 Scheme for SC mapping activity. User defines the rounded shape by specifying only three of four of its vertices.

The geometric rules of determination of the fourth corner point and the rest of rounded, outline shape is shown in Fig. 6.23. The resultant shape in SC mapping of rectangular shape is section of a wheel, i.e. a shape consisting of two concentric arches and two line edges, whose extensions intersect at the centres of arches, see Fig. 6.23, right. Two points – *A* and *B* define one line segment, whereas points *B* and *C* define arched edge, which is perpendicular to the *AB* segment at point *B*. Therefore, the point *O*, which is the centre of arch *BC* lies along the extension of *AB*. The fourth point *D* is found by the intersection of line *CO* (by the definition of shape obtained by SC mapping, line segment *CD* lies on a line passing through *O*) and arch *AD* (whose centre is in point *O*), see Fig. 6.23, right.

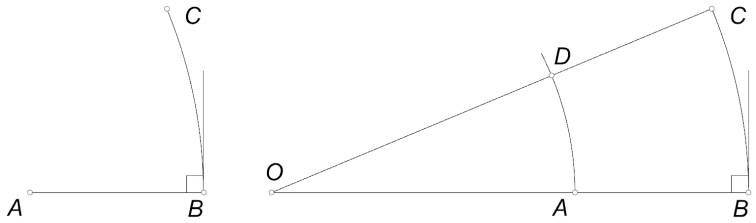

Fig. 6.23 Definition of the rounded shape (section of a wheel) by positioning three vertex points.

The spherical – cylindrical mapping also requires the external space boundary radius (the distance between *O* and *T*, see Fig. 6.24), since the further from the center *O*, the space gets more and more dense, eventually converging into a singularities around a circular boundary. For a specific radius of the first and second outline arc and the angle between line segments the distance between *O* and *T* have to be calculated. Keeping in mind, that SC mapping requires particular alignment of PQ mesh edges in top projection, i.e. only diagonal directions are allowed (45° or -45° to the *x* axis of the coordinate system), the SC mapping image of the diagonal line is part of the circle, that passes through the center point *O* and which is tangent to the border of SC space in point *T*, see Fig. 6.24, 6.25 and 6.26.

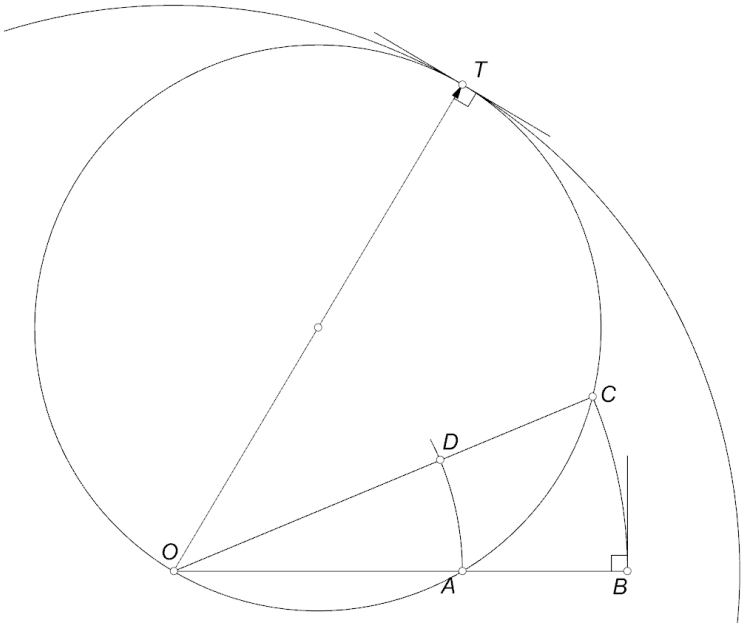

Fig. 6.24 Required shape ABCD*. Point* O *derives from that point.*
Radius OT *derives from the diameter of circle passing through points* O, A *and* C*.*

A circle drawn over SC (spherical – cylindrical) space, passing through the origin point *O* and tangent to the external boundary at the point *T* passes through the points P_1 … P_9, see Fig. 6.25. Each point *P* is the integer point of a SC space. Consequent *P* points are equally spaced and in diagonal array in the SC space. Equivalents of these points in the Cartesian system are consequent points along diagonal of the network – P_n … P_m. It is also known from the properties of SC mapping[85], that points *D*, *B* and P_n … P_m will lie on a common circle after mapping. Therefore, the radius of SC space - |*OT*| - for a specific *A*, *B*, *C* input points is derived from the diameter of a circle passing through points *O*, *A* and *C*.

[85] Points aligned along a straight line which is diagonal to Cartesian coordinate system will lie along a common circle after SC mapping, see Fig. 5.37 on page 124.

Corresponding points along the diagonal of *ABCD* quad from Fig. 6.25, left, are mapped to points P_n on the SC space, see Fig. 6.25, right. Knowing that these original diagonal points are mapped along the black, tangent circle it is only required to know, where exactly on that circle are those points mapped. This information is already implicitly contained in the configuration of user defined *A*, *B* and *C* points, namely in the proportion between straight and arched edges. That relationship between proportions of edge lengths of initial the mesh and the location of that mesh in the SC space is illustrated in Fig. 6.26, where three rectangles with diverse edge proportions are SC mapped. All rectangles have one common dimension α, whereas other dimensions *a*, *b* and *c* are different. The α dimension is transformed into angle between radii of SC space. From the definition, that diagonal lines lie along the tangent circle, consequent rectangles are mapped on various distances from point *O* in order to keep original proportions between edges.

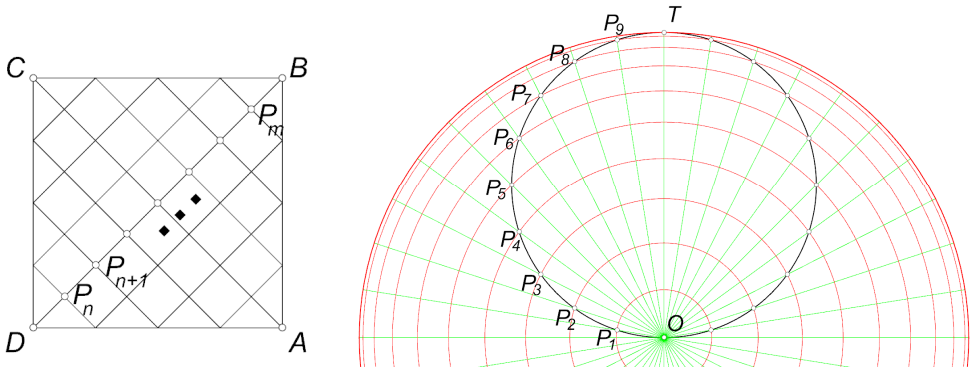

Fig. 6.25 When the base mesh is square (has the same density of vertices in both directions) the diagonal BD *with points* P_n *to* P_m *are mapped along the black circle (right), which is tangent to the boarder of SC space and passes through its centre point* O.

The diagonal directions in Fig. 6.26, left, are suitable for planarity preserving SC mapping only in one case, i.e. for the second, square shape, which diagonal is aligned at 45° according to the *x* direction of coordinate system. However, two other cases also find application, when the base mesh is trimmed in previous activity. Figure 6.27 illustrates a case, when the base mesh was previously trimmed. The unitization of the mesh (anisotropic scaling which aligned corners on particular coordinates) results with a mesh which is not suitable for SC mapping, since its diagonals are not properly aligned.

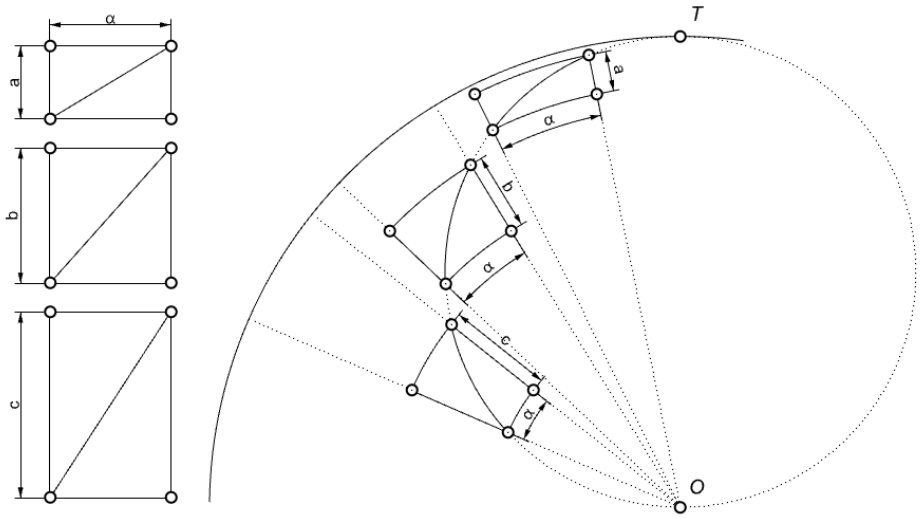

Fig. 6.26 The positioning of resultant section of SC space between centre point O *and external boundary of SC space depends on the edge proportion of initial shape (left).*

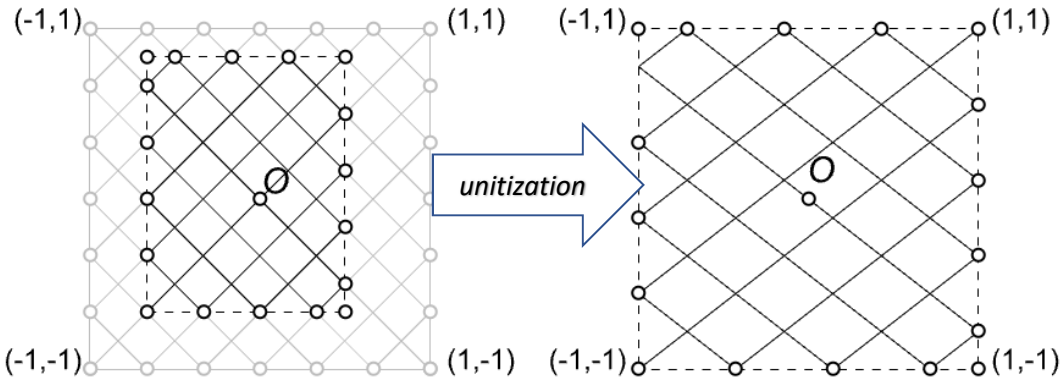

Fig. 6.27 Example of trimming and unitization of a base mesh.
The resultant mesh (right) is no longer suitable for SC mapping, since diagonals are not properly aligned.

In order to bring the unit mesh into a configuration in which it will be eligible for planarity preserving SC mapping, it has to be anisotropically scaled is such a manner, that diagonals are aligned at 45° with respect to the *x* axis of coordinate system. The scaling results with a mesh, which is narrower or wider (depending on the proportion of divisions on each sides), see Fig. 6.28, left. The *y* dimension of the mesh is maintained as 2 units, whereas its *x* dimension is α. The mesh is positioned along the *x* direction in such a manner, that the gaps on both sides to the unit square are both equal to some value β. As φ dimension in SC space is isomorphic, the dimensions α and β are easily converted into angles α' and β' by maintaining the proportions between them, see Fig. 6.28, right. Angle α' in Fig. 6.28, right, is defined by the positions of points *A* and *B*, which are user defined, following by the point *O*, which position is derived from all user defined points. Lines passing through point *O* and points *G* and *H* are defined by angles β', calculated from the proportions between dimensions α and β and angle α'. Following points *E*, *F*, *G* and *H* are at the intersections between newly defined lines and extensions of user defined arches *AB* and *CD*. Aligned diagonal line in Fig. 6.28, left, spans between points *E'* and *G'*, therefore on the SC space the diagonal arch will pass through points *E*, *G* and *O*. Knowing that diagonal arch, tangency point *T* can be found and finally, the radius of desired SC space can be calculated as the distance between points *O* and *T*.

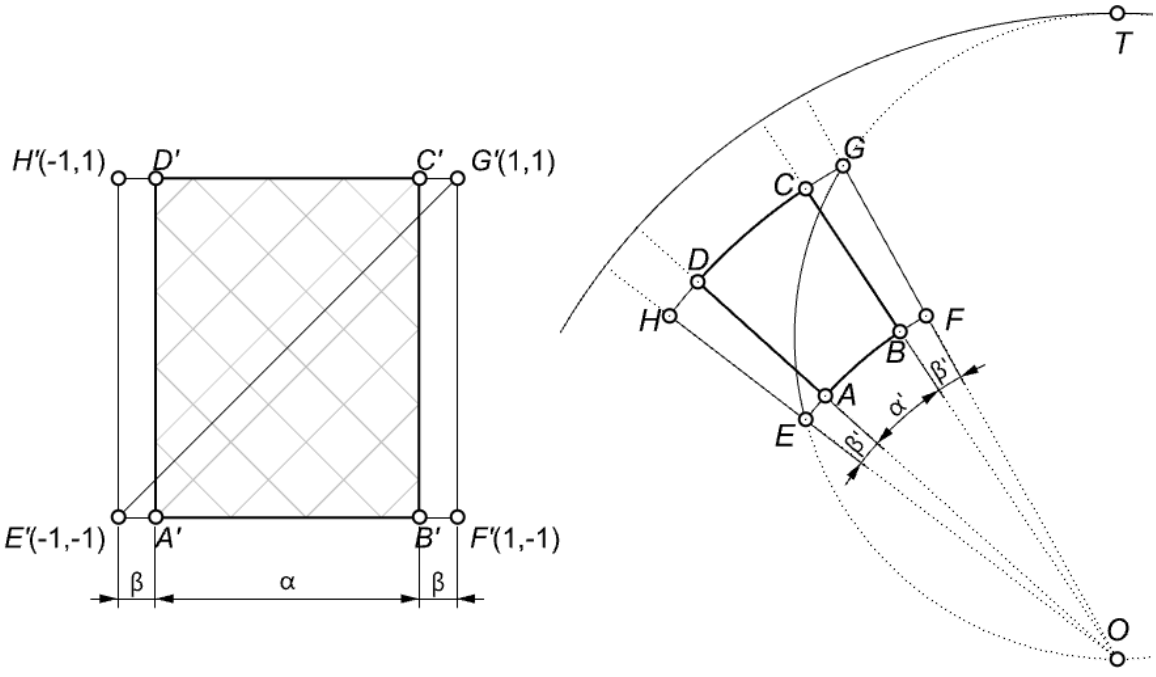

Fig. 6.28 SC mapping of an uneven base mesh. Only A, B *and* C *points are user defined.*

Two examples of application of SC mapping step is shown in Fig. 6.29, where no trimming was applied in previous step. By extension of previously explained procedure, initial base mesh can be trimmed from one, two, three or all sides and in any configuration, see Fig. 6.30 and 6.31.

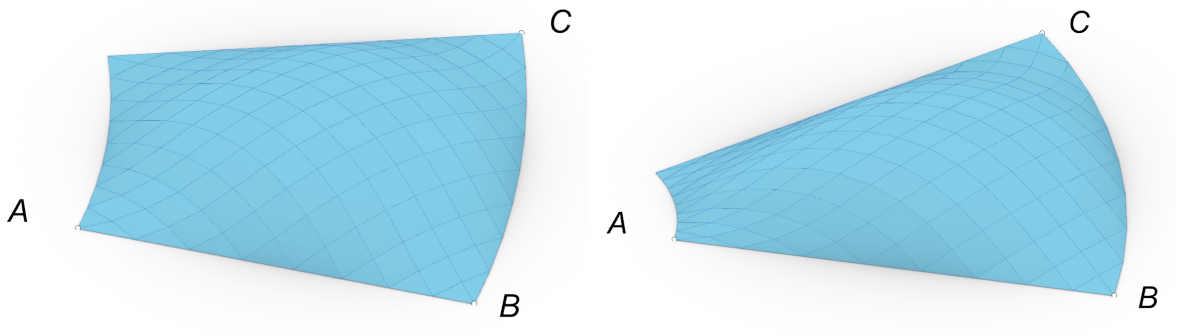

Fig. 6.29 Two examples of SC mapped, untrimmed meshes, user defined by positions of points A, B *and* C.

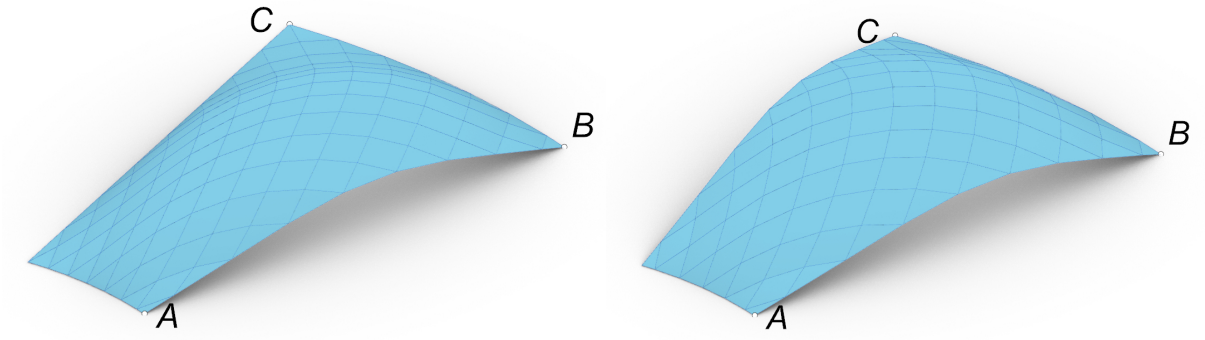

Fig. 6.30 Two examples of SC mapping of previously trimmed meshes - from one (left) and two sides.

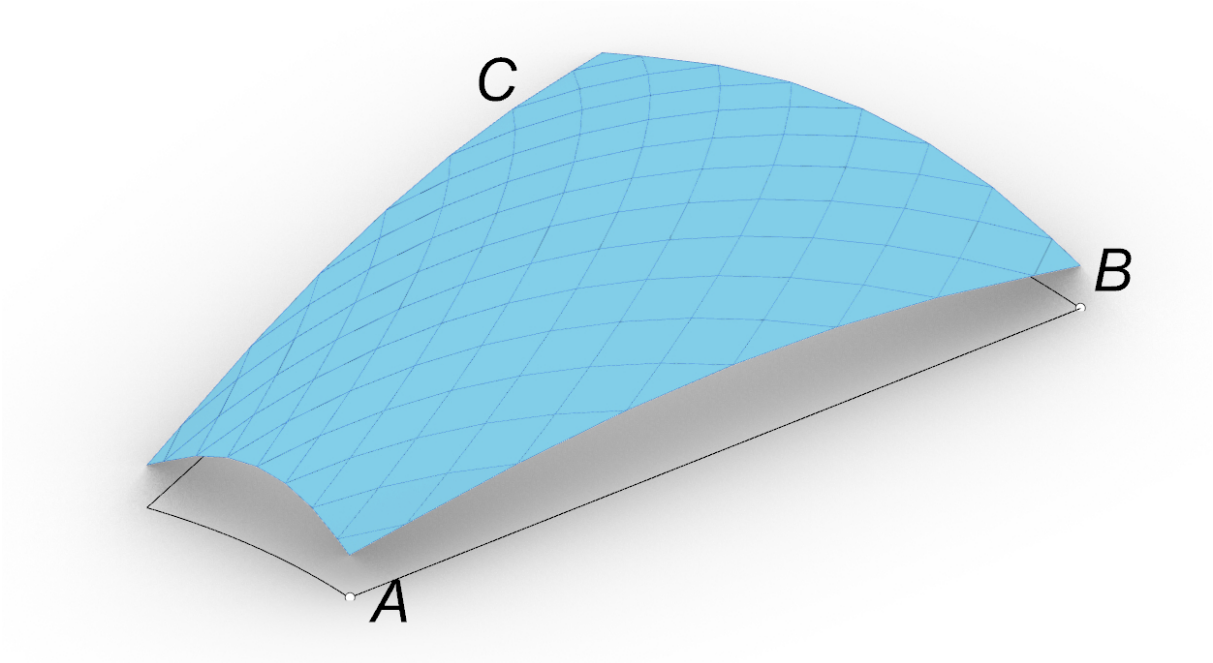

Fig. 6.31 SC mapped PQ mesh, previously trimmed from all four sides.

Aligning SC mapped meshes

In case when the desired base shape is disproportionately rounded quad, whose arched edges are much longer than straight edges, covering mesh may be divided into several sections – each one individually SC mapped, see Fig. 6.32. Sectioning the base form results with meshes, whose individual facets are more proportional, i.e. proportion between diagonals of individual facets are closer to one. When single mesh is mapped onto not sectioned base form, individual facets of mesh are elongated and disproportional, see Fig. 6.32, left.

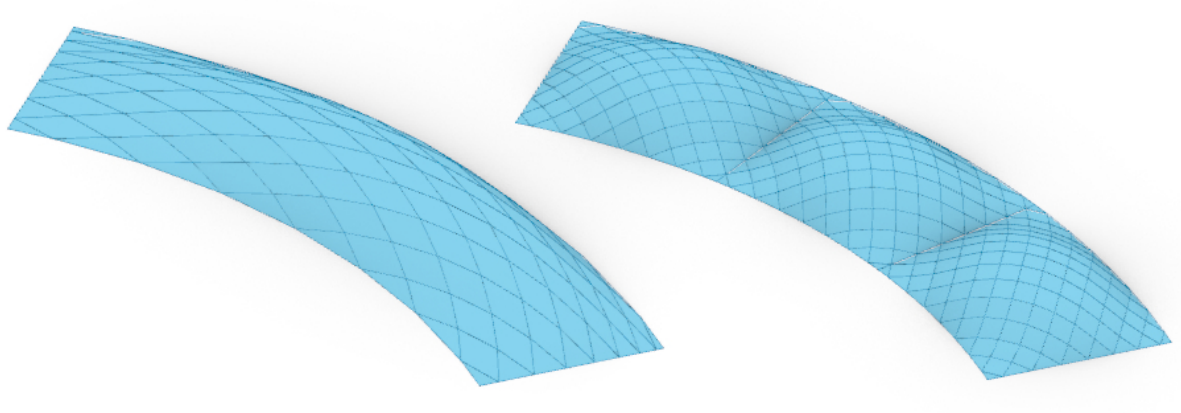

Fig. 6.32 Elongated, rounded base form. Left: single mesh SC mapped on that base form. Right: base form sectioned into three parts.

Meshes mapped onto sectioned base form have one or two edges, which are not supported on perimeter (e.g. by wall). Without trimming the mesh, such unsupported edge is horizontal. However, in previously trimmed mesh, the same unsupported edge is arched as in Fig. 6.33. Arched edge allows for applying arched support beam beneath both adjacent meshes. Structurally, such arched beam have an advantage over straight beam. Greater loads can be transferred by an arched beam than a straight one of the same cross section.

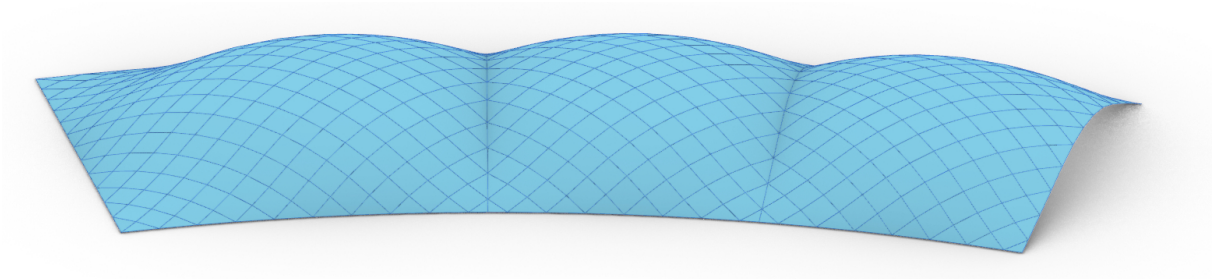

Fig. 6.33 Composition of three SC mapped meshes. The parameters of all SC mappings were selected in such a manner, that corresponding points of neighbouring meshes are incident and the corresponding arched edges have the same radii.

Adjacent meshes with arched edges have the capability for exact matching, i.e. corresponding points of neighboring meshes are exactly incident, see Fig. 6.33. Initial meshes in the above example were generated with the same parameters of unit mesh (slope, quantity, shift) and the same trimming along common edges. However, SC mapping not necessarily have to be performed on the same SC space. The radii of corresponding edges of neighboring meshes can differ and still, corresponding edge vertices of both meshes will be incident, as shown in Fig. 6.34.

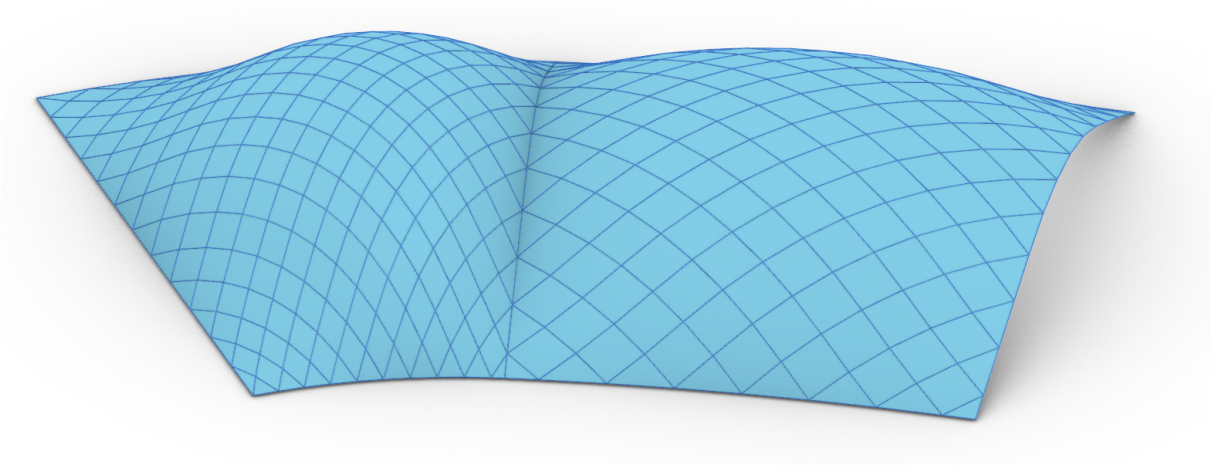

Fig. 6.34 Exact matching of two neighbouring meshes mapped onto different SC spaces. The radii of corresponding edges are different.

6.4.5. Activity 4: Base preserving transformations

Final activity in the design tool of the workflow is composed of the base preserving transformations. All transformations in this group preserve the shape of the base of mesh while allowing to adjust its global form. The group include:

- Anisotropic scale,
- Shear,
- Perspective transformation with *h* parameter.

Each transformation shown in Fig. 6.35 has its individual numerical and vector parameters. Most of these parameters can be combined, allowing the designer to control all base preserving transformations by the position of two points and one numerical value.

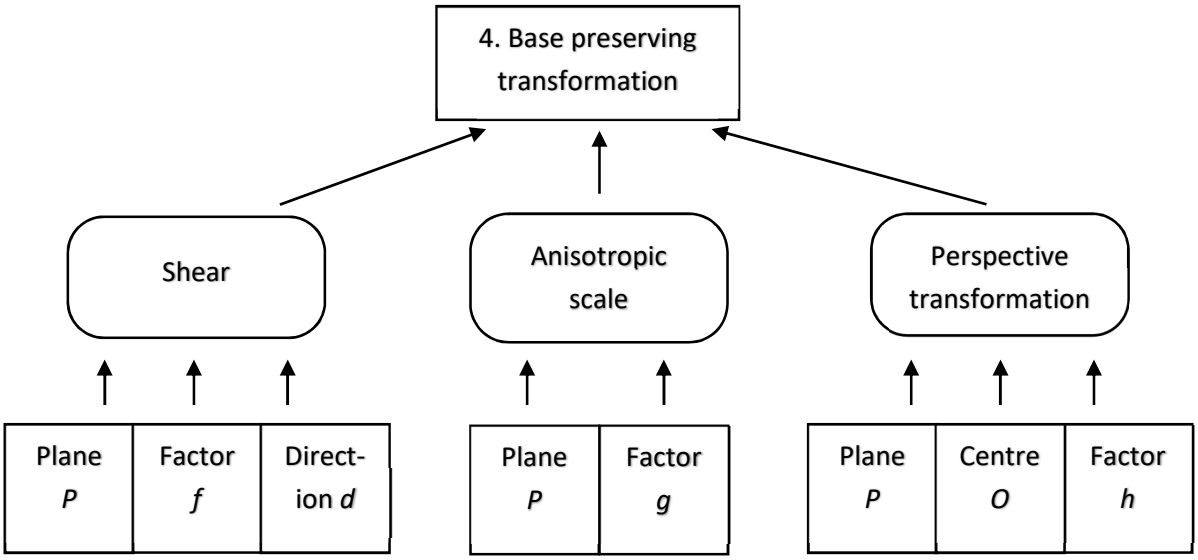

Fig. 6.35 Scheme for base preserving transformations. Each transformation is parametrized by different factors, vectors and planes.

Planes of all transformations are in fact the same, it is the plane containing base of the mesh. Thus, this parameters can be omitted from the list. Factors *f* and *g* parametrizing shear and anisotropic scale transformations can as well be determined by the lengths of some vectors. Shear has a direction parameter *d*, which is a vector, that by the definition has to be parallel to the plane of transformation. In this case it means, that vector *d* is horizontal. Whereas anisotropic scale is parametrized by factor *g*, which can as well be determined by the length of some other vector. Anisotropic scale in this case is a height adjusting transformation, which direction is vertical. Therefore, the vector determining factor *g* has to be vertical as well. Thus, all parameters: *d*, *f* and *g* can be determined by vertical and horizontal components of a vector, which is user defined by positioning of two points – *K* and *L*, see Fig. 6.36.

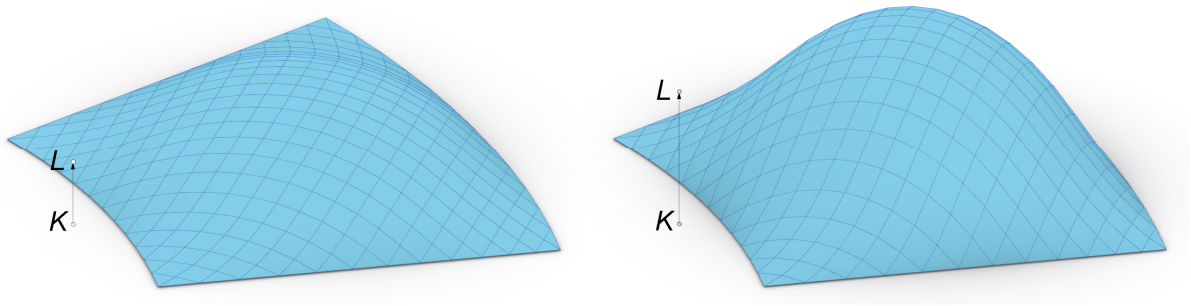

Fig. 6.36 Adjusting height of mesh by manipulating the position of point L *over the ground plane, i.e. only its* z *coordinate is changed.*

Point *K* is constrained to the ground plane and the mesh has unitized height (equal to one). The distance between points *K* and *L* in vertical direction used as factor *g* of anisotropic scale results with the image mesh, whose height is equal exactly *g*. In other words, the peak of the resultant mesh is on the same level as point *L*. Doing so, the designer has the possibility to directly specify one of the most important parameters of the mesh.

Shearing parameters, i.e. factor *f* and direction *d* are also derived from the user defined positions of points *K* and *L* – namely from their top projection, see Fig. 6.37. Direction *d* is the direction of vector $\overrightarrow{KL}$ projected on the ground plane and factor *f* is the length of that projected vector. Perspective view on sheared mesh controlled by the user defined vector $\overrightarrow{KL}$ is shown in Fig. 6.38.

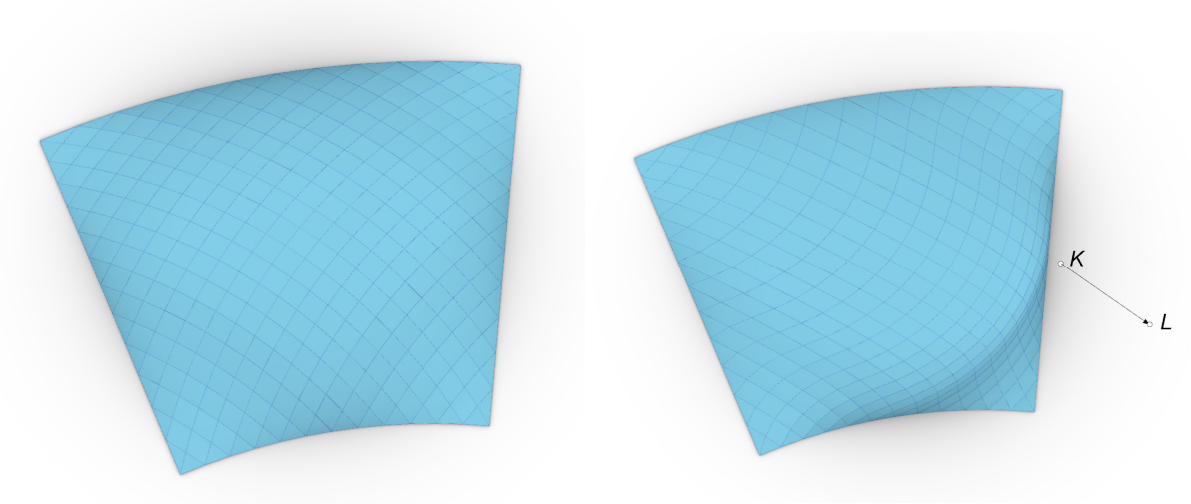

Fig. 6.37 Shearing the mesh by changing the x *and* y *coordinates of point* L*. Top view.*

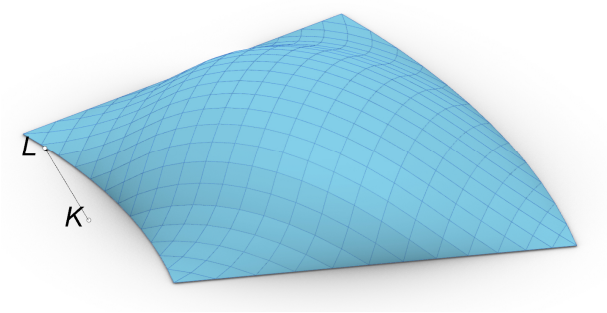

Fig. 6.38 Perspective view on the sheared mesh and KL *vector.*

For the perspective transformation the center point *O* and factor *h* are required. The relevance of location of center point of perspective transformation in vertical direction is highlighted in section 5.2.2.8. Since all parameters of previous transformations were numbers and directions specified by a free vector, the location of points *K* and *L* is irrelevant from these parameters point of view. Therefore point *K* can determine the center of perspective transformation *O*. Factor *h* of perspective transformation remains a separate parameter, whose values are in the range from zero to infinity. Finally, the scheme for base preserving transformation with combined parameters can have a form shown in Fig. 6.39.

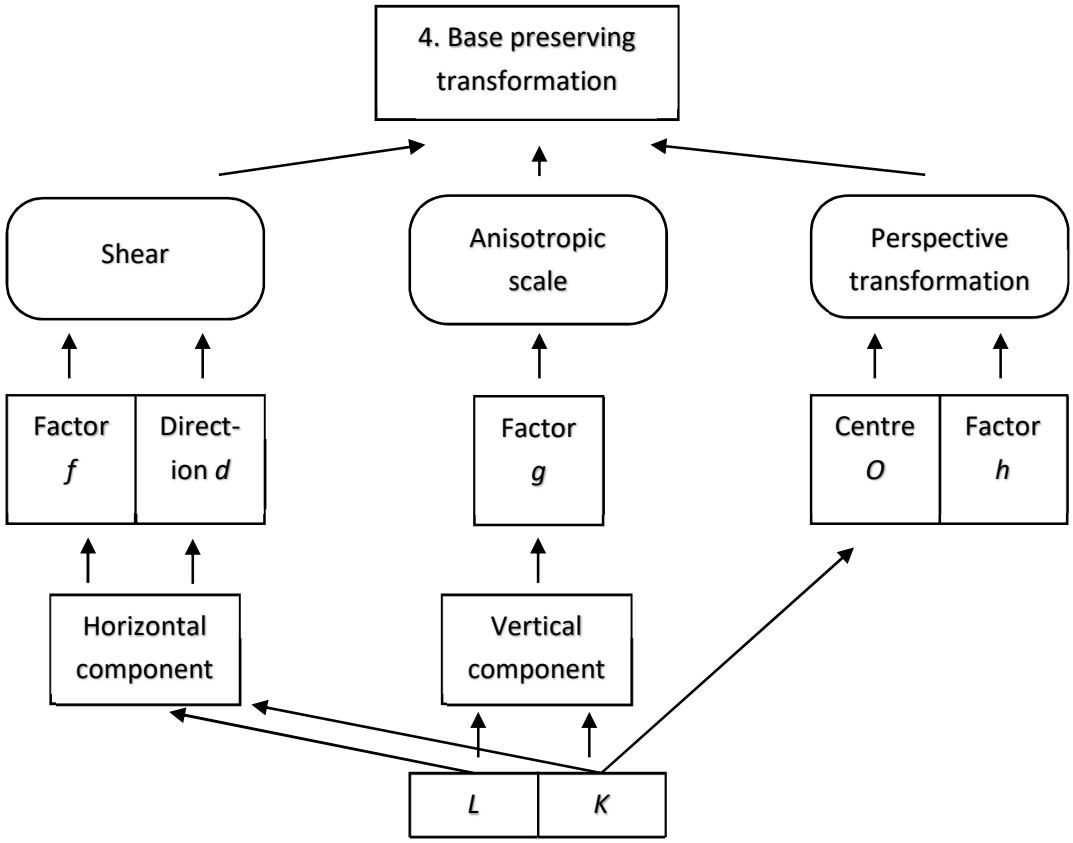

Fig. 6.39 Scheme for base preserving transformations with combined parameters L, K *and* h.

Aligning trimmed edges with shear and perspective transformation

Heterogeneity of SC space results with deflection of the mesh from its center. This deflection is clearly observed on trimmed arch of the mesh, which tilts outwards the circle, see Fig. 6.40, left. This tilt can be corrected by application of shear transformation, making the arch almost symmetrical, see Fig. 6.40, right.

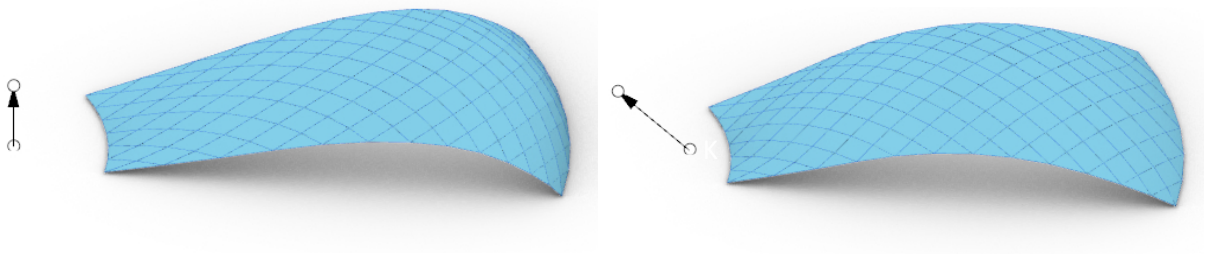

Fig. 6.40 Left: deflection of trimmed, SC mapped mesh. Right: the same mesh corrected by shear transformation.

The shear transformation acts on all vertices of the mesh and translates them in the same direction. Therefore, arch composed of points, which are contained in a common, vertical plane, can be preserved on it by specifying shear direction parallel to that plane. Two adjacent, trimmed meshes can preserve exact adjacency by applying the same shear transformation.

However, if the mesh is trimmed from two sides, it is impossible to keep planarity on both arches, since they lie on different planes which are not parallel, see Fig. 6.41.

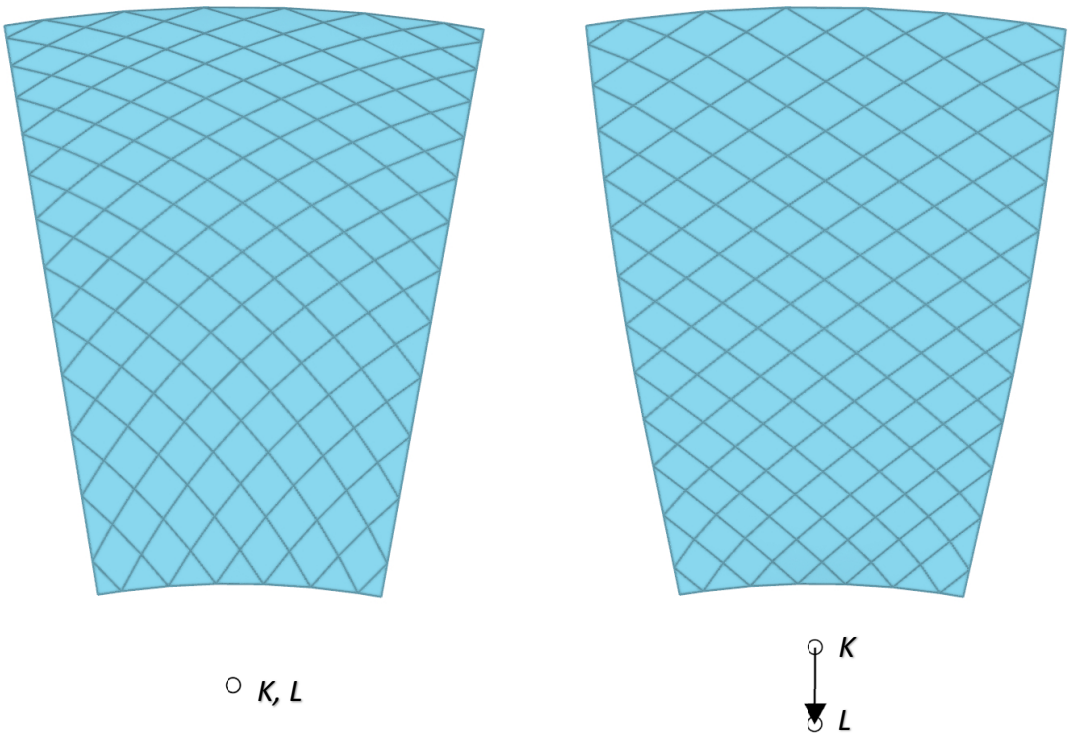

Fig. 6.41 Top view on shear transformed mesh. Edge planarity is distorted.

In contrast to shear transformation which transforms all points in the same direction, the perspective transformation along vertical axis (with parameter *h*, see section 5.2.2.8) transforms points in various directions, depending on their position and the position of the centre point of perspective transformation. As shown in Fig. 6.42 points are shifted along lines passing through them and the designer specified point *L*. Values of relocations relate to the value of parameter *h* and are performed in such a manner, that planarities of facets are preserved. The bundle of those lines[86] have one common point *L*, even, when shear transformation is also applied, see Fig. 6.43. It is worth to emphasize, that centre of perspective transformation is not the point *L*, but the point *K*. Centre point of perspective transformation used for base preserving transformations lies on a common plane with base of transformed mesh, i.e. at the point *K*, which is equivalent to the point *O* from Fig. 5.77 on page 154, whose coordinates are (0,0,0). The designer can define position of point *K* anywhere on a horizontal plane containing base of a mesh, which needs to be maintained. Whereas the location of user defined point *L* not only defines, by the relation with the point *K*, the base preserving transformations such as height adjusting anisotropic scaling and shear transformation, but also has a special property being the centre point of concurrent lines that pass through vertices of the mesh and their projections onto a horizontal plane containing the point *K*, regardless of the value of perspective transformation parameter *h*. Figures 6.42 and 6.43 show the same initial mesh transformed with different values of parameter *h*. Regardless of the value of parameter *h*, the plane projections and orange concurrent lines are always the same and pass through the point *L*.

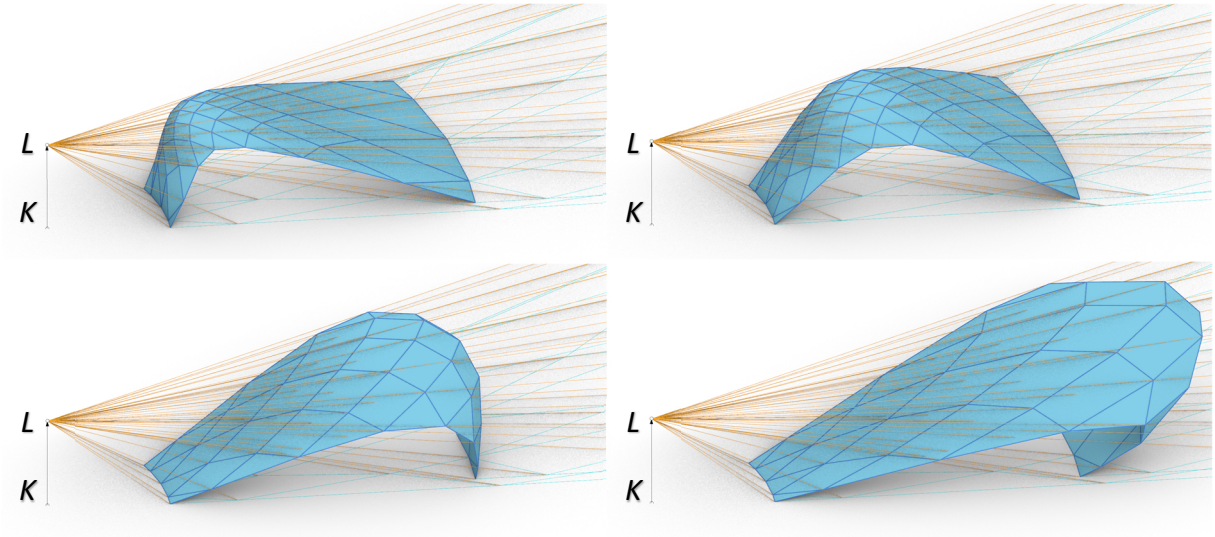

Fig. 6.42 Perspective transformation with parameter h *visualized as shifting the points of mesh along lines radiating from point* L*. Shifting is performed in such a manner that planarity of all facets is preserved. For all four meshes (transformed by means of perspective transformation of the same initial mesh) the images of projection on a horizontal plane form the point* L *are exactly the same.*

[86] Concurrent lines, i.e. a set of lines that intersect at a common point, see (Weisstein 2018c).

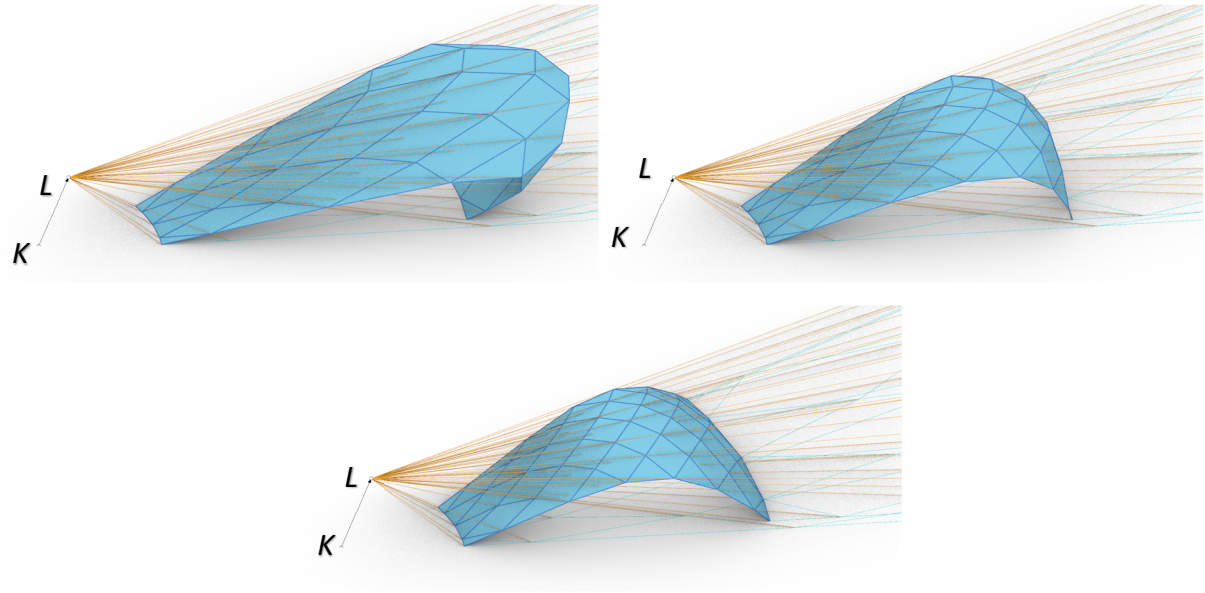

Fig. 6.43 Combination of shear and perspective transformation. The lines radiate from point L*, which is not directly above the point* K*. In all images in this figure only the meshes are different. The locations of points* K*,* L*, orange rays passing through vertices of meshes and the horizontal images of projections are exactly the same.*

In order to apply perspective transformation to a mesh while maintaining all points along trimmed edge on the original, vertical plane, point *L*, which is also the intersection point of the bundle of lines, have to be located on that vertical plane containing trimmed edge, see Fig. 6.44 and 6.45.

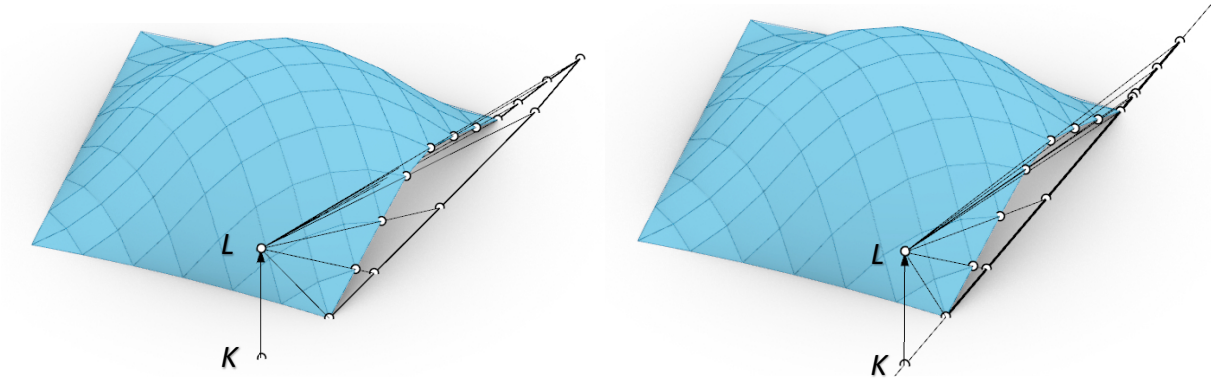

Fig. 6.44 Bundle of lines in perspective transformation create a shadow of edge of the mesh. The shadow is a straight line, when the L *point is located on a common plane with all the edge points (right).*

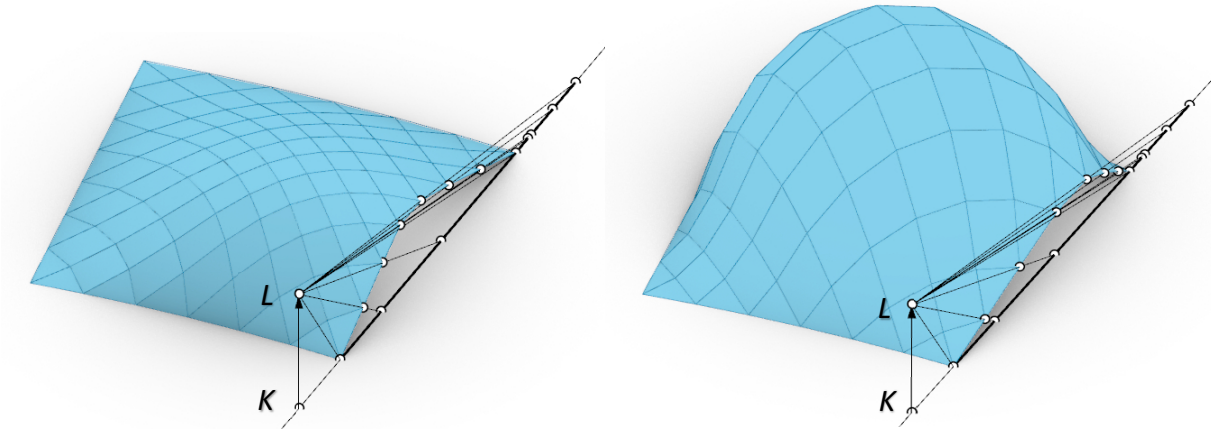

Fig. 6.45 Perspective transformations with L *point located on a plane containing trimmed edge.*

Point *L* located on a plane containing trimmed edge allows to maintain its planarity and vertical setting. In order to maintain planarity and vertical setting for two trimmed edges of one SC mapped edge, point *L* has to be located on both planes containing those edges. Therefore, it has to be located on their intersection, which is a vertical line passing through centre point of SC space, i.e. point *O*.

Central meshes in Figs. 6.46 - 6.49 are trimmed on both sides. Applying perspective transformation, whose centre point is incident with centre of SC spaces on which all meshes were mapped, allows for preserving trimmed edges on original, vertical planes. For comparison with shear transformation see Figs. 6.41 and 6.49.

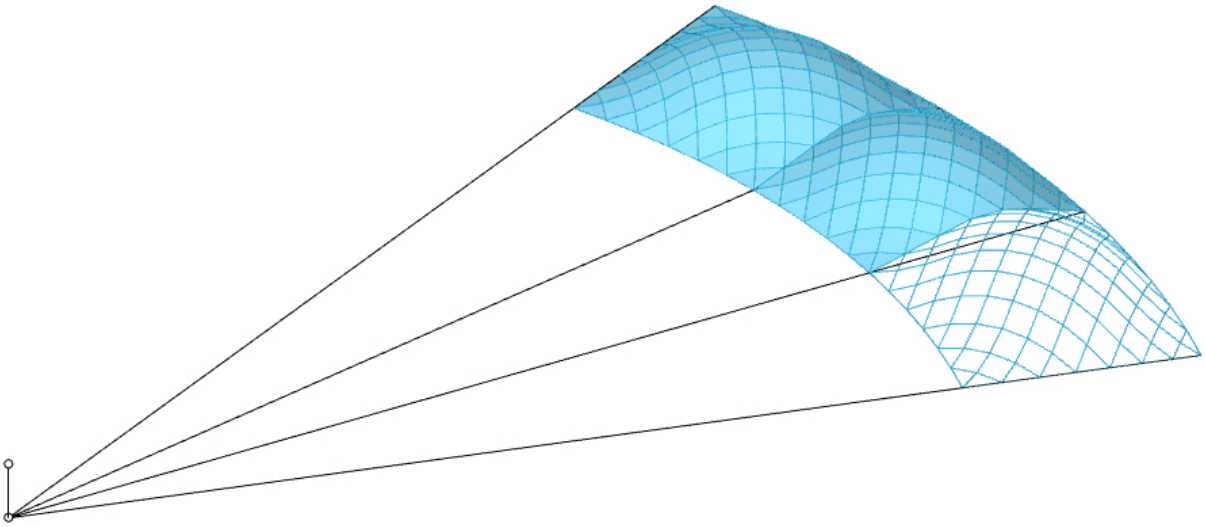

Fig. 6.46 Parallel view of segmented, adjacent meshes.

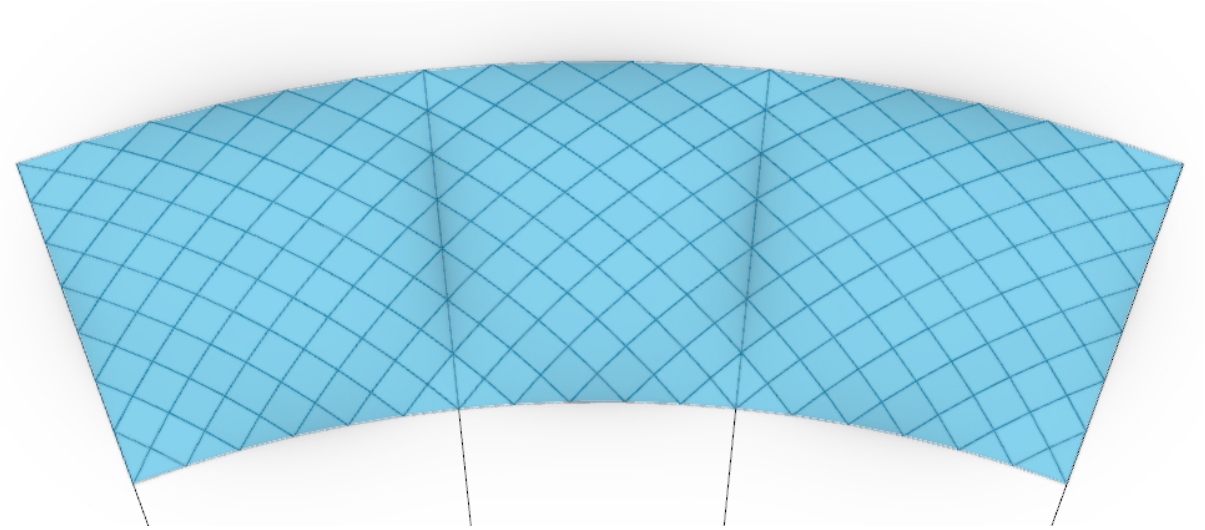

Fig. 6.47 Top view of segmented, adjacent meshes.

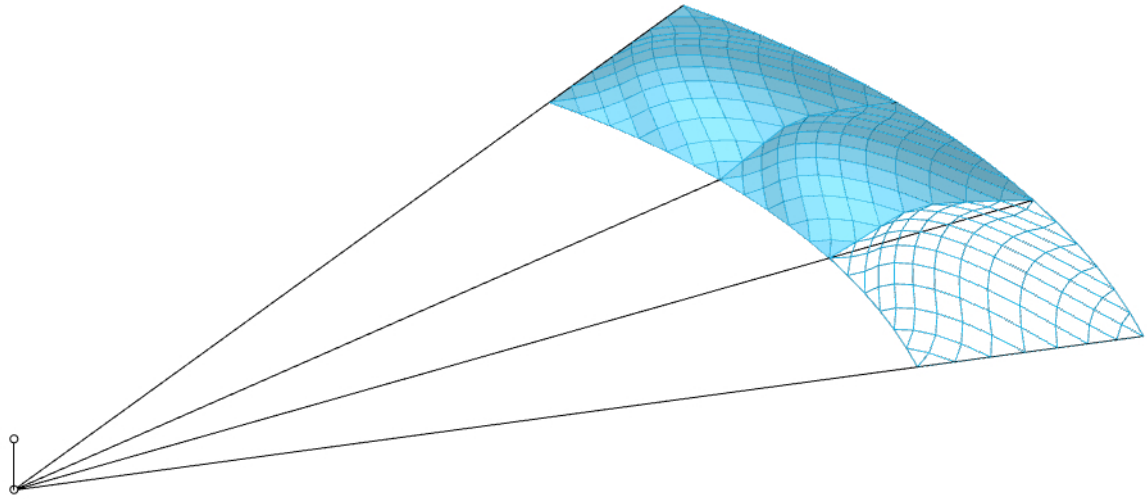

Fig. 6.48 Parallel view of segmented, adjacent meshes.
Perspective transformation along vertical axis performed with the centre above the centre of SC space.

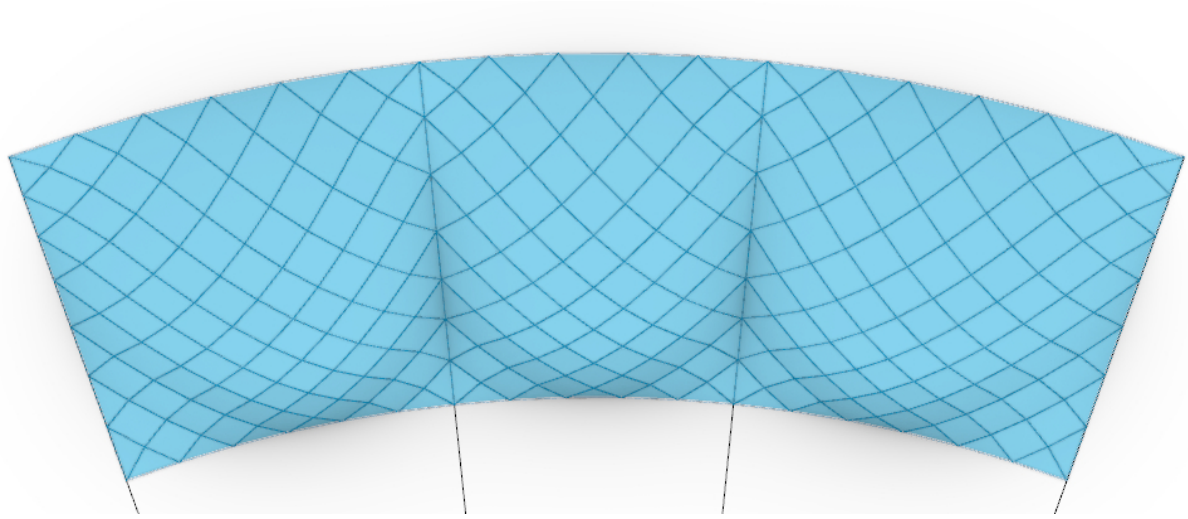

Fig. 6.49 Top view of segmented, adjacent meshes. Perspective transformation along vertical axis performed with the centre above the centre of SC space. The vertical planes containing edges are preserved. High value of parameter h *was intentionally chosen to highlight mentioned property.*

6.5. Implementation of the design tools

Design scenarios were implemented in Grasshopper™ graphical algorithm editor[87]. Each activity has been implemented in Python programming language. Figure 6.50 presents two design tools as a Grasshopper definition assembled from four components each. Component marked in red corresponds to *unit mesh* activity; yellow to *trimming* and green to *base preserving transformations* – these components are shared by both workflows. Component marked in blue stands for *perspective transformation* and purple for *SC mapping*. Remaining components stand for user defined parameters.

[87] Grasshopper is a visual programming language and environment that runs within Rhinoceros 3D CAD application. Homepage of Grasshopper™ is: https://www.grasshopper3d.com/

Numerical parameters are entered using sliders. Points are entered from Rhinoceros 3D[88] interface or directly from Grasshopper environment. Outline for *perspective transformation* is entered as a polyline, i.e. chain of four lines segments not shown in Fig. 6.50. Entered data can also be provided as an output from other algorithms created by the designer. Implementation of the design workflows in Grasshopper environment allows for plugging the output (PQ mesh) into other design, analysis and optimization tools available in this environment, e.g. Karamba3D[89] FEM analysis tool, Galapagos[90] evolutionary solver and others. Output of the design workflows is capable for further processing in Grasshopper environment, i.e.:

- Specifying and optimizing vertex normal vectors (see section 3.5);
- Assigning cross sections;
- Generating the documentation.

Separation of the workflow activities as components allows for reusing them in different scenarios not predicted in this work.

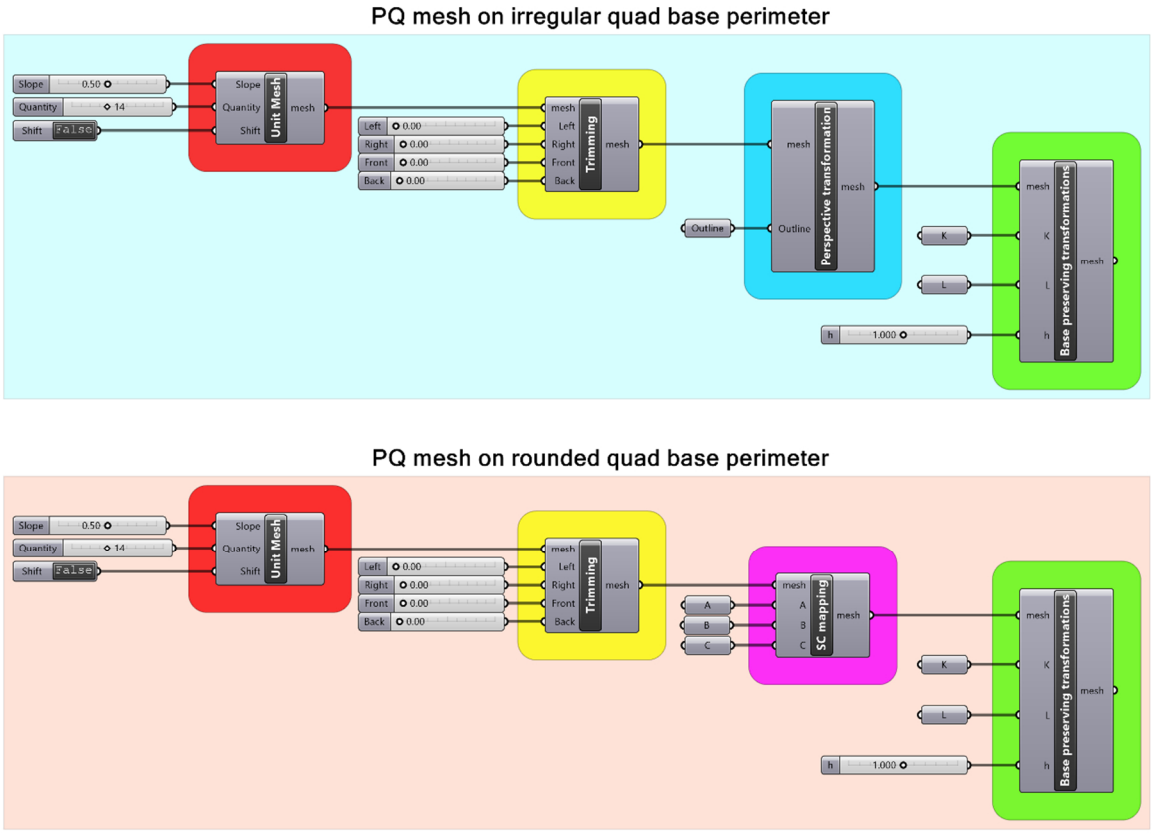

Fig. 6.50 Implementation of design tools as Grasshopper components.

[88] Rhinoceros is a 3D computer graphics and computer-aided design application. Homepage of Rhinoceros is: https://www.rhino3d.com/

[89] Karamba3D is a parametric structural engineering tool which provides analysis of spatial trusses, frames and shells, which is embedded in the Grasshopper. Homepage of Karamba3D is: https://www.karamba3d.com/

[90] Galapagos is a plugin embed in Grasshopper, which provide a generic platform for the application of Evolutionary Algorithms. The details are further discussed in: https://www.grasshopper3d.com/group/galapagos and https://www.grasshopper3d.com/profiles/blogs/evolutionary-principles.

7. Case studies

The tools developed for shaping PQ meshes, briefly described in section 6.5 were tested by using them in designing transparent covers over courtyards of two existing buildings in Wrocław. Both buildings have non-standard shapes of courtyards, for which particular workflows and tools were prepared.

Section 7.1 describes application of the tool for designing PQ meshes over irregular quad base perimeters on case of Department of Human Biology of the Wrocław University.

Section 7.2 describes application of the tool for designing PQ meshes over rounded quad base perimeters on case of the Lower Silesian Governor's Office.

7.1. The grid shell over the courtyard of Collegium Anthropologicum

7.1.1. The design task

Collegium Anthropologicum is a part of the University of Wrocław. Its building is located in the historical part of Wrocław, at Kuźnicza street.

General view on the building is shown in Fig. 7.2, photo from the courtyard is shown in Fig. 7.1, whereas the 3D modelled interior of the courtyard, prepared by the author is shown partially in Fig. 7.3. The form of the courtyard is irregular quadrilateral.

Fig. 7.1 Photo from the courtyard of Collegium Anthropologicum.[91]

[91] Source: https://polska-org.pl/3868296,foto.html?idEntity=4349677

Fig. 7.2 General aerial view on Collegium Anthropogenicum. Source: Google Maps.

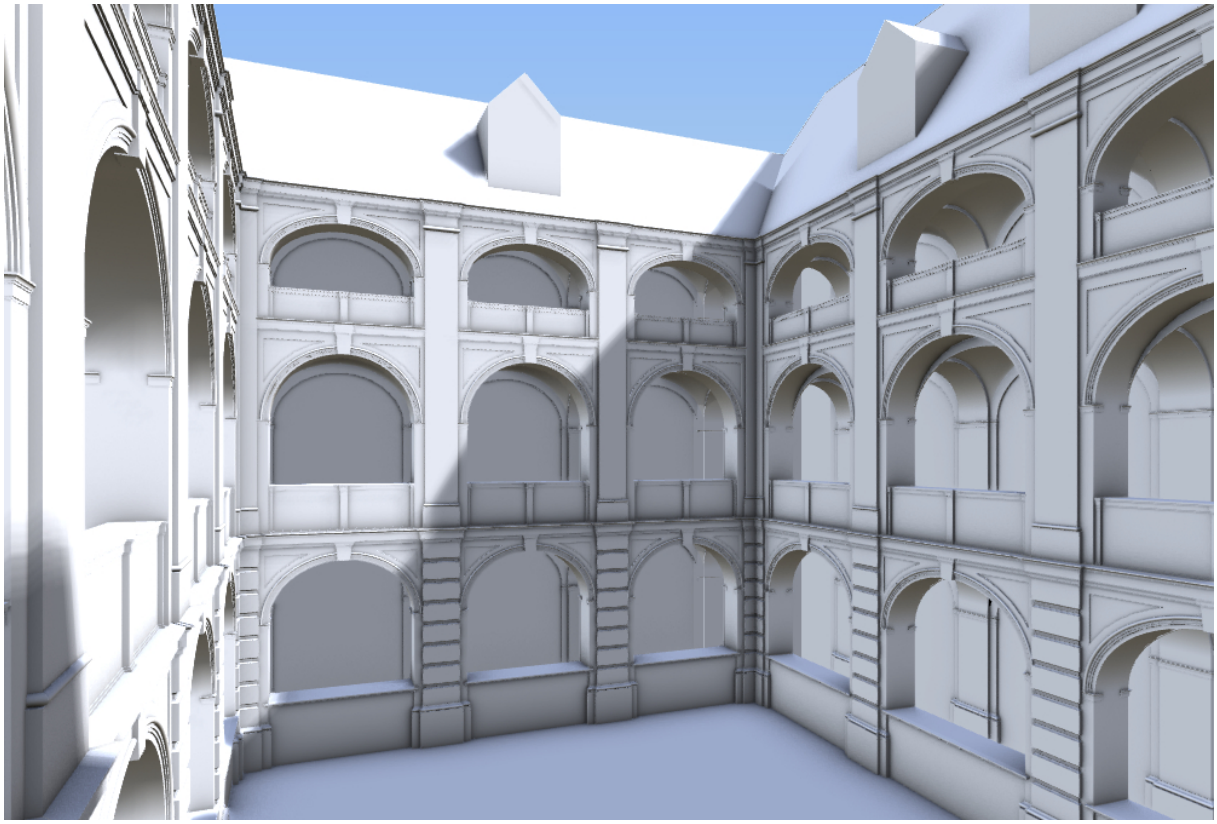

Fig. 7.3 General view on the computer model of the courtyard.

The courtyard is nearly 20 meters long and 12.75 to 13.75 meters wide, see Fig. 7.4.

The objective is to design general geometry for a glazed canopy over the courtyard. The desired geometry is discrete, doubly curved PQ mesh with planar base perimeter. Such geometry is obtained by perspective transformation of translational mesh with planar base 4.1.2 according to the design process described in section 6.3.1.

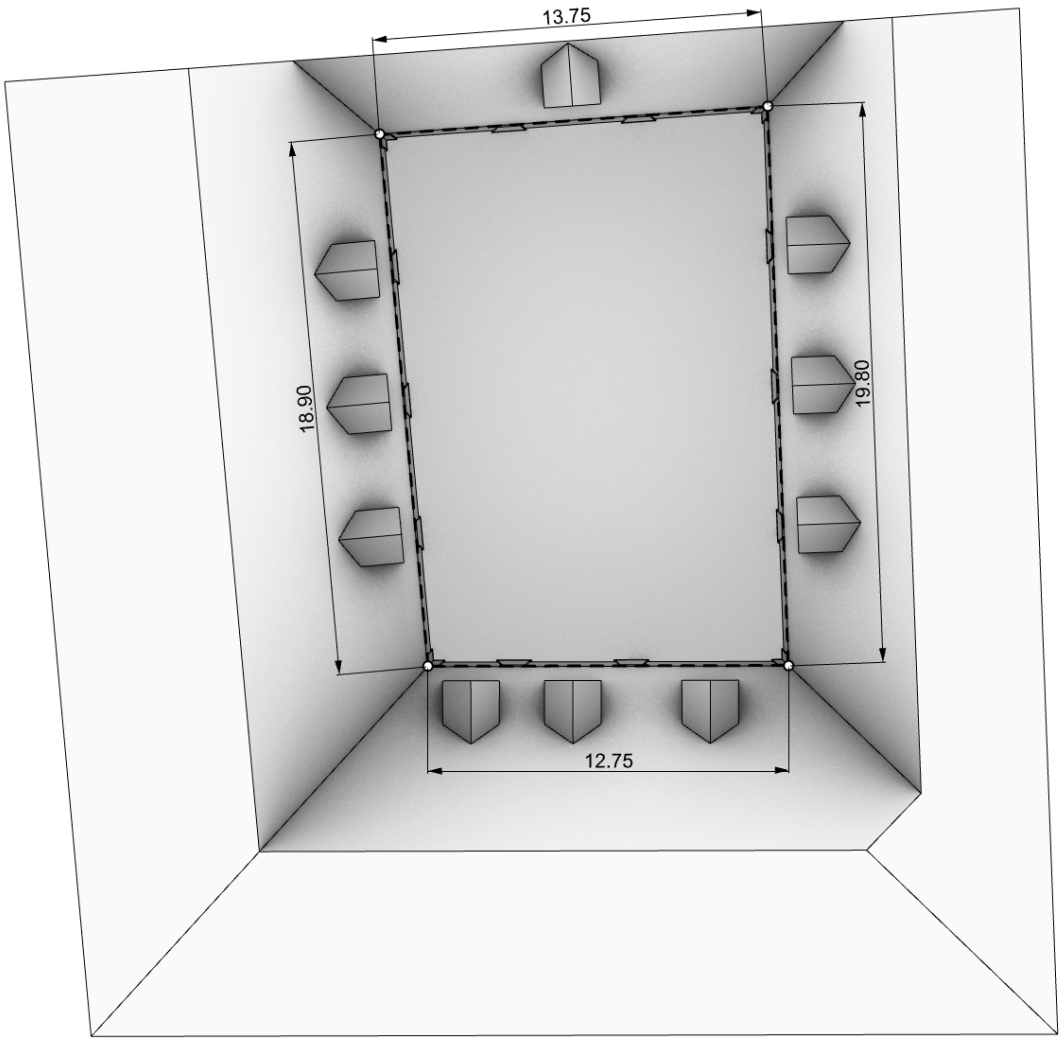

Fig. 7.4 Main dimensions of irregular courtyard.

7.1.2. Description of the activities performed by the designer

In this case study the designer specifies outline of desired base perimeter and performs all necessary transformations using the developed tool. The designer can specify the quantity of facets along edges – in this case the *quantity* parameter is equal to 22, what results in 11 facets along each edge. For this *quantity* value lengths of edges of facets are between 0.8 to 1.4 meters. Slope parameter has value of 0.5 for which the mesh has most smooth form. *Shift* has *false* value. No trimming and no shear transformation is performed. Base preserving transformations are performed to set the height of the mesh at 2,7 meters. Additionally, perspective transformation along vertical axis was performed in order to optimize the lengths of the edges. For the *h* parameter value equal to 1.0, the lengths of facets edges spread from 93 to 124 cm. Slight change of the parameter *h* value to 1.068 result with edges of lengths between 92 to 118 cm, without significant changes of the form, Fig. 7.5.

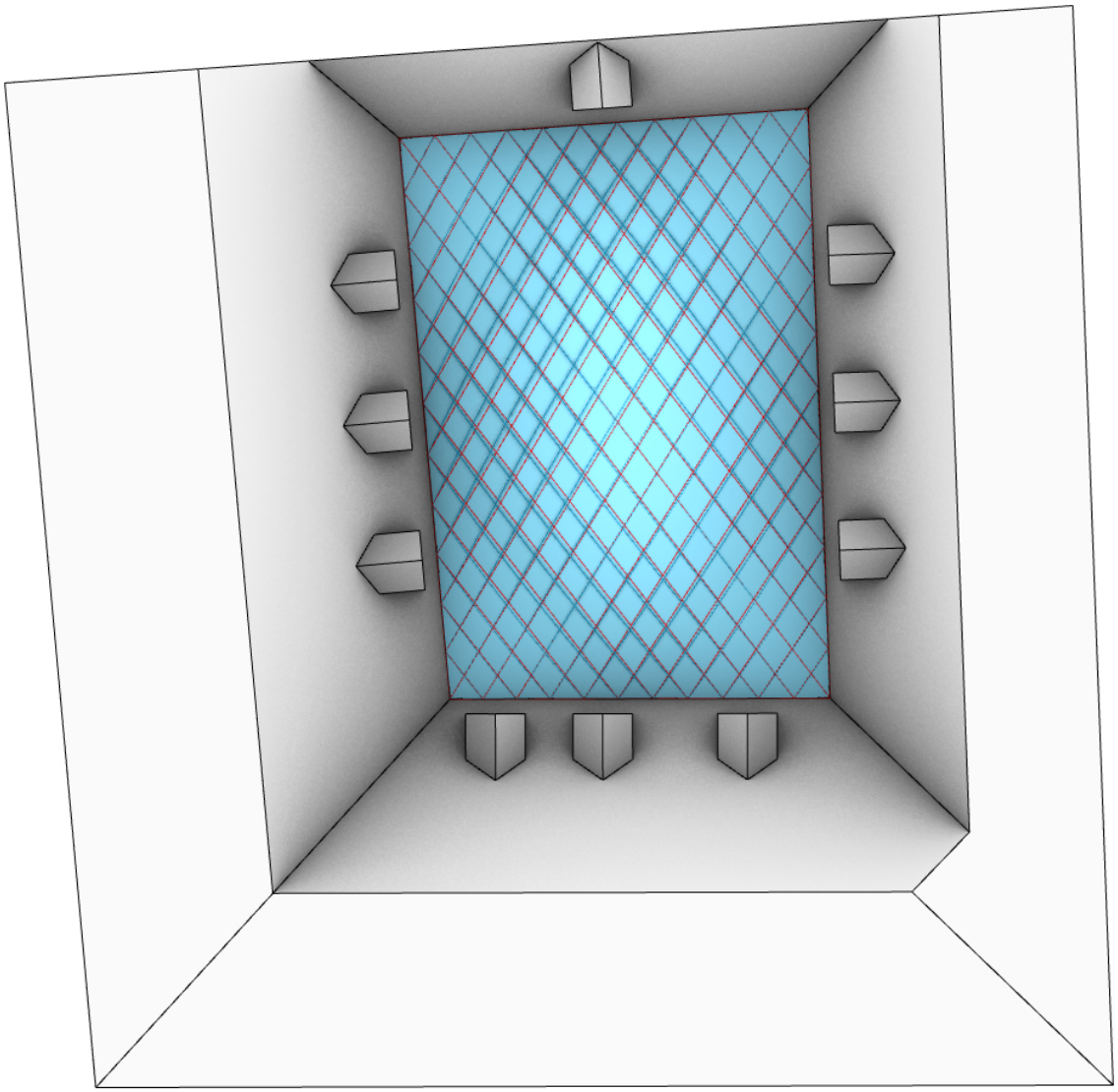

Fig. 7.5 Original mesh edges marked in red, perspective optimized mesh edges marked in blue.

7.1.3. Description of the result

The resultant mesh, shown in Figs. 7.6 and 7.7, is composed of 220 planar quad and 44 triangular facets. Courtyard area of 256 m^2 is covered by a mesh, whose area is 276,6 m^2. Edge lengths of quad glass facets vary from 0,92 to 1,18 meters.

Additional design parameters allow for shape adjustments and mechanical optimizations. The resultant mesh is eligible for torsion optimization (see section 3.5.2), conceptual model was optimized for elimination of geometrical torsion in bars. Obtained mesh is a starting point for further design of structural properties, i.e. cross sections of bars, materials, application of cross-brace stabilizing quads, etc. However, this discussion is out of scope of this work.

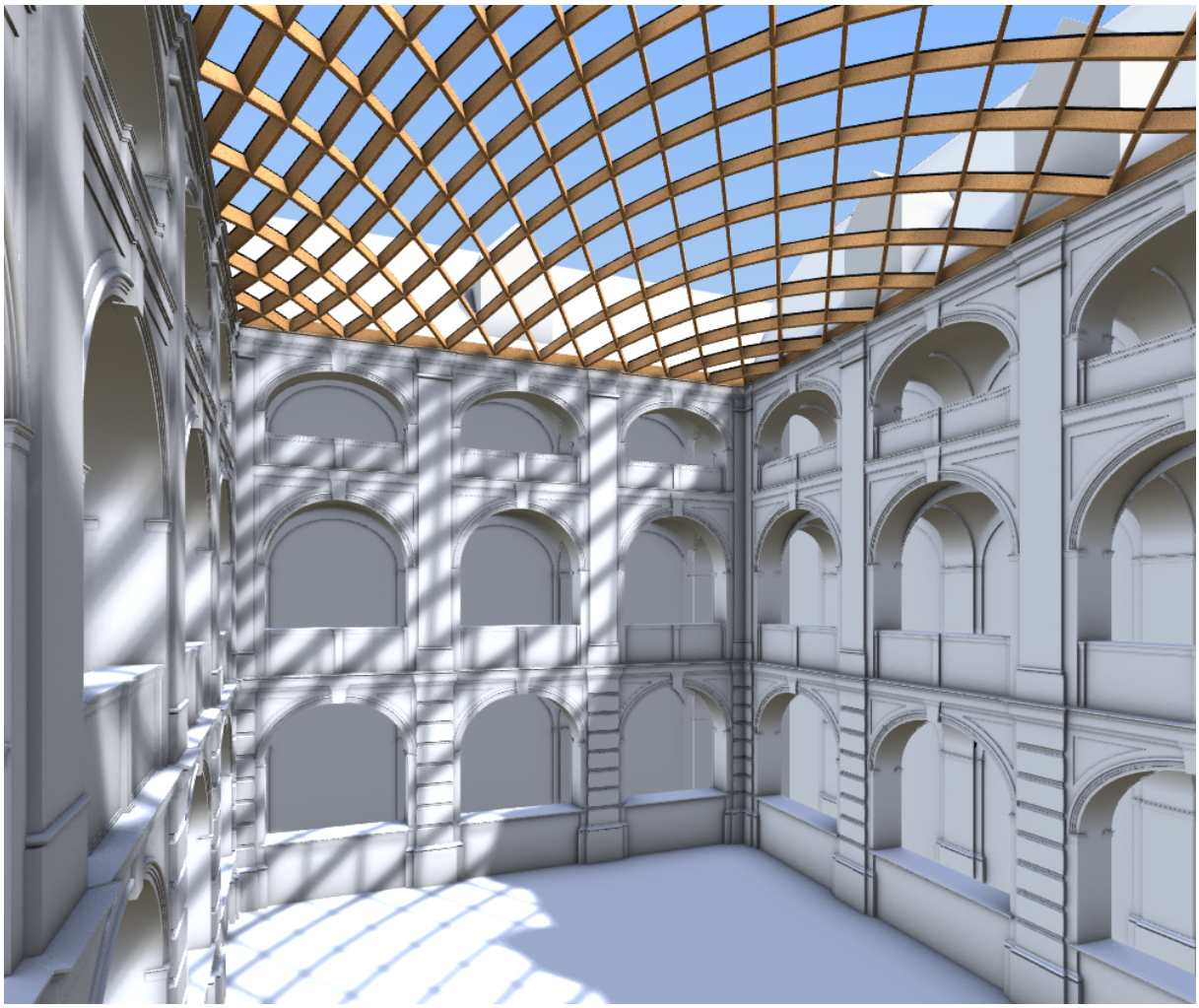

Fig. 7.6 Perspective view from the courtyard. Concept of application of cross sections. All rods are torsion-free.

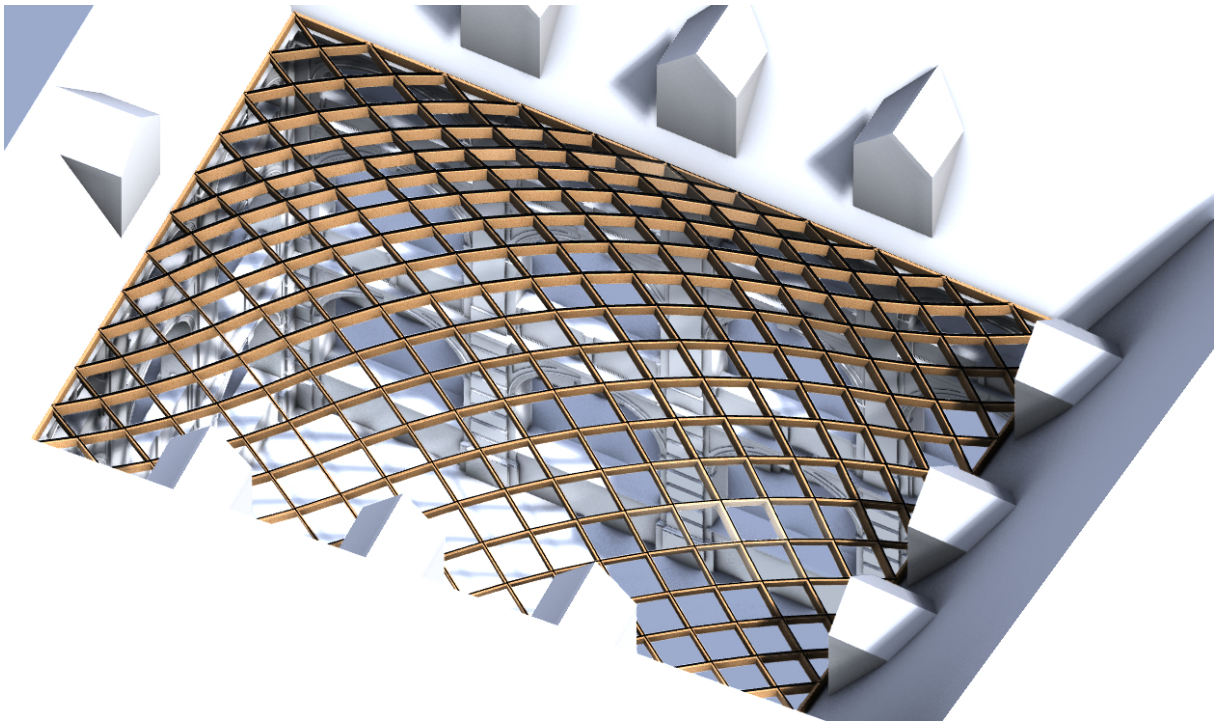

Fig. 7.7 Aerial parallel view on the conceptual model for the glazed grid shell.

7.2. The grid shell over the courtyard of Lower Silesian Voivodeship Office

7.2.1. The design task

The Lower Silesian Voivodeship Office in Wrocław is built along the rounded bank of Odra river. General view on the building is shown in Fig. 7.8 and in Fig. 7.10. The building has the form of a symmetrical, monumental edifice, which is slightly rounded along the longer edge. Inside the block there are three courtyards. The middle courtyard has a rectangular form, whereas two other, symmetrical courtyards are have rounded quad forms. Each one of two symmetrical courtyards consists of two concentric arches (*AB* and *CD*) and two line segment edges (*AD* and *BC*), see Fig. 7.9. The extension of the *AD* passes through the centre point of arched edges - *O*, whereas the extension of the *BC* edge do not intersect with the point *O*.

Fig. 7.8 Aerial view on the Lower Silesian Voivodeship Office. Source: Google Maps.

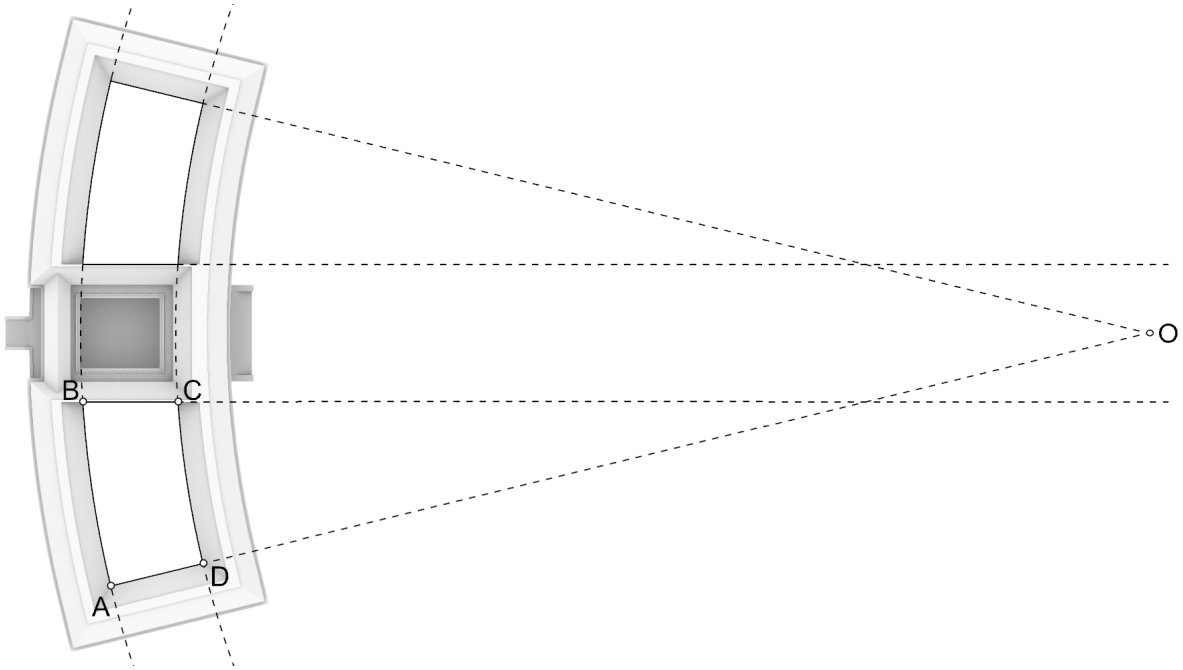

Fig. 7.9 The geometry of rounded courtyards.

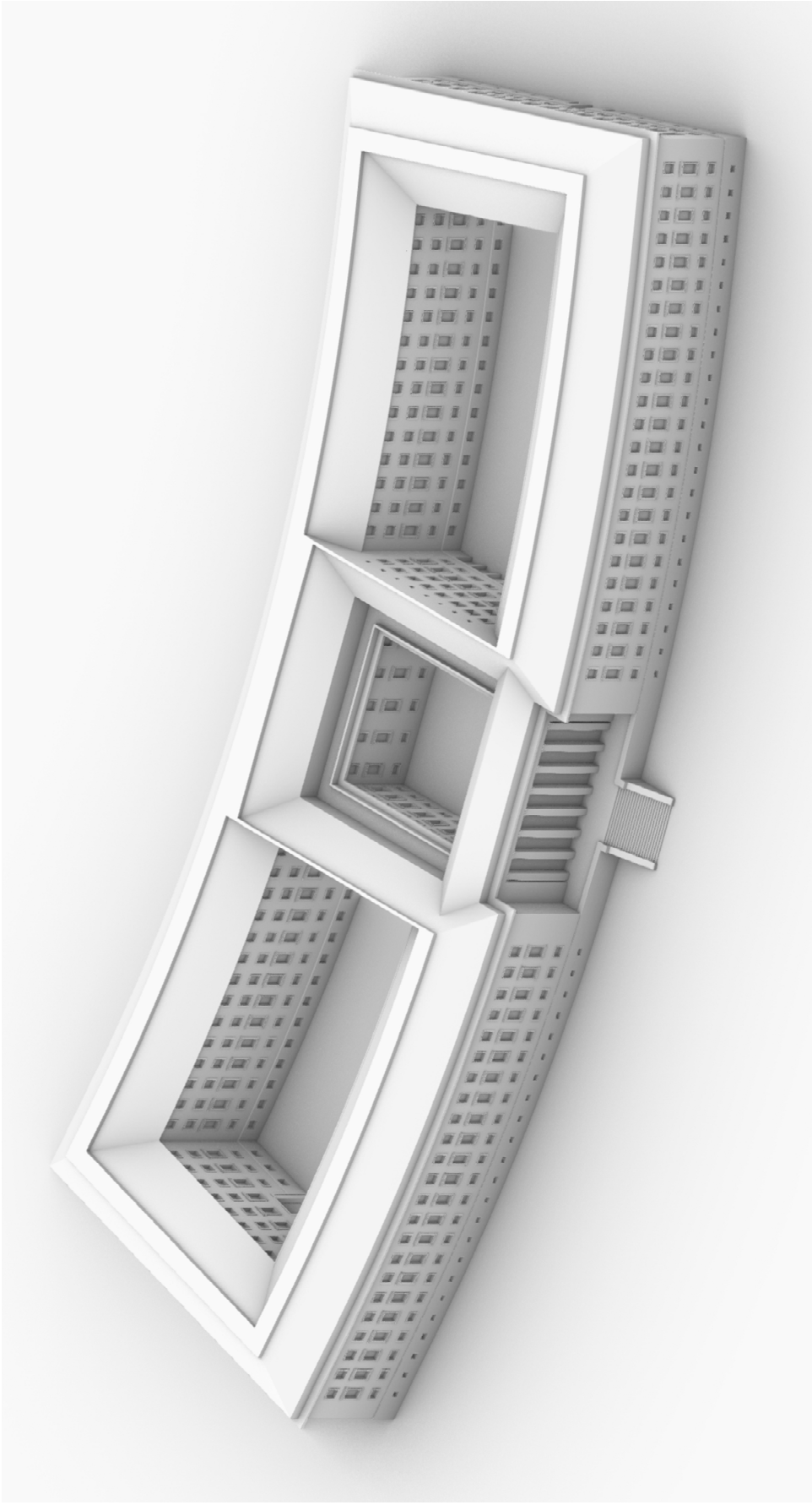

Fig. 7.10 General view on a computer model of the building.

The courtyard is approximately 29 meters wide and 50 to 56 meters long, see Fig. 7.11. The cornice is 19.30 meters and the ridge is 24.50 meters above the level of courtyard, see cross-sections in Fig. 7.12 and 7.12. Three sides of each courtyard are limited by cornice and roof, whereas fourth wall, along the edge *BC* is limited by a wall face.

The objective is to design general geometry for a glazed canopy over one of the side, rounded courtyards. Desired geometry is a composition of discrete, doubly curved PQ meshes. The shape is elongated along rounded edges, therefore more than one mesh is required in order to maintain the proportions of individual facets. Otherwise the facets of the mesh would be unacceptably elongated, i.e. ratio of their diagonals would be far from 1. Adjacent edges of neighbouring meshes may have form of arches obtained by trimming the meshes. One mesh adjacent to the *BC* edge of the courtyard may also be trimmed along that edge, since there is no horizontal cornice. Moreover, trimming allows for obtaining curved edge, which may be adjusted to existing windows over fifth floor.

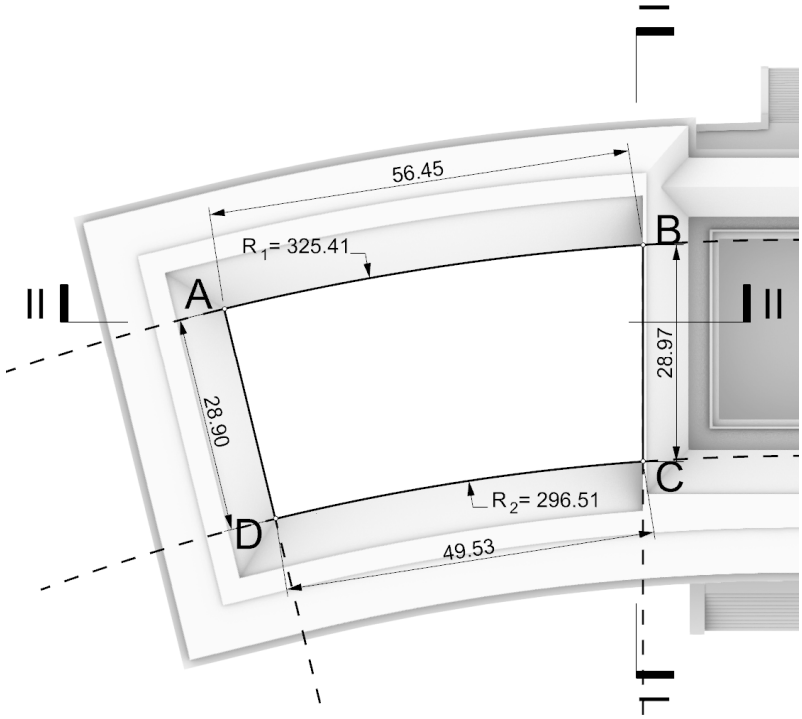

Fig. 7.11 General dimensions of the rounded courtyard.

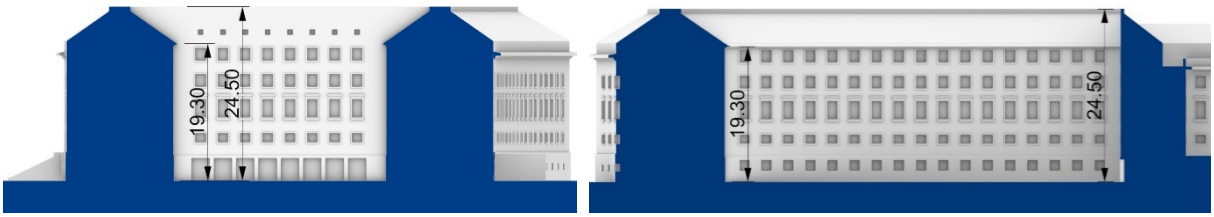

Fig. 7.12 Left: cross-section I – I. *Right: cross-section* II – II.

7.2.2. Description of the activities performed in the design process

Since in this case, the glass roof is composed of two conjugated meshes, the designer have to decide first about values of some parameters. The designer can start from setting the approximate dimension of glass panels. It is known, that one edge of the mesh will run along the *AD* edge, whose span is almost 30 meters. Assuming, that required approximate dimension of a glass panel is 1,3 meters along edge in plan, there should be around 18 panels along that edge. The *quantity* parameter should therefore be set to the value of 36.

Trimming of the edges of both meshes should also be taken into consideration before setting the corner points of SC mapping. In order to align two adjacent meshes perfectly together the direction of axis '2', i.e. the angles between axes '1' – '2' and '2' – '3' are calculated from trimming proportions. Assumption for this case study is that the left mesh 'A' is trimmed along one edge and the right mesh 'B', adjacent to a wall face, is trimmed along two opposite sides. Mesh 'A' has two rows of facets trimmed on the right side, see Fig. 7.13. In order to allow exact alignment between 'A' and 'B' meshes, mesh 'B' is trimmed along the connection with 'A' by two rows of facets as well. Additionally, mesh 'B' is trimmed on the side of the wall by 6,5 rows in order that its edge go over the windows, see Fig. 7.14.

It should be noted that axis '3' is not colinear with the wall on the right side of the courtyard. All axes pass through the centre point of SC spaces and their intersections with arched edges of courtyard indicate parameter points for SC mappings. For that reason, part of the mesh 'B' behind the wall will have to be trimmed and rejected.

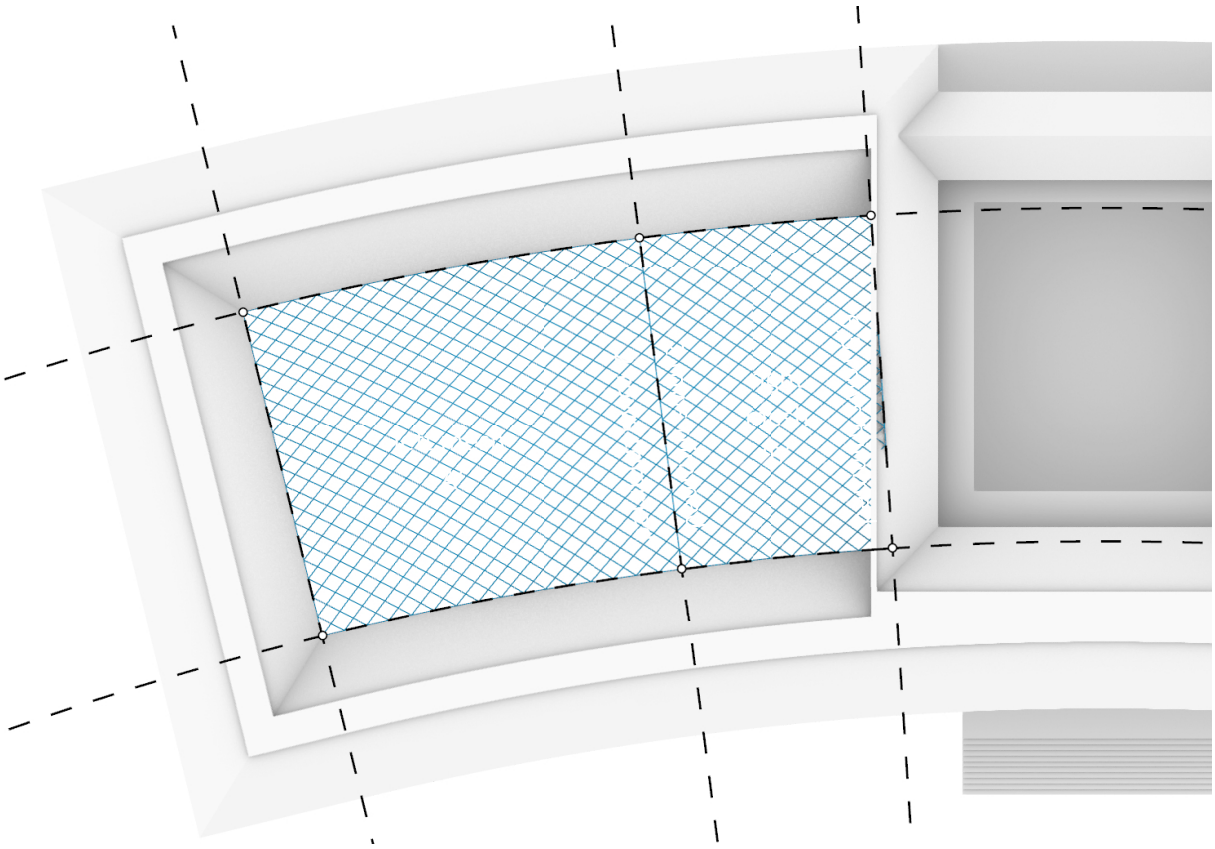

Fig. 7.13 Initial alignment of axes and meshes.

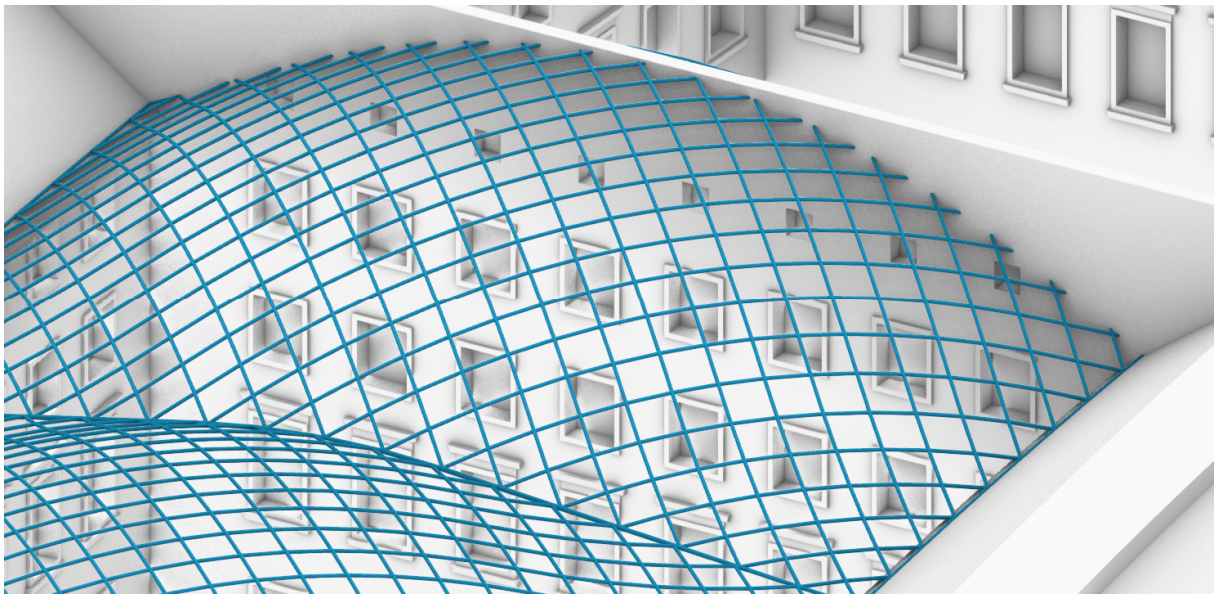

Fig. 7.14 Intersection of the mesh 'B' *with the wall face, over the small windows.*

The mismatching between two adjacent meshes happens, because SC mapping parameters are not the same for both meshes, see Fig. 7.15 and the requirements for matching rounded meshes discussed in section 6.4.4 *Aligning SC mapped meshes*. Although both meshes are mapped on SC spaces, which have the same central point, the spaces have different boundary radii. The boundary radii are derived indirectly from the parameters of meshes (proportions between rows and columns) and destination, corner points. All of these parameters are known, therefore corner points positions can be adjusted, i.e. the points that lie along the axis ‘A’.

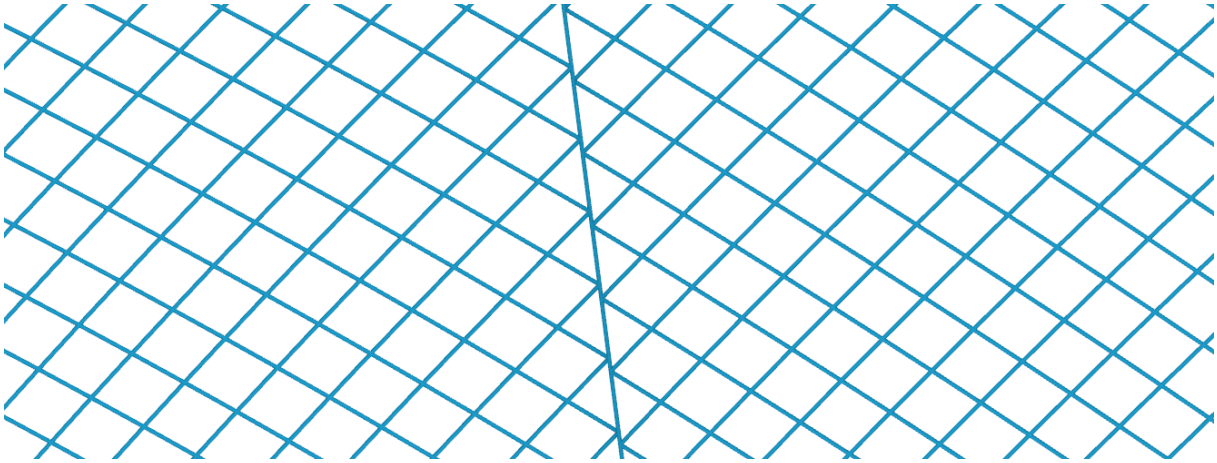

Fig. 7.15 Mismatching of edge points between two adjacent meshes before alignment of the axis '2'.

The angle between axes ‘1’ and ‘3’ is equal to 10.06°. Mesh ‘A’ has 16 and mesh ‘B’ has 9,5 facets along each rounded edges. Hence, each boundary facet along rounded edge should occupy around 0,394°. That means, that mesh ‘A’ should span 6,30° (the angle between axis ‘1’ and ‘2’) and mesh ‘B’ 3,76° (angle between ‘2’ and ‘3’), see Fig. 7.16. Performing the above calculations and adjusting the angles between the axes ensures an exact fit between meshes, see Fig. 7.17. The same rule of proportions between meshes and angles apply for any number of meshes. The algorithm of SC mapping derives parameters of SC space, namely the boundary radius of SC space, automatically from user defined corner points. When the proportions of angles between axes correspond to meshes, the algorithm ensures, that both SC spaces are exactly the same.

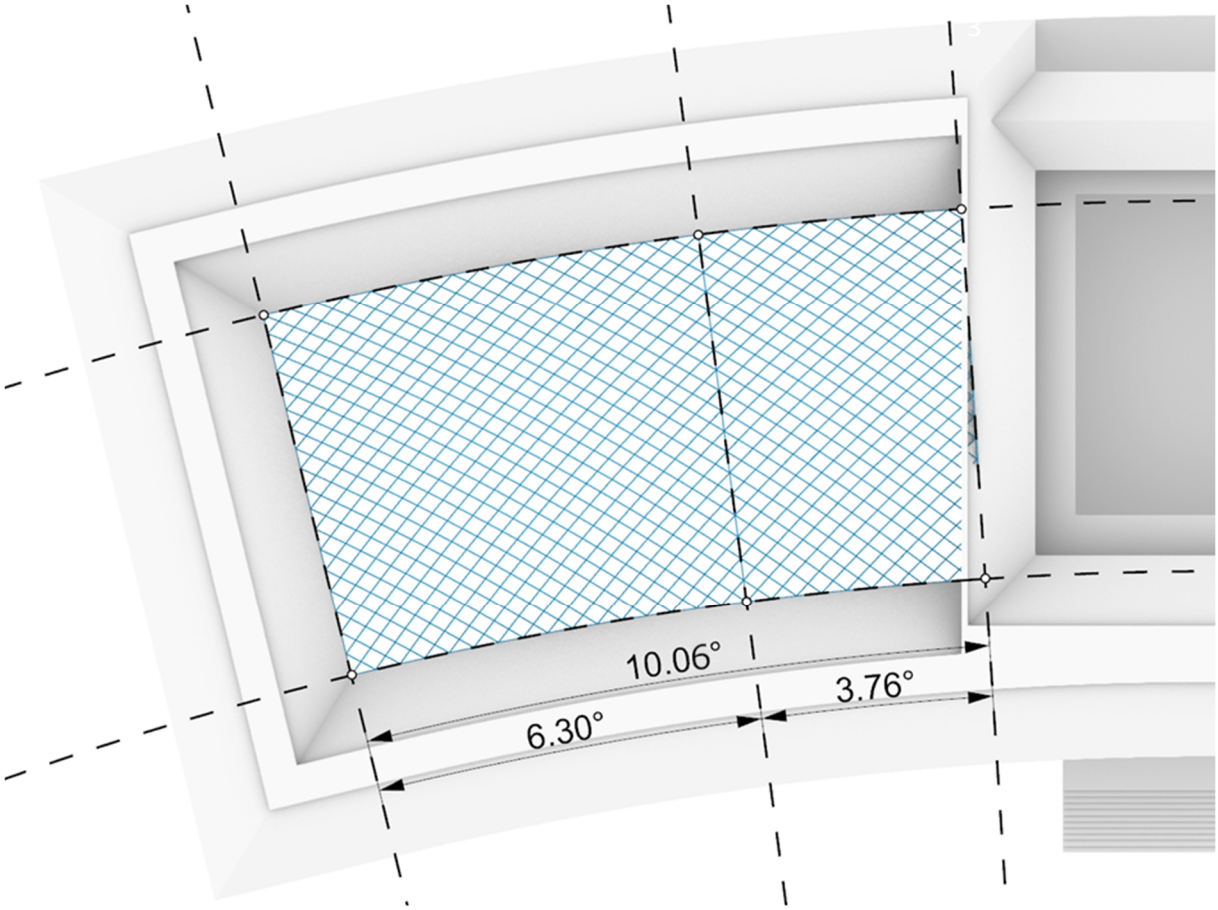

Fig. 7.16 Fitting meshes adjacency by adjusting angles between axes.

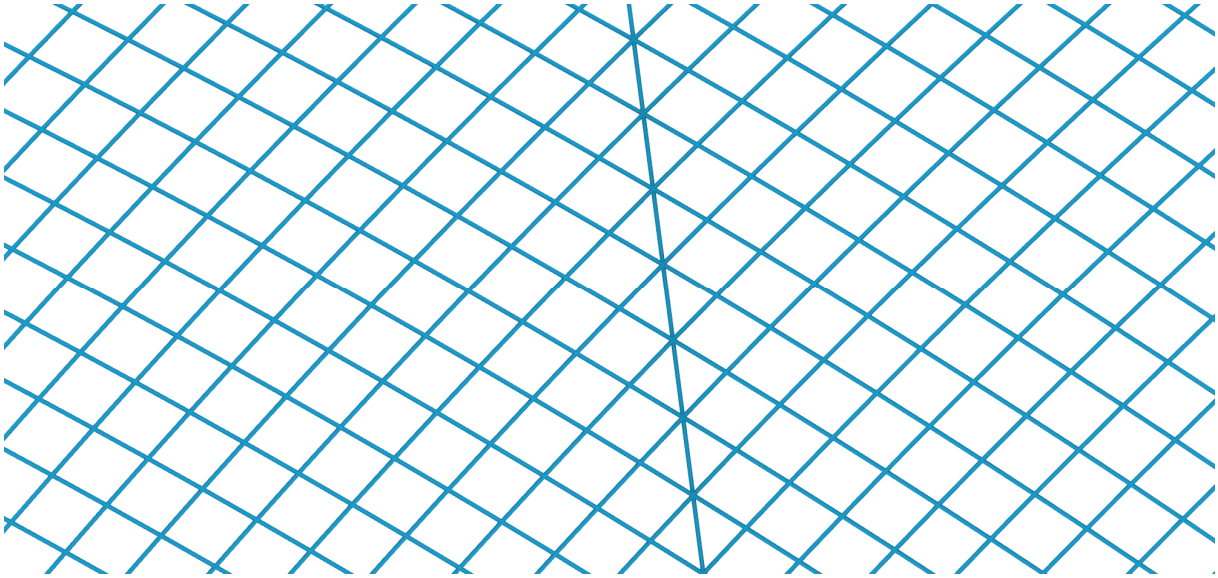

Fig. 7.17 Perfect alignment of neighbouring meshes. Corresponding points on both sides are incident.

In the last step the designer specifies the parameters for *base preserving transformations*. Point *K* is aligned with the centre point of circles and SC spaces (point *O*). Point *L* is located directly above the *K* point. The distance of *L* point above the *K* point is the desired height of the designed mesh, i.e. in this case it can be the difference between the cornice and the ridge of roof, i.e. 5,2 meters, which also assures, that the mesh adjacent to the wall along axis '3' will not protrude over its upper edge and will not go through the top row of small windows, see Fig. 7.18.

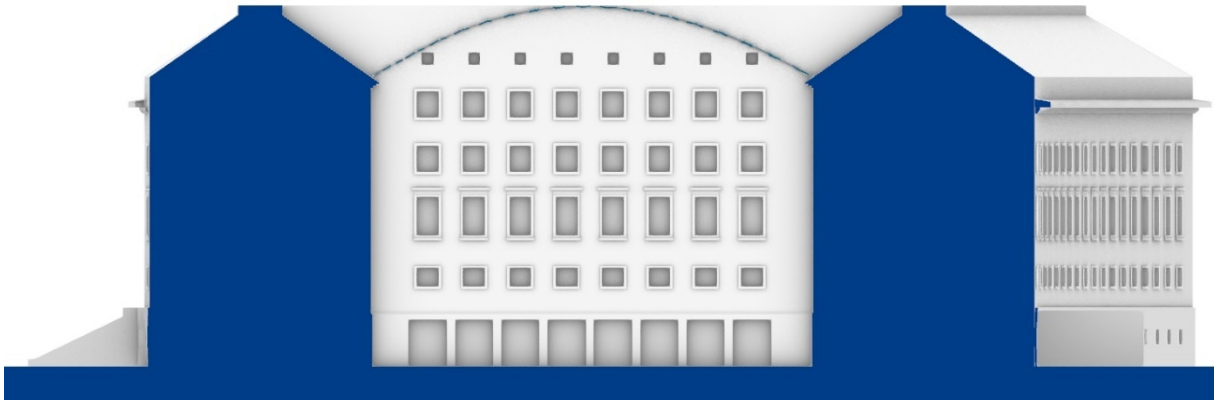

Fig. 7.18 Cross section I -I (see Fig. 7.11) with edge of the mesh traced on the wall face.

7.2.3. Description of the result

The resultant mesh shown in Fig. 7.19 and 7.21 is composed of 857 planar quad and 123 triangular facets. Courtyard area of 1608 m^2 is covered by a mesh, whose area is 1694 m^2. Edge lengths of quad glass facets vary from 1,36 to 1,45 meters.

Additional design parameters allow for shape adjustments and mechanical optimizations. The resultant mesh is eligible of torsion optimization (see section 3.5.2). Obtained mesh is a starting point for further design of structural properties, i.e. cross sections of bars, materials, application of cross-brace stabilizing quads, etc. However, this discussion is out of scope of this work.

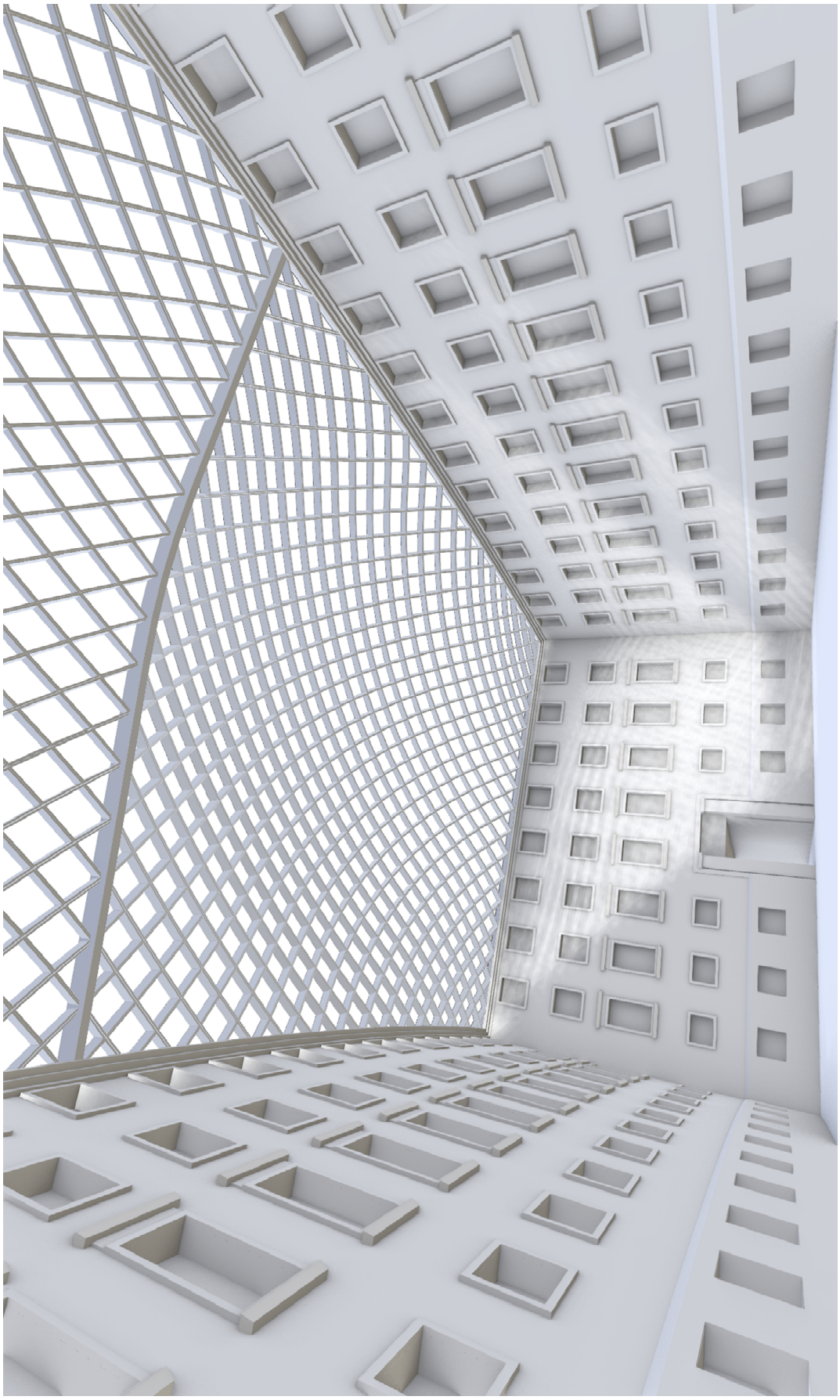

Fig. 7.19 Perspective view from the courtyard. Concept of application of exemplary cross sections and arched beam between sections.

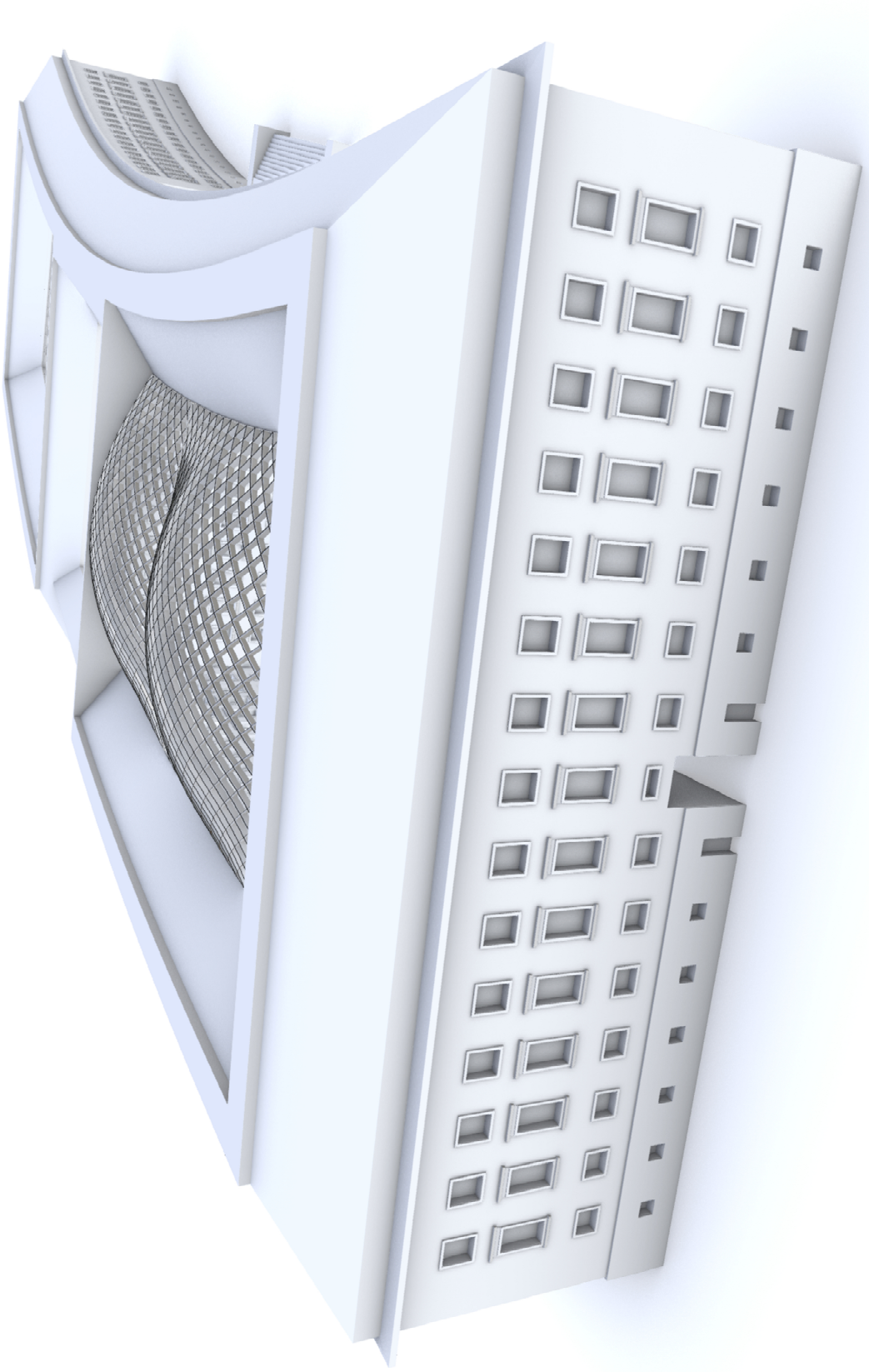

Fig. 7.20 Perspective view from above the building. Concept of application of exemplary cross sections and arched beam between sections.

7.3. Conclusions

With the adoption of bottom-up design paradigm the geometries for grid shells were designed straight away in more favourable topology. Parametrization of the form allows for further exploration and optimization of obtained morphology. In top-down approach the forms for grid shells would have been form found. However, the form obtained by form finding would not necessarily be suitable for PQ tessellation.

Such results are difficult to obtain by using the top-down approach, as illustrated by the following example in Fig. 7.21. A similar, quad based PQ mesh geometry, designed according to the top-down approach is described in *Form-finding and planarisation of glass domes with quad elements* (Estrada and Baldassini 2013). Obtained mesh is a result of predefined tessellation in planar configuration, form-finding of the global form, projection of the predefined tessellation onto a doubly curved form and the planarization of quads in spatial configuration. Final mesh is composed of facets, which deviates from exact planarity.

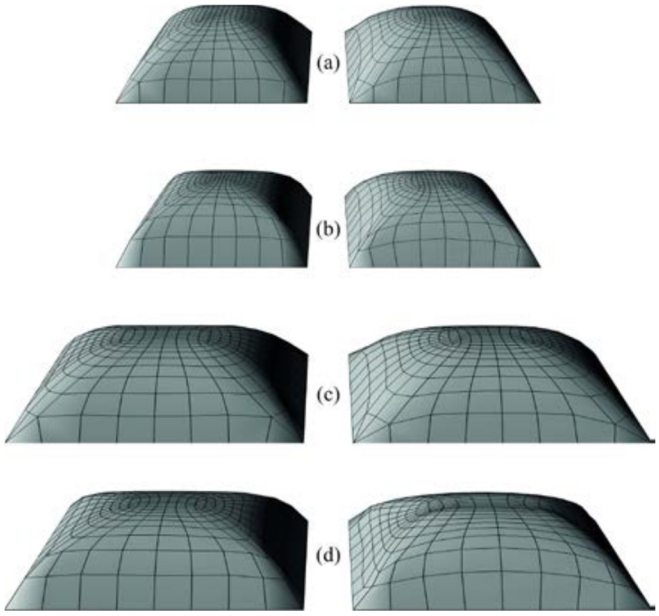

Fig. 7.21 Figure from (Estrada and Baldassini 2013). Square and rectangular domes composed of quasi-PQ facets, designed according to the top-down approach.

Finally, the designs proposed in case studies are characterized by high homogeneity of facets, i.e. regularity of shapes and dimensions.

8. Mechanical performance of doubly curved PQ shells

Previous considerations presented in this work were strictly geometric. However, one of the reasons for which doubly curved PQ grid shells are a subject of interest are their structural properties. In this chapter the mechanical performance of various grid shells based on parametrized forms of translational PQ mesh with planar, rectangular base described in section 4.1.2 is a subject of preliminary static analysis.

8.1. Parametrization of the form

Parametrized form of the translational PQ mesh with planar, rectangular base form depends on the position of the $P_e(a,b)$ extrapolating point. Parameters a and b correspond for its x and y coordinates, see Fig. 8.1.

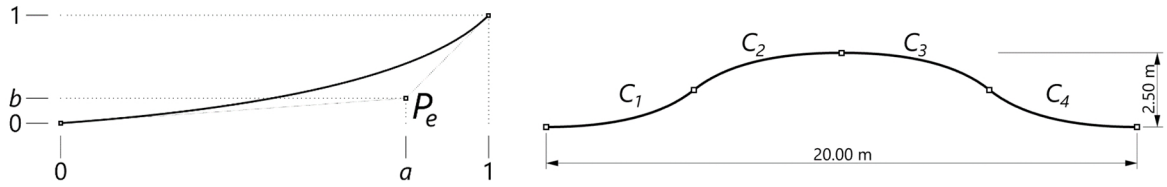

Fig. 8.1 Shape of a profile curve based on the parametrized position of P_e *extrapolating point.*

Examples of possible shapes of profile curves are shown in Fig. 8.2. When the value of parameter b is larger than 0, the profile curve has no curvature continuity in the middle (examples on the right side). If $a = b$ the obtained shape has pyramidal form. Note, that the profiles are anisotropically scaled along x direction in order to fit the profile curve into desired final dimensions, see Fig. 8.1, right.

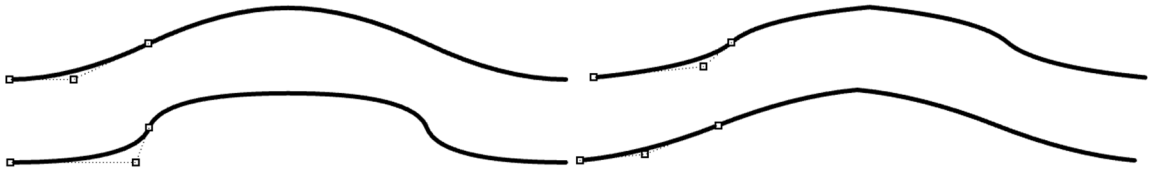

Fig. 8.2 Examples of possible profile curve shapes. For b = 0 *the curvature continuity is preserved (left), for other values of* b *the curvature continuity is broken in the middle of the profile curve (right).*

The space of possible solutions for the possible shapes over P_e parameters is presented in Fig. 8.3. Please note the part of the chart, where the curvilinear networks loose curvature continuity along diagonals and the highly deformed solutions. Also please note pyramidal shapes and doubly curved networks with curvature continuity.

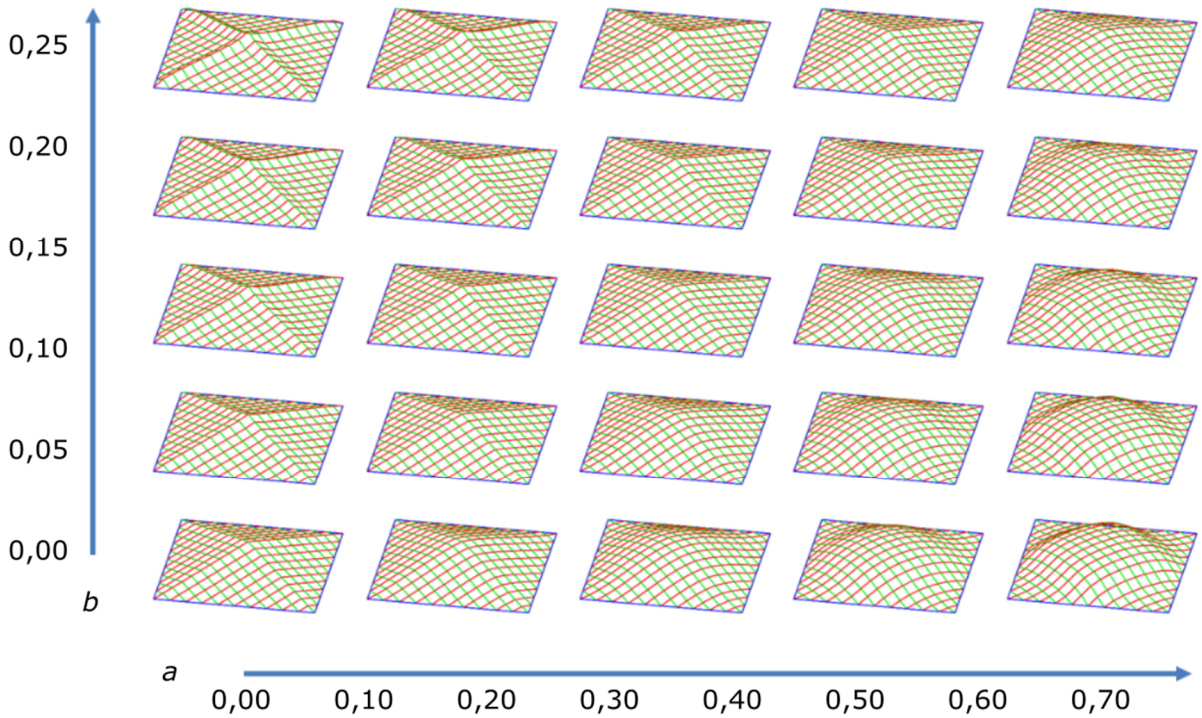

Fig. 8.3 Resultant shapes of PQ meshes depending of parameters a *and* b *or* P_e(a,b) *extrapolating point.*

8.2. Rating of mechanical performance

Initial structural efficiency evaluation of the generated lattice shell was carried out by means of FEM software Karamba (Preisinger 2013). The computational model assumed plane dimensions of the grid A×B = 14.14×14.14 m, the length of each rod in plane – 1.00 m and its cross section – aluminium RHS 100×50×4 mm. The height of the mesh[92] is *H* = 2.50 m. The self-weight of the grid was assumed as the loading. The analyses compared structural behaviour of different meshes generated with various combinations of parameters *a* and *b*. Results of the analyses are presented in the following tables:

- average node translations, see Table 8.1,
- maximal node translations, see Table 8.2,
- maximal axial forces, see Table 8.3,
- maximal bending moments, see Table 8.4,
- maximal shear forces, see Table 8.5.

The results of FEM analyses presented in tables are shown in numerical values and colours. Green colour mean lesser forces or smaller node translation. As seen for the maximal axial forces the best results are obtained for pyramidal shapes and for some combinations of parameters *a* and *b* that create doubly curved grid shells. However, node translations, shear and bending forces analysis prove the superiority of doubly curved shapes over the pyramidal ones. Figure 8.4 shows the value of translations of nodes by the intensity of pink colour. As seen, the parts of shell with less curvature tend to deform more.

[92] Tests were conducted also on meshes with various heights, resulting with three dimensional data sets, however for the value of *H* = 2.5 m, the resultant translations of nodes and forces in rods are the most characteristic.

Table 8.1 Average node translation [mm]

0,25	10,478	9,622	8,761	7,899	7,041	6,189	5,348	4,528	3,739	2,994	2,314	1,769	1,335	0,987	0,735
0,20	8,361	7,550	6,742	5,942	5,157	4,391	3,654	2,957	2,314	1,790	1,365	1,011	0,741	0,550	0,433
0,15	6,432	5,686	4,954	4,244	3,561	2,914	2,314	1,816	1,406	1,052	0,770	0,559	0,408	0,314	0,271
0,10	4,756	4,098	3,467	2,870	2,314	1,846	1,456	1,109	0,821	0,599	0,424	0,294	0,214	0,187	0,206
0,05	3,379	2,828	2,314	1,876	1,511	1,177	0,889	0,663	0,477	0,322	0,205	0,138	0,145	0,189	0,246
0,00	2,314	1,906	1,566	1,252	0,969	0,742	0,555	0,390	0,249	0,142	0,111	0,160	0,231	0,308	0,397
b / a	0,00	0,05	0,10	0,15	0,20	0,25	0,30	0,35	0,40	0,45	0,50	0,55	0,60	0,65	0,70

Table 8.2 Maximal node translation [mm]

0,25	24,213	22,857	21,449	19,984	18,451	16,844	15,158	13,394	11,565	9,691	7,815	6,117	4,521	3,110	1,991
0,20	20,544	19,142	17,687	16,174	14,600	12,966	11,277	9,550	7,815	6,243	4,743	3,370	2,215	1,394	1,100
0,15	16,915	15,494	14,029	12,521	10,974	9,399	7,815	6,379	4,991	3,683	2,525	1,586	1,008	0,815	0,748
0,10	13,487	12,095	10,680	9,250	7,815	6,517	5,252	4,031	2,904	1,949	1,171	0,716	0,550	0,493	0,480
0,05	10,413	9,112	7,815	6,648	5,508	4,391	3,326	2,416	1,618	0,947	0,500	0,326	0,322	0,446	0,732
0,00	7,815	6,765	5,745	4,738	3,758	2,894	2,117	1,413	0,816	0,354	0,343	0,453	0,702	1,121	1,727
b / a	0,00	0,05	0,10	0,15	0,20	0,25	0,30	0,35	0,40	0,45	0,50	0,55	0,60	0,65	0,70

Table 8.3 Maximal axial forces [kN]

0,25	1,027	0,904	0,814	0,725	0,623	0,520	0,514	0,502	0,481	0,487	0,519	0,558	0,579	0,572	0,532
0,20	0,781	0,694	0,595	0,489	0,485	0,476	0,474	0,488	0,519	0,546	0,562	0,558	0,529	0,495	0,580
0,15	0,561	0,470	0,467	0,471	0,478	0,498	0,519	0,537	0,548	0,547	0,527	0,494	0,524	0,631	0,763
0,10	0,470	0,478	0,490	0,505	0,519	0,531	0,538	0,538	0,525	0,496	0,485	0,549	0,651	0,777	0,922
0,05	0,499	0,510	0,519	0,526	0,531	0,530	0,522	0,504	0,482	0,481	0,551	0,642	0,755	0,888	1,038
0,00	0,519	0,523	0,525	0,524	0,519	0,507	0,486	0,474	0,476	0,536	0,613	0,735	0,875	1,023	1,172
b / a	0,00	0,05	0,10	0,15	0,20	0,25	0,30	0,35	0,40	0,45	0,50	0,55	0,60	0,65	0,70

Table 8.4 Maximal bending moments [kNm]

0,25	0,201	0,192	0,183	0,173	0,162	0,153	0,145	0,136	0,127	0,116	0,105	0,093	0,080	0,067	0,058
0,20	0,180	0,172	0,165	0,157	0,149	0,139	0,128	0,117	0,105	0,093	0,080	0,066	0,056	0,048	0,045
0,15	0,168	0,160	0,151	0,141	0,130	0,118	0,105	0,092	0,079	0,066	0,054	0,045	0,039	0,037	0,035
0,10	0,152	0,142	0,131	0,118	0,105	0,092	0,079	0,065	0,052	0,043	0,035	0,029	0,026	0,024	0,022
0,05	0,131	0,118	0,105	0,092	0,078	0,065	0,052	0,041	0,032	0,024	0,019	0,015	0,011	0,009	0,013
0,00	0,105	0,092	0,079	0,065	0,052	0,040	0,030	0,021	0,013	0,007	0,006	0,007	0,011	0,015	0,019
b / a	0,00	0,05	0,10	0,15	0,20	0,25	0,30	0,35	0,40	0,45	0,50	0,55	0,60	0,65	0,70

Table 8.5 Maximal shear forces [kN]

0,25	0,281	0,259	0,237	0,214	0,193	0,173	0,153	0,134	0,119	0,110	0,101	0,092	0,082	0,076	0,070
0,20	0,227	0,208	0,190	0,171	0,153	0,136	0,123	0,112	0,101	0,090	0,080	0,072	0,066	0,062	0,063
0,15	0,187	0,171	0,154	0,139	0,126	0,113	0,101	0,089	0,078	0,069	0,062	0,055	0,054	0,054	0,054
0,10	0,154	0,142	0,128	0,114	0,101	0,088	0,075	0,065	0,056	0,049	0,045	0,043	0,041	0,040	0,039
0,05	0,130	0,115	0,101	0,087	0,073	0,061	0,051	0,043	0,036	0,032	0,029	0,026	0,024	0,023	0,026
0,00	0,101	0,086	0,071	0,058	0,047	0,041	0,035	0,028	0,021	0,015	0,017	0,018	0,022	0,027	0,033
b / a	0,00	0,05	0,10	0,15	0,20	0,25	0,30	0,35	0,40	0,45	0,50	0,55	0,60	0,65	0,70

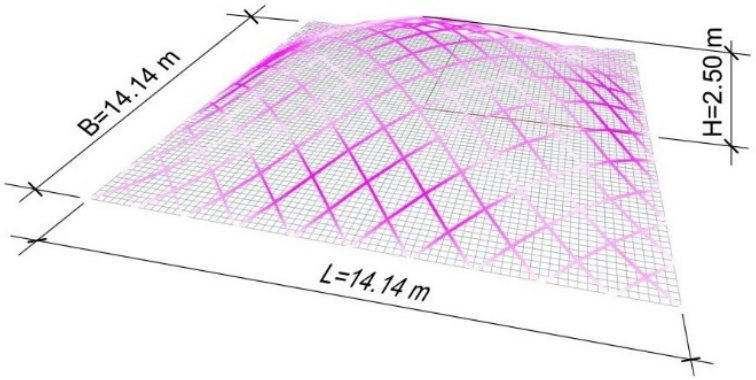

Fig. 8.4 Translations of the nodes shown by the vivid colour.
Greater translations were obtained for the parts of lattice shell with smaller curvatures.

This abbreviated and simplified evaluation of the mechanical properties of the exemplary freeform PQ grid shell justifies the assessment that in these structures both the distribution of internal forces and global deformations are consistent with predictions based on analogy to continuous shell structures. Thanks to the parameterization of the structure, further optimization is possible. One of the possibilities is to choose the shape-generating curves, e.g. by applying *elasticas*, to obtain grid shells with a considerable uniformity of rods effort (Święciak and Tarczewski 2017).

9. Conclusions

The research that was carried out during the preparation of this dissertation allowed to verify theses put forward at the beginning of the work in the falsifiability process. These theses have been proved. All research objectives set out in Chapter 1 have been also accomplished.

9.1. Proven theses of the dissertation

9.1.1. Thesis 1

Analyses of objects representative to the trend of free-form design carried out in the dissertation allowed to follow through the application of free forms in completed objects and define the functions most frequently assigned to them. These are primarily elements of objects that define their visual perception, such as building facades (often in the form of a second skin) and roofing of whole objects or parts thereof, especially courtyard roofs, entrance canopies, etc. A special place among them have grid shells, which on the one hand allow to achieve structural efficiency, and on the other hand provide additional possibilities of shaping the form with transparent fillings. The catalogue of objects that systematize data about them, included in the appendix A-3 to the work, proved to be helpful in drawing conclusions. On the basis of the analysed data on theses 1, it can be concluded that:

> **Among the free formed objects, grid shells occupy a particularly important place and constitute one of the most important groups of structures within this trend. Because they allow to obtain forms with significant spans, they are clearly light, and through large glazing, they are clearly visible, they have become the most frequently implemented objects in this group. These features enabled widespread social acceptance of these new geometric forms, contributing to a large extent to disseminating the freedom of shaping forms in architecture.**

9.1.2. Thesis 2

The analysis of various solutions, taking into account topology, geometry, construction and materials, allowed to state that grid shells whose glass panels are triangular are those that are most often designed and constructed. This solution allows to obtain a smooth mesh on almost any surface, while providing the necessary rigidity of the structure. Grids with such topology are relatively easy to design and can be inscribed in almost any closed contour. Triangular panels defined by grid edges (bars) are always flat. Computer tools for designing such grids are available.

At the same time, many disadvantages of this solution have been discovered. The most important is the complex construction of nodes in whose construction up to six rods are connected. The total number of rods and the roof area occupied by them is also much larger. The triangular glass panels are also smaller. These negative features do not appear in grids of quadrilateral topology. The number of rods connected in one node of such a grid is four, and the relative number of rods is smaller. The visual perception of such structures is much more beneficial. In some respects, they also exhibit more favourable mechanical properties. An important limitation in the design of grids with a quadrilateral topology is the fact that the panels in such a grid are not always flat. For this reason, it is necessary to limit their diversity to a planar quadrilateral (PQ) topology. However, there are limitations in the use of this topology, because it cannot be applied to any previously defined surface. At present, there are no tools available for the design of meshes with such a topology. According to the thesis 2, it can be concluded that:

Among the implemented objects, in which glazed grid shells were applied, structures with a triangular topology dominate. Currently, however, more and more objects are being created with the PQ topology. Although it is more difficult to obtain a grid with PQ topology in the design process, it has many advantages over the triangular topology.

9.1.3. Thesis 3

The dissertation includes a wide description of known methods of shaping PQ grids on free surfaces. These include both those methods already used in practice and those methods that are still theoretical solutions. They have a different range of applications, as well as various advantages and disadvantages. In addition, known methods of transforming of such grids which maintain the planarity of their panels after transformation were analysed. Both the methods of creating grids and the methods of their transformation refer to the methods of discrete geometry.

The results of the research allowed to formulate the author's own original methods of generating PQ grids and methods of their transformation. These methods allow to significantly increase the range of PQ grids' applications. In addition, it was noticed that many restrictions on the use of these grids result from the adopted design methodology, which is described as "top-down". This consists in adapting the mesh to the previously determined free surface. In this approach, many geometric forms of coatings are excluded from the possibility of using PQ divisions. This problem was essentially solved by changing the design methodology to "bottom-up". This consists in generating an output grid with the desired features and then its transformation in order to obtain sufficient compliance with the assumed final surface. According to the thesis 3, it can be concluded that:

By developing appropriate methods for generating and transforming PQ grids and applying bottom-up methodology, they can be effectively designed for various boundary conditions.

9.1.4. Thesis 4

As part of the research, simulations and computer modelling were performed to examine the scope of available PQ mesh forms using known and proposed methods according to the bottom-up methodology. Two case studies proved to be particularly useful, involving designing glazed canopies over internal courtyards in two existing facilities. The analyses carried out showed that the scope of PQ mesh formation is very large and it is possible to adapt them to almost every design situation as well as for triangular-shaped meshes. The condition that enables this is the design in accordance with the bottom-up methodology. Accepting the desired base surface a priori may prevent, and in most cases does prevent, the use of PQ meshes. By transforming, while maintaining the planarity of panels, the initially generated, simple PQ mesh in such a way that it is finally as close as possible to the desired surface, satisfactory architectural results can be obtained. According to the thesis 4, it can be concluded that:

The proposed bottom-up design methodology together with the appropriate tools for generating and transforming PQ grids allows to design PQ grid shells for any design situation, with a small and acceptable limitation of the designer's freedom to shape the general form of such a grid shell.

9.2. Contribution to the field

Freeforms are more and more commonly used in architecture, among them the dominant group are grid shells with transparent filling. For such structures, meshes of bars with the PQ topology are in many respects more favourable than the meshes of bars with a triangular topology. At the same time, however, there were no effective methods for shaping such meshes, allowing their practical application for various boundary conditions.

The design tools proposed in the work and the design methodology based on them allow to definitely extend the scope of using PQ grids in free-form objects. Based on them, practical problems with a high degree of difficulty can be solved.

Considering the number of existing and proposed methods of creating and transforming PQ grids, it is possible to create many scenarios and design tools adequate to the existing design conditions, such as the shape of a courtyard, but also the desired shape of a building's or stadium's facade. The nine methods presented for creating PQ grids can be combined with five methods of their transformation, and two, three, four or five methods can also be used among the transformation methods in a given design tool. The set of five transformation methods gives 32 subsets of their sets, and after multiplying by nine the methods of creating PQ grids, it gives 288 different design tools, each of which includes the method of creating and transforming grids, leading to specific results and giving control over the form of the designed structure.

Additionally, the concept of the PQ mesh design tool presented in the paper provides four auxiliary initial and final transformations that do not eliminate the facets' planarity. Auxiliary transformations can be used in parallel with the basic ones and they are parameterized, additionally increasing the design freedom.

Indirectly, the application of the proposed solutions to design and construct glazed roofs allow for the creation of additional usable spaces within existing buildings, as well as the creation of buffer zones that increase the energy efficiency of buildings. In contrast to the majority of existing solutions for shaping triangular and PQ grid shells, whose accuracy allow for use only in newly designed buildings where the roof form can be coordinated with the form of the building, or in existing buildings' courtyards with shapes, the proposed tools allow for an absolute accuracy of adjusting the form of the PQ grid to the existing, irregular shape of the courtyard. These situations occur especially in the case of historical city centres, in which buildings often have irregular forms and it is not possible to change these conditions by rebuilding them and where, on the other hand, the high building density requires searching for other ways of obtaining additional usable areas.

However, it is also possible to use the proposed tools and methods for shaping PQ grid shells for newly designed objects. By the diversity of available combinations of methods of creating and transforming PQ grids, existing and proposed by the author, consistent with the proposed design tool concept, a wide spectrum of geometrically correct PQ morphologies is available – including glass roofs with other irregular base perimeters, facades and domes. The work also presents the concept of applying both the proposed methods of transformation, i.e. SC and the prospective transformation in order to obtain a PQ grid form with a contour consisting of sections of conic curves, i.e. second degree NURBS curves. This provides a tool for the design of canopies over courtyards with particularly complex perimeters and constraints related to the shape and height of the surrounding walls.

10. Bibliography

Adriaenssens, S., P. Block, D. Veenendaal, and Chris Williams, eds. 2014. *Shell Structures for Architecture: Form Finding and Optimization*. London: Routledge.

Aguilón, François de. 1613. *Opticorum libri sex: philosophiis juxtà ac mathematicis utiles*. http://archive.org/details/opticorumlibrise00agui.

Atauz, Ayse Devrim. 2005. 'Trade, Piracy, and Naval Warfare in the Central Mediterranean: The Maritime History and Archaeology of Malta'. PhD diss., Texas A&M University. http://oaktrust.library.tamu.edu/handle/1969.1/437.

Bagneris, Marine, Bernard Maurin, Alain Marty, and René Motro. 2007. 'Pascalian Forms for Non Standard Architectural Shape Generation'. *IASS Symposium 2007*.

Baldassini, Niccolo. 2008. 'Glazing Technology: The Hidden Side of Freeform Design'. In *Advances in Architectural Geometry 2008*, edited by Helmut Pottmann, Axel Kilian, and Michael Hofer, 41–44. Vienna.

Baldassini, Niccolo, Helmut Pottmann, Jacques Raynaud, and Alexander Schiftner. 2010. 'New Strategies and Developments in Transparent Free-Form Design: From Facetted to Nearly Smooth Envelopes'. *International Journal of Space Structures* 25 (3): 185–97. https://doi.org/10.1260/0266-3511.25.3.185.

Barr, Alan H. 1987. 'Global and Local Deformations of Solid Primitives'. In *Readings in Computer Vision: Issues, Problem, Principles, and Paradigms*, edited by Martin A. Fischler and Oscar Firschein, 661–70. San Francisco: Morgan Kaufmann. https://doi.org/10.1016/B978-0-08-051581-6.50064-7.

Bazylev, V.T. 2002. 'Chebyshev Net'. In *Encyclopedia of Mathematics*. Kluwer Academic Publishers. http://www.encyclopediaofmath.org/index.php?title=Chebyshev_net&oldid=17668.

Bernoulli, Jakob. 1694. 'Curvatura Laminae Elasticae'. *Acta Eruditorum* 13: 262–276.

Block, Philippe, and John Ochsendorf. 2007. 'Thrust Network Analysis: A New Methodology for Three-Dimensional Equilibrium'. *Journal of the International Association for Shell and Spatial Structures* 48 (3): 167–73.

Blomgren, Robert M., and David J. Kasik. 2002. 'Early Investigation, Formulation and Use of NURBS at Boeing'. *ACM SIGGRAPH Computer Graphics* 36 (3): 29–34.

Bobenko, Alexander. 1999. 'Discrete Conformal Maps and Surfaces'. In *Symmetries and Integrability of Difference Equations*, edited by Peter A. Clarkson and Frank W. Nijhoff, 255:97–108. London Mathematical Society Lecture Note Series. Cambridge: Cambridge University Press. https://doi.org/10.1017/CBO9780511569432.009.

Bobenko, Alexander I., Tim Hoffmann, and Boris A. Springborn. 2006. 'Minimal Surfaces from Circle Patterns: Geometry from Combinatorics'. *Annals of Mathematics*, Second Series, 164 (1): 231–264.

Bobenko, Alexander I., Helmut Pottmann, and Johannes Wallner. 2010. 'A Curvature Theory for Discrete Surfaces Based on Mesh Parallelity'. *Mathematische Annalen* 348 (1): 1–24. https://doi.org/10.1007/s00208-009-0467-9.

Bobenko, Alexander I., John M. Sullivan, Peter Schröder, and Günter M. Ziegler, eds. 2008. *Discrete Differential Geometry*. Vol. 38. DMV Seminar. Basel, Boston, Berlin: Birkhäuser Verlag. https://doi.org/10.1007/978-3-7643-8621-4.

Bobenko, Alexander I., and Yuri B. Suris. 2008. *Discrete Differential Geometry. Integrable Structure*. Vol. 98. Graduate Studies in Mathematics. American Mathematical Society.

Bobenko, Alexander I., and Yury B. Suris. 2007. 'On Organizing Principles of Discrete Differential Geometry. Geometry of Spheres'. *Russian Mathematical Surveys* 62 (1): 1–43. https://doi.org/0.1070/RM2007v062n01ABEH004380.

Bobenko, Alexander, and Ulrich Pinkall. 1996. 'Discrete Isothermic Surfaces'. Edited by Rainer Weissauer, Daniel Huybrechts, Hwang Jun-Muk, and Geordie Williamson. *Journal Für Die Reine*

Und Angewandte Mathematik, Crelles Journal, 1996 (475): 187–208. https://doi.org/10.1515/crll.1996.475.187.

Bobenko, Alexander, and Boris Springborn. 2004. 'Variational Principles for Circle Patterns and Koebe's Theorem'. *Transactions of the American Mathematical Society* 356 (2): 659–689. https://doi.org/10.1090/S0002-9947-03-03239-2.

Bradley, Thomas. 1834. *Okładka Practical Geometry, Linear Perspective, and Projection: Including Isometrical Perspective, Projections of the Sphere, and the Projection of Shadows, with Descriptions of the Principal Instruments Used in Geometrical Drawing, &c. ... For the Use of Artists, Architects ... &c*. London: Baldwin and Cradock.

Carter, Robert. 2006. 'Boat Remains and Maritime Trade in the Persian Gulf during the Sixth and Fifth Millennia BC'. *Antiquity* 80 (307): 52–63. https://doi.org/10.1017/S0003598X0009325X.

Catmull, Edwin E., and James H. Clark. 1978. 'Recursively Generated B-Spline Surfaces on Arbitrary Topological Meshes'. *Computer-Aided Design* 10 (6): 350–55. https://doi.org/10.1016/0010-4485(78)90110-0.

Chopine, Ami. 2011. *3D Art Essentials: The Fundamentals of 3D Modeling, Texturing, and Animation*. 1st Edition. Burlington: Focal Press. http://www.crcnetbase.com/isbn/9781136132223.

Cui, Chengwu, Hiroshi Ohmori, and Masaru Sasaki. 2003. 'Computational Morphogenesis of 3D Structures by Extended ESO Method'. *Journal of the International Association for Shell and Spatial Structures* 44 (1): 51–61.

Cutler, Barbara, and Emily Whiting. 2007. 'Constrained Planar Remeshing for Architecture'. In *Proceedings of Graphics Interface 2007*, edited by Christopher G. Healey and Edward Lank, 11–18. Montréal: Canadian Human-Computer Communications Society. https://doi.org/10.1145/1268517.1268522.

Della Francesca, Piero. 1474. *De Prospectiva Pingendi O Perspektywie w Malarstwie*. Edited by Ryszard Mirek. Translated by Zofia Maria Siwecka. Kraków: Universitas.

Desbrun, Mathieu, Eitan Grinspun, Konrad Polthier, Peter Schröder, and Ari Stern. 2006. 'Discrete Differential Geometry: An Applied Introduction'. *ACM SIGGRAPH Course*. https://doi.org/10.1145/1198555.1198660.

DETAIL. 1991. 'Innenhofüberdachung Des Museums Für Hamburgische Geschichte, Hamburg', 1991.

Ding, Hui, and Yao-Zhi Luo. 2013. 'A New Method of Generating Grids on Free-Form Surfaces'. In *Proceedings of IASS 2013: 'Beyond the Limits of Man'*, edited by Jan Bogdan Obrębski and Romuald Tarczewski. Structural Morphology 2: Graphical Statics, Grid Shells. Wrocław. https://www.ingentaconnect.com/content/iass/piass/2013/00002013/00000011/art00004.

Donofrio, Mark. 2016. 'Topology Optimization and Advanced Manufacturing as a Means for the Design of Sustainable Building Components'. *Procedia Engineering* 145: 638–45. https://doi.org/10.1016/j.proeng.2016.04.054.

Douthe, Cyril, Romain Mesnil, Hugo Orts, and Olivier Baverel. 2016. 'New Shapes for Elastic Gridshells Covered by Planar Facets'. In *IASS 2016 Tokyo Symposium: Spatial Structures in the 21st Century*, edited by Ken'ichi Kawaguchi, Makoto Ohsaki, and Toru Takeuchi. Tokyo. https://www.ingentaconnect.com/content/iass/piass/2016/00002016/00000016/art00006.

Eigensatz, Michael, Mario Deuss, Alexander Schiftner, Martin Kilian, Niloy J. Mitra, Helmut Pottmann, and Mark Pauly. 2010. 'Case Studies in Cost-Optimized Paneling of Architectural Freeform Surfaces'. In *Advances in Architectural Geometry 2010*, edited by Cristiano Ceccato, Lars Hesselgren, Mark Pauly, Helmut Pottmann, and Johannes Wallner, 49–72. Vienna: Springer Vienna.

Eisenbach, Philipp, Ragunath Vasudevan, Manfred Grohmann, Klaus Bollinger, and Stephan Hauser. 2014. 'Parapluie - Ultra Thin Concrete Shell Made of UHPC By Activating Membrane Effects'. *Journal of the International Association for Shell and Spatial Structures* 55 (4): 201–12.

Enrique Monzó, Lluís, and Joseph Schwartz. 2017. 'Design of CASTonCAST Shell Structures Based on Load Path Network Method'. *International Journal of Space Structures* 32 (3–4): 216–25. https://doi.org/10.1177/0266351117736650.

Estrada, Giovani, and Niccolò Baldassini. 2013. 'Form-Finding and Planarisation of Glass Domes with Quad Elements'. In *Proceedings of IASS 2013: 'Beyond the Limits of Man'*, edited by Jan Bogdan Obrębski and Romuald Tarczewski. Metal Spatial Structures 1: Buckling and Realization. Wrocław.

Ferenc, Marcin. 2013. 'Muzeum Historii Żydów Polskich'. *Architektura Murator*, no. 6: 38–61.

Foley, James D., Andries van Dam, Steven K. Feiner, and John F. Hughes. 1995. *Computer Graphics Principles and Practice*. Second Edition. The Systems Programming Series. Massachusetts: Addison-Wesley Publishing Company.

Gallier, Jean. 2011. 'Basics of Affine Geometry'. In *Geometric Methods and Applications For Computer Science and Engineering*, 7–63. New York: Springer.

Garrison, Ervan G. 1998. *History of Engineering and Technology: Artful Methods*. 2nd Edition. CRC Press.

Gidófalvy, Kitti, Levente Katula, and Huihuan Ma. 2016. 'Free-Form Grid Shell Structures on Rectangular Plan with Semi-Rigid Socket Joints'. *Journal of the International Association for Shell and Spatial Structures* 57 (4): 295–306. https://doi.org/10.20898/j.iass.2016.190.790.

Glymph, James, Dennis Shelden, Cristiano Ceccato, Judith Mussel, and Hans Schober. 2004. 'A Parametric Strategy for Free-Form Glass Structures Using Quadrilateral Planar Facets'. *Automation in Construction* 13 (2): 187–202. https://doi.org/10.1016/j.autcon.2003.09.008.

Golay, Pascal, Jerry Hambly, and Mary Fugier. 2014. *Rhinoceros v5.0, Level 2, Training Manual*. Robert McNeel & Associates.

Gonzales-Pulido, Francisco, Pablo Vaggione, and Laura A. Ackley. 2002. 'Managing the Construction of the Museo Guggenheim Bilbao (B)'. Student research. Center for Design Informatics, Harvard Design School. http://www.uniroma2.it/didattica/ACALAB2/deposito/case_Guggenheim.pdf.

Goss, Victor Geoffrey Alan. 2003. 'Snap Buckling, Writhing and Loop Formation in Twisted Rods'. PhD diss., London: Center for Nonlinear Dynamics University College London.

Grandine, Thomas A. 2005. 'The Extensive Use of Splines at Boeing'. *SIAM News* 38 (4): 3–6.

Hambleton, Daniel, Crispin Howes, Jonathan Hendricks, John Kooymans, and Halcrow Yolles. 2009. 'Study of Panelization Techniques to Inform Freeform Architecture'. In *Glass Performance Days: Professionals, Products, Processing*, 239–43. Tampere.

Hambleton, Daniel, and Elissa Ross. 2015. 'Exact Face-Offsetting for Polygonal Meshes'. In *Proceedings of the 35th Annual Conference of the Association for Computer Aided Design in Architecture (ACADIA)*, edited by Lonn Combs and Chris Perry, 203–9. Computational Ecologies: Design in the Anthropocene. Cincinnati.

Handy, Richard L. 1973. 'The Igloo and the Natural Bridge as Ultimate Structures'. *Arctic* 26 (4): 276–81.

Hassel, Joshua V. 2016. *Frei Otto - Spanning the Future*. Documentary film.

Helbig, Thorsten, Laurent Giampellegrini, and Matthias Oppe. 2014. '"Carioca Wave" – A free-form steel-and-glass canopy in Rio de Janeiro, Brazil'. *Steel Construction* 7 (4): 252–57. https://doi.org/10.1002/stco.201420033.

Helbig, Thorsten, Jochen Riederer, Florian Kamp, and Matthias Oppe. 2016. 'Free-Form on Every Scale - "Tornado" Roof Structure for Bory Mall, Bratislava, Slovakia'. *Steel Construction* 9 (3): 249–54. https://doi.org/10.1002/stco.201620031.

Hicks, Jim. 1966. 'Close-Up/Piet Hein Bestrides Art and Science'. *LIFE Magazine*, 14 October 1966.

Howarth, Richard. 1996. 'History of the Stereographic Projection and Its Early Use in Geology'. *Terra Nova* 8 (6): 499–513. https://doi.org/10.1111/j.1365-3121.1996.tb00779.x.

Huzefa, Ali. 2013. *Rationalisation of Freeform Glass Façades from Concept to Construction, MSc Dissertation*. University of Bath, Bath, UK.

Jiang, Cagui, Felix Günther, Johannes Wallner, and Helmut Pottmann. 2016. 'Measuring and Controlling Fairness of Triangulations'. In *Advances in Architectural Geometry 2016*, edited by Sigrid Adriaenssens, Fabio Gramazio, Matthias Kohler, Achim Menges, and Mark Pauly, 24–39. Zurich. https://doi.org/10.3218/3778-4.

Jiang, Caigui, Chengcheng Tang, Marko Tomičí, Johannes Wallner, and Helmut Pottmann. 2014. 'Interactive Modeling of Architectural Freeform Structures: Combining Geometry with Fabrication and Statics'. In *Advances in Architectural Geometry 2014*, edited by Philippe Block, Jan Knippers, Niloy J. Mitra, and Wenping Wang, 95–108. Interactive Modeling – Combining Geometry with Fabrication and Statics. London: Springer International Publishing. https://doi.org/10.1007/978-3-319-11418-7.

Jiang, Caigui, Jun Wang, Johannes Wallner, and Helmut Pottmann. 2014. 'Freeform Honeycomb Structures'. Edited by Bedrich Benes and Min Chen. *Computer Graphics Forum* 33 (5): 185–94. https://doi.org/10.1111/cgf.12444.

Krieg, Oliver David, Tobias Schwinn, Achim Menges, Jian-Min Li, Jan Knippers, Annette Schmitt, and Volker Schwieger. 2014. 'Biomimetic Lightweight Timber Plate Shells: Computational Integration of Robotic Fabrication, Architectural Geometry and Structural Design'. In *Advances in Architectural Geometry 2014*, edited by Philippe Block, Jan Knippers, Niloy J. Mitra, and Wenping Wang, 109–125. London: Springer International Publishing.

La Magna, Riccardo, Simon Schleicher, and Jan Knippers. 2016. 'Bending-Active Plates'. In *Advances in Architectural Geometry 2016*, edited by Sigrid Adriaenssens, Fabio Gramazio, Matthias Kohler, Achim Menges, and Mark Pauly, 170–187. Zurich. https://doi.org/10.3218/3778-4.

Lachlan, Robert. 1893. *An Elementary Treatise on Modern Pure Geometry, Chapter XIV: The Theory of Inversion*. London: Macmillan and Company.

Li, Jian-Min, and Jan Knippers. 2015. 'Pattern and Form - Their Influence on Segmental Plate Shells'. In *Proceedings of the International Association for Shell and Spatial Structures (IASS) Symposium 2015: Future Visions*, edited by Jeroen Coenders, Andrew Borgart, and Arno Pronk. Amsterdam.

Li, Yufei, Yang Liu, and Wenping Wang. 2015. 'Planar Hexagonal Meshing for Architecture'. *IEEE Transactions on Visualization and Computer Graphics* 21 (1): 95–106. https://doi.org/10.1109/TVCG.2014.2322367.

Lienhard, Julian. 2014. 'Bending-Active Structures: Form-Finding Strategies Using Elastic Deformation in Static and Kinetic Systems and the Structural Potentials Therein'. PhD diss., Stuttgart: Institut für Tragkonstruktionen und Konstruktives Entwerfen der Universität Stuttgart. http://dx.doi.org/10.18419/opus-107.

Liming, Roy A. 1944. *Practical Analytic Geometry with Applications to Aircraft*. New York: Macmillan. http://hdl.handle.net/2027/wu.89090517988.

Linkwitz, K., H.-J. Schek, and Lothar Gründig. 1974. 'Die Gleichgewichtsberechnung von Seilnetzen Unter Zusatzbedingungen'. *Ingenieur-Archiv* 43 (4): 183–92.

Liu, Yang, Helmut Pottmann, Johannes Wallner, Yong-Liang Yang, and Wenping Wang. 2006. 'Geometric Modeling with Conical Meshes and Developable Surfaces'. *ACM Transactions on Graphics* 25 (3): 681–89.

Liu, Yang, and Wenping Wang. 2008. 'On Vertex Offsets of Polyhedral Surfaces'. In *Advances in Architectural Geometry 2008*, edited by Helmut Pottmann, Axel Kilian, and Michael Hofer, 61–64. Vienna.

Livingston, Clifton W. 1961. 'The Natural Arch, the Fracture Pattern, and the Sequence of Failure in Massive Rocks Surrounding an Underground Opening'. In *The 4th US Symposium on Rock Mechanics (USRMS)*. University Park, Pennsylvania: American Rock Mechanics Association.

Majowiecki, Massimo. 2007. 'Ethics and Structural Reliability in Free-Form Design (FFD)'. *Journal of the International Association for Shell and Spatial Structures* 48 (4): 29–50.

———. 2013. 'Personal Experiences in Structural Architecture: From Form Finding to Free Form Design'. In *Proceedings of IASS 2013: 'Beyond the Limits of Man'*, edited by Jan Bogdan Obrębski and Romuald Tarczewski. Wrocław.

Masson, Yannick, and Laurent Monasse. 2017. 'Existence of Global Chebyshev Nets on Surfaces of Absolute Gaussian Curvature Less than 2π'. *Journal of Geometry* 108 (1): 25–32. https://doi.org/10.1007/s00022-016-0319-1.

Mazzotti, Angelo Alessandro. 2014. 'What Borromini Might Have Known about Ovals. Ruler and Compass Constructions'. *Nexus Network Journal* 16 (2): 389–415. https://doi.org/10.1007/s00004-014-0190-z.

Menard, Raphaël, Etienne Fayette, and Paul Azzopardi. 2013. 'Approximating a Funicular Shape with a Translational Surface, Example of a Glass Canopy'. In *Proceedings of IASS 2013: 'Beyond the Limits of Man'*, edited by Jan Bogdan Obrębski and Romuald Tarczewski. Metal Spatial Structures 1: Buckling and Realization. Wrocław.

Mesnil, Romain. 2017. 'Structural Explorations of Fabrication-Aware Design Spaces for Non-Standard Architecture'. PhD diss., Paris: Université Paris-Est. https://hal-enpc.archives-ouvertes.fr/tel-01510053/document.

Mesnil, Romain, Cyril Douthe, Olivier Baverel, and Bruno Léger. 2015. 'Möbius Geometry and Cyclidic Nets: A Framework for Complex Shape Generation'. In *Proceedings of the International Association for Shell and Spatial Structures (IASS) Symposium 2015: Future Visions*, edited by Jeroen Coenders, Andrew Borgart, and Arno Pronk. Amsterdam.

———. 2016. 'Marionette Mesh: From Descriptive Geometry to Fabrication-Aware Design'. In *Advances in Architectural Geometry 2016*, edited by Sigrid Adriaenssens, Fabio Gramazio, Matthias Kohler, Achim Menges, and Mark Pauly, 62–81. Zurich. https://doi.org/10.3218/3778-4.

———. 2017. 'Generalised Cyclidic Nets for Shape Modelling in Architecture'. *International Journal of Architectural Computing* 15 (2): 148–68. https://doi.org/10.1177/1478077117714917.

Mesnil, Romain, Cyril Douthe, Olivier Baverel, Bruno Léger, and Jean-François Caron. 2015. 'Isogonal Moulding Surfaces: A Family of Shapes for High Node Congruence in Free-Form Structures'. *Automation in Construction* 59 (November): 38–47. http://dx.doi.org/10.1016/j.autcon.2015.07.009.

Mesnil, Romain, Yann Santerre, Cyril Douthe, Olivier Baverel, and Bruno Leger. 2015. 'Generating High Node Congruence in Freeform Structures with Monge's Surfaces'. In *Proceedings of the International Association for Shell and Spatial Structures (IASS) Symposium 2015: Future Visions*, edited by Jeroen Coenders, Andrew Borgart, and Arno Pronk. Amsterdam.

Mortenson, Michael E. 1999. *Mathematics for Computer Graphics Applications*. New York: Industrial Press Inc.

Murray, Peter. 2003. *The Saga of Sydney Opera House: The Dramatic Story of the Design and Construction of the Icon of Modern Australia*. London: Routledge.

Niezabitowska, Elżbieta. 2014. *Metody i Techniki Badawcze w Architekturze*. Gliwice: Wydawnictwo Politechniki Śląskiej.

Nowacki, Horst. 2006. 'Developments in Fluid Mechanics Theory and Ship Design before Trafalgar'. In *Technology of the Ships of Trafalgar: Proceedings of an International Congress Held at the Escuela Técnica Superior de Ingenieros Navales*, edited by Francisco Fernández-González, Larrie D. Ferreiro, and Horst Nowacki. Madrid: ETSI Navales.

Ochsenschlager, Edward. 1998. 'Life on the edge of the marshes', Expedition: The magazine of the University of Pennsylvania, 40 (2): 29–39.

Olaberria, Juan-Pablo. 2014. 'The Conception of Hull Shape by Shell-Builders in the Ancient Mediterranean'. *International Journal of Nautical Archaeology* 43 (2): 351–68. https://doi.org/10.1111/1095-9270.12068.

Oosterhuis, Kas. 2016. 'Parametric Design Is Not a Style'. *Kas Oosterhuis: Observations Opinions Innovations* (blog). 1 December 2016. http://www.oosterhuis.nl/?p=145.

Parekh, Ranjan. 2006. *Principles of Multimedia*. New Delhi: Tata McGraw-Hill.

Petroski, Henry. 1998. 'Engineering: Bilbao'. *American Scientist* 86 (4): 320–25.

Pottmann, Helmut, Andreas Asperl, Michael Hofer, and Axel Kilian. 2007. *Architectural Geometry*. Edited by Daril Bentley. Exton, Pennsylvania: Bentley Institute Press.

Pottmann, Helmut, Sigrid Brell-Cokcan, and Johannes Wallner. 2007. 'Discrete Surfaces for Architectural Design'. In *Curve and Surface Design: Avignon 2006*, edited by Patrick Chenin, Tom Lyche, and Larry L. Schumaker, 213–34. Avignon: Nashboro Press.

Pottmann, Helmut, Michael Eigensatz, Amir Vaxman, and Johannes Wallner. 2015. 'Architectural Geometry'. *Computers & Graphics* 47 (April): 145–64. https://doi.org/10.1016/j.cag.2014.11.002.

Pottmann, Helmut, Philipp Grohs, and Bernhard Blaschitz. 2010. 'Edge Offset Meshes in Laguerre Geometry'. *Advances in Computational Mathematics* 33 (1): 45–73. https://doi.org/10.1007/s10444-009-9119-6.

Pottmann, Helmut, Caigui Jiang, Mathias Höbinger, Jun Wang, Philippe Bompas, and Johannes Wallner. 2015. 'Cell Packing Structures'. *Computer-Aided Design* 60: 70–83. https://doi.org/10.1016/j.cad.2014.02.009.

Pottmann, Helmut, Yang Liu, Johannes Wallner, Alexander Bobenko, and Wenping Wang. 2007. 'Geometry of Multi-Layer Freeform Structures for Architecture'. *ACM Transactions on Graphics* 26 (3): Article No. 65. https://doi.org/10.1145/1276377.1276458.

Pottmann, Helmut, Alexander Schiftner, and Johannes Wallner. 2008. 'Geometry of Architectural Freeform Structures'. In *Proceedings of the 2008 ACM Symposium on Solid and Physical Modeling*, edited by Eric Haines and Morgan McGuire, 15–28. Stony Brook, New York. https://doi.org/10.1145/1364901.1364903.

Pottmann, Helmut, and Johannes Wallner. 2008. 'The Focal Geometry of Circular and Conical Meshes'. *Advances in Computational Mathematics* 29 (3): 249–268. https://doi.org/10.1007/s10444-007-9045-4.

———. 2016. 'Geometry and Freeform Architecture'. In *Mathematics and Society*, edited by Wolfgang König, 131–51. Zürich: European Mathematical Society Publishing House. https://doi.org/10.4171/164-1/9.

Preisinger, Clemens. 2013. 'Linking Structure and Parametric Geometry'. *Architectural Design* 83 (2): 110–13. https://doi.org/10.1002/ad.1564.

Pugnale, Alberto, and Sassone Mario. 2007. 'Morphogenesis and Structural Optimization of Shell Structures with the Aid of a Genetic Algorithm'. *Journal of the International Association for Shell and Spatial Structures* 48 (3): 161–66.

Rieth, Éric. 2003. 'First Archaeological Evidence of the Mediterranean Whole Moulding Ship Design Method: The Example of the Culip VI Wreck, Spain (XIIIth–XIVth C.)'. In *Shipbuilding Practice and Ship Design Methods from the Renaissance to the 18th Century : A Workshop Report*, edited by Horst Nowacki and Matteo Valleriani, 245:9–16. Preprint / Max-Planck-Institut Für Wissenschaftsgeschichte. Berlin: Max-Planck Institute for the History of Science.

Rocha, Pedro, Rui Rodrigues, Franklina M. B. Toledo, and A. Miguel Gomes. 2013. 'Circle Covering Using Medial Axis*'. *IFAC Proceedings Volumes*, 11th IFAC Workshop on Intelligent Manufacturing Systems, 46 (7): 402–7. https://doi.org/10.3182/20130522-3-BR-4036.00081.

Rörig, Thilo, Stefan Sechelmann, Agata Kycia, and Moritz Fleischmann. 2014. 'Surface Panelization Using Periodic Conformal Maps'. In *Advances in Architectural Geometry 2014*, edited by Philippe Block, Jan Knippers, Niloy J. Mitra, and Wenping Wang, 199–214. London: Springer International Publishing.

Ross, Elissa, Daniel Hambleton, and Robert Aish. 2016. 'Face-Offsetting Polygon Meshes with Variable Offset Rates'. In *Advances in Architectural Geometry 2016*, edited by Sigrid Adriaenssens, Fabio Gramazio, Matthias Kohler, Achim Menges, and Mark Pauly, 40–61. Zurich.

Rybczynski, Witold. 2002. 'The Bilbao Effect: Public Competitions for Architectural Commissions Don't Necessarily Produce the Best Buildings'. *The Atlantic*, September 2002.

Sánchez-Alvarez, Jaime. 2002. 'The Geometrical Processing of the Free-Formed Envelopes for The Esplanade Theatres in Singapore'. *Proceedings of the 5th International Conference on Space Structures.*

Sánchez-Alvarez, Jaime, Kamil Schwarnowski, and Christian Wolkowicz. 2013. 'Design and Construction of a Free-Form Reticulated Glazed Canopy'. In *Proceedings of IASS 2013: 'Beyond the Limits of Man'*, edited by Jan Bogdan Obrębski and Romuald Tarczewski. Metal Spatial Structures 1: Buckling and Realization. Wrocław.

Sauer, Robert. 1970. *Differenzengeometrie*. Berlin, Heidelberg: Springer-Verlag.

Schiftner, Alexander, Niccolo Baldassini, Pengbo Bo, and Helmut Pottmann. 2008. 'Architectural Freeform Structures from Single Curved Panels'. In *Advances in Architectural Geometry 2008*, edited by Helmut Pottmann, Axel Kilian, and Michael Hofer, 45–48. Vienna.

Schlaich, Jörg, and Rudolf Bergermann. 1994. 'Conceptual Design of Long-Span Roofs'. *IABSE Reports* 71: 13–24. https://doi.org/10.5169/seals-54113.

Schlaich, Jörg, and Hans Schober. 1992a. *Transparente Netztragwerke: Museum Für Hamburgische Geschichte, Schwimmbad Neckarsulm*. Stahl Und Form. München: Inst. für Internationale Architektur-Dokumentation.

———. 1992b. 'Verglaste Netzkuppeln'. *Bautechnik* 69 (1): 3–10.

———. 1994. 'Glass-Covered Lightweight Spatial Structures'. In *Proceedings of the IASS-ASCE International Symposium*, edited by John F. Abel, John W. Leonard, and Celina U. Penalba. Spatial, Lattice and Tension Structures. Atlanta: New York American Society of Civil Engineers.

———. 1998. 'Glaskuppel Für Die Flusspferde Im Zoo Berlin'. *Stahlbau* 67 (4): 307–12. https://doi.org/10.1002/stab.199800990.

Schlaich, Jörg, Hans Schober, and Kai Kürschner. 2005. 'New Trade Fair in Milan — Grid Topology and Structural Behaviour of a Free-Formed Glass-Covered Surface'. *International Journal of Space Structures* 20 (1): 1–14. https://doi.org/10.1260/0266351054214326.

Schober, Hans. 2003a. 'Freigeformte Netzschalen – Entwurf Und Konstruktion'. *VDI Jahrbuch 'Bautechnik'*, 35–52.

———. 2003b. *Zur Netzschale, Beitrag Im Buch: Das Bosch-Areal, Roland Ostertag*. Karl Krämer Verlag, Stuttgart.

———. 2015a. *Transparent Shells: Form, Topology, Structure*. John Wiley & Sons.

———. 2015b. *Transparent Shells: Form Topology Structure*. Berlin: Wilhelm Ernst & Sohn. 10.1002/9783433605998.

Schober, Hans, and Stefan Justiz. 2012. 'Cabot Circus, Bristol Ebene Viereckknetze Für Freigeformte Glasdächer'. *Stahlbau* 81 (S1): 28–42. https://doi.org/10.1002/stab.201290072.

Schott, Gd. 2008. 'Piero Della Francesca's Projections and Neuroimaging Today'. *The Lancet* 372 (9647): 1378–79. https://doi.org/10.1016/S0140-6736(08)61576-7.

Sechelmann, Stefan, Thilo Rörig, and Alexander I. Bobenko. 2012. 'Quasiisothermic Mesh Layout'. In *Advances in Architectural Geometry 2012*, edited by Lars Hesselgren, Shrikant Sharma, Johannes Wallner, Niccolo Baldassini, Philippe Bompas, and Jacques Raynaud, 243–258. Vienna: Springer.

Sederberg, Thomas W., Jianmin Zheng, Almaz Bakenov, and Ahmad Nasri. 2003. 'T-Splines and T-NURCCs'. *ACM Transactions on Graphics* 22 (3): 477–84. https://doi.org/10.1145/882262.882295.

Shimoda, Masatoshi, Takashi Morimoto, Fuminori Hayashi, and Yang Liu. 2013. 'Non-Parametric Free-Form Optimization for Grid-Shell Structures'. In *Proceedings of IASS 2013: 'Beyond the Limits of Man'*, edited by Jan Bogdan Obrębski and Romuald Tarczewski. Wrocław.

Skylakakis, Stefanos. 2005. 'The Vision of a Guggenheim Museum in Bilbao'. Student research. Center for Design Informatics, Harvard Design School. http://www.gsd.harvard.edu/wp-content/uploads/2016/06/pollalis-case-BilbaoG-CaseA.pdf.

Soeren, Stephan, Jaime Sánchez-Alvarez, and Klaus Knebel. 2004. 'Reticulated Structures on Free-Form Surfaces'. In *Proceedings of IASS 2004: From Models to Realization*, edited by René Motro. Montpellier.

Spitzer, Paul. 1998. 'Harsh Ways: Edward W. Heath and the Shipbuilding Trade'. *The Pacific Northwest Quarterly*, 1998.

Sun, Xiang, Caigui Jiang, Johannes Wallner, and Helmut Pottmann. 2016. 'Vertex Normals and Face Curvatures of Triangle Meshes'. In *Advances in Discrete Differential Geometry*, edited by Alexander I. Bobenko, 267–286. Berlin: Springer. https://doi.org/10.1007/978-3-662-50447-5_8.

Sung, Kelvin, Peter Shirley, and Steven Baer. 2008. *Essentials of Interactive Computer Graphics: Concepts and Implementation*. Wellesley, Massachusetts: A K Peters/CRC Press.

Święciak, Michał, and Romuald Tarczewski. 2015. ‘Topological Optimization of Formworks’ Meshes for Free-Form Surfaces’. In *Advances in Mechanics: Theoretical, Computational and Interdisciplinary Issues*, edited by Michał Kleiber, Tadeusz Burczyński, Krzysztof Wilde, Jarosław Górski, Karol Winkelmann, and Łukasz Smakosz, 577–80. Proceedings of the 3rd Polish Congress of Mechanics and 21st International Conference on Computer Methods in Mechanics. Gdańsk: CRC Press.

———. 2016. ‘Free-Form Structures from Semi-Precast Planar Concrete Elements’. In *IASS 2016 Tokyo Symposium: Spatial Structures in the 21st Century*, edited by Ken’ichi Kawaguchi, Makoto Ohsaki, and Toru Takeuchi. Tokyo.

———. 2017. ‘Relation between Optimal Lattice Shell Shape and Elastic Curve’. In *Proceedings of the 11th International Conference "Shell Structures: Theory and Applications*, edited by Wojciech Pietraszkiewicz and Wojciech Witkowski, 569–72. Gdańsk.

———. 2018. ‘Elasticas in Shaping Architectural Form - a Hypothesis about Borromini’s Approach’. In *Proceedings of IASS Symposium 2018, Creativity in Structural Design*, edited by Sigrid Adriaenssens and Caitlin T. Mueller. Boston.

Tang, Chengcheng, Xiang Sun, Alexandra Gomes, Johannes Wallner, and Helmut Pottmann. 2014. ‘Form-Finding with Polyhedral Meshes Made Simple’. *ACM Transactions on Graphics* 33 (4): Article No.: 70. https://doi.org/10.1145/2601097.2601213.

Tarczewski, Romuald. 2011. *Topologia Form Strukturalnych. Naturalne i Tworzone Przez Człowieka Prototypy Form Konstrukcyjnych w Archtekturze*. Wrocław: Oficyna Wydawnicza Politechniki Wrocławskiej.

Tish, Ghaith. 2015. ‘Computational Techniques For Designing Shell Structures’. In *Proceedings of the International Association for Shell and Spatial Structures (IASS) Symposium 2015: Future Visions*, edited by Jeroen Coenders, Andrew Borgart, and Arno Pronk. Amsterdam.

Townsend, Alastair. 2014. ‘On the Spline: A Brief History of the Computational Curve’. Edited by Jonathon Anderson and Meg Jackson. *International Journal of Interior Architecture + Spatial Design: Applied Geometries* III (3). http://www.alatown.com/spline-history-architecture/.

Troche, Christian. 2008. ‘Planar Hexagonal Meshes by Tangent Plane Intersection’. In *Advances in Architectural Geometry 2008*, edited by Helmut Pottmann, Axel Kilian, and Michael Hofer, 57–60. Vienna.

Veltkamp, Martijn. 2015. ‘The End of Free-Form Design, Long Live Free-Form Design!’ In *Proceedings of the International Association for Shell and Spatial Structures (IASS) Symposium 2015: Future Visions*, edited by Jeroen Coenders, Andrew Borgart, and Arno Pronk. Amsterdam.

Wagner, Ray. 1990. *Mustang Designer Edgar Schmued and the P-51*. New York: Smithsonian Institution.

Wallner, Johannes, Alexander Schiftner, Martin Kilian, Simon Flöry, Mathias Höbinger, Bailin Deng, Qixing Huang, and Helmut Pottmann. 2010. ‘Tiling Freeform Shapes With Straight Panels: Algorithmic Methods’. In *Advances in Architectural Geometry 2010*, edited by Cristiano Ceccato, Lars Hesselgren, Mark Pauly, Helmut Pottmann, and Johannes Wallner, 73–86. Vienna: Springer Vienna.

Wang, Wenping, Johannes Wallner, and Yang Liu. 2007. ‘An Angle Criterion for Conical Mesh Vertices’. *Journal for Geometry and Graphics* 11 (2): 199–208.

Weisstein, Eric W. 2018a. ‘Affine Transformation’. In *Wolfram MathWorld - A Wolfram Web Resource*. http://mathworld.wolfram.com/AffineTransformation.html.

———. 2018b. ‘Angular Defect’. In *Wolfram MathWorld - A Wolfram Web Resource*. http://mathworld.wolfram.com/AngularDefect.html.

———. 2018c. ‘Concurrent’. In *Wolfram MathWorld - A Wolfram Web Resource*. http://mathworld.wolfram.com/Concurrent.html.

———. 2018d. ‘Conformal Mapping’. In *Wolfram MathWorld - A Wolfram Web Resource*. http://mathworld.wolfram.com/ConformalMapping.html.

———. 2018e. ‘Conic Section’. In *Wolfram MathWorld - A Wolfram Web Resource*. http://mathworld.wolfram.com/ConicSection.html.

———. 2018f. ‘Cyclic Quadrilateral’. In *Wolfram MathWorld - A Wolfram Web Resource*. http://mathworld.wolfram.com/CyclicQuadrilateral.html.
———. 2018g. ‘Inversion’. In *Wolfram MathWorld - A Wolfram Web Resource*. http://mathworld.wolfram.com/Inversion.html.
———. 2018h. ‘Inversion Sphere’. In *Wolfram MathWorld - A Wolfram Web Resource*. http://mathworld.wolfram.com/InversionSphere.html.
———. 2018i. ‘Map’. In *Wolfram MathWorld - A Wolfram Web Resource*. http://mathworld.wolfram.com/Map.html.
———. 2018j. ‘NURBS Curve’. In *Wolfram MathWorld - A Wolfram Web Resource*. http://mathworld.wolfram.com/NURBSCurve.html.
———. 2018k. ‘Principal Curvatures’. In *Wolfram MathWorld - A Wolfram Web Resource*. http://mathworld.wolfram.com/PrincipalCurvatures.html.
———. 2018l. ‘Reflection’. In *Wolfram MathWorld - A Wolfram Web Resource*. http://mathworld.wolfram.com/Reflection.html.
———. 2018m. ‘Rotation’. In *Wolfram MathWorld - A Wolfram Web Resource*. http://mathworld.wolfram.com/Rotation.html.
———. 2018n. ‘Shear’. In *Wolfram MathWorld - A Wolfram Web Resource*. http://mathworld.wolfram.com/Shear.html.
———. 2018o. ‘Sphere’. In *Wolfram MathWorld - A Wolfram Web Resource*. http://mathworld.wolfram.com/Sphere.html.
———. 2018p. ‘Superellipsoid’. In *Wolfram MathWorld - A Wolfram Web Resource*. http://mathworld.wolfram.com/Superellipsoid.html.
———. 2018q. ‘Translation’. In *Wolfram MathWorld - A Wolfram Web Resource*. http://mathworld.wolfram.com/Translation.html.
Wester, Ture. 1981. *Structural Order in Space: The Plate-Lattice Dualism*. Copenhagen: Plate Laboratory, Royal Academy of Arts, School of Architecture.
Woltron, Ute, and Gerald Zugmann. 2004. ‘Uniqa Tower, Ein Wahrzeichen Für Wien’,. In *Das Dach Des Platinum Vienna*, 134–45. Vienna: HEP Verlags.
Yang, Yong-Liang, Yi-Jun Yang, Helmut Pottmann, and Niloy J. Mitra. 2011. ‘Shape Space Exploration of Constrained Meshes’. *ACM Transactions on Graphics* 30 (6): Article No.: 124. https://doi.org/10.1145/2070781.2024158.
Zadravec, Mirko, Alexander Schiftner, and Johannes Wallner. 2010. ‘Designing Quad-dominant Meshes with Planar Faces’. *Computer Graphics Forum* 29 (5): 1671–79. https://doi.org/10.1111/j.1467-8659.2010.01776.x.

11. List of figures

A-1 Abstract

A-1.1 The reason for undertaking the research topic

Observing contemporary architectural objects in which coverings are used, especially glazed, in the form of doubly-curved grid shells, it can be noticed that relatively often the use of attractive forms encounters significant implementation restrictions. They affect not only the choice of a particular structural solution but also the perception of the form itself. An example illustrating this problem may be the roofing of the courtyard at the Smithsonian American Art Museum in Washington, named after the founder Kogod Courtyard. This, designed in 2004 by the renowned Foster and Partners office, viewed from the interior (Fig. A-1.1, left) impresses with its lightness, proportions and transparency. The designers obtained this effect, among others, by applying on the slightly wavy surface a grid of rods with square panels, which emphasizes the shape of the roofing, leaving the details of the structure in the background.

Fig. A-1.1 Kogod Courtyard at Smithsonian Art Museum, Washington.
Left: the interior with view from the bottom of the roof[93], right: view of the top of the roof[94].

However, the same cover, viewed from the outside, makes a completely different impression. Individual glass panels protrude beyond the surface, creating a "keyboard" system, a non-smooth surface, the visual effect of which is far from the quiet elegance of the interior (Fig. A-1.1, right). The reason for this is the designer's application of a top-down design methodology, according to which the geometry of the cover surface was first determined and then it was divided using the adopted grid. This approach ignored the fact that not every free formed[95] surface can be divided using flat quadrangles. As a result, in order to preserve the planarity of the panels, the designer was forced to situate them in this way.

Another approach was presented by the same architect, Norman Foster, in the roofing of the Great Court, designed ten years earlier, at the British Museum in London. Here was also used a bar lattice over a doubly-curved smooth surface. However, in this case, the division into triangular panels was adopted, see Fig. A-1.2. Their essential feature is that they are always planar and the resulting cover is smooth, both on the inside and outside.

[93] Source: https://npg.si.edu/visit/kogod-courtyard
[94] Source: https://www.fosterandpartners.com/projects/smithsonian-institution-courtyard/#gallery
[95] The term *freeforms* is also well accepted in literature to describe the design trend

Fig. A-1.2 The roof of the Great Court in British Museum, London.[96]

Why then, in the later project, was a solution used that does not retain this mutual smoothness? The reason is the undoubted advantages of quadrilateral grids. In a nutshell, these are: much lower saturation of the surface with construction elements, and thus greater transparency of the cover, much simpler and therefore easier to make and more reliable nodes, greater ease of ensuring the tightness of the roofing.

The dichotomy: of a triangular division and smooth cover - quadrilateral and non-smooth cover, is not unavoidable. While working on this dissertation, it was found that it is possible to design a smooth quadrangular grid on almost every double-curved surface using the "bottom-up" design methodology. An illustration of this may be the author's original version of the Kogod Courtyard covering designed according to this approach, see Figs. A-1.3 and A-1.4. A quadrangular mesh of rods was used in it, and the obtained surface is smooth on both sides.

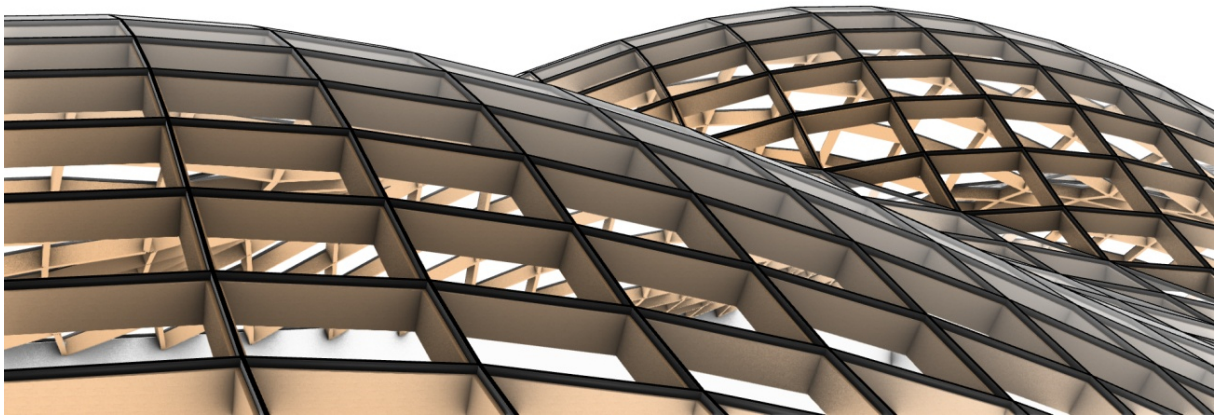

Fig. A-1.3 The proposition for the cover of Kogod Courtyard with smooth, planar quadrilateral cladding, designed with the use of author's methods presented in the work. View of the top of the roof.

[96] Source: https://en.wikipedia.org/wiki/Queen_Elizabeth_II_Great_Court#/media/File:British_Museum_Great_Court,_London,_UK_-_Diliff.jpg

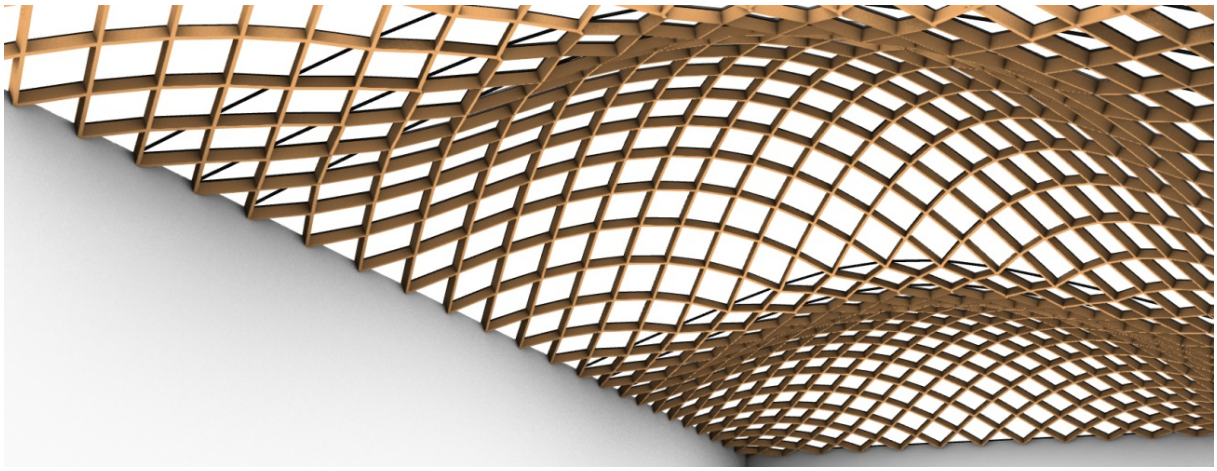

Fig. A-1.4 The proposition for the cover of Kogod Courtyard with smooth, planar quadrilateral cladding, designed with the use of author's methods presented in the work. View of the bottom of the roof.

A-1.2 The subject matter of the work

The subject of the doctoral dissertation is a proprietary development of methodologies and design tools aimed at enabling designers to create geometrically correct glazed grid shells, which are also optimised due to the technological and structural conditions.

The combination of two glass roofs presented above, i.e. the roof over the Kogod Courtyard at the Smithsonian Institute and the proprietary roof concept with a similar shape designed using the proposed methods, shows how the design methods and tools affect the simplification and rationalization of the project. Both roofs are grid shells, i.e. structures that, thanks to the curvature of their form in two directions, can be implemented as structures with very small cross-sectional dimensions of their elements. In turn, the use of four-sided glass panels to cover these roofs has many advantages, such as reducing the saturation of the surface with rods, reducing the mass of the structure, simplifying the nodes and limiting the number of thermal bridges and potential leaks in relation to the most commonly used triangular divisions in doubly-curved glazed roofs. However, while a grid shell with a structurally optimal shape can be easily covered with flat triangular panels, its coverage with quadrangles is not a trivial task. The four vertices of any quadrilateral lying on a curved surface are not at the same time on a common plane, and vice versa – the four vertices of any planar quadrilateral usually do not lie on a curved surface at the same time. For this reason, the use of quadrilateral divisions for any arbitrarily imposed cover surface leads to effects such as in the Kogod Courtyard, where the lack of smoothness of the split was compensated by a specially developed, complicated sealing system. It is worth noting that in practice there are only few proposed solutions involving the use of curved glass panels, despite the fact that this would solve the geometric problem. However, such solutions lead to new problems that are even more difficult to solve, related to the thermal deformability of curved elements and the sealing of panel edges.

The solution proposed in this work is the reversal of the order of activities performed by the designer, who initially develops the surface of the shell (arbitrarily shaped or structurally optimized) and then divides it into panels. Most often it turns out that a rational division into quadrilaterals is not possible and more expensive triangular divisions are the only solution. Instead, the designer can shape the form of the shell by means of the superposition of the methods described in the work to create (methods of formation of) curved, planar quadrilateral grids and methods of transforming them, which maintain

the planarity of individual panels. In this case, the designer first decides about the divisions and then about the form. Thanks to this, with a moderate limitation of freedom in shaping the form, he can be absolutely sure that his project can be implemented using rational technological solutions.

The presented methods and concepts of design tools allow for the reconstruction of designed forms in a geometrically and technologically rational manner and for them to be as close as possible to the initial forms, and also open new possibilities of designing free forms from scratch. The catalogue of existing and proposed methods and tools allows to design not only glazed roofs but also any other structure based on quadrilateral divisions such as facades, glass garden rooms and canopies.

A-1.3 Introduction to the problematic aspects of the work

The design of free forms in architecture is becoming more and more popular thanks to the widespread use of advanced design tools. Historically, free forms are derived from the practice of designing vehicles, i.e. boats, ships, cars and aircrafts.

The history of free forms presented in the work shows how the tools used to design the hulls of boats, ships, and shells of cars and aircraft, always associated with free forms, have become architects' tools and how they influenced the currently adopted design methodology, unfavourable in the author's opinion, forcing the use of less rational technological solutions. Advanced tools dedicated for the design of free forms were first used to design architectural forms during the implementation of the Guggenheim Museum in Bilbao in 1994-1997. The design and implementation of this building required the close cooperation of a team of engineers from the aviation industry who were familiar with their operation, both on the side of the designer as well as the contractors of the facility. The unquestionable commercial success of this realization caused the contemporary phenomenon of the "Bilbao Effect", one aspect of which is the dissemination of free-form designs and the tools for designing them now used by architects. The negative effect of this phenomenon, however, is the omission by many designers of the fact that the forms obtainable using these tools are not adjusted for architectural purposes. Differences between the way vehicles and buildings are implemented imply the need to use different methodologies and design tools. These differences, specified in the work, are listed as follows:

- building partitions are thick and multi-layered, while vehicle hulls/shells are made of material sheets whose thickness in practice is negligible in relation to their other dimensions;
- the seriality of vehicles divides the costs of developing the technology for the number of individual units produced, while the free formed building is implemented once, so its cost must include the development of its technology;
- unlike vehicles whose bodies are made of individual elements produced in large numbers, in free formed buildings (unlike in e.g. mass housing) the used elements not only have individual shapes but are also individually produced;
- vehicles are implemented entirely on production belts within one factory, while free-form buildings are made of components whose dimensions should allow them to be delivered to the construction site and placed in the right place in the constructed building.

These problems were clearly revealed before the Bilbao Effect, during the construction of the Sydney Opera House. Various consequences were revealed, such as the postponing of the completion deadline by 8 years, its almost 100 times exceeding the project implementation budget, but also the first-ever use of computer-based methods on this scale, creating the iconic building symbolizing the continent and the final distinction of the architect Jørn Utzon with the Pritzker Prize. From more than two

hundred submitted competition projects the winning concept consisted only of a general sketch, yet it gained the jury's recognition thanks to its courage in the use of free forms. Among many interpretations and inspirations of the Sydney Opera House's shell forms, one fact is the most convincing, namely that in his youth its designer designed and built yachts together with his father. In one of his interviews Jørn Utzon stated that he equated the lack of a technological barrier between the design and implementation of yachts with its similar lack in the case of buildings. The final solution to the enormous implementation problems was brought about by the use of spatial concrete prefabricates, which were described on a common sphere and therefore repetitive to some degree, also being manufactured near the construction site, instead of monolithic concrete shells as originally assumed by the author of the project.

Although, since then, the technological possibilities of implementing free forms in architecture have significantly increased, these problems are still valid and stand in the way between the architectural concepts and rational possibilities of their implementation. This is because the design tools available to architects have not changed. Successful implementations of free forms in architecture until recently remained in the domain of such well-known projects as the aforementioned roofs over the Grand Courtyard in the British Museum and Kogod Courtyard by Norman Foster and Heydar Aliyev Center in Baku by Zaha Hadid. Both cases required the use of mathematically and algorithmically advanced design methods, individually adjusted to the needs of the projects. The example of the Museum of the History of Polish Jews in Warsaw, described in the work, present technological problems related to the main hall of a building with free-formed walls. It proves that in the case of projects of lesser importance, the ease of creating unique forms using advanced design methods is inversely proportional to the ease of their implementation.

A-1.4 Explanation of the title of the work

The literature review presented in the work does not show a clear definition of free forms used in architecture. For some of the researchers cited, these are forms curved in an irregular manner, which do not have repeatability nor regularity in their fragments. For other researchers, the forms of membrane structures that have the above features do not qualify as free forms, because the freedom of their design is limited by the type of surfaces on which these structures are described. These are the minimal surfaces, i.e. mathematically and physically defined surfaces, by means of external conditions, obtainable in the process of form finding. Consequently, any other form, not only membranes, designed through the process of form finding is not qualified by these researchers as a free form. In this work it is accepted that a free form is a form described on a surface which has double-curvature, regardless of whether it is the result of the structural optimization or sculptural vision of the designer.

The legitimacy of shaping structures in the form of free forms is based on the possibility of implementing them as lightweight constructions. It is thanks to the curvature that shells can be constructed, while the same structure made of flat roof segments must usually be additionally strengthened by using larger cross-sections of rods and the use of spatial trusses.

Currently, one of the most frequently implemented free forms in architecture is glazed grid shells, i.e. single layered lattices consisting of rods, nodes and glass panels. The curvature of such grid shells is discrete, which means that their overall form is curved, i.e. the nodes of the grid shell lie on a curved surface, while its individual components are not curved, i.e. the rods are straight and the panels are flat. The implementation of discrete, doubly-curved grid shells, unlike continuously curved grid shells, may, to a limited extent, make use of the unification of its components. The rods can vary

in lengths and angles between them, but they are straight and the glass panes can have different shapes but are flat.

The topology of grid shells refers to the shape of individual panels and the number of rods converging at each node. The two most commonly used topologies are: triangular (see Fig. A-1.6) and planar quadrilateral (in short PQ; see Fig. A-1.5). Grid shells of triangular topology consist of triangular panels and nodes connecting six rods, while PQ grid shells consist of planar, quadrilateral panels and nodes connecting four rods. The work contains the author's original and other cited researchers' analyses of the differences between these topologies. Among the differences between these topologies the following factors speak to the disadvantage of triangular meshes:

- triangular glass panels are more expensive to produce than quadrilateral ones because they cause more glass waste, and also too small apex angles cause possibilities of cracking;
- in meshes with triangular topology there is a higher ratio of the number of structural elements to the glazing surface than in the grids with PQ topology, compare Figs. A-1.5 and A-1.6;
- the nodes of triangular grids are more complicated and complex than in PQ grids;
- in triangular grids there are more thermal bridges and potential sources of leakage than in PQ grids.

Fig. A-1.5 Cover with PQ grid.

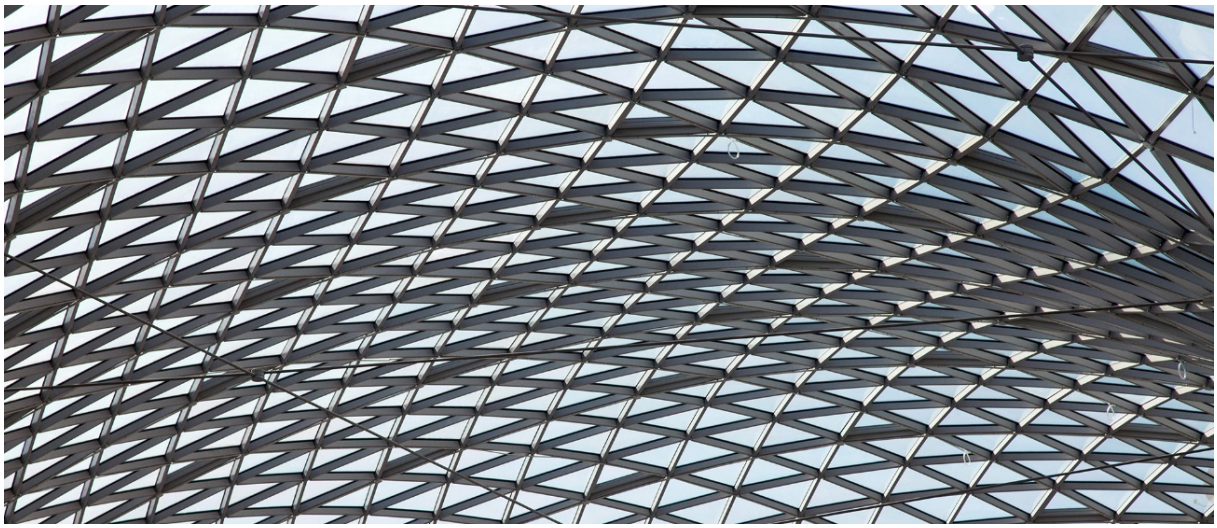

Fig. A-1.6 Cover with triangular grid.

The ease in designing triangular meshes results in an advantage in the number of their implementations, despite the fact that PQ grids are more rational in technological and economic terms. This advantage is caused by the generally accepted methodology, called "top-down", in which the architect creates a free formed surface at the initial stage of project development using the available design tools, on which the grid shell should be described. Because any triangle, regardless of the location of its vertices in space, is flat, the division of any given surface into triangular panels and their adjustment to optimize the lengths of rods allows for an unlimited freedom of shaping the geometric form of the shell. In the case of quadrilateral panels, their planarity is not obvious when placing their vertices on a free formed surface given by the designer. Hence, in this work, it is postulated to use the bottom-up approach, which is based on such shaping of free formed surfaces which right from the start include the possibility of covering them with planar quadrilateral panels. The tools available to architects do not offer sufficient methods for shaping free forms, which in consequence would enable their implementation in the optimal topology.

As a result of the research and analyses carried out, it was found that it is possible to formulate the design methodology, which is called the "bottom-up" approach, and methods for generating and transforming PQ grids shells that will enable their design in practically all cases. The above was the basis for formulating the theses of this doctoral dissertation.

A-1.5 Theses of the work

After the initial, enthusiastic period, just after the "Bilbao Effect", the implementation of many objects based on free forms revealed the problem of separating form from the rationality of structure. Form has become a means of expressing architecture itself, detached from factors related to its implementation. An especially important and interesting example of such free forms are discrete, glazed grid shells realized as glass roofs and facades, which can be shaped as arbitrary, expressive forms or construction-optimized light coatings.

- **Thesis 1**

  Grid shells are one of the main means of expression within the free-form design trend in architecture and belong to the most characteristic and most frequently implemented objects in this group.

- **Thesis 2**

  Free-form grid shells based on planar quadrilateral topology (PQ) have many advantages over grid shells based on a triangular topology.

- **Thesis 3**

  It is possible to develop design tools that allow for the effective design of PQ meshes based on a bottom-up methodology.

- **Thesis 4**

  Guided by the principles of bottom-up design, desirable grid shells can be obtained with a small and acceptable restriction of freedom in shaping their form.

A-1.6 Results of the work

The result of the work is a database of existing and authorial methods of creating and transforming PQ meshes, which form the basis for the development of a comprehensive design system. An appropriate combination of selected methods of creation and transformation allows for the formation of discrete doubly-curved grid shells in PQ topology adapted to the required existing conditions, e.g. the shape of a covered courtyard. The work presents a developed concept of a design tool based on the previously described methods of generating and transforming PQ meshes, and then presents two examples of practical applications of developed tools based on this concept and selected methods of generating and transforming PQ meshes.

As examples of applications developed in accordance with the concept of design tools, two courtyards of buildings existing in Wrocław were selected. The first one is the building of the Lower Silesian Voivodeship Office, which has three courtyards, two of which have the shape of rounded quadrilaterals. For one of them a glass cover has been proposed, see Fig. A-1.7. The proposed solution is based on the PQ mesh translational method and on the author's SC transformation (spherical-cylindrical projection), which accurately transforms the basic grid form into a rounded courtyard form while maintaining the planarity of all facets. The developed tool also contains a number of intermediate steps described in the work, which are supposed to increase the control over the final form of the roof maintained by the designer and at the same time guarantee the geometric correctness of the solution.

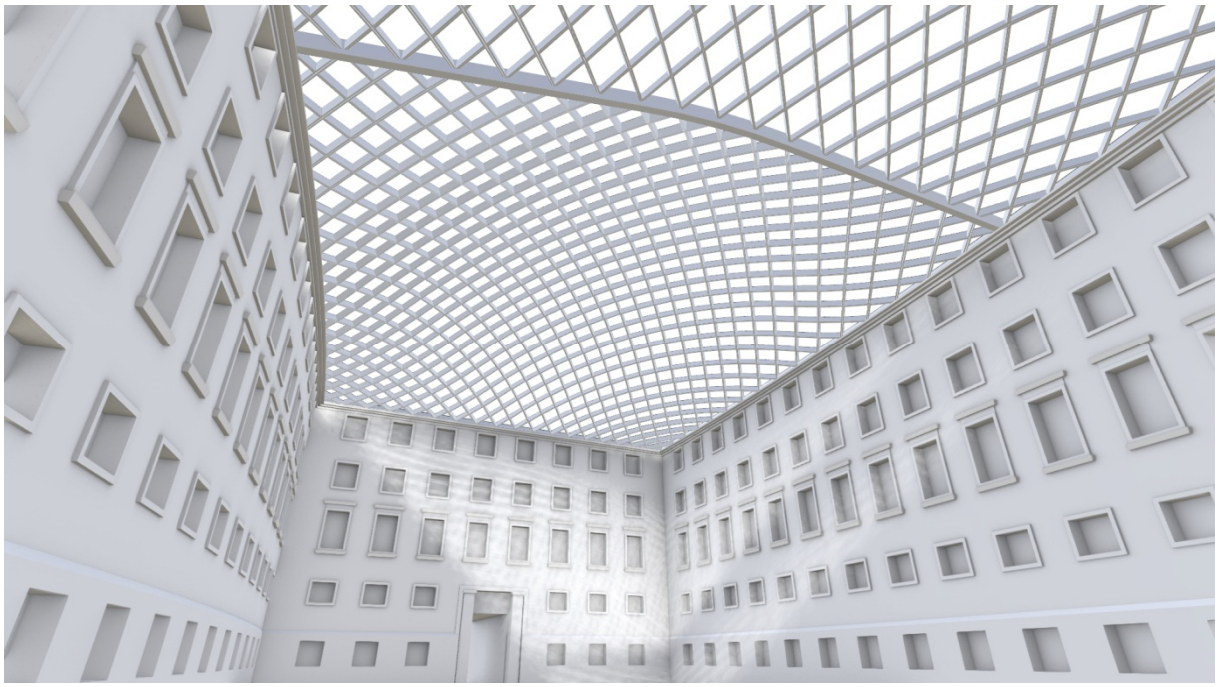

Fig. A-1.7 The proposed cover of the courtyard in the building of the Lower Silesian Voivodeship Office.

The second example concerns the courtyard in the building of the Faculty of Biological Sciences of the University of Wrocław at Kuźnicza street 35. This courtyard has the form of an irregular quadrilateral, and it is surrounded by cloisters that are presently separated from the courtyard by windows. As in the previous case, a tool based on the translational grid creation method and on the author's transformation method, i.e. perspective transformation, was used to design the PQ mesh. This transformation method allows the designer to fit any PQ mesh with a flat, four-sided base, to any four-sided, irregular form of the courtyard, see Fig. A-1.8.

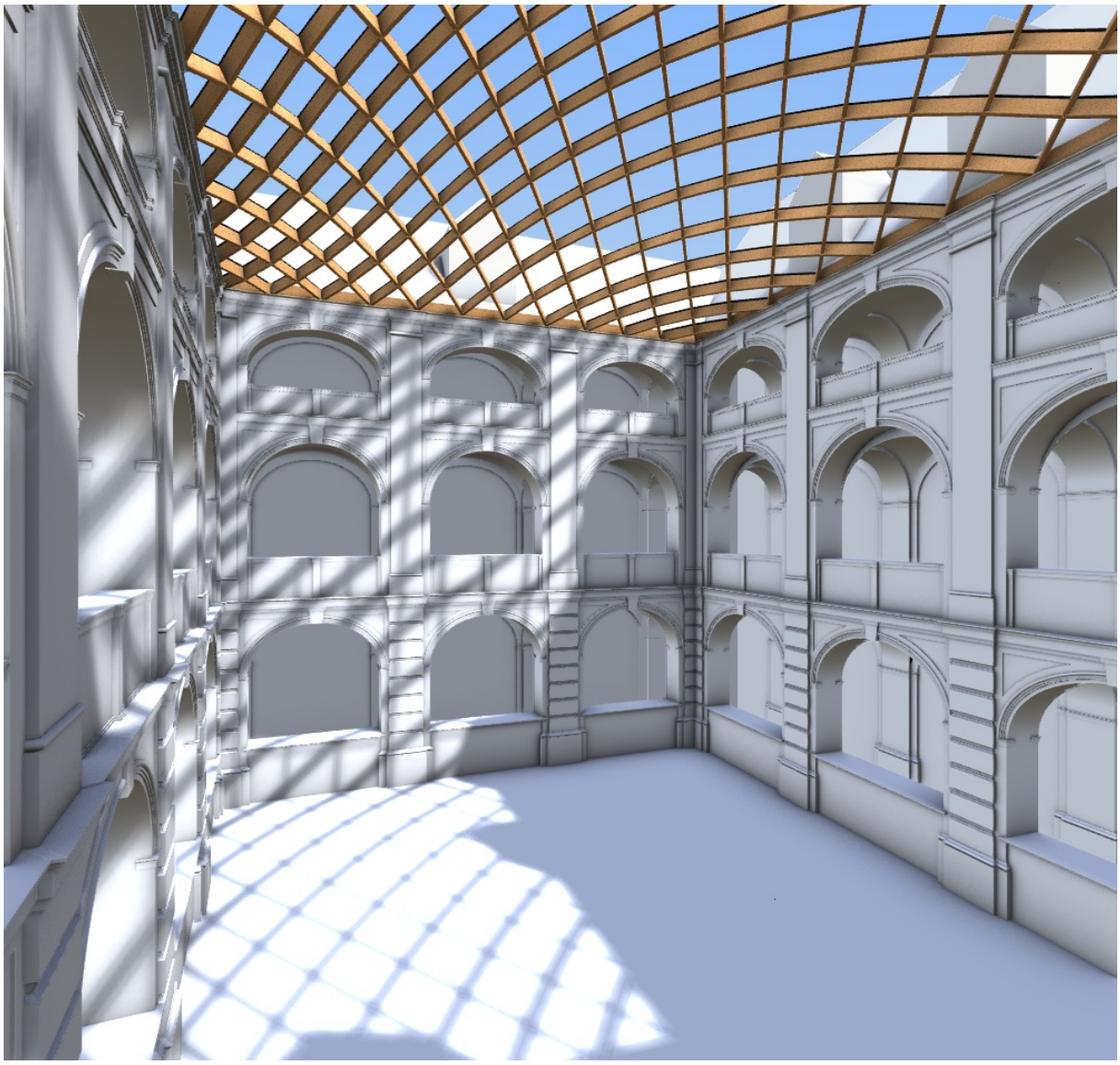

Fig. A-1.8 The proposed cover of the courtyard in the building of the Faculty of Biological Sciences of the University of Wrocław.

In both cases the designer indicates three or four corner points on the plan of the building, depending on the design case, based on which the programmed tool automatically adjusts the relevant transformation parameters. Both tools provide a number of possibilities to modify the form, giving the designer the greatest possible freedom to shape it. The designer, by means of changing the parameter values for the tool, determines the number and distribution of the grid divisions and thus affects the size of the glass panels, the height of the roof, etc. By means of several other parameters, it also affects the shape of the form obtained while maintaining the corner points set at the beginning.

The parameters by which the designer controls the form of the free formed PQ grid shell limit the absolute freedom of shaping, which is peculiar to the top-down design paradigm. However, the freedom of design is only limited to a set of rational morphologies from a geometric point of view. The designer can obtain such forms that are rational from the point of view of realizability. For this reason, one of the researchers in this field of geometry in architecture, Romain Mesnil, calls the "bottom-up" approach the "fabrication aware design".

The available forms of the basic PQ translational mesh with a flat base perimeter parameterized by means of two shaping parameters have been examined in terms of the internal forces values using the finite element method. The results presented in the work prove that the optimal form of the grid shell, in which internal forces have the lowest values, is a doubly-curved form with a high degree of curvature continuity. As a result, a roof of this form can be made of structural elements with smaller cross-sections than in the case of conventional forms, i.e. roofs composed of several flat sections. Above all, thanks to the presented solutions it is possible to shape glass roofs as grid shells rather than space trusses, which in many cases collide with the aesthetics of the building, primarily in the context of courtyards of historic buildings. Use of the tools proposed in the work imply directly into a reduction in the use of materials, in the optimization of form and topology, and ultimately on the economic rationalization of the application of these solutions.

A-1.7 Proven theses of the work

A-1.7.1 Thesis 1

Analyses of objects representative to the trend of free-form design carried out in the dissertation allowed to follow through the application of free forms in completed objects and define the functions most frequently assigned to them. These are primarily elements of objects that define their visual perception, such as building facades (often in the form of a second skin) and roofing of whole objects or parts thereof, especially courtyard roofs, entrance canopies, etc. A special place among them have grid shells, which on the one hand allow to achieve structural efficiency, and on the other hand provide additional possibilities of shaping the form with transparent fillings. The catalogue of objects that systematize data about them, included in the appendix A-3 to the work, proved to be helpful in drawing conclusions. On the basis of the analysed data on theses 1, it can be concluded that:

> **Among the free formed objects, grid shells occupy a particularly important place and constitute one of the most important groups of structures within this trend. Because they allow to obtain forms with significant spans, they are clearly light, and through large glazing, they are clearly visible, they have become the most frequently implemented objects in this group. These features enabled widespread social acceptance of these new geometric forms, contributing to a large extent to disseminating the freedom of shaping forms in architecture.**

A-1.7.2 Thesis 2

The analysis of various solutions, taking into account topology, geometry, construction and materials, allowed to state that grid shells whose glass panels are triangular are those that are most often designed and constructed. This solution allows to obtain a smooth mesh on almost any surface, while providing the necessary rigidity of the structure. Grids with such topology are relatively easy to design and can be inscribed in almost any closed contour. Triangular panels defined by grid edges (bars) are always flat. Computer tools for designing such grids are available.

At the same time, many disadvantages of this solution have been discovered. The most important is the complex construction of nodes in whose construction up to six rods are connected. The total number of rods and the roof area occupied by them is also much larger. The triangular glass panels are also smaller. These negative features do not appear in grids of quadrilateral topology. The number of rods connected in one node of such a grid is four, and the relative number of rods is smaller. The visual perception of such structures is much more beneficial.

In some respects, they also exhibit more favourable mechanical properties. An important limitation in the design of grids with a quadrilateral topology is the fact that the panels in such a grid are not always flat. For this reason, it is necessary to limit their diversity to a planar quadrilateral (PQ) topology. However, there are limitations in the use of this topology, because it cannot be applied to any previously defined surface. At present, there are no tools available for the design of meshes with such a topology. According to the thesis 2, it can be concluded that:

> **Among the implemented objects, in which glazed grid shells were applied, structures with a triangular topology dominate. Currently, however, more and more objects are being created with the PQ topology. Although it is more difficult to obtain a grid with PQ topology in the design process, it has many advantages over the triangular topology.**

A-1.7.3 Thesis 3

The dissertation includes a wide description of known methods of shaping PQ grids on free surfaces. These include both those methods already used in practice and those methods that are still theoretical solutions. They have a different range of applications, as well as various advantages and disadvantages. In addition, known methods of transforming of such grids which maintain the planarity of their panels after transformation were analysed. Both the methods of creating grids and the methods of their transformation refer to the methods of discrete geometry.

The results of the research allowed to formulate the author's own original methods of generating PQ grids and methods of their transformation. These methods allow to significantly increase the range of PQ grids' applications. In addition, it was noticed that many restrictions on the use of these grids result from the adopted design methodology, which is described as "top-down". This consists in adapting the mesh to the previously determined free surface. In this approach, many geometric forms of coatings are excluded from the possibility of using PQ divisions. This problem was essentially solved by changing the design methodology to "bottom-up". This consists in generating an output grid with the desired features and then its transformation in order to obtain sufficient compliance with the assumed final surface. According to the thesis 3, it can be concluded that:

> **By developing appropriate methods for generating and transforming PQ grids and applying bottom-up methodology, they can be effectively designed for various boundary conditions.**

A-1.7.4 Thesis 4

As part of the research, simulations and computer modelling were performed to examine the scope of available PQ mesh forms using known and proposed methods according to the bottom-up methodology. Two case studies proved to be particularly useful, involving designing glazed canopies over internal courtyards in two existing facilities. The analyses carried out showed that the scope of PQ mesh formation is very large and it is possible to adapt them to almost every design situation as well as for triangular-shaped meshes. The condition that enables this is the design in accordance with the bottom-up methodology. Accepting the desired base surface a priori may prevent, and in most cases does prevent, the use of PQ meshes. By transforming, while maintaining the planarity of panels, the initially generated, simple PQ mesh in such a way that it is finally as close as possible to the desired surface, satisfactory architectural results can be obtained. According to the thesis 4, it can be concluded that:

The proposed bottom-up design methodology together with the appropriate tools for generating and transforming PQ grids allows to design PQ grid shells for any design situation, with a small and acceptable limitation of the designer's freedom to shape the general form of such a grid shell.

A-1.8 Conclusions

The design tools proposed in the work and the design methodology based on them allow to definitely extend the scope of using PQ grids in free-form objects. Based on them, practical problems with a high degree of difficulty can be solved.

Considering the number of existing and proposed methods of creating and transforming PQ grids, it is possible to create many scenarios and design tools adequate to the existing design conditions, such as the shape of a courtyard, but also the desired shape of a building's or stadium's facade. The nine methods presented for creating PQ grids can be combined with five methods of their transformation, and two, three, four or five methods can also be used among the transformation methods in a given design tool. The set of five transformation methods gives 32 subsets of their sets, and after multiplying by nine the methods of creating PQ grids, it gives 288 different design tools, each of which includes the method of creating and transforming grids, leading to specific results and giving control over the form of the designed structure.

Additionally, the concept of the PQ mesh design tool presented in the paper provides four auxiliary initial and final transformations that do not eliminate the facets' planarity. Auxiliary transformations can be used in parallel with the basic ones and they are parameterized, additionally increasing the design freedom.

Indirectly, the application of the proposed solutions to design and construct glazed roofs allow for the creation of additional usable spaces within existing buildings, as well as the creation of buffer zones that increase the energy efficiency of buildings. In contrast to the majority of existing solutions for shaping triangular and PQ grid shells, whose accuracy allow for use only in newly designed buildings where the roof form can be coordinated with the form of the building, or in existing buildings' courtyards with shapes, the proposed tools allow for an absolute accuracy of adjusting the form of the PQ grid to the existing, irregular shape of the courtyard. These situations occur especially in the case of historical city centres, in which buildings often have irregular forms and it is not possible to change these conditions by rebuilding them and where, on the other hand, the high building density requires searching for other ways of obtaining additional usable areas.

However, it is also possible to use the proposed tools and methods for shaping PQ grid shells for newly designed objects. By the diversity of available combinations of methods of creating and transforming PQ grids, existing and proposed by the author, consistent with the proposed design tool concept, a wide spectrum of geometrically correct PQ morphologies is available – including glass roofs with other irregular base perimeters, facades and domes. The work also presents the concept of applying both the proposed methods of transformation, i.e. SC and the prospective transformation in order to obtain a PQ grid form with a contour consisting of sections of conic curves, i.e. second degree NURBS curves. This provides a tool for the design of canopies over courtyards with particularly complex perimeters and constraints related to the shape and height of the surrounding walls.

A-2 Streszczenie w języku polskim

A-2.1 Przyczyna podjęcia tematu badawczego

Obserwując współczesne obiekty architektoniczne, w których zastosowane są przekrycia, zwłaszcza przeszklone, w postaci dwukierunkowo zakrzywionych powłok prętowych, można zauważyć, że stosunkowo często stosowanie atrakcyjnych form napotyka na istotne ograniczenia realizacyjne. Mają one wpływ nie tylko na wybór określonego rozwiązania konstrukcyjnego ale również na percepcję samej formy. Przykładem ilustrującym ten problem może być zadaszenie dziedzińca w Smithsonian American Art Museum w Waszyngtonie, od nazwiska fundatora nazywany Kogod Courtyard. To, zaprojektowane w 2004 r. przez renomowane biuro Foster and Partners, zadaszenie, oglądane od wnętrza (Rys. A-2.1, po lewej) imponuje swoją lekkością, proporcjami i transparentnością. Projektanci uzyskali ten efekt m.in. poprzez zastosowanie na lekko falującej powierzchni siatki prętów o panelach czworokątnych, która podkreśla kształt przekrycia, pozostawiając szczegóły konstrukcji na drugim planie.

Rys. A-2.1 Kogod Courtyard w Smithsonian Art Museum w Waszyngtonie.
Po lewej: wnętrze dziedzińca z widokiem na spód dachu[97], po prawej: widok na dach od góry[98].

Jednakże to samo przekrycie, oglądane od zewnątrz, robi zupełnie inne wrażenie. Poszczególne panele szklane wystają poza powierzchnię, tworząc układ „klawiszujący", niegładki, którego efekt wizualny jest daleki od spokojnej elegancji wnętrza (Rys. A-2.1, po prawej). Przyczyną tego jest zastosowanie przez projektanta metodologii projektowania „z góry do dołu" (ang. top-down), zgodnie z którą najpierw została określona geometria powierzchni przekrycia, a następnie została ona podzielona za pomocą przyjętej siatki. W takim podejściu zignorowany został fakt, że nie każdą powierzchnię swobodną można podzielić za pomocą czworokątów płaskich. W rezultacie, chcąc zachować planarność paneli, projektant zmuszony był usytuować je w taki właśnie sposób.

Inne podejście zaprezentował ten sam architekt, Norman Foster, w zaprojektowanym dziesięć lat wcześniej zadaszeniu Wielkiego Dziedzińca w Muzeum Brytyjskim w Londynie. Tam również zastosowana została siatka prętowa na dwukrzywiznowo wygiętej, gładkiej powierzchni. Jednak w tym przypadku przyjęto podział na panele trójkątne, patrz Rys. A-2.2. Ich istotną cechą jest to, że są zawsze planarne i uzyskane przekrycie jest gładkie zarówno od strony wewnętrznej jak i zewnętrznej.

[97] Źródło: https://npg.si.edu/visit/kogod-courtyard
[98] Źródło: https://www.fosterandpartners.com/projects/smithsonian-institution-courtyard/#gallery

Rys. A-2.2 Dach Wielkiego Dziedzińca w Muzeum Brytyjskim, Londyn.[99]

Dlaczego w takim razie w późniejszym projekcie zastosowano rozwiązanie, które nie zachowuje tej obustronnej gładkości? Przyczyną są niewątpliwe zalety siatek czworokątnych. W największym skrócie są to: dużo mniejsze nasycenie powierzchni elementami konstrukcyjnymi, a przez to większa transparentność przekrycia, znacznie prostsze a zatem łatwiejsze do wykonania i bardziej niezawodne węzły, większa łatwość zapewnienia szczelności przekrycia.

Dychotomia: podział trójkątny i przekrycie gładkie —podział czworokątny i przekrycie niegładkie, nie jest nieunikniona. W trakcie pracy nad niniejszą dysertacją stwierdzono, że możliwe jest zaprojektowanie gładkiej siatki czworokątnej na niemal każdej powierzchni dwukrzywiznowej przy zastosowaniu metodologii projektowania „z dołu do góry" (ang. bottom-up). Ilustracją tego może być autorska wersja przekrycia Kogod Courtyard zaprojektowana według takiego podejścia, patrz rysunki A-2.3 i A-2.4. Zastosowana w niej została czworokątna siatka prętów, a uzyskana powierzchnia jest obustronnie gładka.

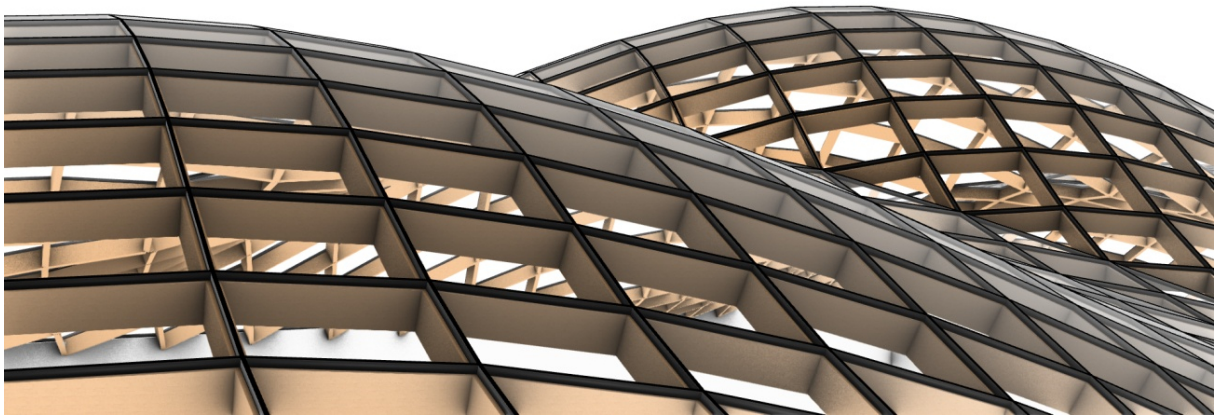

Rys. A-2.3 Propozycja przekrycia dziedzińca Kogod za pomocą gładkich, płaskich, czworobocznych paneli, zaprojektowana przy użyciu autorskich metod przedstawionych w pracy. Widok na dach z góry.

[99] Źródło: https://en.wikipedia.org/wiki/Queen_Elizabeth_II_Great_Court#/media/File:British_Museum_Great_Court,_London,_UK_-_Diliff.jpg

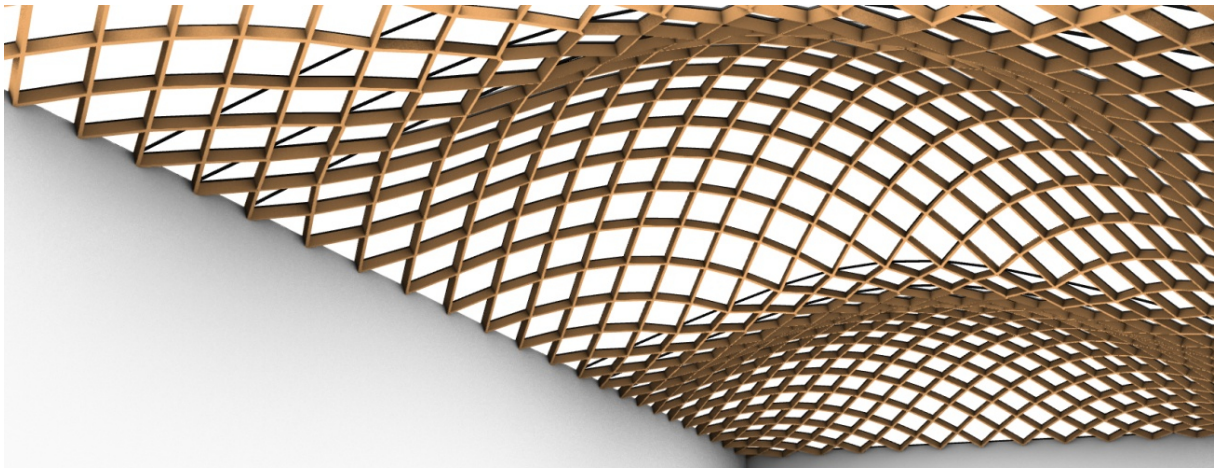

Rys. A-2.4 Propozycja przekrycia dziedzińca Kogod za pomocą gładkich, płaskich, czworobocznych paneli, zaprojektowana przy użyciu autorskich metod przedstawionych w pracy. Widok na dach z dołu.

A-2.2 Tematyka pracy

Tematem rozprawy doktorskiej jest autorskie opracowanie metodologii i narzędzi projektowych mających na celu umożliwienie projektantom tworzenie poprawnych geometrycznie przeszklonych powłok prętowych, które są jednocześnie optymalne ze względu na uwarunkowania technologiczne i konstrukcyjne.

Przedstawione powyżej zestawienie dwóch dachów szklanych, tj. dachu nad Kogod Courtyard w Instytucie Smithsonian oraz autorskiej koncepcji dachu o zbliżonym kształcie zaprojektowanego przy użyciu proponowanych metod, ukazuje jak metody i narzędzia projektowe wpływają na uproszczenie i zracjonalizowanie projektu. Oba dachy są powłokami prętowymi, czyli strukturami, które dzięki zakrzywieniu swojej formy w dwóch kierunkach mogą być realizowane jako struktury o bardzo niewielkich wymiarach przekroju poprzecznego elementów. Z kolei użycie do pokrycia tych dachów czworobocznych paneli szklanych daje wiele korzyści, takich jak zmniejszenie nasycenia powierzchni prętami, zmniejszenie masy konstrukcji, uproszczenie węzłów powłoki prętowej i ograniczenie ilości mostków termicznych oraz potencjalnych miejsc przecieków w stosunku do najczęściej stosowanych w dwukrzywiznowych dachach szklanych podziałów trójkątnych. O ile jednak powłokę o optymalnym konstrukcyjnie kształcie można w łatwy sposób pokryć płaskimi trójkątnymi panelami, to jej pokrycie czworobokami nie jest zadaniem trywialnym. Cztery wierzchołki czworokąta leżące na odwzorowywanej zakrzywionej powierzchni, nie leżą jednocześnie na tej samej płaszczyźnie, i na odwrót – cztery wierzchołki dowolnego czworokąta płaskiego na ogół nie dają się jednocześnie umieścić na odwzorowywanej powierzchni zakrzywionej. Z tego powodu, zastosowanie podziałów czworokątnych dla dowolnej, arbitralnie narzuconej powierzchni przekrycia, prowadzi do efektów takich jak w Kogod Courtyard, gdzie brak gładkości podziału był kompensowany za pomocą specjalnie opracowanego, skomplikowanego systemu uszczelnień. Warto zauważyć, że w praktyce nie są proponowane rozwiązania polegające na zastosowaniu zakrzywionych paneli szklanych, pomimo, że rozwiązywałoby to problem geometryczny. Jednakże takie rozwiązanie prowadziłoby do powstania nowych, jeszcze trudniejszych do rozwiązania problemów, związanych z odkształcalnością termiczną elementów zakrzywionych i uszczelnieniem krawędzi paneli.

Rozwiązaniem proponowanym w niniejszej pracy jest odwrócenie kolejności działań wykonywanych przez projektanta, który standardowo na początku opracowuje powierzchnię powłoki (arbitralnie ukształtowaną lub zoptymalizowaną konstrukcyjnie) a następnie dokonuje jej podziałów na fasety, przy czym najczęściej okazuje się, że nie jest możliwy racjonalny podział na czworoboki

a droższe podziały trójkątne są jedynym rozwiązaniem. Zamiast tego projektant może kształtować formę powłoki za pomocą superpozycji opisanych w pracy metod tworzenia (generowania) zakrzywionych planarnych siatek czworobocznych oraz metod ich przekształcania (transformacji) zachowujących planarność poszczególnych paneli. W tym wypadku w pierwszej kolejności projektant decyduje o podziałach a następnie o formie. Dzięki temu przy umiarkowanym ograniczeniu dowolności w kształtowaniu formy może on mieć zupełną pewność, że jego projekt jest możliwy do zrealizowania przy użyciu racjonalnych rozwiązań technologicznych.

Przedstawione metody oraz koncepcje narzędzi projektowych pozwalają na odtwarzanie zaprojektowanych form w sposób geometrycznie i technologicznie racjonalny oraz jak najbardziej zbliżony do form wyjściowych, a także otwierają nowe możliwości projektowania form swobodnych od podstaw. Katalog istniejących i proponowanych metod oraz narzędzi pozwala na projektowanie dachów szklanych, a także wszelkich innych struktur opartych na podziałach czworobocznych takich jak fasady, ogrody zimowe i wiaty.

A-2.3 Wprowadzenie w problematykę pracy

Projektowanie form swobodnych w architekturze staje się coraz popularniejsze dzięki upowszechnieniu stosowania zaawansowanych narzędzi projektowych. Historycznie formy swobodne wywodzą się z projektowania pojazdów, tj. łodzi, okrętów, samochodów oraz samolotów.

Przedstawiona w pracy historia form swobodnych pokazuje w jaki sposób narzędzia służące do projektowania kadłubów łodzi, statków, samochodów i samolotów, od zawsze związanych z formami swobodnymi, stały się obecnie narzędziami architektów i w jaki sposób wpłynęły one na przyjętą obecnie, niekorzystną zdaniem autora, metodologię projektową wymuszającą stosowanie mniej racjonalnych rozwiązań technologicznych. Zaawansowane narzędzia przeznaczone do projektowania form swobodnych zostały po raz pierwszy użyte do projektowania formy architektonicznej podczas realizacji Muzeum Guggenheima w Bilbao w latach 1994 – 1997. Projekt i realizacja tego budynku wymagały wtedy ścisłego współudziału zespołu inżynierów z branży lotniczej zaznajomionych z ich obsługą zarówno po stronie jednostki projektowej jak i po stronie wykonawców obiektu. Niewątpliwy sukces komercyjny tej realizacji wywołał współczesny fenomen „Efektu Bilbao", którego jednym z czynników jest upowszechnienie projektowania form swobodnych oraz stosowanie przez architektów narzędzi do ich kształtowania. Negatywnym skutkiem tego fenomenu jest jednak pominięcie przez wielu projektantów faktu, że możliwe do uzyskania przy użyciu tych narzędzi formy nie są przystosowane do stosowania w architekturze. Różnice między sposobem realizacji pojazdów i obiektów budowlanych implikują konieczność wykorzystywania różnych metodologii i narzędzi projektowych. Spośród tych różnic w niniejszej pracy wyszczególniono następujące:

- przegrody budowlane posiadają grubość oraz są wielowarstwowe, podczas gdy kadłuby/karoserie pojazdów realizowane są z arkuszy materiałów, których grubość w stosunku ich pozostałych wymiarów jest w praktyce pomijalna;
- seryjność realizowania pojazdów dzieli koszty opracowania technologii na ilość produkowanych egzemplarzy, podczas gdy budynek posiadający formę swobodną realizowany jest jednokrotnie i jego koszt musi obejmować technologię jego opracowania;
- inaczej niż w pojazdach, których karoserie są wykonywane z indywidualnych elementów wytwarzanych w wielkiej liczbie, w budynkach o formach swobodnych (inaczej niż np. w masowym budownictwie mieszkaniowym) stosowane elementy nie tylko mają indywidualne kształty ale również powstają w bardzo małej liczbie egzemplarzy;

- pojazdy realizowane są w całości na taśmach produkcyjnych w obrębie jednej fabryki, natomiast budynki o formach swobodnych realizowane są z elementów składowych, których wymiary powinny pozwalać na ich dostarczenie na plac budowy oraz umieszczenie we właściwym miejscu w realizowanym budynku.

Problemy te wyraźnie ujawniły się jeszcze przed pojawieniem się Efektu Bilbao, podczas realizacji Opery w Sydney, pociągając za sobą szereg konsekwencji takich jak odsunięcie terminu zakończenia realizacji o 8 lat, prawie stukrotne przekroczenie budżetu realizacji projektu, ale także pierwsze w historii użycie w tej skali komputerowych metod analiz konstrukcji, stworzenie symbolu całego kontynentu oraz ostateczne wyróżnienie architekta Jørna Utzona nagrodą Pritzkera. Choć spośród ponad dwustu nadesłanych projektów konkursowych zwycięska koncepcja składała się jedynie z ogólnego szkicu, zdobyła ona uznanie jurorów odwagą w zastosowaniu form swobodnych. Spośród wielu interpretacji i inspiracji form łupin Opery w Sydney przemawia fakt, że ich autor w młodości wspólnie ze swoim ojcem projektował i budował jachty. Sam w jednym z wywiadów stwierdził, że tworząc koncepcję Opery utożsamił brak bariery technologicznej między projektem a realizacją w przypadku jachtów z jej brakiem w przypadku budowli. Ostateczne rozwiązanie olbrzymich problemów realizacyjnych Opery przyniosło zastosowanie opisanych na wspólnej sferze, a więc i w pewnym stopniu powtarzalnych, przestrzennych betonowych prefabrykatów wytwarzanych w pobliżu miejsca realizacji budowli, zamiast powłok jak pierwotnie zakładał autor projektu.

Choć od tamtej pory możliwości technologiczne realizacji form swobodnych w architekturze znacznie się zwiększyły, to wspomniane problemy wciąż są aktualne i stoją na przeszkodzie między koncepcjami architektonicznymi a racjonalnymi możliwościami ich realizacji, ponieważ nie zmieniły się narzędzia projektowe dostępne dla architektów. Pomyślne realizacje form swobodnych w architekturze do niedawna pozostawały w domenie tak znanych projektów jak wspomniany już dach nad Wielkim Dziedzińcem im. Królowej Elżbiety w Muzeum Brytyjskim autorstwa Normana Fostera i Centrum Heydara Aliyeva w Baku autorstwa Zahy Hadid, w obu przypadkach wymagając zastosowania zaawansowanych matematycznie i algorytmicznie metod projektowych indywidualnie dostosowanych do potrzeb projektów. Podany w pracy przykład Muzeum Historii Żydów Polskich w Warszawie opisuje problemy technologiczne związane z realizacją głównego holu budynku posiadającego ściany o formach swobodnych, udowadnia, że w przypadku realizacji mających mniejszą rangę, łatwość w tworzeniu przez architektów wyjątkowych form przy użyciu zaawansowanych metod projektowych jest odwrotnie proporcjonalna do łatwości ich realizacji.

A-2.4 Wyjaśnienie tytułu pracy

Przegląd literatury przedstawiony w pracy nie wykazuje jednoznacznej definicji form swobodnych stosowanych w architekturze. Dla części cytowanych badaczy są to formy zakrzywione w nieregularny sposób, nie posiadające we fragmentach swojej formy powtarzalności. Dla innych badaczy formy konstrukcji membranowych, posiadających powyższe cechy, nie kwalifikują się jako formy swobodne, ponieważ swoboda ich projektowania ograniczona jest przez rodzaj powierzchni na jakich te konstrukcje są opisywane. Są nimi powierzchnie minimalne, czyli matematycznie i fizycznie zdefiniowane za pomocą warunków zewnętrznych powierzchnie możliwe do uzyskania w procesie *form finding*. Konsekwentnie każda inna forma, nie tylko membranowa, zaprojektowana w procesie *form finding* nie jest przez tych badaczy kwalifikowana jako forma swobodna. W niniejszej pracy jako formę swobodną przyjmuję się formę opisaną na powierzchni posiadającej zakrzywienie, stałe lub zmieniające się, w dwóch kierunkach czyli dwukrzywiznową, niezależnie od tego czy jest ona wynikiem optymalizacji konstrukcyjnej, czy rzeźbiarską wizją projektanta.

Zasadność kształtowania struktur w postaci form swobodnych zasadza się na możliwości realizowania ich jako lekkich konstrukcji. To dzięki zakrzywieniu możliwe jest realizowanie powłok, podczas gdy ta sama struktura realizowana z płaskich połaci musi z reguły dodatkowo wzmacniana poprzez zastosowanie większych przekroi prętów oraz zastosowaniem struktur przestrzennych.

Obecnie jednymi z najczęściej realizowanych w architekturze form swobodnych są przeszklone powłoki prętowe, czyli powłoki składające się z prętów, węzłów oraz paneli szklanych. Krzywizna takich powłok prętowych jest dyskretna, co oznacza, że ich ogólna forma jest zakrzywiona czyli węzły siatki leżą na zakrzywionej powierzchni, natomiast jej poszczególne elementy składowe nie są zakrzywione, czyli pręty są proste a panele są płaskie. Realizowanie dyskretnych, dwukrzywiznowych powłok prętowych, w przeciwieństwie do powłok prętowych o stałej krzywiźnie, w ograniczonym stopniu może korzystać z unifikacji ich elementów składowych. Pręty mogą różnić się długościami i kątami między sobą, ale są proste a tafle szklane mogą mieć różne kształty ale są płaskie.

Topologia powłok prętowych odnosi się do kształtu poszczególnych paneli oraz ilości prętów zbiegających się w każdym węźle powłoki. Dwie najczęściej stosowane topologie to: trójkątna (patrz Rys. A-2.6) i planarna czworoboczna (z ang. *planar quadrilateral* – w skrócie PQ; patrz Rys. A-2.5). Powłoki prętowe o topologii trójkątnej składają się z trójkątnych paneli oraz węzłów łączących sześć prętów, natomiast powłoki prętowe o topologii PQ składają się z płaskich, czworobocznych paneli i węzłów łączących cztery pręty. Praca zawiera autorską analizę różnic między tymi topologiami a także opiera się na analizach innych, cytowanych autorów. Spośród różnic między tymi topologiami na niekorzyść siatek trójkątnych przemawiają następujące czynniki:

- panele trójkątne są kosztowniejsze w produkcji niż czworoboczne, gdyż wiążą się w większą ilością odpadów szkła; trudności sprawia też możliwość pękania narożników o zbyt małym kącie wierzchołka;
- w siatkach o topologii trójkątnej jest wyższy stosunek liczby elementów konstrukcyjnych do powierzchni szklenia niż w siatkach o topologii PQ (rysunek poniżej);
- węzły siatek trójkątnych są bardziej skomplikowane i rozbudowane niż w siatkach PQ;
- w siatkach trójkątnych występuje więcej mostków termicznych oraz potencjalnych źródeł nieszczelności niż w siatkach PQ.

Łatwość w projektowaniu siatek trójkątnych przekłada się na przewagę w liczbie ich realizacji, pomimo iż siatki PQ są bardziej racjonalne pod względem technicznym i ekonomicznym. Przewaga ta jest spowodowana przez przyjętą powszechnie metodologię, nazwaną „z góry do dołu”, w której architekt w początkowej fazie opracowywania projektu tworzy za pomocą dostępnych narzędzi projektowych powierzchnię swobodną, na której docelowo ma zostać opisana powłoka prętowa. Ponieważ dowolny trójkąt, niezależnie od lokalizacji jego wierzchołków w przestrzeni jest płaski, to opisanie trójkątnych paneli na zadanej przez architekta powierzchni oraz ich przemieszczanie w celu optymalizacji długości prętów oraz kształtów paneli pozwala na nieograniczoną swobodę kształtowania formy geometrycznej powłoki. W przypadku paneli czworobocznych ich planarność nie jest oczywista przy umieszczeniu ich wierzchołków na odgórnie zadanej przez projektanta formie swobodnej. Stąd w niniejszej pracy postulowane jest stosowanie podejścia oddolnego, które opiera się na takim kształtowaniu powierzchni swobodnych, które oddolnie uwzględnia możliwość wypełnienia ich płaskimi, czworobocznymi panelami. Dostępne dla architektów narzędzia nie oferują wystarczających metod kształtowania form swobodnych, które w konsekwencji umożliwiały by ich realizację w optymalnej topologii.

Rys. A-2.5 Przekrycie z siatką PQ.

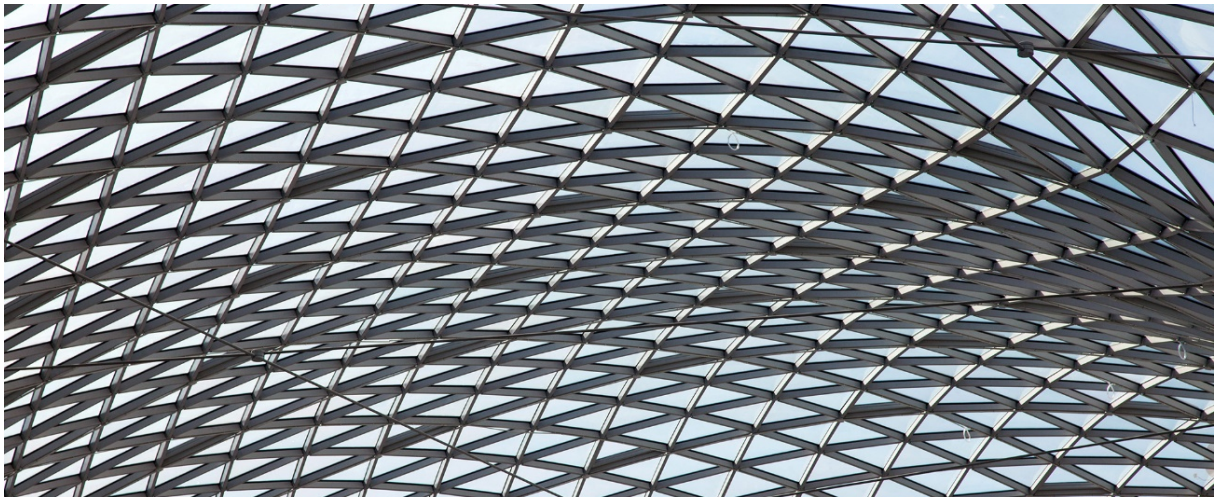

Rys. A-2.6 Przekrycie z siatką trójkątną.

W wyniku przeprowadzonych badań i analiz stwierdzono, że możliwe jest sformułowanie metodologii projektowania, którą nazwano podejściem „z dołu do góry" oraz metod generowania i przekształcania siatek czworokątnych, które umożliwią ich projektowanie w praktycznie wszystkich występujących przypadkach. Powyższe stało się podstawą do sformułowania tez niniejszej rozprawy doktorskiej.

A-2.5 Tezy pracy

Po początkowym, entuzjastycznym okresie tuż po „Efekcie Bilbao" realizacja wielu obiektów opartych na formach swobodnych uwidoczniła problem oderwania formy od racjonalności konstrukcji. Forma stała się środkiem ekspresji architektury samym w sobie, oderwanym od czynników związanych z jej implementacją. Szczególnie istotnym i interesującym przykładem takich form swobodnych są dyskretne, przeszklone powłoki prętowe realizowane jako dachy szklane i fasady, które mogą być kształtowane jako arbitralne, ekspresyjne formy, bądź zoptymalizowane pod względem konstrukcyjnym lekkie powłoki.

- **Teza 1**

  Powłoki prętowe są jednymi z głównych środków wyrazu w obrębie trendu projektowania form swobodnych w architekturze i należą do najbardziej charakterystycznych i najczęściej realizowanych obiektów w tej grupie.

- **Teza 2**

  Powłoki prętowe o formach swobodnych oparte na topologii płaskiej czworobocznej (*planar quadrilateral* – PQ) posiadają wiele zalet w porównaniu do powłok prętowych opartych o topologię trójkątną.

- **Teza 3**

  Możliwe jest opracowanie narzędzi projektowych pozwalających efektywnie projektować powłoki siatki PQ w oparciu o metodologię oddolną.

- **Teza 4**

  Kierując się zasadami projektowania opartego na metodzie oddolnej, pożądane powłoki prętowe można uzyskać przy niewielkim i akceptowalnym ograniczeniu swobody w kształtowaniu ich formy.

A-2.6 Wyniki pracy

Wynikiem pracy jest stworzenie bazy istniejących i autorskich metod tworzenia i przekształcania siatek PQ, które stanowią podstawę opracowania kompleksowego systemu projektowego. Odpowiednie zestawienie wybranych metod tworzenia i przekształcania pozwala na kształtowanie dwukrzywiznowych powłok prętowych o topologii PQ dostosowanych do wymaganych istniejących warunków, np. kształtu zadaszanego dziedzińca. W pracy przedstawiono opracowaną koncepcję narzędzia projektowego opartego na opisanych wcześniej metodach generowania i transformacji siatek PQ, a następnie szczegółowo przedstawiono dwa przykładowe zastosowania praktyczne opracowanych narzędzi oparte na tej koncepcji i wybranych metodach generowania i przekształcania siatek PQ.

Jako przykład aplikacji opracowanych zgodnie z koncepcją narzędzi projektowych wybrano zadaszenia dziedzińców w dwóch istniejących budynkach wrocławskich. Pierwszym z nich jest budynek Dolnośląskiego Urzędu Wojewódzkiego, który posiada aż trzy dziedzińce z których dwa mają kształt zaokrąglonego czworoboku. Dla jednego z nich zaproponowano przeszklone przekrycie przedstawione na rysunku A-2.7. Zaproponowane rozwiązanie opiera się na metodzie translacyjnej tworzenia siatki PQ oraz na autorskim przekształceniu SC (odwzorowaniu sferyczno-cylindrycznym), które dokładnie przekształca podstawową formę siatki do zaokrąglonej formy dziedzińca zachowując planarność wszystkich faset. Opracowane narzędzie zawiera również szereg opisanych w pracy kroków pośrednich, które w założeniu mają zwiększyć kontrolę nad ostateczną formą dachu sprawowaną przez projektanta a jednocześnie gwarantują geometryczną poprawność rozwiązania.

Drugi przykład dotyczy dziedzińca w budynku Wydziału Nauk Biologicznych Uniwersytetu Wrocławskiego przy ul. Kuźniczej 35. Dziedziniec ten posiada formę nieregularnego czworoboku, a otaczają go odcięte obecnie od niego oknami krużganki. Podobnie jak w poprzednim przypadku, do zaprojektowania siatki PQ użyto narzędzie oparte na metodzie translacyjnej tworzenia siatki oraz na autorskiej metodzie przekształcania, tj. transformacji perspektywicznej. Ta metoda przekształcania pozwala na dopasowanie dowolnej siatki PQ o płaskiej, czworobocznej podstawie do dowolnej czworobocznej, nieregularnej formy dziedzińca, patrz Rys. A-2.8.

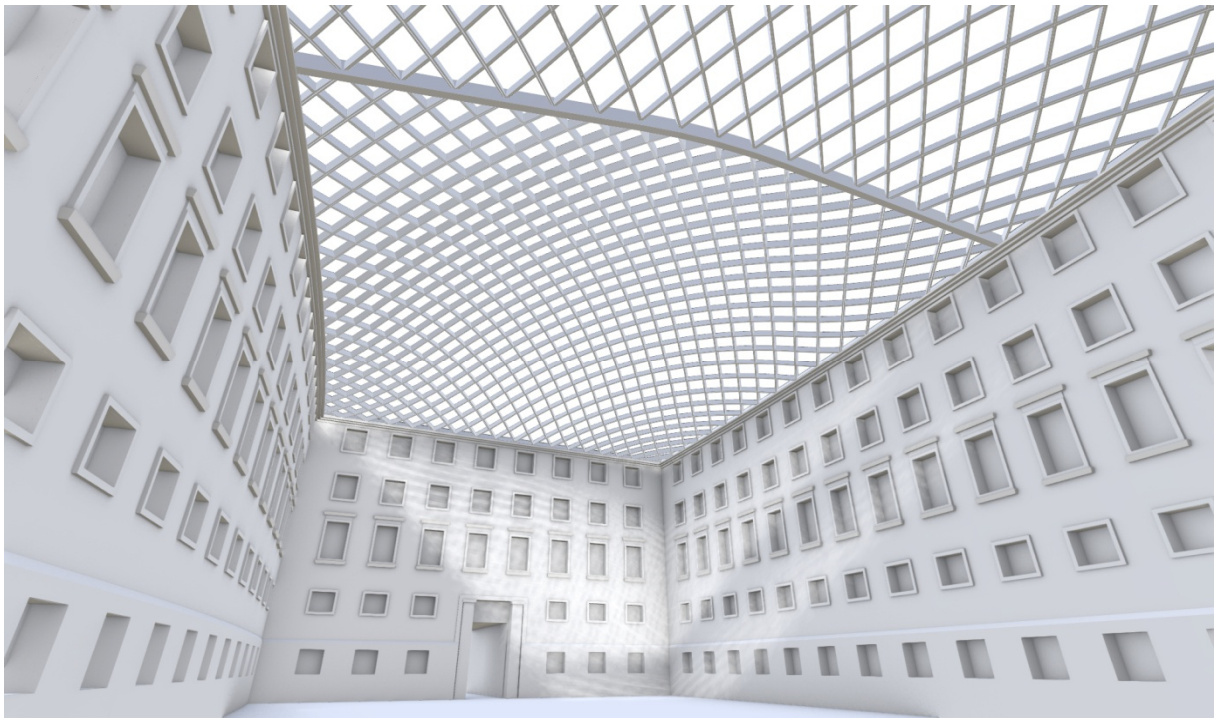

Rys. A-2.7 Propozycja przekrycia dziedzińca budynku siedziby Dolnośląskiego Urzędu Wojewódzkiego we Wrocławiu.

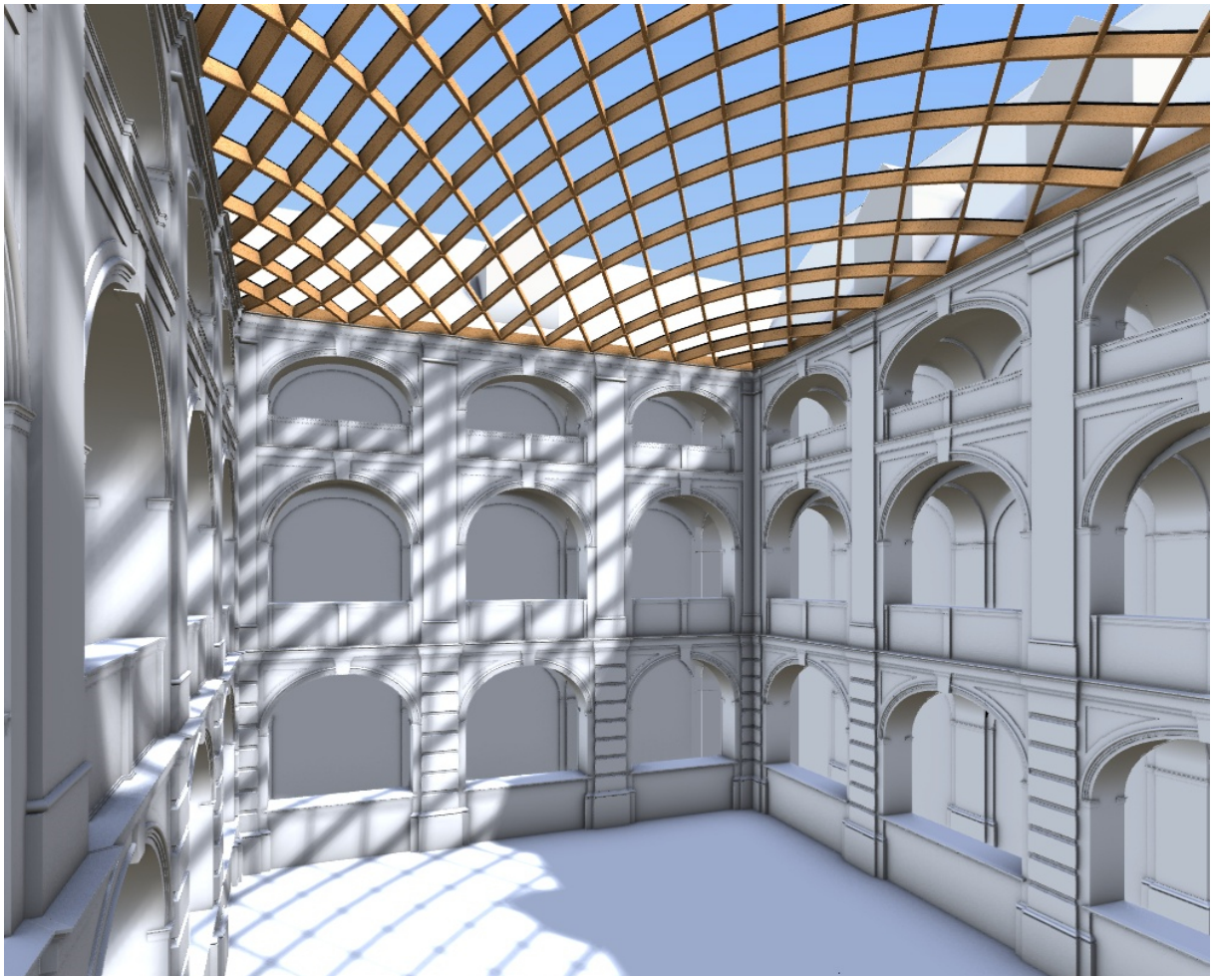

Rys. A-2.8 The proposed cover of the courtyard in the building of the Faculty of Biological Sciences of the University of Wrocław.

W obu przypadkach projektant wskazuje na rzucie budynku trzy lub cztery punkty narożne, zależnie od przypadku projektowego, na podstawie których zaprogramowane narzędzie automatycznie dopasowuje odpowiednie parametry przekształceń. Oba narzędzia zapewniają szereg możliwości modyfikacji formy dając projektantowi jak największą swobodę jej kształtowania. Projektant za pomocą zmiany wartości parametrów dla narzędzia decyduje o ilości i rozmieszczeniu podziałów siatki a tym samym ma wpływ na rozmiary paneli szklanych, wysokości strzałki dachu etc. Za pomocą kilku innych parametrów ma również wpływ na sam kształt otrzymanej formy przy zachowaniu ustalonych na początku jej punktów narożnych.

Parametry za pomocą których projektant kontroluje formę powłoki prętowej PQ ograniczają absolutną swobodę kształtowania charakterystyczną dla paradygmatu projektowania metodą „z góry na dół", lecz ograniczają go do zbioru morfologii racjonalnych z geometrycznego punktu widzenia. Projektant może uzyskać takie formy, które są racjonalne z punktu widzenia realizowalności. Z tego powodu jeden z badaczy w tej dziedzinie geometrii w architekturze, Romain Mesnil, nazywa podejście „z dołu do góry" *fabrication aware design*, czyli projektowanie ze świadomością możliwości wytwórczych.

Dostępne formy podstawowej siatki translacyjnej PQ o płaskiej podstawie sparametryzowane za pomocą dwóch parametrów kształtowania formy zostały zbadane pod względem wartości sił wewnętrznych metodą elementów skończonych. Wyniki przedstawione w pracy dowodzą, że optymalna forma powłoki prętowej, w której siły wewnętrzne mają najmniejsze wartości jest formą dwukrzywiznową o wysokim stopniu ciągłości krzywizny. Dzięki temu dach o takiej formie możliwy jest do zrealizowania z elementów konstrukcyjnych o mniejszych przekrojach niż w przypadku formy konwencjonalnej, tj. ortogonalnej składającej się z układów płaskich połaci, a przede wszystkim jest możliwe kształtowanie dachów szklanych jako powłoki a nie kratownicy przestrzennej, która w wielu przypadkach jest rozwiązaniem kolidującym z estetyką budynku, przede wszystkim w kontekście zabudowywania dziedzińców obiektów zabytkowych. Stosowanie proponowanych w pracy narzędzi przekłada się więc w sposób bezpośredni na zmniejszenie zużycia materiałów, w kwestii optymalizacji formy i topologii, a ostatecznie na racjonalizację ekonomiczną stosowania tych rozwiązań.

A-2.7 Udowodnione tezy pracy

A-2.7.1 Teza 1

Analizy obiektów reprezentatywnych dla trendu projektowania form swobodnych przeprowadzone w rozprawie pozwoliły prześledzić zastosowanie form swobodnych w ukończonych obiektach i zdefiniować najczęściej im przypisywane funkcje. Są to przede wszystkim elementy obiektów, które określają ich wizualną percepcję, takie jak elewacje budynków (często w postaci drugiej skóry) i pokrycia dachowe całych obiektów lub ich części, zwłaszcza zadaszenia dziedzińców, wiaty wejściowe itp. Szczególne miejsce wśród nich zajmują konstrukcje prętowe, które z jednej strony pozwalają na uzyskanie efektywności strukturalnej, a z drugiej dają dodatkowe możliwości kształtowania formy za pomocą przezroczystych wypełnień. Katalog obiektów, które systematyzują dane na ich temat, zamieszczony w Aneksie do pracy, okazał się pomocny w wyciągnięciu wniosków. Na podstawie przenalizowanych danych dotyczących tezy 1 można stwierdzić, że:

Wśród obiektów o formach swobodnych, powłoki prętowe zajmują szczególnie ważne miejsce i stanowią jedną z najważniejszych grup struktur w ramach tego trendu. Ponieważ pozwalają one na uzyskanie form o znacznych rozpiętościach, przy tym są wyraźnie lekkie, a poprzez duże przeszklenia dobrze widoczne, stały się najczęściej realizowanymi obiektami w tej grupie. Cechy te umożliwiły powszechną akceptację społeczną tych nowych form geometrycznych, przyczyniając się w znacznym stopniu do rozpowszechniania swobody kształtowania form w architekturze.

A-2.7.2 Teza 2

Analiza różnych rozwiązań przeprowadzona z uwzględnieniem topologii, geometrii, konstrukcji i materiałów pozwoliła stwierdzić, że najczęściej projektowane i konstruowane są powłoki prętowe, których panele szklane są trójkątne. Takie rozwiązanie pozwala uzyskać gładką siatkę na prawie każdej powierzchni, zapewniając jednocześnie niezbędną sztywność konstrukcji. Siatki o takiej topologii są stosunkowo łatwe do zaprojektowania i mogą być wpisane w prawie każdym zamknięty kontur. Panele trójkątne zdefiniowane przez krawędzie siatki (pręty) są zawsze płaskie. Dostępne są komputerowe narzędzia do projektowania takich siatek.

W tym samym czasie odkryto wiele wad tego rozwiązania. Najważniejsza jest złożona budowa węzłów, w których podłączonych jest do sześciu prętów. Ogólna liczba prętów oraz powierzchnia dachu zajęta przez nie jest również znacznie większa. Trójkątne panele szklane są również mniejsze. Te negatywne cechy nie pojawiają się w siatkach o topologii czworobocznej. Liczba prętów połączonych w jednym węźle takiej siatki wynosi cztery, a względna liczba prętów jest mniejsza. Wizualne postrzeganie takich struktur jest znacznie bardziej korzystne. Pod pewnymi względami wykazują one również bardziej korzystne właściwości mechaniczne. Ważnym ograniczeniem w projektowaniu siatek z topologią czworokątną jest fakt, że panele w takiej siatce nie zawsze są płaskie. Z tego powodu konieczne jest ograniczenie ich różnorodności do topologii płaskiej czworobocznej (PQ – *planar quadrilateral*). Istnieją jednak ograniczenia w stosowaniu tej topologii, ponieważ nie można jej zastosować na każdej zdefiniowanej wcześniej powierzchni. Obecnie nie ma również dostępnych narzędzi do projektowania siatek o takiej topologii. W stosunku do tezy 2, można stwierdzić, że:

Wśród realizowanych obiektów, w których zastosowano przeszklone powłoki prętowe, dominują struktury o topologii trójkątnej. Obecnie jednak powstaje coraz więcej obiektów z topologią PQ. Chociaż trudniej uzyskać go w procesie projektowania, ma wiele istotnych zalet w porównaniu z topologią trójkątną.

A-2.7.3 Teza 3

W rozprawie przeprowadzono szeroką dyskusję na temat znanych metod kształtowania siatek PQ na powierzchniach swobodnych. Obejmują one zarówno metody już stosowane w praktyce, jak i metody, które nadal stanowią rozwiązania teoretyczne. Mają one różny zakres zastosowań, a także różne zalety i wady. Ponadto przeanalizowano znane metody transformacji tych siatek, które zachowują płaskość paneli po transformacji. Zarówno metody tworzenia siatek, jak i metody ich transformacji, odnoszą się do metod geometrii dyskretnej.

Wyniki badań pozwoliły na sformułowanie własnych, oryginalnych metod generowania siatek PQ oraz metod ich transformacji. Metody te pozwalają znacznie zwiększyć zakres zastosowań siatek PQ. Ponadto zauważono, że wiele ograniczeń w stosowaniu tych siatek wynika z przyjętej metodologii projektowania, którą można określić jako "odgórną". Polega ona na dostosowaniu siatki do ustalonej

uprzednio powierzchni swobodnej. W tym podejściu wiele geometrycznych form powłok jest wykluczonych z możliwości zastosowania podziałów PQ. Ten problem został zasadniczo rozwiązany poprzez zmianę metodologii projektowania na "oddolną". Polega ona na wygenerowaniu siatki wyjściowej o pożądanych cechach, a następnie jej transformacji w celu uzyskania wystarczającej zgodności z założoną powierzchnią wyjściową. W odniesieniu do tezy 3, można stwierdzić, że:

> **Opracowując odpowiednie metody generowania i przekształcania siatek PQ oraz stosując metodologię oddolną, można je efektywnie projektować dla różnych warunków brzegowych.**

A-2.7.4 Teza 4

W ramach badań przeprowadzono symulacje i modelowanie komputerowe w celu sprawdzenia zakresu kształtowania siatek PQ przy użyciu znanych i proponowanych metod, z wykorzystaniem metodologii oddolnej. Szczególnie przydatne okazały się dwa studia przypadku, polegające na zaprojektowaniu przeszklonych zadaszeń nad wewnętrznymi dziedzińcami w dwóch istniejących obiektach. Przeprowadzone analizy wykazały, że zakres kształtowania siatek PQ jest bardzo duży i możliwe jest dostosowanie ich do niemal każdej sytuacji projektowej, a także dla siatek o topologii trójkątnej. Warunkiem, który to umożliwia, jest projektowanie zgodnie z metodologią oddolną. Przyjęcie żądanej powierzchni bazowej a priori może uniemożliwić, i w większości przypadków uniemożliwia, wykorzystanie siatek PQ. Przekształcając, przy zachowaniu płaskości paneli, początkowo wygenerowaną, prostą siatkę PQ w taki sposób, że w końcu jest ona jak najbliżej zbliżona do żądanej powierzchni bazowej, można uzyskać satysfakcjonujące wyniki pod względem architektonicznym. W odniesieniu do tezy 4, można stwierdzić, że:

> **Proponowana oddolna metodologia projektowania wraz z odpowiednimi narzędziami o generowania i przekształcania siatek pozwala projektować powłoki prętowe o topologii PQ dla dowolnej sytuacji projektowej, z małym i akceptowalnym ograniczeniem swobody projektanta w zakresie kształtowania ogólnej formy takiej powłoki prętowej.**

A-2.8 Wnioski

Zaproponowane w pracy narzędzia projektowe i bazująca na nich metodologia projektowania pozwalają zdecydowanie rozszerzyć zakres stosowania siatek PQ w obiektach o formie swobodnej. Na ich podstawie można rozwiązywać praktyczne problemy o dużym stopniu trudności.

Biorąc pod uwagę liczbę istniejących oraz proponowanych przez autora pracy metod tworzenia oraz przekształcania siatek PQ możliwe jest stworzenie wielu scenariuszy adekwatnych do istniejących uwarunkowań projektowych jakimi może być na przykład kształt dziedzińca, ale mogą nimi być również kształt fasady budynku lub obudowy stadionu. Dziewięć przedstawionych metod tworzenia siatek PQ może być zestawionych z pięcioma metodami ich przekształceń, przy czym spośród metod przekształceń w danym narzędziu projektowym mogą zostać użyte również dwa, trzy, cztery lub pięć metod jednocześnie. Zbiór pięciu metod przekształcania daje 32 podzbiory ich zestawień, a po pomnożeniu przez dziewięć metod tworzenia siatek PQ daje aż 288 różnych narzędzi projektowania, z których każde obejmuje metodę tworzenia i przekształcania siatek, prowadząc do określonych rezultatów i dając kontrolę nad formą projektowanej struktury.

Dodatkowo koncepcja narzędzia do projektowania siatek PQ przedstawiona w pracy przewiduje po cztery pomocnicze wstępne oraz końcowe transformacje nie likwidujące planarności faset. Transformacje pomocnicze mogą być używane równolegle z podstawowymi i są one sparametryzowane zwiększając dodatkowo swobodę projektowania.

W sposób pośredni stosowanie proponowanych rozwiązań pozwala na tworzenie dodatkowych przestrzeni użytkowych w obrębie istniejących budynków, oraz na tworzenie stref buforowych zwiększających oszczędność energetyczną budynków. W przeciwieństwie do większości istniejących rozwiązań kształtowania powłok prętowych, trójkątnych oraz PQ, dokładność uzyskiwanych rozwiązań pozwala na ich stosowanie w nowo projektowanych budynkach, gdzie forma dachu może zostać skoordynowana z formą budynku, oraz w istniejących budynkach o prostym, regularnym kształcie dziedzińca, proponowane narzędzia oparte na metodach przekształcania pozwalają na absolutną dokładność dostosowania formy siatki PQ do istniejącego, nieregularnego kształtu dziedzińca. Sytuacje te występują szczególnie w przypadku historycznych centrów miast, w których budynki często posiadają nieregularne formy i nie jest możliwa zmiana tych uwarunkowań przez ich przebudowę a z drugiej strony wysoka gęstość zabudowy wymaga poszukiwania innych sposobów uzyskiwania dodatkowych powierzchni użytkowych.

Nie jest jednak wykluczone stosowanie proponowanych narzędzi do kształtowania powłok prętowych PQ w przypadku nowo projektowanych obiektów. Dzięki innym zestawieniom przedstawionych w pracy metod tworzenia i przekształcania siatek PQ, istniejących oraz proponowanych przez autora, zgodnym z proponowaną przez autora koncepcją narzędzia projektowego, możliwe jest szerokie spektrum dostępnych, poprawnych geometrycznie morfologii PQ, w tym dachów szklanych o innych, nieregularnych obrysach, nie tylko planarnych, fasad oraz kopuł. W pracy przedstawiono również koncepcję zastosowania obu zaproponowanych metod przekształcania, tj. SC oraz transformacji perspektywicznej w celu uzyskania formy siatki PQ o obrysie składającym się z odcinków krzywych stożkowych, tj. krzywych NURBS drugiego stopnia. Daje to narzędzie do projektowania zadaszeń nad dziedzińcami o szczególnie złożonym rzucie i ograniczeniach związanych z kształtem i wysokością otaczających ścian.

A-3 Overview of constructed glazed grid shells

This chapter contains an overview of selected constructed glazed grid shells. The overview is divided into three sections considering triangular, PQ and hybrid topologies.

A-3.1 Grid shells based on triangular topology

List of objects in chronological order:

Queen Elizabeth II Great Court

Location: **London**, UK
Date of construction: **1994**
Architecture: **Foster + Partners**, **Norman Foster**, London Structural engineering: **BuroHappold**, Bath, UK; **Zenkner & Handel** (glazing), Graz; **Mike Cook** (structural engineer) Steel & glass construction: **Waagner-Biro**, Vienna; **Qualter, Hall & Co Ltd.**, Barnsley
The roof was designed with the use of sophisticated non-linear form finding methods. Both the geometry and tessellation (alignment of nodes) of the grid shell were subjects of optimization. Although the courtyard's shape is a rectangle the complexity of resultant grid shell is conditioned by the rotunda in the middle of it. Therefore the adopted tessellation had to be a combination of radial and rectangular patterns made of triangles, what had been successfully achieved.
   
Sources of photos: https://www.geograph.org.uk/photo/2067349 https://www.fosterandpartners.com/projects/great-court-at-the-british-museum/

Meeting Hall Flemish Council

Location: **Brussels**, Belgium
Date of construction: **1994**
Architect: **ARROW Architecture and Engineering**, Gent, Belgium Conceptual & construction design: **sbp – Schlaich Bergermann Partner**, Stuttgart, Germany
This glazed roof covers the six sided courtyard with a very irregular shape and sides of different lengths. Support conditions are also complex, since the roof is supported one level above the floor of courtyard, on a horizontal cornice just below second row of windows. High curvature of the shape of roof allowed for the construction of lightweight, single layered structure and placing the Meeting Hall under it. The layout of nodes and members is not regular in top projection, however the continuity of trusses is very consistent, since the positions of individual nodes were optimized.

Source of photo: http://www.arrowarchitecture.be/

New Milan Trade Fair, Vela roof

Location: **Milan**, Italy
Date of construction: **2005**
Architecture: **Massimiliano Fuksas** Structural engineering: **sbp – Schlaich Bergermann Partner**, Stuttgart Engineering: **Hans Schober** (engineer) Steel construction: **Mero GmbH & Co. KG**, Würzburg
The Vela-roof is a 1,3 km long glazed roof containing planar, single- and doubly-curved regions which have synclastic and anticlastic curvatures. The roof is supported by tree-like columns and *volcanos*, i.e. funnels descending from planar regions into the ground level. The diamond pattern creates tessellation on the planar region and was also initially projected on curved regions, however on the later ones the tessellation was optimized by adding diagonal members creating triangular pattern, shifting locations of nodes and changing their valency. The criteria for optimisation were the allowed extreme lengths of members (0,8 to 3,0 m) and the least angle between adjacent members (20°, preferably 30°). Detailed description of the roof design is in (Schlaich, Schober, and Kürschner 2005).

Source of photo: https://www.sbp.de/fileadmin/sbp.de/projects/0605F10876C38E48C1257E7500364FE2_0_1_2109_1221_b_MAX.jpg

Feria Valencia - Foro Sur / Centro de Eventos

Location: **Valencia**, Spain

Date of construction: **2006**

Design: **Tomás Llavador Arquitectos+Ingenieros**, **José María Tomás Llavador**, Valencia
Structural engineering: **Areas Ingenieria y Arquitectura S.L.**, Madrid; **MC2 Estudio de Ingeniería, S.L.**, Madrid
Roof system / Façade: **Mero GmbH & Co. KG**, Würzburg

The roof / facade is in half-oval shape which intersects with orthogonal form of the building on which it stands. It covers four-story high hall and doubles its height by rising over the building. It is a single layered grid shell which is supported along two horizontal edges and one edge placed on vertical wall of the building. On one side the form is cut and closed by vertical façade.

Source of photos: https://www.mero.de/index.php/en/construction-systems/references-en/36-space-structures/89-foro-sur-valencia-spanien-en

Roof over inner courtyard of Odeon

Location: **Munich**, Germany
Date of construction: **2007**
Architecture: **Ackermann and Partner**, Munich Structural engineering: **Knippers Helbig GmbH**, Stuttgart, Berlin, New York
The grid shell covers a courtyard, which three sides are in form of straight lines, whereas the fourth one is a semicircle. Initially the form of roof was modelled as doubly curved NURBS surface on which a regular mesh of equilateral triangles was projected. The mesh created by this projection was used as cable network to simulate inverted hanging model. That form-finding method generated the final, optimized form of the grid shell. Mode details of this procedure are discussed in (Schober 2015b) pp. 163–164.

Source of photo: https://www.sbp.de/en/project/roof-over-inner-courtyard-of-odeon/

Złote tarasy

Location: **Warsaw**, Poland
Date of construction: **2007**
Architecture: **Jon Jerde Partnership**, Venice, Los Angeles, California; **Epstein** Sp. z.o.o., Warszawa Structural design: **Ove Arup & Partners, Zenkner & Handel**, Graz Steel construction: **Waagner-Biro**, Vienna
The structure is arbitrarily shaped and additionally supported by tree-like columns. It is constructed with steel RHS members connected through welding to nodes cut from steel plates, i.e. *End-Face Connectors WABI-1* (Soeren, Sánchez-Alvarez, and Knebel 2004). Facets are almost isosceles right triangles resulting with differentiated lengths of edges.
   
Sources of photos: https://d2qq3nlndk9vv6.cloudfront.net/images_dynam/reference_big/wb_steel_glass_zlote-tarasy_shutterstock_12751525_rgb3.jpg https://www.wacker.com/cms/en/wacker_group/innovations/magazine2013/stahltraeger_im_schaummantel/stahltraeger_schaummantel_1.jsp

Bolton Sixth Form College

Location: **Bolton**, England
Date of construction: **2008**
Architect: **Taylor Young** Roof design and engineering: **Novum Structures**, Menomonee Falls, USA
In this example the assumptions are similar as in previous example, however the tessellation is not regular in top projection. Positions of individual nodes are shifted in order to compromise the continuity of trusses, i.e. rows of members are more continuous than in previous example, and the uniformity of shapes of glass panels. The grid shell is constructed of laminated timber members and tubular steel nodes with fin plate connectors.

Source of photo: https://novumstructures.com/wp-content/uploads/2010/11/project_bolton-sixth-form-college_0.jpg

MyZeil

Location: **Frankfurt**, Germany
Date of construction: **2009**
Architecture: **Massimiliano Fuksas** Structural design: **Knippers Helbig GmbH**, Stuttgart, Berlin, New York Steel construction: **Waagner-Biro AG**, Vienna
The grid shell in MyZeil is composed of façade part, glazed roof and a tunnel connecting both parts. Planar façade is planar composed of diamond shaped, flat cells, whereas the free formed tunnel and glazed roof are tessellated into triangles. Due to large amounts of angular defect the valency of some nodes had to be optimized (reduced) from 6 to 5. A large curvature of the form also causes high heterogeneity of triangles' forms, sizes and member lengths.
   
Sources of photos: https://commons.wikimedia.org/wiki/File:Myzeil-knippershelbig-02.jpg https://files1.structurae.de/files/photos/2621/myzeil_02.jpg

Madrid City Hall

Location: **Madrid**, Spain
Date of construction: **2009**
Architecture: **Arquimática S.L.**, Madrid Structural design: **sbp – Schlaich Bergermann Partner**, Stuttgart Contractor: **Lanik**, San Sebastian, Spain Façade engineering: **Ove Arup & Partners**
The structure is form-found using the idea of catenary surfaces. Due to the geometrically complex shape of the courtyard the triangular topology was adopted. Triangular tessellation of the mesh is composed of almost equilateral triangles resulting with similar lengths of members. The structure is constructed with RHS components connected by nodes using bolted connections.
   
Sources of photos: https://www.arup.com/projects/communications-palace https://www.sbp.de/en/project/palacio-de-comunicaciones-courtyard-roof/

Expo Axis Megastructure

Location: **Shanghai**, China
Date of construction: **2009**
Architecture: **SBA GmbH**, Stuttgart, München, Shanghai; **Hong Li**, **Bianca Nitsch** Structural engineering: **Knippers Helbig GmbH**, Stuttgart, Berlin, New York
The grid shells in Expo Axis Megastructure are in form of funnels supported only at the bottom. The form expands from the bottom ending with top outline which area significantly exceeds the bottom footprint. The tessellation not only include topological aspects like diverse valency of nodes (from 5 to 8, all panels being triangular) compensating angle defect, but also the best possible alignment of nodes in terms of static performance.

Source of photo: https://www.knippershelbig.com/sites/default/files/styles/projekt1494/public/image_project//12421-picture.jpg?itok=hBzgsg3e

Rossignol World Headquarters

Location: **Saint-Jean-de-Moirans**, France
Date of construction: **2009**
Architect: **Hérault Arnod Architectes**, Pantin, France
The grid shell in this example is a façade of generally free formed elevation. It is composed of triangular panels, whose dimensions decrease towards the top. The façade has doubly-curved, synclastic form of small, regular curvature.

Source of photo: http://objektiv-online.de/en/home/projects/project-detail/object/460/

Chenshan Botanical Garden

Location: **Shanghai**, China
Date of construction: **2010**
Architecture: **Auer+Weber+Assoziierte**, Munich Conceptual & construction design: **sbp – Schlaich Bergermann Partner**, Stuttgart
Shape of the structure was a subject of form finding optimization. The grid shell is made of aluminium instead of usually used steel. Due to the large spans, up to 200 m, and joint-less connections the structure required special solutions to compensate considerable thermal expansions.
   
Sources of photos: https://www.sbp.de/en/project/botanical-garden-shanghai/ http://www.auer-weber.de/en/projects/details/buildings-in-the-botanical-garden-shanghai.html

Admirant Eindhoven

Location: **Eindhoven**, Netherlands
Date of construction: **2010**
Architecture: **Massimiliano Fuksas** Structural engineering: **Knippers Helbig GmbH**, Stuttgart, Berlin, New York
The building is completely covered by triangular, doubly curved grid shell containing synclastic and anticlastic regions. The pattern of triangles is visibly regular and their shapes are similar to each other. Four nodes near the top are 5-valent in order to compensate angle defect. Also, in the indentation and narrowing regions the latitude (horizontal) members decline in order to preserve homogeneity of tessellation.

Source of photo: https://upload.wikimedia.org/wikipedia/commons/8/8a/The_Blob_in_Eindhoven%2C_Netherlands.jpg

Glazed roof in Muzeum Armii Krajowej

Location: **Kraków**, Poland
Date of construction: **2011**
Architecture: **AIR Jurkowscy Architekci**, Katowice
The roof is constructed over a courtyard which has regular, rectangular form with elongated proportions. Synclastic double-curvature of the structure allowed for application of lightweight reticulated shell instead of heavier space truss. The grid shell is composed of welded RHS members aligned in two, diagonal directions creating non-planar quadrilateral pattern. Diagonally to each quad cell a bracing rod is added. The layer of glass is composed of triangular panels, which have high similarity of shapes. The glass layer is connected to the structure through spider-like point connectors of one type.
 
Sources of photos: https://archirama.muratorplus.pl/architektura/muzeum-armii-krajowej-w-krakowie-architektura-korespondujaca-z-przeszloscia,67_2329.html https://www.tarsilvex.pl/images/mak.html

Salvador Dali Museum

Location: **Saint Petersburg**, Florida, USA
Date of construction: **2011**
Architecture & engineering: **HOK**, St. Louis, USA Façade system, design and engineering: **Novum Structures**, Menomonee Falls, USA
Grid shell in this example plays a role of a façade smoothly transforming into a glass roof. This structure was designed and tested in scale for resistance to hurricanes. Double curvature strengthens the structure and harmonizes with the aesthetics of works of art presented in the museum. This example emphasizes the fact that even triangular grid shells can be designed according to the bottom-up methodology, due to the fact that the result displays high consistency in the shapes of triangular glass panels as well in the continuity of members given the complexity of the base form, which is normally difficult to achieve while designing according to top-down design rules.

Source of photo: https://novumstructures.com/project/salvador-dali-museum/

Devon Energy World HQ: Oculus Rotunda Skylight

Location: **Oklahoma City**, USA
Date of construction: **2012**
Architecture: **Kendall/Heaton Associates Inc.**, Houston, Texas ; **Pickard Chilton Architects, Inc.**, New Haven, Connecticut Roof design and engineering: **Novum Structures**, Menomonee Falls, USA
The glazed roof is based on a form of geodesic dome with low rise allowing the construction of single layered structure. Tessellation is regular when in top projection, however individual dimensions of members and shapes of glass panels are different. The tessellation regularity is distorted at the perimeter in order to align the vertices and obtain only triangular panels. Therefore, in this grid shell the directions of individual trusses are not straight in top projection.

Source of photo: https://novumstructures.com/project/devon-energy-world-hq-oculus-rotunda-skylight/

Heydar Aliyev International Airport

Location: **Baku**, Azerbaijan
Date of construction: **2013**
Design: **Ove Arup & Partners** Architecture: **Woods Bagot**, Brisbane Structural engineering: **BuroHappold**, Bath, UK Steel construction: **Waagner-Biro AG**, Vienna
Three canopies above the entrances to the terminal are construct as triangular, steel, glazed grid shells – two of which are synclastic and one is anticlastic. The façade of terminal also contains parts with non-planar quadrilateral cells covered with curved glass.
   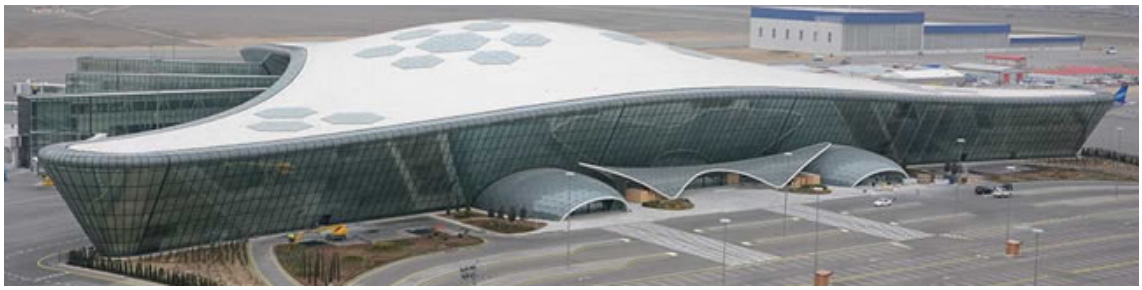
Source of photo: https://www.arch2o.com/wp-content/uploads/2017/10/Arch2O-Heydar-Aliyev-Airport-Woods-Bagot-05.jpg https://en.azvision.az/news/55735/logistics-hub-may-appear-at-baku-int%E2%80%99l-airport.html

Carioca Wave

Location: **Rio de Janeiro**
Date of construction: **2013**
Architecture: **Nir Sivan Architects** Structural design: **Knippers Helbig GmbH**, Stuttgart, Berlin, New York Structural engineering: **Knippers Helbig GmbH**, Stuttgart, Berlin, New York
The form of this structure is a result of evolution, which started from architectural concept assuming more dynamic composition of regions with greater and smaller curvatures and rapid transitions between them. The lack of curvature in some regions would not be able to permit transferring in-plane forces and therefore a slender single-layered structure would not be possible to exist in such a form. Although the form is not a result of form finding, it is optimised in terms of the criteria described above. The result of such optimisation is a form. Which has more homogeneous curvatures. Detailed description of the design is in (Helbig, Giampellegrini, and Oppe 2014)

Source of photo: https://www.knippershelbig.com/sites/default/files/styles/projekt1494/public/image_project//29728-picture.jpg?itok=eNHgQBPA

Ottawa Conference and Event Centre

Location: **Ottawa**, Ontario, Canada
Date of construction: **2013**
Design: **Brisbin Brook Beynon Architects**, Toronto, Canada Façade design and engineering: **Novum Structures**, Menomonee Falls, USA
Freeformed, triangular grid shell wraps the building almost completely around being its dominant and form of expression. Groups of members have consistent directions, e.g. one group is composed of horizontal members only. The curvature of vertical sections of the skin of this building is diverse, from almost straight, vertical sections into far cantilevering parts of façade.
   
Sources of photos: https://novumstructures.com/project/ottowa-conference-and-event-centre/

Tornado Roof in Bory Mall

Location: **Bratislava**, Slovakia
Date of construction: **2014**
Architecture: **Massimiliano Fuksas** Associate architect: **Jančina architekti**, Bratislava Structural engineering: **Knippers Helbig GmbH**, **Thorsten Helbig**, Stuttgart, Berlin, New York Steel construction: **Metal Yapı A.Ş.** (shell), Istanbul
The *Tornado* roof is a grid shell with mixed glazed and opaque cladding, in form of funnel creating a partition between interior and patio of the mall. It is supported at the top and bottom outlines. Depending on the results of non-linear FE analysis varied cross sections of grid members and two node types are used. Less heavily loaded nodes are bolted, whereas more heavily loaded are welded. Detailed description of the roof structure is in (Helbig et al. 2016)

Source of photo: https://www.knippershelbig.com/en/projects/port-mall-shopping-centre

Perdana Garden Canopy

Location: **Kuala Lumpur**, Malaysia
Date of construction: **2014**
Architecture: **GDP Architects Sdn. Bhd.**, Kuala Lumpur Steel construction: **Mero GmbH & Co. KG**, Würzburg
Free formed triangular grid shell is supported on five funnels, which stand on reinforced concrete bases continuing the form of the roof. The curvature of the roof and funnels provide structural stability and allows for wide span coverage.
   
Source of photos: http://gdparchitects.com/2015/?project=perdana-canopy-2

Ak-Asya Mall: Skylights

Location: **Istanbul**, Turkey
Date of construction: **2014**
Design: **Omerler Mimarlik**, Istanbul, Turkey Roof design and engineering: **Novum Structures**, Menomonee Falls, USA
The shape of this glazed roof is composed of two, smoothed surfaces, ruled between two perimeter, concentric arch curves and one wavy ridge curve.
   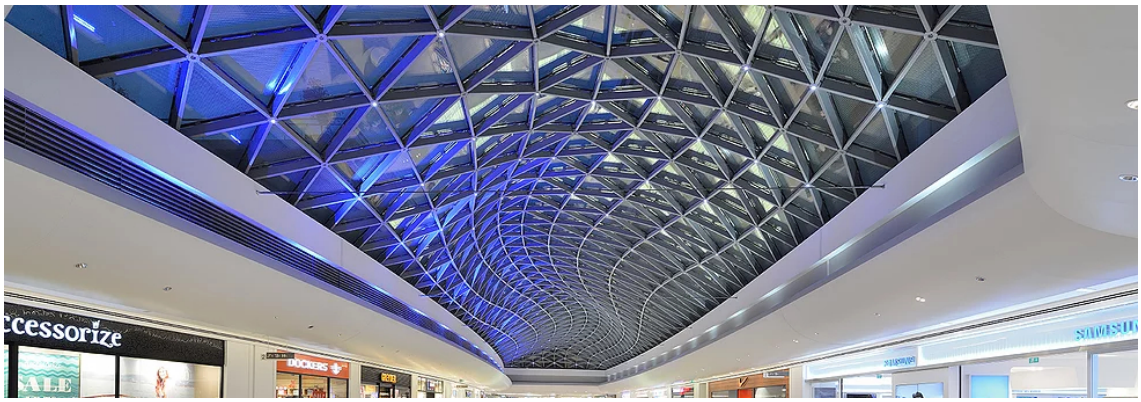
Sources of photos: https://novumstructures.com/project/akasya-mall-skylights/ https://www.omerlermimarlik.com/ak-asya-shopping-mall

Konya Tropical Butterfly Garden

Location: **Konya**, Turkey
Date of construction: **2015**
Architecture & façade engineering: **Ove Arup & Partners**
Single layered, doubly-curved structure is composed of steel lattice shell made of tubular sections in non-planar quadrilateral topology. Over that shell a layer of glass supporting RHS members is added, with one additional diagonal member for each cell of main lattice shell. The structure's double curvature prevents its out-of-plane buckling during seismic activities occurring in that area.

Source of photo: http://www.guardian-inspiration.com/sites/guardian/files/2018-03/KonyaTropicalButterflyGarden_large.jpg

Mall of Africa

Location: **Gauteng**, South Africa
Date of construction: **2016**
Architecture: **MDS Architecture**, Sandton, South Africa Façade design and engineering: **Novum Structures**, Menomonee Falls, USA
Although this grid shell is filled with ETFE pneumatic cushions, which have no planarity restrictions, the tessellation is triangular. This is due to the fact, that the perimeter of this cover has very complex shape consisting of branches and various curves.
   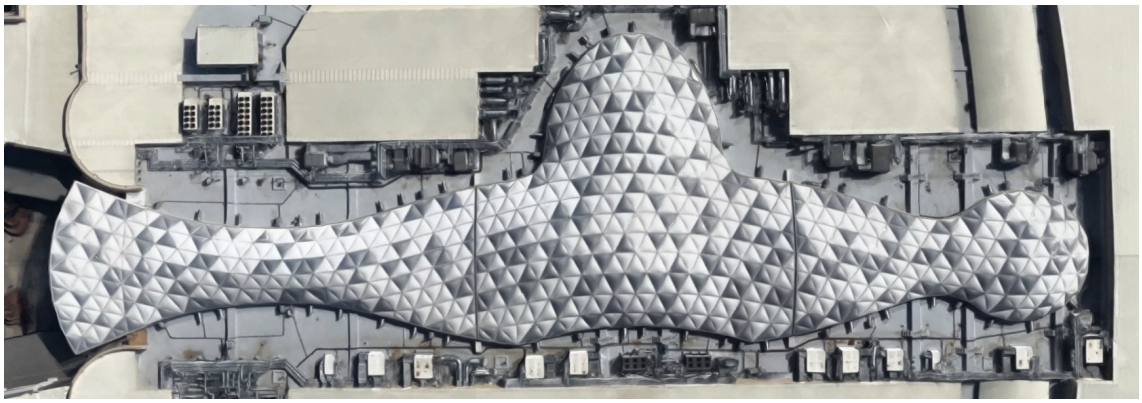
Sources of photos: https://novumstructures.com/project/mall-of-africa/, Google Maps

A-3.2 Grid shells based on PQ topology

List of objects in chronological order:

Museum of Hamburg History

Location: **Hamburg**, Germany
Date of construction: **1989**
Architecture: **von Gerkan Marg und Partner**, Hamburg Structural design and engineering: **sbp – Schlaich Bergermann Partner**, Stuttgart
The roof covers L–shaped courtyard. It is based on mesh composed of two single curved regions and one doubly curved. The generatrixes of both single curved regions were used as directrix and generatrix of the doubly curved region allowing for creating translational PQ mesh. However, that region was also optimized by means of inverted hanging model form-finding method dividing some of the initially planar quads into two triangles or by introduction of cold bent laminated glass, especially near the corners. In order to provide geometrical invariance of quads diagonal cables are introduced. Finally, the cable trusses were introduced to the single curved barrels to replace the second curvature. The design process of this construction is discussed in (Schober 2015b), pp. 44–47.

Source of photo: http://shells.princeton.edu/Ham.html

Swimming Bath Aquatoll

Location: **Neckarsulm**, Germany
Date of construction: **1990**
Architecture: **Kohlmeier und Bechler**, Heilbronn, Germany Conceptual & construction design: **sbp – Schlaich Bergermann Partner**, Stuttgart
The dome was designed with the adoption of translational method resulting with circular plan and members of equal widths, i.e. 1 m. The grid is prestressed by diagonal cables.
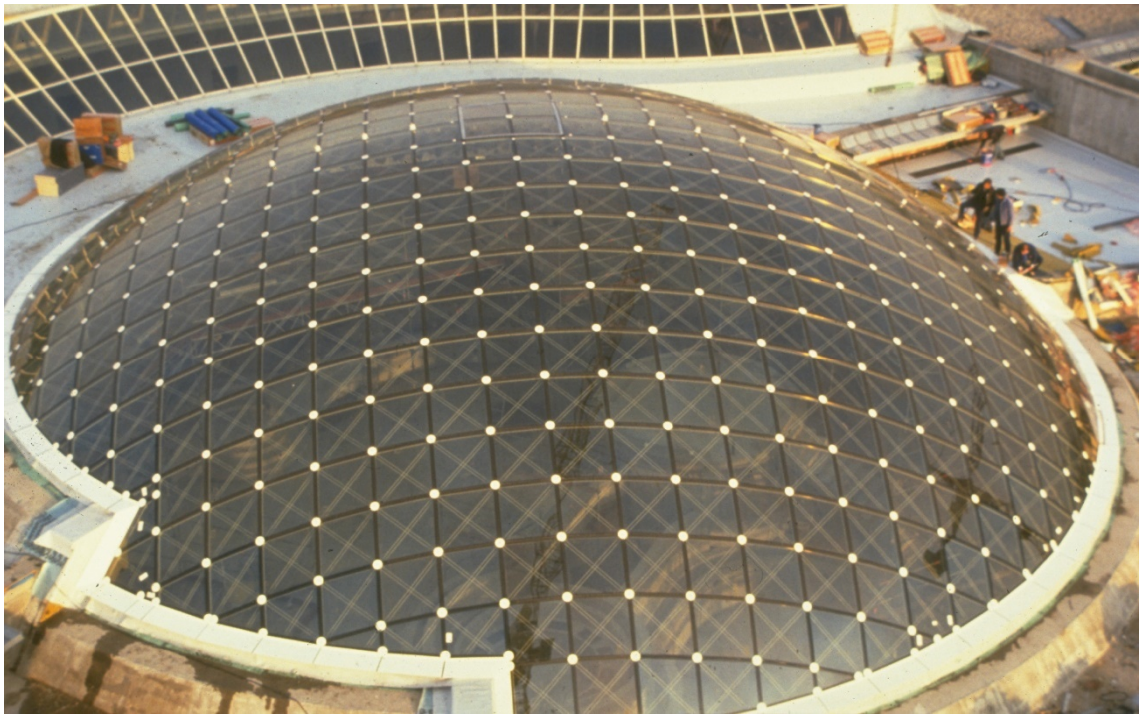   
Source of photos: https://www.sbp.de/en/project/swimming-bath-aquatoll-neckarsulm/

House for Hippopotamus, Zoo Berlin

Location: **Berlin**, Germany
Date of construction: **1996**
Architecture: **J. Gribl**, Munich Conceptual & construction design: **sbp – Schlaich Bergermann Partner**, Stuttgart
Two glass domes and smooth transition between them was achieved thanks to the adoption of translational method for designing PQ grid shells. The generatrix curve is an arch line segment, whereas the directrix curve is composed of three alternately curved arch line segments which create curve of continuous curvature, therefore allowing for generating smooth form of the structure. Part of the generated surface is trimmed by single curved, vertical glass façade resulting with morphologically complex outcome.
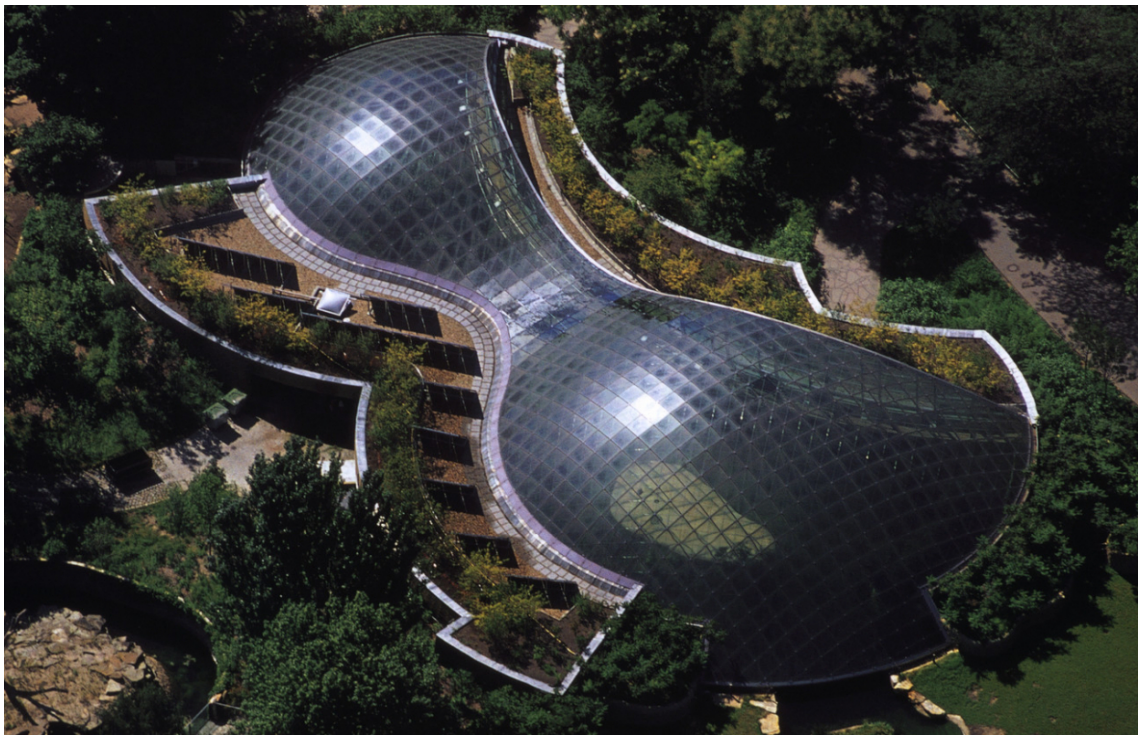   
Source of photos: https://www.sbp.de/en/project/house-for-hippopotamus-zoo-berlin/

Railway Station Frankfurt Airport

Location: **Frankfurt**, Germany
Date of construction: **1999**
Architecture: **Hadi Teherani**, Hamburg, Germany Structural engineering: **INGENIEURBÜRO Dr. Binnewies**, Hamburg, Germany;
The form of this glass shell is supported on the floor level creating the walls and roof of the hall beneath. Smoothness of the surface is obtained by highly consistent is shape rectangular PQ glass panels with structural silicon sealings. Reversed order of layers in the structure additionally emphasize the smoothness from inside, that is glass panels are suspended on spider-like point connectors which are connected to tubular trusses above the layer of glass, outside the dome.
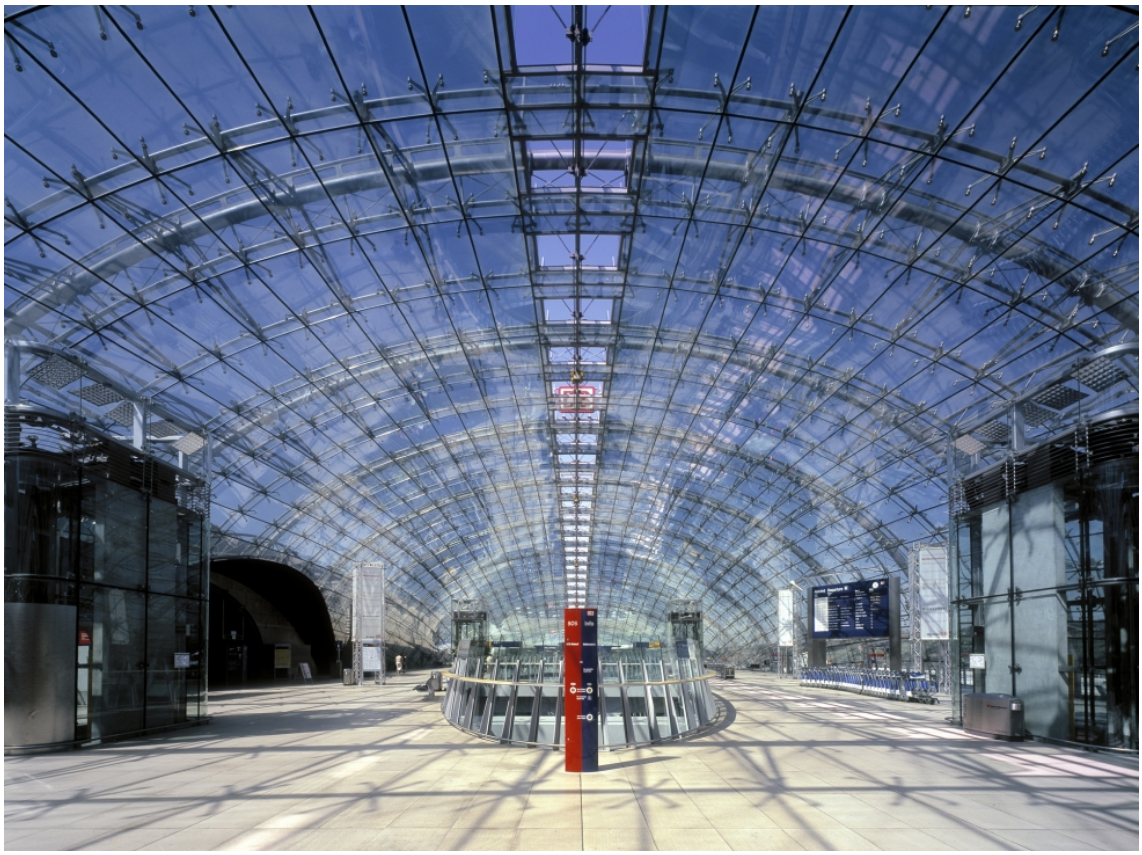
Source of photo: https://commons.wikimedia.org/wiki/Category:Frankfurt_(Main)_Flughafen_Fernbahnhof#/media/File:Frankfurt-Flughafen_2011-08-by-RaBoe-03.jpg

Osaka Maritime Museum

Location: **Osaka**, Japan
Date of construction: **2000**
Architecture: **Aéroports de Paris**, **Paul Andreu**, Paris Structural engineering: **Ove Arup & Partners**, **Tohata Architects & Engineers Inc.**, Japan
The spherical dome is tessellated into PQ topology by loxodromic pattern, i.e. the edges intersect with latitudinal and longitudinal lines at the same angle. The supporting grid shell is constructed in the same pattern, however only half as genes as glazing pattern, i.e. only two opposite vertices of each panel are directly supported. Other vertices of panels are supported on cable network attached to the grid shell. The cable network is composed of cables running in latitudinal and longitudinal directions.
   
Source of photo: https://commons.wikimedia.org/wiki/Category:Osaka_Maritime_Museum#/media/File:Osaka_maritime_museum01s3200.jpg

Great Glass House

Location: **Carmarthenshire**, Wales
Date of construction: **2000**
Architecture: **Foster + Partners**, London Structural engineering: **Anthony Hunt Associates**, London
The structure is designed using translational PQ mesh method. It is a synclastic, doubly-curved structure which is set on round, slightly leaning concrete base. The main trusses of the structure are therefore deviated from the vertical planes.
   
Source of photo: https://www.flickr.com/photos/sevendipity/1375231075/ https://www.fosterandpartners.com/media/2632329/img0_0861_fp138118.jpg?width=1920&quality=85

Bosch Areal

Location: **Stuttgart**, Germany
Date of construction: **2001**
Architecture: **Prof. Ostertag und Vornholt Architekten**, Stuttgart Steel Structure and Glazing: **Mero GmbH & Co. KG**, Würzburg
Single layered grid shell with pre-stressed tensile cables covers area with complex shape between several buildings. Translational base surface is trimmed by walls of adjacent buildings resulting with non-horizontal edges. The structure is additionally reinforced by radial tension trusses.
   
Sources of photos: Google Maps, https://commons.wikimedia.org/wiki/File:Bosch-Areal_Stuttgart_08.jpg

Schubert Club Band Shell

Location: **Saint Paul**, Minnesota, USA
Date of construction: **2002**
Architecture: **Peter Kramer** Associate architects: **James Carpenter Design Associates** Structural engineering: **Shane McCormick; Skidmore, Owings & Merrill**, Chicago; **William F. Baker**
The grid shell has a negatively curved form and tessellation in this example is planar quadrilateral. It is worth emphasizing that the strips of planar quads follow principal curvature lines of the form, see section 3.7.1. In negatively curved forms different alignment of PQ strips would cause to generate planar panels in forms of elongated parallelograms.

Source of photo: https://structurae.net/photos/290221-schubert-club-band-shell

Schlüterhof Roof, German Historical Museum

Location: **Berlin**, Germany
Date of construction: **2002**
Architecture: **I. M. Pei & Partners**, New York; **Eller + Eller Architekten**, Berlin Conceptual & construction design: **sbp – Schlaich Bergermann Partner**, Stuttgart
Translational method was used to obtain doubly curved PQ mesh of this grid shell. Trusses of members are aligned diagonally to the courtyard, which har rectangular shape in plan with two cylindrical extensions at the corners. The doubly curved surface of the grid shell touches the building at corners only, whereas along the edges vertical facades were constructed to close the gaps between building and roof. Each quadrilateral cell is stabilized with two diagonal tensile ties. All glass panels have almost identical shapes and dimensions, i.e. about 1.75 x 1.75 m.


Source of photos: https://www.sbp.de/en/project/schlueterhof-roof-german-historical-museum/

Sage Gateshead

Location: **Gateshead**, UK
Date of construction: **2004**
Architecture: **Foster + Partners**, London Structural engineering: **BuroHappold**, Bath, UK; **Mott MacDonald**, Croydon, UK
The skin of the Sage Gateshead is a PQ scalar-translational grid shell, with glass and opaque cladding. Crosswise the structure is supported by six transverse trusses, two located at the sides leaning out and four inside the structure, located beneath the negatively curved regions of grid shell.
   
Sources of photos: https://commons.wikimedia.org/wiki/File:Sage_Centre_from_North_bank_of_Tyne_-_geograph.org.uk_-_707019.jpg https://upload.wikimedia.org/wikipedia/commons/9/91/Sage_087.jpg

University of Zurich Law Faculty

Location: **Zurich**, Switzerland
Date of construction: **2004**
Design: **Santiago Calatrava Valls AG**, Zürich, Switzerland
Glazed cover of oval courtyard was designed using scale – trans PQ mesh, which is additionally supported along truss running along central ridge.
 
Sources of photos: https://calatrava.com/projects/university-of-zurich-law-faculty-zuerich.html

Wrigley: Global Innovation Center

Location: **Chicago**, Illinois, USA
Date of construction: **2005**
Architecture: **HOK**, St. Louis, USA Roof design and engineering: **Novum Structures**, Menomonee Falls, USA
The grid shell covers a courtyard which has irregular shape composed of six edges. Instead of supporting the roof on the walls it is supported by steel frames composed of mullions and arched beams hidden within vertical glass facades.
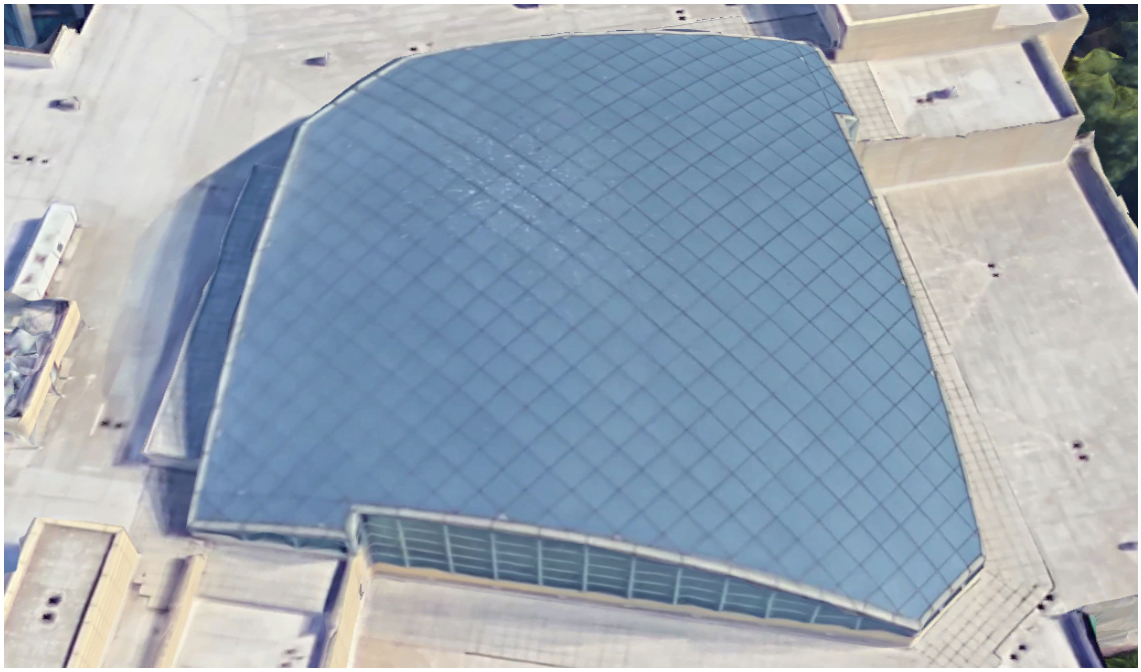   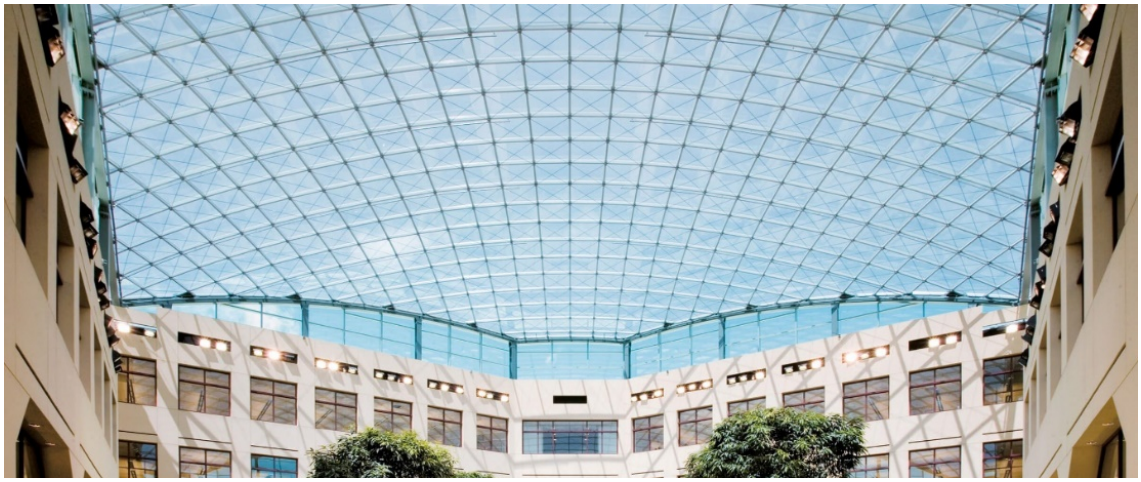
Source of photo: https://novumstructures.com/project/wrigley-global-innovation-center/

Seattle-Tacoma International Airport

Location: **Seattle**, USA
Date of construction: **2005**
Architecture: **Fentress Architects**, Denver, Los Angeles, San Francisco, Washington D.C., Houston Façade design and engineering: **Novum Structures**, Menomonee Falls, USA
The façade is composed of PQ glass panels obtained by rotational method. Each panel is fixed in place by four point, spider connectors, which in turn are retained in place by steel cables running along and across the façade. Due to negative gaussian curvature the façade each cable retaining a joint is curved in different direction, so that the forces perpendicular to it are in balance.
   
Sources of photos: https://novumstructures.com/project/sea-tac-international-airport/ https://commons.wikimedia.org/wiki/File:Glass_Facade_of_Anthony%27s_Restaurant_and_Fish_Bar_at_Sea-Tac_Airport.JPG

Swinhay House

Location: **Swinhay**, UK
Date of construction: **2006**
Architecture: **Roberts Limbrick Architects**, Gloucester, UK
Although the grid shell has triangular topology, the glazing cover is in PQ topology. For each PQ glass panel one diagonal member is applied for the grid shell underneath in alternating directions, creating pattern of pairs of coplanar triangles.
   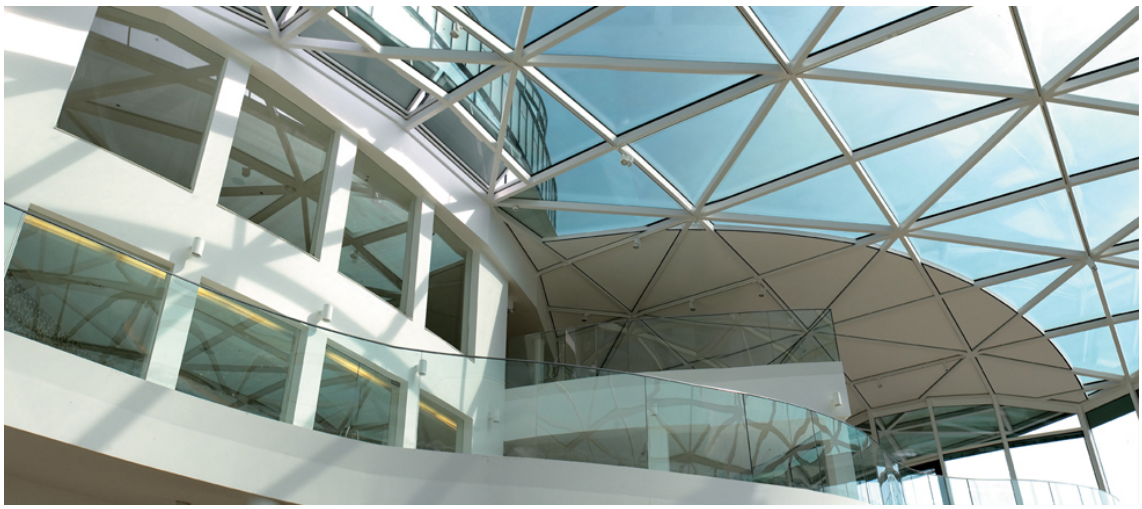
Sources of photos: http://www.homecrux.com/wp-content/gallery/30-million-swinhay-house/30-million-swinhay-house_3.jpg http://www.robertslimbrick.com/wp-content/uploads/2012/12/Swinhay%203.jpg

Elephant House

Location: **Copenhagen**, Denmark
Date of construction: **2008**
Architecture: **Foster + Partners**, London Structural design: **BuroHappold**, Bath, UK
In the Elephant House in Copenhagen there are actually two PQ glass roofs of different sizes, however designed according to similar principles. Individual trusses of these grid shells lie on non-parallel planes. Such effect can be obtained by using the rotational method for PQ mesh generation. Furthermore the axes of rotation are neither vertical nor horizontal, resulting with unobvious, original solution.
   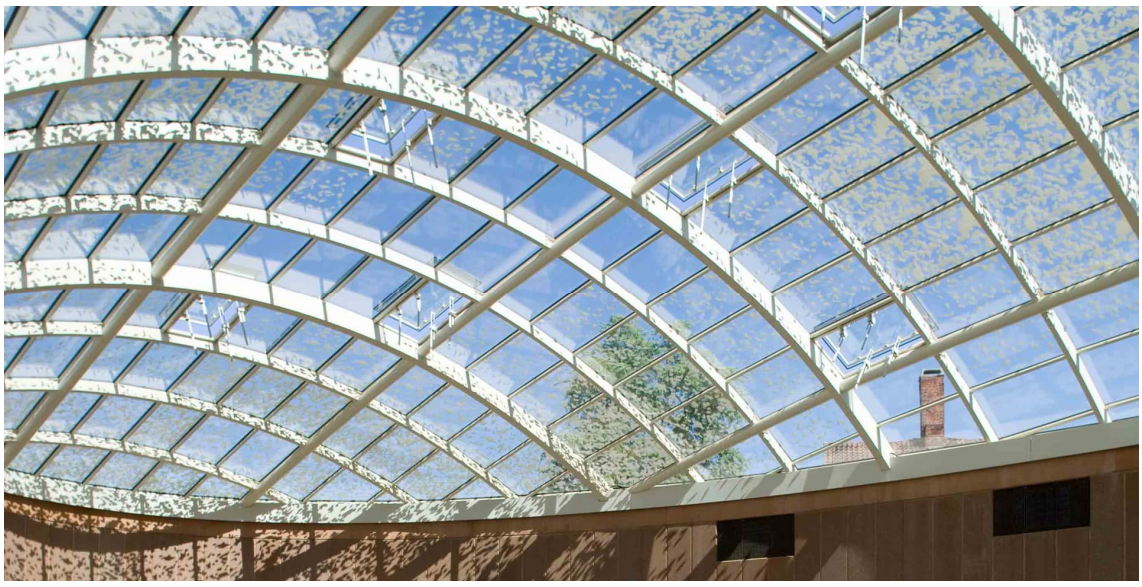
Source of photos: https://www.fosterandpartners.com/projects/elephant-house-copenhagen-zoo/

Cabot Circus

Location: **Bristol**, UK
Date of construction: **2008**
Architecture: **Chapman Taylor LLP Architects Masterplanners**, London Conceptual & roof design: **sbp – Schlaich Bergermann Partner**, Stuttgart
The central roof (shown in picture below) is a doubly-curved, single layer, glazed grid shell in PQ topology obtained by rotational method, where the axis of rotation is neither vertical nor horizontal. Smaller roofs are also doubly curved, PQ, glazed grid shells in both positive and negative gaussian curvatures.

Source of photo: https://www.sbp.de/en/project/cabot-circus-bristol/

Mint Hotel Tower of London

Location: **London**, England
Date of construction: **2010**
Architecture: **Bennetts Associates**, London Roof design and engineering: **Novum Structures**, Menomonee Falls, USA
This low-rise doubly curved PQ grid shell covers quadrilateral courtyard with irregular shape. Edges of the grid shell adjacent to walls are slightly arched. Small curvature values of the lattice shell cause substantial values of support force horizontal components reacting on the walls. However, in case of newly constructed structures, such forces can be provided in the construction of the building.
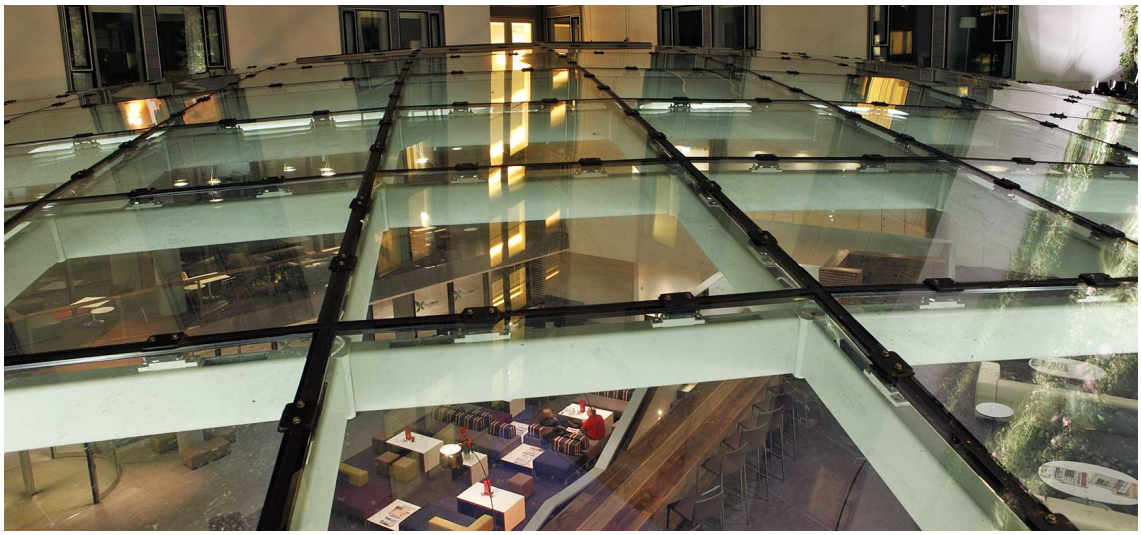   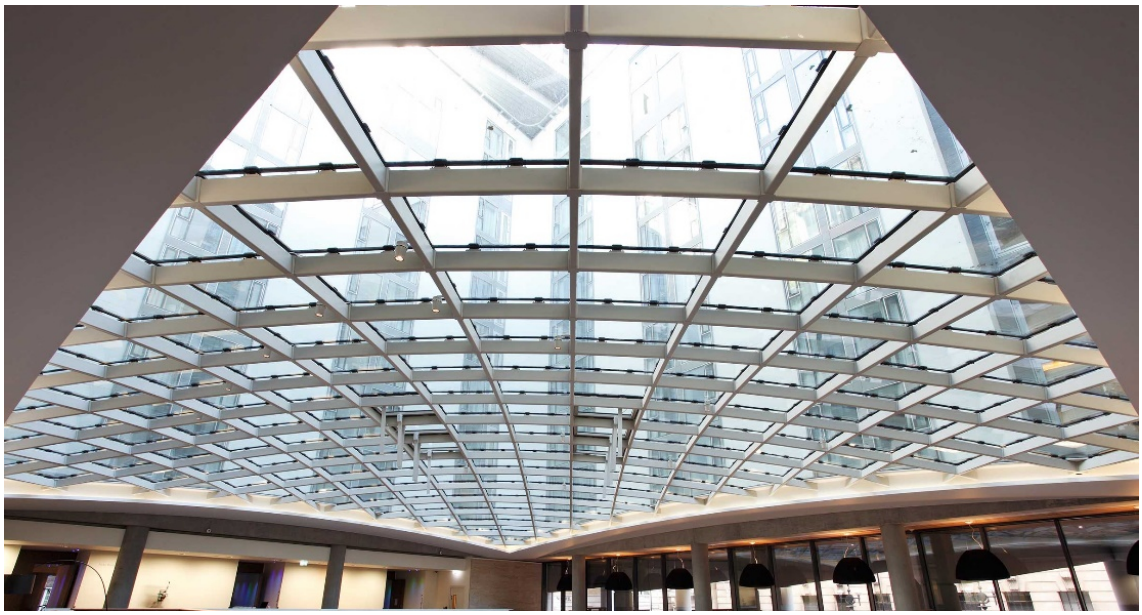
Source of photos: https://novumstructures.com/project/mint-hotel-tower-of-london/

Pearl River Tower

Location: **Guangzhou**, China
Date of construction: **2011**
Architecture: **Adrian Smith + Gordon Gill Architecture** (**AS+GG**), Chicago; **Guangzhou Chengzong Design Institute**, Guangzhou Structural engineering: **Skidmore, Owings & Merrill**, Chicago
The Pearl River Tower belongs to one of the most environmentally friendly building in the world, among other things thanks to its innovative shape. Doubly curved façade divided into three segments direct streams of air blowing from the dominant direction into the channels equipped with power generating turbines. The shape was not only optimized according to these requirements but also taking into consideration the possibility of constructing the facades basing on the PQ tessellations. The segments of facade are based on a rotational PQ meshes and the shapes of individual panels have reasonably unified shapes.
   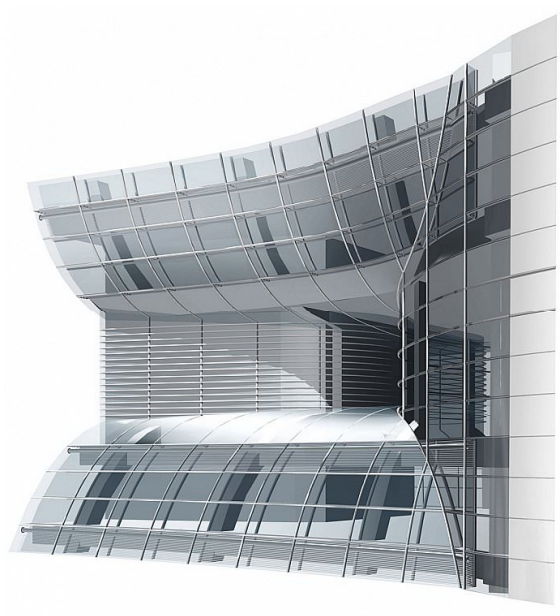   
Source of photos: https://www.som.com/projects/pearl_river_tower

Georgian Parliament Building

Location: **Kutaisi**, Georgia
Date of construction: **2012**
Architecture: **Alberto Domingo Cabo** Structural engineering: **CMD Domingo y Lázaro Ingenieros SL,** Valencia; **Kawaguchi & Engineers: Mamoru Kawaguchi**, **Kenichi Kawaguchi**, Tokyo
Glass cover over the dome of Georgian Parliament Building is tessellated in PQ fashion, which was generated using translational method. The cover is constructed over space truss.
   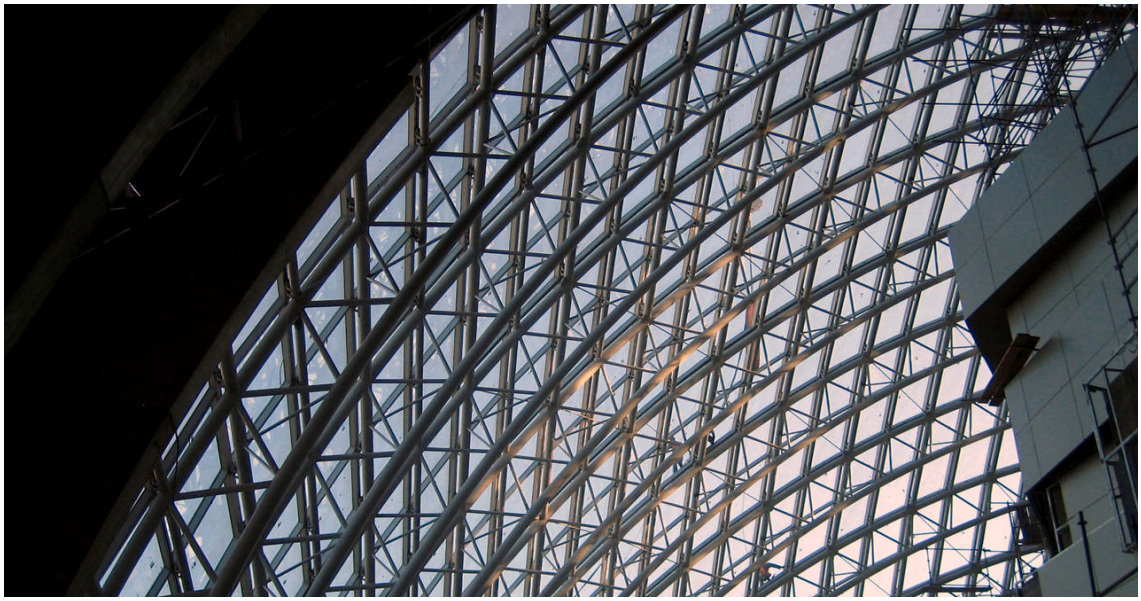
Sources of photos: https://fi.wikipedia.org/wiki/Georgian_parlamentti#/media/File:Parlament_of_Georgia_(Kutaisi)_copy.jpg https://images.adsttc.com/media/images/55e6/db24/8450/b545/5500/1166/slideshow/7-img_6307.jpg?1441192735

Paunsdorf Center glass roofs

Location: **Leipzig**, Germany
Date of construction: **2012**
Conceptual & construction design: **sbp – Schlaich Bergermann Partner**, Stuttgart
Glazing layer has PQ topology obtained by translational method. Each individual panel has the same shape of elongated parallelogram when projected on horizontal plane. Due to the disproportion between lengths of diagonals of glass panels additional member was added along each shorter diagonal creating pattern of proportionally balanced triangles in the grid shell.
 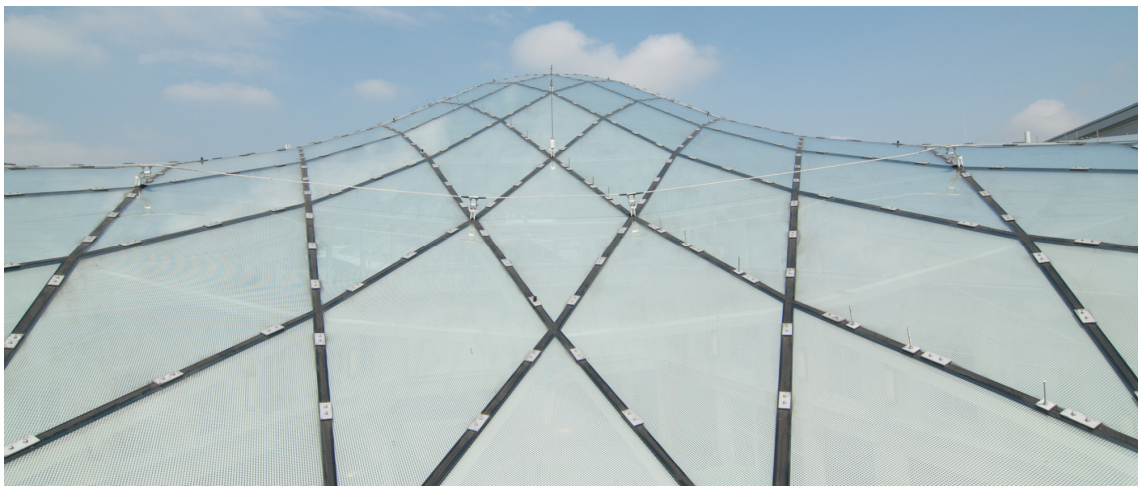
Source of photos: https://www.sbp.de/en/project/glass-roofs-paunsdorf-center-1/

Statoil Regional and International Offices

Location: **Fornebu**, Norway
Date of construction: **2012**
Architecture: **A-lab**, Oslo, Norway
All façades in this buildings are PQ glazed grid shells based on negatively curved, hyperbolic paraboloid surfaces, which are also doubly ruled surfaces. Each one of these surfaces is bounded by four straight edges, which are not placed on a common plane. Although ruled surfaces contain straight lines, structural members of this structures are diagonally aligned to those due to the fact that quadrangles generated by intersections of ruling lines would not be planar. In fact strip of PQ panels are aligned along the smallest and the largest curvatures (see section 3.7.1 describing *conjugate curvature networks* of doubly curved surfaces). Since the surfaces are negatively curved, the value of curvature of straight lines is between the most (positively) and least (negatively) curved directions.
 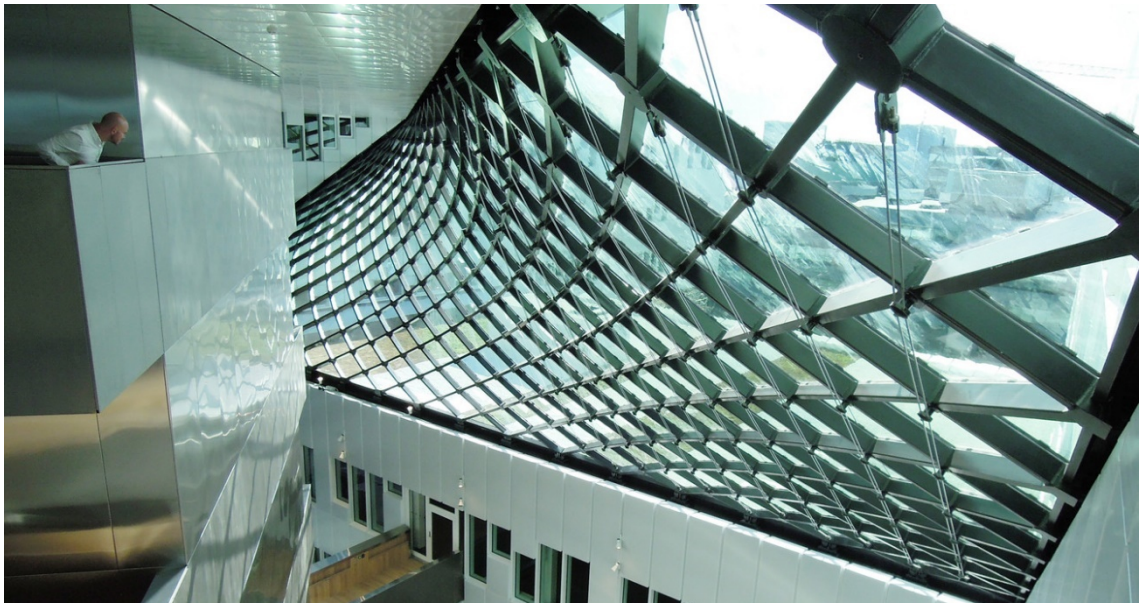
Sources of photos: https://www.archdaily.com/359599/statoil-regional-and-international-offices-a-lab

EGO Roof

Location: **Erbach**, Germany
Date of construction: **2013**
Architecture: **Heusel & Schantz,** Michelstadt, Germany Roof design: **MERO-TSK International GmbH & Co. KG**, Würzburg, Germany
This lightweight glass roof has been formed as translational PQ mesh consisting of positive and negative gaussian curvatures. The roof requires additional supports in forms of tree-like columns. The surface is tessellated in a particular manner, which results with obtaining two types of nodes: four and eight valent. Each PQ cell of the grid shell, not the glass panels, has been diagonally divided by additional member. Individual grid cells are equilateral right triangles, the same in shape from top projection, while in fact there is high diversity in their shapes.
   
Sources of photos: https://www.mero.de/index.php/en/construction-systems/references-en/36-space-structures/720-ego-roof-erbach-wave-in-free-form-en

Trinity

Location: **Leeds**, England
Date of construction: **2013**
Architecture: **Chapman Taylor LLP Architects Masterplanners**, London
The grid shell in PQ topology, obtained by rotational method has high regularity and consistency of shape and tessellation. However it covers a courtyard of highly irregular shape with additional four outgoing hallways. Boundary edges of the roof are therefore curved in plan or spatially curved.

Source of photo: https://www.chapmantaylor.com/projects/trinity-leeds#&gid=1&pid=1

A-3.3 Grid shells based on hybrid topology

List of objects in chronological order:

Robert and Arlene Kogod Courtyard Roof (Smithsonian American Art Museum)

Location: **Washington**, District of Columbia
Date of construction: **2007**
Architecture: **Foster + Partners**, London Façade construction: **Josef Gartner GmbH**
Due to the fact, that the roof cannot be clearly classified neither as planar quadrilateral nor as triangular, it is presented in this section. Although the individual facets are planar quads, corresponding edges of adjacent panels are not colinear and vertices of adjacent panels are not placed in a common point. These two constraints are always satisfied in the other examples in this section. Although the construction acquired the status of an architectural icon it is the only one of its type and such solution was never adopted again due to the costliness and complexity.
   
Sources of photos: https://www.fosterandpartners.com/projects/smithsonian-institution-courtyard/#gallery https://structurae.net/structures/robert-and-arlene-kogod-courtyard-roof-smithsonian-american-art-museum

Dubai Festival City glazed roof

Location: **Dubai**, United Arab Emirates
Date of construction: **2008**
Roof construction: **Waagner-Biro AG**, Vienna
The double curvature of the roof comes from the transverse arch-like profile and the longitudinal curved shape of the hall it covers. Members of the grid shell run in three directions: two diagonal and one longitudinal. The longitudinal members are implemented only in every second row, dividing only half of the original quadrilateral facets. The vertices along longitudinal members are also shifted allowing the planarity of remaining quadrilateral facets. Such solution allowed for reduction of every sixth steel member, simplification of half of all nodes from 6- to 4- valent and finally savings on quadrilateral glass panels manufacturing.
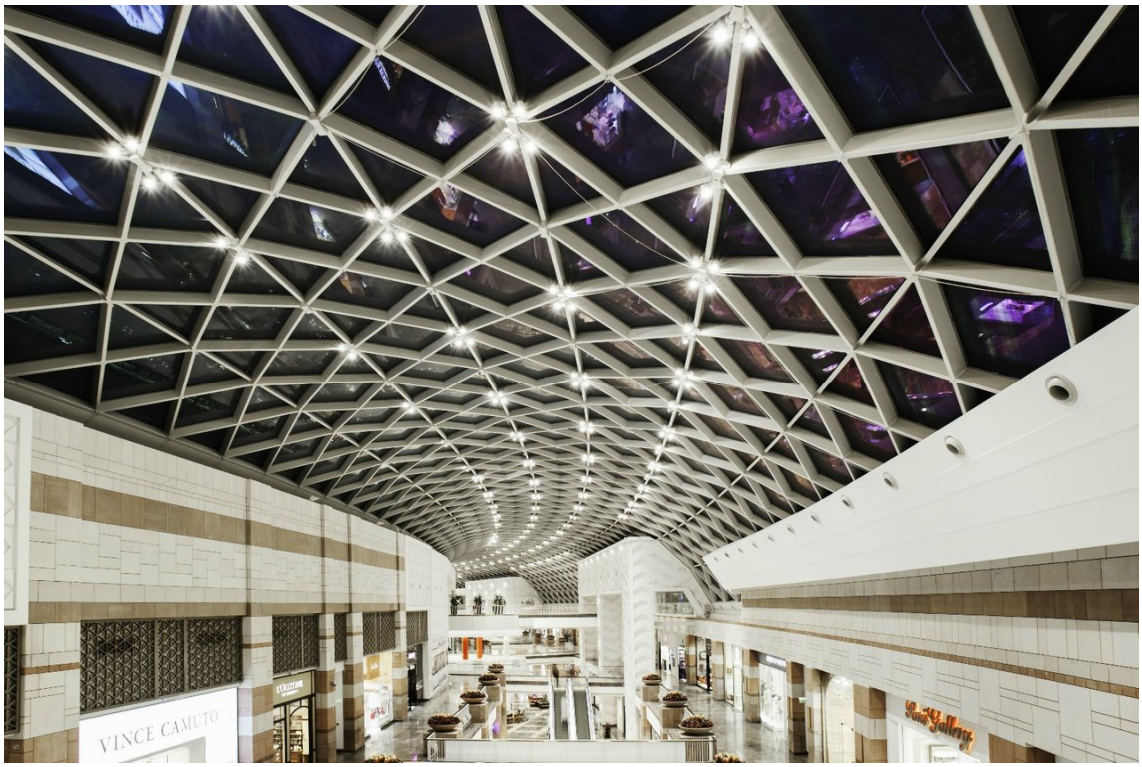
Source of photo: https://www.waagner-biro.com/en/divisions/steel-glass-structures/references/reference/dubai-festival-city

ION Orchard

Location: **Singapore**
Date of construction: **2009**
Architecture: **RSP Architects Planners & Engineers Ltd**, **Benoy** Structural & Façade engineering: **Ove Arup & Partners**
The glazed canopy has arbitrarily free formed shape according to the top-down approach. Its tessellation was optimized, so that only part of the panels are triangular, according to the intrinsic geometrical properties of the surface. However, the shapes of resultant panels are highly irregular, i.e. the quads are sheared and the lengths of members are varied greatly, so are the geometries of nodes. The structure is additionally supported by tree-like columns.

Source of photo: https://www.arup.com/projects/ion-orchard

Bálna CET

Location: **Budapest**, Hungary
Date of construction: **2010**
Architecture: **ONL, Kas Oosterhuis, Ilona Lénárd**, Utrecht, Netherlands Implementation: **Central Industry Group – CIG Architecture**, Osloweg, Netherlands
This structure creates an individual building between two historical buildings. Several grid shells filled with opaque and glass panels form roof and walls. Edges between individual surfaces are visible in the types of cladding and transitions between layouts of grids. The tessellation is not consistent, various shapes and topologies of glass panels are present including PQ panels where it was possible. Transverse tensile members are introduces along the ridges of existing buildings, where part of the grid shell is supported, in order to eliminate horizontal components of support forces.
   
Sources of photos: https://www.archdaily.com/264394/cet-building-onl/502dbe2a28ba0d1b4d00002a-cet-building-onl-photo

Cour Visconti, Louvre

Location: **Paris**, France
Date of construction: **2012**
Architecture: **Mario Bellini** and **Rudy Ricciotti** Structural design: **Waagner-Biro**, Vienna
Although the glazed roof is designed over arbitrarily freeformed surface, its tessellation is highly regular. The top layer of space truss underneath glazing consists of two types of cells filling the surface in a chessboard pattern. The structure was optimized in such a manner, that the vertices of half of the cells were shifted at the expense of the other half of panels, resulting with 50% of PQ panels and 50% of non-PQ panels, which are covered by two triangular glass panels each. The shapes of PQ panels are close to squares whereas triangular panels are right, isosceles triangles. All panels are highly similar in shape. The structure is constructed as steel space truss.
   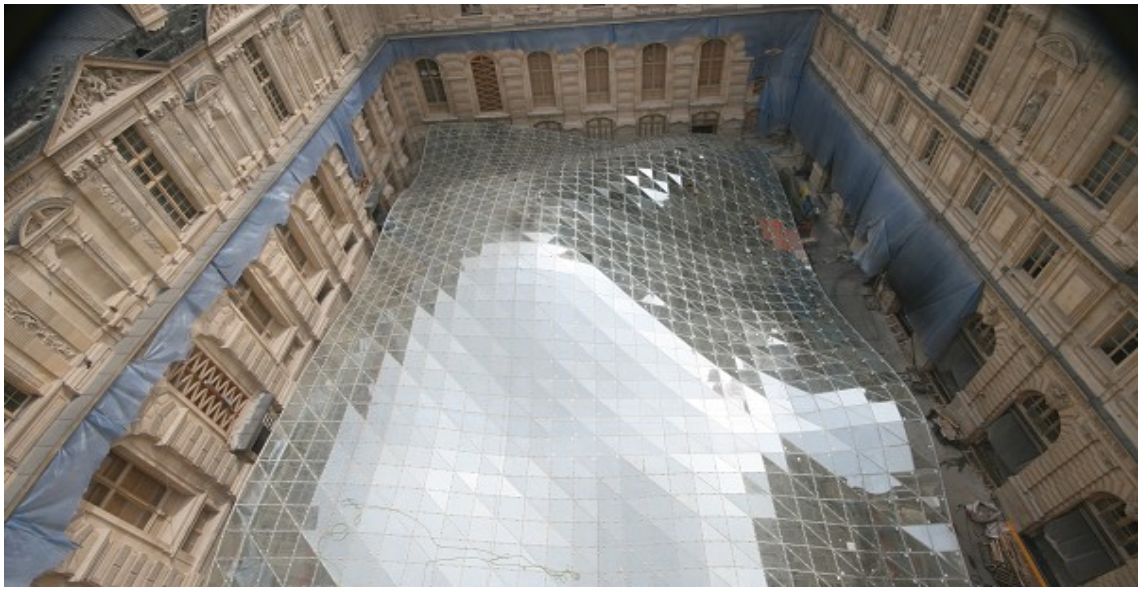
Source of photo: http://www.formakers.eu/media/1.39.1327070323.13413263553745pngpng.png https://files1.structurae.de/files/photos/f011315/das_fertige_glasdach.jpg

Galeria Katowicka

Location: **Katowice**, Poland
Date of construction: **2013**
Architecture: **SUD Architects**, Lyon, France Structural design: **Ove Arup & Partners**
The facade and roof covering the entrance hall of Galeria Katowicka was designed according to the rotational method of generating PQ meshes. Axis of rotation is vertical in this case. The other glass roof in the building include using sweep method (see section 4.1.5) for generating initial PQ mesh, which was later modified to fit the resultant shape into desired shape of corridor walls, making some of the facets non-planar in return.
   
Source of photo: http://www.stekra.pl/static/uploaded_files/galeria-katowicka-6/galeria-katowicka-2.jpg